Dissertation zur Erlangung des Doktorgrades

der Fakultät für Chemie und Pharmazie

der Ludwig-Maximilians-Universität München

Cell Cycle-regulated Signaling and Remodeling at DNA double-strand breaks

Susanne Charlotte Sophie Bantele

aus

Stuttgart, Deutschland

2018

Erklärung

Diese Dissertation wurde im Sinne von § 7 der Promotionsordnung vom 28. November 2011 von Herrn Prof. Dr. Roland Beckmann betreut.

Eidesstattliche Versicherung

Diese Dissertation wurde eigenständig und ohne unerlaubte Hilfe erarbeitet.

München, den 25.10.2018

_____

Susanne C.S. Bantele

Dissertation eingereicht am 17.08.2018

1. Gutachter: Herr Prof. Dr. Roland Beckmann
2. Gutachter: Herr Prof. Dr. Klaus Förstemann

Mündliche Prüfung am 20.09.2018

Table of Contents

List of original publications

Publication 1 | Bantele et al (2017) *eLife*

Bantele, S.C.S., Ferreira, P., Gritenaite, D., Boos, D. & Pfander, B. (2017).Targeting of the Fun30 nucleosome remodeller by the Dpb11 scaffold facilitates cell cycle-regulated DNA end resection. ***eLife***. pii: e21687. doi: 10.7554/eLife.21687.

Publication 2 | Bantele et al., manuscript in revision

Bantele S.C.S., Lisby M., Pfander B. Quantitative signalling mechanisms in response to DNA damage

Publication 3 | Di Cicco et al (2017) *Sci Rep*

Di Cicco, G., **Bantele, S.C.S.**, Reusswig, K-U., Pfander, B. (2017). A cell cycle-independent mode of the Rad9-Dpb11 interaction is induced by DNA damage. ***Sci Rep*** 7(1):11650. doi:10.1038/s41598-017-11937-z.

Publication 4 | Gritenaite et al. (2014) *Genes Dev*

Gritenaite, D., Princz, L. N., Szakal, B., **Bantele, S. C. S.**, Wendeler, L., Schilbach, S., et al. (2014). A cell cycle-regulated Slx4-Dpb11 complex promotes the resolution of DNA repair intermediates linked to stalled replication. ***Genes & Development***, *28*(14), 1604–1619. doi:10.1101/gad.240515.114.

Contribution statement

This thesis comprises the work of my doctoral studies in Dr. Boris Pfander's lab at the MPI of Biochemistry (Martinsried), which was conducted between January 2013 and July 2018. The projects were performed in collaboration with other members of Boris Pfander's lab and the research groups of Prof. Bianca Habermann (Martinsried, Germany), Prof. Joao Matos (Zurich, Swiss), Prof. Michael Lisby (Copenhagen, Denmark), Prof. Dominik Boos (Essen, Germany), and Dr. Dana Branzei (Milan, Italy).

Publication 1 (Bantele et al, *eLife*, 2017)

In this paper, a novel mechanism of cell cycle regulation of DNA end resection at DNA double-strand breaks via the association of the Fun30 chromatin remodeler with the scaffold protein Dpb11 is resolved. I established and performed all experiments except the pulldown assays with human SMARCAD1 and TopBP1 in Figures 9B and 9D, which were performed in the lab of our collaborator Dominik Boos (University of Duisburg, Essen). D. Gritenaite (our lab) helped to establish Fun30-Dpb11 Co-Immunopurification experiments. I prepared all figures and edited the manuscript.

Publication 2 (Bantele *et al*, in revision)

In our current manuscript, we provide the first quantitative study of DNA damage checkpoint activation and elucidate how cells count their DNA damage load. I performed all experiments in this manuscript except for the microscopic analysis of RPA and Ddc1 foci in Figure 4B, which was conducted by M. Lisby (University of Copenhagen). I established all key methodology, prepared all figures and contributed to writing the manuscript.

Publication 3 (Di Cicco et al, *Sci Rep*, 2017)

In this publication, we report a novel mode of the interaction between the scaffold protein Dpb11 and the checkpoint protein Rad9. I contributed to the foundation of this

project and established key methodologies like the Resection Assay and Rad9 Chromatin Immunoprecipitation (ChIP). I generated initial data and materials and commented on the manuscript.

Publication 4 (Gritenaite et al, *Genes Dev*, 2014)

This publication addresses the mechanism of joint molecule resolution at different stages of the cell cycle, in particular by regulation of the Mus81-Mms4 resolvase complex via association with the scaffold protein Dpb11.
I established and performed the RPA foci experiments and analysis presented in Figure 3F, which showed a strong increase of unresolved ssDNA-containing DNA structures in the *slx4-S486A* mutant. I commented on the manuscript.

Abbreviations

3D	3-dimensional
9-1-1	Rad9-Hus1-Rad1 complex
AT	Ataxia talengiectasia
ATP	adenosine triphosphate
BER	base excision repair
BIR	break-induced replication
BRCT	BRCA1 C-terminus
BRCT	carboxy-terminal domain of BRCA1
BS	Bloom syndrome
CDK	cyclin-dependent kinase
ChIP	Chromatin Immunoprecipitation
CK2	Casein kinase 2
CPT	camptothecin
CRISPR	clustered regularly interspaced short palindromic repeats
CUE	coupling of ubiquitin to ER degradation
DDK	Dbf4-dependent kinase
DDR	DNA damage response
DNA	desoxyribonucleic acid
DPC	DNA-protein crosslink

DSB	double-strand break
dsDNA	double-stranded DNA
FA	Fanconi anemia
FHA	forkhead-associated
GC	gene conversion
GCR	gross chromosomal rearrangements
HR	homologous recombination
ICL	interstrand crosslink repair
IR	ionizing radiation
JM	joint molecule
MM	mismatch repair
MMEJ	microhomology-mediated end joining
MMEJ	microhomology mediated end-joining
MRX	Mre11-Rad50-Xrs2
MRX complex	Mre11-Rad50-Xrs2 complex
NBS	Nijmegen breakage syndrome
NER	nucleotide excision repair
NHEJ	non-homologous end joining
OB	oligonucleotide-/oligosaccharide-binding
PIKK	Phosphatidylinositol 3-kinase related
PTM	post-translational modification
qPCR	quantitative PCR
RNR	ribonucleotide reductase
ROS	reactive oxygen species
SAC	spindle assembly checkpoint
SCD	Serine cluster domain
SDSA	synthesis-dependent strand annealing
SSA	single-strand annealing
ssDNA	single-stranded DNA
SWI/SNF	Switch/Sucrose non-fermentable
TAD	topologically associated domain
UV	ultra violet
WT	wildtype
XP	Xeroderma pigmentosum
Y2H	yeast two hybrid

Summary

Maintaining an undamaged, stable genome during DNA transcription, replication and cell division is a pivotal task for cells and therefore governed by a vast variety of surveillance and repair mechanisms. Lesions in genomic DNA are recognized and reported by a signaling network termed DNA damage checkpoint. Subsequently, affected cells stop their cell cycle and activate DNA repair mechanisms in order to clear the genome from DNA lesions and resume the cell cycle with a healthy genome. The molecular pathways coordinating and executing the response to DNA damage are tailored to the nature of the lesion as well as to the cell cycle stage-specific properties of chromosomes. As a consequence, the DNA damage response (DDR) is highly cell cycle-regulated. We are interested in the molecular mechanisms underlying this regulation.

Our entry point to these studies was the scaffold protein Dpb11, which acts as a reader of cell cycle-regulated PTMs set by the major cell cycle kinase CDK (cyclin-dependent kinase). Earlier research has identified two key points of CDK regulation in the DNA damage response: DNA damage checkpoint signaling and DNA repair pathway choice. Intriguingly, both processes are controlled by DNA end processing via resection. Therefore I propose that the cell cycle control of DNA end resection shapes these downstream responses.

Yet, it remained elusive how DNA end resection is ultimately regulated by the cell cycle, how chromatin – the resection substrate – plays into this regulation and how the amount of end resection, which can be viewed as an indicator of the repair status of the DNA lesion, is quantitatively sensed by DNA damage checkpoint proteins and translated in an appropriate signaling response.

In this thesis work, we demonstrate that the nucleosome remodeler Fun30 is targeted to DSBs in a cell cycle-regulated manner by a CDK-dependent complex with Dpb11. By using loss- and gain of function mutants of *FUN30,* which specifically manipulate *FUN30* activity at DSBs, we could establish Fun30 and resected chromatin as decisive bottleneck to end resection (Bantele et al, *eLife* (2017)).

One specific result of DNA end resection is the generation of single-stranded DNA (ssDNA), which is recognized and quantified by the DNA damage checkpoint machinery

in order to signal the presence and severity of a DNA lesion and facilitate its repair. Here, we could dissect two distinctly acting checkpoint circuits, both activated by the apical checkpoint kinase Mec1. Interestingly, we find that only one of them integrates the ssDNA signal generated during resection, while the other was resection-independent. Interestingly, we were able to reveal a synergy between two DNA damage sensors – the 9-1-1 complex and RPA – in counting ssDNA signals, and thus demonstrate a novel role for the 9-1-1 complex as quantitative checkpoint signal sensor at DSBs (Bantele et al, in revision).

Notably, both resection and checkpoint signaling share one central regulator, the scaffold protein Rad9. Rad9 is an antagonist of Fun30, as it inhibits DNA end resection, but at the same time an important checkpoint mediator that recruits the effector kinase Rad53 to DSBs. Current models distinguish between cell cycle-independent chromatin association of Rad9 and a cell cycle-dependent Rad9-Dpb11 interaction, both targeting Rad9 to DSBs. We uncovered a novel mode of the Rad9-Dpb11 interaction. This interaction mode allows cell cycle-independent Dpb11-Rad9 complex formation and suggests a yet unknown function of Rad9 outside of CDK-active cell cycle phases (Di Cicco et al, *Scientific Reports* (2017)).

Previous studies hypothesized putative removal of Rad9 from DSBs by competition with other Dpb11 binders, such as the repair scaffolds Slx4 and Rtt107, which was thought to dampen the DNA damage checkpoint. Here, we demonstrate that rather the Dpb11-Slx4-Rtt107 complex has an active function in DNA repair thus removing DNA lesions, which elicit the checkpoint in the first place. In this context, we describe a cell cycle-dependent multi-protein complex of Dpb11-Slx4-Rtt107 with structure-specific endonucleases, which serves to promote the resolution of joined molecules (for example Holliday junctions) in a spatially and temporally controlled manner (Gritenaite et al, *Genes and Development* (2014)).

Introduction

1.1 Maintenance of genome integrity

Our entire genetic information is stored in the sequence and epigenetic regulation of each cell's genomic DNA. As such, the genomic DNA is a living organism's most valuable biomolecule and needs to be preserved over many cycles of DNA replication and cell division. This presents a major challenge since the DNA is substrate of a number of metabolic processes such as transcription, replication and mitosis and is in this context being exposed from its protective chromatin packaging (Takata et al., 2013). The genome is vulnerable to DNA damage, which can cause mutagenesis, loss of genetic information and finally result in genomic instability if not removed timely and with high precision. It is well known that elevated mutagenesis rates can be correlated with ageing and disease ((Kennedy, Loeb, & Herr, 2012), (Lodato et al., 2018)). The vital importance of fast and error-free DNA repair and maintenance of genome stability is underscored by the connection between malfunctioning DNA repair systems and a prevalence of human diseases, often characterized by predispositions to tumorigenesis or premature ageing (progeria). Prominent examples are Werner Syndrome, Bloom syndrome (BS), Fanconi anemia (FA), Xeroderma pigmentosum (XP), Ataxia talengiectasia (AT), Nijmegen breakage syndrome (NBS), and hereditary ovarian and breast cancer (O'Driscoll, 2012). With growing knowledge about the mechanisms of DNA repair, ever more syndromes connected to failures in these mechanisms emerge (O'Driscoll, 2012).

It is particularly fascinating that the DNA maintains one feature that distinguishes it from all other biomolecules which piece together a cell like proteins, lipids, RNAs and sugars. These cellular components can be degraded and rebuilt from scratch in case they get damaged. In stark contrast, the DNA as unique blueprint and genetic repository must be maintained throughout the entire life of the cell. For this reason, the machineries to detect and repair DNA damages are highly conserved, and underlie sophisticated networks of regulation. Nonetheless, the whole concept of evolution mandates the acquisition of mutations as result of faulty DNA damage repair. DNA damage can

therefore be equally seen as threat to a cell's survival and opportunity to evolve according to the cellular consequence that a particular mutation brings along.

Despite the fact that we know many of the players involved in the DNA damage response (DDR), we only begin to understand their regulation on the molecular level. It is therefore a great motivation to further study the molecular mechanisms that govern the signaling at and repair of DNA damage sites. This thesis focuses on regulatory aspects of the DNA damage response, the cell cycle regulation of protein-protein interactions and their impact on several central processes within the DDR.

1.1.1 Occurrence and nature of DNA lesions

The DNA molecule has two breaking points being affected by damage: The phosphodiester backbone and the nucleobases, which connect the two single strands by forming hydrogen bonds. Different types of DNA lesions range from single nucleotide or nucleobase modifications (abasic sites, deamination, addition of small chemical groups like alkylation or oxidation, or addition of larger chemical groups or protein adducts) over single-strand breaks (SSBs) up to complete disruption of both strands of the DNA double-helix, the so-called DNA double-strand breaks (DSBs) (Fig. 1). Another group of damage comprises intra- or inter-strand crosslinks as generated by radiation or certain chemotherapeutic chemicals.

All kinds of DNA lesions – if not properly repaired – can severely affect function and structure of the DNA and potentially give rise to mutagenic events like point mutations or larger alterations in the DNA sequence. In particular, two-ended DSBs can cause dramatic genome rearrangements (translocations) and loss of genetic information by fusion of wrong ends or mis-guided recombination (Pfeiffer, 1998). Therefore, DSBs are regarded as one of the most deleterious and genotoxic forms of DNA damage.

The sources of DNA lesions can have different origins and can be sub-grouped in external (environmental) and internal (metabolic) sources. External environmental stresses like radiation or exposure to genotoxic chemicals are a common source of DNA damage. Particularly ionizing radiation (IR) threatens the genome integrity since it generates DNA breaks in a direct manner or by producing free water radicals (Sonntag, 2006), which react with the DNA molecule causing single-strand breaks often accompanied by oxidative damage ((Olive, Durand, & Banáth, 1990), (Ward, 1988)). Furthermore, ultraviolet (UV) radiation damages the DNA by inducing the formation of

photo-products like cyclobutane-pyrimidine dimers (CPDs) and 6-4 photoproducts, which both distort the DNA helix (Pearlman, Holbrook, Pirkle, & Kim, 1985), but also by generation of DSBs at sites of clustered oxidative lesions ((Greinert et al., 2012),(R. P. Sinha & Häder, 2002)). Besides these external factors, a variety of aberrant metabolic processes challenge the integrity of the genomic DNA. Among these are reactive nitrogen and oxygen species (ROS) ((Ohshima, Yermilov, Yoshie, & Rubio, 1999), (Cadet & Wagner, 2013)) and errors during DNA replication leading to small deletions, insertions or mismatched bases (Lindahl, 1993).

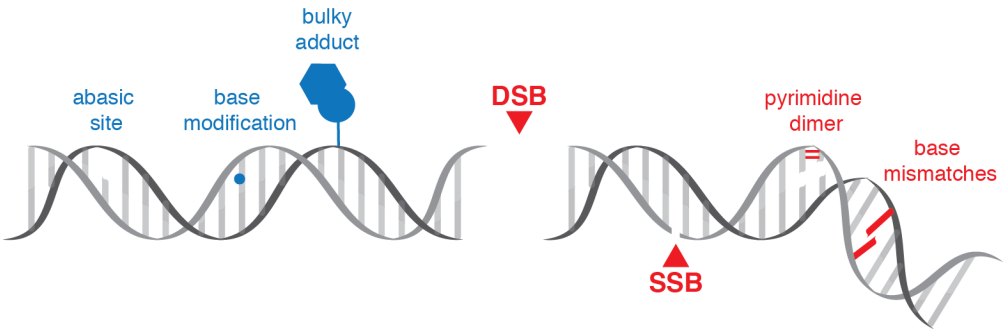

Fig.1 **Overview over different kinds of DNA damage.** DNA lesions can be classified in two categories: lesions affecting single bases which leave the phosphodiester-backbone of the DNA strand intact (blue), and lesions affecting the integrity of one or two DNA strands including the backbone (breakage or distortion, red). Single base lesions comprise abasic sites, chemical modification such as oxidation or methylation, and larger chemical modifications generating bulky adducts. A second class of DNA lesions, by which the conformation and integrity of the DNA helix is affected, comprise DNA double-strand breaks (DSBs), DNA single-strand breaks (SSBs), pyrimidine dimers (such as thymine dimers), inter- and intra-strand crosslinks (not shown in this figure) and base mismatches. Importantly, also single base damages can be converted to SSBs or even single-ended DSBs when clashing with helicases during transcription or DNA replication.

DNA lesions that involve damage of just one DNA strand are repaired by mechanisms that remove the damage site and fill in the missing nucleotides templated by the non-damaged DNA strand, for example during nucleotide excision repair (NER), base excision repair (BER), mismatch repair (MMR) and interstrand-crosslink repair (ICL). Such mechanisms cannot operate at DNA double-strand breaks, at which both DNA strands are broken. For the purpose of this thesis, I will focus on the repair of DNA double-strand breaks in the following.

Importantly, some DSBs are developmentally programmed and deliberately introduced into the genomic DNA, being required for housekeeping DNA metabolism. In those

cases, cells either prevent recognition of the DSB by the DNA damage response machinery or utilize it in a targeted manner to trigger recombination events. The latter is vital to establish diversity in germ cells during meiosis (Longhese, Bonetti, Guerini, Manfrini, & Clerici, 2009) and B- and T-cells by class switch recombination and V(D)J recombination of antibody segments (Arya & Bassing, 2017). Yeast cells additionally use the specific induction of a DSB to switch the mating type by recombination of mating type cassettes (Haber, 2012). In contrast, several other DNA metabolic processes do not trigger recombination. One example are DSBs introduced by topoisomerase II (TopII) during replication (Vos, Tretter, Schmidt, & Berger, 2011). They serve to release topological stress arising before and behind DNA replication forks because of the un- and re-winding of the DNA helix. Finally, DNA intermediates arising during recombination (joined molecules (JMs), such as Holliday junctions) are cleaved by endonucleases to disentangle the repair template and substrate (Dehé & Gaillard, 2017).

1.1.2 Cell cycle checkpoints

The genome is permanently scanned for damages by a network of tightly regulated damage recognition and repair machineries, which are collectively referred to as the DNA damage response (DDR). The general substrate of the DDR network is the genomic DNA in the form of chromosomes. During the cell cycle, chromosomes undergo several structural rearrangements to allow efficient DNA replication and safe division of the resulting sister chromatids in two cells during the anaphase of mitosis. These rearrangements include relaxation and condensation of chromatin, DNA and chromatin modifications, association of accessory proteins and changes in the copy number of the DNA (1n DNA content in G1 versus 2n DNA content after S and in the G2/M phase, Fig. 2 A).

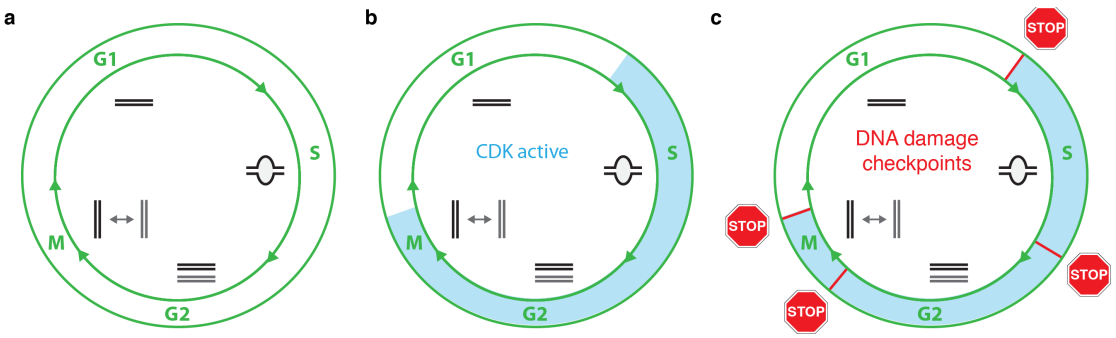

Fig.2 **Genomic DNA rearrangements and DNA damage checkpoint coordination within the cell cycle. (a)** The cell cycle starts with a first gap phase (G1), in which the cell contains a 1n DNA content with relaxed chromatin and which is used to take up nutrients and grow. When the cell is large enough, it starts to re-synthesize its DNA (S phase) in order to duplicate the genome precisely once, so that cells end up with a 2n DNA content. A cell that has finished DNA replication with a fully duplicated genome transits into the second gap phase (G2), which in yeast is negligible and directly moves on to mitosis (M phase). During mitosis, the two replicated sister chromatids of each chromosome are separated to the two daughter cells. To do so, the chromosomes are highly condensed and display the well known X-shaped chromosome structure. Upon completion of anaphase, the cell returns to the gap phase (G1) and relaxes its 1n chromatin. **(b)** The major driver of the cell cycle is the cyclin-dependent kinase (CDK), which becomes activated to set off S-phase, stays active until the meta-to anaphase transition (timeframe of activity shaded in blue) and finally gets switched off to permit the mitotic exit. **(c)** The integrity of the genomic DNA and the successful completion of the previous cell cycle stage is surveilled at each crucial cell cycle transition by so-called DNA damage checkpoints (red STOP signs).

In order to ensure an optimal reaction to occurring DNA lesions in all cell cycle stages, the repair machineries need to be adjusted to these rearrangements.

In general, this is achieved by two fundamental mechanisms. First, the major cell cycle kinase that drives the cell cycle - cyclin-dependent kinase (CDK) - also governs the choice of the correct repair mechanism ((Mathiasen & Lisby, 2014), (Langerak & Russell, 2011), (Symington & Gautier, 2011); as detailed below in paragraph 1.2.1) (Fig. 2 B). Second, the DNA integrity is constantly kept on check by cell cycle stage-specific DNA damage checkpoints, which are signaling networks that are locally assembled and activated at the sites of DNA lesions in order to communicate their presence and severity to the cell (B. Zhou & Elledge, 2000). This becomes particularly important when the lesions cannot be mended instantly. In such cases, the checkpoints stop the cell cycle prior to the transition to the next cell cycle phase and up-regulate DNA repair

mechanisms (Fig. 2 C). This provides a window of time for the cell to repair the lesion and prevents the inheritance of the damaged DNA to the next generation. In case of too severe damage that the cell fails to repair, the checkpoint can trigger cell death.

It is important to note that the term DNA damage checkpoint summarizes a complex network of proteins and signaling pathways, which are diverse in composition and regulation throughout the cell cycle. During G1, two distinct checkpoint mechanisms clear the cell for the entry into the cell cycle. First, the START checkpoint is assessing whether the cell is provided with enough nutrients and large enough to enter a new round of the cell cycle. Additionally, a G1 DNA damage checkpoint can get activated when DNA damage is present (Gerald, Benjamin, & Kron, 2002). After entry into S-phase, an intra-S DNA damage checkpoint that is in parts physically connected with the moving replication forks detects damages present in the replication template or introduced during DNA replication (Branzei & Foiani, 2007). When replication is finished and cells enter mitosis, the resulting doubled genome is scanned for DNA lesions by the mitotic DNA damage checkpoint. Finally, before cells divide, the spindle assembly checkpoint (SAC) controls for correct attachment of the opposing spindle poles to the kinetochores of the chromosomes at the metaphase plane prior to physical separation of the chromosomes (Joglekar, 2016). This synergy between checkpoints controlling proper cell physiology by the START and SAC checkpoints and the DNA damage checkpoints controlling for the integrity of the genomic DNA throughout the cell cycle ensures safe cell propagation.

The following work will focus on the DNA damage checkpoint and its response to DSBs throughout the cell cycle. Both difficult-to-repair lesions persisting too long or a high number of lesions present are situations that seriously challenge the repair machineries. To carry out the repair in a nonetheless faithful and complete manner, the cell requires a time buffer. Providing this time buffer is the major task of the DNA damage checkpoint, and it does so by not only pausing the cell cycle, but also enhancing subsequent DNA repair (Harrison & Haber, 2006)(Fig. 3). To achieve this, the checkpoint effector kinases (yeast Rad53, Chk1 and Dun1) target a plethora of substrates. Outcomes of this regulation are cell cycle arrest by stabilization of the anaphase inhibitor Pds1 (securin) (Cohen-Fix & Koshland, 1997) and a delay of anaphase progression by regulation of

microtubule-associated proteins (Krishnan, Nirantar, Crasta, Cheng, & Surana, 2004). Furthermore, the checkpoint kinases activate the transcriptional up- regulation of repair genes ((Gasch et al., 2001), (Jelinsky & Samson, 1999)) and enhance the expression of ribonucleotide reductase (RNR), an enzyme essential to dNTP production, which establishes adequate dNTPs levels for proper DNA replication and repair (Elledge, Zhou, Allen, & Navas, 1993). Locally, the upstream checkpoint signaling directly facilitates DNA repair by phosphorylating H2A-S129 (then termed γH2A.X or γH2A in yeast)((Downs, Lowndes, Nature, 2000, n.d.), (Nakamura, Du, Redon, & Russell, 2004), (Paull et al., 2000), (Redon et al., 2003)), which constitutes a recruitment platform for repair factors such as Rtt107 ((X. Li et al., 2012), (Ohouo, de Oliveira, Liu, Ma, & Smolka, 2013)) and cohesin ((Unal et al., 2004), (Ström, Lindroos, Shirahige, & Sjögren, 2004)). Once all DNA damage has been removed from the cell, the checkpoint arrest is released allowing cells to re-enter the cell cycle. Figure 3 provides an overview over the global checkpoint response in yeast.

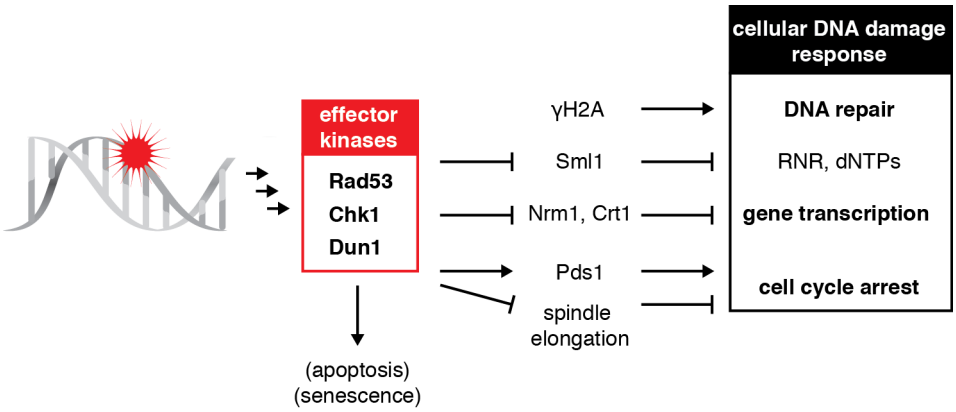

Fig.3 **Targets of the cellular DNA damage checkpoint response.** The DNA damage checkpoint response establishes genome stability by facilitating DNA repair in three ways. While inhibition of cell cycle progression provides a window of time for the cells to act on the DNA lesion, repair factors and dNTP levels are up-regulated. Furthermore, the chromatin modification γH2A marking the DNA damage site helps to recruit repair factors and sustain checkpoint signaling until the DNA lesion is repaired successfully.

The DNA damage checkpoint recognizes specific DNA structures that are generated at DNA lesion sites. The first signals being recognized are unprotected DNA ends. They are bound by the Ku complex ((Paillard & Strauss, 1991), (Blier, Griffith, Craft, & Hardin, 1993), (Griffith, Blier, Mimori, & Hardin, 1992), (Walker, Corpina, & Goldberg,

2001)) and recognized by the MRX complex ((Lisby, Barlow, Burgess, & Rothstein, 2004), reviewed in (Schiller, Seifert, Linke-Winnebeck, & Hopfner, 2014)). Both of them contribute to the stabilization of the DNA end and facilitate the binding of downstream checkpoint and repair factors. The DSB ends can then be further processed by various nuclease activities giving rise to two more molecular structures, which additionally serve as DNA damage signals. First, the concerted action of an endo- and two exonucleases in a process called DNA end resection ((Mimitou & Symington, 2009); chapter 1.2.2) generates 3' single-stranded overhangs by digestion of the 5' DNA strand. Additionally, resection creates a junction of single- to double-stranded DNA (ss-ds-junction). Two distinct checkpoint sensor proteins independently recognize these structures (Kondo, Wakayama, Naiki, Matsumoto, & Sugimoto, 2001; Melo, Cohen, & Toczyski, 2001): single-stranded DNA is rapidly covered by a filament of RPA (Replication Protein A) molecules, while the ss-ds-junction is a signal to load the hetero-trimeric ring-shaped 9-1-1 checkpoint clamp complex. Both sensors act as recruitment anchors for the checkpoint kinase cascade (see chapter 1.2.3).

Sensor proteins are by definition the first factors present at a lesion site and fulfill the important task of marking position and possibly the amount of DNA damage. These two pieces of information are then integrated into the checkpoint signaling cascade and processed to the necessary degree of checkpoint activity, meaning a correlating amount of activated effector kinase molecules that set off the cellular response to the DNA lesion. Since this response stalls the cell proliferation and is energetically cost-intense, cells need to prevent unnecessary activation of the checkpoint.

However, it can be estimated that a single cell accumulates more than 100,000 DNA lesions from endogenous and exogenous sources each day (Ciccia & Elledge, 2010; Hoeijmakers, 2009; LINDAHL & BARNES, 2000). These numbers sum up to almost two new DNA lesions per second per cell. Based on these numbers, it is likely that there is a basal level of DNA damage continuously present in the cell. Yet, cells need to proliferate while ensuring that the integrity of their genetic information is preserved throughout many generations.

The critical challenge therefore is to find a proper balance between tolerance of a certain number of DNA lesions to allow proliferation and activation of the full-blown DNA damage response when the threshold of tolerance is exceeded. In other words, cells must

evaluate whether it is needed to activate the checkpoint or not. This in turn depends on the DNA damage load and the repair efficiency of the present damage.

It has long been known that DNA damage signaling in general follows quantitative rules. In simple terms, one DNA lesions triggers less kinase activity than two or four lesions (Zierhut & Diffley, 2008). In addition, the amount of DSB resection plays a central role in reaching signaling thresholds, since it generates a very important damage signal, the ssDNA. Therefore, resection-proficient cells do activate the checkpoint stronger than resection-deficient cells (Bantele et al, in revision, (Balogun, Truman, & Kron, 2013), (Clerici, Trovesi, Galbiati, Lucchini, & Longhese, 2013)). Overall this suggests a model in which the cells locally assess the damage load, relay this information quantitatively to the global checkpoint effectors, and once a signaling threshold is reached, the full DNA damage response is triggered. To date, the mechanism underlying the quantitative assessment of signaling thresholds on the molecular level remains however elusive.

1.2 The response to DNA double-strand breaks

The cellular response to DNA double-strand breaks can be subdivided in three groups of reactions: recognition and processing of the lesion site, the communication of the presence of the lesion via checkpoint signaling, and the actual repair of the lesion. Importantly, these reactions are tightly interconnected and fully interdependent, and they involve decision-making at several steps. Particularly, the manner in which lesion sites are processed dictates the subsequent repair pathway. Choice of the appropriate repair pathway is essential to successful repair and genome integrity, as it strongly depends on the context of the DSB and cellular conditions such as cell cycle phase. While homologous recombination (HR) is considered to be the most accurate mechanism, it does require a repair template with a homologous donor sequence. This template is usually the sister chromatid generated during replication and therefore only present in post-replicative cell cycle stages. HR in absence of a template fails or leads to mis-targeted recombination events that often go along with global mutagenic events like translocations or gross chromosomal rearrangements (GCR). In any case, genetic material that has been nucleolytically processed and cannot be restored by recombination due to absence of a donor sequence gets irreversibly lost. In diploid cells, the homologous chromosome can

in principle be used as recombination template, however this bears the risk of loss of heterozygosity and is therefore not favoured. Collectively, it is vital for the cell to prevent homologous recombination in absence of a proper template, and in order to do so, the repair pathway choice is tightly controlled during the cell cycle. Key to this regulation is the cell cycle kinase CDK, which becomes active when cells duplicate their genome in order to enter a new round of the cell cycle. In the following chapters I will highlight the molecular details of the mechanisms of the different steps of repair pathway choice, with a specific focus on their cell cycle regulation by CDK.

1.2.1 Double-strand break repair pathways

Cells have two basic regimes of DSB repair at their hands. One option is to repair DSBs by ligation-based mechanisms such as non-homologous end-joining (NHEJ) or micro-homology-mediated end-joining (MMEJ). Alternatively, the broken sequence can be replaced by a copy derived from a homologous sequence in recombination-based repair mechanisms like homologous recombination (HR), synthesis-dependent strand annealing (SDSA), break-induced replication (BIR) and single-strand annealing (SSA). While ligation-dependent repair pathways are considered to be fast but error-prone, recombination is mechanistically more slow and complex but features the immense advantage of being templated and thereby highly accurate. The error-prone nature of ligation is based on the fundamental problem that it is sequence-independent, meaning that two lose ends are being re-connected no matter if DNA was lost or if they belong together in the first place. This in turn has the advantage of being independent of a repair template and therefore of the cell cycle stage in which the DNA damage is inflicted. Figure 4 provides an overview over occurrence and relationships between the different repair pathways (reviewed in (Ranjha, Howard, & Cejka, 2018)).

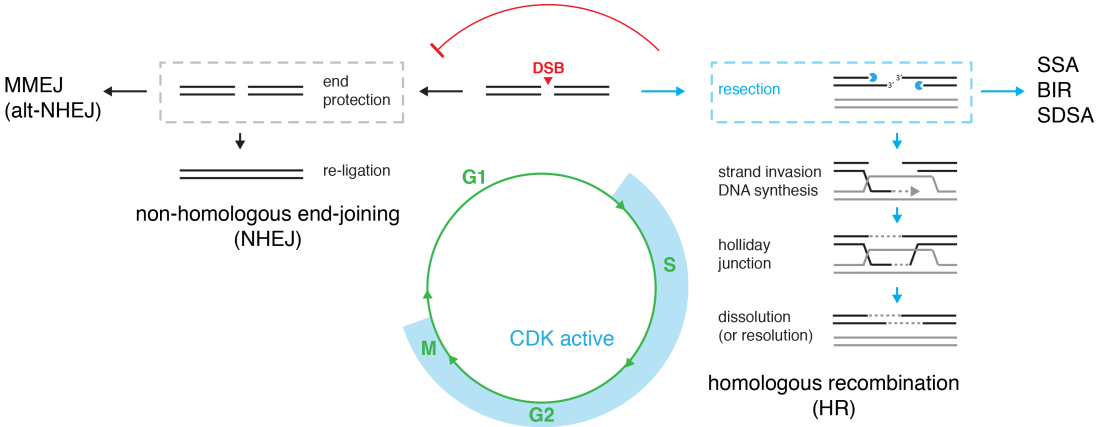

Fig.4 **DNA repair pathway choice within the cell cycle.** DNA repair pathways can be classified in resection-dependent (light blue) and resection-independent (grey) pathways. As resection is activated by CDK, the resection-dependent pathways are restricted to CDK-active cell cycle phases, while the resection-independent repair can occur throughout the cell cycle. Therefore, cells in G1 exclusively rely on NHEJ. Since resection destroys the substrate for ligation-based repair such as NHEJ and MMEJ, it constitutes the switch between repair regimes (red arrow). Once resected, cells are committed to repair by HR, SSA, BIR or SDSA. These sub-pathways mainly rely on length and break-distance of homologous sequences that can be used for annealing or recombination.

For the purpose of this thesis, I will not go into detail about the specifics of the repair pathway sub-groups but talk about gene conversion recombination meaning (GC-) HR and ligation meaning NHEJ. Mechanistically, the processing of the DSB end is the first step in both repair pathways, and is thought to constitute the principle point of pathway choice regulation. While NHEJ requires no or – in case of complex, blocked DNA ends – little processing, homologous recombination needs extensive end processing by DNA end resection. DNA end resection is the nucleolytic digestion of both 5' strands of the DSB ends, generating large stretches of 3' single-stranded overhangs. These overhangs are a crucial structural intermediate of HR, while they strictly prevent repair by NHEJ. In other words, once resection is initiated, the template for HR is generated and at the same time the substrate for NHEJ is being destroyed. Thus, resection is the committing step in HR and therefore the main regulatory element to determine the choice of the correct repair mechanism (Fig. 4). As such, all steps of resection are under tight cell cycle control, as I will detail in the next chapter (chapter 1.2.2).

The physiological balance of repair pathway occurrence is dictated by the cell cycle profile of the affected cell. Budding yeast cells are considered special, for they are highly

active in homologous recombination and use this as the preferred repair pathway of DSBs. In the lab, researchers greatly benefit from this feature of yeast cells since it allows easy and fast genome editing by HR. This however looks completely different in cultured human cells, which are largely post-mitotic with only low rates of recombination and usage of NHEJ as the preferred repair pathway ((Sonoda, Hochegger, Saberi, Taniguchi, & Takeda, 2006), (Mao, Bozzella, Seluanov, & Gorbunova, 2008), (Sargent, Brenneman, & Wilson, 1997)). In particular in the light of recent advances in recombination-based genome editing using CRISPR-Cas9 or similar systems, a low rate of recombination presents the bottleneck to efficiency (Orthwein et al., 2015).

1.2.2 DNA end resection

The process of DNA end resection can be sub-divided in two mechanistically distinct steps; the initiation of resection (or short-range resection) and the more processive long-range resection. The enzymes involved in resection initiation generate but a few hundred basepairs of single-stranded DNA and additionally are specialized to deal with more complex molecular structures that might occur at DSB ends, such as hairpins or adducts (examples are trapped topoisomerases or Spo11-bound meiotic DSBs). It is generally believed that the initiation of resection is the limiting step of the overall resection reaction. The reaction is then handed over to the processive exonucleases carrying out long-range resection, which generates many kilobases of single-stranded DNA (Zhu, Chung, Shim, Lee, & Ira, 2008). Resection as such has two purposes: First, the ssDNA is the key signal for eliciting the cellular DNA damage response. Second, the ssDNA serves as primer for template-dependent DNA repair. How much of ssDNA is ultimately needed to fulfill these tasks is unclear. It has been suggested that as little as 2 kb of homology matched during homology search yield a high recombination rate and increasing the length does not enhance the efficiency further (C.-S. Lee et al., 2016). To date there is no in vivo evidence for a requirement of longer resected tracts. Interestingly, one study suggests that excessive resection can even be inhibitory to recombination (C.-S. Lee et al., 2016). This could be due to either the instability and loss of DNA at the overhanging 3' strand (Zierhut & Diffley, 2008), or due to altered physical properties of an elongated Rad51-coated ssDNA filament that could slow or inhibit homology search. To date it is not known what defines the barriers to DNA end resection, if there actually is such a barrier or if not rather the repair of the lesion ends the resection reaction, and

how loss of genetic information due to excessive resection of long-persisting DSBs is prevented.

1.2.2.1 Initiation of DNA end resection by the MRX/Sae2 complex

Initially, unprotected DNA ends are bound by the Ku complex, which shields them from nucleolytic processing and is therefore an inhibitor of DNA end resection and a pro-NHEJ factor. In G1, Ku blocks the onset of resection and the eviction of Ku and recruitment of the resection machinery are preventing the direct repair of the DNA lesion by NHEJ and present the priming step for HR ((Mimitou & Symington, 2010), (Langerak, Mejia-Ramirez, Limbo, & Russell, 2011)). In the absence of Ku or NHEJ proteins, cells show elevated levels of resection compared to the normally occurring resection in the respective cell cycle stage ((Clerici, Mantiero, Guerini, Lucchini, & Longhese, 2008), (Zierhut & Diffley, 2008)). Besides Ku, a second DNA end-binding protein complex regulates the initiation of resection and was found to be one of the first factors present at DSBs (Lisby et al., 2004): the Mre11-Rad50-Xrs2 complex (MRX). The MRX complex plays roles in DSB end tethering and checkpoint signaling via Xrs2-Tel1 interaction. Through the Mre11 nuclease subunit, it has an additional function during resection initiation. Mre11 has ssDNA endo- and dsDNA exo-nuclease activity in vitro ((Paull & Gellert, 1998), (Hopfner et al., 2000), (Hopfner et al., 2001) and others). At obstructed DSB ends comprising secondary structures like hairpins or larger adducts, the Mre11 endonuclease activity in conjunction with a second endonuclease, Sae2, is required to clear this barrier to facilitate resection initiation ((Clerici, Mantiero, Lucchini, & Longhese, 2006), (Reginato, Cannavo, & Cejka, 2018)). Presumably, Mre11 opens hairpins, which are subsequently cleaved by Sae2 ((Lobachev, Gordenin, & Resnick, 2002), (Lengsfeld, Rattray, Bhaskara, Ghirlando, & Paull, 2007)). The endonuclease activity of Mre11 and its activation by Sae2 become distinctly important for the clearing of DSBs from covalently bound proteins, such as Spo11 during meiosis or trapped topoisomerase cleavage complexes ((Moreau, Ferguson, & Symington, 1999), (Neale, Pan, & Keeney, 2005), (Hoa et al., 2016), (Aparicio, Baer, Gottesman, & Gautier, 2016)).

In contrast, the exonuclease activity of Mre11 is obscure since it generates 5' ss-tails in vitro, while it seems required for the 5'-3' resection generating 3' ss-tails in vivo. Importantly, after stimulation by Sae2, Mre11 can set endonucleolytic cuts in a distance

to the DSB, releasing oligonucleotides. It is therefore tempting to hypothesize that the concerted action of the Mre11 endo- and 3'-5' exonuclease activities in cooperation with the Exo1 5'-3' exonuclease activity serve to generate ssDNA bi-directionally ((Garcia, Phelps, Gray, & Neale, 2011), (Cannavo, Cejka, & Kowalczykowski, 2013)). In cells lacking Mre11 or Sae2, Exo1 is partially able to compensate the defect in resection initiation (D. Nakada, Hirano, & Sugimoto, 2004). Additionally, the MRX complex was shown to recruit long-range resection factors in order to promote efficient long-range resection ((Niu et al., 2010), see chapter 1.2.2.2). Taken together, the MRX can contribute to DNA end resection by two mechanisms: the recruitment of long-range resection factors and the generation of their substrates ((Niu et al., 2010), (Cannavo & Cejka, 2014)).

1.2.2.2 Long-range resection by Exo1- and Sgs1/Dna2- dependent pathways

Long-range resection is defined as the processive, nucleolytic digestion of the 5' strand at DSBs in order to extend the short stretches of 3' ssDNA overhangs generated by the Sae2/Mre11 nucleases in the initiating step of resection. Long-range resection can result in tens of kilobases of ss-overhangs, which are generated with a speed of about 4 kb/h in cycling cells ((Zhu et al., 2008), (Eapen, Sugawara, Tsabar, Wu, & Haber, 2012), (Chung, Zhu, Papusha, Malkova, & Ira, 2010)). There are two independent pathways executing long-range resection, the Exo1- and STR (Sgs1-Top3-Rmi1)/Dna2 pathway ((Mimitou & Symington, 2008), (Gravel, Chapman, Magill, & Jackson, 2008), (Zhu et al., 2008)). In the STR pathway, the RecQ helicase Sgs1 is thought to unwind the DNA while the helicase-nuclease Dna2 digests the 5' strand (Zhu et al., 2008). It is unclear whether the Dna2 helicase activity is required for resection. In vitro studies suggest a translocase-like function of the Dna2 helicase, which seems to contribute to resection efficiency (Levikova, Pinto, & Cejka, 2017). The Dna2 action per se hereby fully depends on Sgs1 and RPA, while its 5'-3' polarity is determined by RPA ((Niu et al., 2010), (Cejka et al., 2010)). The XPG–family exonuclease Exo1 has so far not been genetically linked to a helicase activity, however the human Sgs1 homolog BLM can cooperate with human EXO1 during resection (Nimonkar, Ozsoy, Genschel, Modrich, & Kowalczykowski, 2008). The favoured substrates of Exo1 are 5' ends with a 3' overhang (Cannavo et al., 2013). Although classical models place long-range resection

downstream of the MRX/Sae2-dependent initiation step generating this substrate, Exo1 and Sgs1/Dna2 are able to resect clean cuts as generated by endonucleases in absence of initiation enzymes, however with low efficiency (Llorente & Symington, 2004).

Resection underlies a strong cell cycle control and is mainly acting during cell cycle phases in which CDK is active ((Zierhut & Diffley, 2008), (Barlow, Lisby, & Rothstein, 2008), (Ira et al., 2004), (Trovesi, Falcettoni, Lucchini, Clerici, & Longhese, 2011)). This regulation is essential since once resection is initiated, the DSB is irreversibly channeled to recombination-based repair requiring a repair template ((Ira et al., 2004), (Aylon, Liefshitz, & Kupiec, 2004), (Y. Zhang, Shim, Davis, & Lee, 2009)). To this end, several layers of regulation operate by alteration of the activity of the resection enzymes, their DSB recruitment, and accessory factors which affect resection efficiency. The phosphorylation of resection factors by CDK constitutes the most important layer of resection control. Consequently, resection is suppressed when CDK-dependent enzyme activation lacks. Additionally, end protection by the Ku complex and enhanced activity of NHEJ factors prevent the initiation of resection in G1. When cells enter S phase, CDK phosphorylates several enzymes involved in resection and thereby favors end processing over re-ligation. CDK-dependent phosphorylation of Sae2 ((Huertas, Cortes-Ledesma, Sartori, Aguilera, & Jackson, 2008), (Bonetti, Martina, Clerici, Lucchini, & Longhese, 2009), (Cannavo & Cejka, 2014)) and Dna2 (X. Chen et al., 2011) were shown to play an important role in this regulation. In human cells, also hsEXO1 is target of CDK phosphorylation (Tomimatsu et al., 2017). However, mutants bypassing the CDK-requirement for resection initiation were not able to fully restore efficient resection when CDK was inhibited (Huertas et al., 2008), suggesting the contribution of other CDK substrates. Indeed, by enhancing CDK activity via overexpression of the mitotic cyclin Clb2, the cell cycle regulation of resection can be partially overcome (Clerici et al., 2008). Similarly, the deletion of resection-blocking proteins such as Rad9 and Ku does enhance resection in G1, but can not fully restore resection efficiency (Lazzaro et al., 2008). All current efforts to overcome the cell cycle regulation have been concentrating on the resection nucleases and accessory protein blocks like Ku or Rad9. To date, the role of the resection substrate – the DNA in the context of chromatin – has not been factored in and will be discussed in Chapter 1.3.

1.2.3 Activation of the DNA damage checkpoint

The DNA damage checkpoint is a signal transduction pathway with the major task to communicate occurrence and severity of DNA damage to the cell and activate the subsequent cellular response. It is organized in a kinase cascade that locally assembles on damaged chromatin. This cascade is initiated by the sensor proteins Ku/MRX, RPA and 9-1-1 which specifically associate with damage-specific DNA structures in order to recruit the apical kinases Mec1^{ATR} and Tel1^{ATM} and the mediator proteins Rad9 and Dpb11 providing the platform for further protein binding and regulation. The apical kinases phosphorylate a multitude of substrates at the damage site serving the double purpose of enhancing and regulating further checkpoint and repair protein binding and directly activating the effector kinases. Ultimately, the effector kinase Rad53 is recruited to the lesion site by binding to Rad9. This has two general effects: First, the effector kinase is brought into close proximity with the apical kinases mediating its activation. Second, this physical association of the effector kinase, which is critically required for its activation, provides an essential opportunity for regulation. Figure 5 provides an overview over the DNA damage checkpoint cascade in budding yeast.

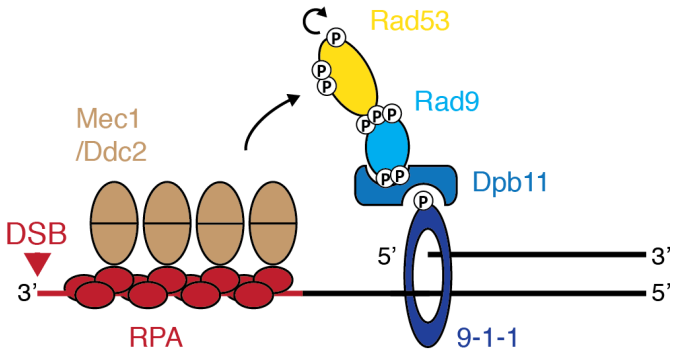

Fig.5 **Architecture of the DNA damage checkpoint cascade.** The DNA damage checkpoint cascade is assembled on the basis of the sensor proteins RPA (red) and 9-1-1 (dark blue). RPA recruits the apical kinase Mec1-Ddc2 (brown), and the synergy of Mec1-and CDK-dependent phosphorylation steps mediates the assembly of the downstream checkpoint factors on 9-1-1. First, the scaffold Dpb11 (middle blue) binds to Mec1-modified 9-1-1 and then binds to CDK-phosphorylated Rad9 (light blue) with its second binding site. Rad9 then interacts with the effector kinase Rad53 (yellow) in a Mec1-dependent manner. Once Rad53 is in place, it becomes phosphorylated and thereby activated by Mec1 and enhanced by auto-phosphorylation.

The assembly of the checkpoint cascade largely follows protein-protein interactions induced by post-translational modifications (PTMs). In yeast, these are mainly phosphorylations, while higher eukaryotes additionally rely on ubiquitin signaling. Regulation of the checkpoint via PTMs has several intriguing advantages.

A crucial aspect, that is vital to how the checkpoint functions, is the possibility of signal amplification by PTMs. In other words, one kinase molecule once activated has the propensity to phosphorylate hundreds of substrate molecules. Quantitatively this has as a consequence, that the checkpoint signal can be adjusted to the appropriate signal strength thoroughly. Qualitatively, this makes the checkpoint a switch-like mechanism, that can be switched on and off extremely fast and efficiently, controlled by the requirement for overcoming specific threshold levels.

Furthermore, each interaction or protein activation facilitated by a PTM can be regulated on several levels: the localization of the enzyme and its substrate, activity of the enzyme and the reversal of the PTM for example by phosphatases. This allows a high sensitivity in fine-tuning of the DNA damage response and the checkpoint in particular.

Taken together, the architecture of the checkpoint kinase cascade is tailored to provide a response that is perfectly adjusted to the needs of the affected cell. In the following subchapters, I will provide the molecular details of each step of DNA damage checkpoint activation and regulation.

1.2.3.1 Role and mechanism of DNA damage sensing

Sensor proteins are the first factors that recognize and mark the lesion, and they do so by having a specific binding affinity for DNA structures being generated by DNA damage. Besides sensing such structures, sensor proteins provide the initial binding platforms for checkpoint and repair at the DSB. At a clean DNA double-strand break, the first structures present are the blunt DNA ends, which are bound and capped by Ku. Here, I will focus on structures and primary sensors that come into play one step later, once resection is ongoing, and which can therefore be rather attributed to the HR repair pathway. Resection reveals 3’ single-stranded DNA, which is rapidly covered by a filament of RPA, a trimeric protein complex consisting of the subunits Rfa1-3. The occurrence of single-stranded DNA is a key damage signal. Although multiple reactions during DNA metabolism generate transient ssDNA intermediates by unwinding of the helix in order to gain access to the genetic information, the DNA is never left uncovered

for reasons of protection, stability and prevention of secondary structure formation. RPA binds to the ssDNA with nanomolar affinity via OB fold domains (oligonucleotide-/oligosaccharide-binding domains) (C. Kim, Paulus, & Wold, 2002). Interestingly, RPA recruitment to ssDNA acts as a positive enhancer of ssDNA formation. RPA prevents secondary structure formation and thereby stabilizes the 3' overhang (H. Chen, Lisby, & Symington, 2013) and enhances the Exo1 processivity (Cannavo et al., 2013). Additionally, it recruits and modulates the activity of Sgs1 and Dna2 at DSBs ((H. Chen et al., 2013), (Cejka et al., 2010), (Niu et al., 2010)).

The second DNA structure that is generated by resection is the ssDNA-dsDNA junction at the border of ongoing resection. This junction stimulates the recruitment of the PCNA-like 9-1-1 checkpoint clamp by a so far not fully understood mechanism. 9-1-1 is a heterotrimeric ring-shaped protein complex of Mec3, Rad17 and Ddc1 encircling the DNA, with the special feature of Ddc1 harboring a C-terminal extension that serves as protein-protein interaction domain. The 9-1-1 complex is loaded in its trimeric form (Majka & Burgers, 2005) by the RFC-Rad24 clamp loader ((Majka, Binz, Wold, & Burgers, 2006), (L. Zou, Liu, & Elledge, 2003)), which is a specialized form of the canonical RFC clamp loader that loads PCNA on replication forks, differing only in the replacement of the Rfc1 subunit by the damage-specific Rad24 subunit (homolog to human RAD17) (Green, Erdjument-Bromage, Tempst, & Lowndes, 2000). 9-1-1 loading requires the presence of RFC-Rad24 and the RPA filament ((Majka et al., 2006), (Ellison & Stillman, 2003), (L. Zou et al., 2003)). Despite the fact that there are multiple protein-protein interactions between Rad24, 9-1-1 and RPA, respectively, the precise placement of the 9-1-1 to the junction and subsequent dynamics of binding are not understood on molecular level. It is particularly elusive how the recognition and binding to the junction is being coordinated with the nucleases that sit on the junction in order to proceed with resection, and whether resection and clamp loading can happen simultaneously or involve a temporary protein binding switch. Furthermore, we do not understand 9-1-1 dynamics in its DNA-loaded state, whether it is stably positioned or can diffuse along the ssDNA or even over the junction on dsDNA. In vitro, the 9-1-1 loading gains its directionality by the influence of RPA. In absence of RPA, the clamp can be loaded to junctions of both directionalities (3'-5' and 5'-3') likewise (Majka et al., 2006). It has also been suggested that 9-1-1 can directly interact with RPA via the C-

terminal tail of the Ddc1 subunit in human cells (X. Wu, Shell, & Zou, 2005), and Ddc1 is in turn involved in stabilizing RPA (Sukhanova, D'Herin, Boiteux, & Lavrik, 2014).

Furthermore, it has been proposed that once loaded, 9-1-1 can slide across dsDNA in vitro (Majka et al., 2006). However, the physiological relevance of this sliding is unclear and needs to be assessed in vivo.

Both checkpoint sensors, RPA and the 9-1-1, facilitate direct binding of checkpoint factors. While RPA is bound by the co-factor Ddc2 (L. Zou & Elledge, 2003), which brings the apical kinase Mec1 to the site of DNA damage ((Cortez, 2001), (Paciotti, Clerici, Lucchini, & Longhese, 2000)), the 9-1-1 fulfills a more complex role. Also the 9-1-1 contributes to the recruitment and stability of Mec1-Ddc2 on the ssDNA, but it furthermore stimulates its kinase activity directly and indirectly by recruiting the checkpoint mediator Dpb11, which itself harbors a Mec1 activating activity. This mechanism is a self-enhancing feedback-loop, as the interaction between the 9-1-1 and Dpb11 is mediated by Mec1-dependent Ddc1 (9-1-1) phosphorylation on T602. The Ddc1- and the Ddc2- dependent sensing pathway were shown to act independently of each other to ensure rapid and sensitive damage recognition ((Melo et al., 2001), (Kondo et al., 2001)). Figure 6 provides details about protein-protein interactions involved in DNA damage sensing mechanisms.

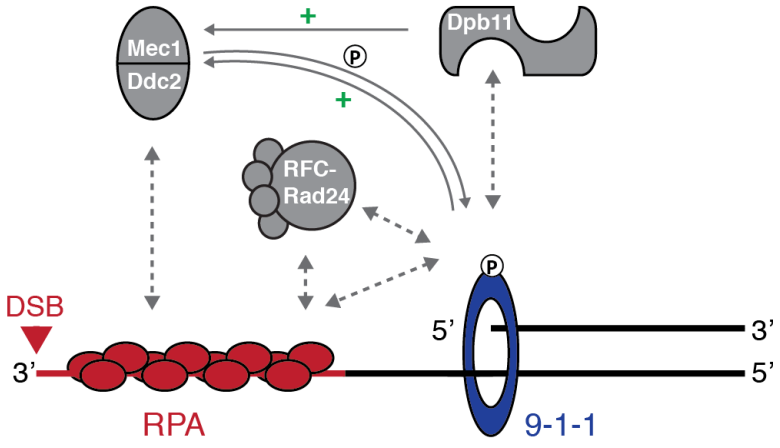

Fig.6 **Functional interactions during the sensing of DNA damage structures.** RPA specifically binds to the ssDNA filament and subsequently interacts with Ddc2 to bring the Mec1 kinase to the DSB. Additionally, RPA interacts with the RFC-Rad24 clamp loader via Rfa1 ((Lindsey-Boltz, Reardon, Wold, & Sancar, 2012), (H. S. Kim & Brill, 2001), (Piya et al., 2015)), which enables loading of the 9-1-1 clamp to the ssDNA-dsDNA junction. To this end, RFC-Rad24 binds the 9-1-1 in an ATP-

dependent manner, and this binding does not require the presence of DNA (Majka & Burgers, 2003). Upon ATP hydrolysis, the 9-1-1 clamp is being released from the clamp loader ((Majka & Burgers, 2003), (Bermudez et al., 2003)). The 9-1-1 clamp itself can interact with RPA and becomes phosphorylated by Mec1 once loaded. This phosphorylation mediates the interaction between 9-1-1 and Dpb11 ((Navadgi-Patil & Burgers, 2009), (J. Lee, Kumagai, & Dunphy, 2007), (Delacroix, Wagner, Kobayashi, Yamamoto, & Karnitz, 2007), (Ohashi, Takeishi, Ueda, & Tsurimoto, 2014)). In turn, 9-1-1 and Dpb11 harbor Mec1-activating domains, which boost Mec1 activity.

One aspect of damage sensing should be specifically highlighted in this context; the involvement of the sensor pathways in transmission of quantitative information. It is established that RPA forms a filament around the ssDNA covering about 20-30 nucleotides per trimer (Sugiyama, Zaitseva, & Kowalczykowski, 1997). Although it is likely that this filament is not strictly continuous, it offers a straight-forward model of how RPA binding can be quantitatively proportional to the amount of resection, and thereby add a quantitative measure to the checkpoint input sensing mechanism. The more ssDNA is formed, the more RPA trimers bind to elongate the RPA filament, and the more Mec1 molecules can be recruited to this filament. In contrast, we do not know whether the 9-1-1 is involved in quantitative damage sensing. It is unclear how many 9-1-1 molecules are present at lesion sites and whether this corresponds to the length of the ssDNA. The activity of both sensor pathways is sufficient to elicit the DNA damage response even in absence of DNA damage (Bonilla, Melo, & Toczyski, 2008), but it is not clear to which extent they feed into overall checkpoint activity by quantitative means. Clearly, the two mechanisms of checkpoint sensing converge in the phosphorylation of Ddc1 by Mec1, and can therefore not be strictly separated when it comes to the quantitative nature of signaling.

1.2.3.2 Regulation of the apical checkpoint kinases Mec1-Ddc2 and Tel1

The apical checkpoint kinases are recruited to DSBs by sensor proteins and become activated at the site of damage in order to phosphorylate a multitude of substrates. These phosphorylation events trigger checkpoint activation by mediating protein-protein interactions and effector kinase activation. The apical kinases belong to the family of PIKK kinases (Phosphatidylinositol 3-kinase related kinases) and specifically phosphorylate Ser/Thr residues in the context of the consensus sequence S/T-Q.

In yeast, the apical PIKK kinases to initiate and control checkpoint signaling are Mec1 ((Naiki, Wakayama, Nakada, Matsumoto, & Sugimoto, 2004), (Grenon, Magill, Lowndes, & Jackson, 2006)), structural homolog of the human ATR; and Tel1 (Gobbini, Cesena, Galbiati, Lockhart, & Longhese, 2013), the ATM homolog. Interestingly, the recruitment mechanisms of Mec1 and Tel1 seem mutually exclusive, so that a partial separation of function can be envisioned. Mec1, which is bound to its co-factor Ddc2 ((Paciotti, Lucchini, Plevani, & Longhese, 1998)), is recruited to the ssDNA-RPA filament via a protein-protein interaction between Ddc2 and RPA (L. Zou & Elledge, 2003). Structural studies suggest a potential interaction mode in which a Mec1-Ddc2 dimer entity (comprising two Mec1 and two Ddc2 molecules) binds to two adjacent RPA molecules with a 1:1 stoichiometry (Deshpande et al., 2017). To date, we do not know about the in vivo stoichiometry of active kinase versus RPA filament length and the binding and activation dynamics, and it is not known whether the activated kinase is locally restricted to the ssDNA or can be soluble and diffuse in order to phosphorylate substrates in a larger radius around the DSB. What is however known is that Mec1 activation occurs locally at the site of the DSB involving several distinct activators (reviewed in (Navadgi-Patil & Burgers, 2011), (Wanrooij & Burgers, 2015), (Wanrooij, Tannous, Kumar, Navadgi-Patil, & Burgers, 2016)). In short, Mec1 is activated by a self-enhancing loop involving the 9-1-1 complex and the Dpb11 checkpoint mediator (see chapter 1.2.3.1), and additionally stimulated by the nuclease Dna2. While the 9-1-1 complex can stimulate Mec1 activity throughout the cell cycle, Dpb11 acts only when CDK is active and Dna2 was suggested to be S-phase specific ((Navadgi-Patil & Burgers, 2011), (Wanrooij & Burgers, 2015)). In contrast to Mec1, Tel1 as its human homolog ATM is stabilized at the DSB ends by direct interaction with the Xrs2 (human Nbs1) subunit of the Mre11-Rad50-Xrs2 complex (MRX, human MRN)((Falck, Coates, & Jackson, 2005), (D. Nakada, Matsumoto, & Sugimoto, 2003), (Mantiero, Clerici, Lucchini, & Longhese, 2007)), which is bound to the DSB end ((Stracker & Petrini, 2011), (R. S. Williams, Williams, & Tainer, 2007), (Rojowska et al., 2014)). The MRX complex is thought to be destabilized at the DSB end once resection has been initiated. Ultimately, this means that the binding mechanism for Tel1 is inactivated at the same time as the binding platform for Mec1 is generated, both by the process of DNA end resection. Thus, resection mediates a kinase switch from Tel1-

dependent to Mec1-dependent kinase activity at the break site (Jazayeri et al., 2006), implying a high level of cell cycle regulation at the step of resection.

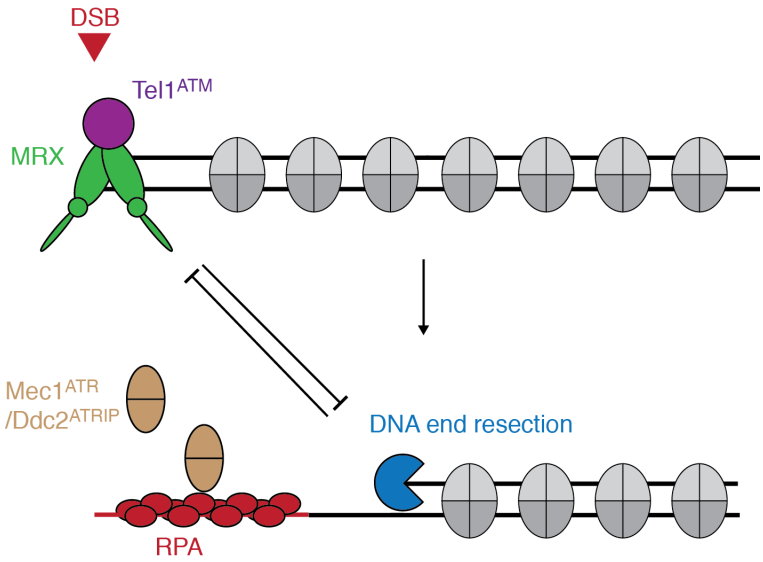

Fig.7 **Apical kinase switch mediated by DNA end resection.** Both yeast apical kinases, Mec1^{ATR}-Ddc2^{ATRIP} (brown) and Tel1^{ATM} (purple), associate with DSBs via protein-protein interactions with checkpoint sensor proteins. Since these sensor proteins (MRX, green; RPA, red) recognize educt (DNA end) and product (ssDNA) of DNA end resection, respectively, resection automatically generates a switch from Tel1- to Mec1-dependent signaling.

In cycling yeast cells, the damage response is therefore mainly governed by Mec1, while deletion of Tel1 has only very mild effects on checkpoint activation (Bantele et al, in revision, (Clerici et al., 2013), (Ira et al., 2004)). Conceptually, as discussed for RPA, the continuous accumulation of Mec1 molecules on the growing RPA filament presents an intuitive mechanism of how ssDNA signal strength can be quantified by the cell. It is however important to note that this model only factors in the presence of the kinase, thereby neglecting the requirement for substrate availability and kinase activation. In other words, it is not known how quantitative the Mec1 activation after RPA recruitment is, and in how far active Mec1 molecules have access to their substrates. Therefore it is not clear, whether Mec1 recruitment alone can fulfill the purpose of ssDNA signal strength quantification.

1.2.4 Mediators in the DNA damage response

A central feature of the DNA damage checkpoint cascade is the utilization of so-called scaffold proteins serving as checkpoint mediators. These scaffolds do not have intrinsic

enzymatic activity themselves but harbor several interaction sites for protein-protein interactions. Thereby, scaffolds act as multifunctional adaptors to physically bring together the checkpoint components like building blocks. Since the interaction sites underlie a regulation by phosphorylation (either cell cycle- specific or damage-dependent), protein scaffolds spatially and temporally coordinate the assembly of specific complexes and thereby offer a handle to modulate signal transduction events. Key to this regulation is the interplay between specific binding sites on the scaffolds and PTMs on their binding partners. It is believed that complexes assembled in this way are rather of dynamic, transient nature, adding additional flexibility to the propagation of checkpoint signals. By this principle mechanism, cells are able to read and integrate several independent pieces of information such as cell cycle stage with the nature, presence and location of a DNA lesion and culminate these pieces of information into a tailored response.

1.2.4.1 Dpb11 as multifunctional CDK reader

The first scaffold protein to be recruited to the DSB is the particularly versatile replication adaptor Dpb11. Yeast Dpb11 has two tandem BRCT repeats at the N-terminus and the middle domain, respectively (BRCT 1+2 and BRCT 3+4), to mediate protein-protein interactions (C. C. Y. Leung & Glover, 2014). With these domains, Dpb11 orchestrates and provides specificity to several processes of DNA metabolism. Among these are initiation of replication (Garcia, Furuya, & Carr, 2005), joint molecule (JM) resolution ((Gritenaite et al., 2014), (Princz et al., 2017)) and DNA damage checkpoint activation (Navadgi-Patil & Burgers, 2008), during which it cooperates with the damage-specific scaffold protein Rad9. Dpb11 is assembled at DSBs via an interaction between its central BRCT3+4 repeat and the Mec1-phosphorylated tail of the 9-1-1 subunit Ddc1 ((Puddu et al., 2008), (Pfander & Diffley, 2011)). For most interactors, the Dpb11 BRCT repeats recognize CDK-dependent phosphorylation sites on the interacting partners, and it is therefore considered to be a reader of CDK activity. This ability to read CDK activity brings Dpb11 into focus of studying cell cycle regulation of DNA metabolism. Fig. 8 summarizes established Dpb11 complexes.

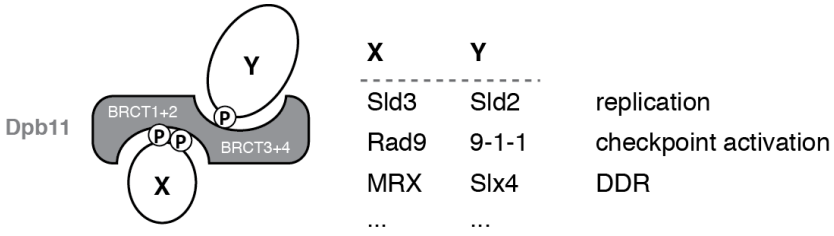

Fig.8 **Dpb11 engages specific protein pairs into ternary complexes during various processes of DNA metabolism.** Dpb11 has two BRCT domains, BRCT1+2 and BRCT3+4, which specifically bind to phosphorylated S/T residues of their interacting partners. The only essential complex formed by Dpb11 is the replication initiation complex with Sld3-Dpb11-Sld2 (Zegerman & Diffley, 2007). In the center of checkpoint signaling, Dpb11 engages in a ternary checkpoint complex with Ddc1 (9-1-1) and Rad9 (Pfander & Diffley, 2011). Further Dpb11 interactors involved in the DNA damage response such as the MRX complex, the scaffold protein Slx4 (Gritenaite et al., 2014) and others (Pfander, unpublished data) were identified.

It is particularly interesting to note that at double-strand breaks, Dpb11 co-localizes partially opposing activities that counteract each other regarding DNA end resection and checkpoint activation. As such, the Dpb11 complexes may provide a buffering system, which can be tipped towards activating or inhibiting the respective activity dependent on the current needs and thereby adds to the fine-tuning of the DDR ((S. Bantele, Ferreira, Gritenaite, Boos, & Pfander, 2017), (Cussiol, Jablonowski, Yimit, Brown, & Smolka, 2015), (Gritenaite et al., 2014), (Y. Liu et al., 2017)).

Both checkpoint scaffolds, Rad9 and Dpb11, are evolutionary conserved up to humans. Human TopBP1^{Dpb11} harbors nine instead of four BRCT domains and is recruited to DSBs in a similar manner as the yeast Dpb11 (Wardlaw, Carr, & Oliver, 2014). However, its interaction with Rad9^{Ddc1} depends on constitutive CK2-dependent instead of damage-induced phosphorylation of Rad9^{Ddc1}, and this interaction occurs via BRCT1+2 instead of BRCT3+4 in yeast (Takeishi et al., 2010). It has been proposed that human TopBP1 instead can directly interact with ssDNA-RPA, potentially facilitating its recruitment to DSBs (Acevedo, Yan, & Michael, 2016).

1.2.4.2 Dual role of the checkpoint scaffold Rad9

Rad9 (structurally and functionally equivalent to human MDC1/BRCA1/53BP1) has been the first checkpoint player being identified (Weinert & Hartwell, 1988). Surprisingly, however, we still do not understand all aspects of its regulation and

function. Rad9 associates with damaged chromatin upon Mec1-/Tel1-dependent hyper-phosphorylation ((Vialard, 1998), (Emili, 1998)), which depends on the formation of a ternary checkpoint complex comprising Mec1, Rad9 and Dpb11 (Pfander & Diffley, 2011). Currently, two distinct Rad9 recruitment pathways are established. Rad9 is recruited to DSBs upon CDK phosphorylation (Granata et al., 2010) on S462 and T474 by direct interaction with Dpb11 BRCT1+2 (Dpb11 pathway) (Pfander & Diffley, 2011). Such a cell cycle regulation of Rad9-Dpb11 binding has first been observed in fission yeast (Du, Nakamura, & Russell, 2006). Alternatively, Rad9 can directly bind modified histones in order to localize to DSBs (histone pathway) in a dual mode (Toh et al., 2006). More precisely, it recognizes the damage-specific, Mec1/Tel1-dependent phosphorylation mark γH2A (H2A phospho-S129; mammalian γH2A.X) ((Hammet, Magill, Heierhorst, & Jackson, 2007), (Javaheri et al., 2006)), which spreads around a DSB over up to 50 kb (Shroff et al., 2004), with its BRCT repeats. Additionally, Rad9 recognizes histone H3 when K79 is methylated by the methyltransferase Dot1 ((van Leeuwen, Gafken, & Gottschling, 2002), (Wysocki et al., 2005), (Giannattasio, Lazzaro, Plevani, & Muzi-Falconi, 2005)) via its Tudor domain (Grenon et al., 2007). This dual binding mode is conserved to the human functional ortholog, 53BP1, which binds H4K20me2 (Botuyan et al., 2006) and H2AK15ub (Fradet-Turcotte et al., 2013) with its Tudor- and UDR (ubiquitination-dependent recruitment motif)- domains, respectively. The histone pathway of yeast Rad9 recruitment is thought to operate cell cycle-independent being reinforced by the Dpb11 pathway in cell cycle stages where CDK is active. Fig. 9 provides an overview over protein-protein interactions that regulate Rad9 at DSBs.

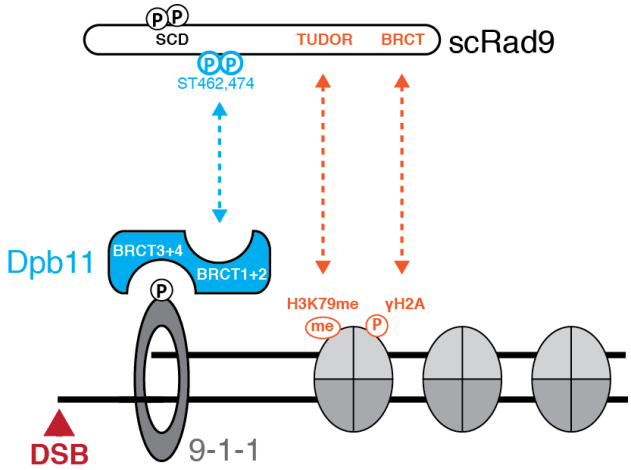

Fig.9 **Rad9 is recruited to DSBs by two pathways.** Upon phosphorylation of ST462,474 by CDK, Rad9 can bind to the BRCT1+2 of Dpb11 and thereby engage in a ternary checkpoint complex (blue). This recruitment pathway is therefore cell cycle-regulated and termed the "Dpb11 pathway". Additionally, Rad9 recognized modified histones in a bivalent mode, with its TUDOR domain binding to methylated H3K79 and its C-terminal BRCT domain binding to γH2A (orange). This recruitment pathway is not dependent on the cell cycle and termed the "histone pathway".

After DSB localization, Rad9 becomes hyper-phosphorylated by Mec1 on multiple S/T-Q motifs within an N-terminal SCD cluster region, which is then recognized by the Rad53^{Chk2} FHA (forkhead-associated) domain in order to recruit Rad53 to the DSB and mediate its subsequent activation by Mec1 ((Emili, 1998), (Sun, Hsiao, Fay, & Stern, 1998), (Vialard, 1998), (Schwartz et al., 2002), (Sweeney et al., 2005)). It has been suggested that Rad9 oligomerizes upon damage-dependent phosphorylation and thereby further contributes to the Rad53 enrichment at DSBs, stimulating its auto-phosphorylation (Usui, Foster, & Petrini, 2009). In addition, the second effector kinase Chk1 is activated by Rad9 in a similar way as Rad53 (Y. Sanchez et al., 1999).

Besides its central role in checkpoint activation, recent studies established Rad9 and its functional homolog 53BP1 as inhibitors of DNA end resection (Symington, 2014). While deletion of Rad9 strongly enhances resection efficiency in G2/M, it requires additional deletion of Ku in G1 to overcome the barrier to resection ((Lazzaro et al., 2008), (Trovesi et al., 2011), (Ferrari et al., 2015), Bantele et al, in revision). Genetics suggest that it is rather the histone-related Rad9 sub-pool acting as resection inhibitor, but the mechanism remains unknown. One possibility would be the physical blocking of nuclease progression through the chromatin by histone-bound Rad9 itself or Rad9-dependent stabilization of the chromatin structure. This model raises another interesting

question. Rad9 is recruited to histones after DNA damage in a cell cycle-independent manner. As consequence, the Rad9-dependent inhibition of resection should be present throughout the cell cycle. Yet, mitotic cells are highly resection-active, implying an active mechanism of Rad9 removal in G2/M in order to allow efficient DNA end resection. This aspect will be further discussed in Chapter 1.3.

1.2.4.3 The DNA repair scaffolds Slx4 and Rtt107

Similar to Dpb11, Rtt107 (Esc4) is a BRCT repeat containing scaffold protein required for the response to DNA damage and stalled replication forks ((Hang & Zhao, 2016), (G. P. Leung, Brown, Glover, & Kobor, 2016)). Like Rad9, Rtt107 can be localized to sites of DNA damage by two mechanisms: the direct interaction with γH2A (X. Li et al., 2012) and the recruitment into a multiprotein complex together with yet another scaffolding protein, Slx4. Both Rtt107 and Slx4 play a conserved role in the response to stalled replication forks and seem to act in a concerted manner. Slx4 binds to the structure-specific endonucleases Slx1 and Rad1-Rad10 and thereby supports the resolution of joint molecule (JM) structures arising during the repair of stalled replication forks and as recombination intermediates ((Fricke & Brill, 2003), (Toh et al., 2010)). Slx4-Slx1 associate in a higher order complex with Dpb11 and Rtt107 bridged by Slx4, and this association critically depends on phosphorylation by several kinases. DNA damage-dependent phosphorylation is required for the complex association (Flott & Rouse, 2005), as well as CDK-dependent phosphorylation of Slx4 on S486 (Ohouo, Bastos de Oliveira, Almeida, & Smolka, 2010). This multiprotein complex has a proposed role in DNA damage checkpoint regulation in early G2/M phase, as it might potentially affect the assembly dynamics of the 9-1-1-Dpb11-Rad9 checkpoint complex ((Ohouo et al., 2013), (Cussiol et al., 2015)). Interestingly, Rtt107 additionally coordinates the regulated activation of another nuclease activity, the structure-specific endonuclease Mus81-Mms4, which acts on Holliday junctions. In order to prevent untimely and mistargeted DNA cleavage by the Rtt107-associated nucleases, their recruitment and activation must be tightly controlled. To date it is poorly understood by which molecular mechanism the different nuclease activities centering around the Rtt107-Slx4-Dpb11 core are coordinated with the cell cycle, and how their activity is controlled in a spatial and temporal manner.

1.3 Role of Chromatin in the DSB Response

The genomic DNA is organized in a DNA-Protein complex called chromatin. The main protein components of chromatin are histone proteins building the globular core around which the DNA is wrapped, and harboring additional N- and C-terminal extensions that are often targeted by PTMs for architectural and regulatory functions. Eukaryotic cells use two molecules of four core histones (H2A, H2B, H3 and H4), respectively, to first build histone dimers (H2A/B and H3/H4), which then assemble in a histone octamer. Each octamer is being wrapped by 146 bp of DNA and this structure is then termed a nucleosome. Single nucleosomes are interconnected by a short stretch of DNA and additionally stabilized by the linker histone H1, often decorated with high-mobility group (HMG) proteins. The chain of nucleosomes, also referred to as "beads on a string", further coils up in a regulated manner to form a 30 nm fiber, which is additionally condensed during mitosis generating the well-known X-shaped mitotic chromosome structures. In yeast, the chromosomes are spatially organized within the nucleus in a manner, whereby centromeres cluster opposite of the telomeres in proximity to the spindle pole body (SPB). Packaging the DNA in order to fit it into the nucleus and stabilization and protection of the DNA molecule are obvious functions of chromatin. However, a much more complex and active role of chromatin during almost all DNA metabolic processes is evident. It has long been known that chromatin helps regulating the activity of the DNA molecule, on the one hand by enabling the formation of sub-compartments characterized by euchromatin (an open, active form of chromatin) or heterochromatin (a more dense and inaccessible form of chromatin), and on the other hand by a whole variety of regulatory modifications summarized as epigenetics. Epigenetics describes the regulation of DNA loci as achieved by PTM modification of DNA and histone proteins, both events which in turn mediate binding of accessory proteins and chromatin regulators to facilitate or suppress transcription of the respective gene locus. The propagation and maintenance of such epigenetic modifications is a major challenge for the cell during DNA replication and can determine the fate of the cell and path of differentiation. In contrast to sites of transcription, which are defined by sequence, DNA lesions occur at random positions and have to be dealt with according to the chromatin state and cellular condition.

Traditionally, nucleosomes have rather been viewed as a barrier to the DNA damage response, restricting the accessibility of the DNA to repair and signaling proteins. The "access – repair – restore" model ((Green & Almouzni, 2002), (Soria, Polo, & Almouzni, 2012)) describes the necessity to remove nucleosomes prior to repair and subsequently restore the chromatin in its original composition and structure once DNA repair is finished. However, this view has dramatically changed in the past ten years, when it has become evident that chromatin actively participates in damage signaling and repair. To this end, chromatin serves as PTM-regulated recruitment platform to enhance and modulate the binding and increase the local concentration of DDR factors, and therefore the "access" phase is now rather termed the "prime" phase (Soria et al., 2012). Finally, we begin to understand the impact of remodeling of chromatin in the context of DNA damage. This chapter will highlight the mechanisms by which chromatin and chromatin remodeling are involved in the DDR with a focus on DNA end resection, and how this converges with the cell cycle regulation of the DDR.

1.3.1 Chromatin as substrate in the DNA damage response

The substrate for all steps in the DNA damage response is chromatin. Accordingly, chromatin actively participates in damage signaling by different mechanisms. First, damage-specific post-translational modifications of the protruding histone tails, but also the histone bodies, serve to alter chromatin structure in order to prime it for the repair and to directly recruit DDR proteins. The most prominent example is the γH2A (human γH2A.X) mark, which is one of the first targets of the apical checkpoint kinases $Mec1^{ATR}$/$Tel1^{ATM}$ at DSBs, spreading over large regions around a lesion site ((Shroff et al., 2004), (Rogakou, Pilch, Orr, Ivanova, & Bonner, 1998)). γH2A then recruits the checkpoint mediator and resection inhibitor $Rad9^{53BP1}$ (chapter 1.2.4.2), the repair scaffold Rtt107 (X. Li et al., 2012), and cohesion ((Unal et al., 2004), (Ström et al., 2004)), which is involved in stabilizing sister chromatids to facilitate homology search during HR. Furthermore, a number of chromatin remodelers were suggested to be localized to DSBs by γH2A binding ((Paull et al., 2000), chapter 1.3.4).

γH2A is required to sustain checkpoint signaling, most likely by stabilizing Rad9, a mechanism that is conserved to the human checkpoint mediator MDC1 (Stucki et al., 2005). Collectively, the data suggest that γH2A maintains the checkpoint in an active state rather than contributing to de novo checkpoint factor recruitment and activation

((Celeste et al., 2003), (Nakamura et al., 2004), (Downey & Durocher, 2006)). Alternatively, γH2A could have a non-essential checkpoint function, leading to a faster recovery in γH2A mutants after low doses of DNA damage.

Notably, γH2A appears to be stably maintained in damaged chromatin without major turnover ((J.-A. Kim, Kruhlak, Dotiwala, Nussenzweig, & Haber, 2007), (Tsabar et al., 2015)). Therefore, the alleviation of checkpoint-mediated cell cycle arrest after successful DNA repair requires the removal of γH2A, which critically depends on de-phosphorylation by several phosphatases, such as PP4 and Ptc2/3 in yeast ((Keogh et al., 2006), (S. Nakada, Chen, Gingras, & Durocher, 2008), (J. A. Kim, Hicks, Li, Tay, & Haber, 2011)). Taken together, γH2A levels appear to be primarily determined by the damage kinases and not by its phosphatase-dependent de-phosphorylation. Due to its ubiquitous nature, γH2A.X is widely used as biomarker for the presence of DNA damage, and has gained particular clinical importance as biodosimeter for measuring DNA damage inflicted during chemotherapy (reviewed in (Redon et al., 2012)). Besides γH2A, a corresponding modification of H2B (phospho-T129) has recently been described (C.-S. Lee, Lee, Legube, & Haber, 2013), but a possible function during DSB repair yet has to be elucidated.

Other histone tail modifications with a potential role in the DNA damage response comprise acetylation, methylation and ubiquitylation. Acetylation in general has the propensity to control chromatin compaction, as it introduces negative charges that are thought to weaken the DNA-histone interactions or disrupt the folding of chromosomes and therefore open up the chromatin for transcription or repair. As an example, the acetylation of H3K56 by the Rtt109 histone acetyltransferase confers resistance towards genotoxic agents ((Ozdemir et al., 2005), (Masumoto, Hawke, Kobayashi, & Verreault, 2005)) and was shown to enrich after DNA damage. H3K56 acetylation was connected to re-positioning of nucleosomes after DNA repair allowing checkpoint recovery (C.-C. Chen et al., 2008), and to contribute to HR repair template choice by promoting the usage of the sister chromatid for recombination (Muñoz-Galván, Jimeno, Rothstein, & Aguilera, 2013). During both DNA repair and DNA replication, the H3K56 acetylation mark is required for complete chromatin reconstitution and resolution of Rad52 foci (Wurtele et al., 2012).

Methylation in contrast is often but not always counteracting the adverse effect to histone acetylation by compacting chromatin, as exemplified by methyl-H3K9, the most prominent mark of heterochromatin. On top of regulating chromatin structure, histone methylation by the Dot1 methyltransferase affects the DDR. While this mark is apparently not regulated in a DNA damage-dependent fashion, it is required to target Rad9 to damaged chromatin ((Wysocki et al., 2005), (Grenon et al., 2007); chapter 1.2.4.2). Therefore, the H3K79me mark appears to cooperate with γH2A. Together, both are essential to Rad9-dependent checkpoint signaling ((Giannattasio et al., 2005), (Toh et al., 2006)). The H3K79me modification by Dot1 is facilitated through H2B-K123 ubiquitylation via Rad6/Bre1 ((Robzyk, 2000), (Wood, Schneider, Dover, Johnston, & Shilatifard, 2003)). Interestingly, H3K79 methylation is cell cycle-regulated with high levels of di-methylated H3K79 during mitosis in yeast and the exact inversed fluctuation in human cells (Feng et al., 2002). In how far this cell cycle regulation plays a role in the DNA damage response is not understood (Schulze et al., 2009). In fission yeast and humans, the recruitment modes of the Rad9 homologs Crb2 and 53BP1 are similar and involve di-methylation of H4K20 ((Botuyan et al., 2006), (Pei et al., 2011)). While Crb2 is thought to be specific for H4K20me, also methyl-H3K79 was shown to interact with human 53BP1 (Huyen et al., 2004). In addition, Dot1 methylation of H3K79 might add to the DSB repair by enhancing cohesin recruitment in order to facilitate recombination (Conde et al., 2009).

In human cells, a central regulatory cascade underlying checkpoint signaling is the multi-step ubiquitylation of several targets by the E3 RING ubiquitin ligases RNF8 and RNF168. In short, H1 ubiquitylation by RNF8 recruits RNF168, which subsequently ubiquitylates H2AK13 and H2AK15, both of which contribute to the recruitment of the human Rad9 ortholog 53BP1 (for a detailed review, see (Panier & Durocher, 2009), (Panier & Durocher, 2013)).

Along with PTM modification of the canonical histones, cells can incorporate histone variants in nucleosomes independent of DNA replication and thereby alter their function. In mammals, the most prominent histone variant connected to the DDR is H2A.X, which harbours the phosphorylation site for γH2A.X and replaces canonical H2A in about 2-25% of all nucleosomes throughout the whole genome (Rogakou et al., 1998), strongly dependent on tissue type and cellular context. In yeast, this

phosphorylation takes place in the canonical H2A tail and a corresponding variant is therefore absent. Yet, another H2A variant – Htz1 or mammalian H2A.Z – has a well-established function in the DDR ((Kalocsay, Hiller, & Jentsch, 2009), (Lademann, Renkawitz, Pfander, & Jentsch, 2017), (Xu et al., 2012)). Htz1 is specifically incorporated around DSBs by the chromatin remodeler Swr1 and required for re-location of DSBs to perinuclear anchor sites in a manner that depends on Htz1 SUMOylation ((Kalocsay et al., 2009), (Horigome et al., 2016)). In turn, Htz1 is removed by Ino80, and the interplay between Swr1 and Ino80 to balance Htz1 levels contributes to genome stability and DNA damage checkpoint control via γH2A stabilization (Papamichos-Chronakis, Krebs, & Peterson, 2006). During HR, Htz1 controls the step of presynaptic filament formation (Lademann et al., 2017). Additionally, some studies describe early functions enhancing DNA end resection and checkpoint activation (Kalocsay et al., 2009). Other H2A variants that only exist in higher eukaryotes, such as macroH2A, contribute to DNA repair pathway choice by facilitating the accumulation of BRCA1 on damaged chromatin, a pro-HR factor (Khurana et al., 2014).

Collectively, the definition of the nucleosome structure and function by histone PTMs and incorporation of histone variants is an integral part of the DNA damage response, adding additional layers of regulation to DNA end resection, checkpoint activation and DNA repair.

1.3.2 Chromatin and DNA end resection

The digestion of one DNA strand during end resection requires nucleases to access the DNA. There are two fundamental mechanisms by which chromatin can influence DNA end resection. First, chromatin can directly physically block nuclease access or progression. Second, chromatin can recruit accessory proteins to stimulate or suppress resection. In vitro data suggest that chromatin impedes resection (Adkins, Niu, Sung, & Peterson, 2013). However, it has not been demonstrated in vivo that nucleosomes actually do present a barrier to resection, nor has it been unambiguously shown that nucleosomes are evicted during the process. In fact, the relative loss of histones at regions of active transcription appears to be significantly higher than at DNA lesion sites, strongly pointing towards the residual presence of histones at resected loci ((Boeger, Griesenbeck, Strattan, & Kornberg, 2003), (Shroff et al., 2004), (Bennett, Papamichos-

Chronakis, & Peterson, 2013)). In vitro studies suggest that nucleosomes can slow down nucleases, and this inhibition seems to have more pronounced effects on the Exo1-dependent resection pathway than on the STR/Dna2 pathway (Adkins et al., 2013). While Exo1 is blocked by nucleosomes, STR/Dna2 mainly requires a nucleosome-free "entrance gap" to carry out resection (Adkins et al., 2013). This finding is perhaps not surprising, since in these in vitro studies, there is no helicase supporting Exo1, while Dna2 cooperates with the Sgs1 helicase and it could therefore be speculated that Sgs1 promotes access for Dna2 to nucleosomal DNA. Notably, while the sheer presence of nucleosomes appears to counteract resection in these assays, unmodified nucleosomes lacking PTMs and accessory proteins were used, which most likely reflect only poorly the actual chromatin, which is substrate of resection in vivo. Interestingly, in vitro and in vivo, the histone variant Htz1 seems to enhance specifically Exo1-dependent resection (Adkins et al., 2013). Furthermore, in vitro studies have shown that per se, nucleosome octamers can assemble on single-stranded DNA de novo and are also retained on the ssDNA after Sgs1-dependent resection (Adkins et al., 2017). Intriguingly, such ssDNA-nucleosome assemblies are more flexible than dsDNA-nucleosome structures, a feature that could potentially also play a role during subsequent repair steps (Adkins et al., 2017). In vivo, this question is difficult to address since cells lacking histones are not viable. First insights about the role of chromatin during resection in vivo can be derived from experiments using chromatin remodeler mutants as discussed below (chapters 3.4 and 3.5). To date, mobilization of only one histone directly at the DSB was observed in vivo, potentially by sliding or eviction ((Shim et al., 2007), (Tsabar, Hicks, Tsaponina, & Haber, 2016)), and there is no solid evidence for greater histone loss at DSBs.

The second mechanism – recruitment of non-histone chromatin interactors affecting resection efficiency – has emerged recently as an important control mechanism, but remains mechanistically elusive. The checkpoint mediator Rad9 as well as its human homolog 53BP1, which both bind to histones after DNA damage (chapter 1.2.4.2), block resection. Phenotypically, Rad9 counter-acts the activity of the nucleosome remodeler Fun30 during end resection ((X. Chen et al., 2012), chapter 1.3.5), and Fun30 becomes fully dispensable for efficient resection when Rad9 is depleted. Interestingly, both proteins are targeted by CDK to enhance their DNA binding, suggesting a cell cycle-dependent regulation of a pro- and an anti-resection factor. How

this antagonism manifests in the control of resection, and by which mechanism Rad9 and its orthologs could inhibit resection on a molecular level, is under investigation.

1.3.3 Chromatin architecture influences the DDR

Besides local effects of nucleosomes and nucleosome binders on the DNA damage response, also the global architecture of chromatin and the larger chromosomal context in which a DSB occurs play a decisive role in the repair process. Factoring in is local chromatin structure (for example eu- versus heterochromatin), the mobility of the DSB ends, the location of the repair donor with respect to the lesion site (here, we can distinguish between intra-or inter-chromosomal recombination), and the 3D conformation of the affected locus.

It has been long known that chromatin is not fixed in position but features plasticity (Marshall et al., 1997). Chromatin is inherently restricted in free diffusion, and this restriction derives from anchoring to nuclear structures, ATP levels, inter- and intra-nucleosomal interactions, size of the chromosome (Neumann et al., 2012), nucleosome density (Hauer et al., 2017) and sister chromatid cohesion (Dion, Kalck, Seeber, Schleker, & Gasser, 2013). Upon DNA damage, chromatin visibly expands (Adam et al., 2016). The induction of a DSB provokes changes in the physical properties and enhances plasticity not only of the affected genomic locus, but also genome-wide ((Seeber, Dion, & Gasser, 2013a), (Hauer et al., 2017), (Dion, Kalck, Horigome, Towbin, & Gasser, 2012)). DSBs and likewise uncapped telomeres occupy a larger area in the nucleus compared to undamaged loci ((Dion et al., 2012), (Miné-Hattab & Rothstein, 2012), (Savage, 1996), (Dimitrova, Chen, Spector, & de Lange, 2008)). It has been demonstrated that DSBs become mobilized and are translocated to the nuclear periphery if not repaired in time ((Nagai et al., 2008), (Oza, Jaspersen, Miele, Dekker, & Peterson, 2009)). Such mobilization is a double-sided coin: DSB repair efficiency during HR apparently benefits from DSB mobility, most likely because it drives homology search ((Agmon, Liefshitz, Zimmer, Fabre, & Kupiec, 2013), (C.-S. Lee et al., 2016)). Importantly, this is not due to constitutive pairing of homologous loci, but happens in a damage-induced manner (Miné-Hattab & Rothstein, 2012). The re-localization of DSBs to the nuclear periphery, either to NPCs or Mps3 anchors, has a great benefit. It shifts the lesion from a random position into a defined environment, allowing the cell to channel the DSB repair to specific repair pathways. More precisely, at the nuclear

periphery recombination is repressed while template-switching, non-precise NHEJ and BIR are promoted ((Swartz, Rodriguez, & King, 2014), (Horigome et al., 2016)). On the downside, enhanced DSB mobility has the potential to increase unwanted recombination and result in genomic instability ((Roukos et al., 2013), (Aten et al., 2004)). The mechanism of DSB mobilization is not yet fully established, but it seems to rely on the DNA damage checkpoint activation by $Mec1^{ATR}$ (Hauer et al., 2017) or ATM in mammals (Lottersberger, Karssemeijer, Dimitrova, & de Lange, 2015). Work in yeast proposes that Mec1 stimulates the Ino80 chromatin remodeler, which would then induce removal of histones from the damaged chromatin followed by proteasomal degradation and thereby enhance its mobility (Hauer et al., 2017). Studies in mammalian cells similarly report histone eviction at sites of DNA lesions (Adam et al., 2016). Lastly, histone loss has been linked to checkpoint activation via the Rad53 effector kinase, implying a positive feedback loop in the DNA damage response (Gunjan & Verreault, 2003). In addition to inducing histone loss, Rad53 was reported to uncouple kinetochore attachments and thereby to enhance local and global chromatin mobility (Strecker et al., 2016).

The dependency on an active checkpoint seems an appropriate means to balance benefits for repairing long-persisting DSBs with the threat to genome instability by mistargeted recombination. To date, there is however a discrepancy in published data regarding whether DSB mobility is beneficial for homology search, and most likely the cellular conditions and nature of DNA damage induction is an underestimated component of the subsequent HR-dependent repair and effect of DSB mobility ((Strecker et al., 2016), (Neumann et al., 2012), (Rudin & Haber, 1988)).

Intriguingly, it is not only the chromatin changes induced by DNA damage that can affect DSB repair, but also the chromosome conformation that was established before the damage occurred. Recent studies have described so-called topologically associated domains (TADs), defined as loci that are in close spatial proximity, potentially physically tethered, but not necessarily adjacent in the primary sequence or on the same chromosome ((Caron et al., 2015), (Caron et al., 2012), (Aymard et al., 2017)). The propagation of checkpoint signals such as γH2A appears to be restricted to a TAD and as such clearly distributes in three dimensions instead of linearly along the broken chromosome. This model goes along with observations in yeast, where the monitoring of

homology search by Rad51 recombinase ChIP revealed spreading of Rad51 and γH2A guided by 3D clustering ((Renkawitz, Lademann, Kalocsay, & Jentsch, 2013b),(Agmon et al., 2013)).

A principle challenge for the cell are DNA lesions occurring in repetitive DNA sequences such as telomere or centromeric repeats. In order to prevent unwanted recombination between repeats and the resulting genomic instability (Peng & Karpen, 2008), these regions are typically heterochromatic or otherwise restricted as exemplified by the compartmentalization of rDNA repeats to the nucleolus in yeast. It has been shown that while recombination can act on heterochromatic loci, this occurs only after they become physically separated, so that repair can be carried out without losing repeats ((Chiolo et al., 2011), (Chiolo, Tang, Georgescu, & Costes, 2013)). Similarly, rDNA repeats have to be moved out of the restrictive environment of the nucleolus in order to complete DSB repair, and for both rDNA and heterochromatic repeats, the Smc5/6 complex is required to do so ((Torres-Rosell, Machin, & Aragón, 2005), (Torres-Rosell et al., 2007)). Additionally, chromatin remodelers help to open the heterochromatin structure in order to support strand invasion during HR ((M. Sinha & Peterson, 2009), chapter 1.3.4.2).

1.3.4 Remodeling of DNA double-strand breaks

ATP-dependent nucleosome remodelers are large, mostly multiprotein-containing machineries that modify the properties of chromatin by sliding, evicting and spacing nucleosomes on the DNA, or by altering its composition via histone dimer or octamer exchange, using the energy released by ATP hydrolysis. First insights about the function of chromatin remodelers have emerged from studies of gene transcription. Nucleosome remodelers were observed to bind to DNA lesions and are therefore thought to be involved in the DNA damage response. However, until now there is relatively little mechanistic understanding about chromatin remodeling at DNA damage sites. It seems reasonable to assume that functions during transcription can be extrapolated and applied to the DNA damage response.

Over time, chromatin remodeling was shown to influence a vast variety of distinct steps during DSB processing, signaling and repair (reviewed in (Seeber, Hauer, & Gasser, 2013b)). In this chapter, individual nucleosome remodelers are discussed regarding their activity at DSBs. These are subdivided in early remodeling steps, mainly thought to

enhance DDR protein binding, and late remodeling steps with potentially more complex functions reaching several kilobases into the chromatin adjacent to the DNA damage site.

1.3.4.1 Early DSB remodeling

Ku and the MRX complex immediately bind DSB ends in order to initiate ligation-based repair (NHEJ) or DNA end resection, as discussed earlier. These recruitment steps require opening of the local chromatin structure, and indeed, nucleosomes were shown to be repositioned around DSBs ((Kent, Chambers, & Downs, 2007), (Shim et al., 2007), (Liang, Qiu, Ratnakumar, & Laurent, 2007)). RSC, a SWI2/SNF2 remodeler of the Snf2-like family, was shown to change nucleosome positioning around DSBs by sliding (Kent et al., 2007) prior to and independent of DNA end resection, and this repositioning is needed to allow Ku and MRX binding (Shim et al., 2007), as well as for apical checkpoint kinase recruitment and checkpoint activation (Liang et al., 2007). As a consequence, the efficiency of the entire downstream break processing, signaling and repair seems hampered in absence of RSC (Shim et al., 2007). Defects in resection initiation in cells with impeded RSC activity are minor and can be attributed to lacking Mre11 enrichment at the DSB (Chambers & Downs, 2012). Notably, also the Swi/Snf remodeler appears to enhance MRX binding to DSBs, with similar phenotypes as RSC mutants (Wiest, Houghtaling, Sanchez, Tomkinson, & Osley, 2017). Overall, the current model of RSC function during early DSB repair steps pictures nucleosome mobilization by RSC as general enhancer of DDR factor recruitment, consistent with RSC contributing to NHEJ and HR ((Shim et al., 2007), (Chambers & Downs, 2012)).
Two remodelers of the Swr1-like family of SWI2/SNF2 remodelers are the conserved Ino80 and Swr1 complexes, which are the key regulators of Htz1 levels in chromatin. As discussed earlier, the histone variant Htz1 (H2A.Z) plays a multifaceted role in the DNA damage response. Htz1 is incorporated into chromatin by Swr1 (Luk et al., 2010), and this reaction is being reversed by Ino80 (Papamichos-Chronakis, Watanabe, Rando, & Peterson, 2011). Both remodelers are required for resistance against genotoxic agents ((Kobor et al., 2004), (Shen, Mizuguchi, Hamiche, & Wu, 2000)). Interestingly, the removal of canonical H2A/H2B seems to be at least partially uncoupled from the deposition of Htz1/H2B dimers, since Swr1 induces genome instability in absence of Htz1, most likely thanks to incomplete remodeling (Morillo-Huesca, Clemente-Ruiz, Andújar, & Prado, 2010).

Similar to the mild defect in resection initiation in cells with defective RSC function, Ino80 seems to contribute to resection initiation to a limited extent ((van Attikum, Fritsch, & Gasser, 2007), (X. Chen et al., 2012), (Lademann et al., 2017)). Both remodelers are dispensable for later resection steps and initial resection defects are additive with mutants specifically affecting long-range resection (X. Chen et al., 2012). In conclusion, current models place Ino80 and RSC in the initiating step of resection, while other remodeling activities contribute to processive resection as discussed in the next section. This model is supported by the finding that repair pathways such as single-strand annealing (SSA), which specifically rely on long-range resection, are not affected by mutants in Ino80 or RSC (Eapen et al., 2012).

1.3.4.2 Late DSB remodeling

In addition to establishment of open, accessible chromatin close to the DSB, also later steps in the DDR require chromatin changes. This sub-chapter focuses on two particular reactions, which both involve large parts of the damaged chromosome or even the whole genome, and therefore impose an enhanced need for chromatin restructuring: long-range DNA end resection and homology search during HR.

Until recently, there has been no chromatin remodeler associated with enhancing long-range resection, and it was unclear whether at all and if yes, to what extent additional remodeling or helicase activity besides Sgs1 is required to support long-range resection. A series of pioneering studies in 2012 has elucidated a pivotal, conserved role of the nucleosome remodeler Fun30/SMARCAD1 in the Exo1- and Sgs1-dependent long-range resection of DNA double-strand breaks and resection-coupled repair ((X. Chen et al., 2012), (Eapen et al., 2012), (Costelloe et al., 2012)), as discussed further in the next chapter.

Homology search describes the complex task for the DSB ends to find and pair with a homologous donor sequence, which can be located anywhere in the genome, in order to initiate the templated DNA synthesis that will restore the sequence. Due to the complexity of this step, homology search was coined the “search for the needle in the haystack” ((Renkawitz et al., 2013b), (Renkawitz, Lademann, & Jentsch, 2013a)). Homology search requires the loading of the recombinase Rad51, which forms a filament around the resected DNA replacing RPA in a Rad52-dependent manner. Availability of Rad51 for specific DSB localization is ensured by the single-subunit Swi/Snf-family

remodeler Rad54, which displaces Rad51 from unspecific binding sites ((Chi et al., 2011), (M. Sinha & Peterson, 2009)) and establishes stability of the resulting Rad51 filament (Ceballos & Heyer, 2011). Rad51 assembly by Rad54 is ATP-independent (Wolner & Peterson, 2005) and apparently acts in a self-enhancing manner, as Rad51 does stimulate Rad54 DSB-binding (Dion et al., 2012). To date it is not clear how the two ssDNA-binding proteins coexist on the single-stranded DSB overhang. Rad51 filament formation drives homology search and a recent study nicely demonstrates that Rad51 spreading from a DSB critically depends on Htz1 removal by Ino80 ((Lademann et al., 2017), (Tsukuda, Fleming, Nickoloff, & Osley, 2005)). A similar requirement for Ino80-dependent H2A.Z removal to complete HR was observed in human cells ((Tsukuda et al., 2009), (Alatwi & Downs, 2015)), suggesting a conserved function of Ino80 at the step of synaptic filament formation. Indeed, control of H2A.Z occupancy by Ino80 and Swr1 is required for genomic stability ((Papamichos-Chronakis et al., 2011), (Van, Williams, Kunkel, & Peterson, 2015)).

Rad54 also appears to act after strand invasion, as conclusion of HR-dependent repair is dependent on Rad54, which is required for ATP-dependent histone mobilization prior to gap fill DNA synthesis ((Sugawara, Wang, & Haber, 2003), (Wolner & Peterson, 2005)).

The last step in the DSB repair process is the restoration of chromatin. Notably, the two H3-H4 histone chaperones Asf1 and Caf1, which both have well-defined functions during the re-establishment of chromatin after replication and transcription ((Tyler et al., 1999), (Tyler et al., 2001)), are similarly involved the re-establishment of nucleosome occupancy at repaired DNA damage sites in yeast and mammalian cells ((J. A. Kim & Haber, 2009), (Soria et al., 2012), (Tsabar et al., 2016), (Mello et al., 2002)).

1.3.5 The chromatin remodeler Fun30^{SMARCAD1}

The Snf2-like Etl1-subfamily, single-subunit chromatin remodeler Fun30 (function unknown now) and its fission yeast homolog Fft3 have been characterized for their role in silencing of certain gene loci and preserving heterochromatic structures, the repression of unwanted transcription over centromeres, repression of euchromatin formation, distribution of the histone variant Htz1, and for a general function in chromatin organization at centromeres and subtelomeric regions ((Steglich et al., 2015), (Strålfors, Walfridsson, Bhuiyan, & Ekwall, 2011), (Neves-Costa, Will, Vetter, Miller, & Varga-

Weisz, 2009), (Byeon et al., 2013), (Durand-Dubief et al., 2012), (Yu, Zhang, & Bi, 2011)). First insights into an actual molecular mechanism behind these functions was provided recently by Taneja et al (2017), who showed that fission yeast Fun30, Fft3, inhibits histone turnover in heterochromatin, thereby preserving density of heterochromatic histone marks. Generally it is likely that Fun30 homologs act during transcription, replication and DNA repair, as they were shown to directly interact with proteins involved in these processes ((Taneja et al., 2017), (J. Lee et al., 2017), (Rowbotham et al., 2011)).

In vitro, Fun30 possesses nucleosome sliding and histone dimer exchange activity ((Awad, Ryan, Prochasson, Owen-Hughes, & Hassan, 2010), (Byeon et al., 2013)). The gene-repressive function of Fun30 was described to be due to Fun30-mediated changes in the 5' flanking region of affected genes, to which Fun30 was also shown to localize, most likely catalyzed by ATP-dependent nucleosome sliding (Byeon et al., 2013). Fun30 purifies as homodimer and its ATPase activity is being stimulated likewise by naked and chromatinized DNA (Awad et al., 2010). When compared to the in vitro activity of RSC, it seems that the primary reaction catalyzed by Fun30 is H2A/H2B dimer exchange (Awad et al., 2010). Therefore, it is not unlikely to assume that Fun30 could also be involved in the incorporation or removal of Htz1, consistent with a described role in genome-wide Htz1 distribution particularly to ensure centromere structure and function (Durand-Dubief et al., 2012). Furthermore, Fun30 possesses remarkable sequence homology with the Ino80 and Swr1 chromatin remodelers (Flaus, 2006), which themselves exchange Htz1-containing dimers.

Notably, Fun30 is one of few single-subunit chromatin remodelers, which needs to unite all catalytic and regulatory assets in one polypeptide chain. Its domain structure can be roughly divided in a catalytic domain at the C-terminus comprising Walker DNA binding motifs in conjunction with a helC helicase domain, thus comprising the Snf2 nucleosome remodeling domain, and a regulatory unit at the N-terminus (Fig. 10). The N-terminus harbours protein-protein interaction sites such as a CUE domain and CDK consensus phosphorylation sites (S20, S28, S34), suggesting that Fun30 might be subjected to cell cycle control by CDK phosphorylation ((Ubersax et al., 2003), (X. Chen et al., 2016)). The catalytic domain of Fun30 was structurally analyzed revealing a Fun30-specific insert that might support functional alterations compared to other Snf2

remodelers (L. Liu & Jiang, 2017). Fun30 is functionally conserved from yeast to higher eukaryotes, and human Fun30 (SMARCAD1, formerly human helicase 1; hHel1) has been analogously implicated in chromatin silencing and compaction. It is remarkable that besides the catalytic domain, all Fun30 homologs carry one or more CUE domains, which are putative binding sites for ubiquitylated proteins. Interaction partners of these CUE domains on Fun30 still need to be elucidated (Neves-Costa et al., 2009).

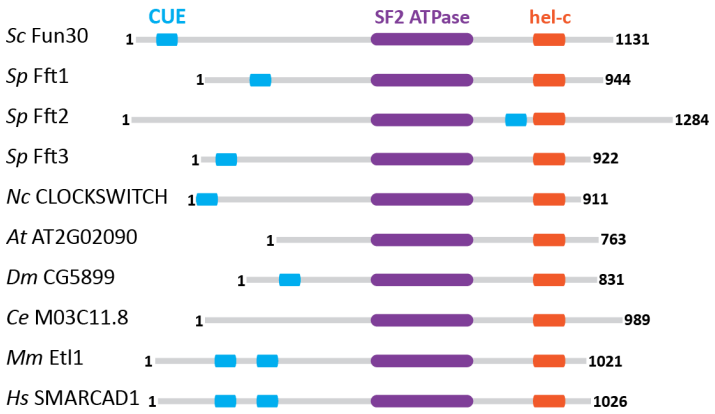

Fig.10 **Domain structure of Fun30 and its homologs** (modified from (Neves-Costa et al., 2009)). All homologs of Fun30 execute nucleosome remodeling via a central SF2 ATPase (purple) in synergy with a hel-c helicase domain (orange). Additionally, except for the plant and worm Fun30, an N-terminal CUE domain (blue) was mapped in all homologs.

Fun30 has first been connected to the DNA damage response by the observation that *fun30Δ* mutants are sensitive to the topoisomerase I inhibitor camptothecin (Neves-Costa et al., 2009), which generates covalent DNA-topoisomerase I adducts. It was also identified in a screen searching for genes that would affect gene targeting efficiency (X. Chen et al., 2012). As gene targeting requires functional homologous recombination and resection, this phenotype is consistent with a resection defect of *fun30Δ* mutants. Based on this seminal discovery by Chen et al (2012), Fun30 was characterized as resection-promoting chromatin remodeler ((Eapen et al., 2012), (X. Chen et al., 2012), (Costelloe et al., 2012)). Importantly, Fun30 could be specifically attributed to the long-range resection pathway, as it supports resection beyond 5 kb without affecting the initiation of resection, consistent with deficiencies in repair pathways relying on long-range resection (X. Chen et al., 2012). This specificity distinguishes Fun30 from other chromatin remodelers implicated in early steps of DNA end resection (chapter 1.3.4).

Despite the growing understanding of the importance of Fun30-dependent chromatin remodeling for DNA end resection, there is a number of intriguing questions yet to be answered. Fun30 has been demonstrated to localize genome-wide and specifically to telomeric and centromeric regions, gene-flanking regions at both ends ((Durand-Dubief et al., 2012), (Byeon et al., 2013)), and to DNA double-strand breaks ((Eapen et al., 2012), (X. Chen et al., 2012), (S. Bantele et al., 2017)). In vitro, Fun30 displays the propensity to bind to histone H2A (Eapen et al., 2012) and was suggested to preferentially interact with nucleosomes that are placed on single-stranded DNA (Adkins et al., 2017). However, we do not understand how Fun30 is specifically targeted to DNA double-strand breaks, how this targeting is integrated within the cell cycle, and by which molecular mechanism Fun30 acts to enhance DNA end resection once it has been recruited to the DSB.

Objectives of these studies

Targeting of the Fun30 nucleosome remodeller by the Dpb11 scaffold facilitates cell cycle-regulated DNA end resection.

Bantele, S.C.S., Ferreira, P., Gritenaite, D., Boos, D. & Pfander, B.

eLife. pii: e21687. doi: 10.7554/eLife.21687 (2017).

DNA end resection is the nucleolytic degradation of the 5' ends at DNA double-strand breaks, which uncovers long stretches of single-stranded DNA needed for homologous recombination (HR). Therefore, this type of DSB processing constitutes the critical switch between ligation-dependent DSB repair and HR. Resection must be kept under tight cell cycle control, as aberrant resection in cells that have not yet duplicated chromosomes during S-phase and therefore do not possess a suitable recombination donor can cause large genome rearrangements and ultimately corrupts genome stability. Past research has identified a multitude of mechanisms by which resection is cell cycle-regulated, all of which target the enzymes executing resection and none the substrate of resection, damaged chromatin. In a series of seminal publications, the chromatin remodeler Fun30 was found to specifically support resection ((Eapen et al., 2012), (X. Chen et al., 2012), (Costelloe et al., 2012)). However, it was unclear whether this process is under cell cycle control. In this work, we identified Fun30 as a target of cell cycle-dependent CDK phosphorylation, and therefore set out to establish the molecular mechanism of this regulation, with a focus on Fun30 targeting to DSBs, and to which extent it contributes to the overall cell cycle regulation of DNA end resection.

Quantitative signaling mechanisms in response to DNA damage.

Bantele S.C.S., Lisby M. and Pfander B.

manuscript in revision

Every cell frequently encounters damages to its DNA, and therefore has to constantly monitor its "DNA damage status" so that a suitable response can be set off. High damage loads or difficult-to-repair lesions persisting for a long time call for cell cycle arrest and up-regulation of DNA repair activity, both of which are triggered by activation of the DNA damage checkpoint. At the same time, cells need to grow and proliferate when the damage load is tolerable.

Taken together, DNA damage checkpoint activation needs to balance genome integrity with proliferation. The basic phenomenon that gives a measure of the cells' damage load is the occurrence of single-stranded DNA, a typical structure generated at lesion sites that accumulates locally at long-persisting damage sites (for example DSBs) and when quantified could serve as a global signal of the cellular DNA damage load. Cells use sensor proteins to signal the presence of ssDNA in the cell ((Bonilla et al., 2008), (Kondo et al., 2001)), but whether and how these signals are quantified is unknown. A possible quantitative sensor could be the recruitment of the checkpoint initiator kinase Mec1-Ddc2 to RPA-covered ssDNA (Deshpande et al., 2017). However, we found that a distinct Mec1 phosphorylation target –the histone mark γH2A – does not quantitatively respond to the ssDNA signal. Here, we set out to characterize the two modes of Mec1 signaling and moreover to unveil the molecular mechanism underlying the quantitative reading of the ssDNA signal and according transmission of DNA damage checkpoint signals.

A cell cycle-independent mode of the Rad9-Dpb11 interaction is induced by DNA damage.

Di Cicco, G., Bantele, S.C.S., Reusswig, K-U. and Pfander, B.

Sci Rep 7(1):11650. doi:10.1038/s41598-017-11937-z (2017).

Rad9 fulfills two distinct functions at DNA double-strand breaks. First, it mediates checkpoint activation and second, it inhibits DNA end resection. While resection and thus probably also the associated Rad9 activity are cell cycle regulated, the DNA damage checkpoint has to be able to become active throughout the entire cell cycle. Thus, the two Rad9 functions might have distinct cell cycle requirements.

Interestingly, Rad9 associates with damaged chromatin via two pathways. First, it can bind to histones in a damage-dependent and cell cycle-independent mode ((Hammet et al., 2007), (Grenon et al., 2007)). Second, it associates with Dpb11 upon cell cycle-dependent phosphorylation of Rad9 by CDK, which occurs in S-, G2-, and M-phases of the cell cycle (Pfander & Diffley, 2011). So far it was not clear, whether the Rad9-Dpb11 interaction can also take place in G1 and whether such an interaction would influence resection and checkpoint signaling.

Furthermore, it was not clear whether the two Rad9 DSB recruitment pathways act independently or interact, and if certain functions of Rad9 can be specifically attributed to one of the two complexes.

We identified a new Rad9 recruitment mode that mediates interaction between Rad9 and Dpb11 in G1. Interestingly, this interaction requires DNA damage and the same CDK sites on Rad9 as the cell cycle-regulated interaction, however occurs when CDK is inactive. In this study, we set out to identify the genetic and cellular requirements for this novel Rad9-Dpb11 complex formation and clarify its role during DNA end resection and checkpoint activation.

A cell cycle-regulated Slx4-Dpb11 complex promotes the resolution of DNA repair intermediates linked to stalled replication.

Gritenaite, D., Princz, L. N., Szakal, B., Bantele, S. C. S., Wendeler, L., Schilbach, S., Habermann B.H., Matos J., Lisby M., Branzei D. and Pfander B.

Genes & Development, *28*(14), 1604–1619. doi:10.1101/gad.240515.114. (2014).

The scaffold protein Dpb11 acts as a reader of CDK-dependent PTMs, and thereby engages in a number of specific protein-protein complexes, all of which serve to assemble proteins in a cell cycle-regulated manner. Dpb11-mediated complexes govern a variety of DNA metabolic processes such as DNA replication, repair and damage signaling. One of these Dpb11 complexes involves the DNA damage scaffold proteins Slx4 and Rtt107 (Ohouo et al., 2013).

In this project, we aimed to elucidate the mechanism by which this multi-scaffold protein complex regulates the structure-specific endonuclease Mus81-Mms4 within the cell cycle. Complex formation between Dpb11 and Slx4/Rtt107 was suggested to have a function as dampener of the DNA damage checkpoint by direct competition with the checkpoint-essential Dpb11-Rad9 complex (Ohouo et al., 2013). Therefore, my specific aim for this work was to analyse the connection between DNA damage checkpoint activity and its potential regulation by Dpb11-Slx4-Rtt107. In particular, I asked whether mutants abolishing the interaction between Dpb11 and Slx4 would affect checkpoint activity after exposure to MMS relative to the number of lesion sites.

Cumulative Thesis: Summary of publications

Publication 1 | Targeting of the Fun30 nucleosome remodeller by the Dpb11 scaffold facilitates cell cycle-regulated DNA end resection.

Bantele, S.C.S., Ferreira, P., Gritenaite, D., Boos, D. & Pfander, B.
eLife. pii: e21687. doi: 10.7554/eLife.21687 (2017).

DSB repair by HR requires a homologous DNA template, which is usually the sister chromatid. As G1 cells lack this recombination template, it is strictly necessary to restrict resection and HR to cell cycle phases outside of G1. So far, studies analyzing the cell cycle regulation of resection have focused on the cell cycle regulation of resection nucleases.

In this paper, we show that the actual bottleneck in the resection reaction lies within the resection substrate itself, the damaged chromatin. We demonstrate that the chromatin remodeler Fun30, which is essential to efficient long-range resection, becomes targeted by CDK and then interacts with the scaffold protein Dpb11. This interaction is strictly required for the resection-promoting function of Fun30.

A Dpb11 interaction-deficient mutant of Fun30, which contains non-phosphorylatable alanines in stead of the CDK-targeted serines is not properly recruited to DSBs and fails to support DNA end resection and resection-coupled DSB repair.

We furthermore show that Fun30 and Dpb11 engage in a complex with the 9-1-1 checkpoint clamp, which thereby brings Fun30 to its place of action at the DSB. Importantly, we achieve a hyper-activation of DNA end resection by making the Fun30-Dpb11-9-1-1 complex constitutive (using a covalent protein fusion between 9-1-1 and Fun30). Intriguingly, this mutant condition also leads to a bypass of DNA end resection, which is activated in G1. These data do not only support the hypothesis that chromatin is a barrier to resection and therefore actively influences DNA repair pathway choice, but also provides the first genetic tool to ectopically activate resection independent of the cell cycle.

The human Fun30 homolog SMARCAD1 was reported to function in DNA end resection, too. Here, we show that the interaction between the Dpb11 homolog TOPBP1 and SMARCAD1, its CDK regulation and the Fun30^{SMARCAD1} interaction surface are highly conserved, suggesting that human and yeast cells share this regulatory mechanism.

Overall, we therefore propose a model by which CDK-dependent recruitment of Fun30^{SMARCAD1} to DSBs through interaction with Dpb11^{TOPBP1} is key to the regulation of Fun30 at DNA double-strand breaks and is an essential factor in the cell cycle regulation of DNA end resection.

Publication 2 | Quantitative signaling mechanisms in response to DNA damage.

Bantele S.C.S., Lisby M. and Pfander B.

manuscript in revision

Cells have to accurately judge their DNA damage load in order to make decisions such as whether cell cycle arrest and up-regulation of DNA repair are required or not. In other words: cells have to quantify their damage load.

With this paper we provide the first study of quantitative aspects of checkpoint signaling at DSBs. We report that the apical checkpoint kinase Mec1, which is recruited to DSBs in a manner that depends on RPA-ssDNA – generated by DNA end resection, feeds into two distinct signaling circuits. On the one hand, it mediates – in the local circuit – phosphorylation of H2A (γH2A). On the other hand it phosphorylates and triggers activation of the checkpoint effector kinase Rad53 and thereby participates in the global checkpoint circuit.

Interestingly, we observe that while the global checkpoint signaling strongly depends on the amount of ssDNA, the local signaling circuit seems to be irresponsive to changes in the ssDNA signal. Consequently, the recruitment of the apical kinase Mec1 cannot be the only determinant of the quantitative checkpoint output.

Moreover, we find that the checkpoint clamp 9-1-1 is a quantitative sensor for the amount of the ssDNA signal. Importantly, artificial hyper-activation of 9-1-1-dependent

signaling using a covalent protein fusion of 9-1-1 and its downstream target Rad9 leads to checkpoint hyper-activation, even under conditions where less Mec1 apical kinase is recruited. By uncoupling Mec1 recruitment from 9-1-1-dependent checkpoint activation we establish the 9-1-1 complex as a key sensor for the quantification of checkpoint input signals and their transmission to the effector kinase.

Publication 3 | A cell cycle-independent mode of the Rad9-Dpb11 interaction is induced by DNA damage.

Di Cicco, G., **Bantele, S.C.S.**, Reusswig, K-U. and Pfander, B.
Sci Rep 7(1):11650. doi:10.1038/s41598-017-11937-z (2017).

Rad9 is a central DNA damage checkpoint mediator with a dual functionality at DSBs: it activates global checkpoint signaling and blocks end resection throughout the cell cycle. So far, it is unclear whether and which of these functions require cell cycle regulation of Rad9, as both activities are present throughout the cell cycle.

Interestingly, one Rad9 DSB recruitment mechanism appears to be cell cycle regulated. This pathway involves the CDK-dependent phosphorylation of Rad9 on two CDK consensus sites S462 and T474, which once phosphorylated are bound by the Dpb11 N-terminal BRCT repeats.

We find that these Rad9 CDK sites cannot be phosphorylated solely by CDK, but also in a DNA damage-induced manner, even in G1 – when CDK is inactive. Most likely, this phosphorylation involves a chromatin-associated kinase, since chromatin recruitment of Rad9 is required for its phosphorylation. Following this phosphorylation, Rad9 is then able to interact with Dpb11 independently of the cell cycle phase.

The DNA damage-dependent interaction between Rad9 and Dpb11 in G1 is neither required for the DNA damage checkpoint, nor for inhibition of DNA end resection. Yet, this work clearly shows that the current model of two separate and independent checkpoint pathways needs to be revised, which opens the possibility for a new mechanism of regulation of the scaffold protein Rad9 that could likely also apply to other DNA damage response proteins.

Publication 4 | A cell cycle-regulated Slx4-Dpb11 complex promotes the resolution of DNA repair intermediates linked to stalled replication.

Gritenaite, D., Princz, L. N., Szakal, B., **Bantele, S. C. S.**, Wendeler, L., Schilbach, S., Habermann B.H., Matos J., Lisby M., Branzei D. and Pfander B.
Genes & Development, *28*(14), 1604–1619. doi:10.1101/gad.240515.114. (2014).

The resolution of joint molecules generated during template-switch at stalled replication forks involves the endonuclease complex Mus81-Mms4. We identified a two-step mechanism, by which the action of Mus81-Mms4 on JMs is coordinated and regulated within the cell cycle. First, we found that the two scaffold proteins Slx4 and Dpb11 interact after Slx4 is phosphorylated by CDK on S486, and this complex formation is required for the response to replication fork-stalling agents such as MMS. In a second step facilitated by the Polo kinase Cdc5 in late mitosis, this complex binds to Mus81-Mms4, requiring Cdc5-dependent Mms4 phosphorylation. Thus, two regulatory branches governed by CDK and Cdc5, respectively, converge in the control of the Mus81-Mms4 nuclease to allow efficient resolution of joint molecules in mitosis and unhampered progression of DNA replication and subsequent chromosome segregation.
Interestingly, in absence of the Dpb11-Slx4 complex, the DNA damage checkpoint is hyper-activated and it was previously suggested that the prime function of Slx4 is that of a checkpoint regulator, for example by interfering with Dpb11 binding to Rad9. Here, we demonstrate, however, that in the absence of the Dpb11-Slx4 complex DNA lesions/DNA repair intermediates accumulate. More precisely, we could demonstrate that specific structures containing RPA-ssDNA after MMS exposure are highly enriched in cells expressing a non-phosphorylatable mutant of *SLX4*, which cannot interact with Dpb11 anymore. Our work therefore offers an alternative mechanism in which Slx4 does not target the checkpoint directly, but rather indirectly by the removal of DNA repair intermediates.

Discussion

1 Cell cycle regulation of DNA end resection

A vast variety of studies have demonstrated the strict repression of DNA end resection in cell cycle stages with low CDK activity in order to prevent genomic instability induced by spurious recombination. However, we still lack sufficient mechanistic understanding of both short- and long-range resection and their cell cycle regulation to be able to overcome this regulation. Current models appreciate the influence of chromatin and chromatin-bound factors as regulators of resection efficiency, while they view activation of the resection enzymes as central targets of CDK regulation. To date it remains a central question in the field which aspects of regulation on the enzymes – such as activating phosphorylations by CDK – synergize with cell cycle- and damage-dependent changes in the substrate of the reaction, damaged chromatin, to generate efficient resection rates when needed but strictly prevent unwanted resection. Accordingly, an efficient bypass of the cell cycle regulation of DNA end resection has not been accomplished yet.

Besides in vitro studies, first evidence for the crucial role of chromatin as resection inhibitor in vivo stems from the observation that the chromatin remodeler Fun30 seems critical for efficient DNA end resection. The direct involvement of a chromatin remodeler in facilitating resection implies a potential function of the remodeled substrate, damaged chromatin, in the repression of resection. Likewise, these data suggest that chromatin changes catalyzed by Fun30 shift the chromatin into a resection-permissive conformation.

Here, I will discuss the cell cycle regulation of Fun30 and how our novel understanding of Fun30 regulation adds a decisive piece to the puzzle of overcoming the cell cycle regulation of DNA end resection.

1.1 Fun30 DSB recruitment mechanisms

Enzymes acting at DNA double-strand breaks are positively regulated from two angles: their recruitment to DSBs, and their activation. In the case of Fun30, these two steps are merged since the Fun30 enzymatic activity is stimulated by chromatin or DNA ((Awad et al., 2010), (Byeon et al., 2013)), and we do not know about additional factors influencing the activity of Fun30. Therefore, understanding the mechanism of DSB recruitment of Fun30 is key to understanding its regulation. Moreover, trying to gain knowledge about the role of a chromatin remodeler at DSBs imposes an additional challenge: we cannot use deletion mutants, as they exhibit highly pleiotropic phenotypes. Changes in damage-independent chromatin organization, transcription of certain genes, silencing and chromatin composition as caused by deletion of remodeler/s (subunits) might impact on the DSB-related phenotypes without necessarily being directly linked to the action of the remodeler at the DSB.

1.1.1 Fun30 targeting by the Dpb11-9-1-1 complex

With our work, we established two extremely powerful tools to address this problem. By elucidating the molecular mechanism of Fun30 recruitment via binding to 9-1-1-Dpb11 after CDK-dependent phosphorylation on Fun30 (Fig. 11a), we were able to generate a highly specific separation-of-function mutant of Fun30 (*fun30-SS20,28AA*), which exclusively abolishes the DSB-related Fun30 functions in enhancing DNA end resection and resection-coupled repair, without impacting on other chromatin changes such as silencing, which are compromised in *fun30Δ* mutants (S. Bantele et al., 2017). Using this separation-of-function mutant, we are now equipped to study the molecular function of Fun30 at DSBs.

Importantly, we were also able to generate a gain-of-function mutant exploiting the newly discovered recruitment pathway, by directly fusing Fun30 to the 9-1-1 complex subunit Ddc1, which naturally would bind to Dpb11 and thereby promote Fun30 recruitment. This artificial construct, the *DDC1-FUN30* fusion, strongly stabilizes Fun30 at DSBs and therefore enhances its local concentration (S. Bantele et al., 2017). As discussed below, using this fusion as a tool did not only prove extreme value for studying Fun30, but also elucidated the critical impact of Fun30 targets on DNA end resection.

So far, these genetic backgrounds are the only available separation-of-function mutants of chromatin remodelers at DSBs, providing a unique opportunity to study remodeling at DSBs. Alternatively, one could make use of the requirement of histone modifications or variants for remodeler recruitment, as for example γH2A mutation or *htz1Δ* (human H2A.Z) depletion. Such approaches have the fundamental disadvantage of strongly impacting on many aspects of chromatin regulation and therefore help us very little to understand DSB remodeling. A similar strategy to target the Ino80 remodeler has been published recently, however this system uses an "anchor away" strategy by LacO-lacI-mediated tethering and therefore requires ectopic introduction of the operator repeats in the genome, representing a less physiological environment as achieved in our system ((Neumann et al., 2012),(S. Bantele et al., 2017)).

1.1.2 Alternative Fun30 DSB recruitment mechanisms

Despite the fact that Dpb11-dependent Fun30 targeting clearly constitutes the basis for Fun30 cell cycle regulation, it seems not to be the only mechanism stabilizing Fun30 at DSBs (Fig. 11). We observed residual binding of Fun30 to DSBs in ChIP experiment using mutants that would specifically abrogate the 9-1-1-Dpb11-Fun30 complex formation, such as the *ddc1-T602A* and the *dpb11Δ SLD3-dpb11ΔN* mutant (S. Bantele et al., 2017). It is therefore plausible that other protein-protein interactions add to Fun30 stability at DSBs.

Previous studies showed an interaction between Fun30 and histone H2A, with a preference for un-phosphorylated H2A over γH2A (Eapen et al., 2012). This interaction could serve two needs: association with chromatin and molecular basis for Fun30-dependent nucleosome remodeling. For the association with nucleosomes, the proposed dimerization of Fun30 allowing the interaction with both H2A subunits of the nucleosome might play a role (Fig. 11b). So far, we do not understand the requirements for Fun30 dimerization (for example involvement of PTMs) and thus a dimerization-deficient mutant is not available to address this question.

However, there are several other potential recruitment pathways for Fun30 to DSBs. First, biochemical analysis has shown that Fun30 directly binds to the resection-related proteins Exo1, Dna2 and RPA (X. Chen et al., 2012)(Fig. 11c). Although the biological importance of these interactions is not clear, it is extremely exciting to imagine a self-enhancing loop within DNA end resection, by which Fun30 promotes resection and

consequently more Fun30 gets recruited. There is one observation arguing in favor of this model. In the *fun30-SSAA* mutant, in which Fun30 can't bind to Dpb11 anymore, we observe a stronger DNA binding defect at positions distal to the break, while recruitment to break-proximal locations seems hardly affected (S. Bantele et al., 2017), arguing for a mechanism involving the resected chromatin, on which RPA is located. It is still possible that nucleosomes are involved, as current research is suggesting the presence of nucleosomes in single-stranded DNA (Adkins et al., 2017).

Yet another hypothesis for how Fun30 gets recruited to chromatin in addition to Dpb11-dependent targeting stems from research on the mammalian homolog of Fun30, SMARCAD1. Both proteins harbor one or – in case of SMARCAD1 – two N-terminal CUE domains, which interact with ubiquitylated proteins (Fig. 11d). The SMARCAD1 CUE domains interact with BRCA1-ubiquitylated H2A, and this interaction promotes DSB binding of SMARCAD1 and is essential to enhancement of DNA end resection by SMARCAD1 (Densham et al., 2016). However, such a mechanism is unlikely to be evolutionary conserved, since mutation of the yeast Fun30 CUE domain does neither affect DNA binding, nor enhancement of DNA end resection. However, recruitment pathways could be synergistic and it remains to be tested whether the reduced DSB binding of *fun30-SSAA* is further enhanced by CUE domain mutation. The interaction partners of the Fun30 CUE domain remain to be elucidated, but it seems unlikely that CUE-mediated interactions play an important role at DSBs, as they neither affect DSB binding, nor Fun30 activity or contribute to conferring DNA damage resistance ((S. Bantele et al., 2017),(X. Chen et al., 2012)).

Possible Fun30 recruitment and stabilization mechanisms at DSBs are summarized in Figure 11.

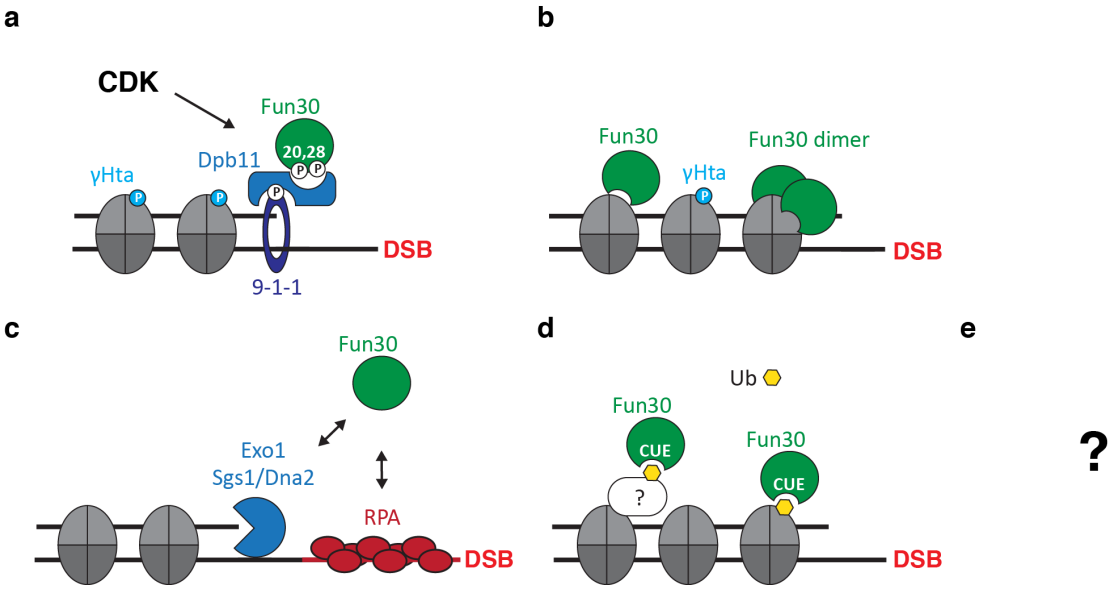

Fig.11 **Model of putative recruitment pathways to target and stabilize Fun30 at DNA double-strand breaks.** (**a**) Cell cycle-dependent Fun30 targeting via the 9-1-1-Dpb11-Fun30 complex. (**b**) Direct interaction between Fun30 and histones, either as a monomer or a dimer. (**c**) Protein-protein interactions of Fun30 with Exo1, Dna2 and RPA. (**d**) CUE-dependent recognition of modified histones or histone-bound proteins by Fun30. (**e**) So-far unknown mechanisms contributing to Fun30 targeting.

1.1.3 Conservation of the Fun30-Dpb11 interaction

While the CUE-dependent targeting seems newly evolved, the CDK-dependent regulation of Fun30 is highly conserved and also depends on CDK phosphorylation of SMARCAD1 to promote TopBP1 binding (S. Bantele et al., 2017). We did not only identify the responsible phosphorylation site on T71, but also generated a chimera merging the TopBP1-interaction surface of SMARCAD1 with the catalytic domain of Fun30. This chimera was fully able to rescue DNA damage sensitivity of *fun30Δ* cells in vivo, emphasizing the remarkably high degree of conservation of the Fun30-Dpb11 complex (S. Bantele et al., 2017). Whether the regulation of resection by CDK is similarly exploiting this interaction in human cells as it does in yeast will be focus of future research.

Both yeast Fun30 and human SMARCAD1 are targeted by DNA damage-dependent phosphorylation. While ATM-mediated SMARCAD1 phosphorylation contributes to its DNA binding ((Densham et al., 2016),(Chakraborty et al., 2018)), it remains unclear

which role Mec1/Tel1-dependent Fun30 phosphorylation plays, as it is largely dispensable for DSB recruitment (X. Chen et al., 2012).

Despite the fact that several molecular mechanisms might contribute to Fun30 recruitment and stabilization around DNA double-strand breaks, the 9-1-1-Dpb11-Fun30 complex is the only mechanism subjected to cell cycle regulation that we know of to date and therefore fulfills a unique, essential role in the targeting of Fun30 and the cell cycle regulation of DNA end resection.

1.2 Cell cycle regulation of resection by the Dpb11-Fun30 complex

Fun30 has been identified as a substrate of CDK phosphorylation ((Ubersax et al., 2003),(X. Chen et al., 2016)) and previous studies showed that CDK is required to recruit Fun30 to DSBs and promote DNA end resection ((X. Chen et al., 2016), (X. Chen et al., 2012)), however by a so-far unknown mechanism. In our work, we do not only provide the molecular mechanism of this CDK regulation, but also introduce a Fun30-hyperactivating mutant that is able to bypass this regulation and uncouple Fun30-dependent resection from the cell cycle (S. Bantele et al., 2017). More precisely, we force-recruit Fun30 to DSBs using a covalent fusion between the 9-1-1 checkpoint clamp subunit Ddc1 and Fun30, taking advantage of the Fun30 recruitment mechanism we identified in our work (S. Bantele et al., 2017). The fusion achieves two effects. First, it bypasses the CDK-dependent phosphorylation of Fun30 and thereby the CDK requirement for Fun30 DSB recruitment. Second, it bypasses yet another, DNA damage-dependent phosphorylation of Ddc1, and thereby greatly stabilizes and concentrates Fun30, leading to an increased activity at DSBs. Consequently, the *DDC1-FUN30* fusion hyperactivates Fun30 throughout the cell cycle.

Other approaches to uncouple resection from cell cycle regulation targeting the Sae2 nuclease with a CDK phosphorylation-mimicking mutant or the inhibitory Ku complex by *yku70Δ* deletion were less efficient ((S. Bantele et al., 2017),(Trovesi et al., 2011)). Notably, both Sae2 and Ku are involved in initiation of resection. Consistent with an exclusive function of Fun30 as a long-range resection enhancer, combination of the *yku70Δ* deletion or the *sae2-S267E* phospho-mimicking version with the Fun30 CDK-

bypass fusion additively enhances the overall resection efficiency ((S. Bantele et al., 2017); Bantele and Pfander, unpublished data).

1.2.1 Characterization of resection phenotypes by RPA ChIP

In order to assess resection phenotypes, we quantified the RPA-coated ssDNA. To this end, we performed RPA ChIPs to a stable, inducible DSB. Here, it is crucial to distinguish between the spreading of RPA into chromatin and the fold-enrichment of RPA. The spreading of RPA correlates with the reach of DNA end resection and this is substantiated by a concurrent loss of DNA at these sites due to resection. The interpretation of the fold enrichment of RPA is more difficult. ChIP qPCR signals derive from millions of DSBs being averaged, and as resection initiation is a stochastic event, we always look at a heterogenic signal. Therefore, the fold enrichment can either represent the amount of cells that have gone through resection at this location at the time being measured, or a lower level of resection at the respective location in all cells of the population. This distinction would require single cell assays such as microscopic analysis of RPA foci, which has been successfully used before ((Gritenaite et al., 2014), Bantele and Pfander, in revision).

1.2.2 Fun30 substrates as key barrier to end resection

In the hyperactive *DDC1-FUN30* fusion mutant we observe a strong enhancement of RPA spreading from a DSB throughout the cell cycle, which reaches G2M-like distances in G1 arrested cells and strongly pushes resection further compared to WT cells (S. Bantele et al., 2017). However, the fold enrichment of RPA in the G1-arrested mutant does not reach the levels measured in G2M WT cells.

We interpret this result as follows: Unambiguously, the enhanced RPA spreading throughout the cell cycle shows that Fun30 targets are limiting to end resection throughout the cell cycle, and this limitation can be overcome with our fusion mutant. Despite being hyper-active, this mutant does not act un-physiologically. On the one hand, the mutant only causes to G2M-like RPA spreading in G1 in the sub-population of cells, which have initiated resection, and this is reflected by the mild increase of the RPA fold enrichment. On the other hand, also non-homologous end-joining remains unchanged. Thirdly, all effects of the *DDC1-FUN30* fusion depend on the catalytic activity of Fun30 and are lost in an ATPase mutant (S. Bantele et al., 2017).

Taken together, these data do not only establish chromatin as a main regulator of resection efficiency, but also show that the cell cycle regulation of Fun30 by the 9-1-1-Dpb11 targeting complex are a pivotal aspect of cell cycle regulation of DNA end resection and might constitute the bottleneck to the onset of long-range resection.

Besides the biological implications of this work, overcoming resection barriers is of tremendous interest to biologists. Tools like the *DDC1-FUN30* fusion could prove invaluable to enhance the efficiency of gene targeting methodologies based on recombination, such as CRISPR-Cas9, particularly in post-mitotic cells. Indeed, first attempts to enhance gene targeting efficiency in human cells involve removal of the resection inhibitor 53BP1 (Orthwein et al., 2015), an ortholog of yeast Rad9, which is potentially the main target of Fun30/SMARCAD1 on damaged chromatin, as discussed below. It is highly tempting to test whether a *hRad9-SMARCAD1* fusion or an *H2A-SMARCAD1* fusion protein would allow resection and gene targeting in G1 in the presence of 53BP1, and hopefully future experiments will test this possibility.

1.3 Enzymatic function of Fun30 at DSBs

1.3.1 Putative histone dimer exchange by Fun30

It is established that the SWI/SNF ATPase activity of Fun30 is critically required for promoting DNA long-range resection (X. Chen et al., 2012). Together with the fact that Fun30 has the highest sequence similarity to the SWR1/Ino80 remodelers, which among others exchange H2A/H2B dimers and H2A.Z/H2B dimers, and that it seems to be active in histone dimer exchange in vitro itself (Awad et al., 2010), it seems plausible that histone dimer exchange by Fun30 could be involved in enhancing end resection (Fig. 12a). Whether this is directed against specific dimer compositions, for example in H2A.Z deposition or removal, or removal of γH2A - containing dimers, is not clear. Interestingly, Fun30 has a binding preference between non-phosphorylated and γH2A-phosphorylated H2A (Eapen et al., 2012), and we observe an increase of the γH2A ChIP enrichment in *fun30Δ* cells that is most likely not due to the resection defect since it does not display in break-proximal regions as expected for resection-deficient mutants, but all over the measured γH2A domain (Bantele and Pfander, unpublished data). We observe

the same increase in γH2A on chromatin when performing chromatin fractionation in *fun30Δ* mutant cells (Bantele and Pfander, unpublished data).

Interestingly, in vitro, Fun30 shows a higher affinity to nucleosomes on single- than on double-stranded DNA (Adkins et al., 2017). Thus, a potential model could suggest an ssDNA-H2A-dependent Fun30 binding mechanism that acts to enhance Fun30 recruitment during resection and might contribute to the removal of γH2A on resected DNA in addition to the (partial) histone loss. A direct testing of this hypothesis is however not trivial, as all DSB-related *FUN30* mutants cause resection defects, which in turn generate higher levels of γH2A.

When the phosphorylatable serine in H2A is mutated to prevent γH2A formation, resection efficiency is enhanced ((Eapen et al., 2012), (Clerici et al., 2013)). Previous studies have established Rad9 and its human ortholog 53BP1 as well as the fission yeast homolog Crb2 as resection inhibitors ((Chapman, Sossick, Boulton, & Jackson, 2012), (Ferrari et al., 2015), (Bonetti et al., 2015), (Symington, 2016), (Leland, Chen, Zhao, Wharton, & King, 2018)). γH2A provides a binding site for Rad9 homologs on damaged chromatin ((Hammet et al., 2007), (Javaheri et al., 2006)), and could therefore explain the enhanced resection in γH2A-deficient cells by removal of Rad9 from damaged chromatin.

1.3.2 Antagonistic action of Fun30 and Rad9

Intriguingly, genetic data suggest that Rad9 and Fun30 are counteracting each other ((S. Bantele et al., 2017),(X. Chen et al., 2012)), and cells lacking Fun30 recruit more Rad9 to DSBs and vice versa. These data raise the possibility that Fun30 acts by removing Rad9 from chromatin, either directly or indirectly by removing Rad9 binding sites as discussed in the previous subchapter (Fig. 12a,b).

It is particularly interesting that besides the chromatin-associated Rad9 recruitment pathway, also the Dpb11-dependent Rad9 recruitment might be corrupted by Fun30, as Rad9 and Fun30 bind to the same BRCT repeat 1+2 of Dpb11 ((S. Bantele et al., 2017),(Pfander & Diffley, 2011)). So far we do not have evidence for binding competition on Dpb11, as Rad9 overexpression does not weaken the Yeast Two-Hybrid interaction between Dpb11 and Fun30 (Bantele and Pfander, unpublished data). Still, binding competition on H2A cannot be excluded to date (Fig.12c).

Whether a potential γH2A removal by Fun30 is directed or just a byproduct of the enhanced enrichment of γH2A around DSBs is not clear. Similarly, a potential specificity towards H2A.Z-containing histone dimers has not been tested yet and could generate a similar decrease in γH2A levels. So far, we do not observe changes in the turnover of H2A.Z in damaged chromatin in mutants lacking Fun30 (Bantele and Pfander, unpublished data).

Importantly, the mechanism by which Fun30 promotes efficient DNA end resection at DSBs is fully elusive to date and a potential histone dimer exchange is only one possible mechanism.

In general, data do argue against a mechanism by which Fun30 would catalyze one particular step of the resection reaction, since resection defects in *fun30Δ* mutants can be compensated by overexpression of *EXO1* ((Eapen et al., 2012), (Costelloe et al., 2012), (X. Chen et al., 2012)). Thus we believe that Fun30 rather primes the chromatin for resection by transforming it into a more resection-permissive state, potentially by alleviating Rad9 inhibition.

If truly Rad9 is the key antagonist of Fun30, one could also envision a more direct eviction mechanism acting on Rad9. Figure 12 provides an overview over possible mechanisms by which Fun30 might enhance resection and oppose Rad9 inhibition.

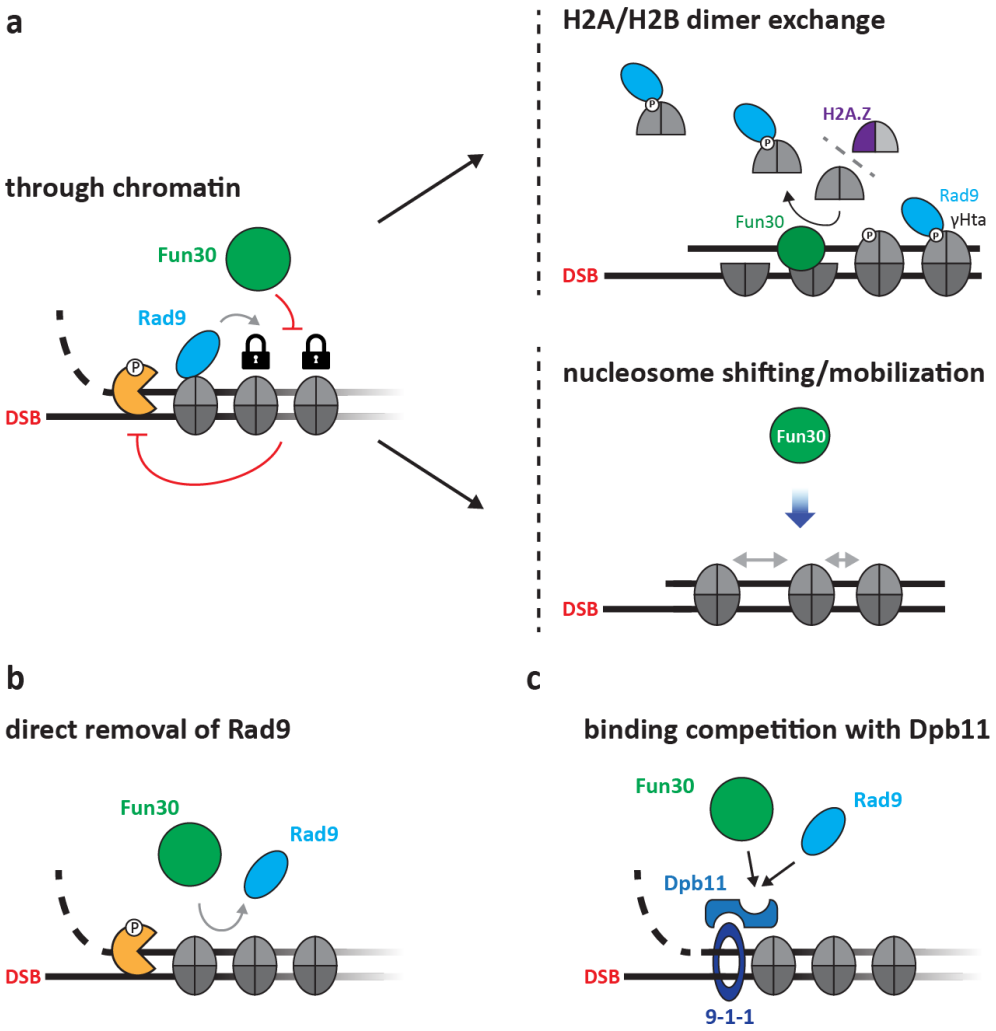

Fig.12 **Model of possible mechanisms of resection enhancement by Fun30, opposing the Rad9-dependent obstruction.** (**a**) Fun30 could counteract Rad9 indirectly through chromatin changes, for example H2A/H2B dimer exchange concomitant with changes in the nucleosome composition, particularly γH2A and H2A.Z, or by nucleosome mobilization potentially rendering it a worse binding platform for Rad9. (**b**) Alternatively, a direct removal of Rad9 by Fun30 involving the Fun30 ATPase and helicase activity could be envisioned. (**c**) Thirdly, a binding competition between Fun30 and Rad9, either on Dpb11 BRCT1+2 or on H2A could be possible.

1.3.3 Mechanism of Rad9 resection inhibition

We showed in our study that clearly the Fun30 target at DSBs, potentially Rad9, strongly contributes to resection inhibition throughout the cell cycle (S. Bantele et al., 2017). We favor a model in which this inhibition is present in all cell cycle phases. When CDK becomes active and mediates resection enzyme activation on the one hand, and Fun30 recruitment on the other hand, the inhibition is overcome. Two findings

support this model. First, Rad9 binding to histones is not subject of cell cycle regulation. Second, we clearly demonstrate in our new manuscript that γH2A is not cell cycle-regulated either (Bantele et al, in revision). Therefore, histone-bound Rad9 is a bona fide candidate for a constitutive resection inhibitor.

As mentioned before, Rad9 can also be recruited to DSBs via CDK-dependent interaction with Dpb11 (Pfander & Diffley, 2011). Three arguments point towards histone-bound rather than Dpb11-bound Rad9 as resection inhibitor. First, we have little evidence for a binding competition between Rad9 and Fun30 on Dpb11 (Bantele and Pfander, unpublished data). Second, mutation of the Rad9 CDK sites interacting with Dpb11 does not affect end resection (di Cicco, Bantele, Reusswig, & Pfander, 2017). Third, the deletion of Rad9 also enhances resection in G1 when CDK is inactive (Trovesi et al., 2011).

Another argument supporting this model stems from the observation that similar to γH2A mutation, the deletion of the Dot1 methyl-transferase, which generates the second binding site for Rad9 on chromatin (methyl-H3K79), increases the efficiency of end resection (Lazzaro et al., 2008). All together, genetics suggest that the H3/H2A-Rad9 complex acts as the resection-inhibiting unit.

It is particularly puzzling that we also do not understand the mechanism by which Rad9 inhibits resection, and whether this converges to the same target as Fun30 or works completely independent. Several scenarios are possible. Histone-bound Rad9 could alter the chromatin structure and thereby make it a worse substrate for the resection nucleases (Fig. 13d). Alternatively, Rad9 itself could physically block the passage of the nucleases and prevent their progression into chromatin (Fig. 13a). Thirdly, Rad9 could impede Fun30-dependent chromatin remodeling (Fig. 13c).

Similar to the *DDC1-FUN30* hyperactive fusion system, we generated a *DDC1-RAD9* fusion and to our great surprise, this fusion is a very strong resection inhibitor (Bantele et al, in revision). These data are particularly interesting since the *DDC1-RAD9* fusion is most likely not associated with chromatin but accumulates via the 9-1-1 complex. This raises the possibility for yet another potential mechanism by which Rad9 could inhibit resection. A well-established binding partner of Rad9 at DSBs is the checkpoint effector kinase Rad53, which indeed is hyper-activated in the *DDC1-RAD9* fusion mutant (Bantele et al, in revision). Previous experiments suggest that Rad53 might trigger a

negative feedback inhibition on resection by phosphorylating Exo1 in order to dampen its activity (Morin et al., 2008). However, we do not observe hyper-resection in cells lacking Rad53 (Bantele and Pfander, unpublished data). As Rad9 itself is a protein scaffold, it could recruit a so far unknown protein to DSBs, which negatively affects resection (Fig. 13b).

Figure 13 summarizes potential modes of Rad9 resection inhibition.

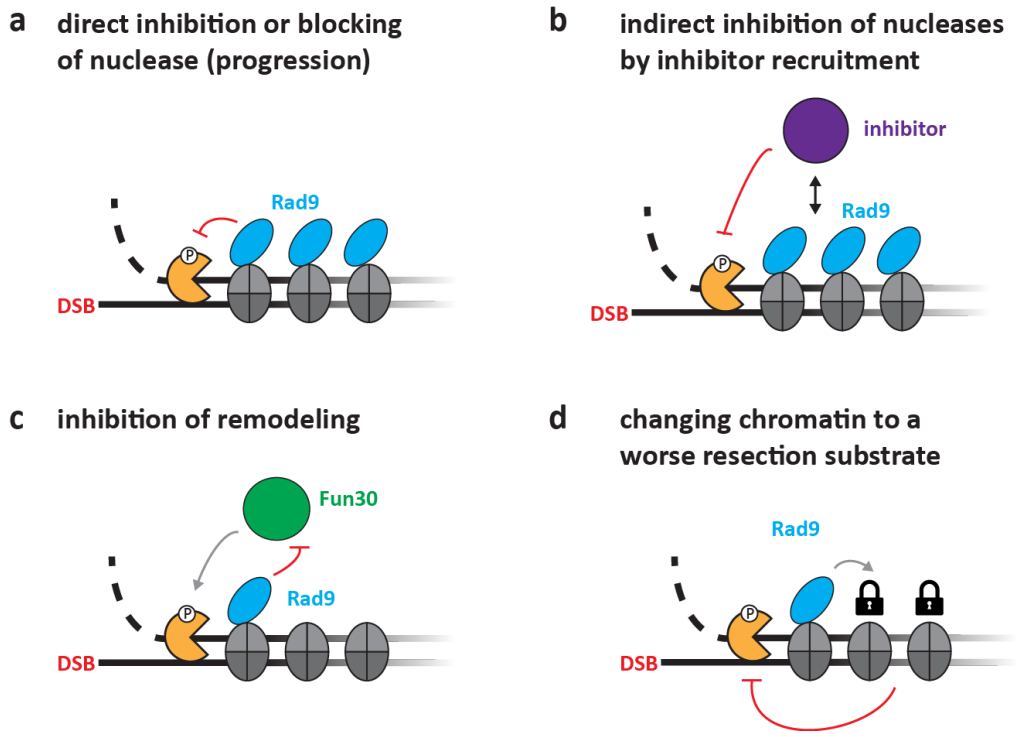

Fig.13 **Model of possible mechanisms of resection inhibition by Rad9** (**a**) Rad9 could either inhibit the nucleases or physically block the progression of the nucleases, acting s a roadblock. (**b**) Rad9 could act as a protein scaffold and recruit resection inhibiting activities, as for example Rad53. (**c**) Rad9 might inhibit Fun30-dependent remodeling, either by preventing chromatin access, or by directly inhibiting Fun30 activity. (**d**) Finally, Rad9-bound chromatin might change in its physical properties in a way that it becomes a worse substrate for DNA end resection, for example by compaction.

1.3.4 Conservation of chromatin-related resection regulation

Interestingly, the antagonistic action of Fun30 and Rad9 appears to be conserved to the mammalian homologs SMARCAD1 and 53BP1 ((Densham et al., 2016), (Costelloe et al., 2012)). SMARCAD1 depletion leads to 53BP1 stabilization at DSBs generated by laser cuts, and this depends on the CUE domains and ATPase activity of SMARCAD1, suggesting an active role of SMARCAD1 in repositioning 53BP1 (Densham et al.,

2016). Whether such an eviction is direct or an indirect effect of SMARCAD1-dependent nucleosome remodeling is not clear. Similar to yeast, 53BP1 depletion renders SMARCAD1/Fun30 function dispensable (Densham et al., 2016). In addition to the discussed roles during repressing long-range resection, Rad9 as well as 53BP1 have been recently implicated with suppressing the initiation of resection.

In human cells, we have a better understanding of the mechanistic details of 53BP1-dependent resection inhibition. As both 53BP1 and the resection-enhancing counterpart BRCA1 are recruited in a ubiquitylation-dependent manner, 53BP1 accumulates one of its effectors, RIF1, which impedes chromatin binding of BRCA1 and consequently blocks SMARCAD1 accumulation and the onset of resection ((Escribano-Díaz et al., 2013), (Densham et al., 2016)). Once CtIP becomes activated by CDK, it replaces RIF1 from chromatin, facilitating cell cycle-regulated end resection.

Intriguingly, the inhibition of resection in mammalian cells seems to be enforced in G1 by yet another, 53BP1-independent mechanism. Human cells employ a negative feedback regulation in which the helicase HELB is recruited to RPA-ssDNA and inhibits both Exo1- and Dna2-dependent resection. When CDK becomes active at the onset of S phase, HELB is displaced from ssDNA and permits processive resection (Tkáč et al., 2016).

1.3.5 Resection pathway-specificity of Fun30

Yet another interesting aspect of Fun30 function is whether it generally enhances all resection pathways or is specifically coupled to one of the two pathways. This idea is primed by the fact that the Dna2 nuclease is genetically linked to the Sgs1 helicase activity during end resection, while the redundant resection pathway carried out by the Exo1 nuclease seems to act without strict requirement for a helicase activity at DSBs. These differential requirements also reflect in in vitro experiments, where purified Exo1 alone can carry out DSB resection, while Dna2 requires among others the STR complex (Adkins et al., 2013).

In contrast to yeast Exo1, human Exo1 seems to readily cooperate with helicases. Previous studies showed that in vitro, the human RecQ helicases BLM and WRN stimulate hExo1 activity by direct interaction, which supposedly facilitates targeting of the exonuclease to its substrates ((Nimonkar et al., 2008), (Aggarwal, Sommers, Morris, & Brosh, 2010)). Moreover, in the absence of RNaseH2, hExo1 synergizes with the

helicase Srs2 in the removal of Top1-dependent nicks at sites of aberrant insertion of ribonucleoside monophosphates into the DNA (Potenski, Niu, Sung, & Klein, 2014).
Fun30 possesses a conserved, helicase-like domain (Flaus, 2006), but it is not clear to date whether Fun30 does at all act as a helicase in vivo. Current genetic data argue against a pathway-specific action of Fun30 since DNA damage sensitivity and resection efficiency are both additively affected when the *fun30Δ* deletion is combined with mutants of either of the two resection pathways, *exo1Δ* or *sgs1Δ* ((Eapen et al., 2012), (Costelloe et al., 2012), Bantele and Pfander, unpublished data).

1.4 Repair pathway regulation by Fun30 and Rad9

The initiation of resection constitutes the decision point between NHEJ and HR. Therefore, mutants affecting the initiation of resection are able to shift this balance and result in altered repair pathway usage, potentially with genotoxic consequences. As discussed, Fun30 clearly is not involved in this early step of resection and in agreement with that, neither mutants with decreased, nor with increased Fun30 activity do affect rates of NHEJ ((Eapen et al., 2012),(S. Bantele et al., 2017)).
Importantly, also the different recombination-based repair pathways have different requirements for resection efficiency. Gene conversion (GC) only requires short stretches of ssDNA ((C.-S. Lee et al., 2016)), although it is possible that longer overhangs might promote recombination. In contrast, single-strand annealing (SSA) requires the efficient resection of longer DNA tracts, depending on the positioning of the annealing site. In fact, while Fun30 seems dispensable for SSA with a 5 kb spacer between the DSB and the annealing site, it is vital for completion of SSA with a 25 kb spacer, indicating that resection efficiency is not sufficient to pass through 25 kb of chromatin in absence of Fun30 ((Eapen et al., 2012), (S. Bantele et al., 2017)).
SSA and also MMEJ, which both rely on removal of DNA tracts separating a homologous region to the break site from the actual DSB, go along with DNA loss and are as such the highly mutagenic alternatives to gene conversion once a DSB has initiated resection. In contrast, NHEJ is a much safer repair alternative as it has reasonable accuracy with only a low rate of small deletions or mutations (0.06% at a clean DSB (S. Bantele et al., 2017)). Consequently, controlling the switch between homology-directed

repair pathways may be as crucial for genome integrity as the switch between NHEJ and HR.

Notably, deregulation of Fun30 has only minor effects on the overall prevalence of NHEJ events at clean DSBs, however it increases the rate of mutagenic NHEJ about 50-fold ((S. Bantele et al., 2017)). The mechanism of these mutagenic events is not clear and the role of Fun30 during the execution of NHEJ is not yet understood.

Interestingly, a recent study discovered a similar role of the Rad9 ortholog 53BP1 in balancing the usage of GC and SSA in human cells (Ochs et al., 2016). The authors observe that the hyper-resection, occurring when levels of 53BP1 are artificially low, triggers a shift from gene conversion to SSA. Since also in human cells, $53BP1^{Rad9}$ is opposed by $SMARCAD1^{Fun30}$, it would be highly tempting to test whether deregulation of SMARCAD1 affects the balance between GC and SSA likewise. Such a finding would further emphasize the tremendous importance of properly balancing repair pathway choice.

Together, these data suggest that a two-step surveillance mechanism at DSBs controlling (a) the usage of NHEJ versus HR at the step of resection initiation and (b) the usage of GC versus SSA at the step of long-range resection efficiency is at place in order to ensure the usage of the respective high-fidelity repair pathway.

1.5 Roles of Fun30/SMARCAD1 beyond DSBs

1.5.1 Fun30 in the response to camptothecin

One facet of *FUN30* phenotypes is exceptionally fascinating and fully elusive until now. Cells with compromised Fun30 function or lacking interaction between Fun30 and Dpb11 are exclusively sensitive to the topoisomerase 1 inhibitor Camptothecin (CPT), but not to any other DNA damaging drugs ((S. Bantele et al., 2017)). CPT stalls the covalently linked Top1-DNA intermediate that occurs naturally transiently during the catalytic cycle of Top1 and by this generates DNA-protein crosslinks (DPCs). Such crosslinks present an obstacle to other DNA metabolic machineries and can cause single- and secondary double-strand breaks upon collision with transcription and replication machineries as well as stalled replication forks.

The Top1-DNA adducts are either directly hydrolysed by tyrosyl-DNA phosphodiesterase (Tdp1), cleaved at the DNA part by the MRX complex or removed in a protease-dependent manner by the Wss1/SPARTAN protease ((Stingele, Schwarz, Bloemeke, Wolf, & Jentsch, 2014), (Stingele et al., 2016), (Lopez-Mosqueda et al., 2016)).

Given the DSB resection function, genetic interactions between Fun30 and the MRX complex are inherently difficult to analyse. However, *fun30Δ* cells display additive genetic interactions upon cronic exposure to CPT with the respective protease, Wss1, as well as Tdp1, suggesting functions in parallel pathways (Bantele and Pfander, unpublished data). Additionally, *fun30Δ* cells are not sensitive to other forms of DNA-protein crosslinks such as induced by formaldehyde treatment (Bantele and Pfander, unpublished data). It seems therefore unlikely that Fun30 generally enhances repair of DPCs by the canonical repair pathways, but rather is specifically linked to topoisomerase1-dependent DNA damage, potentially in the context of stalled replication forks. This idea is substantialized by the observation that CPT-induced checkpoint activation is prolonged in cells lacking *FUN30* and this is restricted to Rad53 activation during S-phase (Bantele and Pfander, unpublished data).

Interestingly, dealing with replication fork stalling by other drugs like MMS or HU does not require Fun30 ((S. Bantele et al., 2017)). Taken together, it will be highly interesting to study the role of Fun30 at Top1-stalled replication forks and Top1-dependent DPCs.

1.5.2 Involvement of Fun30 in DNA mismatch repair

Besides Top1-DPC removal and DSB end resection, Fun30 might very well impact on other DNA repair-related processes. Genetic screening has revealed interactions with a vast variety of chromatin modifying complexes such as the histone acetyl transferase Rtt109, components of the NuA4, SAS, NatA and SAGA histone acetyl transferases, base and nucleotide excision repair proteins, replication fork components and chromatin remodeling factors such as Rad54, the RSC, ISWI and Ino80 chromatin remodeling complexes ((Costanzo et al., 2010), (Krogan et al., 2003), (Krogan et al., 2006), (Collins et al., 2007), (Beltrao et al., 2009)). A recent study describes a genetic link between Fun30 and enzymes connected to mismatch repair (MMR), Msh2,3 and 6 (Terui et al., 2018). Intriguingly, the human Fun30 homolog SMARCAD1 has recently been linked to MMR. Both yeast Fun30 and SMARCAD1 seem to be involved in the disposition of

nucleosomes around mismatched basepairs, opposing the activity of Caf1 (Terui et al., 2018). The proposed mechanism depends on the MMR factor Msh2 and is important for the following repair of the lesion (Terui et al., 2018). Furthermore, Msh2 was shown to be involved specifically in HR-dependent DSB repair ((Franchitto et al., 2003), (Pichierri, Franchitto, Piergentili, Colussi, & Palitti, 2001)) and is required for CPT recovery in human cells (Burdova, Mihaljevic, Sturzenegger, Chappidi, & Janscak, 2015), offering an alternative explanation for the genetic interaction with Fun30.
Altogether, future studies should be directed towards a universal understanding of Fun30 functions and dissect whether the chromatin changes catalysed by Fun30/SMARCAD1 are identical at lesions of all different natures or whether specific mechanisms of regulation funnel Fun30 activity dependent on the origin of the lesion.

1.6 Establishing a genetic toolbox to study regulation of DNA end resection, chromatin dynamics during end resection, and mechanism of the Rad9-Fun30 axis

On a final note regarding our studies of Fun30 and its role in resection enhancement, it should be emphasized that the artificial protein fusions we generated during this study may constitute invaluable tools for future studies on DNA resection ((S. Bantele et al., 2017); Bantele et al, in revision,(di Cicco et al., 2017)). Figure 14 shows the ability of these covalent protein fusions to manipulate DNA end resection.

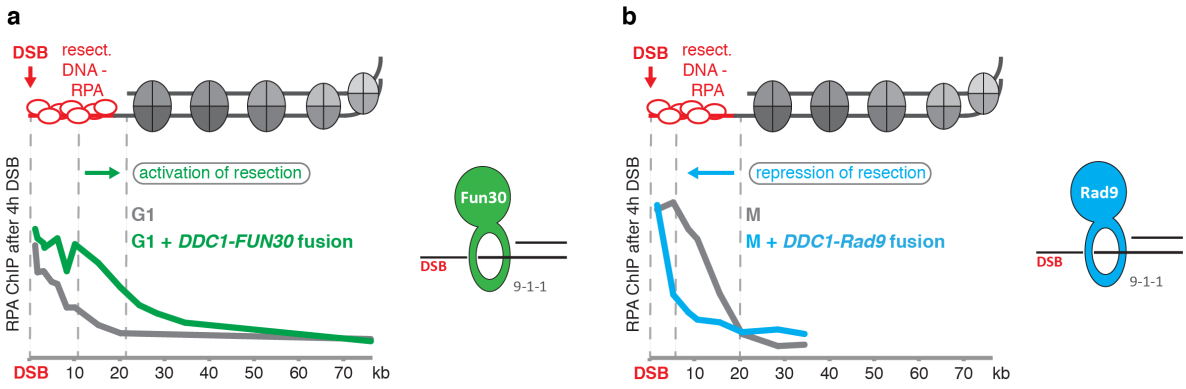

Fig.14. **The toolbox of Ddc1 fusion proteins.** (**a**) Force-localization of Fun30 by the *DDC1-FUN30* fusion induces hyper-resection throughout the cell cycle (not shown here), and uncouples resection from its cell cycle regulation by promoting a G2M-like resection range in G1-arrested cells.

(**b**) Force-localization of Rad9 by the *DDC1-RAD9* fusion effectively represses resection in G2M arrested cells.

We are only beginning to understand, whether chromatin changes are accompanying or preceding end resection, and to distinguish between changes required for or induced by end resection is inherently difficult.

Ddc1 fusion proteins offer the genetic means to on the hand make chromatin susceptible or repressive towards end resection and on the other hand to analyze resection uncoupled from its cell cycle regulation ((S. Bantele et al., 2017); Bantele et al, in revision). This offers the potential to find novel factors involved in resection regulation and to gain a comprehensive understanding of resection-associated changes in chromatin. To take it one step further, other enzymatic activities might be targeted to DSB using the Ddc1 fusion strategy in order to investigate their impact on DSB-related processes, resection being only one of them. In conclusion, we believe that the Ddc1 fusions will have future impact on our research field that goes beyond the biological findings we present in our studies here.

2 DNA damage checkpoint signaling mechanisms

2.1 Regulation of Mec1 and its substrates

We showed that independent of the extent of DNA end resection and CDK activity, a subset of Mec1 targets, represented by γH2A, is phosphorylated to similar levels, even under extreme conditions such as the absence of long-range resection (*exo1Δ sgs1Δ* cells) or upon hyper-resection (*DDC1-FUN30* cells) (Fig. 15) (Bantele et al, in revision). As Mec1 kinase recruitment requires resection, a major question arising from our data is how such dramatically different amounts of Mec1 kinase at a DSB can lead to the same amount of phosphorylation of substrate molecules, and how Mec1 targets differ?

2.1.1 Dynamics of γH2A phosphorylation during resection

γH2A (H2A phospho-S129) is one of the earliest Mec1 kinase targets and decorates a broad region around a DSB, ranging from around 20 kb in yeast to several hundreds of kb in human cells ((Shroff et al., 2004),(S. Bantele et al., 2017), (Rogakou et al., 1998)).

This region can be subdivided in two: the resected region comprising RPA-ssDNA, and the adjacent intact chromatin (Fig. 15). These two regions behave profoundly different regarding the dynamics of γH2A phosphorylation. In this section, the inverse relationship between resection and γH2A signal intensity will be discussed below as well as potential mechanisms underlying resection-independent spreading of γH2A into the adjacent chromatin. Together, both phenomena show that γH2A phosphorylation is primarily regulated from the side of the substrate, but not from the side of the kinase.

In the resected area, we observe a pronounced correlation of resection with γH2A signal loss (Fig. 15; Bantele et al, in revision). Accordingly, γH2A is greatly enriched at break-proximal regions in absence of resection. γH2A phosphorylation depends on the availability of H2A for the kinase reaction. According to the prevalent model, histones are at least partially evicted during DNA end resection, creating a respective lack of H2A substrate in the resected region. It is therefore likely that histone loss in resected regions reflects in a decreased γH2A signal.

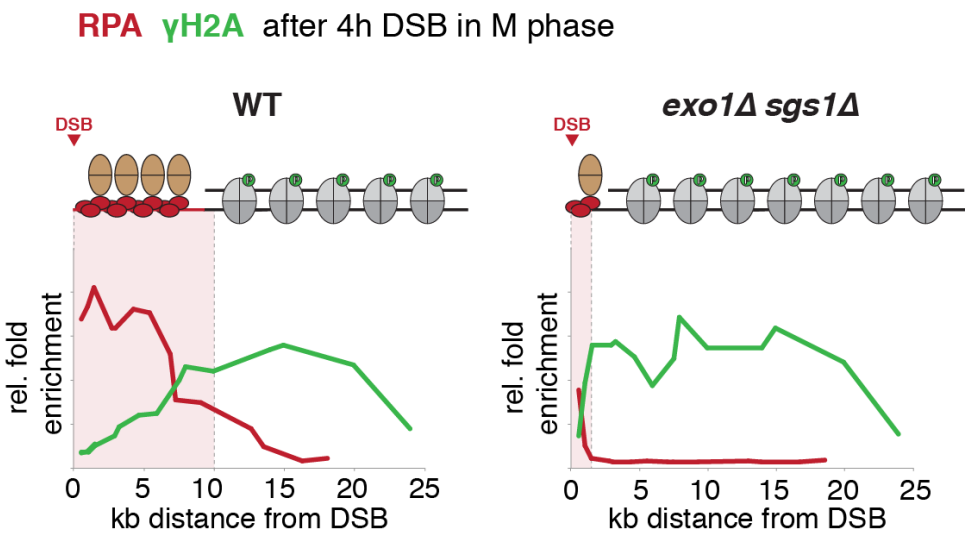

Fig.15. **Anti-correlation between RPA and γH2A ChIP signals at a DSB.** RPA ChIP signals (red) demark the border of resection, which is around 10 kb from the DSB in WT mitotic cells after 4 hours of break induction (left panel) and at under 1 kb in *exo1Δsgs1Δ* mitotic cells (right panel). Correspondingly, the γH2A ChIP signals (green) remain unchanged at regions beyond the resection border, while they show a decrease at RPA-enriched ssDNA. In regions outside of RPA enrichment, which are supposedly double-stranded and have not undergone resection yet, the signals are highly similar between both conditions.

It is currently under debate to which degree histones are being lost around a DSB. Notably, we observe almost complete loss of the γH2A signal directly at the DSB (Fig. 15; Bantele et al, in revision). Should this be representative of histone loss, these data would point towards major histone loss in these regions. In vitro data suggest the existence of nucleosomes in single-stranded DNA (Adkins et al., 2017), but whether they are being bypassed by the resecting nucleases or deposited after resection is not clear. One could speculate that such an ssDNA-nucleosome complex could participate in signaling actively or indirectly by alteration of the physical properties of the ssDNA. Indeed, single-stranded DNA tracts, which are assembled with nucleosomes in vitro, seem to adapt structural features similar to normal double-stranded nucleosomes but display a more dynamic behavior (Adkins et al., 2017).

In vivo experiments suggest a rather moderate loss of histones around DSBs, compared to the complete removal at transcriptional start sites ((Bennett et al., 2013), (van Attikum et al., 2007), (C.-C. Chen et al., 2008), (Boeger et al., 2003). A recent study proposes that histones are actively deposited on resected DNA and subsequently facilitate Rad51 loading and completion of recombination (Huang et al., 2018). However, due to the ubiquitous presence of histones on the DNA, histone ChIPs are inherently difficult to analyse and normalize, calling for a more sophisticated methodology to finally determine occupancy and dynamics of nucleosomes on resected DNA.

2.1.2 The bottleneck to γH2A phosphorylation

Outside the region of resection we measure highly similar γH2A signals independently of the amount of ssDNA (Fig. 15; Bantele et al, in revision). In contrast, proteins involved in the Rad53 activation cascade do strongly depend on DNA end resection for their recruitment to DSBs and their subsequent Mec1 activation (Bantele et al, in revision). Thus, Mec1 activity seems to target those factors by a different mechanism than γH2A. This apparent contradiction suggests the presence of distinct, parallel Mec1 signaling mechanisms operating at DSBs.

A central question arising from these data is how – if not by channeling of Mec1 activity – γH2A phosphorylation is limited. In our work we ruled out redundancy between the apical kinases Mec1 and Tel1 as well as saturation of H2A molecules to account for this enigmatic relationship (Bantele et al, in revision). As neither substrate nor enzyme seem to limit the γH2A phosphorylation reaction, additional factors must play in. The

phosphorylation reaction requires the physical encounter of the Mec1 kinase with its substrate, and these encounters are limiting to the rate of the γH2A phosphorylation. Here, three potential factors influencing contact frequencies between Mec1 and H2A are discussed.

First, DSBs are not locally fixed structures but have a certain propensity to move in the nucleus. Compared to undamaged DNA loci, DSBs can probe a larger volume in the nucleus ((Dion et al., 2012), (Miné-Hattab & Rothstein, 2012)). Mechanistically, this boils down to DNA damage checkpoint-dependent histone loss enhancing DSB mobility (Hauer et al., 2017). The precise mechanism of this DSB mobility enhancement remains to be clarified. In principle, DSB end-tethered Mec1 kinase could reach H2A substrates in a wider radius when the DSB is more mobile, and consequently mutants interfering with the DSB mobilization could restrict the γH2A domain. However, using checkpoint-dead cells such as the *rad9Δ* or *rad53Δ* mutant, we could not observe changes in γH2A levels or spreading and therefore exclude enhancement of DSB mobility as a major factor influencing γH2A levels (Bantele et al, in revision).

Second, chromatin is organized in distinct 3D volumes, forming so-called topologically associated domains (TADs) ((Caron et al., 2012), (Caron et al., 2015), (Aymard et al., 2017)). In human cells it was shown earlier that γH2A spreads within the confinement of TADs (Caron et al., 2012). Until now, we do not have access to genome contact data after a DSB in yeast, and studies correlating 3D contacts of DNA loci with DSB-related events such as repair efficiency used 3D contact maps of undamaged yeast cells as a reference ((R. W. Wang, Lee, & Haber, 2017), (Duan et al., 2010)). While such an approach might give first insights into correlations between local events such as γH2A modification with the chromosome conformation, a genome-wide mapping of γH2A and 3D contacts from the same conditions will finally be required to draw conclusions. In principle, Mec1 has the propensity to act in trans ((Renkawitz et al., 2013b), (C.-S. Lee et al., 2013)), which is a basic requirement for the proposed mechanism to work, and we therefore think a TAD-guided definition of the γH2A domain is not unlikely.

Third, localization and amount of activated Mec1 molecules will obviously be decisive to shape the γH2A signal. Mec1 requires recruitment to ssDNA meditated via a direct interaction between RPA and the Mec1 cofactor Ddc2 in order to get activated. However, we have no understanding of whether all Mec1 molecules recruited to DSBs

are being activated, and whether active Mec1 stays bound to the ssDNA or can be released afterwards to reach substrates by diffusion. Such a diffusion mechanism would generate a "cloud" of Mec1 activity, which would not necessarily be different in size and activity between cells that resect to different extents.

One aspect of our γH2A ChIP data argues in favor of such a mechanism. We usually measure timecourse experiments, in which we monitor protein recruitment or γH2A phosphorylation around a DSB within four hours. We typically observe two effects: first, the enrichment of the protein gets higher. Second, the protein moves into chromatin away from the DSB in a vectorial manner, and this coincides with resection. This movement is perfectly explained by checkpoint protein localization to the borders of resection or resected DNA. Notably, we observe a completely different behavior for γH2A, which also increases over time, but evenly rises over the entire γH2A domain, without showing any vectorial movement along the chromosome arm. This observation can give us several hints towards Mec1 substrate regulation. The "cloud" model of Mec1 activity would readily explain the phenomenon of the homogenously distributed γH2A enrichment, as most likely Mec1 diffusion is faster than the γH2A phosphorylation reaction, and could therefore reach H2A molecules all over the diffusion radius with a relatively similar timing. As we cannot distinguish between the spreading of Mec1 activity by Mec1 diffusion or by TAD formation experimentally, both mechanisms could contribute to in cis and trans spreading of γH2A.

Overall, Mec1 substrate phosphorylation is therefore not dependent on Mec1 regulation but rather Mec1 phosphorylation could be viewed as being primarily channeled from the side of its substrates, as very few Mec1 molecules seem sufficient to phosphorylate its substrates at the DSB (Bantele et al, in revision). In agreement with this model, checkpoint proteins of the Rad53 activation cascade, such as 9-1-1, Dpb11 and Rad9, which do depend on resection, require a primary recruitment step in order to be available for Mec1 phosphorylation. This recruitment step constitutes the basis for the regulation by resection, and not necessarily Mec1 kinase activity. In contrast, H2A is inherently present around the DSB and as such a more direct readout for Mec1 activity.

If this model was true, overall Mec1 activity would be similar whenever a DSB is present, independent of the amounts of resection, and the pool of DSB recruited Mec1 does not

inherently correlate with the pool of active Mec1. Consequently, one could make every Mec1 substrate a resection-independent substrate by bypassing the resection-dependent recruitment step, for example by addition of a γH2A binding domain.

On the contrary, one could artificially generate a γH2A-like phosphorylation event that is resection-dependent by fusing the H2A histone tail to one of the checkpoint proteins that requires resection for its DSB association. Future studies using these tools therefore have the potential to provide deeper understanding of the ultimate point of regulation of the Mec1 kinase reactions at DSBs.

2.1.3 Local and global Mec1 signaling circuits

The differential regulation of Mec1 substrates demonstrates that Mec1 feeds into at least two distinct signaling circuits, one that follows quantitative inputs in the form of the amount of ssDNA generated by DNA end resection and activates the effector kinase to a proportional degree, and another that does not integrate quantitative information but is activated at every lesion site likewise. We think that the purposes of these two circuits are global, quantitative checkpoint activation, and local regulation of damage repair (Fig. 16; Bantele et al, in revision).

γH2A representing the local circuit was indeed demonstrated to act locally, as it is regulated individually at each lesion site where it coordinates DNA repair ((Tsabar et al., 2015), (J.-A. Kim et al., 2007)), and independently of other lesion sites is required for efficient DNA repair ((Unal et al., 2004), (Downs, Lowndes, & Jackson, 2000)). Currently, there is no evidence for communication of γH2A signals from different sites. We therefore term the resection-independent γH2A signaling mechanism the "local" checkpoint circuit (Fig. 16a).

In contrast, Rad53 activation very well responds to the amount of resection ((Mantiero et al., 2007), (Zierhut & Diffley, 2008)), and this sensitive response is essential to balance out cell proliferation and genome maintenance. As activated Rad53 targets a large variety of checkpoint effectors and this is not locally connected to the DSB after its activation, we term this checkpoint signaling pathway the "global" circuit (Fig. 16b).

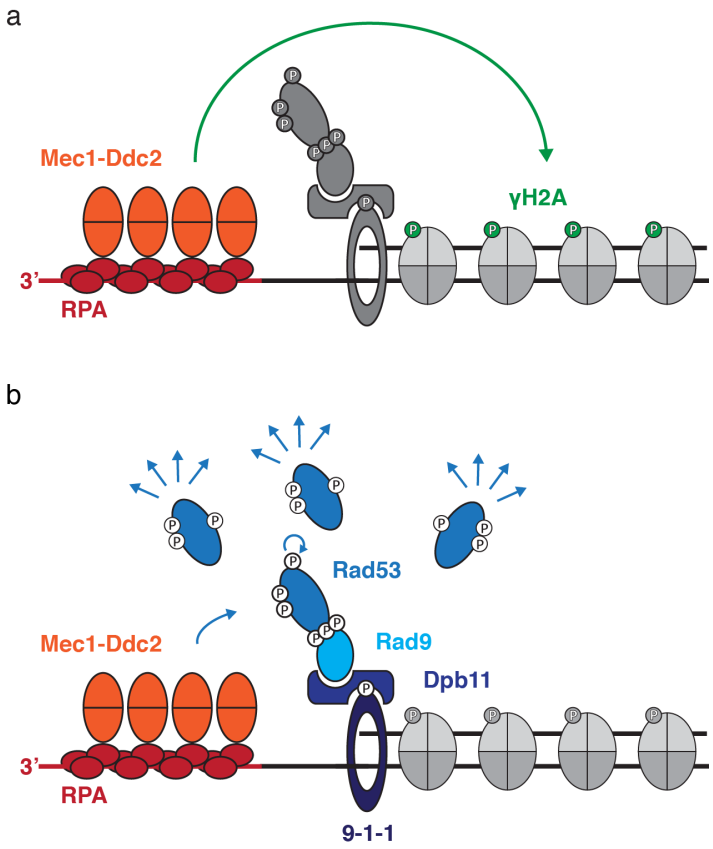

Fig.16. **Model of local and global DNA damage checkpoint signaling circuits.** Mec1-Ddc2 triggers (**a**) local checkpoint signaling to ensure efficient repair of the lesion, as for example γH2A phosphorylation. Local signaling is not responsive to the extent of resection and does not participate in Rad53 activation. In parallel, Mec1-Ddc2 sets off the global checkpoint response (**b**), which cumulates in Rad53 activation and acts proportional to the extent of resection.

Previous studies have raised the possibility that checkpoint signaling is cell cycle-regulated not only due to resection, but also because of other mechanisms. Indeed in S-phase, where inherently high levels of RPA-ssDNA are present, full Rad53 activation requires a higher damage load compared to in mitosis, providing a tailored checkpoint response that prevents unwanted checkpoint activation by single-stranded replication intermediates ((Shimada, Pasero, & Gasser, 2002), (Tercero, Longhese, & Diffley, 2003)). If this was true, the tolerance towards the presence of ssDNA as checkpoint activator would be adjusted to the basal level of ssDNA in the respective cell cycle stage.

Taken together, the mechanistic separation of events that mediate repair and events that mediate global signaling at DSBs establishes a buffering system in which the cell initiates the full repair force from the moment a lesion is introduced, while the cost-intense global

response acts as emergency signal when fast repair fails. As these two branches of signaling are mechanistically separated but elicited by the same kinase, it is inversely ensured that no matter what, both signaling circuits are in principle ready to react.
From these ideas several highly interesting questions arise. How are signaling thresholds defined in the cell? Is the global checkpoint response coordinated genome-wide, and how do locally separated lesions communicate with each other? And finally, it remains unresolved by which molecular mechanism the damage load of a cell is being quantitatively read. This last point will be discussed in the following.

2.2 Signal integration by checkpoint sensor proteins

2.2.1 Contribution of checkpoint input signals

DNA damage checkpoint activation follows a threshold-based mechanism and therefore requires quantitative sensing of input signals, i.e. damage-specific DNA structures. A very important checkpoint signal is RPA-ssDNA, which in case of DSBs is generated processively by end resection as long as the lesion remains unrepaired. A second damage signal is the ssDNA-dsDNA junction at the border of resection. In a simplified view, one such structure exists per DSB end and therefore is not suited to measure lesion persistence. However, it is tempting to speculate that discontinuous resection could include new entrypoints for example by the endonuclease activity of the MRX-Sae2 complex and as such also ss-dsDNA junctions could accumulate over time and provide a signal that correlates with the amount of end resection.
Thus, RPA-ssDNA and potentially ss-dsDNA junctions provide necessary features to be quantitative checkpoint input signals that rise in number at long-persisting DSBs, providing the mechanistic foundation for a selective, quantitatively adjusted checkpoint response.

2.2.2 The checkpoint sensors Ddc2 and Ddc1

The checkpoint is equipped with two sensor proteins that are characterized by direct binding to the damage-specific structures. The first sensor is the Mec1 cofactor Ddc2, which directly binds RPA-ssDNA. The second sensor is the 9-1-1 checkpoint clamp consisting of Ddc1, Rad17 and Mec3, that specifically associates with ss-dsDNA

junctions. Both checkpoint sensor complexes accumulate at DSBs via distinct mechanisms and independent of each other ((Melo et al., 2001), (Kondo et al., 2001)). Ddc2-Mec1 directly binds to RPA and is therefore a good candidate for a quantitative checkpoint sensor, reflecting the amount of RPA-ssDNA. Our data demonstrate for the first time that the 9-1-1 is a quantitative checkpoint sensor as well. In this section, the potential roles of both sensor pathways in quantifying checkpoint inputs are discussed.

We define checkpoint activity by the amount of effector kinase activation, which is mediated through a Mec1-activated kinase cascade assembly on 9-1-1. As detailed in the previous chapter, we have evidence that at least in the case of γH2A very little Mec1 is sufficient for full phosphorylation (Bantele et al, in revision). In strong contrast, the recruitment of the checkpoint complex comprising Dpb11, Rad9, and the effector kinase Rad53 on the 9-1-1 complex is strictly dependent on resection and quantitatively increases with ongoing resection (Bantele et al, in revision). Although it might seem trivial, a central question is to how this increase of the 9-1-1-dependent checkpoint cascade at a DSB is achieved. Here, I would like to provide two plausible hypotheses.

9-1-1 has been suggested to be loaded at ss-dsDNA junctions (Majka & Burgers, 2003), and it was shown in vitro that it can diffuse along the DNA in the loaded state (Majka et al., 2006). Whether diffusion happens in vivo, and if yes, whether the 9-1-1 can enter chromatinized regions or RPA-ssDNA filaments, should be assessed in future research. Independent of this potential relocalization of 9-1-1, subsequent loading of several clamp molecules in a time- and resection-dependent manner would lead to an accumulation of 9-1-1 that reflects the progression of resection. Such progressive loading guided by RPA-ssDNA generation could be supported by the direct protein-protein interaction between RPA and Rad24-RFC, the 9-1-1-specific clamp loader (Lindsey-Boltz et al., 2012). In this model, the growing RPA-ssDNA filament would enrich the clamp loader, which subsequently would catalyze consecutive rounds of 9-1-1 loading, causing a quantitative enrichment of 9-1-1 (and consequently the whole checkpoint effector cascade) on the resecting DSB.

Alternatively, a discontinuous resection mechanism involving several internal resection start sites with the corresponding ss-dsDNA junctions could provide the basis for resection-dependent 9-1-1 enrichment. In this model, each resection tract would interact

with Rad24-RFC and harbor two ss-dsDNA junctions with the propensity to load 9-1-1. Obviously, one could envision also a combination of both models, with consecutive loading of 9-1-1 molecules on multiple resected tracts. Figure 17 visualizes the factors that may contribute to resection-dependent 9-1-1 loading.

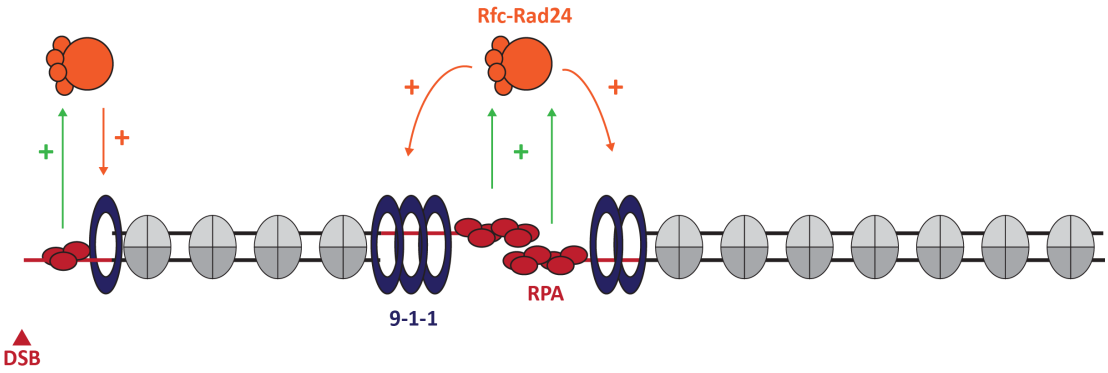

Fig.17. **Model for a putative mechanism of resection-dependent 9-1-1 loading.** Resection could promote a corresponding amount of 9-1-1 loading by enhancing the local concentration of the 9-1-1 clamp loader Rad24-RFC (orange) via direct interaction with RPA (red). Such a mechanism could be enhanced in a discontinuous resection mode, where several ss-dsDNA junctions are available for 9-1-1 loading.

With our work we would like to put forward a new model of quantitative checkpoint input signal sensing (Bantele et al, in revision). Two components are required to set off the checkpoint signaling: Mec1 kinase activation and Rad53 recruitment via 9-1-1. Each of these steps is supported by one checkpoint sensor with the potential of being a quantitative sensor. Intriguingly, the Ddc2-Mec1-dependent step occurs upstream of the Ddc1-Rad53-dependent step, the latter additionally depending on Mec1-catalyzed phosphorylations on Ddc1, Rad9 and Rad53. Together, both sensor pathways converge at the step of Ddc1 (9-1-1) phosphorylation. A model of the two checkpoint sensor pathways and their interconnection is presented in Figure 18.

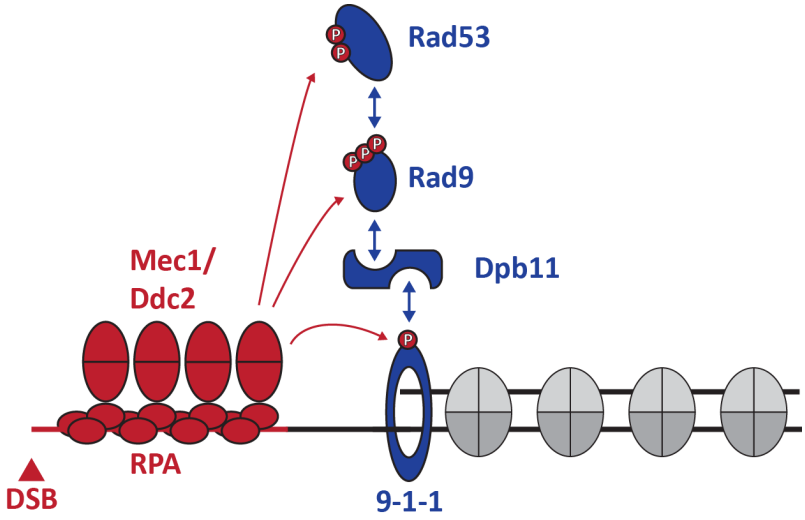

Fig.18. **Dissection of Ddc2- and 9-1-1-dependent sensing pathways.** The Ddc2-dependent checkpoint sensor pathway (red) reads the length of the RPA filament and accumulates the apical Mec1 kinase activity at the DSB. Independently of Mec1-Ddc2, the 9-1-1 sensor is loaded to ss-dsDNA junctions and assembles the checkpoint cascade in consecutive recruitment steps (blue), which mostly require Mec1-dependent phosphorylation. Therefore, Ddc2- and Ddc1-mediated sensing pathways converge on checkpoint protein phosphorylation downstream of Mec1 recruitment.

As discussed before, Mec1 most likely contributes to, but alone is not decisive for making this step proportional to the amount of resection (Bantele et al, in revision). Here, I would like to discuss a piece of evidence showing that manipulation of the 9-1-1 sensing can modulate the checkpoint output, even when Ddc2 sensing is partially reduced.

We utilized two different fusion proteins to enhance Rad53 activation independent of resection by manipulation of the Ddc1-, but not the Mec1-dependent signaling (Bantele et al, in revision). First, we fused Dpb11 to Rad9. This mutant background partially blocks resection and at the same times stabilizes Rad9-Rad53 at DSBs. Additionally, in this mutant Rad53 is hyperactive despite the fact that only minimal amounts of Mec1 are present (Bantele et al, in revision).

These data make two points: First, Mec1 phosphorylation appears to be saturated at the step of Ddc1 phosphorylation. Second, enhancing the 9-1-1-dependent sensing by hyper-recruitment of the 9-1-1 downstream factors leads to hyper-activation of the checkpoint, demonstrating the strong ability of the 9-1-1 axis to modulate Rad53 activation levels. In a reciprocal experiment, where we up-regulate Mec1-dependent signaling by inducing hyper-resection using the *DDC1-FUN30* fusion protein, the checkpoint is normal.

Correspondingly, when we further enhance the 9-1-1 signaling axis using the even more potent *DDC1-RAD9* fusion, which at the same time also strictly blocks resection and Mec1 loading, we achieve even higher checkpoint hyper-activation (Bantele et al, in revision).

Lastly, an argument that weakens the model that Mec1-Ddc2 itself acts as quantitative checkpoint sensor comes from the existence of a second apical checkpoint kinase – Tel1. Intriguingly, Tel1 can not only target the same substrates as Mec1 with a certain degree of redundancy, but moreover is inhibited by resection as it is recruited to DSBs via the MRX complex. In principle, one could therefore propose that this inverse regulation might ensure a constant level of kinase activity at the break independent of its resection status. In how far such a redundancy plays a role on checkpoint substrates in vivo still needs to be assessed.

Collectively, these data support a model by which the 9-1-1 complex is recruited to DSBs in a resection-dependent manner and modulates the quantitative checkpoint output. Whether Mec1-Ddc2 can also act as quantitative sensor in checkpoint signaling as would be intuitive based on its interaction with RPA needs to be tested.

References

Acevedo, J., Yan, S., & Michael, W. M. (2016). Direct Binding to Replication Protein A (RPA)-coated Single-stranded DNA Allows Recruitment of the ATR Activator TopBP1 to Sites of DNA Damage. *The Journal of Biological Chemistry*, *291*(25), 13124–13131. http://doi.org/10.1074/jbc.M116.729194

Adam, S., Dabin, J., Chevallier, O., Leroy, O., Baldeyron, C., Corpet, A., et al. (2016). Real-Time Tracking of Parental Histones Reveals Their Contribution to Chromatin Integrity Following DNA Damage. *Molecular Cell*, *64*(1), 1–15. http://doi.org/10.1016/j.molcel.2016.08.019

Adkins, N. L., Niu, H., Sung, P., & Peterson, C. L. (2013). Nucleosome dynamics regulates DNA processing. *Nature Publishing Group*, *20*(7), 836–842. http://doi.org/10.1038/nsmb.2585

Adkins, N. L., Swygert, S. G., Kaur, P., Niu, H., Grigoryev, S. A., Sung, P., et al. (2017). Nucleosome-like, Single-stranded DNA (ssDNA)-Histone Octamer Complexes and the Implication for DNA Double Strand Break Repair. *The Journal of Biological Chemistry*, *292*(13), 5271–5281. http://doi.org/10.1074/jbc.M117.776369

Aggarwal, M., Sommers, J. A., Morris, C., & Brosh, R. M., Jr. (2010). Delineation of WRN helicase function with EXO1 in the replicational stress response. *DNA Repair*, *9*(7), 765–776. http://doi.org/10.1016/j.dnarep.2010.03.014

Agmon, N., Liefshitz, B., Zimmer, C., Fabre, E., & Kupiec, M. (2013). Effect of nuclear architecture on the efficiency of double-strand break repair. *Nature Publishing Group*, *15*(6), 694–699. http://doi.org/10.1038/ncb2745

Alatwi, H. E., & Downs, J. A. (2015). Removal of H2A.Z by INO80 promotes homologous recombination. *EMBO Reports*, *16*(8), 986–994. http://doi.org/10.15252/embr.201540330

Aparicio, T., Baer, R., Gottesman, M., & Gautier, J. (2016). MRN, CtIP, and BRCA1 mediate repair of topoisomerase II–DNA adducts. *The Journal of Cell Biology*, *212*(4), 399–408. http://doi.org/10.1083/jcb.201504005

Arya, R., & Bassing, C. H. (2017). V(D)J Recombination Exploits DNA Damage Responses to Promote Immunity. *Trends in Genetics*, *33*(7), 479–489. http://doi.org/10.1016/j.tig.2017.04.006

Aten, J. A., Stap, J., Krawczyk, P. M., van Oven, C. H., Hoebe, R. A., Essers, J., & Kanaar, R. (2004). Dynamics of DNA double-strand breaks revealed by clustering of damaged chromosome domains. *Science (New York, N.Y.)*, *303*(5654), 92–95. http://doi.org/10.1126/science.1088845

Awad, S., Ryan, D., Prochasson, P., Owen-Hughes, T., & Hassan, A. H. (2010). The Snf2 homolog Fun30 acts as a homodimeric ATP-dependent chromatin-remodeling enzyme. *The Journal of Biological Chemistry*, *285*(13), 9477–9484. http://doi.org/10.1074/jbc.M109.082149

Aylon, Y., Liefshitz, B., & Kupiec, M. (2004). The CDK regulates repair of double-strand breaks by homologous recombination during the cell cycle. *Embo Journal*, *23*(24), 4868–4875. http://doi.org/10.1038/sj.emboj.7600469

Aymard, F., Aguirrebengoa, M., Guillou, E., Javierre, B. M., Bugler, B., Arnould, C., et al. (2017). Genome-wide mapping of long-range contacts unveils clustering of DNA

double-strand breaks at damaged active genes. *Nature Publishing Group*, *24*(4), 353–361. http://doi.org/10.1038/nsmb.3387

Balogun, F. O., Truman, A. W., & Kron, S. J. (2013). DNA resection proteins Sgs1 and Exo1 are required for G1 checkpoint activation in budding yeast. *DNA Repair*, *12*(9), 1–10. http://doi.org/10.1016/j.dnarep.2013.06.003

Bantele, S., Ferreira, P., Gritenaite, D., Boos, D., & Pfander, B. (2017). Targeting of the Fun30 nucleosome remodeller by the Dpb11 scaffold facilitates cell cycle-regulated DNA end resection. *Elife*, *6*, e21687. http://doi.org/10.7554/eLife.21687

Barlow, J. H., Lisby, M., & Rothstein, R. (2008). Differential regulation of the cellular response to DNA double-strand breaks in G1. *Molecular Cell*, *30*(1), 73–85. http://doi.org/10.1016/j.molcel.2008.01.016

Beltrao, P., Trinidad, J. C., Fiedler, D., Roguev, A., Lim, W. A., Shokat, K. M., et al. (2009). Evolution of phosphoregulation: comparison of phosphorylation patterns across yeast species. *PLoS Biology*, *7*(6), e1000134. http://doi.org/10.1371/journal.pbio.1000134

Bennett, G., Papamichos-Chronakis, M., & Peterson, C. L. (2013). DNA repair choice defines a common pathway for recruitment of chromatin regulators. *Nature Communications*, *4*, 602–2010. http://doi.org/10.1038/ncomms3084

Bermudez, V. P., Lindsey-Boltz, L. A., Cesare, A. J., Maniwa, Y., Griffith, J. D., Hurwitz, J., & Sancar, A. (2003). Loading of the human 9-1-1 checkpoint complex onto DNA by the checkpoint clamp loader hRad17-replication factor C complex in vitro. *Proceedings of the National Academy of Sciences*, *100*(4), 1633–1638. http://doi.org/10.1073/pnas.0437927100

Blier, P. R., Griffith, A. J., Craft, J., & Hardin, J. A. (1993). Binding of Ku protein to DNA. Measurement of affinity for ends and demonstration of binding to nicks. *The Journal of Biological Chemistry*, *268*(10), 7594–7601.

Boeger, H., Griesenbeck, J., Strattan, J. S., & Kornberg, R. D. (2003). Nucleosomes unfold completely at a transcriptionally active promoter. *Molecular Cell*, *11*(6), 1587–1598.

Bonetti, D., Martina, M., Clerici, M., Lucchini, G., & Longhese, M. P. (2009). Multiple Pathways Regulate 3Ã¢â‚¬Â² Overhang Generation at S. cerevisiae Telomeres. *Molecular Cell*, *35*(1), 70–81. http://doi.org/10.1016/j.molcel.2009.05.015

Bonetti, D., Villa, M., Gobbini, E., Cassani, C., Tedeschi, G., & Longhese, M. P. (2015). Escape of Sgs1 from Rad9 inhibition reduces the requirement for Sae2 and functional MRX in DNA end resection. *EMBO Reports*, *16*(3), 351–361. http://doi.org/10.15252/embr.201439764

Bonilla, C. Y., Melo, J. A., & Toczyski, D. P. (2008). Colocalization of Sensors Is Sufficient to Activate the DNA Damage Checkpoint in the Absence of Damage. *Molecular Cell*, *30*(3), 267–276. http://doi.org/10.1016/j.molcel.2008.03.023

Botuyan, M. V., Lee, J., Ward, I. M., Kim, J.-E., Thompson, J. R., Chen, J., & Mer, G. (2006). Structural Basis for the Methylation State-Specific Recognition of Histone H4-K20 by 53BP1 and Crb2 in DNA Repair. *Cell*, *127*(7), 1361–1373. http://doi.org/10.1016/j.cell.2006.10.043

BRANZEI, D., & FOIANI, M. (2007). Interplay of replication checkpoints and repair proteins at stalled replication forks. *DNA Repair*, *6*(7), 994–1003. http://doi.org/10.1016/j.dnarep.2007.02.018

Burdova, K., Mihaljevic, B., Sturzenegger, A., Chappidi, N., & Janscak, P. (2015). The Mismatch-Binding Factor MutSβ Can Mediate ATR Activation in Response to

DNA Double-Strand Breaks. *Molecular Cell*, *59*(4), 603–614. http://doi.org/10.1016/j.molcel.2015.06.026

Byeon, B., Wang, W., Barski, A., Ranallo, R. T., Bao, K., Schones, D. E., et al. (2013). The ATP-dependent Chromatin Remodeling Enzyme Fun30 Represses Transcription by Sliding Promoter-proximal Nucleosomes. *The Journal of Biological Chemistry*, *288*(32), 23182–23193. http://doi.org/10.1074/jbc.M113.471979

Cadet, J., & Wagner, J. R. (2013). DNA base damage by reactive oxygen species, oxidizing agents, and UV radiation. *Cold Spring Harbor Perspectives in Biology*, *5*(2), a012559–a012559. http://doi.org/10.1101/cshperspect.a012559

Cannavo, E., & Cejka, P. (2014). Sae2 promotes dsDNA endonuclease activity within Mre11-Rad50-Xrs2 to resect DNA breaks. *Nature*, *514*(7520), 122–125. http://doi.org/10.1038/nature13771

Cannavo, E., Cejka, P., & Kowalczykowski, S. C. (2013). Relationship of DNA degradation by Saccharomyces cerevisiae Exonuclease 1 and its stimulation by RPA and Mre11-Rad50-Xrs2 to DNA end resection. *Proceedings of the National Academy of Sciences*, *110*(18), E1661–E1668. http://doi.org/10.1073/pnas.1305166110

Caron, P., Aymard, F., Iacovoni, J. S., Briois, S., Canitrot, Y., Bugler, B., et al. (2012). Cohesin protects genes against γH2AX Induced by DNA double-strand breaks. *PLoS Genetics*, *8*(1), e1002460. http://doi.org/10.1371/journal.pgen.1002460

Caron, P., Choudjaye, J., Clouaire, T., Bugler, B., Daburon, V., Aguirrebengoa, M., et al. (2015). Non-redundant Functions of ATM and DNA-PKcs in Response to DNA Double-Strand Breaks. *Cell Reports*, *13*(8), 1598–1609. http://doi.org/10.1016/j.celrep.2015.10.024

Ceballos, S. J., & Heyer, W.-D. (2011). Functions of the Snf2/Swi2 family Rad54 motor protein in homologous recombination. *Biochimica Et Biophysica Acta*, *1809*(9), 509–523. http://doi.org/10.1016/j.bbagrm.2011.06.006

Cejka, P., Cannavo, E., Polaczek, P., Masuda-Sasa, T., Pokharel, S., Campbell, J. L., & Kowalczykowski, S. C. (2010). DNA end resection by Dna2–Sgs1–RPA and its stimulation by Top3–Rmi1 and Mre11–Rad50–Xrs2. *Nature*, *467*(7311), 112–116. http://doi.org/10.1038/nature09355

Celeste, A., Fernandez-Capetillo, O., Kruhlak, M. J., Pilch, D. R., Staudt, D. W., Lee, A., et al. (2003). Histone H2AX phosphorylation is dispensable for the initial recognition of DNA breaks. *Nature Cell Biology*, *5*(7), 675–U51. http://doi.org/10.1038/ncb1004

Chakraborty, S., Pandita, R. K., Hambarde, S., Mattoo, A. R., Charaka, V., Ahmed, K. M., et al. (2018). SMARCAD1 Phosphorylation and Ubiquitination Are Required for Resection during DNA Double-Strand Break Repair. *iScience*, *2*, 123–135. http://doi.org/10.1016/j.isci.2018.03.016

Chambers, A. L., & Downs, J. A. (2012). The RSC and INO80 Chromatin-Remodeling Complexes in DNA Double-Strand Break Repair. In *Mechanisms of DNA Repair* (Vol. 110, pp. 229–261). Elsevier. http://doi.org/10.1016/B978-0-12-387665-2.00009-2

Chapman, J. R., Sossick, A. J., Boulton, S. J., & Jackson, S. P. (2012). BRCA1-associated exclusion of 53BP1 from DNA damage sites underlies temporal control of DNA repair. *Journal of Cell Science*, *125*(15), 3529–3534. http://doi.org/10.1242/jcs.105353

Chen, C.-C., Carson, J. J., Feser, J., Tamburini, B., Zabaronick, S., Linger, J., & Tyler, J. K. (2008). Acetylated lysine 56 on histone H3 drives chromatin assembly after

repair and signals for the completion of repair. *Cell*, *134*(2), 231–243. http://doi.org/10.1016/j.cell.2008.06.035

Chen, H., Lisby, M., & Symington, L. S. (2013). RPA coordinates DNA end resection and prevents formation of DNA hairpins. *Molecular Cell*, *50*(4), 589–600. http://doi.org/10.1016/j.molcel.2013.04.032

Chen, X., Cui, D., Papusha, A., Zhang, X., Chu, C.-D., Tang, J., et al. (2012). The Fun30 nucleosome remodeller promotes resection of DNA double-strand break ends. *Nature*, *489*(7417), 576–580. http://doi.org/10.1038/nature11355

Chen, X., Niu, H., Chung, W.-H., Zhu, Z., Papusha, A., Shim, E. Y., et al. (2011). Cell cycle regulation of DNA double-strand break end resection by Cdk1-dependent Dna2 phosphorylation. *Nature Publishing Group*, *18*(9), 1015–1019. http://doi.org/10.1038/nsmb.2105

Chen, X., Niu, H., Yu, Y., Wang, J., Zhu, S., Zhou, J., et al. (2016). Enrichment of Cdk1-cyclins at DNA double-strand breaks stimulates Fun30 phosphorylation and DNA end resection. *Nucleic Acids Research*, *44*(6), 2742–2753. http://doi.org/10.1093/nar/gkv1544

Chi, P., Kwon, Y., Visnapuu, M.-L., Lam, I., Santa Maria, S. R., Zheng, X., et al. (2011). Analyses of the yeast Rad51 recombinase A265V mutant reveal different in vivo roles of Swi2-like factors. *Nucleic Acids Research*, *39*(15), 6511–6522. http://doi.org/10.1093/nar/gkr297

Chiolo, I., Minoda, A., Colmenares, S. U., Polyzos, A., Costes, S. V., & Karpen, G. H. (2011). Double-Strand Breaks in Heterochromatin Move Outside of a Dynamic HP1a Domain to Complete Recombinational Repair. *Cell*, *144*(5), 732–744. http://doi.org/10.1016/j.cell.2011.02.012

Chiolo, I., Tang, J., Georgescu, W., & Costes, S. V. (2013). Nuclear dynamics of radiation-induced foci in euchromatin and heterochromatin. *Mutation Research - Fundamental and Molecular Mechanisms of Mutagenesis*, *750*(1-2), 56–66. http://doi.org/10.1016/j.mrfmmm.2013.08.001

Chung, W.-H., Zhu, Z., Papusha, A., Malkova, A., & Ira, G. (2010). Defective resection at DNA double-strand breaks leads to de novo telomere formation and enhances gene targeting. *PLoS Genetics*, *6*(5), e1000948. http://doi.org/10.1371/journal.pgen.1000948

Ciccia, A., & Elledge, S. J. (2010). The DNA damage response: making it safe to play with knives. *Molecular Cell*, *40*(2), 179–204. http://doi.org/10.1016/j.molcel.2010.09.019

Clerici, M., Mantiero, D., Guerini, I., Lucchini, G., & Longhese, M. P. (2008). The Yku70-Yku80 complex contributes to regulate double-strand break processing and checkpoint activation during the cell cycle. *EMBO Reports*, *9*(8), 810–818. http://doi.org/10.1038/embor.2008.121

Clerici, M., Mantiero, D., Lucchini, G., & Longhese, M. P. (2006). The Saccharomyces cerevisiae Sae2 protein negatively regulates DNA damage checkpoint signalling. *EMBO Reports*, *7*(2), 212–218. http://doi.org/10.1038/sj.embor.7400593

Clerici, M., Trovesi, C., Galbiati, A., Lucchini, G., & Longhese, M. P. (2013). Mec1/ATR regulates the generation of single-stranded DNA that attenuates Tel1/ATM signaling at DNA ends. *The EMBO Journal*, *25*, n/a–n/a. http://doi.org/10.1002/embj.201386041

Cohen-Fix, O., & Koshland, D. (1997). The anaphase inhibitor of Saccharomyces cerevisiae Pds1p is a target of the DNA damage checkpoint pathway. *Proceedings of*

the National Academy of Sciences, *94*(26), 14361–14366. http://doi.org/10.1073/pnas.94.26.14361

Collins, S. R., Miller, K. M., Maas, N. L., Roguev, A., Fillingham, J., Chu, C. S., et al. (2007). Functional dissection of protein complexes involved in yeast chromosome biology using a genetic interaction map. *Nature*, *446*(7137), 806–810. http://doi.org/10.1038/nature05649

Conde, F., Refolio, E., Cordon-Preciado, V., Cortes-Ledesma, F., Aragón, L., Aguilera, A., & San-Segundo, P. A. (2009). The Dot1 histone methyltransferase and the Rad9 checkpoint adaptor contribute to cohesin-dependent double-strand break repair by sister chromatid recombination in Saccharomyces cerevisiae. *Genetics*, *182*(2), 437–446. http://doi.org/10.1534/genetics.109.101899

Cortez, D. (2001). ATR and ATRIP: Partners in Checkpoint Signaling. *Science (New York, N.Y.)*, *294*(5547), 1713–1716. http://doi.org/10.1126/science.1065521

Costanzo, M., Baryshnikova, A., Bellay, J., Kim, Y., Spear, E. D., Sevier, C. S., et al. (2010). The genetic landscape of a cell. *Science (New York, N.Y.)*, *327*(5964), 425–431. http://doi.org/10.1126/science.1180823

Costelloe, T., Louge, R., Tomimatsu, N., Mukherjee, B., Martini, E., Khadaroo, B., et al. (2012). The yeast Fun30 and human SMARCAD1 chromatin remodellers promote DNA end resection. *Nature*, *489*(7417), 581–584. http://doi.org/10.1038/nature11353

Cussiol, J. R., Jablonowski, C. M., Yimit, A., Brown, G. W., & Smolka, M. B. (2015). Dampening DNA damage checkpoint signalling via coordinated BRCT domain interactions. *Embo Journal*, *34*(12), 1704–1717. http://doi.org/10.15252/embj.201490834

Dehé, P.-M., & Gaillard, P.-H. L. (2017). Control of structure-specific endonucleases to maintain genome stability. *Nature Publishing Group*, *18*(5), 315–330. http://doi.org/10.1038/nrm.2016.177

Delacroix, S., Wagner, J. M., Kobayashi, M., Yamamoto, K.-I., & Karnitz, L. M. (2007). The Rad9-Hus1-Rad1 (9-1-1) clamp activates checkpoint signaling via TopBP1. *Genes & Development*, *21*(12), 1472–1477. http://doi.org/10.1101/gad.1547007

Densham, R. M., Garvin, A. J., Stone, H. R., Strachan, J., Baldock, R. A., Daza-Martin, M., et al. (2016). Human BRCA1–BARD1 ubiquitin ligase activity counteracts chromatin barriers to DNA resection. *Nature Publishing Group*, *23*(7), 647–655. http://doi.org/10.1038/nsmb.3236

Deshpande, I., Seeber, A., Shimada, K., Keusch, J. J., Gut, H., & Gasser, S. M. (2017). Structural Basis of Mec1-Ddc2-RPA Assembly and Activation on Single-Stranded DNA at Sites of Damage. *Molecular Cell*, *68*(2), 431–445.e5. http://doi.org/10.1016/j.molcel.2017.09.019

di Cicco, G., Bantele, S. C. S., Reusswig, K.-U., & Pfander, B. (2017). A cell cycle-independent mode of the Rad9-Dpb11 interaction is induced by DNA damage. *Scientific Reports*, *7*(1), 1447–11. http://doi.org/10.1038/s41598-017-11937-z

Dimitrova, N., Chen, Y.-C. M., Spector, D. L., & de Lange, T. (2008). 53BP1 promotes non-homologous end joining of telomeres by increasing chromatin mobility. *Nature*, *456*(7221), 524–528. http://doi.org/10.1038/nature07433

Dion, V., Kalck, V., Horigome, C., Towbin, B. D., & Gasser, S. M. (2012). Increased mobility of double-strand breaks requires Mec1, Rad9 and the homologous recombination machinery. *Nature Cell Biology*, *14*(5), 502–509. http://doi.org/10.1038/ncb2465

Dion, V., Kalck, V., Seeber, A., Schleker, T., & Gasser, S. M. (2013). Cohesin and the nucleolus constrain the mobility of spontaneous repair foci. *EMBO Reports*, *14*(11), 984–991. http://doi.org/10.1038/embor.2013.142

Downey, M., & Durocher, D. (2006). gammaH2AX as a checkpoint maintenance signal. *Cell Cycle (Georgetown, Tex.)*, *5*(13), 1376–1381. http://doi.org/10.4161/cc.5.13.2899

Downs, J. A., Lowndes, N. F., & Jackson, S. P. (2000). A role for Saccharomyces cerevisiae histone H2A in DNA repair. *Nature*, *408*(6815), 1001–1004. http://doi.org/10.1038/35050000

Downs, J. A., Lowndes, N. F., Nature, S. J., 2000. (n.d.). A role for Saccharomyces cerevisiae histone H2A in DNA repair. *Nature.com*

Du, L.-L., Nakamura, T. M., & Russell, P. (2006). Histone modification-dependent and -independent pathways for recruitment of checkpoint protein Crb2 to double-strand breaks. *Genes & Development*, *20*(12), 1583–1596. http://doi.org/10.1101/gad.1422606

Duan, Z., Andronescu, M., Schutz, K., McIlwain, S., Kim, Y. J., Lee, C., et al. (2010). A three-dimensional model of the yeast genome. *Nature*, *465*(7296), 363–367. http://doi.org/10.1038/nature08973

Durand-Dubief, M., Will, W. R., Petrini, E., Theodorou, D., Harris, R. R., Crawford, M. R., et al. (2012). SWI/SNF-Like Chromatin Remodeling Factor Fun30 Supports Point Centromere Function in S. cerevisiae. *PLoS Genetics*, *8*(9), e1002974–19. http://doi.org/10.1371/journal.pgen.1002974

Eapen, V. V., Sugawara, N., Tsabar, M., Wu, W.-H., & Haber, J. E. (2012). The Saccharomyces cerevisiae chromatin remodeler Fun30 regulates DNA end resection and checkpoint deactivation. *Molecular and Cellular Biology*, *32*(22), 4727–4740. http://doi.org/10.1128/MCB.00566-12

Elledge, S. J., Zhou, Z., Allen, J. B., & Navas, T. A. (1993). DNA damage and cell cycle regulation of ribonucleotide reductase. *BioEssays : News and Reviews in Molecular, Cellular and Developmental Biology*, *15*(5), 333–339. http://doi.org/10.1002/bies.950150507

Ellison, V., & Stillman, B. (2003). Biochemical characterization of DNA damage checkpoint complexes: clamp loader and clamp complexes with specificity for 5' recessed DNA. *PLoS Biology*, *1*(2), E33. http://doi.org/10.1371/journal.pbio.0000033

Emili, A. (1998). MEC1-dependent phosphorylation of Rad9p in response to DNA damage. *Molecular Cell*, *2*(2), 183–189.

Escribano-Díaz, C., Orthwein, A., Fradet-Turcotte, A., Xing, M., Young, J. T. F., Tkáč, J., et al. (2013). A Cell Cycle-Dependent Regulatory Circuit Composed of 53BP1-RIF1 and BRCA1-CtIP Controls DNA Repair Pathway Choice. *Molecular Cell*, *49*(5), 872–883. http://doi.org/10.1016/j.molcel.2013.01.001

Falck, J., Coates, J., & Jackson, S. P. (2005). Conserved modes of recruitment of ATM, ATR and DNA-PKcs to sites of DNA damage. *Nature*, *434*(7033), 605–611. http://doi.org/10.1038/nature03442

Feng, Q., Wang, H., Ng, H. H., Erdjument-Bromage, H., Tempst, P., Struhl, K., & Zhang, Y. (2002). Methylation of H3-lysine 79 is mediated by a new family of HMTases without a SET domain. *Current Biology*, *12*(12), 1052–1058.

Ferrari, M., Dibitetto, D., De Gregorio, G., Eapen, V. V., Rawal, C. C., Lazzaro, F., et al. (2015). Functional interplay between the 53BP1-ortholog Rad9 and the Mre11

complex regulates resection, end-tethering and repair of a double-strand break. *PLoS Genetics*, *11*(1), e1004928. http://doi.org/10.1371/journal.pgen.1004928

Flaus, A. (2006). Identification of multiple distinct Snf2 subfamilies with conserved structural motifs. *Nucleic Acids Research*, *34*(10), 2887–2905. http://doi.org/10.1093/nar/gkl295

Flott, S., & Rouse, J. (2005). Slx4 becomes phosphorylated after DNA damage in a Mec1/Tel1-dependent manner and is required for repair of DNA alkylation damage. *The Biochemical Journal*, *391*(Pt 2), 325–333. http://doi.org/10.1042/BJ20050768

Fradet-Turcotte, A., Canny, M. D., Escribano-Díaz, C., Orthwein, A., Leung, C. C. Y., Huang, H., et al. (2013). 53BP1 is a reader of the DNA-damage- induced H2A Lys 15 ubiquitin mark. *Nature*, *498*(7456), 50–54. http://doi.org/10.1038/nature12318

Franchitto, A., Pichierri, P., Piergentili, R., Crescenzi, M., Bignami, M., & Palitti, F. (2003). The mammalian mismatch repair protein MSH2 is required for correct MRE11 and RAD51 relocalization and for efficient cell cycle arrest induced by ionizing radiation in G2 phase. *Oncogene*, *22*(14), 2110–2120. http://doi.org/10.1038/sj.onc.1206254

Fricke, W. M., & Brill, S. J. (2003). Slx1-Slx4 is a second structure-specific endonuclease functionally redundant with Sgs1-Top3. *Genes & Development*, *17*(14), 1768–1778. http://doi.org/10.1101/gad.1105203

Garcia, V., Furuya, K., & Carr, A. M. (2005). Identification and functional analysis of TopBP1 and its homologs. *DNA Repair*, *4*(11), 1227–1239. http://doi.org/10.1016/j.dnarep.2005.04.001

Garcia, V., Phelps, S. E. L., Gray, S., & Neale, M. J. (2011). Bidirectional resection of DNA double-strand breaks by Mre11 and Exo1. *Nature*, *479*(7372), 241–244. http://doi.org/10.1038/nature10515

Gasch, A. P., Huang, M., Metzner, S., Botstein, D., Elledge, S. J., & Brown, P. O. (2001). Genomic Expression Responses to DNA-damaging Agents and the Regulatory Role of the Yeast ATR Homolog Mec1p. *Molecular Biology of the Cell*, *12*(10), 2987–3003. http://doi.org/10.1091/mbc.12.10.2987

Gerald, J., Benjamin, J. M., & Kron, S. J. (2002). Robust G1 checkpoint arrest in budding yeast: dependence on DNA damage signaling and repair. *Journal of Cell Science*, *115*(8), 1749–1757.

Giannattasio, M., Lazzaro, F., Plevani, P., & Muzi-Falconi, M. (2005). The DNA damage checkpoint response requires histone H2B ubiquitination by Rad6-Bre1 and H3 methylation by Dot1. *The Journal of Biological Chemistry*, *280*(11), 9879–9886. http://doi.org/10.1074/jbc.M414453200

Gobbini, E., Cesena, D., Galbiati, A., Lockhart, A., & Longhese, M. P. (2013). Interplays between ATM/Tel1 and ATR/Mec1 in sensing and signaling DNA double-strand breaks. *DNA Repair*, *12*(10), 791–799. http://doi.org/10.1016/j.dnarep.2013.07.009

Granata, M., Lazzaro, F., Novarina, D., Panigada, D., Puddu, F., Abreu, C. M., et al. (2010). Dynamics of Rad9 Chromatin Binding and Checkpoint Function Are Mediated by Its Dimerization and Are Cell Cycle–Regulated by CDK1 Activity. *PLoS Genetics*, *6*(8), e1001047–14. http://doi.org/10.1371/journal.pgen.1001047

Gravel, S., Chapman, J. R., Magill, C., & Jackson, S. P. (2008). DNA helicases Sgs1 and BLM promote DNA double-strand break resection. *Genes & Development*, *22*(20), 2767–2772. http://doi.org/10.1101/gad.503108

Green, C. M., & Almouzni, G. (2002). When repair meets chromatin. First in series on

chromatin dynamics. *EMBO Reports*, *3*(1), 28–33. http://doi.org/10.1093/embo-reports/kvf005

Green, C. M., Erdjument-Bromage, H., Tempst, P., & Lowndes, N. F. (2000). A novel Rad24 checkpoint protein complex closely related to replication factor C (vol 10, pg 39, 2000). *Current Biology*, *10*(4), R171–R171.

Greinert, R., Volkmer, B., Henning, S., Breitbart, E. W., Greulich, K. O., Cardoso, M. C., & Rapp, A. (2012). UVA-induced DNA double-strand breaks result from the repair of clustered oxidative DNA damages. *Nucleic Acids Research*, *40*(20), 10263–10273. http://doi.org/10.1093/nar/gks824

Grenon, M., Costelloe, T., Jimeno, S., O'Shaughnessy, A., FitzGerald, J., Zgheib, O., et al. (2007). Docking onto chromatin via theSaccharomyces cerevisiae Rad9 Tudor domain. *Yeast*, *24*(2), 105–119. http://doi.org/10.1002/yea.1441

Grenon, M., Magill, C. P., Lowndes, N. F., & Jackson, S. P. (2006). Double-strand breaks trigger MRX- and Mec1-dependent, but Tel1-independent, checkpoint activation. *FEMS Yeast Research*, *6*(5), 836–847. http://doi.org/10.1111/j.1567-1364.2006.00076.x

Griffith, A. J., Blier, P. R., Mimori, T., & Hardin, J. A. (1992). Ku polypeptides synthesized in vitro assemble into complexes which recognize ends of double-stranded DNA. *The Journal of Biological Chemistry*, *267*(1), 331–338.

Gritenaite, D., Princz, L. N., Szakal, B., Bantele, S. C. S., Wendeler, L., Schilbach, S., et al. (2014). A cell cycle-regulated Slx4-Dpb11 complex promotes the resolution of DNA repair intermediates linked to stalled replication. *Genes & Development*, *28*(14), 1604–1619. http://doi.org/10.1101/gad.240515.114

Gunjan, A., & Verreault, A. (2003). A Rad53 kinase-dependent surveillance mechanism that regulates histone protein levels in S. cerevisiae. *Cell*, *115*(5), 537–549. http://doi.org/10.1038/nrm1297

Haber, J. E. (2012). Mating-Type Genes and MAT Switching in Saccharomyces cerevisiae. *Genetics*, *191*(1), 33–64. http://doi.org/10.1534/genetics.111.134577

Hammet, A., Magill, C., Heierhorst, J., & Jackson, S. P. (2007). Rad9 BRCT domain interaction with phosphorylated H2AX regulates the G1 checkpoint in budding yeast. *EMBO Reports*, *8*(9), 851–857. http://doi.org/10.1038/sj.embor.7401036

Hang, L., & Zhao, X. (2016). The Rtt107 BRCT scaffold and its partner modification enzymes collaborate to promote replication. *Nucleus (Austin, Tex.)*, *7*(4), 346–351. http://doi.org/10.1080/19491034.2016.1201624

Harrison, J. C., & Haber, J. E. (2006). Surviving the breakup: the DNA damage checkpoint. *Annual Review of Genetics*, *40*(1), 209–235. http://doi.org/10.1146/annurev.genet.40.051206.105231

Hauer, M. H., Seeber, A., Singh, V., Thierry, R., Sack, R., Amitai, A., et al. (2017). Histone degradation in response to DNA damage enhances chromatin dynamics and recombination rates. *Nature Publishing Group*, *24*(2), 99–107. http://doi.org/10.1038/nsmb.3347

Hoa, N. N., Shimizu, T., Zhou, Z. W., Wang, Z.-Q., Deshpande, R. A., Paull, T. T., et al. (2016). Mre11 Is Essential for the Removal of Lethal Topoisomerase 2 Covalent Cleavage Complexes. *Molecular Cell*, *64*(3), 580–592. http://doi.org/10.1016/j.molcel.2016.10.011

Hoeijmakers, J. H. J. (2009). DNA damage, aging, and cancer. *The New England Journal of Medicine*, *361*(15), 1475–1485. http://doi.org/10.1056/NEJMra0804615

Hopfner, K. P., Karcher, A., Shin, D., Fairley, C., Tainer, J. A., & Carney, J. P. (2000).

Mre11 and Rad50 from Pyrococcus furiosus: Cloning and Biochemical Characterization Reveal an Evolutionarily Conserved Multiprotein Machine. *Journal of Bacteriology*, *182*(21), 6036–6041. http://doi.org/10.1128/JB.182.21.6036-6041.2000

Hopfner, K.-P., Karcher, A., Craig, L., Woo, T. T., Carney, J. P., & Tainer, J. A. (2001). Structural Biochemistry and Interaction Architecture of the DNA Double-Strand Break Repair Mre11 Nuclease and Rad50-ATPase. *Cell*, *105*(4), 473–485. http://doi.org/10.1016/S0092-8674(01)00335-X

Horigome, C., Bustard, D. E., Marcomini, I., Delgoshaie, N., Tsai-Pflugfelder, M., Cobb, J. A., & Gasser, S. M. (2016). PolySUMOylation by Siz2 and Mms21 triggers relocation of DNA breaks to nuclear pores through the Slx5/Slx8 STUbL. *Genes & Development*, *30*(8), 931–945. http://doi.org/10.1101/gad.277665.116

Huang, T.-H., Fowler, F., Chen, C.-C., Shen, Z.-J., Sleckman, B., & Tyler, J. K. (2018). The Histone Chaperones ASF1 and CAF-1 Promote MMS22L-TONSL-Mediated Rad51 Loading onto ssDNA during Homologous Recombination in Human Cells. *Molecular Cell*, *69*(5), 1–20. http://doi.org/10.1016/j.molcel.2018.01.031

Huertas, P., Cortes-Ledesma, F., Sartori, A. A., Aguilera, A., & Jackson, S. P. (2008). CDK targets Sae2 to control DNA-end resection and homologous recombination. *Nature*, *455*(7213), 689–692. http://doi.org/10.1038/nature07215

Huyen, Y., Zgheib, O., Ditullio, R. A., Gorgoulis, V. G., Zacharatos, P., Petty, T. J., et al. (2004). Methylated lysine 79 of histone H3 targets 53BP1 to DNA double-strand breaks. *Nature*, *432*(7015), 406–411. http://doi.org/10.1038/nature03114

Ira, G., Pellicioli, A., Balijja, A., Wang, X., Fiorani, S., Carotenuto, W., et al. (2004). DNA end resection, homologous recombination and DNA damage checkpoint activation require CDK1. *Nature*, *431*(7011), 1011–1017. http://doi.org/10.1038/nature02964

Javaheri, A., Wysocki, R., Jobin-Robitaille, O., Altaf, M., Côté, J., & Kron, S. J. (2006). Yeast G1 DNA damage checkpoint regulation by H2A phosphorylation is independent of chromatin remodeling. *Proceedings of the National Academy of Sciences of the United States of America*, *103*(37), 13771–13776. http://doi.org/10.1073/pnas.0511192103

Jazayeri, A., Falck, J., Lukas, C., Bartek, J., Smith, G. C. M., Lukas, J., & Jackson, S. P. (2006). ATM- and cell cycle-dependent regulation of ATR in response to DNA double-strand breaks. *Nature Cell Biology*, *8*(1), 37–45. http://doi.org/10.1038/ncb1337

Jelinsky, S. A., & Samson, L. D. (1999). Global response of Saccharomyces cerevisiae to an alkylating agent. *Proceedings of the National Academy of Sciences*, *96*(4), 1486–1491. http://doi.org/10.1073/pnas.96.4.1486

Joglekar, A. (2016). A Cell Biological Perspective on Past, Present and Future Investigations of the Spindle Assembly Checkpoint. *Biology*, *5*(4), 44–19. http://doi.org/10.3390/biology5040044

Kalocsay, M., Hiller, N. J., & Jentsch, S. (2009). Chromosome-wide Rad51 Spreading and SUMO-H2A.Z-Dependent Chromosome Fixation in Response to a Persistent DNA Double-Strand Break. *Molecular Cell*, *33*(3), 335–343. http://doi.org/10.1016/j.molcel.2009.01.016

Kennedy, S. R., Loeb, L. A., & Herr, A. J. (2012). Somatic mutations in aging, cancer and neurodegeneration. *Mechanisms of Ageing and Development*, *133*(4), 118–126.

http://doi.org/10.1016/j.mad.2011.10.009
Kent, N. A., Chambers, A. L., & Downs, J. A. (2007). Dual chromatin remodeling roles for RSC during DNA double strand break induction and repair at the yeast MAT locus. *The Journal of Biological Chemistry*, *282*(38), 27693–27701. http://doi.org/10.1074/jbc.M704707200
Keogh, M.-C., Kim, J.-A., Downey, M., Fillingham, J., Chowdhury, D., Harrison, J. C., et al. (2006). A phosphatase complex that dephosphorylates gammaH2AX regulates DNA damage checkpoint recovery. *Nature*, *439*(7075), 497–501. http://doi.org/10.1038/nature04384
Khurana, S., Kruhlak, M. J., Kim, J., Tran, A. D., Liu, J., Nyswaner, K., et al. (2014). A macrohistone variant links dynamic chromatin compaction to BRCA1-dependent genome maintenance. *CellReports*, *8*(4), 1049–1062. http://doi.org/10.1016/j.celrep.2014.07.024
Kim, C., Paulus, B. F., & Wold, M. S. (2002). Interactions of human replication protein A with oligonucleotides. *Biochemistry*, *33*(47), 14197–14206. http://doi.org/10.1021/bi00251a031
Kim, H. S., & Brill, S. J. (2001). Rfc4 Interacts with Rpa1 and Is Required for Both DNA Replication and DNA Damage Checkpoints in Saccharomyces cerevisiae. *Molecular and Cellular Biology*, *21*(11), 3725–3737. http://doi.org/10.1128/MCB.21.11.3725-3737.2001
Kim, J. A., & Haber, J. E. (2009). Chromatin assembly factors Asf1 and CAF-1 have overlapping roles in deactivating the DNA damage checkpoint when DNA repair is complete. *Proceedings of the National Academy of Sciences*, *106*(4), 1151–1156. http://doi.org/10.1073/pnas.0812578106
Kim, J. A., Hicks, W. M., Li, J., Tay, S. Y., & Haber, J. E. (2011). Protein Phosphatases Pph3, Ptc2, and Ptc3 Play Redundant Roles in DNA Double-Strand Break Repair by Homologous Recombination. *Molecular and Cellular Biology*, *31*(3), 507–516. http://doi.org/10.1128/MCB.01168-10
Kim, J.-A., Kruhlak, M., Dotiwala, F., Nussenzweig, A., & Haber, J. E. (2007). Heterochromatin is refractory to gamma-H2AX modification in yeast and mammals. *The Journal of Cell Biology*, *178*(2), 209–218. http://doi.org/10.1083/jcb.200612031
Kobor, M. S., Venkatasubrahmanyam, S., Meneghini, M. D., Gin, J. W., Jennings, J. L., Link, A. J., et al. (2004). A protein complex containing the conserved Swi2/Snf2-related ATPase Swr1p deposits histone variant H2A.Z into euchromatin. *PLoS Biology*, *2*(5), E131. http://doi.org/10.1371/journal.pbio.0020131
Kondo, T., Wakayama, T., Naiki, T., Matsumoto, K., & Sugimoto, K. (2001). Recruitment of Mec1 and Ddc1 checkpoint proteins to double-strand breaks through distinct mechanisms. *Science*, *294*(5543), 867–870. http://doi.org/10.1126/science.1063827
Krishnan, V., Nirantar, S., Crasta, K., Cheng, A. Y. H., & Surana, U. (2004). DNA Replication Checkpoint Prevents Precocious Chromosome Segregation by Regulating Spindle Behavior. *Molecular Cell*, *16*(5), 687–700. http://doi.org/10.1016/j.molcel.2004.11.001
Krogan, N. J., Cagney, G., Yu, H., Zhong, G., Guo, X., Ignatchenko, A., et al. (2006). Global landscape of protein complexes in the yeast Saccharomyces cerevisiae. *Nature*, *440*(7084), 637–643. http://doi.org/10.1038/nature04670
Krogan, N. J., Keogh, M.-C., Datta, N., Sawa, C., Ryan, O. W., Ding, H., et al. (2003). A Snf2 family ATPase complex required for recruitment of the histone H2A variant

Htz1. *Molecular Cell*, *12*(6), 1565–1576.
Lademann, C. A., Renkawitz, J., Pfander, B., & Jentsch, S. (2017). The INO80 Complex Removes H2A.Z to Promote Presynaptic Filament Formation during Homologous Recombination. *CellReports*, *19*(7), 1294–1303. http://doi.org/10.1016/j.celrep.2017.04.051
Langerak, P., & Russell, P. (2011). Regulatory networks integrating cell cycle control with DNA damage checkpoints and double-strand break repair. *Philosophical Transactions of the Royal Society B: Biological Sciences*, *366*(1584), 3562–3571. http://doi.org/10.1098/rstb.2011.0070
Langerak, P., Mejia-Ramirez, E., Limbo, O., & Russell, P. (2011). Release of Ku and MRN from DNA Ends by Mre11 Nuclease Activity and Ctp1 Is Required for Homologous Recombination Repair of Double-Strand Breaks. *PLoS Genetics*, *7*(9), e1002271. http://doi.org/10.1371/journal.pgen.1002271
Lazzaro, F., Sapountzi, V., Granata, M., Pellicioli, A., Vaze, M., Haber, J. E., et al. (2008). Histone methyltransferase Dot1 and Rad9 inhibit single-stranded DNA accumulation at DSBs and uncapped telomeres. *The EMBO Journal*, *27*(10), 1502–1512. http://doi.org/10.1038/emboj.2008.81
Lee, C.-S., Lee, K., Legube, G., & Haber, J. E. (2013). Dynamics of yeast histone H2A and H2B phosphorylation in response to a double-strand break. *Nature Structural & Molecular Biology*, *21*(1), 103–109. http://doi.org/10.1038/nsmb.2737
Lee, C.-S., Wang, R. W., Chang, H.-H., Capurso, D., Segal, M. R., & Haber, J. E. (2016). Chromosome position determines the success of double-strand break repair. *Proceedings of the National Academy of Sciences of the United States of America*, *113*(2), E146–54. http://doi.org/10.1073/pnas.1523660113
Lee, J., Choi, E. S., Seo, H. D., Kang, K., Gilmore, J. M., Florens, L., et al. (2017). Chromatin remodeller Fun30Fft3 induces nucleosome disassembly to facilitate RNA polymerase II elongation. *Nature Communications*, *8*, 14527. http://doi.org/10.1038/ncomms14527
Lee, J., Kumagai, A., & Dunphy, W. G. (2007). The Rad9-Hus1-Rad1 checkpoint clamp regulates interaction of TopBP1 with ATR. *The Journal of Biological Chemistry*, *282*(38), 28036–28044. http://doi.org/10.1074/jbc.M704635200
Leland, B. A., Chen, A. C., Zhao, A. Y., Wharton, R. C., & King, M. C. (2018). Rev7 and 53BP1/Crb2 prevent RecQ helicase-dependent hyper-resection of DNA double-strand breaks. *Elife*, *7*, 5497. http://doi.org/10.7554/eLife.33402
Lengsfeld, B. M., Rattray, A. J., Bhaskara, V., Ghirlando, R., & Paull, T. T. (2007). Sae2 Is an Endonuclease that Processes Hairpin DNA Cooperatively with the Mre11/Rad50/Xrs2 Complex. *Molecular Cell*, *28*(4), 638–651. http://doi.org/10.1016/j.molcel.2007.11.001
Leung, C. C. Y., & Glover, J. N. M. (2014). BRCT domains. *Cell Cycle*, *10*(15), 2461–2470. http://doi.org/10.4161/cc.10.15.16312
Leung, G. P., Brown, J. A. R., Glover, J. N. M., & Kobor, M. S. (2016). Rtt107 BRCT domains act as a targeting module in the DNA damage response. *DNA Repair*, *37*, 22–32. http://doi.org/10.1016/j.dnarep.2015.10.007
Levikova, M., Pinto, C., & Cejka, P. (2017). The motor activity of DNA2 functions as an ssDNA translocase to promote DNA end resection. *Genes & Development*, *31*(5), 493–502. http://doi.org/10.1101/gad.295196.116
Li, X., Liu, K., Li, F., Wang, J., Huang, H., Wu, J., & Shi, Y. (2012). Structure of C-terminal tandem BRCT repeats of Rtt107 protein reveals critical role in interaction

with phosphorylated histone H2A during DNA damage repair. *The Journal of Biological Chemistry*, *287*(12), 9137–9146. http://doi.org/10.1074/jbc.M111.311860

Liang, B., Qiu, J., Ratnakumar, K., & Laurent, B. C. (2007). RSC Functions as an Early Double-Strand-Break Sensor in the Cell's Response to DNA Damage. *Current Biology*, *17*(16), 1432–1437. http://doi.org/10.1016/j.cub.2007.07.035

Lindahl, T. (1993). Instability and decay of the primary structure of DNA. *Nature*, *362*(6422), 709–715. http://doi.org/10.1038/362709a0

LINDAHL, T., & BARNES, D. E. (2000). Repair of endogenous DNA damage. *Cold Spring Harbor Symposia on Quantitative Biology*, *65*(0), 127–133. http://doi.org/10.1101/sqb.2000.65.127

Lindsey-Boltz, L. A., Reardon, J. T., Wold, M. S., & Sancar, A. (2012). In VitroAnalysis of the Role of Replication Protein A (RPA) and RPA Phosphorylation in ATR-mediated Checkpoint Signaling. *The Journal of Biological Chemistry*, *287*(43), 36123–36131. http://doi.org/10.1074/jbc.M112.407825

Lisby, M., Barlow, J. H., Burgess, R. C., & Rothstein, R. (2004). Choreography of the DNA damage response: spatiotemporal relationships among checkpoint and repair proteins. *Cell*, *118*(6), 699–713. http://doi.org/10.1016/j.cell.2004.08.015

Liu, L., & Jiang, T. (2017). Crystal structure of the ATPase-C domain of the chromatin remodeller Fun30 from Saccharomyces cerevisiae. *Acta Crystallographica. Section F, Structural Biology Communications*, *73*(Pt 1), 9–15. http://doi.org/10.1107/S2053230X16019269

Liu, Y., Cussiol, J. R., Dibitetto, D., Sims, J. R., Twayana, S., Weiss, R. S., et al. (2017). TOPBP1 Dpb11plays a conserved role in homologous recombination DNA repair through the coordinated recruitment of 53BP1 Rad9. *The Journal of Cell Biology*, *216*(3), 623–639. http://doi.org/10.1083/jcb.201607031

Llorente, B., & Symington, L. S. (2004). The Mre11 Nuclease Is Not Required for 5“ to 3” Resection at Multiple HO-Induced Double-Strand Breaks. *Molecular and Cellular Biology*, *24*(21), 9682–9694. http://doi.org/10.1128/MCB.24.21.9682-9694.2004

Lobachev, K. S., Gordenin, D. A., & Resnick, M. A. (2002). The Mre11 Complex Is Required for Repair of Hairpin-Capped Double-Strand Breaks and Prevention of Chromosome Rearrangements. *Cell*, *108*(2), 183–193. http://doi.org/10.1016/S0092-8674(02)00614-1

Lodato, M. A., Rodin, R. E., Bohrson, C. L., Coulter, M. E., Barton, A. R., Kwon, M., et al. (2018). Aging and neurodegeneration are associated with increased mutations in single human neurons. *Science (New York, N.Y.)*, *359*(6375), 555–559. http://doi.org/10.1126/science.aao4426

Longhese, M. P., Bonetti, D., Guerini, I., Manfrini, N., & Clerici, M. (2009). DNA double-strand breaks in meiosis: checking their formation, processing and repair. *DNA Repair*, *8*(9), 1127–1138. http://doi.org/10.1016/j.dnarep.2009.04.005

Lopez-Mosqueda, J., Maddi, K., Prgomet, S., Kalayil, S., Marinovic-Terzic, I., Terzic, J., & Dikic, I. (2016). SPRTN is a mammalian DNA-binding metalloprotease that resolves DNA-protein crosslinks. *Elife*, *5*, 179. http://doi.org/10.7554/eLife.21491

Lottersberger, F., Karssemeijer, R. A., Dimitrova, N., & de Lange, T. (2015). 53BP1 and the LINC Complex Promote Microtubule-Dependent DSB Mobility and DNA Repair. *Cell*, *163*(4), 880–893. http://doi.org/10.1016/j.cell.2015.09.057

Luk, E., Ranjan, A., FitzGerald, P. C., Mizuguchi, G., Huang, Y., Wei, D., & Wu, C. (2010). Stepwise Histone Replacement by SWR1 Requires Dual Activation with

Histone H2A.Z and Canonical Nucleosome. *Cell*, *143*(5), 725–736. http://doi.org/10.1016/j.cell.2010.10.019

Majka, J., & Burgers, P. (2003). Yeast Rad17/Mec3/Ddc1: A sliding clamp for the DNA damage checkpoint. *Proceedings of the National Academy of Sciences of the United States of America*, *100*(5), 2249–2254. http://doi.org/10.1073/pnas.0437148100

Majka, J., & Burgers, P. M. (2005). Function of Rad17/Mec3/Ddc1 and its partial complexes in the DNA damage checkpoint. *DNA Repair*, *4*(10), 1189–1194. http://doi.org/10.1016/j.dnarep.2005.07.008

Majka, J., Binz, S. K., Wold, M. S., & Burgers, P. M. J. (2006). Replication protein A directs loading of the DNA damage checkpoint clamp to 5'-DNA junctions. *The Journal of Biological Chemistry*, *281*(38), 27855–27861. http://doi.org/10.1074/jbc.M605176200

Mantiero, D., Clerici, M., Lucchini, G., & Longhese, M. P. (2007). Dual role for Saccharomyces cerevisiae Tel1 in the checkpoint response to double-strand breaks. *EMBO Reports*, *8*(4), 380–387. http://doi.org/10.1038/sj.embor.7400911

Mao, Z., Bozzella, M., Seluanov, A., & Gorbunova, V. (2008). Comparison of nonhomologous end joining and homologous recombination in human cells. *DNA Repair*, *7*(10), 1765–1771. http://doi.org/10.1016/j.dnarep.2008.06.018

Marshall, W. F., Straight, A., Marko, J. F., Swedlow, J., Dernburg, A., Belmont, A., et al. (1997). Interphase chromosomes undergo constrained diffusional motion in living cells. *Current Biology*, *7*(12), 930–939.

Masumoto, H., Hawke, D., Kobayashi, R., & Verreault, A. (2005). A role for cell-cycle-regulated histone H3 lysine 56 acetylation in the DNA damage response. *Nature*, *436*(7048), 294–298. http://doi.org/10.1038/nature03714

Mathiasen, D. P., & Lisby, M. (2014). Cell cycle regulation of homologous recombination in Saccharomyces cerevisiae. *FEMS Microbiology Reviews*, *38*(2), 172–184. http://doi.org/10.1111/1574-6976.12066

Mello, J. A., Sillje, H., Roche, D., Kirschner, D. B., Nigg, E. A., & Almouzni, G. (2002). Human Asf1 and CAF-1 interact and synergize in a repair-coupled nucleosome assembly pathway. *EMBO Reports*, *3*(4), 329–334. http://doi.org/10.1093/embo-reports/kvf068

Melo, J. A., Cohen, J., & Toczyski, D. P. (2001). Two checkpoint complexes are independently recruited to sites of DNA damage in vivo. *Genes & Development*, *15*(21), 2809–2821. http://doi.org/10.1101/gad.903501

Mimitou, E. P., & Symington, L. S. (2008). Sae2, Exo1 and Sgs1 collaborate in DNA double-strand break processing. *Nature*, *455*(7214), 770–774. http://doi.org/10.1038/nature07312

Mimitou, E. P., & Symington, L. S. (2009). DNA end resection: Many nucleases make light work. *DNA Repair*, *8*(9), 983–995. http://doi.org/10.1016/j.dnarep.2009.04.017

Mimitou, E. P., & Symington, L. S. (2010). Ku prevents Exo1 and Sgs1-dependent resection of DNA ends in the absence of a functional MRX complex or Sae2. *The EMBO Journal*, *29*(19), 3358–3369. http://doi.org/10.1038/emboj.2010.193

Miné-Hattab, J., & Rothstein, R. (2012). Increased chromosome mobility facilitates homology search during recombination. *Nature Publishing Group*, *14*(5), 510–517. http://doi.org/10.1038/ncb2472

Moreau, S., Ferguson, J. R., & Symington, L. S. (1999). The Nuclease Activity of Mre11 Is Required for Meiosis but Not for Mating Type Switching, End Joining, or

Telomere Maintenance. *Molecular and Cellular Biology*, *19*(1), 556–566. http://doi.org/10.1128/MCB.19.1.556

Morillo-Huesca, M., Clemente-Ruiz, M., Andújar, E., & Prado, F. (2010). The SWR1 histone replacement complex causes genetic instability and genome-wide transcription misregulation in the absence of H2A.Z. *PloS One*, *5*(8), e12143. http://doi.org/10.1371/journal.pone.0012143

Morin, I., Ngo, H.-P., Greenall, A., Zubko, M. K., Morrice, N., & Lydall, D. (2008). Checkpoint-dependent phosphorylation of Exo1 modulates the DNA damage response. *Embo Journal*, *27*(18), 2400–2410. http://doi.org/10.1038/emboj.2008.171

Muñoz-Galván, S., Jimeno, S., Rothstein, R., & Aguilera, A. (2013). Histone H3K56 acetylation, Rad52, and non-DNA repair factors control double-strand break repair choice with the sister chromatid. *PLoS Genetics*, *9*(1), e1003237. http://doi.org/10.1371/journal.pgen.1003237

Nagai, S., Dubrana, K., Tsai-Pflugfelder, M., Davidson, M. B., Roberts, T. M., Brown, G. W., et al. (2008). Functional targeting of DNA damage to a nuclear pore-associated SUMO-dependent ubiquitin ligase. *Science (New York, N.Y.)*, *322*(5901), 597–602. http://doi.org/10.1126/science.1162790

Naiki, T., Wakayama, T., Nakada, D., Matsumoto, K., & Sugimoto, K. (2004). Association of Rad9 with Double-Strand Breaks through a Mec1-Dependent Mechanism. *Molecular and Cellular Biology*, *24*(8), 3277–3285. http://doi.org/10.1128/MCB.24.8.3277-3285.2004

Nakada, D., Hirano, Y., & Sugimoto, K. (2004). Requirement of the Mre11 complex and exonuclease 1 for activation of the Mec1 signaling pathway. *Molecular and Cellular Biology*, *24*(22), 10016–10025. http://doi.org/10.1128/MCB.24.22.10016-10025.2004

Nakada, D., Matsumoto, K., & Sugimoto, K. (2003). ATM-related Tel1 associates with double-strand breaks through an Xrs2-dependent mechanism. *Genes & Development*, *17*(16), 1957–1962. http://doi.org/10.1101/gad.1099003

Nakada, S., Chen, G. I., Gingras, A.-C., & Durocher, D. (2008). PP4 is a gamma H2AX phosphatase required for recovery from the DNA damage checkpoint. *EMBO Reports*, *9*(10), 1019–1026. http://doi.org/10.1038/embor.2008.162

Nakamura, T. M., Du, L.-L., Redon, C., & Russell, P. (2004). Histone H2A phosphorylation controls Crb2 recruitment at DNA breaks, maintains checkpoint arrest, and influences DNA repair in fission yeast. *Molecular and Cellular Biology*, *24*(14), 6215–6230. http://doi.org/10.1128/MCB.24.14.6215-6230.2004

Navadgi-Patil, V. M., & Burgers, P. M. (2008). Yeast DNA Replication Protein Dpb11 Activates the Mec1/ATR Checkpoint Kinase. *The Journal of Biological Chemistry*, *283*(51), 35853–35859. http://doi.org/10.1074/jbc.M807435200

Navadgi-Patil, V. M., & Burgers, P. M. (2009). A tale of two tails: activation of DNA damage checkpoint kinase Mec1/ATR by the 9-1-1 clamp and by Dpb11/TopBP1. *DNA Repair*, *8*(9), 996–1003. http://doi.org/10.1016/j.dnarep.2009.03.011

Navadgi-Patil, V. M., & Burgers, P. M. (2011). Cell-cycle-specific activators of the Mec1/ATR checkpoint kinase. *Biochemical Society Transactions*, *39*(2), 600–605. http://doi.org/10.1042/BST0390600

Neale, M. J., Pan, J., & Keeney, S. (2005). Endonucleolytic processing of covalent protein-linked DNA double-strand breaks. *Nature*, *436*(7053), 1053–1057. http://doi.org/10.1038/nature03872

Neumann, F. R., Dion, V., Gehlen, L. R., Tsai-Pflugfelder, M., Schmid, R., Taddei, A., & Gasser, S. M. (2012). Targeted INO80 enhances subnuclear chromatin movement and ectopic homologous recombination. *Genes & Development*, *26*(4), 369–383. http://doi.org/10.1101/gad.176156.111

Neves-Costa, A., Will, W. R., Vetter, A. T., Miller, J. R., & Varga-Weisz, P. (2009). The SNF2-Family Member Fun30 Promotes Gene Silencing in Heterochromatic Loci. *PloS One*, *4*(12), e8111–13. http://doi.org/10.1371/journal.pone.0008111

Nimonkar, A. V., Ozsoy, A. Z., Genschel, J., Modrich, P., & Kowalczykowski, S. C. (2008). Human exonuclease 1 and BLM helicase interact to resect DNA and initiate DNA repair. *Proceedings of the National Academy of Sciences*, *105*(44), 16906–16911. http://doi.org/10.1073/pnas.0809380105

Niu, H., Chung, W.-H., Zhu, Z., Kwon, Y., Zhao, W., Chi, P., et al. (2010). Mechanism of the ATP-dependent DNA end-resection machinery from Saccharomyces cerevisiae. *Nature*, *467*(7311), 108–111. http://doi.org/10.1038/nature09318

O'Driscoll, M. (2012). Diseases associated with defective responses to DNA damage. *Cold Spring Harbor Perspectives in Biology*, *4*(12), a012773–a012773. http://doi.org/10.1101/cshperspect.a012773

Ochs, F., Somyajit, K., Altmeyer, M., Rask, M.-B., Lukas, J., & Lukas, C. (2016). 53BP1 fosters fidelity of homology-directed DNA repair. *Nature Publishing Group*, *23*(8), 714–721. http://doi.org/10.1038/nsmb.3251

Ohashi, E., Takeishi, Y., Ueda, S., & Tsurimoto, T. (2014). Interaction between Rad9–Hus1–Rad1 and TopBP1 activates ATR–ATRIP and promotes TopBP1 recruitment to sites of UV-damage. *DNA Repair*, *21*, 1–11. http://doi.org/10.1016/j.dnarep.2014.05.001

Ohouo, P. Y., Bastos de Oliveira, F. M., Almeida, B. S., & Smolka, M. B. (2010). DNA damage signaling recruits the Rtt107-Slx4 scaffolds via Dpb11 to mediate replication stress response. *Molecular Cell*, *39*(2), 300–306. http://doi.org/10.1016/j.molcel.2010.06.019

Ohouo, P. Y., de Oliveira, F. M. B., Liu, Y., Ma, C. J., & Smolka, M. B. (2013). DNA-repair scaffolds dampen checkpoint signalling by counteracting the adaptor Rad9. *Nature*, *493*(7430), 120–124. http://doi.org/10.1038/nature11658

Ohshima, H., Yermilov, V., Yoshie, Y., & Rubio, J. (1999). DNA Damage Induced by Reactive Nitrogen Species. In *Advances in DNA Damage and Repair* (pp. 329–339). Boston, MA: Springer US. http://doi.org/10.1007/978-1-4615-4865-2_27

Olive, P. L., Durand, R. E., & Banáth, J. P. (1990). Heterogeneity in Radiation-Induced DNA Damage and Repair in Tumor and Normal Cells Measured Using the "Comet" Assay. *Radiation Research*, *122*(1), 86. http://doi.org/10.2307/3577587

Orthwein, A., Noordermeer, S. M., Wilson, M. D., Landry, S., Enchev, R. I., Sherker, A., et al. (2015). A mechanism for the suppression of homologous recombination in G1 cells. *Nature*, *528*(7582), 422–426. http://doi.org/10.1038/nature16142

Oza, P., Jaspersen, S. L., Miele, A., Dekker, J., & Peterson, C. L. (2009). Mechanisms that regulate localization of a DNA double-strand break to the nuclear periphery. *Genes & Development*, *23*(8), 912–927. http://doi.org/10.1101/gad.1782209

Ozdemir, A., Spicuglia, S., Lasonder, E., Vermeulen, M., Campsteijn, C., Stunnenberg, H. G., & Logie, C. (2005). Characterization of lysine 56 of histone H3 as an acetylation site in Saccharomyces cerevisiae. *The Journal of Biological Chemistry*, *280*(28), 25949–25952. http://doi.org/10.1074/jbc.C500181200

Paciotti, V., Clerici, M., Lucchini, G., & Longhese, M. P. (2000). The checkpoint protein Ddc2, functionally related to S. pombe Rad26, interacts with Mec1 and is regulated by Mec1-dependent phosphorylation in budding yeast. *Genes & Development*, *14*(16), 2046–2059.

Paciotti, V., Lucchini, G., Plevani, P., & Longhese, M. P. (1998). Mec1p is essential for phosphorylation of the yeast DNA damage checkpoint protein Ddc1p, which physically interacts with Mec3p. *Embo Journal*, *17*(14), 4199–4209. http://doi.org/10.1093/emboj/17.14.4199

Paillard, S., & Strauss, F. (1991). Analysis of the mechanism of interaction of simian Ku protein with DNA. *Nucleic Acids Research*, *19*(20), 5619–5624.

Panier, S., & Durocher, D. (2009). Regulatory ubiquitylation in response to DNA double-strand breaks. *DNA Repair*, *8*(4), 436–443. http://doi.org/10.1016/j.dnarep.2009.01.013

Panier, S., & Durocher, D. (2013). Push back to respond better: regulatory inhibition of the DNA double-strand break response. *Nature Publishing Group*, *14*(10), 661–672. http://doi.org/10.1038/nrm3659

Papamichos-Chronakis, M., Krebs, J. E., & Peterson, C. L. (2006). Interplay between Ino80 and Swr1 chromatin remodeling enzymes regulates cell cycle checkpoint adaptation in response to DNA damage. *Genes & Development*, *20*(17), 2437–2449. http://doi.org/10.1101/gad.1440206

Papamichos-Chronakis, M., Watanabe, S., Rando, O. J., & Peterson, C. L. (2011). Global regulation of H2A.Z localization by the INO80 chromatin-remodeling enzyme is essential for genome integrity. *Cell*, *144*(2), 200–213. http://doi.org/10.1016/j.cell.2010.12.021

Paull, T. T., & Gellert, M. (1998). The 3“ to 5” exonuclease activity of Mre 11 facilitates repair of DNA double-strand breaks. *Molecular Cell*, *1*(7), 969–979.

Paull, T. T., Rogakou, E. P., Yamazaki, V., Kirchgessner, C. U., Gellert, M., & Bonner, W. M. (2000). A critical role for histone H2AX in recruitment of repair factors to nuclear foci after DNA damage. *Current Biology*, *10*(15), 886–895.

Pearlman, D. A., Holbrook, S. R., Pirkle, D. H., & Kim, S. H. (1985). Molecular models for DNA damaged by photoreaction. *Science*, *227*(4692), 1304–1308.

Pei, H., Zhang, L., Luo, K., Qin, Y., Chesi, M., Fei, F., et al. (2011). MMSET regulates histone H4K20 methylation and 53BP1 accumulation at DNA damage sites. *Nature*, *470*(7332), 124–128. http://doi.org/10.1038/nature09658

Peng, J. C., & Karpen, G. H. (2008). Epigenetic regulation of heterochromatic DNA stability. *Current Opinion in Genetics & Development*, *18*(2), 204–211. http://doi.org/10.1016/j.gde.2008.01.021

Pfander, B., & Diffley, J. F. X. (2011). Dpb11 coordinates Mec1 kinase activation with cell cycle-regulated Rad9 recruitment. *The EMBO Journal*, *30*(24), 4897–4907. http://doi.org/10.1038/emboj.2011.345

Pfeiffer, P. (1998). The mutagenic potential of DNA double-strand break repair. *Toxicology Letters*, *96-97*(1-2), 119–129. http://doi.org/10.1016/S0378-4274(98)00058-7

Pichierri, P., Franchitto, A., Piergentili, R., Colussi, C., & Palitti, F. (2001). Hypersensitivity to camptothecin in MSH2 deficient cells is correlated with a role for MSH2 protein in recombinational repair. *Carcinogenesis*, *22*(11), 1781–1787.

Piya, G., Mueller, E. N., Haas, H. K., Ghospurkar, P. L., Wilson, T. M., Jensen, J. L., et al. (2015). Characterization of the Interaction between Rfa1 and Rad24 in

Saccharomyces cerevisiae. *PloS One*, *10*(2), e0116512–24. http://doi.org/10.1371/journal.pone.0116512

Potenski, C. J., Niu, H., Sung, P., & Klein, H. L. (2014). Avoidance of ribonucleotide-induced mutations by RNase H2 and Srs2-Exo1 mechanisms. *Nature*, *511*(7508), 251–254. http://doi.org/10.1038/nature13292

Princz, L. N., Wild, P., Bittmann, J., Aguado, F. J., Blanco, M. G., Matos, J., & Pfander, B. (2017). Dbf4-dependent kinase and the Rtt107 scaffold promote Mus81-Mms4 resolvase activation during mitosis. *The EMBO Journal*, *36*(5), 664–678. http://doi.org/10.15252/embj.201694831

Puddu, F., Granata, M., Di Nola, L., Balestrini, A., Piergiovanni, G., Lazzaro, F., et al. (2008). Phosphorylation of the Budding Yeast 9-1-1 Complex Is Required for Dpb11 Function in the Full Activation of the UV-Induced DNA Damage Checkpoint. *Molecular and Cellular Biology*, *28*(15), 4782–4793. http://doi.org/10.1128/MCB.00330-08

Ranjha, L., Howard, S. M., & Cejka, P. (2018). Main steps in DNA double-strand break repair: an introduction to homologous recombination and related processes. *Chromosoma*, *6*(38), e1001160–28. http://doi.org/10.1007/s00412-017-0658-1

Redon, C. E., Weyemi, U., Parekh, P. R., Huang, D., Burrell, A. S., & Bonner, W. M. (2012). γ-H2AX and other histone post-translational modifications in the clinic. *Biochimica Et Biophysica Acta*, *1819*(7), 743–756. http://doi.org/10.1016/j.bbagrm.2012.02.021

Redon, C., Pilch, D. R., Rogakou, E. P., Orr, A. H., Lowndes, N. F., & Bonner, W. M. (2003). Yeast histone 2A serine 129 is essential for the efficient repair of checkpoint-blind DNA damage. *EMBO Reports*, *4*(7), 678–684. http://doi.org/10.1038/sj.embor.embor871

Reginato, G., Cannavo, E., & Cejka, P. (2018). Physiological protein blocks direct the Mre11–Rad50–Xrs2 and Sae2 nuclease complex to initiate DNA end resection. *Genes & Development*, *31*(23-24), 2325–2330. http://doi.org/10.1101/gad.308254.117

Renkawitz, J., Lademann, C. A., & Jentsch, S. (2013a). γH2AX spreading linked to homology search. *Cell Cycle (Georgetown, Tex.)*, *12*(16), 2526–2527. http://doi.org/10.4161/cc.25836

Renkawitz, J., Lademann, C. A., Kalocsay, M., & Jentsch, S. (2013b). Monitoring Homology Search during DNA Double-Strand Break Repair In Vivo. *Molecular Cell*, *50*(2), 261–272. http://doi.org/10.1016/j.molcel.2013.02.020

Robzyk, K. (2000). Rad6-Dependent Ubiquitination of Histone H2B in Yeast. *Science (New York, N.Y.)*, *287*(5452), 501–504. http://doi.org/10.1126/science.287.5452.501

Rogakou, E. P., Pilch, D. R., Orr, A. H., Ivanova, V. S., & Bonner, W. M. (1998). DNA double-stranded breaks induce histone H2AX phosphorylation on serine 139. *The Journal of Biological Chemistry*, *273*(10), 5858–5868.

Rojowska, A., Lammens, K., Seifert, F. U., Direnberger, C., Feldmann, H., & Hopfner, K.-P. (2014). Structure of the Rad50 DNA double-strand break repair protein in complex with DNA. *The EMBO Journal*, *33*(23), 2847–2859. http://doi.org/10.15252/embj.201488889

Roukos, V., Voss, T. C., Schmidt, C. K., Lee, S., Wangsa, D., & Misteli, T. (2013). Spatial dynamics of chromosome translocations in living cells. *Science (New York, N.Y.)*, *341*(6146), 660–664. http://doi.org/10.1126/science.1237150

Rowbotham, S. P., Barki, L., Neves-Costa, A., Santos, F., Dean, W., Hawkes, N., et al. (2011). Maintenance of Silent Chromatin through Replication Requires SWI/SNF-like Chromatin Remodeler SMARCAD1. *Molecular Cell*, *42*(3), 285–296. http://doi.org/10.1016/j.molcel.2011.02.036

Rudin, N., & Haber, J. E. (1988). Efficient repair of HO-induced chromosomal breaks in Saccharomyces cerevisiae by recombination between flanking homologous sequences. *Molecular and Cellular Biology*, *8*(9), 3918–3928.

Sanchez, Y., Bachant, J., Wang, H., Hu, F., Liu, D., Tetzlaff, M., & Elledge, S. J. (1999). Control of the DNA damage checkpoint by chk1 and rad53 protein kinases through distinct mechanisms. *Science*, *286*(5442), 1166–1171.

Sargent, R. G., Brenneman, M. A., & Wilson, J. H. (1997). Repair of site-specific double-strand breaks in a mammalian chromosome by homologous and illegitimate recombination. *Molecular and Cellular Biology*, *17*(1), 267–277.

Savage, J. (1996). Insight into sites. *Mutation Research-Reviews in Genetic Toxicology*, *366*(2), 81–95.

Schiller, C. B., Seifert, F. U., Linke-Winnebeck, C., & Hopfner, K. P. (2014). Structural Studies of DNA End Detection and Resection in Homologous Recombination. *Cold Spring Harbor Perspectives in Biology*, *6*(10), a017962–a017962. http://doi.org/10.1101/cshperspect.a017962

Schulze, J. M., Jackson, J., Nakanishi, S., Gardner, J. M., Hentrich, T., Haug, J., et al. (2009). Linking Cell Cycle to Histone Modifications: SBF and H2B Monoubiquitination Machinery and Cell-Cycle Regulation of H3K79 Dimethylation. *Molecular Cell*, *35*(5), 626–641. http://doi.org/10.1016/j.molcel.2009.07.017

Schwartz, M. F., Duong, J. K., Sun, Z. X., Morrow, J. S., Pradhan, D., & Stern, D. F. (2002). Rad9 phosphorylation sites couple Rad53 to the Saccharomyces cerevisiae DNA damage checkpoint. *Molecular Cell*, *9*(5), 1055–1065.

Seeber, A., Dion, V., & Gasser, S. M. (2013a). Checkpoint kinases and the INO80 nucleosome remodeling complex enhance global chromatin mobility in response to DNA damage. *Genes & Development*, *27*(18), 1999–2008. http://doi.org/10.1101/gad.222992.113

Seeber, A., Hauer, M., & Gasser, S. M. (2013b). Nucleosome remodelers in double-strand break repair. *Current Opinion in Genetics & Development*, *23*(2), 174–184. http://doi.org/10.1016/j.gde.2012.12.008

Shen, X., Mizuguchi, G., Hamiche, A., & Wu, C. (2000). A chromatin remodelling complex involved in transcription and DNA processing. *Nature*, *406*(6795), 541–544. http://doi.org/10.1038/35020123

Shim, E. Y., Hong, S. J., Oum, J.-H., Yanez, Y., Zhang, Y., & Lee, S. E. (2007). RSC mobilizes nucleosomes to improve accessibility of repair machinery to the damaged chromatin. *Molecular and Cellular Biology*, *27*(5), 1602–1613. http://doi.org/10.1128/MCB.01956-06

Shimada, K., Pasero, P., & Gasser, S. M. (2002). ORC and the intra-S-phase checkpoint: a threshold regulates Rad53p activation in S phase. *Genes & Development*, *16*(24), 3236–3252. http://doi.org/10.1101/gad.239802

Shroff, R., Arbel-Eden, A., Pilch, D., Ira, G., Bonner, W. M., Petrini, J. H., et al. (2004). Distribution and dynamics of chromatin modification induced by a defined DNA double-strand break. *Current Biology*, *14*(19), 1703–1711. http://doi.org/10.1016/j.cub.2004.09.047

Sinha, M., & Peterson, C. L. (2009). Chromatin dynamics during repair of chromosomal DNA double-strand breaks. *Epigenomics*, *1*(2), 371–385. http://doi.org/10.2217/epi.09.22

Sinha, R. P., & Häder, D.-P. (2002). UV-induced DNA damage and repair: a review. *Photochemical & Photobiological Sciences*, *1*(4), 225–236. http://doi.org/10.1039/b201230h

Sonntag, von, C. (2006). Ionizing Radiation Damage to DNA (Vol. 10). Weinheim, Germany: Wiley-VCH Verlag GmbH & Co. KGaA. http://doi.org/10.1002/3527600906.mcb.200400108

Sonoda, E., Hochegger, H., Saberi, A., Taniguchi, Y., & Takeda, S. (2006). Differential usage of non-homologous end-joining and homologous recombination in double strand break repair. *DNA Repair*, *5*(9-10), 1021–1029. http://doi.org/10.1016/j.dnarep.2006.05.022

Soria, G., Polo, S. E., & Almouzni, G. (2012). Prime, Repair, Restore: The Active Role of Chromatin in the DNA Damage Response. *Molecular Cell*, *46*(6), 722–734. http://doi.org/10.1016/j.molcel.2012.06.002

Steglich, B., Strålfors, A., Khorosjutina, O., Persson, J., Smialowska, A., Javerzat, J.-P., & Ekwall, K. (2015). The Fun30 Chromatin Remodeler Fft3 Controls Nuclear Organization and Chromatin Structure of Insulators and Subtelomeres in Fission Yeast. *PLoS Genetics*, *11*(3), e1005101–21. http://doi.org/10.1371/journal.pgen.1005101

Stingele, J., Bellelli, R., Alte, F., Hewitt, G., Sarek, G., Maslen, S. L., et al. (2016). Mechanism and Regulation of DNA-Protein Crosslink Repair by the DNA-Dependent Metalloprotease SPRTN. *Molecular Cell*, *64*(4), 688–703. http://doi.org/10.1016/j.molcel.2016.09.031

Stingele, J., Schwarz, M. S., Bloemeke, N., Wolf, P. G., & Jentsch, S. (2014). A DNA-Dependent Protease Involved in DNA-Protein Crosslink Repair. *Cell*, *158*(2), 327–338. http://doi.org/10.1016/j.cell.2014.04.053

Stracker, T. H., & Petrini, J. H. J. (2011). The MRE11 complex: starting from the ends. *Nature Reviews Molecular Cell Biology*, *12*(2), 90–103. http://doi.org/10.1038/nrm3047

Strålfors, A., Walfridsson, J., Bhuiyan, H., & Ekwall, K. (2011). The FUN30 chromatin remodeler, Fft3, protects centromeric and subtelomeric domains from euchromatin formation. *PLoS Genetics*, *7*(3), e1001334. http://doi.org/10.1371/journal.pgen.1001334

Strecker, J., Gupta, G. D., Zhang, W., Bashkurov, M., Landry, M.-C., Pelletier, L., & Durocher, D. (2016). DNA damage signalling targets the kinetochore to promote chromatin mobility. *Nature Cell Biology*, *18*(3), 281–290. http://doi.org/10.1038/ncb3308

Ström, L., Lindroos, H. B., Shirahige, K., & Sjögren, C. (2004). Postreplicative Recruitment of Cohesin to Double-Strand Breaks Is Required for DNA Repair. *Molecular Cell*, *16*(6), 1003–1015. http://doi.org/10.1016/j.molcel.2004.11.026

Stucki, M., Clapperton, J. A., Mohammad, D., Yaffe, M. B., Smerdon, S. J., & Jackson, S. P. (2005). MDC1 directly binds phosphorylated histone H2AX to regulate cellular responses to DNA double-strand breaks. *Cell*, *123*(7), 1213–1226. http://doi.org/10.1016/j.cell.2005.09.038

Sugawara, N., Wang, X., & Haber, J. E. (2003). In vivo roles of Rad52, Rad54, and Rad55 proteins in Rad51-mediated recombination. *Molecular Cell*, *12*(1), 209–219.

Sugiyama, T., Zaitseva, E. M., & Kowalczykowski, S. C. (1997). A Single-stranded DNA-binding Protein Is Needed for Efficient Presynaptic Complex Formation by the Saccharomyces cerevisiaeRad51 Protein. *The Journal of Biological Chemistry*, *272*(12), 7940–7945. http://doi.org/10.1074/jbc.272.12.7940

Sukhanova, M. V., D'Herin, C., Boiteux, S., & Lavrik, O. I. (2014). Interaction of Ddc1 and RPA with single-stranded/double-stranded DNA junctions in yeast whole cell extracts: Proteolytic degradation of the large subunit of replication protein A in ddc1Δ strains. *DNA Repair*, *22*, 30–40. http://doi.org/10.1016/j.dnarep.2014.07.002

Sun, Z., Hsiao, J., Fay, D. S., & Stern, D. F. (1998). Rad53 FHA domain associated with phosphorylated Rad9 in the DNA damage checkpoint. *Science*, *281*(5374), 272–274.

Swartz, R. K., Rodriguez, E. C., & King, M. C. (2014). A role for nuclear envelope-bridging complexes in homology-directed repair. *Molecular Biology of the Cell*, *25*(16), 2461–2471. http://doi.org/10.1091/mbc.E13-10-0569

Sweeney, F. D., Yang, F., Chi, A., Shabanowitz, J., Hunt, D. F., & Durocher, D. (2005). Saccharomyces cerevisiae Rad9 acts as a Mec1 adaptor to allow Rad53 activation. *Current Biology*, *15*(15), 1364–1375. http://doi.org/10.1016/j.cub.2005.06.063

Symington, L. S. (2014). End resection at double-strand breaks: mechanism and regulation. *Cold Spring Harbor Perspectives in Biology*, *6*(8), a016436–a016436. http://doi.org/10.1101/cshperspect.a016436

Symington, L. S. (2016). Mechanism and regulation of DNA end resection in eukaryotes. *Critical Reviews in Biochemistry and Molecular Biology*, *51*(3), 195–212. http://doi.org/10.3109/10409238.2016.1172552

Symington, L. S., & Gautier, J. (2011). Double-strand break end resection and repair pathway choice. *Annual Review of Genetics*, *45*(1), 247–271. http://doi.org/10.1146/annurev-genet-110410-132435

Takata, H., Hanafusa, T., Mori, T., Shimura, M., Iida, Y., Ishikawa, K., et al. (2013). Chromatin Compaction Protects Genomic DNA from Radiation Damage. *PloS One*, *8*(10), e75622–11. http://doi.org/10.1371/journal.pone.0075622

Takeishi, Y., Ohashi, E., Ogawa, K., Masai, H., Obuse, C., & Tsurimoto, T. (2010). Casein kinase 2-dependent phosphorylation of human Rad9 mediates the interaction between human Rad9-Hus1-Rad1 complex and TopBP1. *Genes to Cells : Devoted to Molecular & Cellular Mechanisms*, *15*(7), 761–771. http://doi.org/10.1111/j.1365-2443.2010.01418.x

Taneja, N., Zofall, M., Balachandran, V., Thillainadesan, G., Sugiyama, T., Wheeler, D., et al. (2017). SNF2 Family Protein Fft3 Suppresses Nucleosome Turnover to Promote Epigenetic Inheritance and Proper Replication. *Molecular Cell*, *66*(1), 1–20. http://doi.org/10.1016/j.molcel.2017.02.006

Tercero, J. A., Longhese, M. P., & Diffley, J. F. X. (2003). A Central Role for DNA Replication Forks in Checkpoint Activation and Response. *Molecular Cell*, *11*(5), 1323–1336. http://doi.org/10.1016/S1097-2765(03)00169-2

Terui, R., Nagao, K., Kawasoe, Y., Taki, K., Higashi, T. L., Tanaka, S., et al. (2018). Nucleosomes around a mismatched base pair are excluded via an Msh2-dependent reaction with the aid of SNF2 family ATPase Smarcad1. *Genes & Development*, *32*(11-12), 806–821. http://doi.org/10.1101/gad.310995.117

Tkáč, J., Xu, G., Adhikary, H., Young, J. T. F., Gallo, D., Escribano-Diaz, C., et al.

(2016). HELB Is a Feedback Inhibitor of DNA End Resection. *Molecular Cell*, *61*(3), 405–418. http://doi.org/10.1016/j.molcel.2015.12.013

Toh, G. W. L., O'Shaughnessy, A. M., Jimeno, S., Dobbie, I. M., Grenon, M., Maffini, S., et al. (2006). Histone H2A phosphorylation and H3 methylation are required for a novel Rad9 DSB repair function following checkpoint activation. *DNA Repair*, *5*(6), 693–703. http://doi.org/10.1016/j.dnarep.2006.03.005

Toh, G. W. L., Sugawara, N., Dong, J., Toth, R., Lee, S. E., Haber, J. E., & Rouse, J. (2010). Mec1/Tel1-dependent phosphorylation of Slx4 stimulates Rad1-Rad10-dependent cleavage of non-homologous DNA tails. *DNA Repair*, *9*(6), 718–726. http://doi.org/10.1016/j.dnarep.2010.02.013

Tomimatsu, N., Mukherjee, B., Hardebeck, M. C., Ilcheva, M., Camacho, C. V., Harris, J. L., et al. (2017). Phosphorylation of EXO1 by CDKs 1 and 2 regulates DNA end resection and repair pathway choice. *Nature Communications*, *5*, 1–10. http://doi.org/10.1038/ncomms4561

Torres-Rosell, J., Machin, F., & Aragón, L. (2005). Smc5-Smc6 complex preserves nucleolar integrity in S. cerevisiae. *Cell Cycle (Georgetown, Tex.)*, *4*(7), 868–872. http://doi.org/10.4161/cc.4.7.1825

Torres-Rosell, J., Sunjevaric, I., De Piccoli, G., Sacher, M., Eckert-Boulet, N., Reid, R., et al. (2007). The Smc5–Smc6 complex and SUMO modification of Rad52 regulates recombinational repair at the ribosomal gene locus. *Nature Cell Biology*, *9*(8), 923–931. http://doi.org/10.1038/ncb1619

Trovesi, C., Falcettoni, M., Lucchini, G., Clerici, M., & Longhese, M. P. (2011). Distinct Cdk1 requirements during single-strand annealing, noncrossover, and crossover recombination. *PLoS Genetics*, *7*(8), e1002263. http://doi.org/10.1371/journal.pgen.1002263

Tsabar, M., Eapen, V. V., Mason, J. M., Memisoglu, G., Waterman, D. P., Long, M. J., et al. (2015). Caffeine impairs resection during DNA break repair by reducing the levels of nucleases Sae2 and Dna2. *Nucleic Acids Research*, *43*(14), 6889–6901. http://doi.org/10.1093/nar/gkv520

Tsabar, M., Hicks, W. M., Tsaponina, O., & Haber, J. E. (2016). Re-establishment of nucleosome occupancy during double-strand break repair in budding yeast. *DNA Repair*, *47*, 1–9. http://doi.org/10.1016/j.dnarep.2016.09.005

Tsukuda, T., Fleming, A. B., Nickoloff, J. A., & Osley, M. A. (2005). Chromatin remodelling at a DNA double-strand break site in Saccharomyces cerevisiae. *Nature*, *438*(7066), 379–383. http://doi.org/10.1038/nature04148

Tsukuda, T., Lo, Y.-C., Krishna, S., Sterk, R., Osley, M. A., & Nickoloff, J. A. (2009). INO80-dependent chromatin remodeling regulates early and late stages of mitotic homologous recombination. *DNA Repair*, *8*(3), 360–369. http://doi.org/10.1016/j.dnarep.2008.11.014

Tyler, J. K., Adams, C. R., Chen, S. R., Kobayashi, R., Kamakaka, R. T., & Kadonaga, J. T. (1999). The RCAF complex mediates chromatin assembly during DNA replication and repair. *Nature*, *402*(6761), 555–560. http://doi.org/10.1038/990147

Tyler, J. K., Collins, K. A., Prasad-Sinha, J., Amiott, E., Bulger, M., Harte, P. J., et al. (2001). Interaction between the Drosophila CAF-1 and ASF1 chromatin assembly factors. *Molecular and Cellular Biology*, *21*(19), 6574–6584. http://doi.org/10.1128/MCB.21.19.6574-6584.2001

Ubersax, J. A., Woodbury, E. L., Quang, P. N., Paraz, M., Blethrow, J. D., Shah, K., et al. (2003). Targets of the cyclin-dependent kinase Cdk1. *Nature*, *425*(6960), 859–

864. http://doi.org/10.1038/nature02062
Unal, E., Arbel-Eden, A., Sattler, U., Shroff, R., Lichten, M., Haber, J. E., & Koshland, D. (2004). DNA damage response pathway uses histone modification to assemble a double-strand break-specific cohesin domain. *Molecular Cell*, *16*(6), 991–1002. http://doi.org/10.1016/j.molcel.2004.11.027
Usui, T., Foster, S. S., & Petrini, J. H. J. (2009). Maintenance of the DNA-Damage Checkpoint Requires DNA-Damage-Induced Mediator Protein Oligomerization. *Molecular Cell*, *33*(2), 147–159. http://doi.org/10.1016/j.molcel.2008.12.022
van Attikum, H., Fritsch, O., & Gasser, S. M. (2007). Distinct roles for SWR1 and INO80 chromatin remodeling complexes at chromosomal double-strand breaks. *Embo Journal*, *26*(18), 4113–4125. http://doi.org/10.1038/sj.emboj.7601835
van Leeuwen, F., Gafken, P. R., & Gottschling, D. E. (2002). Dot1p modulates silencing in yeast by methylation of the nucleosome core. *Cell*, *109*(6), 745–756.
Van, C., Williams, J. S., Kunkel, T. A., & Peterson, C. L. (2015). Deposition of histone H2A.Z by the SWR-C remodeling enzyme prevents genome instability. *DNA Repair*, *25*, 9–14. http://doi.org/10.1016/j.dnarep.2014.10.010
Vialard, J. E. (1998). The budding yeast Rad9 checkpoint protein is subjected to Mec1/Tel1-dependent hyperphosphorylation and interacts with Rad53 after DNA damage. *The EMBO Journal*, *17*(19), 5679–5688. http://doi.org/10.1093/emboj/17.19.5679
Vos, S. M., Tretter, E. M., Schmidt, B. H., & Berger, J. M. (2011). All tangled up: how cells direct, manage and exploit topoisomerase function. *Nature Reviews Molecular Cell Biology*, *12*(12), 827–841. http://doi.org/10.1038/nrm3228
Walker, J. R., Corpina, R. A., & Goldberg, J. (2001). Structure of the Ku heterodimer bound to DNA and its implications for double-strand break repair. *Nature*, *412*(6847), 607–614. http://doi.org/10.1038/35088000
Wang, R. W., Lee, C.-S., & Haber, J. E. (2017). Position effects influencing intrachromosomal repair of a double-strand break in budding yeast. *PloS One*, *12*(7), e0180994–13. http://doi.org/10.1371/journal.pone.0180994
Wanrooij, P. H., & Burgers, P. M. (2015). Yet another job for Dna2: Checkpoint activation. *DNA Repair*, *32*, 1–7. http://doi.org/10.1016/j.dnarep.2015.04.009
Wanrooij, P. H., Tannous, E., Kumar, S., Navadgi-Patil, V. M., & Burgers, P. M. (2016). Probing the Mec1ATR Checkpoint Activation Mechanism with Small Peptides. *The Journal of Biological Chemistry*, *291*(1), 393–401. http://doi.org/10.1074/jbc.M115.687145
Ward, J. F. (1988). DNA Damage Produced by Ionizing Radiation in Mammalian Cells: Identities, Mechanisms of Formation, and Reparability (Vol. 35, pp. 95–125). Elsevier. http://doi.org/10.1016/S0079-6603(08)60611-X
Wardlaw, C. P., Carr, A. M., & Oliver, A. W. (2014). TopBP1: A BRCT-scaffold protein functioning in multiple cellular pathways. *DNA Repair*, *22*, 165–174. http://doi.org/10.1016/j.dnarep.2014.06.004
Weinert, T., & Hartwell, L. (1988). The RAD9 gene controls the cell cycle response to DNA damage in Saccharomyces cerevisiae. *Science*, *241*(4863), 317–322. http://doi.org/10.1126/science.3291120
Wiest, N. E., Houghtaling, S., Sanchez, J. C., Tomkinson, A. E., & Osley, M. A. (2017). The SWI/SNF ATP-dependent nucleosome remodeler promotes resection initiation at a DNA double-strand break in yeast. *Nucleic Acids Research*, *45*(10), 5887–5900. http://doi.org/10.1093/nar/gkx221

Williams, R. S., Williams, J. S., & Tainer, J. A. (2007). Mre11–Rad50–Nbs1 is a keystone complex connecting DNA repair machinery, double-strand break signaling, and the chromatin templateThis paper is one of a selection of papers published in this Special Issue, entitled 28th International West Coast Chromatin and Chromosome Conference, and has undergone the Journal's usual peer review process. *Biochemistry and Cell Biology = Biochimie Et Biologie Cellulaire*, *85*(4), 509–520. http://doi.org/10.1139/O07-069

Wolner, B., & Peterson, C. L. (2005). ATP-dependent and ATP-independent roles for the Rad54 chromatin remodeling enzyme during recombinational repair of a DNA double strand break. *The Journal of Biological Chemistry*, *280*(11), 10855–10860. http://doi.org/10.1074/jbc.M414388200

Wood, A., Schneider, J., Dover, J., Johnston, M., & Shilatifard, A. (2003). The Paf1 complex is essential for histone monoubiquitination by the Rad6-Bre1 complex, which signals for histone methylation by COMPASS and Dot1p. *The Journal of Biological Chemistry*, *278*(37), 34739–34742. http://doi.org/10.1074/jbc.C300269200

Wu, X., Shell, S. M., & Zou, Y. (2005). Interaction and colocalization of Rad9/Rad1/Hus1 checkpoint complex with replication protein A in human cells. *Oncogene*, *24*(29), 4728–4735. http://doi.org/10.1038/sj.onc.1208674

Wurtele, H., Kaiser, G. S., Bacal, J., St-Hilaire, E., Lee, E.-H., Tsao, S., et al. (2012). Histone H3 lysine 56 acetylation and the response to DNA replication fork damage. *Molecular and Cellular Biology*, *32*(1), 154–172. http://doi.org/10.1128/MCB.05415-11

Wysocki, R., Javaheri, A., Allard, S., Sha, F., Cote, J., & Kron, S. J. (2005). Role of Dot1-Dependent Histone H3 Methylation in G1 and S Phase DNA Damage Checkpoint Functions of Rad9. *Molecular and Cellular Biology*, *25*(19), 8430–8443. http://doi.org/10.1128/MCB.25.19.8430-8443.2005

Xu, Y., Ayrapetov, M. K., Xu, C., Gursoy-Yuzugullu, O., Hu, Y., & Price, B. D. (2012). Histone H2A.Z controls a critical chromatin remodeling step required for DNA double-strand break repair. *Molecular Cell*, *48*(5), 723–733. http://doi.org/10.1016/j.molcel.2012.09.026

Yu, Q., Zhang, X., & Bi, X. (2011). Roles of chromatin remodeling factors in the formation and maintenance of heterochromatin structure. *The Journal of Biological Chemistry*, *286*(16), 14659–14669. http://doi.org/10.1074/jbc.M110.183269

Zegerman, P., & Diffley, J. F. X. (2007). Phosphorylation of Sld2 and Sld3 by cyclin-dependent kinases promotes DNA replication in budding yeast. *Nature*, *445*(7125), 281–285. http://doi.org/10.1038/nature05432

Zhang, Y., Shim, E. Y., Davis, M., & Lee, S. E. (2009). Regulation of repair choice: Cdk1 suppresses recruitment of end joining factors at DNA breaks. *DNA Repair*, *8*(10), 1235–1241. http://doi.org/10.1016/j.dnarep.2009.07.007

Zhou, B., & Elledge, S. J. (2000). The DNA damage response: putting checkpoints in perspective. *Nature*, *408*(6811), 433–439. http://doi.org/10.1038/35044005

Zhu, Z., Chung, W.-H., Shim, E. Y., Lee, S. E., & Ira, G. (2008). Sgs1 helicase and two nucleases Dna2 and Exo1 resect DNA double-strand break ends. *Cell*, *134*(6), 981–994. http://doi.org/10.1016/j.cell.2008.08.037

Zierhut, C., & Diffley, J. F. X. (2008). Break dosage, cell cycle stage and DNA replication influence DNA double strand break response. *The EMBO Journal*, *27*(13), 1875–1885. http://doi.org/10.1038/emboj.2008.111

Zou, L., & Elledge, S. J. (2003). Sensing DNA damage through ATRIP recognition of RPA-ssDNA complexes. *Science (New York, N.Y.)*, *300*(5625), 1542–1548. http://doi.org/10.1126/science.1083430

Zou, L., Liu, D., & Elledge, S. J. (2003). Replication protein A-mediated recruitment and activation of Rad17 complexes. *Proceedings of the National Academy of Sciences*, *100*(24), 13827–13832. http://doi.org/10.1073/pnas.2336100100

Acknowledgements

I would like to express my deep gratitude to my PhD supervisor and mentor Boris Pfander. Thank you for your enthusiastic guidance, being open for my ideas and supporting me in my scientific development. I am lucky that you cared so much about our work and were always available for discussions and advice. Thanks for trusting me to swim with the sharks of the DNA repair field from the very beginning.

I would like to particularly thank Stefan Jentsch, for letting us be a part of your scientific family and establishing an inspiring, stimulating environment along with generous support. I was very impressed with your intuition when it came to implications of scientific ideas and your passion for molecular details and mechanisms, and I have greatly benefitted from your influence.

I thank my PhD committee Prof. Klaus Förstemann, Prof. Elena Conti, Prof. Julian Stingele, PD Dr. Dietmar Martin, Prof. Karl-Peter Hopfner and particularly my doctoral supervisor at the LMU, Prof. Roland Beckmann.
Furthermore, I thank the members of my TAC committee Prof. Andreas Ladurner, Prof. Stephan Gruber and Prof. Philipp Korber for their valuable input at all stages of my projects.

I am especially grateful for the immense experimental support from Uschi, for your excellent work and great times as your bench neighbor. Thanks for adventurous car rides, one of which ended with a journey from UK to US.

Thanks also to the technicians of the Jentsch department Sven, Dirk, Katrin, Ulla, Jochen, Alex, Massimo and Ruzika as well as Klara for their valuable support.

Moreover, I would like to thank all scientific collaborators that contributed to the success of our work; Dominik Boos, Pedro Ferreira, Dalia Gritenaite for invaluable contributions to the Fun30 project, and Michael Lisby for fantastic microscopy on the checkpoint project. Furthermore, I would like to thank LAFUGA, Tobias Straub, Assa Yeroslawitz and Claudio Lademann for help with measuring and analyzing ChIP-chip and ChIP-seq data, members of the MPI Core Facility for Mass Spec and Sequencing and Zuzana Storchova for support with RPA foci microscopy and cell culture.

Major personal and scientific happiness and success during my PhD would not have been possible without my colleagues who contributed with scientific discussions and bench company, the mandatory coffee breaks, occasional Snakebites and overall friendship. Here, I would like to thank all members of the Molecular Cell Biology department of Stefan Jentsch, Zuzana Storchova, Karl Duderstadt and Boris Pfander. I had great times working side-by-side with everyone in the MCB department and later the NWG wing. Thanks for inspiring discussions, help whenever needed and a fun time in and outside the lab. A special thanks goes to Jörg, Max and Claudio from Stefan's lab, for teaching me my favourite method and the cheerful company.

A great thanks goes to my colleagues from Boris' lab over the years (aka the Sharkaromyces); Uschi, Lissa, Giulia, Fabi, Dalia, Kalle, Martina, Lorenzo, Julia, Leo and my students Jenny, Clara and Ryan. I appreciate our team spirit and great atmosphere in the lab.
I particularly thank Dalia, you raised me from baby PhD to lab granny and you became family to me. Special thanks goes to Kalle, for being my tower of strength in the lab and a great friend along the whole journey (the Sam to my Frodo). No thanks instead for maintaining our Mount Diabetes. Thanks to Julia for coffee telepathy and being my partner in crime during acquisition of new lab equipment. Thank you Martina and Lorenzo for bringing along the italian spirit, great cakes by Martina and philosophical talks with Lorenzo. Leo, have fun with Fun.

I would like to express my gratitude to the IMPRS school run by Hans-Jörg, Maxi and Ingrid for providing a framework of lectures and workshops that greatly complemented the PhD work.

I am grateful for my PhD fellowship awarded by the FCI, for believing in our work and providing financial support to realize our projects.

Finally, a warm thanks goes to my friends and family for love, support, understanding and distraction during the time of my PhD. Special thanks to my mum, my brother and grandparents for believing in me and supporting me unconditionally, for giving me the freedom to find my own way and backing me up when necessary. Without you this would not have been possible.

Publications and manuscripts

2014

Gritenaite, D., Princz, L. N., Szakal, B., **Bantele, S. C. S.**, Wendeler, L., Schilbach, S., et al. (2014). A cell cycle-regulated Slx4-Dpb11 complex promotes the resolution of DNA repair intermediates linked to stalled replication. ***Genes and Development***, *28*(14), 1604–1619. doi:10.1101/gad.240515.114.

2017

Bantele, S.C.S., Ferreira, P., Gritenaite, D., Boos, D. & Pfander, B. (2017).Targeting of the Fun30 nucleosome remodeller by the Dpb11 scaffold facilitates cell cycle-regulated DNA end resection. ***eLife***. pii: e21687. doi: 10.7554/eLife.21687.

Di Cicco, G., **Bantele, S.C.S.**, Reusswig, K-U., Pfander, B. (2017). A cell cycle-independent mode of the Rad9-Dpb11 interaction is induced by DNA damage. ***Scientific Reports*** 7(1):11650. doi:10.1038/s41598-017-11937-z.

manuscript in revision

Bantele S.C.S., Lisby M., Pfander B. Quantitative signalling mechanisms in response to DNA damage.

eLIFE elifesciences.org

RESEARCH ARTICLE

Targeting of the Fun30 nucleosome remodeller by the Dpb11 scaffold facilitates cell cycle-regulated DNA end resection

Susanne CS Bantele[1], Pedro Ferreira[2], Dalia Gritenaite[1], Dominik Boos[2], Boris Pfander[1]*

[1]DNA Replication and Genome Integrity, Max Planck Institute of Biochemistry, Martinsried, Germany; [2]Centre for Medical Biotechnology, Molecular Genetics II, University Duisburg-Essen, Essen, Germany

Abstract DNA double strand breaks (DSBs) can be repaired by either recombination-based or direct ligation-based mechanisms. Pathway choice is made at the level of DNA end resection, a nucleolytic processing step, which primes DSBs for repair by recombination. Resection is thus under cell cycle control, but additionally regulated by chromatin and nucleosome remodellers. Here, we show that both layers of control converge in the regulation of resection by the evolutionarily conserved Fun30/SMARCAD1 remodeller. Budding yeast Fun30 and human SMARCAD1 are cell cycle-regulated by interaction with the DSB-localized scaffold protein Dpb11/TOPBP1, respectively. In yeast, this protein assembly additionally comprises the 9-1-1 damage sensor, is involved in localizing Fun30 to damaged chromatin, and thus is required for efficient long-range resection of DSBs. Notably, artificial targeting of Fun30 to DSBs is sufficient to bypass the cell cycle regulation of long-range resection, indicating that chromatin remodelling during resection is underlying DSB repair pathway choice.
DOI: 10.7554/eLife.21687.001

***For correspondence:** bpfander@biochem.mpg.de

Competing interests: The authors declare that no competing interests exist.

Funding: See page 17

Received: 21 September 2016
Accepted: 03 January 2017
Published: 12 January 2017

Reviewing editor: Gregory Ira, Baylor College of Medicine, United States

Introduction

DNA end resection – the nucleolytic digestion of the 5' strands of a DSB – is essential for the initiation of homologous recombination (HR) or related recombination-based mechanisms (reviewed in [***Cejka, 2015***; ***Symington, 2014***; ***Symington and Gautier, 2011***]). At the same time, resection interferes with ligation-based repair (non-homologous end-joining, NHEJ) and thus is the critical step for repair pathway choice. In mitotically dividing cells, recombination-based repair critically depends on the presence of a sister-chromatid. DSB repair pathway choice and accordingly DNA end resection are therefore highly regulated during the cell cycle: in G1 phase, little resection occurs and NHEJ is therefore favoured. Conversely, in S, G2 and M phase, resection is up-regulated and HR becomes more prevalent (***Cejka, 2015***; ***Ira et al., 2004***; ***Symington, 2014***; ***Symington and Gautier, 2011***).

The nucleases that mediate resection can be subdivided into resection initiation (by Mre11-Rad50-Xrs2 and Sae2 in budding yeast) and long-range resection (by Exo1 or Dna2 with Sgs1-Top3-Rmi1 in budding yeast) pathways (***Cannavo and Cejka, 2014***; ***Cejka et al., 2010***; ***Mimitou and Symington, 2008***; ***Niu et al., 2010***; ***Zhu et al., 2008***). So far, Sae2 and Dna2 were shown to be cell cycle - controlled by cyclin-dependent kinase (CDK) phosphorylation in yeast (***Chen et al., 2011***; ***Huertas et al., 2008***) and EXO1 in human cells (***Tomimatsu et al., 2014***). Notably, however, a bypass of this control is not sufficient to allow efficient end resection to occur in G1, suggesting that other factors may be involved in the cell cycle control of DNA end resection.

eLife digest DNA is continually exposed to chemicals and radiation that cause various forms of DNA damage. One of the most toxic forms of DNA damage is the double strand break, in which both strands of the double helix are broken. These breaks can be mended in two ways: by directly joining the broken ends together, or via a process called homologous recombination. In homologous recombination, a duplicate DNA molecule is used as a template to repair the broken DNA strands. These duplicates only form during particular phases of the cell division cycle, which limits when homologous recombination can take place.

A cell can choose which pathway it uses to repair double strand breaks. However, the first step of homologous recombination – trimming the broken DNA ends in a process called resection – commits a cell to the homologous recombination repair pathway. Cell cycle kinases regulate the cell division cycle and control DNA end resection. This control takes two forms: on the one hand by regulating whether the enzymes that trim the DNA ends are active; and on the other hand by regulating the remodelling of the structure into which DNA is packaged, which is called chromatin. However, it is not known which of these two targets is the limiting factor that determines whether homologous recombination occurs.

A protein called Fun30 that remodels chromatin had been found to be important for promoting resection in budding yeast. Bantele et al. now reveal how the activity of Fun30 is regulated by the cell cycle to limit extensive resection to certain cell cycle phases, where homologous recombination is wanted. During those stages, cell cycle kinases add phosphate groups to Fun30. This enables Fun30 to engage in a protein complex that directs Fun30 to the site of a double strand break to facilitate the resection process.

Bantele et al. also studied artificial versions of Fun30 that were directly fused to components of the protein complex, and so bypassed the controls that limit homologous recombination to particular phases of the cell cycle. These forms of Fun30 enabled resection to take place in phases of the cell cycle where it does not normally occur. This suggests that the remodelling of chromatin by Fun30 is a critical step at which resection is regulated by the cell cycle.

Further experiments showed that the cell cycle regulation of human proteins that are equivalent to Fun30 and another protein in the resection complex is similar to that seen for the yeast proteins. In the future, knowing how these proteins are regulated during resection could help researchers to develop new gene editing methods based on homologous recombination that can be used in cells at any stage of the cell cycle.

DOI: 10.7554/eLife.21687.002

Resection is also influenced by the surrounding chromatin. Nucleosomes themselves can be inhibitory to resection enzymes (**Adkins et al., 2013**). Additionally, nucleosome-associated proteins such as budding yeast Rad9 or its functional ortholog in humans, 53BP1, can inhibit resection (**Bunting et al., 2010**; **Lazzaro et al., 2008**; **Trovesi et al., 2011**). Consistent with a barrier function of chromatin and/or Rad9, nucleosome remodellers are recruited to DSBs and promote resection, although the mechanism is poorly understood (**Bennett and Peterson, 2015**; **Bennett et al., 2013**; **Chai et al., 2005**; **Morrison et al., 2004**; **van Attikum et al., 2007**, **2004**). The Swr1-like family remodeller Fun30 (SMARCAD1 in humans) was found to be a critical regulator of resection (**Chen et al., 2012**; **Costelloe et al., 2012**; **Eapen et al., 2012**). Fun30 localizes to chromatin surrounding DSBs and *fun30*△ mutant cells show a pronounced defect in long-range resection (**Chen et al., 2012**; **Costelloe et al., 2012**; **Eapen et al., 2012**). Importantly, also SMARCAD1 promotes DNA end resection in human cells, suggesting evolutionary conservation (**Costelloe et al., 2012**). Fun30 itself is a substrate for CDK phosphorylation (**Chen et al., 2012**, **2016**; **Ubersax et al., 2003**), but it has remained unclear by which mechanism Fun30 function is regulated during the cell cycle, how Fun30 is targeted to DNA lesions and if this regulation imposes a bottleneck in the regulation of DNA end resection.

Here, we show that CDK phosphorylation enables Fun30 to form a complex with the phosphoprotein-binding scaffold protein Dpb11 and the DNA damage sensor 9-1-1. Formation of this complex is required for proper localization of Fun30 and for efficient long-range resection in M

phase cells. Notably, when we bypass the CDK requirement by directly fusing Fun30 to a subunit of the 9-1-1 complex, we observe long-range resection even in G1–arrested cells. This suggests that the cell cycle regulation of long-range resection can be bypassed solely by artificially targeting Fun30 to DSBs. Finally, we show that also human SMARCAD1 binds to TOPBP1 (human ortholog of Dpb11) in a CDK phosphorylation-dependent manner that involves conserved interaction surfaces, suggesting that the formation of a Fun30-Dpb11 complex is a conserved mechanism of cell cycle regulation that could control DNA end resection and repair pathway choice throughout eukaryotes.

Results

Cell cycle-dependent targeting of Fun30 by Dpb11

We identified Fun30 in a two-hybrid screen for interactors of the scaffold protein Dpb11. Dpb11 is a critical regulator of genome stability in budding yeast and as such is found in several distinct protein complexes (**Gritenaite et al., 2014**; **Ohouo et al., 2010**, **2013**; **Pfander and Diffley, 2011**; **Puddu et al., 2008**; **Tanaka et al., 2007**; **Zegerman and Diffley, 2007**). Crucial for the formation of these complexes are the two tandem BRCT domains of Dpb11, which are phospho-protein binding modules (**Leung and Glover, 2011**) specific for discrete sets of phosphorylation-dependent interactors. In case of Fun30, the interaction is mediated by BRCT1+2, but not BRCT3+4 (**Figure 1A**, **Figure 1—figure supplement 1**). Using Dpb11 expressed from the strong GPD promoter, we also observed an interaction between Fun30^{3FLAG} and Dpb11 in co-immunoprecipitation (Co-IP) experiments (**Figure 1B**). All Dpb11 complexes characterized so far are cell cycle-regulated (**Gritenaite et al., 2014**; **Ohouo et al., 2013**; **Pfander and Diffley, 2011**; **Tanaka et al., 2007**; **Zegerman and Diffley, 2007**). Thus, we tested the interaction between Dpb11 and Fun30 from cells at different cell cycle stages. We observed that Fun30 interacted with Dpb11 only during late S to M phase, but not in G1 (**Figure 1B–C**, **Figure 1—figure supplement 2**) and this interaction was not influenced by DNA damage (**Figure 1D**).

Since Fun30 is phosphorylated by CDK (**Chen et al., 2012**, **2016**; **Ubersax et al., 2003**) and Dpb11 was shown to bind several CDK targets (**Gritenaite et al., 2014**; **Pfander and Diffley, 2011**; **Tanaka et al., 2007**; **Zegerman and Diffley, 2007**), we tested if CDK phosphorylation mediates the Fun30-Dpb11 interaction. Indeed, upon CDK inhibition (using the *cdc28-as1* allele and 1-NMPP1 inhibition) Dpb11 binding to Fun30 was strongly reduced (**Figure 1E**). Accordingly, purified Fun30^{3FLAG} was able to interact with ^{GST}Dpb11-BRCT1+2 in vitro but only after pre-phosphorylation by CDK (**Figure 1F**), suggesting that the Fun30-Dpb11 interaction as well as its regulation by CDK phosphorylation are direct. Therefore, we sought to identify the CDK phosphorylation sites on Fun30, which are relevant for Dpb11 binding. Interaction mapping using truncated constructs placed the Dpb11 interaction site close to the N-terminus of Fun30 (**Figure 1G**, **Figure 1—figure supplement 3**). Within this region, we identified S20 as well as S28 as critical residues for the Fun30-Dpb11 interaction by two-hybrid and Co-IP binding assays using non-phosphorylatable versions of Fun30 (**Figure 1H–I**, **Figure 1—figure supplement 4**). This suggests that phosphorylation of both residues may create a composite binding surface for Dpb11 BRCT1+2, perhaps similar to the Dpb11-binding surfaces on Rad9 and Sld3 (**Pfander and Diffley, 2011**; **Tanaka et al., 2007**; **Zegerman and Diffley, 2007**; **Zegerman et al., 2010**).

It seemed likely that Dpb11 is involved in targeting Fun30 to DNA lesions. We therefore tested recruitment of *WT* Fun30^{3FLAG} or the corresponding *fun30-SSAA* variant to a site-specific, non-repairable DSB using chromatin immunoprecipitation (ChIP). Indeed, we observed that Fun30-SSAA binding to regions distal of the DSB was reduced compared to *WT* (8–20 kb, **Figure 1J**, **Figure 1—figure supplement 5**), while both versions bound similarly to the immediate vicinity of the DSB (1–3 kb, **Figure 1J**, **Figure 1—figure supplement 5**). This result thus confirms recent observations showing a DSB recruitment defect of *fun30-S20A* and *fun30-S28A* mutants (**Chen et al., 2016**).

Importantly, we could expand these data by generating an experimental tool, which restores the Fun30-Dpb11 interaction in a phosphorylation-independent manner. Since conventional phosphomimetic mutations failed to promote binding (data not shown), we generated a covalent fusion of the Fun30-SSAA protein directly to Dpb11△N lacking BRCT1+2 (*FUN30-AA-DPB11-276-C* expressed as the only copy of Fun30 from the endogenous promoter, referred to as *FUN30-*

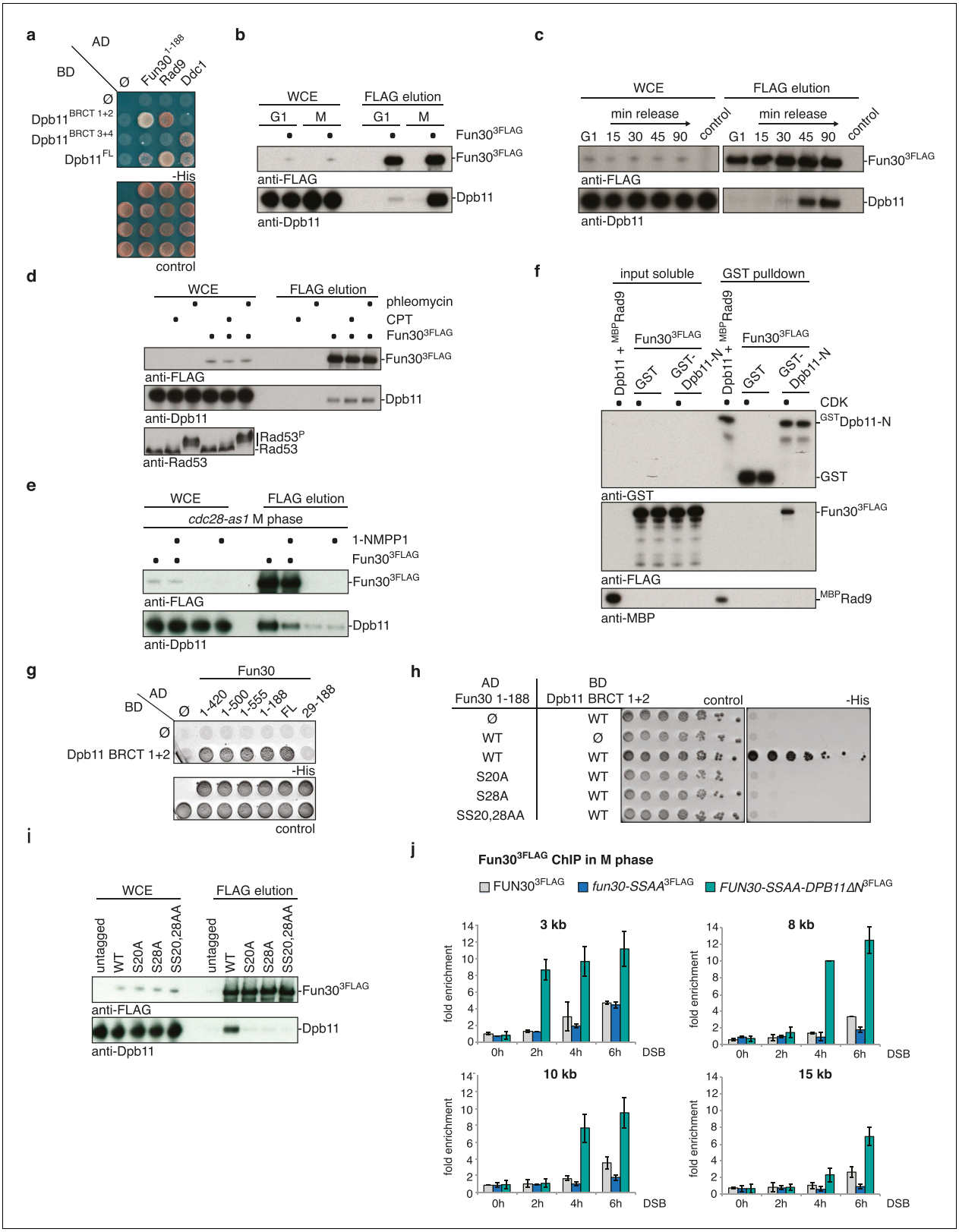

Figure 1. Fun30 and Dpb11 interact in a cell cycle- and CDK phosphorylation-dependent manner and this targets Fun30 to DSBs. (**a**) Two-hybrid assay with GAL4-AD and -BD constructs as indicated reveals a physical interaction between the N-terminal region of Fun30 (aa 1–188) and the BRCT1+2 domain of Dpb11. Rad9 and Ddc1 represent known interactors of BRCT1+2 and BRCT3+4, respectively. (**b–e**) Characterization of the Fun30-Dpb11 interaction by Fun30^{3FLAG} Co-IP experiments. Dpb11 was expressed from the strong, constitutive GPD promoter. (**b**) Fun30^{3FLAG} specifically binds

Figure 1 continued on next page

Figure 1 continued

Dpb11 in cells arrested in M but not G1 phase. (**c**) Fun30^{3FLAG} purified from cells synchronously progressing through the cell cycle binds Dpb11 only at 45' and 90' time points corresponding to late S and M phase (***Figure 1—figure supplement 2*** for FACS analysis and western analysis of cell cycle progression). (**d**) No enhancement of the Fun30-Dpb11 interaction by CPT or phleomycin treatment as measured by Fun30^{3FLAG} Co-IP. For DNA damage treatment, 50 µM CPT or 50 µg/ml phleomycin were added to asynchronously dividing yeast cells. DNA damage checkpoint activation was measured by Rad53 phosphorylation in IP extracts (lowest blot panel). (**e**) CDK inhibition using the *cdc28-as1* allele and 1-NMPP1 treatment diminishes the Fun30^{3FLAG}-Dpb11 interaction in M phase arrested cells. (**f**) Purified Fun30 interacts with a BRCT1+2 fragment of Dpb11 in the presence of CDK phosphorylation. Purified Fun30^{3FLAG} or the positive control ^{MBP}Rad9 (***Pfander and Diffley, 2011***) were incubated with a model CDK and ATP before binding to bead-bound ^{GST}Dpb11 BRCT1+2. (**g**) Mapping analysis of the two-hybrid interaction between Fun30 and Dpb11 reveals a binding site close to the N-terminus of Fun30. (**h–i**) Putative CDK sites on Fun30 (S20 and S28) are required for Dpb11 binding. (**h**) Two-hybrid assay as in (**a**) but in five-fold serial dilution and with *WT*, *S20A*, *S28A* and *SS20,28AA* variants of Gal4-AD-Fun30$^{1-188}$. (**i**) Co-IP as in (**b**) but with mutant variants of Fun30^{3FLAG} growing asynchronously. (**j**) Efficient Fun30 localization to damaged chromatin requires the Dpb11-Fun30 interaction. ChIP of Fun30^{3FLAG} to chromatin locations 3, 8, 10 and 15 kb distant of a non-repairable DSB induced at the MAT locus in M phase-arrested cells. *fun30* mutants were expressed from the endogenous promoter as only copy of *FUN30*. The *FUN30-DPB11* fusion contains *fun30-SSAA* and *dpb11△N* mutations. *WT*, *fun30-SSAA* and *FUN30-DPB11 fusion* cells were crosslinked at indicated timepoints after DSB induction. Plotted values represent means from two independent experiments, error bars represent standard deviations.

DOI: 10.7554/eLife.21687.003

The following figure supplements are available for figure 1:

Figure supplement 1. Expression control of two-hybrid constructs used in ***Figure 1A***.

DOI: 10.7554/eLife.21687.004

Figure supplement 2. Control of the cell cycle states of the experiment in ***Figure 1C***.

DOI: 10.7554/eLife.21687.005

Figure supplement 3. Expression control of two-hybrid constructs used in ***Figure 1G***.

DOI: 10.7554/eLife.21687.006

Figure supplement 4. Expression control of two-hybrid constructs used in ***Figure 1H***.

DOI: 10.7554/eLife.21687.007

Figure supplement 5. Efficient Fun30 localization to damaged chromatin requires the Dpb11-Fun30 interaction.

DOI: 10.7554/eLife.21687.008

DPB11 fusion in the following). Importantly, the fusion protein localized efficiently to damaged chromatin and thus restored the defect of the *fun30-SSAA* mutation (***Figure 1J***, ***Figure 1—figure supplement 5***). This finding suggests that the interaction with Dpb11 is indeed involved in targeting Fun30 to DSBs and that the covalent fusion is sufficient to bypass the CDK regulation of Fun30. Notably, DSB recruitment of the Fun30-Dpb11 fusion protein was stronger than Fun30 consistent with the replacement of a transient, PTM-dependent interaction by a covalent interaction. Therefore, we reason that the *FUN30-DPB11* fusion deregulates Fun30 in two ways: first, it uncouples Fun30 from its cell cycle regulation. Second, it leads to enhanced DSB localization to DSBs, thus potentially enhancing Fun30 activity at damaged chromatin.

We also note that the apparently normal recruitment of Fun30-SSAA to the immediate vicinity of the DSB could be explained by an additional CDK phosphorylation-independent, but resection-dependent recruitment mechanism, such as via binding to RPA (***Chen et al., 2012***). Our data thus suggest the existence of two Fun30–targeting mechanisms: one that is Dpb11-dependent and recruits Fun30 to sites of ongoing resection, and a second that is Dpb11-independent and tethers Fun30 to DNA that has already been resected.

The Fun30-Dpb11 complex is required for efficient long-range resection

We utilized our system of abolishing and constitutively forcing Fun30 binding to Dpb11 in order to investigate the biological function of the Dpb11-dependent Fun30 targeting mechanism and its role in regulating DNA end resection. We measured resection at an HO-induced, non-repairable DSB in M phase-arrested cells using the combined read-out of (a) the accumulation of the ssDNA-binding protein RPA (***Figure 2A***, upper panel) around the DSB by ChIP and (b) the specific DNA loss (occurring due to ssDNA formation, ***Figure 2A***, lower panel). Indeed, compared to *WT* cells, *fun30△* mutants showed a pronounced defect in long-range resection, visible by a reduced spreading of both RPA-ChIP and DNA loss, to regions greater than 10 kb away from the break (***Figure 2A***, ***Figure 2—figure supplement 1***), confirming previous observations (***Chen et al., 2011***, ***2012***; ***Costelloe et al., 2012***; ***Eapen et al., 2012***). Notably, the same defect in long-range resection

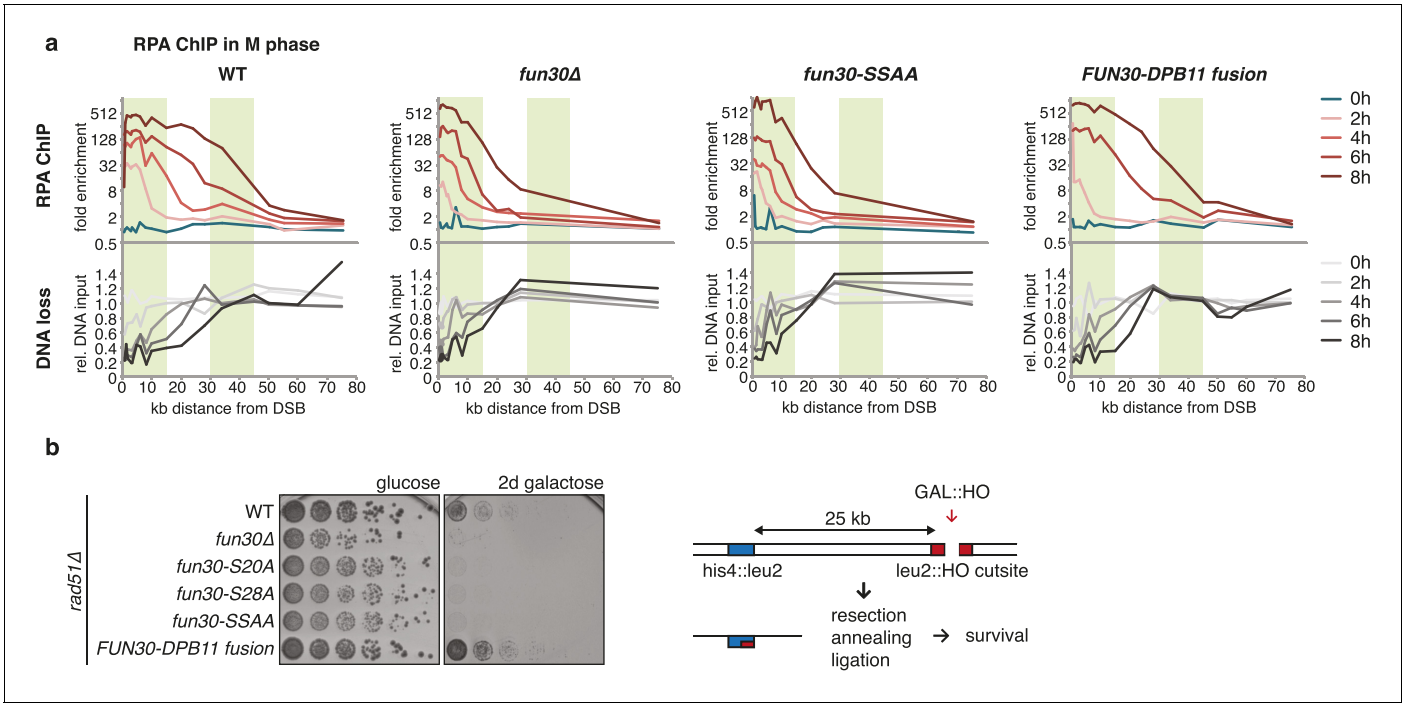

Figure 2. The Fun30-Dpb11 complex is required for efficient long-range resection. (**a**) Long-range resection of a DSB is dependent on the Fun30-Dpb11 interaction. A non-repairable DSB at MAT was induced in M phase-arrested *WT*, *fun30*△, *fun30-SSAA* and *FUN30-DPB11* fusion strains and DNA end resection measured at indicated times. Upper panel: fold enrichment of a given locus in an RPA ChIP relative to undamaged control loci. Lower panel: DNA loss relative to control loci located in non-damaged chromatin. (**b**) Single-strand annealing (SSA) is dependent on the Fun30-Dpb11 interaction. *FUN30* mutants as indicated were combined with the *rad51*△ deletion, a DSB at the leu2::HO cutsite was induced by plating cells on galactose. Cells need to resect 25 kb up to the homologous his4::leu2 locus in order to survive by SSA.

DOI: 10.7554/eLife.21687.009

The following figure supplement is available for figure 2:

Figure supplement 1. The Fun30-Dpb11 interaction is required for efficient long-range resection.

DOI: 10.7554/eLife.21687.010

was also observed in the Dpb11-binding deficient *fun30-SSAA* mutant and was fully restored by the *FUN30-DPB11* fusion (***Figure 2A***, ***Figure 2—figure supplement 1***). To corroborate these findings, we also analysed resection-dependent DSB repair in a single-strand annealing (SSA) assay, where cellular survival upon an HO-induced DSB in the absence of Rad51 critically depends on the efficient resection of 25 kb of DNA (***Figure 2B***, [***Vaze et al., 2002***]). In fact, Dpb11-binding deficient *fun30* mutants were deficient in SSA-mediated survival and this defect was completely rescued by covalent fusion of Fun30-SSAA to Dpb11 (***Figure 2B***). Thus, the CDK-regulated interaction between Fun30 and Dpb11 is required for efficient long-range resection as well as subsequent resection-coupled repair.

Fun30 participates in chromatin organization in the absence of DNA damage (***Neves-Costa et al., 2009***) and previous studies could therefore not rule out the possibility that the DNA end resection defect of the *fun30*△ mutant is a consequence of general changes in chromatin organization (***Chen et al., 2012***; ***Costelloe et al., 2012***; ***Eapen et al., 2012***). However, we found that the *fun30-SSAA* mutant (unlike the *fun30*△ mutant) did not display any defect in silencing at telomeres or at the silent mating type locus and thus differs from the *fun30*△ mutant (***Figure 3***). The *fun30-SSAA* mutant thus separates Fun30 functions and the associated resection phenotype of this mutant therefore provides strong support for a direct role of Fun30 and the Fun30-Dpb11 complex during DNA end resection.

Mutants with DNA end resection defects such as *exo1*△ *sgs1*△, *sae2*△ or *fun30*△ are hypersensitive towards the Top1 inhibitor camptothecin (CPT) (***Chen et al., 2012***; ***Costelloe et al., 2012***; ***Eapen et al., 2012***; ***Neves-Costa et al., 2009***) (***Figure 4A–C***), most likely because of repair defects

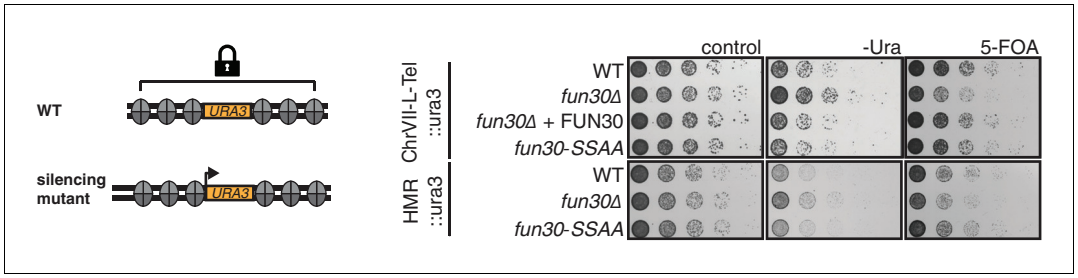

Figure 3. The Fun30-Dpb11 interaction is not involved in Fun30-dependent gene silencing at telomeric heterochromatin and a silent mating type locus. The silencing defect of the *fun30*Δ mutant is not recapitulated by the *fun30-SSAA* mutant. Two silencing tester strains were used: the first (upper panels) had URA3 integrated in telomeric heterochromatin at the end of the left arm of chromosome VII, the second (lower panels) had URA3 integrated at the HML silent mating type locus. A silencing defect leads to enhanced growth on –Ura medium and less growth on medium supplemented with 5-FOA (e.g. *fun30*Δ). Shown is a spotting in 5-fold serial dilutions on non-selective medium, medium lacking uracil or containing 5-FOA.

DOI: 10.7554/eLife.21687.011

of replication-borne DSBs at CPT-induced Top1 stall sites. Indeed, also the *fun30-SSAA* mutant showed hyper-sensitivity to CPT albeit not as strong as the *fun30* deletion. Importantly, the CPT sensitivity of *fun30-SSAA* was rescued by expressing the covalent *FUN30-DPB11* fusion (***Figure 4A***, ***Figure 4—figure supplement 1***), emphasizing again the importance of the Fun30-Dpb11 interaction for DSB repair.

Genetic evidence suggests that Fun30 may promote DNA end resection by antagonizing the resection inhibitor Rad9 (***Chen et al., 2012***). Similar to what has been described for the *fun30*△ mutant, we observed that the CPT-hypersensitivity of the *fun30-SSAA* was suppressed by an additional *rad9* deletion (***Figure 4D***), suggesting that the Fun30-Dpb11 complex antagonizes Rad9. Interestingly, Rad9 also binds to Dpb11, and Fun30 and Rad9 share the same interaction site on Dpb11 (***Pfander and Diffley, 2011***). While it is currently unknown whether Dpb11-associated Rad9

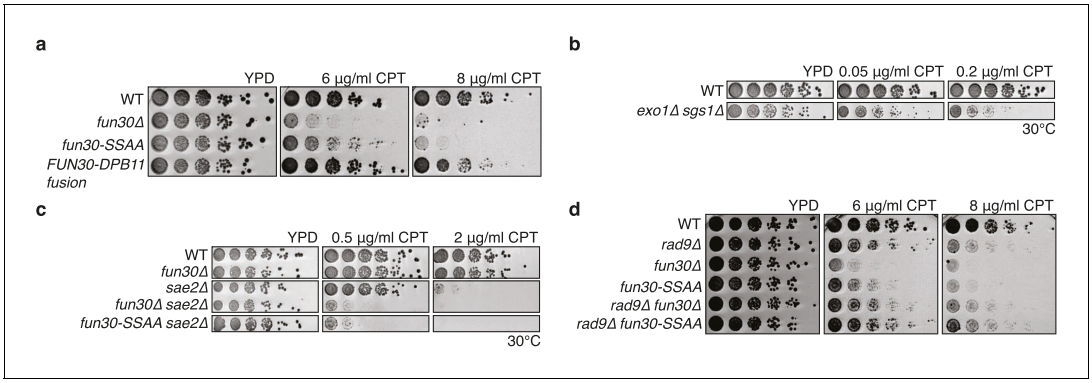

Figure 4. The Fun30-Dpb11 interaction is required for the response towards CPT, as is functional long- and short-range resection. (**a**) The Fun30-Dpb11 interaction is required for the response towards CPT. *WT*, *fun30*△, *fun30-SSAA* and *FUN30-DPB11 fusion* were spotted in five-fold serial dilutions on plates containing indicated amounts of CPT and incubated at 37°C for two days. (**b**) A double mutant of *exo1*Δ and *sgs1*Δ is hyper-sensitive to low doses of CPT. Spotting in 5-fold serial dilutions was incubated for two days at 30°C. (**c**) The *fun30*Δ/*fun30-SSAA* mutants enhance the CPT hypersensitivity of *sae2*Δ mutants. Cells were spotted in 5-fold serial dilutions and incubated for two days at 30°C. (**d**) A *rad9*Δ deletion rescues CPT hypersensitivity of *fun30*Δ and *fun30-SSAA* mutant alleles.

DOI: 10.7554/eLife.21687.012

The following figure supplements are available for figure 4:

Figure supplement 1. Mutants of Fun30 show no discernable phenotype upon chronic exposure to HU, MMS or phleomycin.

DOI: 10.7554/eLife.21687.013

Figure supplement 2. The catalytic activity of Fun30 is required for the suppression of the CPT phenotype in the context of the *FUN30-DPB11 fusion*.

DOI: 10.7554/eLife.21687.014

(in contrast to nucleosome-associated Rad9) contributes to the inhibition of DNA end resection, the overlapping binding site raised the possibility that Fun30 may interfere with Rad9 function via competition. Therefore, in order to exclude that the *FUN30-DPB11* fusion rescues resection simply by blocking the Rad9-Dpb11 interaction, we inactivated the ATPase activity of Fun30 by a Walker A motif mutation (K603R) in the context of the *FUN30-DPB11* fusion and found the K603R mutant fusion did not restore *WT* resistance to CPT (***Figure 4—figure supplement 2***). Therefore, competition does not explain the effects of the *FUN30-DPB11* fusion and the catalytic activity of Fun30 is required for the resection-promoting function of the Fun30-Dpb11 complex. Overall, these data thus suggest that cell cycle-regulated targeting of Fun30 by Dpb11 is required for efficient DNA end resection.

The 9-1-1 complex targets Fun30 to DSBs and – as artificial fusion with Fun30 - can be utilized to promote long-range resection in G1

In several organisms, recruitment of Dpb11 and its orthologs to DSBs has been shown to be facilitated by the 9-1-1 complex (***Delacroix et al., 2007***; ***Du et al., 2006***; ***Furuya et al., 2004***; ***Pfander and Diffley, 2011***; ***Puddu et al., 2008***), a signalling platform (***Parrilla-Castellar et al., 2004***) which is loaded at DNA damage sites. Given that 9-1-1 interacts with BRCT3+4 of Dpb11 (***Wang and Elledge, 2002***), we tested whether Dpb11 could simultaneously bind to Fun30 and 9-1-1. Indeed, Fun30^{3FLAG} co-precipitated the 9-1-1 subunits Mec3 and Ddc1 and this binding was absent in cells arrested in G1 or in the respective Dpb11 interaction-deficient mutants (*ddc1-T602A* or *fun30-SSAA*; ***Figure 5A–B***, ***Figure 5—figure supplement 1***). We thus conclude that Fun30, Dpb11 and 9-1-1 can form a ternary complex, which is regulated by the cell cycle stage (model in ***Figure 5—figure supplement 2***). Moreover, we observed a reduction of the Fun30 binding in the proximity of a DSB by ChIP, when we interfered either with the 9-1-1-Dpb11 interaction (*ddc1-T602A* mutant) or with the Fun30-Dpb11 interaction (*SLD3-DPB11ΔN* mutant strain, which expresses as only copy of *DPB11* a truncated version of Dpb11 lacking the Fun30 binding site, ***Zegerman and Diffley, 2007***), further supporting a role of 9-1-1 in targeting Fun30 to DSBs (***Figure 5C***).

Given that Dpb11 seems to function as an adaptor between Fun30 and 9-1-1, we also generated a covalent fusion of Fun30-SSAA and the 9-1-1 subunit Ddc1 (referred to as *DDC1-FUN30* fusion). Also this fusion rescued the CPT phenotype of the *fun30-SSAA* mutant in a manner that depended on the catalytic activity of Fun30 (***Figure 6A***, ***Figure 6—figure supplement 1***). The *DDC1-FUN30* fusion targeted Fun30 even more efficiently to damaged chromatin than the *FUN30-DPB11* fusion and, notably, the corresponding strain was able to survive at very high CPT concentrations, where little growth could be detected even for *WT* cells, indicating that the *DDC1-FUN30* fusion promotes hyper-resistance to CPT (***Figure 6A***). It is thus possible to at least partially overcome the limits of cellular resistance to CPT by providing very efficient targeting of Fun30 to damaged chromatin and uncoupling it from cell cycle control.

DNA end resection is up-regulated in S, G2, M phases of the cell cycle, thus shifting the DSB repair pathway choice from NHEJ to recombination-dependent mechanisms (***Cejka, 2015***; ***Symington and Gautier, 2011***). Previous efforts to bypass this regulation have focussed on nucleases (***Huertas et al., 2008***). Thus, we tested if the CDK-regulation of Fun30 may contribute to the cell cycle regulation of DNA end resection or may even be a limiting factor for this regulation. We used the *DDC1-FUN30* fusion, which in contrast to *WT* Fun30 efficiently localized to a DSB in G1 (***Figure 6B***, ***Figure 6—figure supplement 3***). This indicates that the fusion may in principle allow Fun30 to act on damaged chromatin in G1, consistent with 9-1-1 being loaded to damaged chromatin in G1 (***Barlow et al., 2008***; ***Janke et al., 2010***). Indeed, the *DDC1-FUN30* fusion protein promoted resection in G1 to a significantly larger reach compared to *WT* Fun30, since RPA recruitment could be observed up to 25 kb distance from the DSB (***Figure 6C***, ***Figure 6—figure supplement 3***). Notably, the spreading of resection under the *DDC1-FUN30* conditions was even more pronounced than in *WT* cells arrested in M phase (***Figure 6C***, ***Figure 6—figure supplement 3***). This effect is thus consistent with the very efficient targeting of Fun30 to DNA damage sites by the *DDC1-FUN30* fusion. This hyperactivation of resection thus indicates that forced tethering of Fun30 to DSB sites is able to bypass the bottleneck that limits long-range resection in G1.

It needs to be pointed out that within the resected region the fold enrichment of RPA recruitment and the extent of DNA loss was not restored to similar levels as observed in M phase (***Figure 6C***).

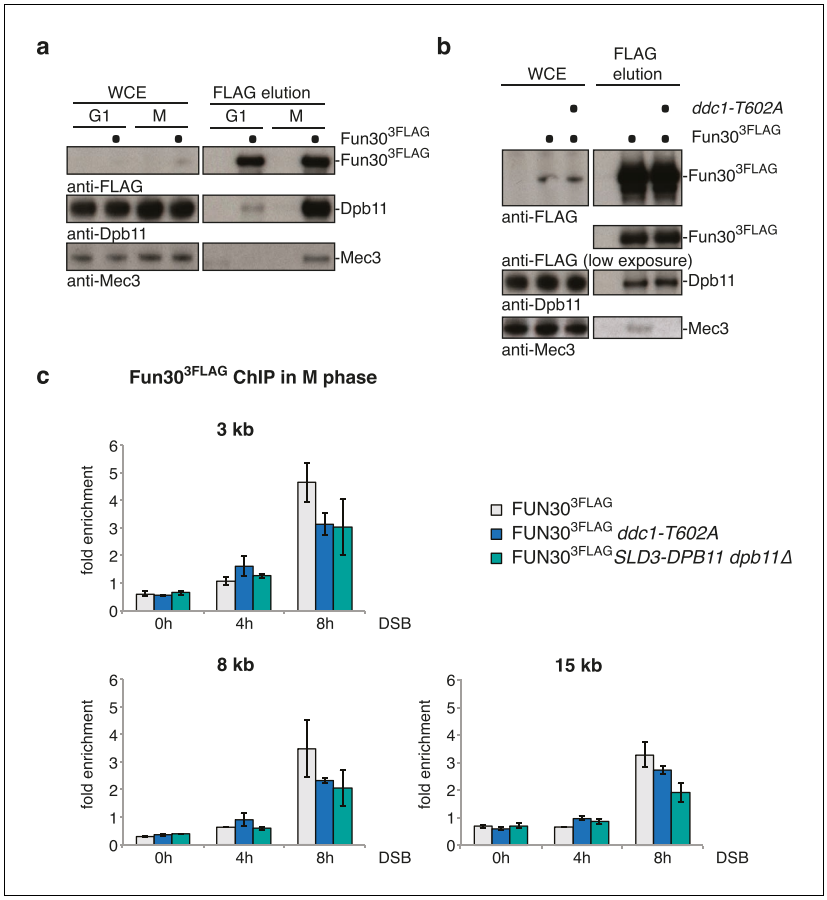

Figure 5. The 9-1-1 complex forms a ternary complex with Fun30-Dpb11. (**a**) Fun30, Dpb11 and 9-1-1 form a ternary complex. The 9-1-1 subunit Mec3 interacts with Fun30^{3FLAG} when purified from M phase cells, where also Dpb11 binds to Fun30. (**b**) The *ddc1-T602A* mutation abolishes binding of Mec3 to Fun30-Dpb11 in Fun30^{3FLAG} Co-IPs, but leaves the Fun30-Dpb11 interaction intact. (**c**) Mutants disrupting the interaction between 9-1-1 and Dpb11 (*ddc1-T602A*) or Fun30 and Dpb11 (*SLD3-dpb11ΔN*, lacks Fun30 binding site, only copy of Dpb11) impair efficient localization of Fun30 to DSBs in Fun30^{3FLAG} ChIPs of M phase-arrested cells. Experiment performed as in ***Figure 1J***, plotted values represent means of two independent experiments, error bars represent standard deviations.

DOI: 10.7554/eLife.21687.015

The following figure supplements are available for figure 5:

Figure supplement 1. The interaction between Fun30 and 9-1-1 depends on mutual interactions with Dpb11, suggesting that Dpb11 forms a molecular bridge in the Fun30-Dpb11-9-1-1 complex.

DOI: 10.7554/eLife.21687.016

Figure supplement 2. Model of the Fun30-Dpb11-9-1-1 association and its regulation.

DOI: 10.7554/eLife.21687.017

Moreover, precise ligation of a cut plasmid by NHEJ did not appear to be influenced by the *DDC1-FUN30* fusion (***Figure 7***). These data thus suggest that the overall cell cycle regulation of DNA end resection was not bypassed completely, presumably because other resection proteins and in particular resection initiation are additional targets of cell cycle regulation (***Albuquerque et al., 2008***; ***Chen et al., 2011***; ***Huertas et al., 2008***; ***Pfander and Diffley, 2011***; ***Zhang et al., 2009***). We therefore compared G1 resection in the *DDC1-FUN30* strain to another mutant – *sae2-S267E* – that is thought to at least partially bypass the CDK regulation of resection initiation (***Cannavo and Cejka, 2014***; ***Huertas, 2010***). Notably, the *sae2-S267E* mutant showed no increase in the reach of resection and only led to a slight increase in the fold enrichment of the RPA ChIP, both in *WT* and *DDC1-FUN30* background (***Figure 8***). Overall, these data are thus consistent with a model, whereby *sae2-S267E* partially bypasses the cell cycle regulation of resection initiation, while the *DDC1-FUN30*

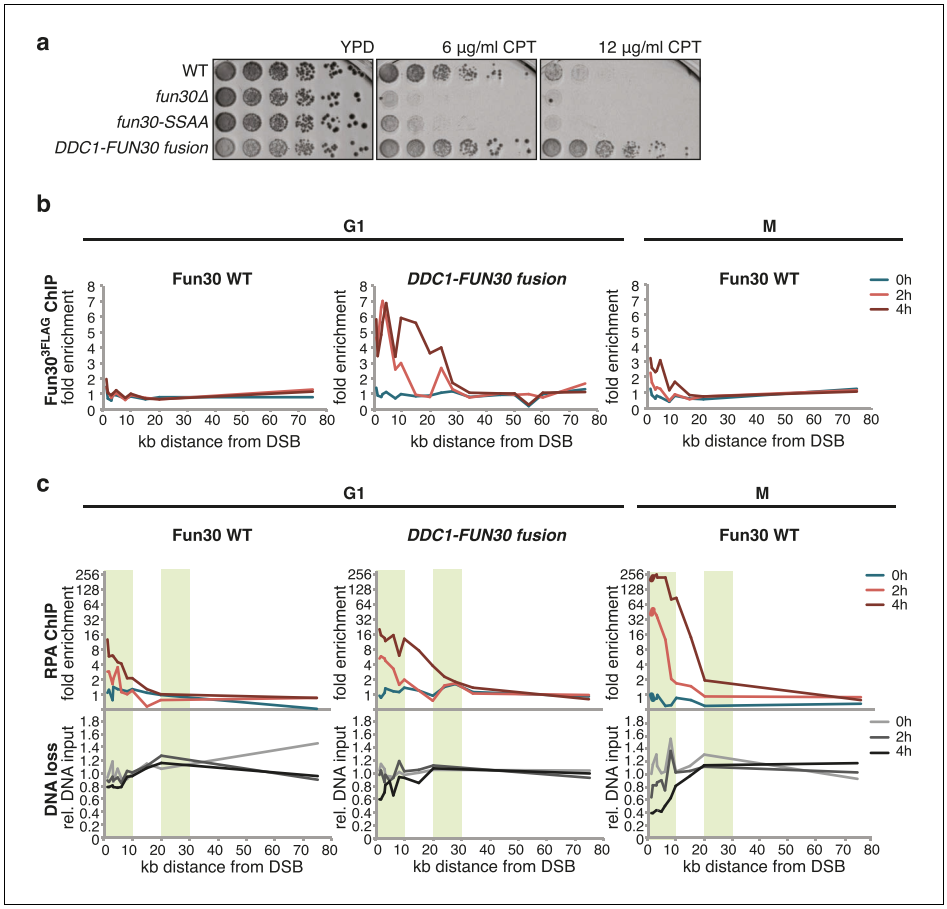

Figure 6. A covalent fusion of Fun30 to the 9-1-1 subunit Ddc1 generates a bypass of the cell cycle regulation of long-range resection. (**a**) The *DDC1-FUN30* fusion confers cellular hyper-resistance to CPT. Spotting of indicated strains as in ***Figure 4A***, but using CPT concentrations of up to 12 µg/ml. (**b**) The *DDC1-FUN30* fusion localizes efficiently to a DSB in G1-arrested cells. Fun30^{3FLAG} ChIPs from *WT*, *fun30-SSAA*, *FUN30-DPB11* and *DDC1-FUN30* cells as in ***Figure 1J***, but from G1 or M phase-arrested cells. Additional Fun30^{3FLAG} ChIP data can be found in ***Figure 6—figure supplement 3***. (**c**) The *DDC1-FUN30* fusion enhances long-range resection in G1-arrested cells. Resection assay as in ***Figure 2A***, but with G1 or M phase-arrested cells. Additional resection assay data can be found in ***Figure 6—figure supplement 3***.

DOI: 10.7554/eLife.21687.018

The following figure supplements are available for figure 6:

Figure supplement 1. The *DDC1-FUN30 fusion* rescues the CPT sensitivity of the *fun30*△ mutant in a manner that depends on the Fun30 catalytic activity.

DOI: 10.7554/eLife.21687.019

Figure supplement 2. Flow cytometric analysis of DNA content for experiments shown in ***Figure 6B–C*** and ***Figure 6—figure supplement 3***.

DOI: 10.7554/eLife.21687.020

Figure supplement 3. The *DDC1-FUN30 fusion* protein efficiently localizes to DSBs and promotes hyper-resection in M phase as well as allowing long-range resection in G1 phase.

DOI: 10.7554/eLife.21687.021

fusion bypasses the cell cycle regulation of long-range resection. This highlights that chromatin has a barrier function towards resection and that formation of the Fun30-Dpb11 complex is the limiting step that needs to be up-regulated during recombination-permissive cell cycle phases in order to overcome this barrier.

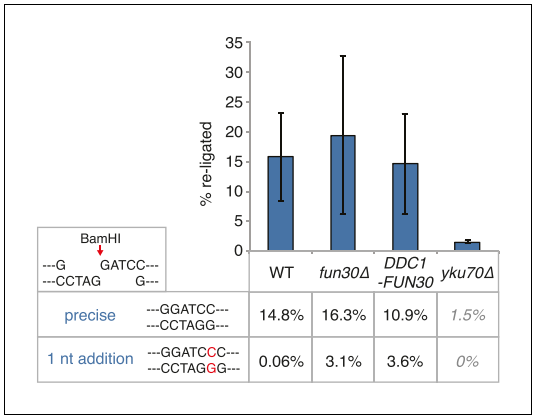

Figure 7. The *DDC1-FUN30* fusion does not significantly inhibit non-homologous end-joining (NHEJ). Precise re-ligation of BamHI-cut pRS316 as measured by cell viability on SC-Ura plates and subsequent sequencing of single colonies was dependent on Ku70 but not significantly affected in *DDC1-FUN30* of *fun30*Δ mutant cells. Plotted are values from three independent experiments representing the viability rate of cells on SC-Ura plates relative to the total cell number and the transformation efficiency of the mock-digested plasmid. Error bars represent standard deviations.

DOI: 10.7554/eLife.21687.022

Conservation of Fun30 regulation to human SMARCAD1

Fun30's role in promoting DNA end resection is conserved to its human ortholog SMARCAD1 (***Costelloe et al., 2012***; ***Densham et al., 2016***). Strikingly, in an independent screen we identified an N-terminal fragment of SMARCAD1 (aa 55–274) as interactor of TOPBP1 (using a TOPBP1 BRCT0-2 construct), the human ortholog of Dpb11. Furthermore, we found this interaction to require the phospho-protein binding sites of TOPBP1 BRCT1+2 (***Figure 9A***, ***Figure 9—figure supplement 1***). We verified the SMARCAD1-TOPBP1 interaction in a pulldown approach using purified GST-TOPBP1-BRCT0/1/2 fragments and in vitro phosphorylation of cell extracts with purified CDK. GFP-SMARCAD1-55-445 bound efficiently to GST-TOPBP1-BRCT0/1/2, but only after addition of active CDK to the cell extract (***Figure 9B***). This suggests that CDK phosphorylation promotes the interaction, similar to the regulation in yeast. We therefore queried for the TOPBP1 interaction site on SMARCAD1 using mutagenesis of CDK consensus motifs. Using this approach, we found that the T71A variant, but none of the other S/TP site mutants tested caused strongly reduced TOPBP1 binding in two-hybrid and Co-IP (***Figure 9C–D***, ***Figure 9—figure supplement 2***). These data therefore suggest that SMARCAD1 interacts with TOPBP1 via the CDK-site T71. To our surprise, we observed in two-hybrid experiments that human SMARCAD1 also interacted with yeast Dpb11 and in a manner that was dependent on the T71 phosphorylation site (***Figure 9E***, ***Figure 9—figure supplement 3***), despite low sequence conservation. This raised the possibility that SMARCAD1 and FUN30 could also functionally complement each other. Expression of SMARCAD1 from the inducible GAL-promoter lead only to a slight suppression of the CPT sensitivity of a *fun30*△ strain (data not shown), suggesting that there is an aspect of Fun30 function or regulation that is not recapitulated by SMARCAD1. In contrast, when we generated a SMARCAD1-Fun30 chimera lacking the Dpb11-binding region of Fun30 but containing the TOPBP1-binding region of SMARCAD1 (SMARCAD1-1-300-FUN30-30-C), this chimera was largely able to rescue the CPT sensitivity of the *fun30*△ mutant (***Figure 9F***, ***Figure 9—figure supplement 5***). In contrast, the

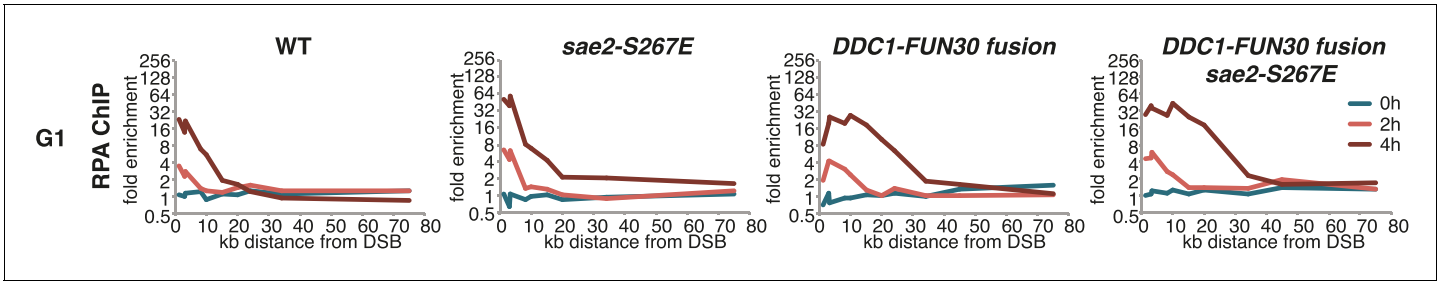

Figure 8. The *DDC1-FUN30* fusion specifically enhances long-range resection in G1, while the *sae2-S267E* phospho-mimicry leads to a small increase in resection initiation. The *sae2-S267E* mutant has little effect on the spreading of DNA end resection in G1, but slightly stimulates the RPA fold enrichment in *WT* and the *DDC1-FUN30* fusion mutant. This suggests that *sae2-S267E* in contrast to the *DDC1-FUN30* fusion does not affect long-range resection. DNA end resection in the indicated strains was analysed by RPA ChIP as in ***Figure 5C*** but with G1 arrested cells.

DOI: 10.7554/eLife.21687.023

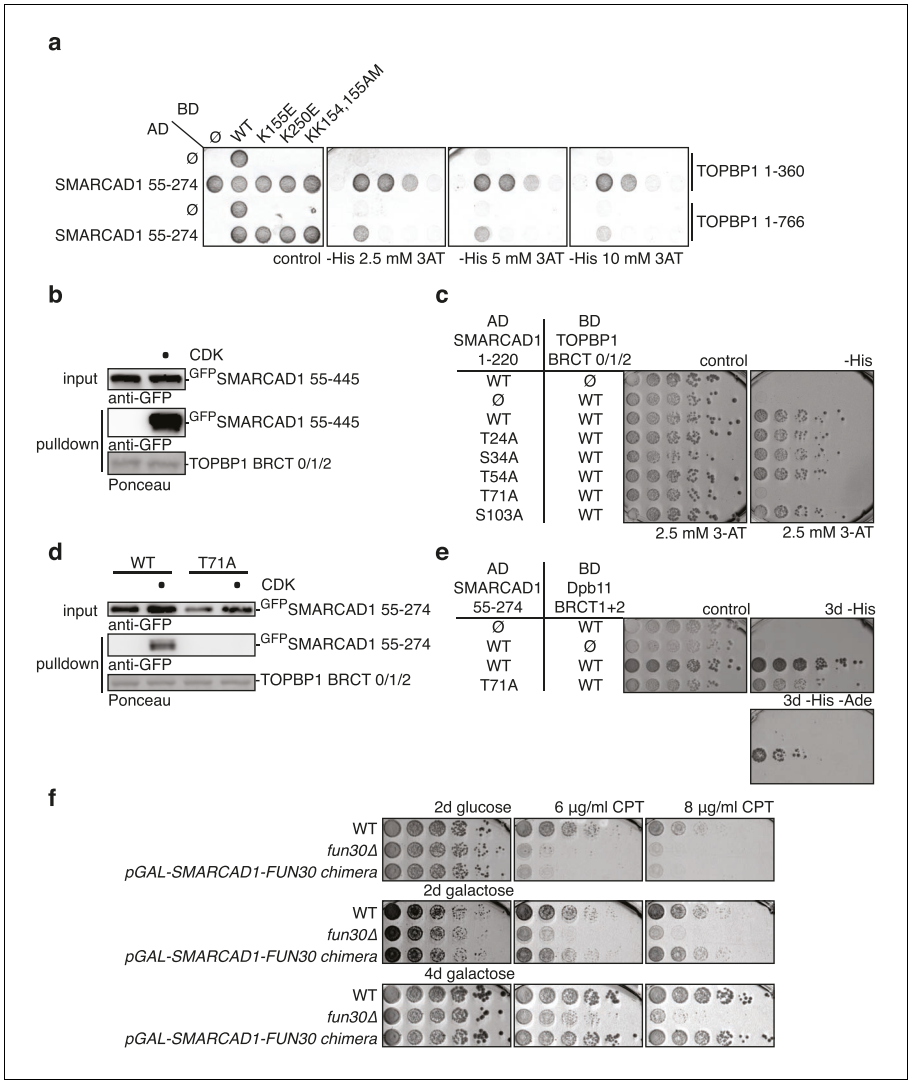

Figure 9. Yeast Fun30 and human SMARCAD1 underlie a conserved regulation. (**a**) SMARCAD1 and TOPBP1 interact and their interaction depends on functional phospho-binding pockets in BRCT1 and BRCT2 of TOPBP1. lexA-BD TOPBP1 1–360 (harbouring BRCT0/1/2) or lexA-BD TOPBP1 1–766 (harbouring BRCT0-5) were tested as *WT* versions or as *K155E, KK154,155AM* (affecting BRCT1) or *K250E* (affecting BRCT2) mutant derivatives. Interaction was tested against the Gal4-AD SMARCAD1 55–274. 3AT was added to –His plates to suppress auto-activation and to increase the stringency of the two-hybrid. Two-hybrid interactions with the lexA-BD TOPBP1 1–360 construct were generally stronger compared to lexA-BD TOPBP1 1–766, leading to milder effects of the K155E and K250E single-mutants, particularly at low 3AT concentrations. (**b**) SMARCAD1 interacts with TOPBP1 after CDK phosphorylation. ^{GFP}SMARCAD1 (55-445) was bound to a ^{GST}TOPBP1 BRCT0/1/2 construct after phosphorylation with CDK. This CDK-dependent interaction was seen with several N-terminal SMARCAD1 constructs, but not with FL, perhaps due to low expression. (**c–d**) Threonine 71 of SMARCAD1, a putative CDK phosphorylation site, is required for TOPBP1 binding. (**c**) Two-hybrid analysis of ^{AD}SMARCAD1 (1-220) and phospho-mutant derivatives to ^{BD}TOPBP1 BRCT0/1/2. (**d**) Co-IP as in (**a**), but additionally using a T71A variant of ^{GFP}SMARCAD1 (55-274). (**e**) Dpb11 can bind to human SMARCAD1, and T71 is important for the interaction. Two-hybrid analysis as in (**b**), but using a ^{BD}Dpb11 BRCT1+2 construct. (**f**) A SMARCAD1-Fun30 chimera lacking the Dpb11-binding site of Fun30, but containing the TOPBP1-binding site of SMARCAD1 restores sensitivity to CPT. The SMARCAD1-Fun30 chimera is expressed from the pGAL1-10 promoter and induced by galactose. Spotting on CPT medium as in ***Figure 4A***.

DOI: 10.7554/eLife.21687.024

The following figure supplements are available for figure 9:

Figure supplement 1. The interaction between SMARCAD1 and TOPBP1 depends on functional phospho-binding pockets in BRCT1 and 2 of TOPBP1.

DOI: 10.7554/eLife.21687.025

Figure 9 continued on next page

Figure 9 continued

Figure supplement 2. Threonine 71 of SMARCAD1, a putative CDK phosphorylation site, is required for TOPBP1 binding.

DOI: 10.7554/eLife.21687.026

Figure supplement 3. Dpb11 can bind to human SMARCAD1, and T71 is important for the interaction.

DOI: 10.7554/eLife.21687.027

Figure supplement 4. A SMARCAD-FUN30 chimera lacking the Dpb11 binding site of Fun30 but containing the putative TOPBP1 binding site of SMARCAD1 restores sensitivity to CPT, while expression of the Fun30 construct lacking the Dpb11 binding site does not.

DOI: 10.7554/eLife.21687.028

Figure supplement 5. Expression control of the SMARCAD1-FUN30 chimera in ***Figure 9F***.

DOI: 10.7554/eLife.21687.029

Figure supplement 6. Expression control of the SMARCAD1-FUN30 chimera, FUN30-30-C and GFP-FUN30 30-C in ***Figure 9—figure supplement 4*** .

DOI: 10.7554/eLife.21687.030

Fun30-30-C fragment alone was unable to provide a rescue and showed reduced protein stability as well (without tag or GFP-tagged, figure ***Figure 9—figure supplements 4,6***). This experiment may thus indicate that the TOPBP1-binding region of SMARCAD1 could replace the Dpb11-binding region of Fun30 in vivo. Overall, we therefore conclude from the data in ***Figure 9*** that the Fun30/SMARCAD1 interaction with Dpb11/TOPBP1, its regulation by CDK phosphorylation and the corresponding interaction surfaces show a remarkable conservation over more than a billion years of eukaryotic evolution.

Discussion

Our study reveals that the function of Fun30/SMARCAD1 at DSBs is cell cycle-regulated via interaction with Dpb11/TOPBP1. In budding yeast, this interaction seems to facilitate localization of Fun30 to damaged chromatin in a manner that depends on the 9-1-1 complex. Notably, other interactions may also contribute to Fun30 targeting or function, given that Fun30 was shown to interact with RPA and nucleases (***Chen et al., 2012***) and that SMARCAD1 was recently shown to interact with H2A-ubiquitin (***Densham et al., 2016***). Importantly, however, our data suggests that the interaction with Dpb11 and 9-1-1 is essential for the resection function of Fun30 during the cell cycle. In contrast to the Fun30-Dpb11 complex, the other interactions are seemingly cell cycle-independent and future research will need to show whether they are at all critical for Fun30/SMARCAD1 function.

Once recruited to a lesion, Fun30 will then promote the action of the long-range resection machinery by generating resection-permissive chromatin. It seems clear that Fun30 antagonizes the resection inhibitor Rad9 (***Chen et al., 2012***), but different, non-exclusive mechanisms remain possible. For example, Fun30 could directly remove Rad9 from DNA damage sites or render Rad9-containing chromatin resection-permissive, but also could interfere with Rad9 recruitment by changing chromatin composition. We predict that our system of forced targeting Fun30 to damaged chromatin will be useful to discriminate between these possibilities in the future.

It is furthermore possible that a direct competition for Dpb11 binding between Fun30 and Rad9 contributes to the functional antagonism, similar to what has been suggested for Slx4 and Rad9 (***Cussiol et al., 2015***; ***Dibitetto et al., 2016***; ***Ohouo et al., 2013***). Dpb11 thus interacts with pro- and anti-resection factors, and the same is true for TOPBP1 (***Cescutti et al., 2010***; ***Moudry et al., 2016***). It will thus be interesting to figure out in the future, how binding of potential antagonizing factors is balanced.

Overall, our data suggest that at least two layers of cell cycle regulation of DNA end resection can be distinguished. First, nucleases and nuclease-associated factors are substrate for CDK phosphorylation (***Chen et al., 2011***; ***Huertas et al., 2008***) and this may directly activate these enzymes, as has for example been shown for the endonuclease activity of MRX-Sae2 (***Cannavo and Cejka, 2014***). Second, chromatin and nucleosome remodellers may be regulated in a way that generates resection-permissive chromatin at damage sites in cell cycle phases when resection is favoured. The Fun30-Dpb11 complex clearly falls in this second category, as does perhaps Rad9/53BP1, the cell

cycle regulation of which we are only beginning to understand (**Cescutti et al., 2010**; **Pfander and Diffley, 2011**). Notably, deregulation of the second layer such as in the experiments with the *DDC1-FUN30* fusion has so far been the most successful strategy to bypass the cell cycle regulation of DNA end resection (**Figure 6**). This emphasizes the importance of resection regulation by its chromatin substrate and suggests that chromatin (more specifically the Fun30 target on chromatin) is the factor that limits long-range resection in G1 phase cells.

Experimentally manipulating DSB repair pathway choice is a key challenge for future research, because it may allow gene targeting in G1/post-mitotic cells, which are currently refractory to this type of approach, since HR is inefficient under these conditions (**Orthwein et al., 2015**). Notwithstanding the overall complexity of DSB repair pathway choice, our results suggest that modification of the DSB-surrounding chromatin by Fun30/SMARCAD1 should be explored further – particularly in higher eukaryotes – as a tool to experimentally channel DSBs into the HR pathway independently of cell cycle stage.

Materials and methods

Yeast strains, cell lines and plasmids

All yeast strains used in this study derive from W303 MATa (strains listed in **Supplementary file 1A**) and were constructed using standard methods (**Janke et al., 2004**). Cells were grown in YP glucose or YP raffinose media at 30˚C. For sensitivity spottings on camptothecin, plates were incubated at 37˚C for 2 days. The inhibitor-sensitive CDK allele *cdc28-as1* (**Bishop et al., 2000**) was inhibited by supplementing 1NM-PP1 (final concentration 1.5 µM) to the medium. Cell cycle synchronization was performed using alpha-factor (5µg/ml) or nocodazole (5µg/ml) for 2–3 hr.

HEK293-T cells were used in mammalian cell culture experiments. Cells were obtained from the cell services facility of CRUKs London Research Institute, authenticated using STR profiling (Promega Mannheim, Germany) and species determination. They were also tested negative for mycoplasma contamination.

For molecular cloning, genes were amplified from yeast genomic DNA and inserted in plasmids using the In-Fusion HD cloning kit (Clontech Saint-Germain-en-Laye, France). For site-directed mutagenesis, a PCR-based protocol with mutagenic oligonucleotides was used. All plasmids used in this study are listed in **Supplementary file 1B**.

Yeast two-hybrid interaction assays

The yeast two-hybrid analyses of the protein-protein interactions were performed using either the Gal4-based plasmid system (pGAD-C1, pGBD-C1 [**James et al., 1996**]) in PJ69-7a cells, or the lexA-based plasmid system (pBTM116, Clontech Saint-Germain-en-Laye, France) in L40 cells (Invitrogen Schwerte, Germany).

Transformants were spotted in serial (1:5) or single dilution either on SC-Leu-Trp plates (control) or on SC-Leu-Trp-His plates (selection) and grown at 30˚C for 2–4 days. For a specific interaction between TOPBP1 1–360 and SMARCAD1 55–247, spotting plates were supplemented with different concentrations of 3-Amino-1,2,4-triazole (3-AT) (2.5–10 mM). To assess the phosphorylation-specific interaction between SMARCAD1 and Dpb11, cells were additionally spotted on SC-Leu-Trp-His-Ade plates.

All experiments (**Figure 1A,G and H**; **Figure 9A,C,E**) were performed in three technical repetitions per biological repetition (spotting of the same yeast cultures on three separate selection plates) and each interaction was observed in several (2-10) independent experiments (a biological replicate corresponds to a fresh transformation of the Y2H expression vectors, raising of the transformed cells and spotting on selective plates).

Fun30 Co-Immunoprecipitation

Yeast cells were freshly transformed with pUK1 (pAG416 GPD-Dpb11) and grown to log-phase (OD_{600} 0.5) in SC-Ura medium + 2% glucose (YPD) at 30˚C. Cells were cell cycle synchronized as describe above, the arrest was controlled by flow cytometry. To release cells from G1 (**Figure 1C**, **Figure 1—figure supplement 2**), BAR1+ cells were synchronized with 5 µg/ml alpha-factor, washed

twice in pre-warmed SC-Ura medium and resuspended in pre-warmed SC-Ura medium supplemented with nocodazole.

For preparation of extracts, 300 OD yeast cells were harvested, washed in ice-cold sorbitol buffer (1 M sorbitol, 25 mM Hepes pH 7.6), and resuspended in 2 ml lysis buffer with protease and phosphatase inhibitors (100 mM Hepes, 200 mM KOAc, 0.1 % NP-40, 10% glycerol, 2 mM β-mercaptoethanol, 100 nM ocadaic acid, 10 mM NaF, 20 mM β-glycerophosphate, 400 µM PMSF, 4 µM aprotinin, 4 mM benzamidin, 400 µM leupeptin, 300 µM pepstatin A) and prepared for lysis using a Spex Sample Prep cryo mill. The extracts were cleared by centrifugation and incubated with anti--FLAG agarose resin (Sigma Munich, Germany) for 30 min (4°C, rotation). After six washes with lysis buffer, Fun30-^{3FLAG} was eluted twice with 0.5 mg/ml 3X FLAG peptide (Sigma Munich, Germany). The elutions were pooled and proteins were precipitated with TCA prior to analysis on 4–12% NuPAGE gradient gels (Invitrogen Schwerte, Germany) and standard Western blotting.

Yeast in vivo co-immunoprecipitation experiments were not performed in technical replicates. The number of biological replicates (fresh transformation with the GPD-Dpb11 overexpressing plasmid, raising of the cells, lysis and IP) was two or more, with the exception of ***Figures 1C*** and ***5B***, ***Figure 5—figure supplement 1***.

Protein purification

Purification of bacterially expressed CDK2/cycA$^{\Delta N170}$

CDK/cycA was purified as described previously (***Brown et al., 1995***).

Purification of Fun30 from S. cerevisiae

YSB784 was grown in 6 L YP medium + 2% raffinose at 30°C until mid-log phase before expression was induced by addition of 2% galactose. After 3 hr of induction, yeast cells were harvested and washed with 1 M Sorbitol + 25 mM HEPES pH 7.6. Cells were resuspended in 20 ml of Lysis Buffer (500 mM NaCl, 100 mM HEPES pH 7.6, 0.1% NP-40, 10% glycerol, 2 mM β-mercaptoethanol, 400 µM PMSF, 4 µM aprotinin, 4 mM benzamidin, 400 µM leupeptin, 300 µM pepstatin A, 1x complete protease inhibitor cocktail, EDTA-free) and frozen to drops in liquid nitrogen. Cells were lysed using a cryo mill (Spex Sample Prep). The lysate was thawed and cleared by centrifugation. The extract was incubated with 2 ml equilibrated slurry of anti-FLAG M2 resin (Sigma Munich, Germany). After 2 hr of incubation, the resin was washed six times with 15 CV of lysis buffer. Two elution steps were performed by adding 2 ml 0.5 mg/mL 3FLAG peptide in lysis buffer and incubation for 30 min at 4°C. Next, Fun30^{3FLAG} was further purified using a 1 ml MonoQ column. To this end, Fun30 was first brought to 100 mM NaCl, bound to the column and eluted on a 100 mM to 1 M salt gradient over 20 CV. Fun30 containing fractions were pooled, snap-frozen and stored at −80°C.

Purification of GST-Dpb11 1–275 from E.coli

GST-Dpb11-1-275 was purified as described previously (***Pfander and Diffley, 2011***).

Purification of GST-TOPBP1-1-360 from E.coli

GST-TOPBP1-1-360 was purified as described previously (***Boos et al., 2011***).

In vitro analysis of protein-protein interactions

In vitro experiments (***Figure 1F***; ***Figure 9B,D***) as depicted were performed once, but confirmed in several different experimental setups (***Figure 9B and D***).

In vitro CDK phosphorylation and pulldown of Fun30

For in vitro pulldown of Fun30 with Dpb11 after in vitro CDK phosphorylation, GST-Dpb11-N or GST (approx. 18 µg per reaction) were immobilized on Sepharose beads for 1 hr at 4°C. The beads were washed twice in lysis buffer (200 mM KOAc, 100 mM HEPES KOH pH 7.6, 10% glycerol, 0.1% NP-40, 2 mM β-mercaptoethanol) and resuspended in 100 µl lysis buffer per reaction. For phosphorylation of Fun30 and Rad9 (control), 5 µg purified protein per reaction were dialyzed against lysis buffer (4°C) and supplied with 4 mM ATP and 5 mM MgOAc. Buffer or CDK (2.5 µg per reaction) were added and the reactions were incubated for 30 min at 24°C. Then, the pre-bound Dpb11/GST-beads were added to the phosphorylated proteins and incubated for 1 hr at 4°C. The beads were washed

five times in lysis buffer and eluted by boiling in 2x Laemmli buffer. Proteins were separated by SDS-PAGE and analyzed with standard Western Blotting techniques.

In vitro CDK phosphorylation and pulldown of SMARCAD1

CDK-dependent pulldowns of SMARCAD1-TOPBP1 (***Figure 9B and D***) were carried out as described (***Boos et al., 2011***) for TRESLIN-TOPBP1 with modifications. HEK293T cells were transfected with pCS2-SMARCAD1-55-275 or pCS2-SMARCAD1-55-445 (carrying an N-terminal GFP tag) and native cell lysates were prepared by lysing the cell pellets in 5x lysis buffer (20 mM HEPES pH 7.5, 250 mM KCl, 0.1% Triton X-100, 5 mM β-mercaptoethanol, 5% glycerol and Complete EDTA-free Protease Inhibitor Cocktail (Roche Mannheim, Germany)). For CDK phosphorylation, the extract was supplemented with 5 mM ATP, 5 mM $MgCl_2$ and approx. 67 ng/µl cycA/CDK2 or buffer (as control) and incubated for 5 min at 25˚C. 200 µl of cell extract were incubated with approx. 10 µg immobilized GST-TopBP1-BRCT0/1/2 for 2 hr at 4˚C. The beads were washed with lysis buffer and WCE and bound material were analysed by SDS PAGE, Western Blotting and ponceau staining.

Chromatin immunoprecipitation (ChIP) and qPCR analysis

For chromatin immunoprecipitation of Fun30 and RPA, cells were grown in YP-Raffinose to an OD of 0.5 and - as indicated for the individual experiments- cell cycle arrest was induced. A double-strand break was introduced by inducing the HO endonuclease from the galactose promoter by addition of galactose to the cultures (2% final). 100 ml samples were crosslinked with formaldehyde (final 1%) for 16 min at indicated timepoints and the reaction was quenched with glycine. Cells were harvested by centrifugation, washed in ice-cold PBS and snap-frozen (RPA ChIPs) or directly processed (Fun30-^{3FLAG} ChIPs). For lysis, cell pellets were resuspended in 800 µl lysis buffer (50 mM HEPES KOH pH 7.5, 150 mM NaCl, 1 mM EDTA, 1% Triton X-100, 0.1% Na-deoxycolate, 0.1% SDS) and grinded with zirconia beads using a bead beating device. The chromatin was sonified to shear the DNA to a size of 200–500 bp. Subsequently the extracts were cleared by centrifugation, 1% was taken as input sample and 40% were incubated with either anti FLAG M2 magnetic beads (Sigma Munich, Germany) for 2 hr (Fun30-^{3FLAG} ChIPs) or 1.5 hr with anti RFA antibody (AS07-214, Agrisera Vännäs, Sweden) followed by 30 min with Dynabeads ProteinA (Invitrogen Schwerte, Germany, for RPA ChIPs). The beads were washed 3x in lysis buffer, 2x in lysis buffer with 500 mM NaCl, 2x in wash buffer (10 mM Tris-Cl pH 8.0, 0.25 M LiCl, 1 mM EDTA, 0.5% NP-40, 0.5% Na-deoxycholate) and 2x in TE pH 8.0. DNA-protein complexes were eluted in 1% SDS, proteins were removed with Proteinase K (3 hr, 42˚C) and crosslinks were reversed (8 hr or overnight, 65˚C). The DNA was subsequently purified using phenol-chloroform extraction and ethanol precipitation and quantified by quantitative PCR (Roche LightCycler480 System, KAPA SYBR FAST 2x qPCR Master Mix, KAPA Biosystems London, UK) at indicated positions with respect to the DNA double-strand break. As control, 2–3 control regions on other chromosomes were quantified and used for normalization.

Chromatin Immunoprecipitation (ChIP) experiments were generally performed in technical replicates (on the qPCR level, each sample was measured three times). Our experimental design (excluding ***Figure 1J*** and figure ***Figure 1—figure supplement 5***) includes further replicates, which can be considered as technical as well as biological replicates: we took samples at different timepoints after induction of the DNA break, which showed a consistent trend over the experiment. Additionally, we measured signals with 15–20 qPCR primer pairs over the damaged chromosome including three control regions on unaffected chromosomes. Therefore, we plot results from single experiments and timepoints and do not include error bars. Nonetheless, 2–6 repetitions (independent cell growth and crosslinking) were performed for mutants analysed in ***Figure 2A***; ***Figure 6B–C***; ***Figure 2—figure supplement 1***, ***Figure 8*** with the exception of ***Figure 6—figure supplement 3***. The ChIP experiment in ***Figure 1J*** and figure ***Figure 1—figure supplement 5*** was performed three times, error bars represent the standard deviation.

Yeast growth assays

Yeast growth assays (DNA damage sensitivity spottings ***Figures 2B*** and ***4A–D***; ***Figure 6A***, ***9F***; ***Figure 4—figure supplements 1,2***; ***Figure 6—figure supplement 1***; ***Figure 9—figure supplement 5*** and *URA3* silencing assay ***Figure 3***) were performed in three technical repetitions per biological repetition (spotting of the same yeast cultures on three separate selection plates), biological

replicates refer to raising of the mutant strains and spotting on plates with indicated conditions. The genotypes were additionally confirmed by comparing several clones of each strain. Each experiment was spotted with three technical replicates.

Single strand annealing spotting assay

Derivates of the YMV80 strain (**Vaze et al., 2002**) carrying a 25 kb spacer between a galactose-inducible HO cutsite and repair locus with a *rad51*△ deletion to prevent DSB repair by gene conversion were grown to stationary phase in YP-Raffinose and spotted in a 5-fold serial dilution on plates containing glucose or galactose. The plates were incubated for 2–3 days at 30˚C.

DNA damage sensitivity spotting assay

Cells were grown to stationary phase in YP-Glucose and spotted in a 5-fold serial dilution on plates containing camptothecin (concentrations as indicated, typically between 4 and 12 µg/ml) or other drugs at the indicated concentrations. The plates were incubated for 2 days at 30˚C or 37˚C (for camptothecin, if not indicated differently).

Plasmid re-ligation assay

In order to assay for precise non-homologous end-joining, 40 OD of transformation-competent yeast cells were transformed with 500 ng BamHI-linearized or mock-digested pRS316. Transformed cells were plated in a five-fold serial dilution on SC-Ura and SC-complete agar plates and grown for two days. Clones on plates containing 50–200 clones were counted to calculate the re-ligation rate (ratio of clones from +BamHI –Ura by +BamHI +Ura divided by the equivalent ratio of mock digested plasmid transformations). Each sample was plated in triplicates and the experiment was independently repeated three times. Error bars represent standard deviations.

50–75 clones from the BamHI-digest transformation on –Ura plates were sequenced to analyse the precise NHEJ event. We found that the majority of cells had precisely re-joined the BamHI overhangs, with a subset having added a single G-C basepair at the cutsite (shown as rate in %). *yku70*Δ cells are NHEJ-deficient and showed very low NHEJ rates with exclusively precisely re-joined plasmid sequences, indicating that this number represents the background of uncut plasmid in the reactions.

Acknowledgements

We thank U Kagerer for technical assistance, J Willmann for early contributions to the project, J Diffley for support of the initial TopBP1 two hybrid screen, J Diffley, J Haber, P Huertas, S Jackson, K-U Reusswig, L Symington for antibodies, plasmid constructs and strains, P Becker, S Gruber, S Jentsch and members of the Jentsch and Pfander labs for stimulating discussion and critical reading of the manuscript. The Fun30-Dpb11 and the SMARCAD1-TOPBP1 interactions were discovered in two-hybrid screens by Hybrigenics, Paris, France. This work was supported by the German Research Council (DFG; project grant PF794/3–1, to BP) and the Max Planck Society (to BP), by the NRW Rueckkehrerprogramm from the MIWF of the state of North Rhine-Westphalia (to DB). SCSB was supported by a Chemiefonds stipend of the FCI. The Pfander lab is associated with the DFG-funded collaborative research cluster SFB1064 Chromatin Dynamics.

Additional information

Funding

Funder	Grant reference number	Author
Deutsche Forschungsgemeinschaft	Project Grant, PF794/3-1	Boris Pfander
Max-Planck-Gesellschaft		Boris Pfander
Fonds der Chemischen Industrie	Fellowship	Susanne CS Bantele
NRW Rueckkehrerprogramm from the state of North-Rhine-		Dominik Boos

Westphalia

The funders had no role in study design, data collection and interpretation, or the decision to submit the work for publication.

Author contributions

SCSB, Conceptualization, Investigation, Methodology, Writing—review and editing, Conceived and designed research, Performed experiments, Analysed the data, Reviewed and edited the manuscript; PF, Investigation, Methodology, Writing—review and editing, Performed human cell culture experiments shown in Fig. 9B+D, Analysed the data, Edited the manuscript; DG, Investigation, Methodology, Writing—review and editing, Performed experiments, Analysed the data, Approved the manuscript; DB, Investigation, Methodology, Writing—review and editing, Identified SMARCAD1-TOPBP1 interaction, Performed human cell culture experiments shown in Fig. 9B+D, Analysed the data and edited the manuscript; BP, Conceptualization, Investigation, Methodology, Writing—original draft, Writing—review and editing, Conceived and designed research, Performed experiments, Analysed the data, Wrote the manuscript

Author ORCIDs

Boris Pfander, http://orcid.org/0000-0003-2180-5054

Additional files

Supplementary files

• Supplementary file 1. Yeast strains used in this study. (A) Table 1 lists all *S.cerevisiae* yeast strains used in this study, their relevant genotypes and the source. (B) Table 2. Plasmids used in this study. Table 2 lists all yeast plasmids and mammalian expression vectors used in this study and their relevant features.

DOI: 10.7554/eLife.21687.031

References

Adkins NL, Niu H, Sung P, Peterson CL. 2013. Nucleosome dynamics regulates DNA processing. *Nature Structural & Molecular Biology* **20**:836–842. doi: 10.1038/nsmb.2585, PMID: 23728291

Albuquerque CP, Smolka MB, Payne SH, Bafna V, Eng J, Zhou H. 2008. A multidimensional chromatography technology for in-depth phosphoproteome analysis. *Molecular & Cellular Proteomics* **7**:1389–1396. doi: 10.1074/mcp.M700468-MCP200, PMID: 18407956

Barlow JH, Lisby M, Rothstein R. 2008. Differential regulation of the cellular response to DNA double-strand breaks in G1. *Molecular Cell* **30**:73–85. doi: 10.1016/j.molcel.2008.01.016, PMID: 18406328

Bennett G, Papamichos-Chronakis M, Peterson CL. 2013. DNA repair choice defines a common pathway for recruitment of chromatin regulators. *Nature Communications* **4**:2084. doi: 10.1038/ncomms3084, PMID: 23811932

Bennett G, Peterson CL. 2015. SWI/SNF recruitment to a DNA double-strand break by the NuA4 and Gcn5 histone acetyltransferases. *DNA Repair* **30**:38–45. doi: 10.1016/j.dnarep.2015.03.006, PMID: 25869823

Bishop AC, Ubersax JA, Petsch DT, Matheos DP, Gray NS, Blethrow J, Shimizu E, Tsien JZ, Schultz PG, Rose MD, Wood JL, Morgan DO, Shokat KM. 2000. A chemical switch for inhibitor-sensitive alleles of any protein kinase. *Nature* **407**:395–401. doi: 10.1038/35030148, PMID: 11014197

Boos D, Sanchez-Pulido L, Rappas M, Pearl LH, Oliver AW, Ponting CP, Diffley JF. 2011. Regulation of DNA replication through Sld3-Dpb11 interaction is conserved from yeast to humans. *Current Biology* **21**:1152–1157. doi: 10.1016/j.cub.2011.05.057, PMID: 21700459

Brown NR, Noble MEM, Endicott JA, Garman EF, Wakatsuki S, Mitchell E, Rasmussen B, Hunt T, Johnson LN. 1995. The crystal structure of cyclin A. *Structure* **3**:1235–1247. doi: 10.1016/S0969-2126(01)00259-3

Bunting SF, Callén E, Wong N, Chen HT, Polato F, Gunn A, Bothmer A, Feldhahn N, Fernandez-Capetillo O, Cao L, Xu X, Deng CX, Finkel T, Nussenzweig M, Stark JM, Nussenzweig A. 2010. 53BP1 inhibits homologous recombination in Brca1-deficient cells by blocking resection of DNA breaks. *Cell* **141**:243–254. doi: 10.1016/j.cell.2010.03.012, PMID: 20362325

Cannavo E, Cejka P. 2014. Sae2 promotes dsDNA endonuclease activity within Mre11-Rad50-Xrs2 to resect DNA breaks. *Nature* **514**:122–125. doi: 10.1038/nature13771, PMID: 25231868

Cejka P, Cannavo E, Polaczek P, Masuda-Sasa T, Pokharel S, Campbell JL, Kowalczykowski SC. 2010. DNA end resection by Dna2-Sgs1-RPA and its stimulation by Top3-Rmi1 and Mre11-Rad50-Xrs2. *Nature* **467**:112–116. doi: 10.1038/nature09355, PMID: 20811461

Cejka P. 2015. DNA end resection: Nucleases team up with the right partners to initiate homologous recombination. *Journal of Biological Chemistry* **290**:22931–22938. doi: 10.1074/jbc.R115.675942, PMID: 26231213

Cescutti R, Negrini S, Kohzaki M, Halazonetis TD. 2010. TopBP1 functions with 53bp1 in the G1 DNA damage checkpoint. *The EMBO Journal* **29**:3723–3732. doi: 10.1038/emboj.2010.238, PMID: 20871591

Chai B, Huang J, Cairns BR, Laurent BC. 2005. Distinct roles for the RSC and swi/Snf ATP-dependent chromatin remodelers in DNA double-strand break repair. *Genes & Development* **19**:1656–1661. doi: 10.1101/gad.1273105, PMID: 16024655

Chen X, Cui D, Papusha A, Zhang X, Chu CD, Tang J, Chen K, Pan X, Ira G. 2012. The Fun30 nucleosome remodeller promotes resection of DNA double-strand break ends. *Nature* **489**:576–580. doi: 10.1038/nature11355, PMID: 22960743

Chen X, Niu H, Chung WH, Zhu Z, Papusha A, Shim EY, Lee SE, Sung P, Ira G. 2011. Cell cycle regulation of DNA double-strand break end resection by Cdk1-dependent Dna2 phosphorylation. *Nature Structural & Molecular Biology* **18**:1015–1019. doi: 10.1038/nsmb.2105, PMID: 21841787

Chen X, Niu H, Yu Y, Wang J, Zhu S, Zhou J, Papusha A, Cui D, Pan X, Kwon Y, Sung P, Ira G. 2016. Enrichment of Cdk1-cyclins at DNA double-strand breaks stimulates Fun30 phosphorylation and DNA end resection. *Nucleic Acids Research* **44**:2742–2753. doi: 10.1093/nar/gkv1544

Costelloe T, Louge R, Tomimatsu N, Mukherjee B, Martini E, Khadaroo B, Dubois K, Wiegant WW, Thierry A, Burma S, van Attikum H, Llorente B. 2012. The yeast Fun30 and human SMARCAD1 chromatin remodellers promote DNA end resection. *Nature* **489**:581–584. doi: 10.1038/nature11353, PMID: 22960744

Cussiol JR, Jablonowski CM, Yimit A, Brown GW, Smolka MB. 2015. Dampening DNA damage checkpoint signalling via coordinated BRCT domain interactions. *The EMBO Journal* **34**:1704–1717. doi: 10.15252/embj.201490834, PMID: 25896509

Delacroix S, Wagner JM, Kobayashi M, Yamamoto K, Karnitz LM. 2007. The Rad9-Hus1-Rad1 (9-1-1) clamp activates checkpoint signaling via TopBP1. *Genes & Development* **21**:1472–1477. doi: 10.1101/gad.1547007, PMID: 17575048

Densham RM, Garvin AJ, Stone HR, Strachan J, Baldock RA, Daza-Martin M, Fletcher A, Blair-Reid S, Beesley J, Johal B, Pearl LH, Neely R, Keep NH, Watts FZ, Morris JR. 2016. Human BRCA1-BARD1 ubiquitin ligase activity counteracts chromatin barriers to DNA resection. *Nature Structural & Molecular Biology* **23**:647–655. doi: 10.1038/nsmb.3236, PMID: 27239795

Dibitetto D, Ferrari M, Rawal CC, Balint A, Kim T, Zhang Z, Smolka MB, Brown GW, Marini F, Pellicioli A. 2016. Slx4 and Rtt107 control checkpoint signalling and DNA resection at double-strand breaks. *Nucleic Acids Research* **44**:669–682. doi: 10.1093/nar/gkv1080, PMID: 26490958

Du LL, Nakamura TM, Russell P. 2006. Histone modification-dependent and -independent pathways for recruitment of checkpoint protein Crb2 to double-strand breaks. *Genes & Development* **20**:1583–1596. doi: 10.1101/gad.1422606, PMID: 16778077

Eapen VV, Sugawara N, Tsabar M, Wu WH, Haber JE. 2012. The Saccharomyces cerevisiae chromatin remodeler Fun30 regulates DNA end resection and checkpoint deactivation. *Molecular and Cellular Biology* **32**:4727–4740. doi: 10.1128/MCB.00566-12, PMID: 23007155

Furuya K, Poitelea M, Guo L, Caspari T, Carr AM. 2004. Chk1 activation requires Rad9 S/TQ-site phosphorylation to promote association with C-terminal BRCT domains of Rad4TOPBP1. *Genes & Development* **18**:1154–1164. doi: 10.1101/gad.291104, PMID: 15155581

Gritenaite D, Princz LN, Szakal B, Bantele SC, Wendeler L, Schilbach S, Habermann BH, Matos J, Lisby M, Branzei D, Pfander B. 2014. A cell cycle-regulated Slx4-Dpb11 complex promotes the resolution of DNA repair intermediates linked to stalled replication. *Genes & Development* **28**:1604–1619. doi: 10.1101/gad.240515.114, PMID: 25030699

Huertas P, Cortés-Ledesma F, Sartori AA, Aguilera A, Jackson SP. 2008. CDK targets Sae2 to control DNA-end resection and homologous recombination. *Nature* **455**:689–692. doi: 10.1038/nature07215, PMID: 18716619

Huertas P. 2010. DNA resection in eukaryotes: deciding how to fix the break. *Nature Structural & Molecular Biology* **17**:11–16. doi: 10.1038/nsmb.1710, PMID: 20051983

Ira G, Pellicioli A, Balijja A, Wang X, Fiorani S, Carotenuto W, Liberi G, Bressan D, Wan L, Hollingsworth NM, Haber JE, Foiani M. 2004. DNA end resection, homologous recombination and DNA damage checkpoint activation require CDK1. *Nature* **431**:1011–1017. doi: 10.1038/nature02964, PMID: 15496928

James P, Halladay J, Craig EA. 1996. Genomic libraries and a host strain designed for highly efficient two-hybrid selection in yeast. *Genetics* **144**:1425–1436. PMID: 8978031

Janke C, Magiera MM, Rathfelder N, Taxis C, Reber S, Maekawa H, Moreno-Borchart A, Doenges G, Schwob E, Schiebel E, Knop M. 2004. A versatile toolbox for PCR-based tagging of yeast genes: new fluorescent proteins, more markers and promoter substitution cassettes. *Yeast* **21**:947–962. doi: 10.1002/yea.1142, PMID: 15334558

Janke R, Herzberg K, Rolfsmeier M, Mar J, Bashkirov VI, Haghnazari E, Cantin G, Yates JR, Heyer WD. 2010. A truncated DNA-damage-signaling response is activated after DSB formation in the G1 phase of Saccharomyces cerevisiae. *Nucleic Acids Research* **38**:2302–2313. doi: 10.1093/nar/gkp1222, PMID: 20061370

Lazzaro F, Sapountzi V, Granata M, Pellicioli A, Vaze M, Haber JE, Plevani P, Lydall D, Muzi-Falconi M. 2008. Histone methyltransferase Dot1 and Rad9 inhibit single-stranded DNA accumulation at DSBs and uncapped telomeres. *The EMBO Journal* **27**:1502–1512. doi: 10.1038/emboj.2008.81, PMID: 18418382

Leung CCY, Glover JNM. 2011. BRCT domains. *Cell Cycle* **10**:2461–2470. doi: 10.4161/cc.10.15.16312

Meijsing SH, Ehrenhofer-Murray AE. 2001. The silencing complex SAS-I links histone acetylation to the assembly of repressed chromatin by CAF-I and Asf1 in Saccharomyces cerevisiae. *Genes & Development* **15**:3169–3182. doi: 10.1101/gad.929001, PMID: 11731480

Mimitou EP, Symington LS. 2008. Sae2, Exo1 and Sgs1 collaborate in DNA double-strand break processing. *Nature* **455**:770–774. doi: 10.1038/nature07312, PMID: 18806779

Morrison AJ, Highland J, Krogan NJ, Arbel-Eden A, Greenblatt JF, Haber JE, Shen X. 2004. INO80 and gamma-H2AX interaction links ATP-dependent chromatin remodeling to DNA damage repair. *Cell* **119**:767–775. doi: 10.1016/j.cell.2004.11.037, PMID: 15607974

Moudry P, Watanabe K, Wolanin KM, Bartkova J, Wassing IE, Watanabe S, Strauss R, Troelsgaard Pedersen R, Oestergaard VH, Lisby M, Andújar-Sánchez M, Maya-Mendoza A, Esashi F, Lukas J, Bartek J. 2016. TOPBP1 regulates RAD51 phosphorylation and chromatin loading and determines PARP inhibitor sensitivity. *The Journal of Cell Biology* **212**:281–288. doi: 10.1083/jcb.201507042

Neves-Costa A, Will WR, Vetter AT, Miller JR, Varga-Weisz P. 2009. The SNF2-family member Fun30 promotes gene silencing in heterochromatic loci. *PLoS One* **4**:e8111. doi: 10.1371/journal.pone.0008111, PMID: 19956593

Niu H, Chung WH, Zhu Z, Kwon Y, Zhao W, Chi P, Prakash R, Seong C, Liu D, Lu L, Ira G, Sung P. 2010. Mechanism of the ATP-dependent DNA end-resection machinery from Saccharomyces cerevisiae. *Nature* **467**:108–111. doi: 10.1038/nature09318, PMID: 20811460

Ohouo PY, Bastos de Oliveira FM, Almeida BS, Smolka MB. 2010. DNA damage signaling recruits the Rtt107-Slx4 scaffolds via Dpb11 to mediate replication stress response. *Molecular Cell* **39**:300–306. doi: 10.1016/j.molcel.2010.06.019, PMID: 20670896

Ohouo PY, Bastos de Oliveira FM, Liu Y, Ma CJ, Smolka MB, de Oliveira FMB, Smolka MB. 2013. DNA-repair scaffolds dampen checkpoint signalling by counteracting the adaptor Rad9. *Nature* **493**:120–124. doi: 10.1038/nature11658, PMID: 23160493

Orthwein A, Noordermeer SM, Wilson MD, Landry S, Enchev RI, Sherker A, Munro M, Pinder J, Salsman J, Dellaire G, Xia B, Peter M, Durocher D. 2015. A mechanism for the suppression of homologous recombination in G1 cells. *Nature* **528**:422–426. doi: 10.1038/nature16142, PMID: 26649820

Parrilla-Castellar ER, Arlander SJ, Karnitz L. 2004. Dial 9-1-1 for DNA damage: the Rad9-Hus1-Rad1 (9-1-1) clamp complex. *DNA Repair* **3**:1009–1014. doi: 10.1016/j.dnarep.2004.03.032, PMID: 15279787

Pfander B, Diffley JF. 2011. Dpb11 coordinates Mec1 kinase activation with cell cycle-regulated Rad9 recruitment. *The EMBO Journal* **30**:4897–4907. doi: 10.1038/emboj.2011.345, PMID: 21946560

Puddu F, Granata M, Di Nola L, Balestrini A, Piergiovanni G, Lazzaro F, Giannattasio M, Plevani P, Muzi-Falconi M. 2008. Phosphorylation of the budding yeast 9-1-1 complex is required for Dpb11 function in the full activation of the UV-induced DNA damage checkpoint. *Molecular and Cellular Biology* **28**:4782–4793. doi: 10.1128/MCB.00330-08, PMID: 18541674

Singer MS, Kahana A, Wolf AJ, Meisinger LL, Peterson SE, Goggin C, Mahowald M, Gottschling DE. 1998. Identification of high-copy disruptors of telomeric silencing in saccharomyces cerevisiae. *Genetics* **150**:613–632. PMID: 9755194

Symington LS, Gautier J. 2011. Double-strand break end resection and repair pathway choice. *Annual Review of Genetics* **45**:247–271. doi: 10.1146/annurev-genet-110410-132435, PMID: 21910633

Symington LS. 2014. End resection at double-strand breaks: mechanism and regulation. *Cold Spring Harbor Perspectives in Biology* **6**:a016436. doi: 10.1101/cshperspect.a016436, PMID: 25085909

Tanaka S, Umemori T, Hirai K, Muramatsu S, Kamimura Y, Araki H. 2007. CDK-dependent phosphorylation of Sld2 and Sld3 initiates DNA replication in budding yeast. *Nature* **445**:328–332. doi: 10.1038/nature05465, PMID: 17167415

Thomas BJ, Rothstein R. 1989. Elevated recombination rates in transcriptionally active DNA. *Cell* **56**:619–630. doi: 10.1016/0092-8674(89)90584-9, PMID: 2645056

Tomimatsu N, Mukherjee B, Catherine Hardebeck M, Ilcheva M, Vanessa Camacho C, Louise Harris J, Porteus M, Llorente B, Khanna KK, Burma S. 2014. Phosphorylation of EXO1 by CDKs 1 and 2 regulates DNA end resection and repair pathway choice. *Nature Communications* **5**:3561. doi: 10.1038/ncomms4561, PMID: 24705021

Trovesi C, Falcettoni M, Lucchini G, Clerici M, Longhese MP. 2011. Distinct Cdk1 requirements during single-strand annealing, noncrossover, and crossover recombination. *PLoS Genetics* **7**:e1002263. doi: 10.1371/journal.pgen.1002263, PMID: 21901114

Ubersax JA, Woodbury EL, Quang PN, Paraz M, Blethrow JD, Shah K, Shokat KM, Morgan DO. 2003. Targets of the cyclin-dependent kinase Cdk1. *Nature* **425**:859–864. doi: 10.1038/nature02062, PMID: 14574415

van Attikum H, Fritsch O, Gasser SM. 2007. Distinct roles for SWR1 and INO80 chromatin remodeling complexes at chromosomal double-strand breaks. *The EMBO Journal* **26**:4113–4125. doi: 10.1038/sj.emboj.7601835, PMID: 17762868

van Attikum H, Fritsch O, Hohn B, Gasser SM. 2004. Recruitment of the INO80 complex by H2A phosphorylation links ATP-dependent chromatin remodeling with DNA double-strand break repair. *Cell* **119**:777–788. doi: 10.1016/j.cell.2004.11.033, PMID: 15607975

Vaze MB, Pellicioli A, Lee SE, Ira G, Liberi G, Arbel-Eden A, Foiani M, Haber JE. 2002. Recovery from checkpoint-mediated arrest after repair of a double-strand break requires Srs2 helicase. *Molecular Cell* **10**:373–385. doi: 10.1016/S1097-2765(02)00593-2, PMID: 12191482

Wang H, Elledge SJ. 2002. Genetic and physical interactions between DPB11 and DDC1 in the yeast DNA damage response pathway. *Genetics* **160**:1295–1304. PMID: 11973288

Zegerman P, Diffley JF, Zhong Y, Nellimoottil T, Peace JM, Knott SRV, Villwock SK, Yee JM, Jancuska JM, Rege S, Tecklenburg M, Sclafani RA. 2010. Checkpoint-dependent inhibition of DNA replication initiation by Sld3 and Dbf4 phosphorylation. *Nature* **467**:474–478. doi: 10.1038/nature09373, PMID: 20835227

Zegerman P, Diffley JF. 2007. Phosphorylation of Sld2 and Sld3 by cyclin-dependent kinases promotes DNA replication in budding yeast. *Nature* **445**:281–285. doi: 10.1038/nature05432, PMID: 17167417

Zhang Y, Shim EY, Davis M, Lee SE. 2009. Regulation of repair choice: Cdk1 suppresses recruitment of end joining factors at DNA breaks. *DNA Repair* **8**:1235–1241. doi: 10.1016/j.dnarep.2009.07.007, PMID: 19699692

Zhu Z, Chung WH, Shim EY, Lee SE, Ira G. 2008. Sgs1 helicase and two nucleases Dna2 and Exo1 resect DNA double-strand break ends. *Cell* **134**:981–994. doi: 10.1016/j.cell.2008.08.037, PMID: 18805091

eLIFE elifesciences.org

RESEARCH ARTICLE

Figures and figure supplements

Targeting of the Fun30 nucleosome remodeller by the Dpb11 scaffold facilitates cell cycle-regulated DNA end resection

Susanne CS Bantele *et al*

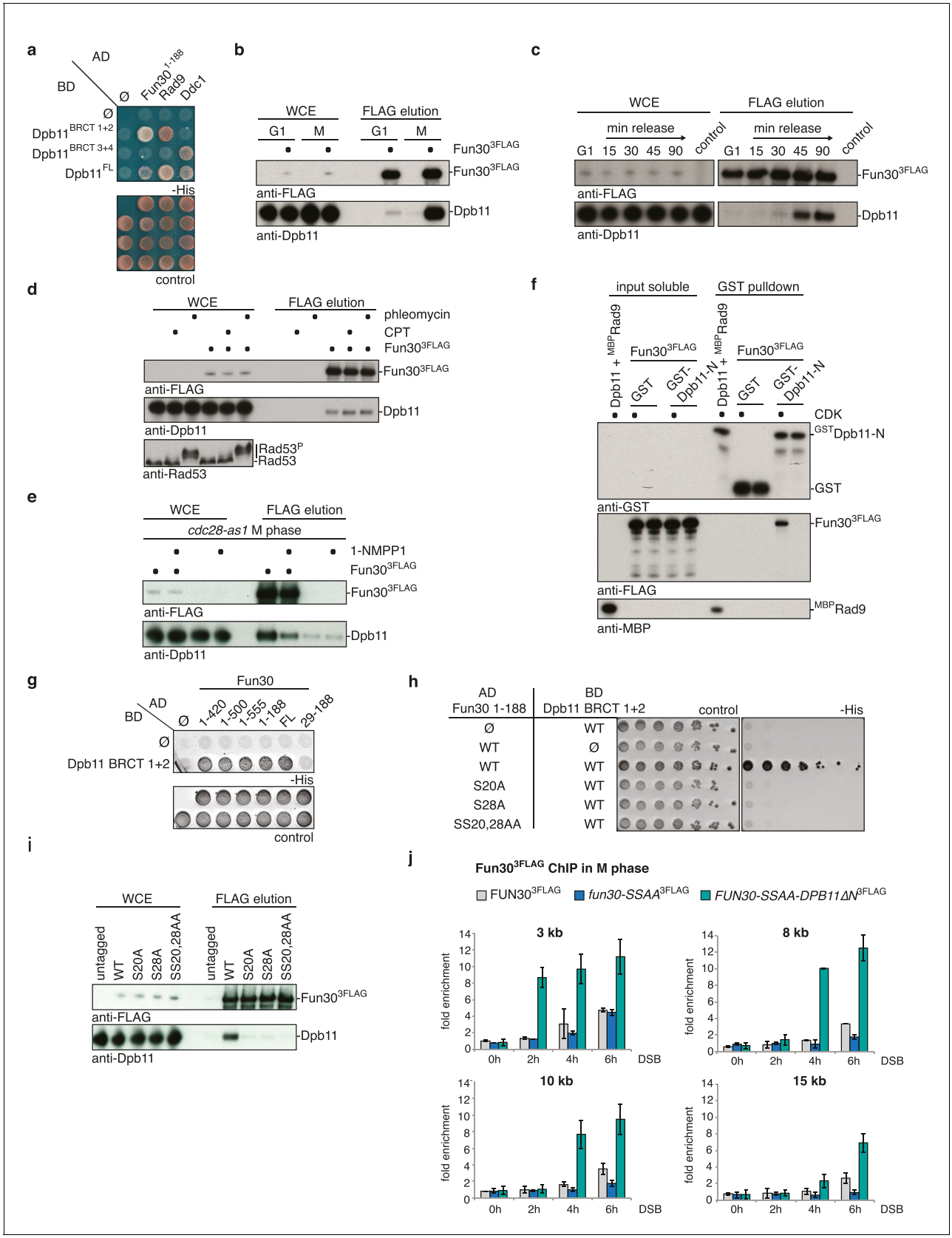

Figure 1. Fun30 and Dpb11 interact in a cell cycle- and CDK phosphorylation-dependent manner and this targets Fun30 to DSBs. (**a**) Two-hybrid assay with GAL4-AD and -BD constructs as indicated reveals a physical interaction between the N-terminal region of Fun30 (aa 1–188) and the BRCT1+2

Figure 1 continued on next page

Figure 1 continued

domain of Dpb11. Rad9 and Ddc1 represent known interactors of BRCT1+2 and BRCT3+4, respectively. (**b–e**) Characterization of the Fun30-Dpb11 interaction by Fun30^{3FLAG} Co-IP experiments. Dpb11 was expressed from the strong, constitutive GPD promoter. (**b**) Fun30^{3FLAG} specifically binds Dpb11 in cells arrested in M but not G1 phase. (**c**) Fun30^{3FLAG} purified from cells synchronously progressing through the cell cycle binds Dpb11 only at 45' and 90' time points corresponding to late S and M phase (***Figure 1—figure supplement 2*** for FACS analysis and western analysis of cell cycle progression). (**d**) No enhancement of the Fun30-Dpb11 interaction by CPT or phleomycin treatment as measured by Fun30^{3FLAG} Co-IP. For DNA damage treatment, 50 µM CPT or 50 µg/ml phleomycin were added to asynchronously dividing yeast cells. DNA damage checkpoint activation was measured by Rad53 phosphorylation in IP extracts (lowest blot panel). (**e**) CDK inhibition using the *cdc28-as1* allele and 1-NMPP1 treatment diminishes the Fun30^{3FLAG}-Dpb11 interaction in M phase arrested cells. (**f**) Purified Fun30 interacts with a BRCT1+2 fragment of Dpb11 in the presence of CDK phosphorylation. Purified Fun30^{3FLAG} or the positive control ^{MBP}Rad9 (***Pfander and Diffley, 2011***) were incubated with a model CDK and ATP before binding to bead-bound ^{GST}Dpb11 BRCT1+2. (**g**) Mapping analysis of the two-hybrid interaction between Fun30 and Dpb11 reveals a binding site close to the N-terminus of Fun30. (**h–i**) Putative CDK sites on Fun30 (S20 and S28) are required for Dpb11 binding. (**h**) Two-hybrid assay as in (**a**) but in five-fold serial dilution and with *WT*, *S20A*, *S28A* and *SS20,28AA* variants of Gal4-AD-Fun30$^{1-188}$. (**i**) Co-IP as in (**b**) but with mutant variants of Fun30^{3FLAG} growing asynchronously. (**j**) Efficient Fun30 localization to damaged chromatin requires the Dpb11-Fun30 interaction. ChIP of Fun30^{3FLAG} to chromatin locations 3, 8, 10 and 15 kb distant of a non-repairable DSB induced at the MAT locus in M phase-arrested cells. *fun30* mutants were expressed from the endogenous promoter as only copy of *FUN30*. The *FUN30-DPB11* fusion contains *fun30-SSAA* and *dpb11△N* mutations. *WT*, *fun30-SSAA* and *FUN30-DPB11 fusion* cells were crosslinked at indicated timepoints after DSB induction. Plotted values represent means from two independent experiments, error bars represent standard deviations.

DOI: 10.7554/eLife.21687.003

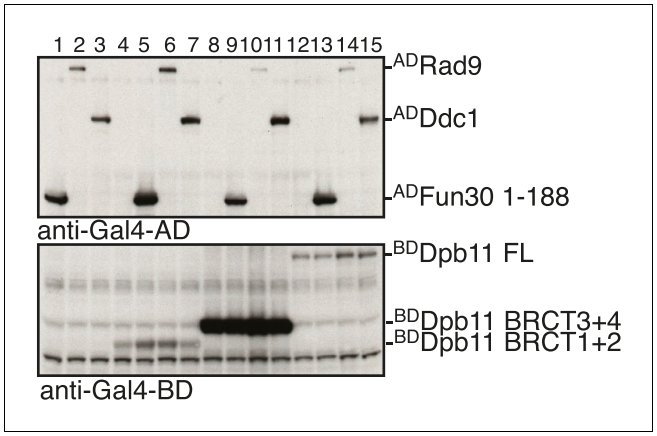

Figure 1—figure supplement 1. Expression control of two-hybrid constructs used in ***Figure 1A***. Two-hybrid constructs are detected with anti-Gal4-AD (AD-Fun30 1–188, AD-Ddc1, AD-Rad9) and with anti-Gal4-BD (for BD-Dpb11 constructs) antibodies.
DOI: 10.7554/eLife.21687.004

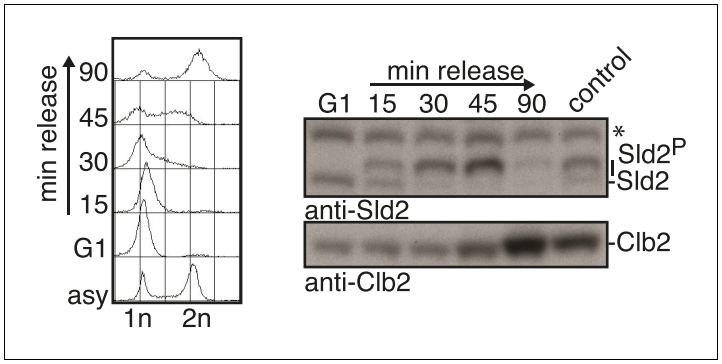

Figure 1—figure supplement 2. Control of the cell cycle states of the experiment in ***Figure 1C***. Left panel: DNA content measurements with FACS. Right panel: Western Blot analysis using S/M-phase (hyperphosphorylated Sld2) or M-phase (Clb2) markers. Asterisk indicates a cross reactive band.
DOI: 10.7554/eLife.21687.005

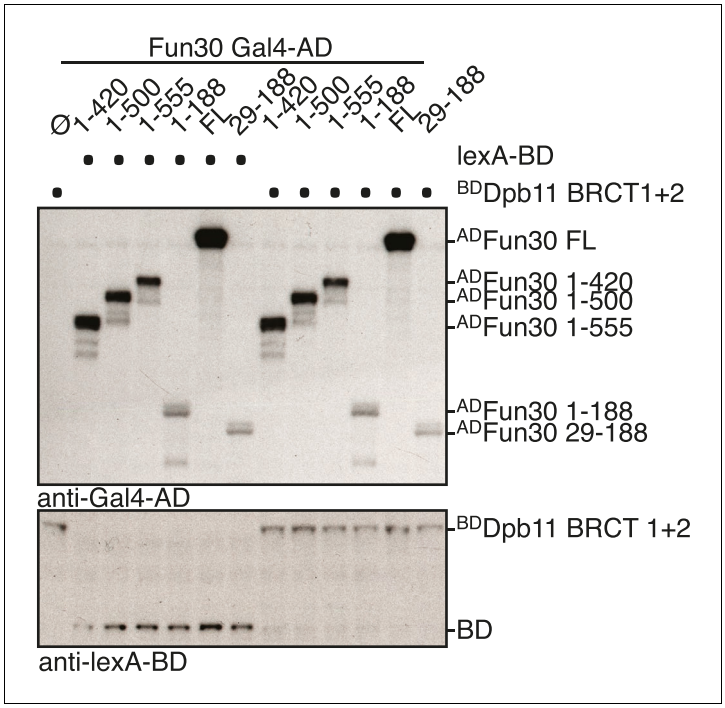

Figure 1—figure supplement 3. Expression control of two-hybrid constructs used in ***Figure 1G***. Two-hybrid constructs are detected with anti-Gal4-AD (AD-Fun30 constructs) and with anti-lexA-BD (for BD-Dpb11 BRCT1 +2 construct) antibodies.

DOI: 10.7554/eLife.21687.006

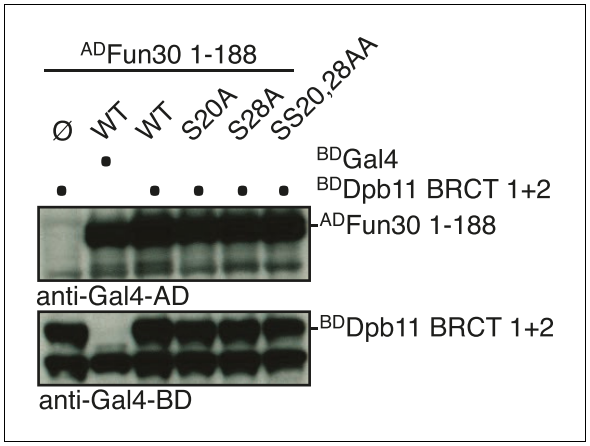

Figure 1—figure supplement 4. Expression control of two-hybrid constructs used in ***Figure 1H***. Two-hybrid constructs are detected with anti-Gal4-AD (AD-Fun30 1–188 and mutant derivatives) and with anti-Gal4-BD (for BD-Dpb11 BRCT1 +2 constructs) antibodies.
DOI: 10.7554/eLife.21687.007

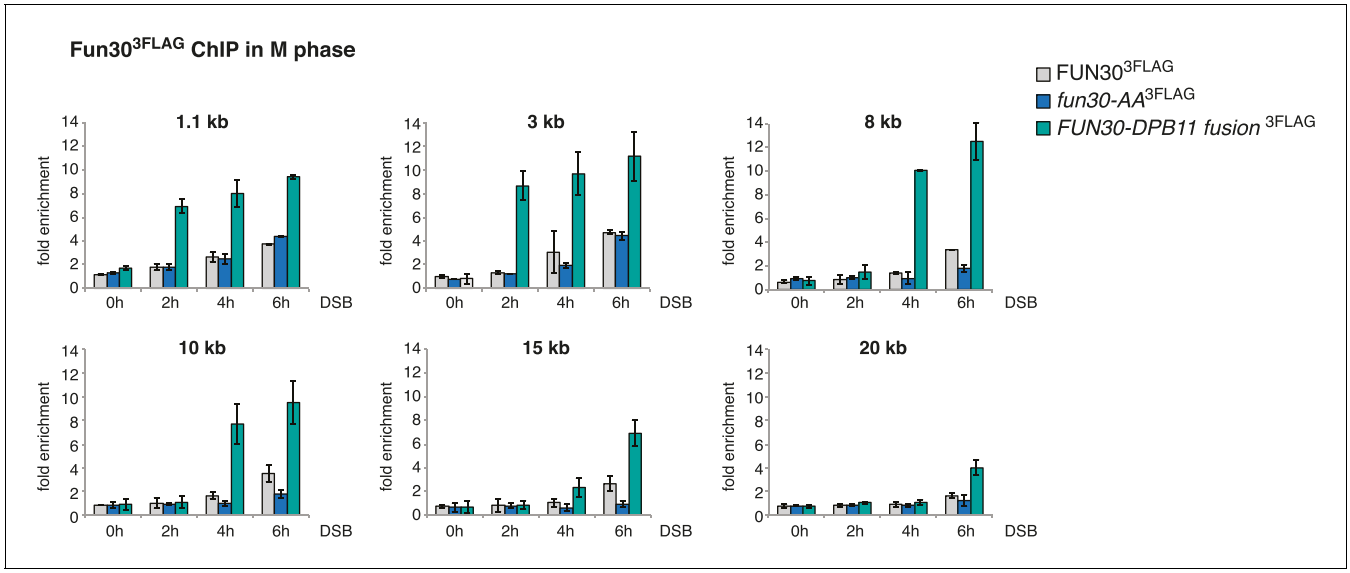

Figure 1—figure supplement 5. Efficient Fun30 localization to damaged chromatin requires the Dpb11-Fun30 interaction. ChIP of Fun30^{3FLAG} to chromatin in proximity of a non-repairable DSB induced at the MAT locus in M phase arrested cells. Same experiment as in ***Figure 1J***, using *WT*, *fun30-SSAA* and *FUN30-DPB11 fusion* cells, but here Fun30 ChIP is shown at additional loci (1.1, 3, 8, 10, 15 and 20 kb distance from break). Cells were crosslinked at distinct time points after DSB induction. Plotted values represent error bars from three independent experiments.
DOI: 10.7554/eLife.21687.008

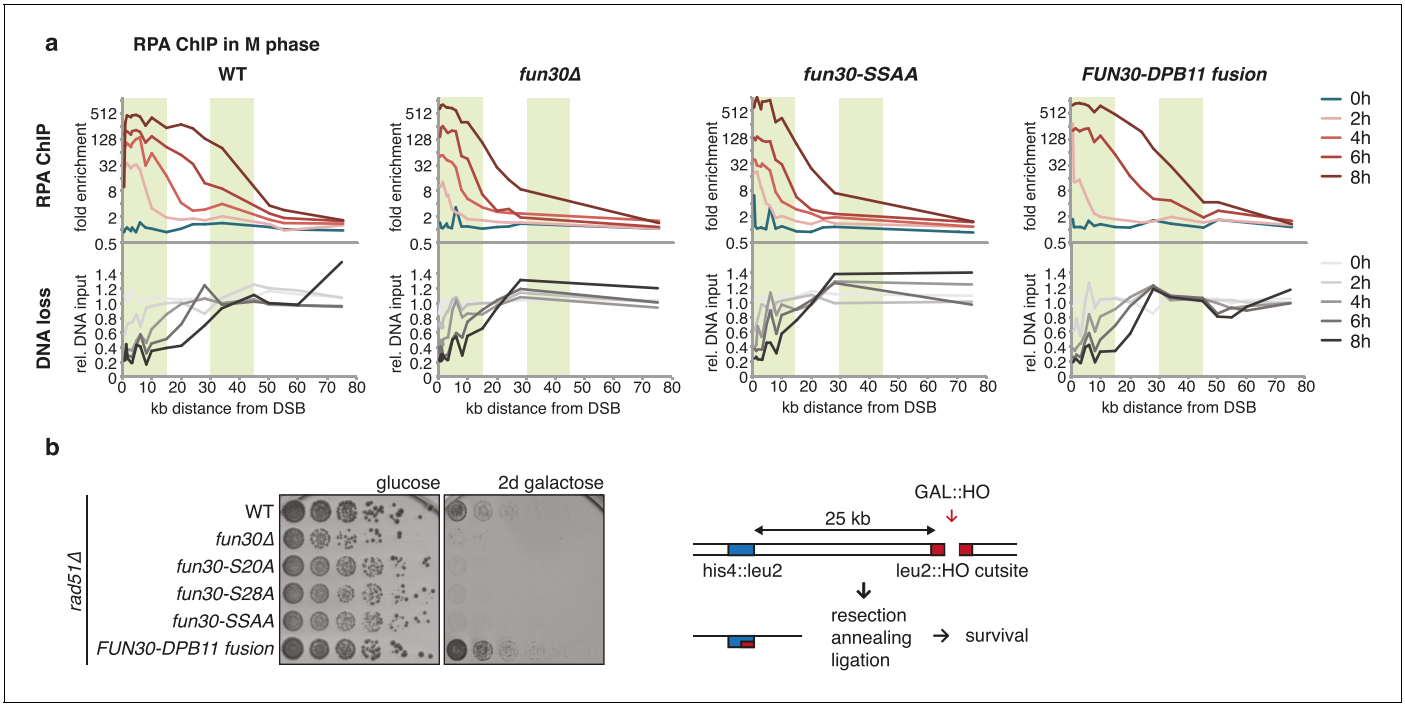

Figure 2. The Fun30-Dpb11 complex is required for efficient long-range resection. (**a**) Long-range resection of a DSB is dependent on the Fun30-Dpb11 interaction. A non-repairable DSB at MAT was induced in M phase-arrested *WT*, *fun30*△, *fun30-SSAA* and *FUN30-DPB11* fusion strains and DNA end resection measured at indicated times. Upper panel: fold enrichment of a given locus in an RPA ChIP relative to undamaged control loci. Lower panel: DNA loss relative to control loci located in non-damaged chromatin. (**b**) Single-strand annealing (SSA) is dependent on the Fun30-Dpb11 interaction. *FUN30* mutants as indicated were combined with the *rad51*△ deletion, a DSB at the leu2::HO cutsite was induced by plating cells on galactose. Cells need to resect 25 kb up to the homologous his4::leu2 locus in order to survive by SSA.

DOI: 10.7554/eLife.21687.009

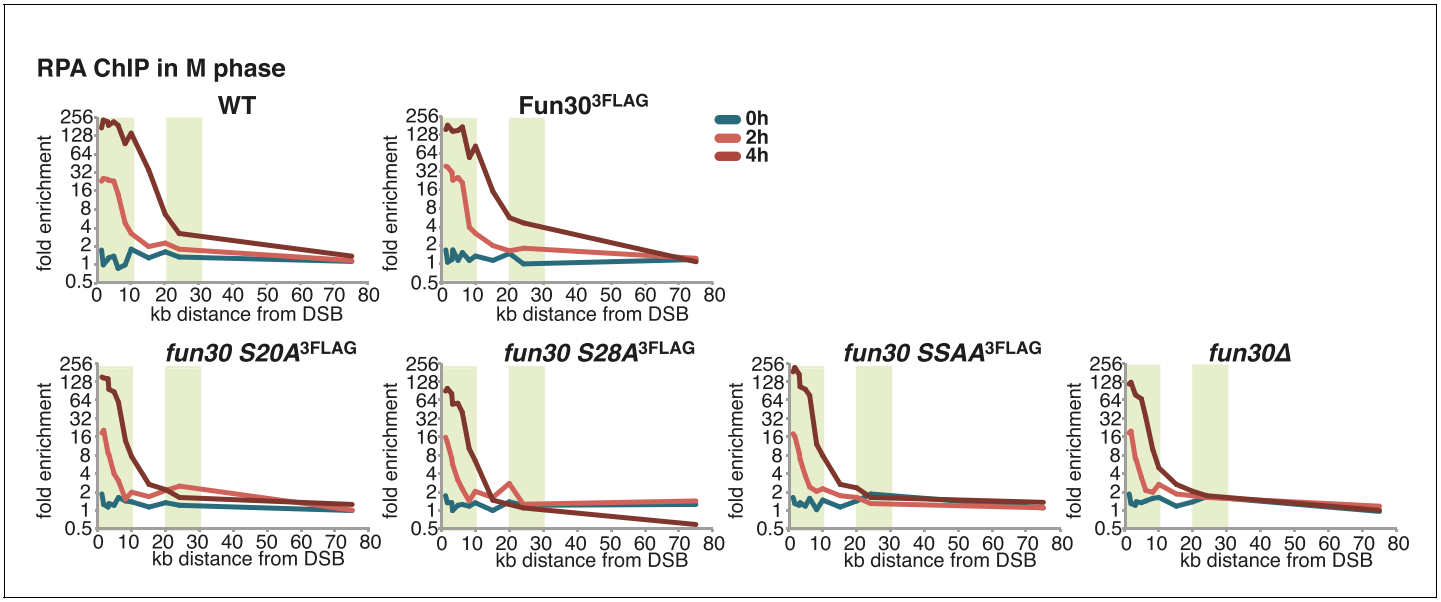

Figure 2—figure supplement 1. The Fun30-Dpb11 interaction is required for efficient long-range resection. Long-range resection of a site-specific DSB is partially deficient in CDK-phosphorylation site mutants that are deficient in the Fun30-Dpb11 interaction. A non-repairable DSB at MAT was induced in M-phase arrested *WT*, *fun30-S20A*^{3FLAG}, *fun30-S28A*^{3FLAG}, *fun30-SSAA*^{3FLAG} and *fun30*Δ cells. DNA end resection was measured at indicated time points by RPA ChIP. Plotted is the fold enrichment of a given locus relative to three undamaged control loci.

DOI: 10.7554/eLife.21687.010

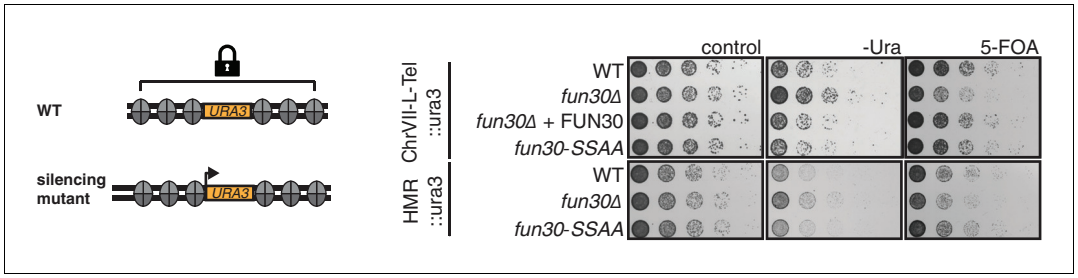

Figure 3. The Fun30-Dpb11 interaction is not involved in Fun30-dependent gene silencing at telomeric heterochromatin and a silent mating type locus. The silencing defect of the *fun30Δ* mutant is not recapitulated by the *fun30-SSAA* mutant. Two silencing tester strains were used: the first (upper panels) had URA3 integrated in telomeric heterochromatin at the end of the left arm of chromosome VII, the second (lower panels) had URA3 integrated at the HML silent mating type locus. A silencing defect leads to enhanced growth on –Ura medium and less growth on medium supplemented with 5-FOA (e.g. *fun30Δ*). Shown is a spotting in 5-fold serial dilutions on non-selective medium, medium lacking uracil or containing 5-FOA.

DOI: 10.7554/eLife.21687.011

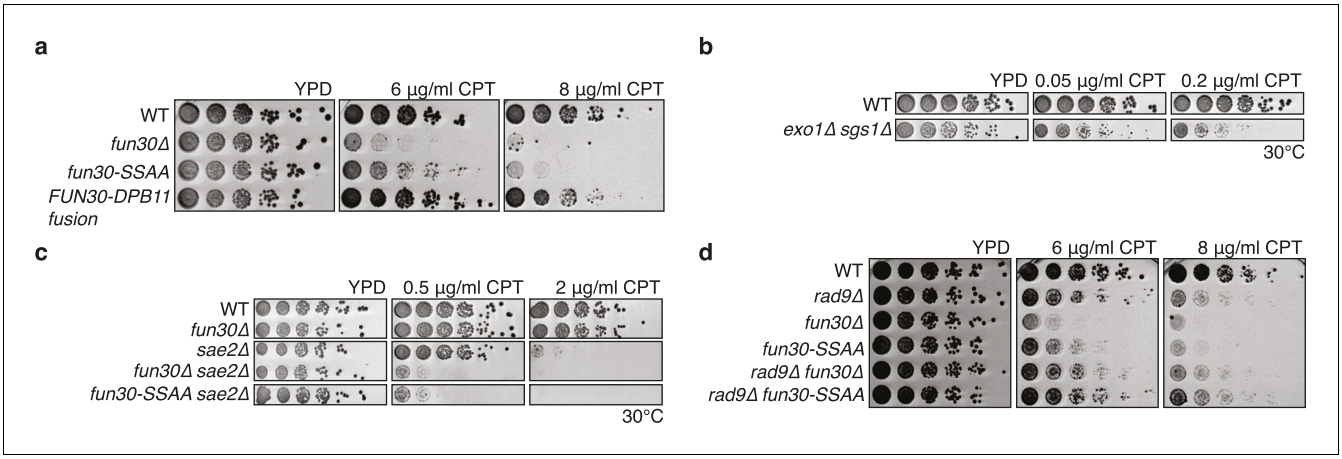

Figure 4. The Fun30-Dpb11 interaction is required for the response towards CPT, as is functional long- and short-range resection. (**a**) The Fun30-Dpb11 interaction is required for the response towards CPT. *WT*, *fun30△*, *fun30-SSAA* and *FUN30-DPB11 fusion* were spotted in five-fold serial dilutions on plates containing indicated amounts of CPT and incubated at 37˚C for two days. (**b**) A double mutant of *exo1Δ* and *sgs1Δ* is hyper-sensitive to low doses of CPT. Spotting in 5-fold serial dilutions was incubated for two days at 30˚C. (**c**) The *fun30Δ/fun30-SSAA* mutants enhance the CPT hyper-sensitivity of *sae2Δ* mutants. Cells were spotted in 5-fold serial dilutions and incubated for two days at 30˚C. (**d**) A *rad9Δ* deletion rescues CPT hyper-sensitivity of *fun30Δ* and *fun30-SSAA* mutant alleles.

DOI: 10.7554/eLife.21687.012

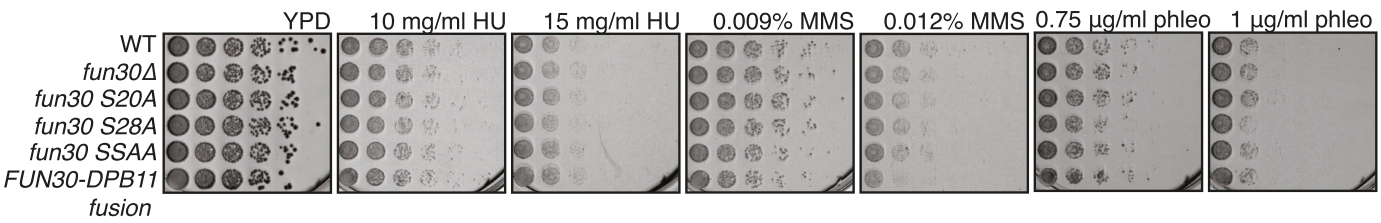

Figure 4—figure supplement 1. Mutants of Fun30 show no discernable phenotype upon chronic exposure to HU, MMS or phleomycin. Spotting in 5-fold serial dilutions on medium containing indicated dosages of DNA damaging agents. Plates were incubated two days at 30°C.
DOI: 10.7554/eLife.21687.013

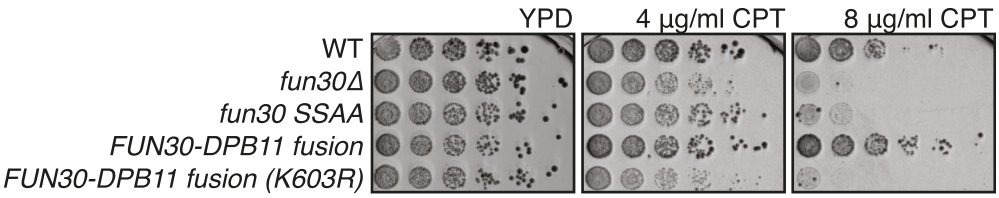

Figure 4—figure supplement 2. The catalytic activity of Fun30 is required for the suppression of the CPT phenotype in the context of the *FUN30-DPB11 fusion*. Spotting of strains with indicated genotypes in 5-fold serial dilutions on CPT containing medium. The K603R mutation is located in the Walker A motif of Fun30. Plates were incubated for two days at 37°C.

DOI: 10.7554/eLife.21687.014

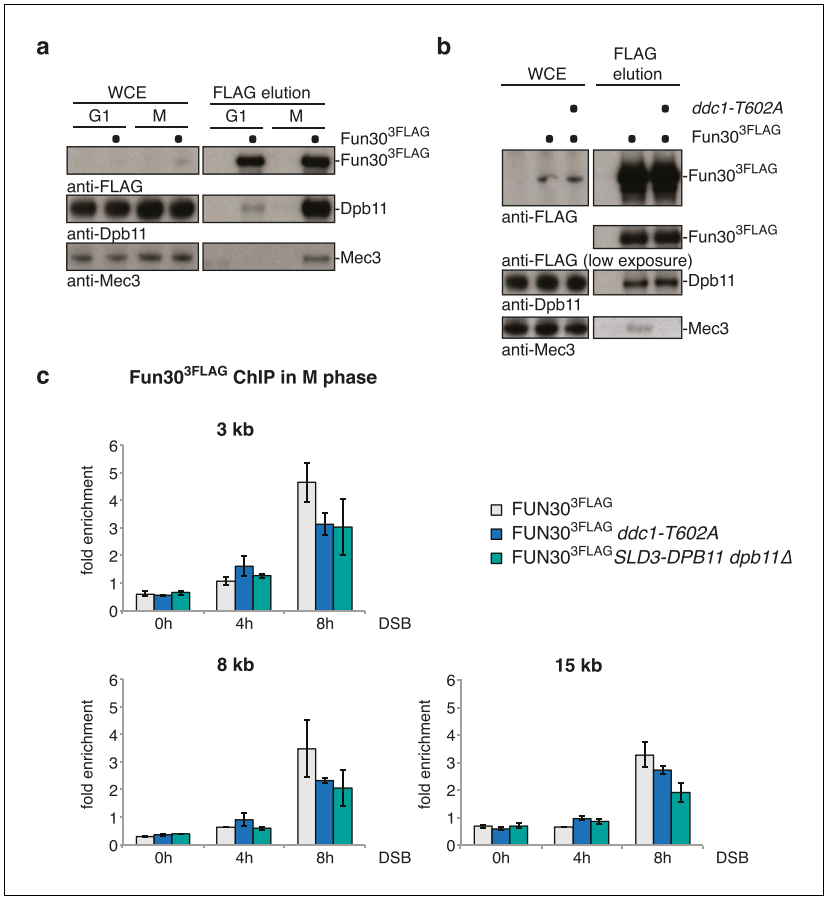

Figure 5. The 9-1-1 complex forms a ternary complex with Fun30-Dpb11. (**a**) Fun30, Dpb11 and 9-1-1 form a ternary complex. The 9-1-1 subunit Mec3 interacts with Fun30^{3FLAG} when purified from M phase cells, where also Dpb11 binds to Fun30. (**b**) The *ddc1-T602A* mutation abolishes binding of Mec3 to Fun30-Dpb11 in Fun30^{3FLAG} Co-IPs, but leaves the Fun30-Dpb11 interaction intact. (**c**) Mutants disrupting the interaction between 9-1-1 and Dpb11 (*ddc1-T602A*) or Fun30 and Dpb11 (*SLD3-dpb11ΔN*, lacks Fun30 binding site, only copy of Dpb11) impair efficient localization of Fun30 to DSBs in Fun30^{3FLAG} ChIPs of M phase-arrested cells. Experiment performed as in ***Figure 1J***, plotted values represent means of two independent experiments, error bars represent standard deviations.

DOI: 10.7554/eLife.21687.015

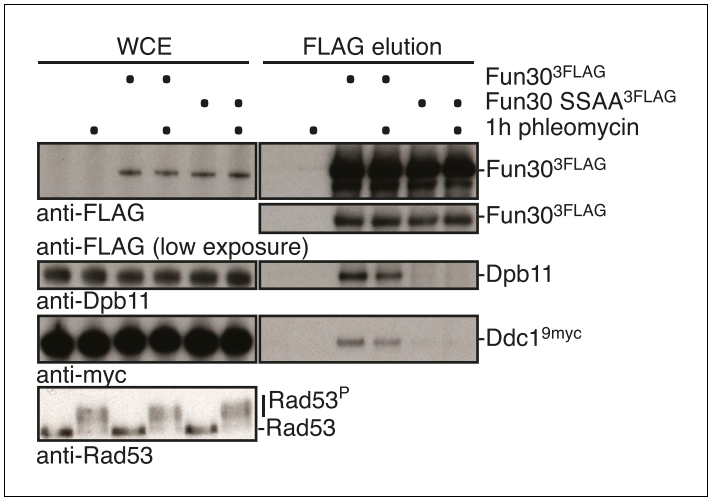

Figure 5—figure supplement 1. The interaction between Fun30 and 9-1-1 depends on mutual interactions with Dpb11, suggesting that Dpb11 forms a molecular bridge in the Fun30-Dpb11-9-1-1 complex. The *fun30-SSAA* mutation abolishes binding of Dpb11 and also Ddc1^{9myc} in Fun30^{3FLAG} Co-IPs. Cells were either left untreated or treated with 50 µg/ml phleomycin, which induced the DNA damage checkpoint (Rad53 activation), but did not influence Dpb11 or Ddc1 binding.

DOI: 10.7554/eLife.21687.016

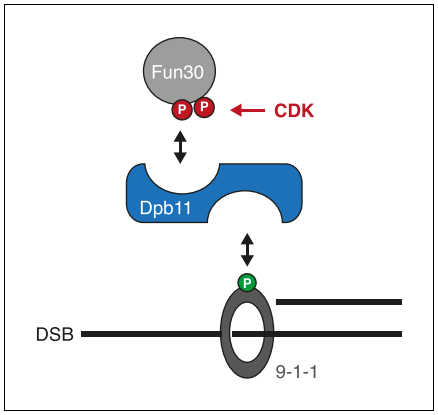

Figure 5—figure supplement 2. Model of the Fun30-Dpb11-9-1-1 association and its regulation.
DOI: 10.7554/eLife.21687.017

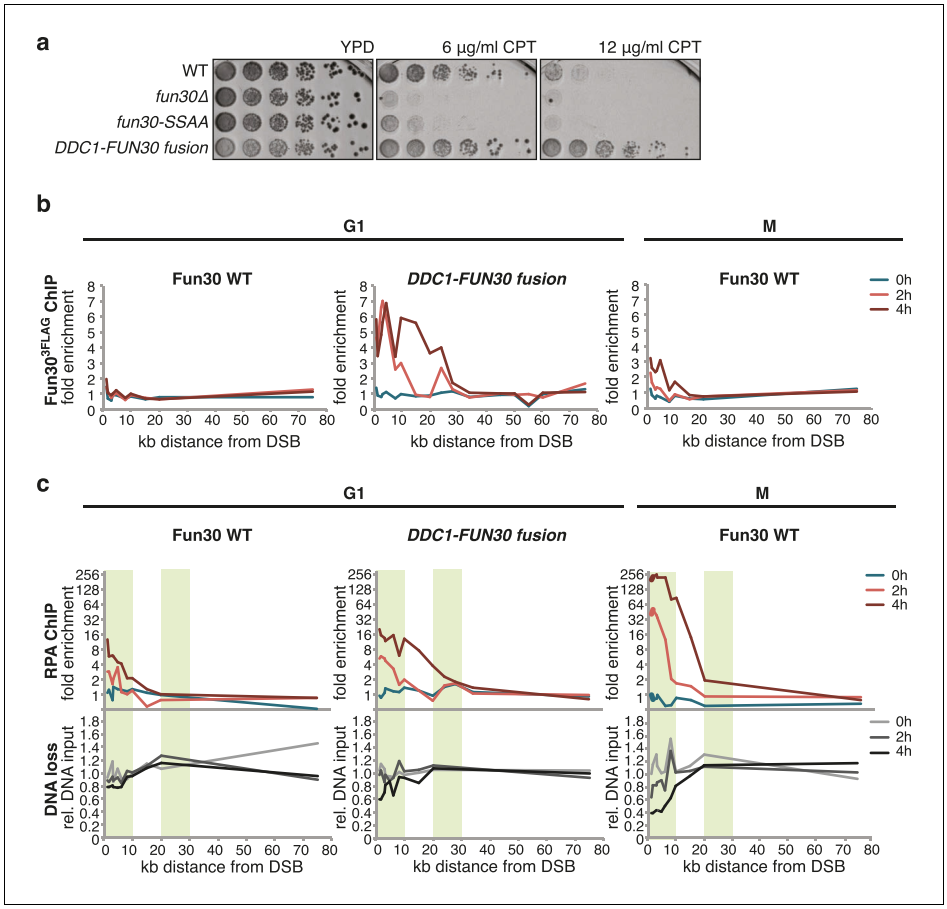

Figure 6. A covalent fusion of Fun30 to the 9-1-1 subunit Ddc1 generates a bypass of the cell cycle regulation of long-range resection. (**a**) The *DDC1-FUN30* fusion confers cellular hyper-resistance to CPT. Spotting of indicated strains as in ***Figure 4A***, but using CPT concentrations of up to 12 µg/ml. (**b**) The *DDC1-FUN30* fusion localizes efficiently to a DSB in G1-arrested cells. Fun30^{3FLAG} ChIPs from *WT*, *fun30-SSAA*, *FUN30-DPB11* and *DDC1-FUN30* cells as in ***Figure 1J***, but from G1 or M phase-arrested cells. Additional Fun30^{3FLAG} ChIP data can be found in ***Figure 6—figure supplement 3***. (**c**) The *DDC1-FUN30* fusion enhances long-range resection in G1-arrested cells. Resection assay as in ***Figure 2A***, but with G1 or M phase-arrested cells. Additional resection assay data can be found in ***Figure 6—figure supplement 3***.

DOI: 10.7554/eLife.21687.018

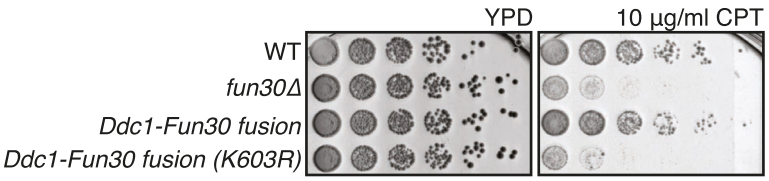

Figure 6—figure supplement 1. The *DDC1-FUN30 fusion* rescues the CPT sensitivity of the *fun30△* mutant in a manner that depends on the Fun30 catalytic activity. *WT*, *fun30Δ*, *DDC1-FUN30 fusion* and *DDC1-FUN30 (K603R) fusion* mutants are spotted on CPT as in ***Figure 4A***.

DOI: 10.7554/eLife.21687.019

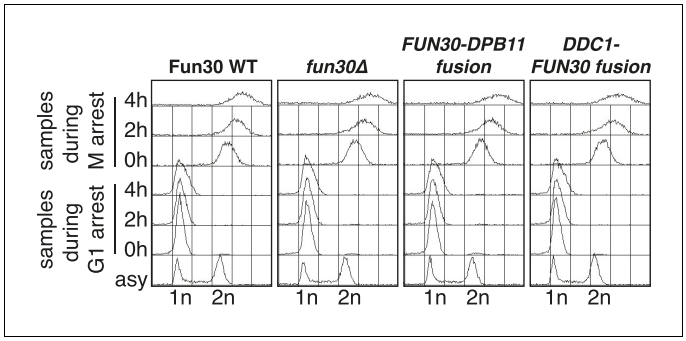

Figure 6—figure supplement 2. Flow cytometric analysis of DNA content for experiments shown in ***Figure 6B–C*** and ***Figure 6—figure supplement 3***.

DOI: 10.7554/eLife.21687.020

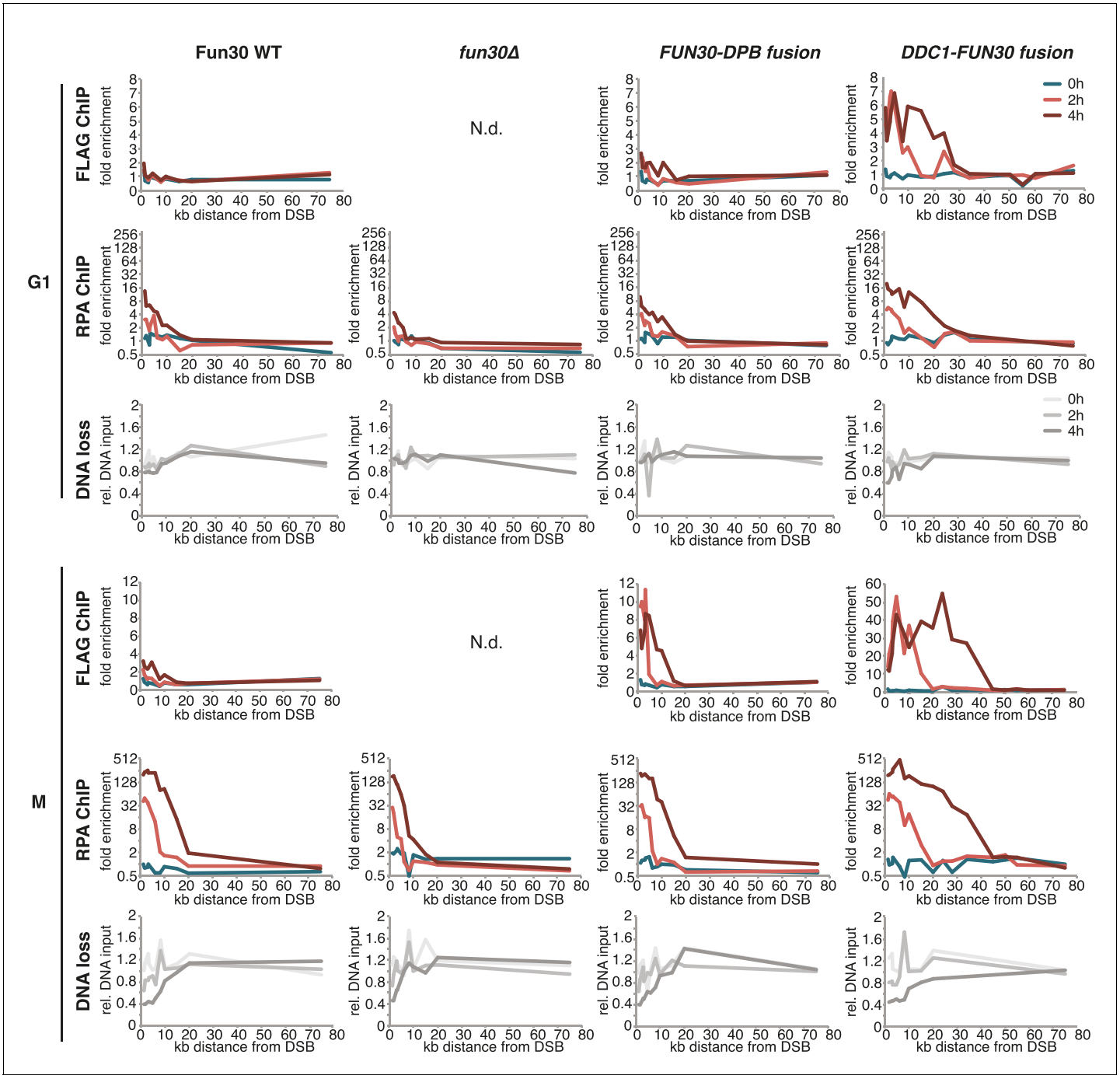

Figure 6—figure supplement 3. The *DDC1-FUN30 fusion* protein efficiently localizes to DSBs and promotes hyper-resection in M phase as well as allowing long-range resection in G1 phase. Cells (*WT, fun30Δ and DDC1-FUN30 fusion*) were arrested in G1 or M phase prior to DSB induction. Fun30 localization was investigated by anti-FLAG ChIP after break induction (upper panels). DNA end resection was investigated by the combined read-out of RPA ChIP and DNA loss (lower panels).

DOI: 10.7554/eLife.21687.021

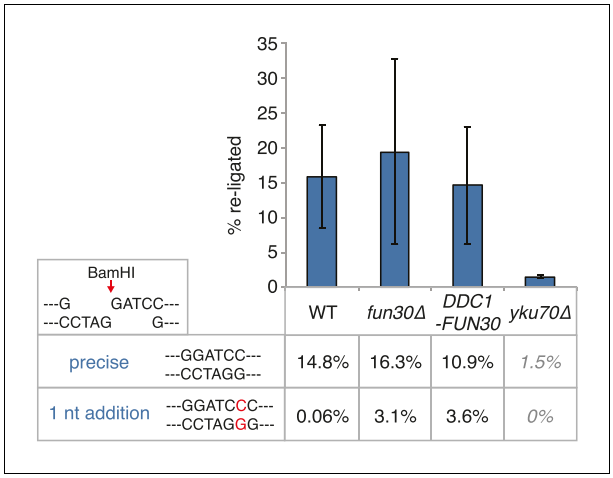

Figure 7. The *DDC1-FUN30* fusion does not significantly inhibit non-homologous end-joining (NHEJ). Precise re-ligation of BamHI-cut pRS316 as measured by cell viability on SC-Ura plates and subsequent sequencing of single colonies was dependent on Ku70 but not significantly affected in *DDC1-FUN30* of *fun30*Δ mutant cells. Plotted are values from three independent experiments representing the viability rate of cells on SC-Ura plates relative to the total cell number and the transformation efficiency of the mock-digested plasmid. Error bars represent standard deviations.

DOI: 10.7554/eLife.21687.022

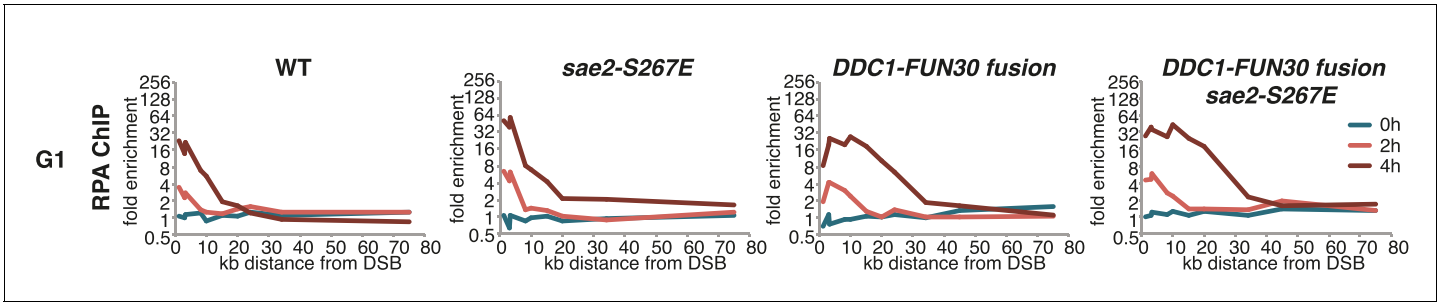

Figure 8. The *DDC1-FUN30* fusion specifically enhances long-range resection in G1, while the *sae2-S267E* phospho-mimicry leads to a small increase in resection initiation. The *sae2-S267E* mutant has little effect on the spreading of DNA end resection in G1, but slightly stimulates the RPA fold enrichment in *WT* and the *DDC1-FUN30* fusion mutant. This suggests that *sae2-S267E* in contrast to the *DDC1-FUN30* fusion does not affect long-range resection. DNA end resection in the indicated strains was analysed by RPA ChIP as in ***Figure 5C*** but with G1 arrested cells.
DOI: 10.7554/eLife.21687.023

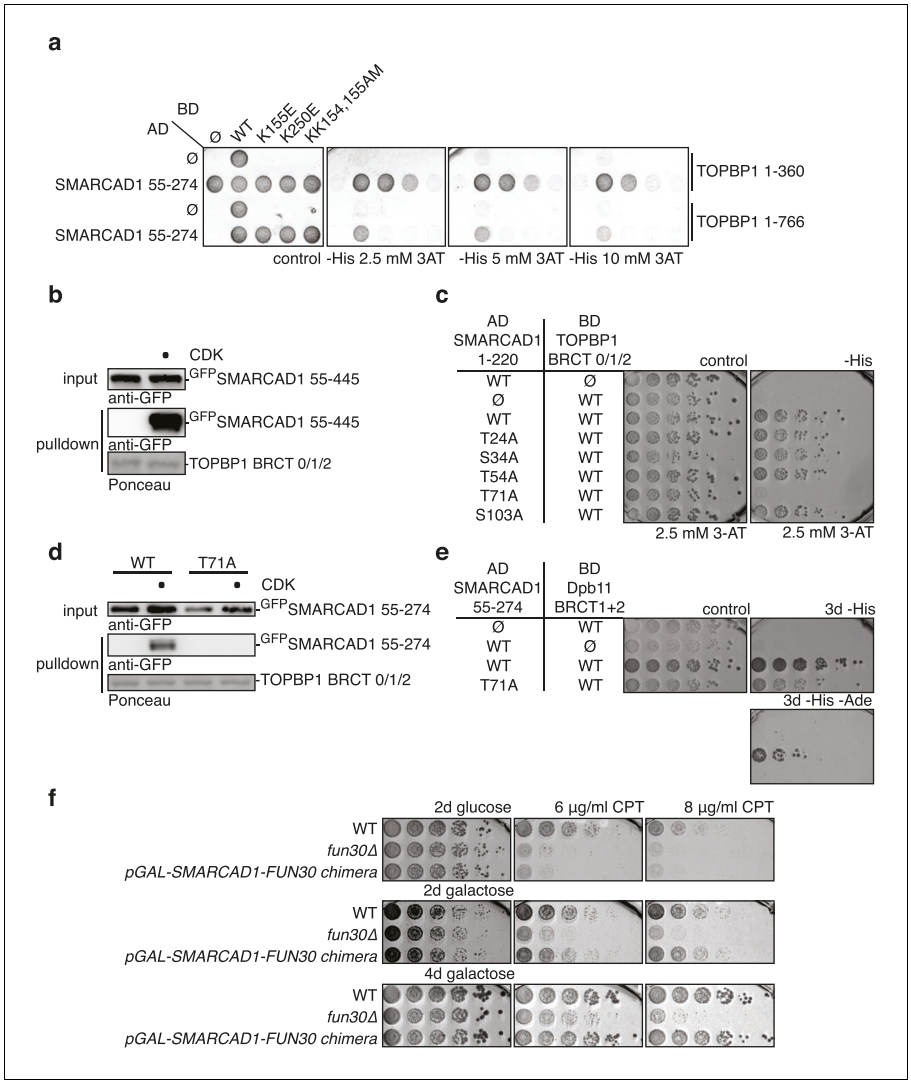

Figure 9. Yeast Fun30 and human SMARCAD1 underlie a conserved regulation. (**a**) SMARCAD1 and TOPBP1 interact and their interaction depends on functional phospho-binding pockets in BRCT1 and BRCT2 of TOPBP1. lexA-BD TOPBP1 1–360 (harbouring BRCT0/1/2) or lexA-BD TOPBP1 1–766 (harbouring BRCT0-5) were tested as *WT* versions or as *K155E, KK154,155AM* (affecting BRCT1) or *K250E* (affecting BRCT2) mutant derivatives. Interaction was tested against the Gal4-AD SMARCAD1 55–274. 3AT was added to –His plates to suppress auto-activation and to increase the stringency of the two-hybrid. Two-hybrid interactions with the lexA-BD TOPBP1 1–360 construct were generally stronger compared to lexA-BD TOPBP1 1–766, leading to milder effects of the K155E and K250E single-mutants, particularly at low 3AT concentrations. (**b**) SMARCAD1 interacts with TOPBP1 after CDK phosphorylation. ^{GFP}SMARCAD1 (55-445) was bound to a ^{GST}TOPBP1 BRCT0/1/2 construct after phosphorylation with CDK. This CDK-dependent interaction was seen with several N-terminal SMARCAD1 constructs, but not with FL, perhaps due to low expression. (**c–d**) Threonine 71 of SMARCAD1, a putative CDK phosphorylation site, is required for TOPBP1 binding. (**c**) Two-hybrid analysis of ^{AD}SMARCAD1 (1-220) and phospho-mutant derivatives to ^{BD}TOPBP1 BRCT0/1/2. (**d**) Co-IP as in (**a**), but additionally using a T71A variant of ^{GFP}SMARCAD1 (55-274). (**e**) Dpb11 can bind to human SMARCAD1, and T71 is important for the interaction. Two-hybrid analysis as in (**b**), but using a ^{BD}Dpb11 BRCT1+2 construct. (**f**) A SMARCAD1-Fun30 chimera lacking the Dpb11-binding site of Fun30, but containing the TOPBP1-binding site of SMARCAD1 restores sensitivity to CPT. The SMARCAD1-Fun30 chimera is expressed from the pGAL1-10 promoter and induced by galactose. Spotting on CPT medium as in ***Figure 4A***.
DOI: 10.7554/eLife.21687.024

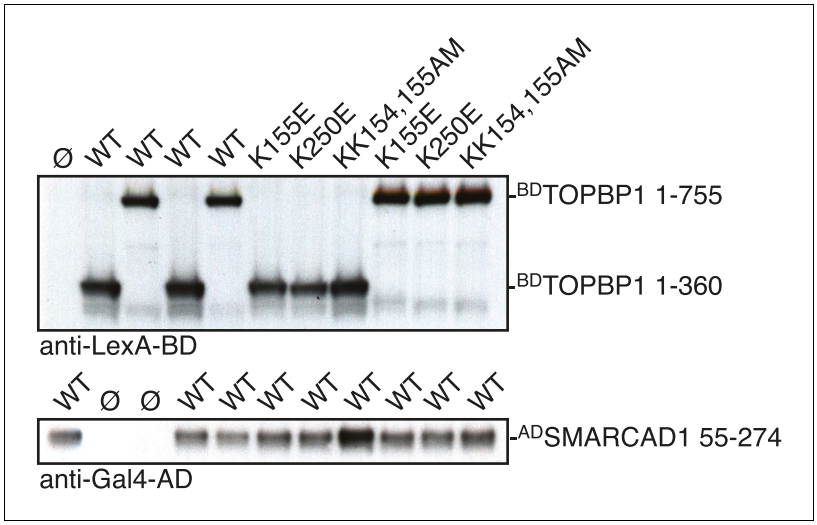

Figure 9—figure supplement 1. The interaction between SMARCAD1 and TOPBP1 depends on functional phospho-binding pockets in BRCT1 and 2 of TOPBP1. Expression control for two-hybrid constructs in ***Figure 9A*** using anti-lexA-BD and anti-Gal4-AD antibodies.
DOI: 10.7554/eLife.21687.025

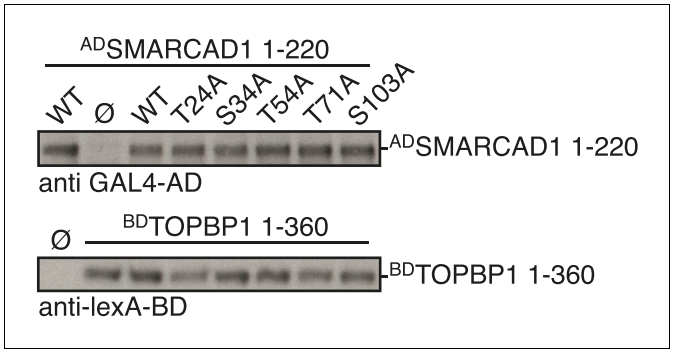

Figure 9—figure supplement 2. Threonine 71 of SMARCAD1, a putative CDK phosphorylation site, is required for TOPBP1 binding. Expression control for two-hybrid constructs in ***Figure 9C*** using anti-lexA-BD and anti-Gal4-AD antibodies.

DOI: 10.7554/eLife.21687.026

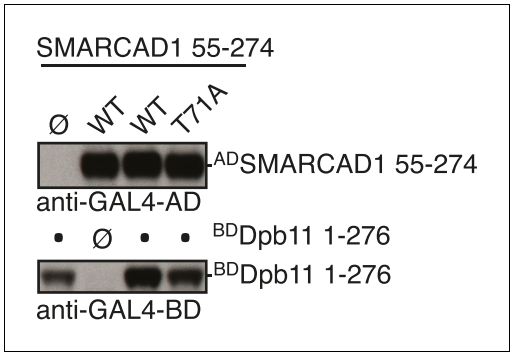

Figure 9—figure supplement 3. Dpb11 can bind to human SMARCAD1, and T71 is important for the interaction. Expression control for two-hybrid constructs in ***Figure 9E*** using anti-Gal4-BD and anti-Gal4-AD antibodies.
DOI: 10.7554/eLife.21687.027

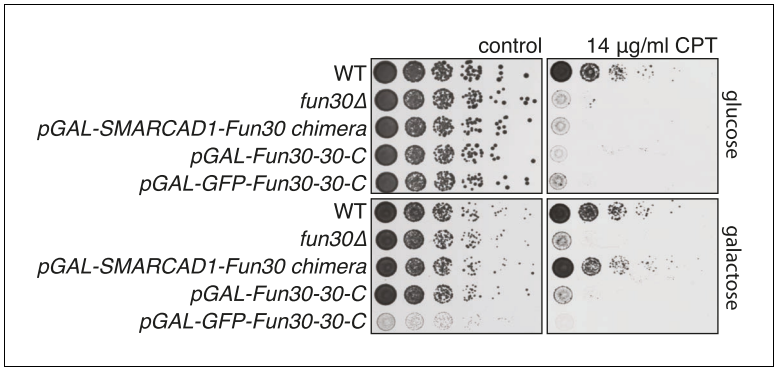

Figure 9—figure supplement 4. A SMARCAD-FUN30 chimera lacking the Dpb11 binding site of Fun30 but containing the putative TOPBP1 binding site of SMARCAD1 restores sensitivity to CPT, while expression of the Fun30 construct lacking the Dpb11 binding site does not. The SMARCAD1-FUN30 chimera, FUN30 30–C and GFP-FUN30 30–C constructs are expressed from the pGAL1-10 promoter and induced by galactose. Spotting on CPT medium as in ***Figure 4A***.

DOI: 10.7554/eLife.21687.028

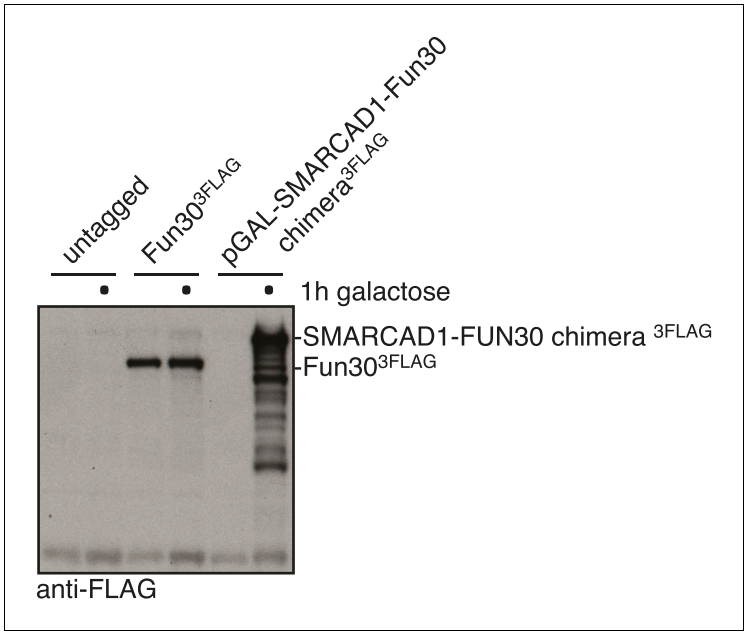

Figure 9—figure supplement 5. Expression control of the SMARCAD1-FUN30 chimera in ***Figure 9F***. SMARCAD1-FUN30 ^{3FLAG} chimerais expressed from the GAL1-10 promoter by addition of galactose. Fun30 ^{3FLAG} expressed from the endogenous promoter serves as control to visualize expression levels of the chimera.
DOI: 10.7554/eLife.21687.029

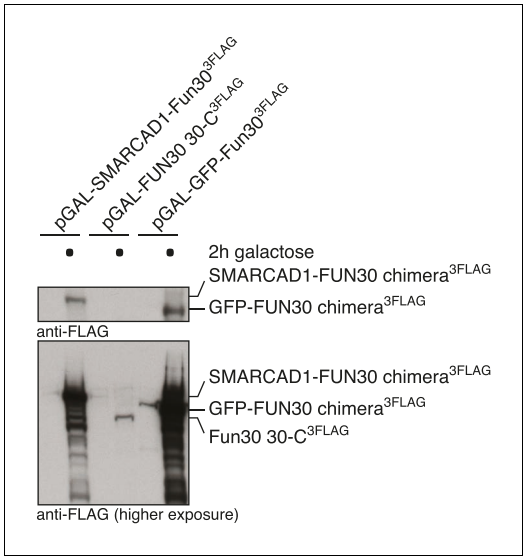

Figure 9—figure supplement 6. Expression control of the SMARCAD1-FUN30 chimera, FUN30-30-C and GFP-FUN30 30-C in ***Figure 9—figure supplement 4*** . SMARCAD1-FUN30^{3FLAG} chimera, FUN30-30-C and GFP-FUN30 30 C are expressed from the GAL1-10 promoter by addition of galactose, which however leads to a stronger expression of the chimera constructs than the truncated FUN30 fragment alone.
DOI: 10.7554/eLife.21687.030

Supplementary file 1

Table 1. Yeast strains used in this study.

Strain	Relevant genotype	Source
W303a	MATa ade2-1 ura3-1 his3-11,15 trp1-1 leu2-3,112 can1-100	(Thomas and Rothstein, 1989)
pJ69-7a	MATa trp1-Δ901 leu2-3,112 901 ura3-52 his3-Δ200 gal4Δ gal8Δ GAL2-ADE2 LYS2::GAL1-HIS3 met2::GAL7-lacZ	(James et al, 1996)
YSB117	MATa lys1Δ::natNT2 pep4Δ::LEU2 bar1Δ::TRP1	this study
YSB220	MATa lys1Δ::natNT2 pep4Δ::LEU2 bar1Δ::TRP1 Fun30-3FLAG::hphNT1	this study
YBP388	MATa pep4Δ::LEU2	this study
YSB760	MATa pep4Δ::LEU2 Fun30-3FLAG::hphNT1	this study
YSB707	MATa cdc28-as1 bar1Δ::trp1 pep4Δ::leu2 Fun30-3FLAG	this study
YSB708	MATa cdc28-as1 bar1Δ::trp1 pep4Δ::leu2	this study
YSB714	MATa bar1Δ::TRP1 pep4Δ::LEU2 natNT2::Fun30-S20A-3FLAG::hphNT1	this study
YSB718	MATa bar1Δ::TRP1 pep4Δ::LEU2 natNT2::Fun30-S28A-3FLAG::hphNT1	this study
YSB719	MATa bar1Δ::TRP1 pep4Δ::LEU2 natNT2::Fun30-SS20,28AA-3FLAG::hphNT1	this study
YSB723	MATa bar1Δ::TRP1 pep4Δ::LEU2 natNT2:: Fun30-SS20,28AA-dpb11ΔN-3FLAG::hphNT1	this study
YSB745	MATa bar1Δ::TRP1 pep4Δ::LEU2 Fun30-3FLAG::hphNT1	this study
YSB743	MATa hmlΔ::prS hmrΔ::pRS bar1Δ::trp1 pGal-HO::ade3 Fun30-3FLAG::hphNT1	this study
YSB725	MATa hmlΔ::prS hmrΔ::pRS bar1Δ::trp1 pGal-HO::ade3 natNT2::Fun30-S20A-3FLAG::hphNT1	this study
YSB727	MATa hmlΔ::prS hmrΔ::pRS bar1Δ::trp1 pGal-HO::ade3 natNT2::Fun30-S28A-3FLAG::hphNT1	this study
YSB728	MATa hmlΔ::prS hmrΔ::pRS bar1Δ::trp1 pGal-HO::ade3 natNT2::Fun30-SS20,28AA-3FLAG::hphNT1	this study
YSB731	MATa hmlΔ::prS hmrΔ::pRS bar1Δ::trp1 pGal-HO::ade3 natNT2::Fun30-SS20,28AA-dpb11ΔN-3FLAG::hphNT1	this study
L40	MATa his3Δ200 trp1-901 leu2-3,112 ade2 LYS2::(4lexAop-HIS3) URA3::(8lexAop-lacZ) GAL4	Invitrogen
YSB782	MATa bar1Δ::TRP1 pep4Δ::LEU2 natNT2::Fun30-SS20,28AA-3FLAG::hphNT1 ddc1-9myc::kanMX4	this study
YSB771	MATa lys1Δ::natNT2 pep4Δ::LEU2 bar1Δ::TRP1 ddc1-9myc::kanMX4	this study
YSB772	MATa lys1Δ::natNT2 pep4Δ::LEU2 bar1Δ::TRP1 Fun30-3FLAG::hphNT1 ddc1-9myc::kanMX4	this study
YSB753	MATa bar1Δ::TRP1 pep4Δ::LEU2 Fun30-3FLAG::hphNT1 ddc1-T602A::kanMX4	this study
YSB517	MATa hmlΔ::prS hmrΔ::pRS bar1Δ::trp1 pGal-HO::ade3	this study
YSB525	MATa hmlΔ::prS hmrΔ::pRS bar1Δ::trp1 pGal-HO::ade3 fun30Δ::hphNT1	this study
YSB260	YMV80 rad51Δ::hphNT1	this study

YSB329	YMV80 fun30-S20A::TRP1 rad51Δ::hphNT1	this study
YSB330	YMV80 fun30-S28A::TRP1 rad51Δ::hphNT1	this study
YSB331	YMV80 fun30-SS20,28AA::TRP1 rad51Δ::hphNT1	this study
YSB253	YMV80 fun30Δ::kanMX4 rad51Δ::hphNT1	this study
UCC3511	hmr::URA3	(Singer et al, 1996)
YSB248	hmr::URA3 fun30Δ::hphNT1	this study
YSB335	hmr::URA3 fun30Δ::hphNT1 Fun30 SS20,28AA::LEU2	this study
AEY1017	ChrVII-L-TEL::URA3	(Meijsing et al, 2001)
YSB246	ChrVII-L-TEL::URA3 fun30Δ::hphNT1	this study
YSB294	ChrVII-L-TEL::URA3 fun30Δ::hphNT1 Fun30::TRP1	this study
YSB297	ChrVII-L-TEL::URA3 fun30Δ::hphNT1 Fun30 SS20,28AA::TRP1	this study
YSB314	MATa lys1Δ::natNT2 pep4Δ::LEU2 bar1Δ::TRP1 fun30Δ::hphNT1	this study
YJW031	MATa rad9Δ::kanMX4	this study
YDG148	MATa fun30Δ::hphNT1	this study
YSB183	MATa fun30Δ::hphNT1 Fun30 SS20,28AA::TRP1	this study
YJW032	MATa fun30Δ::hphNT1 rad9Δ::kanMX4	this study
YJW035	MATa fun30Δ::hphNT1 rad9Δ::kanMX4 Fun30 SS20,28AA::TRP1	this study
YSB758	MATa fun30Δ::kanMX4	this study
YSB761	MATa fun30Δ::kanMX4 Ddc1-Fun30- SS20,28AA-3FLAG::hphNT1	this study
YSB777	MATa fun30Δ::kanMX4 Ddc1-Fun30- SS20,28AA-K603R-3FLAG::hphNT1	this study
YSB791	MATa bar1Δ::TRP1 pep4Δ::LEU2 natNT2:: Fun30-SS20,28AA-K603R-dpb11ΔN-3FLAG::hphNT1	this study
YSB797	MATa hmlΔ::prS hmrΔ::pRS bar1Δ::trp1 pGal-HO::ade3 fun30Δ::kanMX4 Ddc1-Fun30- SS20,28AA-3FLAG::hphNT1	this study
YSB819	MATa fun30Δ::kanMX4 pGAL-SMARCAD1 1-300-FUN30 30-C-3FLAG::URA3	this study
YSB784	MATa bar1Δ::TRP1 pep4Δ::LEU2 GAL4 pGAl1-10 Fun30-3FLAG::HIS3	this study
YSB910	MATa hmlΔ::prS hmrΔ::pRS bar1Δ::trp1 pGal-HO::ade3 Fun30-3FLAG::hphNT1 ura3::Sld3-dpb11ΔN dpb11Δ::kanMX4	this study
YSB911	MATa fun30Δ::kanMX4 pGAL-GFP-FUN30 30-C-3FLAG::URA3	this study
YSB832	MATa hmlΔ::prS hmrΔ::pRS bar1Δ::trp1 pGal-HO::ade3 yku70Δ::natNT2	this study

Table 2. Plasmids used in this study.

name	description
pDG1	pGAD-C1 Fun30 1-188
pAD25	pGAD-C1 Rad9
pAD30	pGAD-C1 Ddc1
pBD23	pGBD-C1 Dpb11
pBD26	pGBD-C1 Dpb11 1-276
pUK211	pB66 Dpb11 271-582
pGAD-C1	pGAD-C1 (James et al, 1996)
pGBD-C1	pGBD-C1 (James et al, 1996)
pUK1	pAG416 GPD-Dpb11
pBP91	pMALp2x RAD9
pKR347	pRS303 Fun30-3FLAG pGAL1-10 GAL4 (Fun30 ORF codon optimized for yeast expression)
pBP48	pGex4T1 DPB11 1-275
pSB035	pGAD-C1 Fun30 1-188 S20A
pSB036	pGAD-C1 Fun30 1-188 S28A
pSB029	pGAD-C1 Fun30 1-188 SS20,28AA
pSB075	pGAD-C1 Fun30 29-188
pAP3	pGAD-C1 Fun30
pKS8	pGAD-C1 Fun30 1-420
pKS10	pGAD-C1 Fun301-500
pKS12	pGAD-C1 Fun30 1-555
pSB181	pBTM116 Dpb11 1-276
pSB31	pRS304 Fun30 S20A
pSB32	pRS304 Fun30 S28A
pSB33	pRS304 Fun30 SS20,28AA
pSB140	pRS304 Fun30 SS20,28AA-Dpb11 276-C
pSB38	pRS305 Fun30 SS20,28AA
pDB104	pB27 TOPBP1 1-360
pSB190	pB6 SMARCAD1 1-220
pSB191	pB6 SMARCAD1 1-220 T24A
pSB192	pB6 SMARCAD1 1-220 S34A
pSB193	pB6 SMARCAD1 1-220 T54A
pSB194	pB6 SMARCAD1 1-220 T71A
pSB195	pB6 SMARCAD1 1-220 T103A
pSB205	pB6 SMARCAD1 55-274
pSB174	pB6 SMARCAD1 55-274 T71A
pSB189	Yiplac211 pGAL-SMARCAD1 1-300-FUN30 30-C-3FLAG
pSB196	Yiplac211 pGAL-FUN30 30-C-3FLAG
pSB247	Yiplac211 pGAL-GFP-FUN30 30-C-3FLAG
pSB242	Yiplac211 pSld3-oSld3-dpb11ΔN
pSB206	pB27 TOPBP1 1-766
pSB197	pB27 TOPBP1 1-360 K155E
pSB198	pB27 TOPBP1 1-360 KK154,155AM
pSB199	pB27 TOPBP1 1-360 K250E
pSB202	pB27 TOPBP1 1-766 K155E
pSB203	pB27 TOPBP1 1-766 KK154,155AM
pSB204	pB27 TOPBP1 1-766 K250E

pPF345	pCS2-GFP-SMARCAD1-55-445
pPF348	pCS2-GFP-SMARCAD1-55-274
pPF351	pCS2-GFP-SMARCAD1-55-274-T71A

Quantitative signalling mechanisms in response to DNA damage

Susanne C. S. Bantele1, Michael Lisby2, and Boris Pfander1*

1 - Max Planck Institute of Biochemistry, DNA Replication and Genome Integrity, Martinsried, Germany
2 - Department of Biology, University of Copenhagen, DK-2200, Copenhagen N, Denmark

Running title: Quantitative signal transduction mechanisms triggered by DNA damage

Key Words: DNA damage checkpoint, Signal transduction, Double strand break, DNA end resection, cell cycle, post-translational modification, genome stability

* Corresponding author:
e-mail: bpfander@biochem.mpg.de
Tel: +49 (0)89-85783050
FAX: +49 (0)89-85783022

The DNA damage checkpoint senses the presence of DNA lesions and controls the cellular response thereto. A crucial DNA damage signal is single-stranded DNA (ssDNA), which is frequently found at sites of DNA damage and recruits the sensor checkpoint kinase Mec1-Ddc2. However, how this signal – and therefore the cells' DNA damage load – is quantified, is poorly understood.

Here, we use genetic manipulation of DNA end resection at a site-specific DNA double-strand break (DSB) in budding yeast to generate quantitatively different DNA damage (ssDNA) signals. Interestingly, two major targets of the Mec1-Ddc2 kinase – Rad53 and γH2A – differ in their dependency on the ssDNA signal, indicating distinct signalling circuits within the checkpoint. The "local" checkpoint signalling circuit leading to γH2A phosphorylation is non-quantitative and unresponsive to increased amounts of damage-associated Mec1-Ddc2 kinase. In contrast, the "global" checkpoint signalling circuit, which triggers Rad53 activation, integrates the ssDNA signal in a quantitative manner.

We find that in the global circuit not only Mec1-Ddc2, but also the 9-1-1 co-sensor complex is recruited to DNA damage sites in a manner that correlates with ssDNA signal strength. Intriguingly, we can uncouple global checkpoint activation from the amount of Mec1-Ddc2 kinase at the lesion by using mutant conditions that hyper-activate the 9-1-1 signalling axis and at the same time reduce the amount of damage-associated Mec1-Ddc2 kinase. We therefore propose that a key function of the 9-1-1 complex and the downstream checkpoint mediators is to generate a checkpoint response, which is quantitative and proportional to the cellular DNA damage load.

Introduction

DNA damage elicits a signalling response termed the DNA damage checkpoint. Once activated, the checkpoint induces several global changes to cell physiology, including cell cycle arrest, transcriptional up-regulation of DNA repair genes and modulation of DNA replication pathways [1-4]. Furthermore, the checkpoint locally controls DNA repair [5,6].

Sensing of DNA damage occurs by so-called apical or sensor kinases, which are recruited to specific DNA structures arising at DNA lesions. Budding yeast has two apical kinases: Mec1-Ddc2 (orthologs of human ATR-ATRIP) and Tel1 (ortholog of human ATM). Tel1 recognizes DNA double strand breaks (DSBs) by interaction with the DSB-binding Mre11-Rad50-Xrs2 complex [7-9], while Mec1-Ddc2 senses the presence of single stranded DNA (ssDNA) via interaction with RPA [10,11]. ssDNA can be readily found at many lesion sites due to damage processing (for example DNA end resection) or stalling of replication forks [12,13]. In fact, in budding yeast, the response to DSBs is even dominated by Mec1-Ddc2 due to high resection rates [14]. Upon sensing of the damage site, the apical kinases trigger a kinase cascade, which leads to phosphorylation and activation of downstream acting factors. Among them are the Rad53 and Chk1 effector kinases, which mediate cell-wide responses [4,15], or histone H2A, which upon phosphorylation forms the γH2A mark of damaged chromatin [16]. In this context, the apical checkpoint kinases face two tasks. On the one hand, they directly phosphorylate factors in the vicinity of the lesion site and thereby control the local response. On the other hand, they facilitate activation of the effector kinases, which after activation will localize throughout the entire nucleus and even into the cytoplasm [17] and phosphorylate checkpoint effectors. Thereby apical kinases set off the global response, although in indirect fashion.

Additionally, so-called mediators are required for checkpoint activation. Among these, the 9-1-1 complex is loaded at the boarder of the ssDNA region (ss-dsDNA junction) by the Rad24-RFC clamp loader complex in a manner that appears independent of Mec1-Ddc2 association [17-20]. The 9-1-1 complex serves as a platform for the association of additional checkpoint mediators (the 9-1-1 axis), such as Dpb11 (TOPBP1 in human) and Rad9 (53BP1 in human), which are critically required for recruitment, phosphorylation and activation of the effector kinase Rad53 [21-27]. Notably, the checkpoint is artificially activated even in the absence of DNA damage, if Mec1-Ddc2 and the 9-1-1 complex are forced to colocalize on chromatin, suggesting a sensor/co-sensor relationship [28].

It is logical to assume that the checkpoint not only qualitatively senses the presence of DNA lesions, but that quantitative signalling inputs are utilized to shape the cellular response to DNA

damage. A highly quantitative signal integration is necessary, given the abundant occurrence of DNA lesions (with estimates ranging to up to 100,000 lesions per day in a human cell, [29,30]). Most likely, cells are never entirely free of DNA lesions and thus require a dose-dependent response with a defined threshold of a tolerable DNA damage load. However, we do currently not understand how DNA damage signals are quantified.

Here, we investigate how the checkpoint quantifies the ssDNA signal at DNA damage sites. To this end we utilized a system of an enzyme-induced DSB in budding yeast [31], which allowed us to manipulate the amount of ssDNA formed at a DSB using genetic manipulation of the DNA end resection process. Intriguingly, we find that specific checkpoint targets respond differently to quantitatively different ssDNA signals. Local γH2A phosphorylation appears unresponsive to changes in the ssDNA signal, while activation of the Rad53 effector kinase responds very strongly to changes in the ssDNA signal. Quantitative signal transduction appears to depend on at least to factors, as we observe that association not only of the Mec1-Ddc2 kinase but also of the 9-1-1 complex and its downstream factors correlate with the ssDNA signal. Notably, we find that artificial hyper-activation of the 9-1-1 axis triggers hyper-activation of the Rad53 effector kinase. This occurs even under conditions of reduced Mec1-Ddc2 association, suggesting that the 9-1-1 complex acts as a quantitative sensor of the ssDNA signal.

Results

Single-stranded DNA is a universal DNA damage signal [1-3]. To investigate how the ssDNA signal is quantified, we studied the checkpoint response to a single site-specific DSB. At DSBs, 3' ssDNA is generated by DNA end resection, a processive, nucleolytic digestion of the 5' strand [32]. Formation of ssDNA therefore is an active process, which allows genetic manipulation of the ssDNA signal using DNA end resection mutants. In order to induce a site-specific DSB at the MAT locus, we used galactose-induced expression of the HO-endonuclease [31]. In M phase arrested cells, DSB induction resulted in processive DNA end resection that reached up to 20 kb distal of the DSB in a 4h timecourse, as visualized by ChIP against RPA (Fig. 1A). In contrast, *exo1Δ sgs1Δ* cells deficient in long-range resection restricted ssDNA formation to less than 1.5 kb (Fig. 1A, see also [33-35]). Mec1-Ddc2 directly interacts with RPA [10]. Consistently, in *exo1Δ sgs1Δ* cells Mec1-Ddc2 association with the DNA damage site was strongly reduced and correlated with the amount of the ssDNA signal (Fig. 1A). Due to its direct interaction with RPA [10], Mec1-Ddc2 was our best candidate for a quantitative sensor of the ssDNA signal. Therefore, we expected the checkpoint response to be diminished in resection-defective *exo1Δ sgs1Δ* cells.

Indeed, *exo1Δ sgs1Δ* cells were unable to phosphorylate and activate the Rad53 effector kinase over the time course of our experiment (Fig. 1B, see also [35,36]). In contrast, when we looked at another Mec1-Ddc2 phosphorylation target - histone H2A - using ChIP with an antibody specific for the γH2A mark, we surprisingly observed highly similar induction of γH2A phosphorylation in *WT* and *exo1Δ sgs1Δ* cells (Fig. 1A). This suggests that γH2A phosphorylation is neither quantitatively responding to the amount of ssDNA signal (in the range tested), nor to the amount of damage-associated Mec1-Ddc2.

The only differences in γH2A formation were observed close to the DSB (up to 7.6 kb for the 4h timepoint, Fig 1A), where the γH2A ChIP signal was consistently lower in WT than *exo1Δ sgs1Δ* cells. Given that RPA and γH2A ChIP signals appear anti-correlated (see Fig. S1A for an overlay), we suggest that this reduction in the γH2A signal occurs due to loss of histones on resected DNA. Otherwise, the γH2A ChIP signals (50-100 kb of DNA to both sides of the DSB on the broken chromosome) were remarkably similar in *WT* and *exo1Δ sgs1Δ*, also when we measured γH2A distribution using either ChIP-qPCR (Fig, S1B) or over the entire damaged chromosome using ChIP-seq methodology (Fig. 1C, Fig. S1C-E). We also found this robustness of γH2A distribution to be independent of the availability of a donor template for repair (Fig. S2A).

To ensure that the observed effects were not influenced by the mutant background used, we employed cell cycle arrest as an alternative means to manipulate the ssDNA signal. Consistent with DNA end resection being highly cell cycle-regulated, we observed very little RPA at the DNA damage site in *WT* cells that were arrested in G1 consistent with a strongly reduced ssDNA signal (Fig. 1D). Accordingly, Mec1-Ddc2 association and Rad53 activation were impaired in G1-arrested cells, as has been observed before (Fig. 1D-E, [37]). In contrast, γH2A phosphorylation was induced to similar extent in G1 and M arrested cells (Fig. 1D), suggesting that γH2A phosphorylation is unresponsive to changes of the strength of the ssDNA signal and the amount of Mec1-Ddc2 associated with the DNA lesion during the cell cycle. We also find a very similar pattern of γH2A phosphorylation, when a DSB is introduced at another genomic location (Chr. VI, close to ARS607, Fig. S2B). Moreover, we see a damage-dependent, but ssDNA signal-unresponsive association of Rtt107 (Fig, S2C), which serves as a proxy for γH2A phosphorylation, as it directly binds to the γH2A mark [38].

Finally, we manipulated DNA end resection using mutants in the resection agonist Fun30 and the resection antagonist Rad9 [39-43]. Fun30 and Rad9 are recruited in a manner that depends on interaction with Dpb11-Ddc1 [22,39,44], and we have previously shown that covalent protein fusions with Dpb11 or Ddc1 can be used to artificially target Rad9 or Fun30 to DSBs and hyper-

activate their respective function as resection regulators [39,45]. We find that the Ddc1-Fun30 fusion hyper-activated DNA end resection similar to a *RAD9* deletion, whereas the Ddc1-Rad9 fusion blocked resection to an even greater extent than a *FUN30* deletion (Fig. 1F,G). However, the damage-induced formation of γH2A was unchanged in these mutants (Fig. 1F,G).

Previous studies have shown that Mec1-Ddc2, and apical checkpoint kinases in general, have a dual function in the local response at the lesion site and in the global, cell-wide response via activation of the effector kinases [4,15]. Our data collectively show that the two best-characterized outputs of these responses, phosphorylated Rad53 and γH2A, have fundamentally different dependencies on the strength of the ssDNA signal. We hypothesize that the signalling circuits leading to phosphorylation of Rad53 and to phosphorylation of H2A are different (see Fig. S3 for a model). We will refer to the circuit leading to γH2A phosphorylation as local checkpoint circuit, since it is involved in controlling local action of repair factors. The circuit leading to Rad53 phosphorylation we will refer to as global checkpoint circuit, as it controls the cell-wide checkpoint response. Notably, our data indicate that already minimal ssDNA signals are able to elicit a full-blown local response that does not appear to correlate with the strength of the ssDNA signal. In contrast, the global response appears to feature a dose-dependent relation with the ssDNA signal.

Given that signalling in the local checkpoint circuit appeared to occur independent of DNA end resection and the ssDNA signal, we tested other factors that might quantitatively determine γH2A phosphorylation. First, we tested whether H2A phosphorylation sites adjacent to the DSB were saturated. We noted that the γH2A ChIP signal increased over the timepoints of our experiments (Fig. 1A, 1D, 2A), strongly arguing against saturation. Additionally, we addressed saturation by reducing the density of H2A phosphorylation sites on chromatin. We made use of the fact that H2A is expressed from two gene copies (*HTA1* and *HTA2*) in budding yeast and that both copies contribute similarly to the pool of H2A protein (1/3 and 2/3, [46]). By introducing the *S129STOP* mutation in either *HTA1* or *HTA2* we therefore reduced the amount of H2A phosphorylation sites on chromatin accordingly. Yet, γH2A phosphorylation after DSB induction was highly similar in *WT*, *hta1-S129STOP* and *hta2-S129STOP* cells (Fig. 2A), suggesting that phosphorylation sites are not limiting.

Second, we tested the possibility that the two sensor kinases Mec1-Ddc2 and Tel1 might differentially contribute to γH2A phosphorylation in resection-proficient and –deficient conditions. A resection-dependent switch from Tel1 to Mec1-Ddc2 is well-documented [16,17,47] and Tel1 activity might compensate for Mec1-Ddc2 in absence of resection. In contrast, we

observed that the overall γH2A ChIP signal after DSB induction was unchanged in *tel1Δ* and *tel1Δ exo1Δ sgs1Δ* cells, with the exception of the region closest to the break, which is directly affected by histone loss due to resection (Fig. 2A). Furthermore, we observed only a minor role for Tel1 in γH2A phosphorylation in response to phleomycin-induced DNA breaks (Fig. S4A). However, the γH2A phosphorylation signal in ChIP was largely abolished in the absence of Mec1 (Fig. S4B; this includes basal levels of γH2A phosphorylation without DSB induction, Fig. S4C).

Lastly, we tested whether any of the established Mec1 activators [22,25,26,48,49] was involved in γH2A phosphorylation and may influence the γH2A ChIP signal. We used a *dna2-WYAA ddc1Δ* strain to abolish Mec1 activation by either Dpb11, Ddc1 or Dna2. In these cells Ddc1 is absent, Dpb11 fails to be recruited to DSBs and Dna2 cannot interact with Mec1-Ddc2 [21,49,50]. However, while we observed a slight reduction in DNA end resection, the γH2A phosphorylation signal after DSB induction was not influenced (Fig. 2C). Consistently, we observed normal phleomycin-induced γH2A phosphorylation in *ddc1Δ*, *dpb11ΔC* and *dna2-WYAA* cells even in absence of Tel1 (Fig. S4D), indicating that γH2A phosphorylation is independent of the known Mec1 activators.

Overall, our data are consistent with a model in which limited amounts of Mec1-Ddc2 are sufficient to facilitate efficient γH2A phosphorylation and γH2A phosphorylation occurs independent of additional activators or checkpoint mediators. We furthermore note that H2A and Mec1-Ddc2 (Fig. 1A) are anchored at specific locations within the damaged chromosome. Thereby, enzyme substrate encounters will be dependent on chromosome architecture and perhaps mobility of these locations [51-56], which may pose a bottleneck to γH2A phosphorylation.

Mec1-Ddc2 association with the damaged chromosome mirrored the ssDNA signal and correlated with Rad53 phosphorylation (Fig. 1A,B). Thus, Mec1-Ddc2 levels at the DSB correlate with signalling in the global checkpoint circuit. Given our results on γH2A phosphorylation, we questioned whether other factors may contribute to the quantitative transduction of the ssDNA signal in the global checkpoint circuit. Notably, Rad53 phosphorylation in response to DSBs is dependent on additional checkpoint proteins, namely the 9-1-1 complex (consisting of Ddc1, Mec3 and Rad17 in budding yeast) and the scaffold proteins Dpb11 and Rad9. For each we tested localization to the DSB by ChIP and found that in *exo1Δ sgs1Δ* cells, localization of all three factors was restricted to the resected DSB end and was overall reduced (Fig. 3A). Also in resection-deficient G1 cells we observed a reduction of DSB recruitment for the 9-1-1 subunit Ddc1 and Dpb11 (Fig. S5A). These data show that the DSB association of checkpoint mediators is influenced by the amount of ssDNA and resection.

We therefore reasoned that the 9-1-1 axis could be involved in the quantitative transduction of the ssDNA signal. Previous data suggested that of all checkpoint mediators, the 9-1-1 complex is furthest upstream [17,21,22,50]. Our data are in agreement with this model, since we observed a loss of the DSB association for Dpb11 or Rad9 in *ddc1-T602A* cells (Fig. 3B).

We therefore followed the hypothesis that 9-1-1 acts as a quantitative sensor of the ssDNA signal and tested DSB association of the 9-1-1 complex in single cells. In case of an HO-induced DSB we could follow the association of proteins with the DSB as the appearance of a single, HO-dependent focus. (Fig. 3D, S5B, see also [17,20,57,58]). In M phase-arrested cells, we observed an increase in the number of cells containing an RPA focus (Rfa1-CFP) over time (>50%, 4h after HO induction). In contrast, in a G1 arrest much fewer cells showed an RPA focus (<12%, 4h after HO induction), suggesting that already the presence of an RPA focus is a good indicator of whether cells engage in DNA end resection (Fig. 3E, S5C). Interestingly, the large majority of M phase cells with an RPA focus contained a colocalizing 9-1-1 focus, supporting the idea that the 9-1-1 complex may localize to ssDNA and act as an ssDNA sensor. To determine quantitative association we measured the fluorescence intensity of colocalizing Rfa1-CFP and Ddc1-YFP foci as an indicator of the number of recruited protein molecules. Notably, we find that HO-induced foci accumulate Ddc1-YFP over time in M phase, as they do for RPA (Fig. 3F). Futhermore, we find a correlation (R^2 = 0.37) between the number of DSB-recruited 9-1-1 and RPA 4h after induction of resection (Fig. 3G), suggesting that the ssDNA signal translates into quantitative association not only of RPA and Mec1-Ddc2, but also of 9-1-1. We also note that the abundance of DSB-associated 9-1-1 complexes and RPA differs by at least an order of magnitude (Fig. 3F, S5D). The DSB foci contain between 300-2000 molecules of RPA 4h after DSB induction, consistent with resection rates of 4-5 kb/h [33] and an RPA footprint of 20/30 bases [59]. At the same time, they accumulate fewer than 30 9-1-1 molecules (Fig. 3F, S5D). Overall, we conclude that resecting DSBs accumulate proportional amounts of ssDNA-bound RPA (and by inference Mec1-Ddc2) and 9-1-1 complexes over time, suggesting that cells may combine both pieces of information to accordingly shape the global checkpoint response.

Our data thus indicates that not only Mec1-Ddc2, but also the 9-1-1 complex and its downstream factors (the 9-1-1 axis) associate with DSBs in a manner that correlates with the ssDNA signal. We wanted to test whether the 9-1-1 complex contributes to transduction of the ssDNA signal in a quantitative manner. Therefore, we enhanced 9-1-1-dependent signalling by expressing a covalent fusion of the 9-1-1 complex to its downstream factor Rad9 (Ddc1-Rad9 fusion). These cells showed markedly enhanced Rad9 recruitment to the DSB compared to WT cells (Fig. 4A). Moreover, resection was blocked and consequently also Ddc2-Mec1 recruitment,

consistent with the role of Rad9 as resection inhibitor (Fig. 1F-G, Fig. 4A). Intriguingly, and despite the decrease of the ssDNA signal and concomitant decrease in Mec1-Ddc2 recruitment, global checkpoint signalling as determined by Rad53 phosphorylation was hyper-activated (Fig. 4B). Thus, mutant conditions, which show enhanced 9-1-1 signalling and decreased Mec1-Ddc2 DSB recruitment hyper-activate the global checkpoint, suggesting that loading of the 9-1-1 complex and signalling along the 9-1-1 axis quantitatively contribute to global checkpoint signalling.

The Ddc1-Rad9 fusion bypasses the phosphorylation of the 9-1-1 complex by Mec1-Ddc2. Therefore, we utilized a second construct, in which Rad9 is fused to Dpb11 (Rad9-dpb11ΔN fusion, [22,45]) and which is at least partly dependent on 9-1-1/Ddc1 phosphorylation by Mec1-Ddc2 (Fig. S6A). Cells expressing this fusion protein showed a remarkably similar phenotype as the Ddc1-Rad9 fusion mutant. Rad9 recruitment to the DSB was increased, while Mec1-Ddc2 recruitment and DNA end resection were decreased. Importantly, however, global checkpoint signalling was hyper-activated (Fig. 1F-G, Fig. 4C-D). In summary, we discovered synthetic conditions that boost signalling specifically in the 9-1-1 axis. These conditions lead to hyper-activated global checkpoint signalling despite decreased recruitment of Mec1-Ddc2. This establishes the 9-1-1 complex as a quantitative sensor of the ssDNA signal, which appears to be limiting for Rad53 activation and signalling in the global checkpoint circuit.

Discussion

DNA damage checkpoint signalling involves a two-layered control in the form of apical and effector kinases. Interestingly, the apical kinases do not only transduce the checkpoint signal to the effector kinases, but phosphorylate checkpoint targets on their own. Targets of apical and effector kinases can be distinguished by their localization. Apical kinase targets such as histone H2A act locally on the damaged chromosome and can be visualized as a focus surrounding the site of the DNA damage [16]. The effector kinases in contrast act cell-wide after a local activation step [4,17,60]. Our study demonstrates a second fundamental difference, as we find that the DNA damage signal (single-stranded DNA) is quantified differentially in the two signalling circuits. The "local" checkpoint circuit leading to γH2A phosphorylation is hypersensitive and already fully active at low (<1.5 kb) ssDNA signals. In contrast, the "global" checkpoint circuit leading to phosphorylation and activation of the Rad53 effector kinase is able to quantitatively respond to a broad range of ssDNA signals and at even >20 kb of ssDNA is not fully active.

Our data is thus consistent with a model, in which the DNA damage checkpoint is not a single pathway, but rather an amalgamation of at least two distinct signalling circuits that can be discriminated by their ability to quantify DNA damage (Fig. S3). It seems plausible that the local checkpoint response needs to be sensitive to the presence of DNA damage in order to steer local DNA repair, but not necessarily needs to integrate the DNA damage signal quantitatively. The global checkpoint response in contrast needs to accurately quantify the cellular DNA damage load in order to control cell-wide processes, such as cell cycle progression or DNA replication.

For the local circuit we find that γH2A phosphorylation sites are not saturated under our experimental conditions (Fig. 2A), suggesting that a bottleneck is limiting H2A phosphorylation, which is neither the amount of damage-associated kinase, nor the availability of phosphorylation sites. We furthermore ruled out that this bottleneck may be posed by any of the known Mec1 activators. One possibility is that this bottleneck is formed by chromosome architecture and mobility. Given that substrate and kinase are tethered to specific chromosomal locations, chromosome mobility may contribute to the frequency of substrate-kinase-encounters [52-56]. However, mutants known to markedly decrease chromosome mobility such as the *RAD9* deletion mutant [53] do not impact on the γH2A phosphorylation in our experiments (Fig. 1F and G). In an alternative model, active Mec1-Ddc2 molecules are not strictly tethered to the ssDNA stretch and can target substrates within a certain diffusion range. In this case, chromosome architecture, but not necessarily mobility will impact on the spreading of γH2A. In fact, data from mammalian cells point towards restriction of the γH2A signal within

topologically associated domains [51]. We suggest therefore that chromosome architecture and perhaps mobility could influence how far the γH2A damage mark spreads into chromatin and could as such shape the response quantitatively.

The global signalling circuit leading to the activation of the Rad53 effector kinase is more complex. Most critically, it involves so-called mediator proteins (9-1-1 complex, Dpb11 and Rad9; 9-1-1 signalling axis), which facilitate signal transduction to the effector kinase. Importantly, DNA damage recruitment of Mec1-Ddc2 and the 9-1-1 complex occur by separate mechanisms [10,19,20,28]. Therefore, the global DNA damage signalling circuit relies on two independent DNA damage sensors [20,28]. Qualitatively, the involvement of two sensors (sensor and co-sensor, respectively) provides for a fail-safe mechanism. Our data suggest, however, that additionally the involvement of two sensors is critical to quantify the ssDNA signal and to yield a proportional response.

How can it be envisioned that the 9-1-1 complex quantitatively senses the ssDNA signal? First of all, formation of a DSB-associated 9-1-1 focus was shown to depend on RPA [17]. Our ChIP data suggest that the 9-1-1 complex associates – possibly in its loaded, DNA encircling form – with the area of resection, where it colocalizes with RPA. This suggests that the 9-1-1 encircles ssDNA. It is possible that 9-1-1 is loaded on ssDNA, perhaps guided by a strong interaction between RPA and the Rad24-RFC clamp loader complex [61], at discontinuities in the RPA filament. However, biochemical studies rather suggest that 9-1-1 is loaded at 5' ss-dsDNA junctions, the leading edge of DNA end resection [18,19]. It is currently unclear, how 9-1-1 loading at the 5' ss-dsDNA junction is coordinated with the activity of resecting nucleases, but most likely this would involve dissociation of the nucleases. After loading and dissociation of the clamp loader, the 9-1-1 could subsequently slide into the ssDNA region. In the dynamic setting of ongoing resection, consecutive cycles of 9-1-1 loading could thereby generate a 9-1-1 signal on resected DNA that correlates with the amount of ssDNA.

We conclude that a main task of all upstream factors (apical kinase, co-sensor and scaffolds) in the global checkpoint circuit is to relay the DNA damage signal to the checkpoint effectors in a quantitative manner. This will allow cells to integrate the DNA damage load over the entire genome and tailor an appropriate cell-wide response. Such a mechanism appears essential given the abundance of endogenous DNA damage [29,30], where checkpoint signalling will typically arise at multiple DNA damage sites. Importantly, by generating a global checkpoint response that correlates with the ssDNA signal, different types of DNA lesions with different ssDNA signals will contribute differentially to the overall checkpoint response, depending on how much ssDNA is formed. Moreover, this mechanism also hyper-sensitizes the global checkpoint

response to S-phase, since an abundant ssDNA signal is formed by replication fork stalling, consistent with the essential function of Mec1-Ddc2 and Rad53 in S phase regulation.

Lastly, we note that certain cell-wide responses such as cell cycle arrest or – in higher eukaryotes – apoptosis [29] are binary switches. This implies the existence of thresholds, above which a certain response is triggered. We are only beginning to understand the quantitative nature of checkpoint signalling, but it will be critical to reveal how such thresholds are formed, how big a DNA damage load cells tolerate and whether these thresholds differ between organisms, cell types or during development. We think that this question is also of central relevance for our understanding of cancer development, since the DNA damage checkpoint forms an important barrier that is often overcome by mutation during tumorigenesis [62,63].

Acknowledgements

We thank Uschi Schkölziger for technical assistance, the sequencing unit of the Laboratory for Functional Genome Analysis (LAFUGA) at LMU Munich for performing next generation sequencing, Assa Yeroslaviz and Tobias Straub for bioinformatic analysis of NGS data, Giovanni Cardone and the MPIB imaging facility for help in data representation, Petr Cejka, Jörg Renkawitz and members of the Pfander lab for stimulating discussion and critical reading of the manuscript. This work was supported by the German Research Council (DFG; project grant PF794/1-1, PF794/3-1 to BP) and the Max Planck Society (to BP), by the Danish Agency for Science, Technology and Innovation (DFF), the Danish National Research Foundation (DNRF115), and the Villum Foundation (to ML). SCB was supported by a Chemiefonds stipend of the FCI.

Author contributions

SCB and BP conceived and designed research. ML performed the microscopy experiments of Fig. 3D-G and S5B-D. All other experiments were performed by SCB. All authors analysed the data. BP wrote the paper, SCB and ML contributed to writing.

Competing financial interests

The authors declare that they have no competing financial interests.

Online Methods

Yeast strains and plasmids

All yeast strains used in this study derive from W303 MATa (strains listed in Supplemental Table 1) and were constructed using standard methods [64]. Cells were grown in YP glucose or YP raffinose media at 30 °C. Cell cycle synchronization was performed using alpha-factor or nocodazole for 2-3 hours and controlled by Flow Cytometry.

For molecular cloning, genes were amplified from yeast genomic DNA and inserted in plasmids using the In-Fusion HD cloning kit (Clontech). For site-directed mutagenesis, a PCR-based protocol with mutagenic oligonucleotides was used. All plasmids used in this study are listed in Supplemental Table 2.

Chromatin Immunoprecipitation (ChIP) and qPCR analysis

For chromatin immunoprecipitation of γH2A, FLAG-tagged proteins and RPA, cells were grown in YP-Raffinose to an OD of 0.5 and –as indicated for the individual experiments- cell cycle arrest was induced. A double-strand break was introduced by inducing the HO endonuclease from the galactose promoter by addition of galactose to the cultures (2% final). 100 ml samples were crosslinked with formaldehyde (final 1%) for 16 min at indicated timepoints and the reaction was quenched with glycine. Cells were harvested by centrifugation, washed in ice-cold PBS and snap-frozen. For lysis, cell pellets were resuspended in 800 µl lysis buffer (50 mM HEPES KOH pH 7.5, 150 mM NaCl, 1 mM EDTA, 1% Triton X-100, 0.1% Na-deoxycolate, 0.1% SDS) and grinded with zirconia beads using a bead beating device. The chromatin was sonified to shear the DNA to a size of 200-500 bp. Subsequently the extracts were cleared by centrifugation, 1% was taken as input sample and 40% were incubated with either anti FLAG M2 magnetic beads (Sigma) for 2 hours or 1.5 hours with anti RFA (AS07-214, Agrisera) or anti γH2A (ab15083, Abcam) antibody followed by 30 min with additional Dynabeads ProteinA (Invitrogen, for RPA and γH2A ChIPs). The beads were washed 3x in lysis buffer, 1x in lysis buffer with 500 mM NaCl, 1x in wash buffer (10 mM Tris-Cl pH 8.0, 0.25 M LiCl, 1 mM EDTA, 0.5% NP-40, 0.5% Na-deoxycholate) and 1x in TE pH 8.0. DNA-protein complexes were eluted in 1% SDS, proteins were removed with Proteinase K (3h, 42°C) and crosslinks were reversed (8h or overnight, 65°C). The DNA was subsequently purified using phenol-chloroform extraction and ethanol precipitation and quantified by quantitative PCR (Roche LightCycler480 System, KAPA SYBR FAST 2x qpCR Master Mix, KAPA Biosystems) at indicated positions with

401 respect to the DNA double-strand break. As control, 2-3 control regions on other chromosomes
402 were quantified.
403
404 **Chromatin Immunoprecipitation (ChIP) and sequencing analysis**
405 For the ChIP-seq experiment shown in Fig. 1C and S1C-E, cells were treated as described above
406 for the ChIP-qPCR experiments. Before de-crosslinking of eluted DNA-protein complexes,
407 samples were digested with RNAse A. The sequencing library was prepared using the MicroPlax
408 Library Preparation kit v2 (Diagenode) according to the manufacturers manual. Size analysis
409 and sequencing were performed by the genomics division of the LAFUGA lab (GeneCenter,
410 Munich). The sequencing data was analysed in collaboration with Assa Yeroslawitz and plotted
411 using the Integrative Genome Browser (IGB) software.
412
413 **Western Blot analysis of γH2A and Rad53 activation**
414 For protein detection by Western Blot, 1 OD of cells were harvested at the indicated time points
415 and snap frozen. Protein lysates were prepared by glass bead lysis and subsequent TCA
416 precipitation. For analysis of γH2A, samples were run on pre-cast NuPage gels (4-12% Bis-Tris,
417 Invitrogen) using MES buffer for 35 min at 200 V. To detect checkpoint activation by analysis of
418 the Rad53 phosphorylation shift, samples were run on 10% SDS-PAGE gels for 180 min at 160
419 V. Western blotting was performed with standard methods. The γH2A phosphorylation was
420 detected using anti γH2A (Abcam, ab15083) antibody, for Rad53 shift detection anti Rad53
421 (Abcam, ab104232) was used. As loading control, the membranes were washed and re-
422 incubated with anti-PGK1 antibody (22D5C8, Invitrogen).
423
424 **Yeast live cell imaging**
425 Rfa1 was tagged with cyan fluorescent protein (CFP, clone W7) and Ddc1 with yellow
426 fluorescent protein (YFP, clone 10C) [17]. For live cell microscopy of Rfa1 and Ddc1 recruitment to
427 an HO-induced DSB, cells were grown shaking in liquid SC+Ade medium (synthetic complete
428 medium supplemented with 100 µg/ml adenine) with 2% raffinose at 25°C to OD600 = 0.2–0.3
429 and arrested either in G1 phase with 10 µg/ml α-factor or in M phase with 15 µg/ml nocodazole
430 for 2 hours before addition of galactose to a final concentration of 2%. Cells were processed for
431 fluorescence microscopy at the indicated times after addition of galactose as described
432 previously [65]. Fluorophores were visualized on a Deltavision Elite microscope (Applied
433 Precision, Inc) equipped with a 100X objective lens (Olympus U-PLAN S-APO, NA 1.4), a cooled
434 Evolve 512 EMCCD camera (Photometrics, Japan), and an Insight solid-state illumination source

(Applied Precision, Inc). Images were acquired using softWoRx (Applied Precision, Inc) software. Image analysis and fluorescence intensity quantification were done using Volocity software (PerkinElmer) and presented as scatter plots using Prism software (GraphPad software, Inc.). Images were pseudocoloured according to the approximate emission wavelength of the fluorophores.

Table 1. Yeast strains:

Strain	Relevant genotype	Source
W303a	MATa ade2-1 ura3-1 his3-11,15 trp1-1 leu2-3,112 can1-100	[1]
YSB117	MATa lys1Δ::natNT2 pep4Δ::LEU2 bar1Δ::TRP1	this study
YSB5	MATa HML hmrΔ::pRS bar1Δ::trp1 pGal-HO::ade3	this study
YSB147	MATa HML hmrΔ::pRS bar1Δ::trp1 pGal-HO::ade3 exo1Δ::natNT2 sgs1Δ::kanMX4	this study
YSB87	MATa HML hmrΔ::pRS bar1Δ::trp1 pGal-HO::ade3 Ddc2-3FLAG::hphNT1	this study
YSB380	MATa HML hmrΔ::pRS bar1Δ::trp1 pGal-HO::ade3 exo1Δ::natNT2 sgs1Δ::kanMX4 Ddc2-3FLAG::hphNT1	this study
YSB633	MATa HML hmrΔ::pRS bar1Δ::trp1 HOcs-ChrIV::hphNT1 pGal-HO::ade3 exo1Δ::natNT2 sgs1Δ::kanMX4	this study
YSB643	MATa HML hmrΔ::pRS bar1Δ::trp1 pGal-HO::ade3 HOcs-ChrIV::hphNT1	this study
YSB336	MATa HML hmrΔ::pRS bar1Δ::trp1 pGal-HO::ade3 fun30Δ::kanMX4	this study
YSB6	MATa HML hmrΔ::pRS bar1Δ::trp1 pGal-HO::ade3 rad9Δ::hphNT1	this study
YSB1046	MATa HML hmrΔ::pRS bar1Δ::trp1 pGal-HO::ade3 fun30Δ::kanMX4 Ddc1-Fun30-3FLAG::hphNT1	this study
YSB1064	MATa HML hmrΔ::pRS bar1Δ::trp1 pGal-HO::ade3 Yiplac128-Ddc1-Rad9-3FLAG::LEU2	this study
YSB165	MATa HML hmrΔ::pRS bar1Δ::trp1 pGal-HO::ade3 tel1Δ::hphNT1	this study
YSB245	MATa HML hmrΔ::pRS bar1Δ::trp1 pGal-HO::ade3 sml1Δ::kanMX4 mec1Δ::hphNT1	this study
YSB374	MATa HML hmrΔ::pRS bar1Δ::trp1 pGal-HO::ade3 sml1Δ::kanMX4 mec1Δ::hphNT1 sgs1Δ::natNT2 exo1Δ::ura3	this study
YSB371	MATa HML hmrΔ::pRS bar1Δ::trp1 pGal-HO::ade3 tel1Δ::hphNT1 sgs1Δ::natNT2 exo1Δ::ura3	this study
YSB1098	MATa HML hmrΔ::pRS bar1Δ::trp1 pGal-HO::ade3 hta1-S129STOP::hphNT1	this study
YSB1100	MATa HML hmrΔ::pRS bar1Δ::trp1 pGal-HO::ade3 hta2-S129STOP::kanMX4	this study
YSB171	MATa HML hmrΔ::pRS bar1Δ::trp1 pGal-HO::ade3 Ddc1-3FLAG::hphNT1	this study
YSB243	MATa HML hmrΔ::pRS bar1Δ::trp1 pGal-HO::ade3 exo1::natNT2 sgs1::kanMX4 Ddc1-3FLAG::hphNT1	this study
YSB15	MATa HML hmrΔ::pRS bar1Δ::trp1 pGal-HO::ade3 Dpb11-3FLAG::natNT2	this study
YSB381	MATa HML hmrΔ::pRS bar1Δ::trp1 pGal-HO::ade3 exo1::natNT2	this study

	sgs1::kanMX4 Dpb11-3FLAG::hphNT1	
YSB9	MATa HML hmrΔ::pRS bar1Δ::trp1 pGal-HO::ade3 Rad9-3FLAG::hphNT1	this study
YSB146	MATa HML hmrΔ::pRS bar1Δ::trp1 pGal-HO::ade3 exo1::natNT2 sgs1::kanMX4 Rad9-3FLAG::hphNT1	this study
YSB210	MATa HML hmrΔ::pRS bar1Δ::trp1 pGal-HO::ade3 Dpb11-3FLAG::natNT2 ddc1-T602A::hphNT1	this study
YSB75	MatA ade3::pGAL::HO bar1Δ::TRP1 hmlΔ::pRS-1 hmrΔpRS-2 Rad9-3FLAG::hphNT1 ddc1-T602A:: natNT2	this study
YSB218	MATa HML hmrΔ::pRS bar1Δ::trp1 pGal-HO::ade3 Rtt107-3FLAG::hphNT1	this study
YSB219	MATa HML hmrΔ::pRS bar1Δ::trp1 pGal-HO::ade3 exo1Δ::natNT2 sgs1Δ::kanMX4 Rtt107-3FLAG::hphNT1	this study
YSB388	MatA ade3::pGAL::HO bar1Δ::TRP1 HML hmrΔpRS-2 Rtt107-3FLAG::natNT2 ddc1-T602A::natNT2	this study
YSB404	MatA ade3::pGAL::HO bar1Δ::TRP1 HML hmrΔpRS-2 Ddc1-3FLAG::hphNT1 lys1Δ::ura3 pep4Δ::leu2	this study
YSB1105	MATa HML hmrΔ::pRS bar1Δ::trp1 pGal-HO::ade3 Ddc2-9myc::hphNT1	this study
YSB1106	MATa HML hmrΔ::pRS bar1Δ::trp1 pGal-HO::ade3 Yiplac128-Ddc1-Rad9-3FLAG::LEU2 Ddc2-9myc::hphNT1	this study
YSB1107	MATa HML hmrΔ::pRS bar1Δ::trp1 pGal-HO::ade3 Rad9-dpb11ΔN-3FLAG::kanMX4	this study
YSB1108	MATa HML hmrΔ::pRS bar1Δ::trp1 pGal-HO::ade3 Rad9-dpb11ΔN-3FLAG::kanMX4 ddc1-T602A::natNT2	this study
YCZ173	ade3::P_{GAL}::HO ARS607::HOcs::KanMX bar1Δ::TRP1 hmlΔ::pRS-1 hmrΔ::pRS-2 matHOcsΔ::pBR-1	[66]
YSB517	MATa hmlΔ::prS hmrΔ::pRS bar1Δ::trp1 pGal-HO::ade3	this study
YSB519	hmlΔ::prS hmrΔ::pRS bar1Δ::trp1 pGal-HO::ade3 exo1Δ::natNT2 sgs1Δ::kanMX4	this study
YSB522	bar1Δ::trp1 pGal-HO::ade3	this study
YSB524	bar1Δ::trp1 pGal-HO::ade3 exo1Δ::natNT2 sgs1Δ::kanMX4	this study
YSB397	MATa HML hmrΔ::pRS bar1Δ::trp1 pGal-HO::ade3 dpb11ΔC::hphNT1	this study
YSB412	MATa HML hmrΔ::pRS bar1Δ::trp1 pGal-HO::ade3 dpb11ΔC::hphNT1 tel1Δ::kanMX4	this study
YSB406	MATa HML hmrΔ::pRS bar1Δ::trp1 pGal-HO::ade3 ddc1Δ::kanMX4	this study
YSB413	MATa HML hmrΔ::pRS bar1Δ::trp1 pGal-HO::ade3 ddc1Δ::kanMX4 tel1Δ::natNT2	this study
YSB407	MATa HML hmrΔ::pRS bar1Δ::trp1 pGal-HO::ade3 dna2Δ::hphNT1 Yiplac211-dna2-WYAA::URA3	this study
YSB414	MATa HML hmrΔ::pRS bar1Δ::trp1 pGal-HO::ade3 dna2Δ::hphNT1 Yiplac211-dna2-WYAA::URA3 tel1Δ::natNT2	this study
YSB408	MATa HML hmrΔ::pRS bar1Δ::trp1 pGal-HO::ade3 dna2Δ::hphNT1 Yiplac211-dna2-WYAA::URA3 ddc1Δ::kanMX4	this study
ML891-5A	MATa ADE2 ade3::pGAL::HO trp1-1 hmrΔpRS-2 DDC1-4ala-YFP RFA1-8ala-CFP RAD5	this study
W5094-1C	MATa ADE2 trp1-1 LYS2 RAD52-YFP RAD5	[67](
ML187-1D	MATa ADE2 trp1-1 LYS2 RAD52-CFP RAD5	this study

Table 2: Plasmids:

name	description
pSB251	Yiplac128-pDdc1-Ddc1-Rad9-3FLAG
pSB143	Yiplac211-pDna2o+t WY128,130AA

Main Figure Legends:

Figure 1

Differential regulation of DNA damage checkpoint effectors: DSB-induced γH2A phosphorylation is independent of DNA end resection, while Rad53 phosphorylation is resection-dependent.

(A) Different amounts of Mec1-Ddc2 kinase on the damaged DNA phosphorylate H2A with similar efficiency. A non-repairable DSB at MAT was induced by Gal-HO expression in M phase-arrested *WT* and long-range deficient *exo1Δ sgs1Δ* strains and protein recruitment was measured at indicated times. Upper panel: fold enrichment of a given locus in an RPA ChIP relative to undamaged control loci. All RPA ChIPs in this paper were performed using an anti-RFA antibody directed against all three subunits of RPA. Middle panel: Mec1-Ddc2 kinase recruitment. In order to detect Mec1-Ddc2, a ChIP against Ddc2-3FLAG was performed using an anti-FLAG antibody. Lower panel: H2A-S129 phosphorylation (γH2A phosphorylation). γH2A phosphorylation was measured with an antibody directed against S129-phosphorylated H2A. The experiment was performed with different numbers of biological replicates, the RPA ChIP three times, the Ddc2 ChIP once, and the γH2A ChIP four times.

(B) The checkpoint kinase Rad53 is activated in a resection-dependent manner. Western blot detecting the phosphorylation-dependent shift of activated Rad53 with an anti-Rad53 antibody. The samples were obtained at indicated time points after Gal-HO induction in M phase-arrested cells.

(C) γH2A phosphorylation around a DSB is not dependent on DNA resection. Overlay of ChIP-seq profiles of γH2A phosphorylation around a DSB at the MAT locus in *WT* cells (blue) and *exo1Δ sgs1Δ* cells (purple). The enrichment is plotted relative to the whole genome average. The DSB was induced for 4h in M phase-arrested cells.

(D,E) γH2A phosphorylation is not influenced by the cell cycle. *WT* strains as in (a), but cells were arrested either in G1 by alpha-factor treatment (left panel), or in M phase by nocodazole treatment (right panel). The experiment was performed with different numbers of biological replicates, the RPA and Ddc2 ChIPs three times and the Ddc2 ChIP twice. **(E)** Western blot analysis of Rad53 activation as in (B), but with G1- and M phase -arrested cells.

(F) Genetic manipulation of DNA end resection by de-regulation of the resection regulators Fun30 and Rad9 does not affect γH2A phosphorylation around a DSB.

WT cells, strains with hyper-active resection (*rad9Δ, DDC1-FUN30 fusion*), or strains with inhibited resection (*fun30Δ, DDC1-RAD9 fusion*) were arrested in M phase and a DSB was

induced. The two fusion proteins carry a 3FLAG tag at their C-terminus for detection. Resection (left panel, ChIP against RPA) and γH2A phosphorylation (right panel, ChIP against H2A-S129 phosphorylation) were measured at indicated time points. The experiment was performed in independent biological duplicates.

(G) Overlay of ChIP-qPCR traces of RPA and γH2A after 4h of DSB induction from panel (F). The blue lines represent enrichments in WT cells, while strains with resection defects are depicted in red and hyper-resecting strains in shades of green.

Figure 2

γH2A phosphorylation is unresponsive to the ssDNA signal, but not because of phosphorylation site saturation, contribution of the sensor kinase Tel1 or the involvement of any known Mec1 activator.

(A) The number of γH2A phosphorylation sites (H2A-S129) on chromatin is not limiting to γH2A phosphorylation efficiency. γH2A phosphorylation was measured in strains with either normal γH2A phosphorylation site availability (*WT*) or in strains in which the number of phosphorylation sites is reduced by mutation of either one of the two H2A coding genes (*hta1-S129STOP, hta2-S129STOP,* respectively).

(B) γH2A is mainly phosphorylated by Mec1-Ddc2. ChIP-qPCR analysis of γH2A phosphorylation around a DSB in M phase. *WT*, *tel1Δ* and *tel1Δ exo1Δ sgs1Δ* mutant strains were analysed at indicated timepoints.

(C) Specific Mec1 activators do not influence γH2A phosphorylation. ChIP-qPCR analysis of DNA resection (upper panels, RPA ChIPs) and γH2A phosphorylation (lower panels, γH2A ChIPs) in *WT* cells and *dna2-WYAA ddc1Δ* mutant cells arrested in M phase.

Figure 3

The 9-1-1 complex is a quantitative sensor of the ssDNA signal.

(A) The major checkpoint cascade proteins 9-1-1 (Ddc1), Dpb11 and Rad9 are recruited to a DSB in a resection-dependent manner. ChIP-qPCR analysis of *WT* (left panel) or *exo1Δ sgs1Δ* (right panel) strains arrested in M phase at indicated time points. Ddc1, Dpb11 and Rad9 were tagged at the C-terminus with 3FLAG tags, respectively, and the ChIP was subsequently performed against the FLAG tag.

(B,C) 9-1-1 (Ddc1) phosphorylation site T602 is required to recruit the checkpoint factors Rad9 and Dpb11 (9-1-1 axis). **(B)** *WT* and *ddc1-T602A* cells (right panels) were arrested in M phase and protein recruitment was analysed by ChIP-qPCR. To this end, Rtt107, Rad9 and Dpb11 were C-terminally tagged with a 3FLAG tag, which was used as affinity tag for the ChIP experiment. **(C)** Analysis of Rad53 phosphorylation by Western Blot against Rad53 as in Fig. 1B, but in *WT* and *ddc1-T602A* cells.

(D) Ddc1 and RPA form DSB-induced foci. Representative microscopy images from the Rfa1- and Ddc1-foci analysis. A DSB was induced at the MAT locus in M phase-arrested cells using Gal-HO and cells were microscopically analysed for Ddc1-YFP foci (yellow, left panel) and Rfa1-CFP foci (blue, second to the left panel) at indicated times. An overlay of both imaging channels is shown in panel three and a bright field image of the yeast cells in panel four. Pictures represent cells before DSB induction (upper line) and 4 hours after DSB induction (lower line).

(E) Ddc1 and RPA foci formation depends on DNA end resection. Plots show the percentage of cells with foci at 0, 2 and 4 hours after DSB induction, values are from the same experiment as in (D). After 4 hours, about 55% of M phase-arrested cells show foci, while only 15% of cells in G1 show foci. In both cases, most of the foci contain Ddc1 and RPA (black fraction). Error bars represent 95% confidence intervals.

(F) RPA and Ddc1 recruitment to a DSB increases over time. Scatter plot depicting the number of RPA (left graph) or Ddc1 (right graph) molecules per focus after 2 hours DSB (left, respectively) and 4 hours DSB (right, respectively). We quantified the number of molecules per focus using nucleus-wide signals of Rfa1-CFP and Ddc1-YFP (normalized against Rad52-CFP/YFP signals (Fig. S5D)) as standard. Same experiment as in (D) and (E). The red lines represent the mean, error bars represent 95% confidence intervals.

(G) Correlation of the recruitment of RPA and Ddc1 to a DSB. Scatter plot showing the number of Ddc1-YFP molecules plotted against the number of Rfa1-CFP molecules per focus. Same experiment as (D)-(F). The black line represents a linear regression line with the corresponding 95% confidence intervals in red.

Figure 4

Mutant conditions that hyper-activate the 9-1-1 axis lead to hyper-activation of the effector kinase Rad53, despite reduced Mec1-Ddc2 recruitment to the DSB.

(A) A covalent Ddc1-Rad9 interaction hyper-recruits Rad9 and blocks Mec1-Ddc2 kinase recruitment to a DSB. *WT* cells and cells expressing a *Ddc1-Rad9-fusion* (same fusion as used in

Fig. 1F+G) were arrested in M phase and analysed at indicated times. ChIP-qPCR measurements of Mec1-Ddc2 recruitment (upper panels, ChIP directed against Ddc2-3FLAG using an anti-FLAG antibody) and Rad9 recruitment to a DSB (lower panels, ChIP directed against Rad9 or the fusion which both carry a 3FLAG tag for detection).

(B) Rad53 activation in response to a DSB is strongly enhanced in *Ddc1-Rad9-fusion* cells. Western blot analysis of Rad53 activation at indicated times after DSB induction, strains as in (A).

(C) A covalent Rad9-Dpb11 fusion protein enhances Rad9 recruitment to the DSB and blocks DNA end resection. *WT* cells and cells expressing a *Rad9-dpb11ΔN-fusion* (lacking BRCT 1+2 of Dpb11 which normally bind to Rad9) were arrested in M phase and analysed at indicated timepoints. ChIP-qPCR measurements of DNA resection (upper panels) and Rad9 recruitment to a DSB (lower panels). To measure Rad9 recruitment, the fusion and Rad9, respectively, were tagged C-terminally with a 3FLAG tag.

(D) Rad53 activation in response to a DSB is enhanced in *Rad9-dpb11ΔN-fusion* cells. Western blot analysis of Rad53 activation at indicated times after DSB induction, strains as in (C).

Supplemental Figure Legends:

Figure S1

γH2A phosphorylation is not correlating with ssDNA signal strength.

(A) RPA and γH2A enrichments around a DSB are anti-correlated, suggesting that resection as read by RPA enrichment evicts histones and thereby the substrate for γH2A phosphorylation. Overlay of RPA (red) and γH2A (blue) ChIP signals after 4h of DSB in *WT* (left panel) and *exo1Δ sgs1Δ* cells (right panel) cells arrested in M phase.

(B) γH2A phosphorylation spreads over a large distance from a DSB (>75 kb) in *WT* and *exo1Δ sgs1Δ cells.* With the exception of the area of resection (Fig. S1A), resection has no influence on γH2A phosphorylation. ChIP-qPCR analysis of *WT* cells or *exo1Δ sgs1Δ* cells after 4h of DSB induction.

γH2A phosphorylation and RPA enrichment around two distinct DSBs anti-correlate in ChIP-seq experiments (C) and depend on the presence of the DSBs (D).

(C) Overlay of ChIP-seq profiles from the same experiment as shown in Fig. 1C. RPA enrichments are plotted in blue, γH2A phosphorylation is plotted in yellow. The positions of the HO-induced DSBs on chromosome 3 (upper two panels) and chromosome 4 (lower two panels)

are indicated by the red dotted line. *WT* cells (upper traces) are compared with *exo1Δ sgs1Δ* mutant cells (lower traces).

(D) ChIP-seq profiles of the 0h time point before induction of DSB. Samples were obtained in the same experiment as data shown in Fig. 1B and Fig. S1A. Analysis of the enrichment of RPA (upper panel, respectively) and γH2A phosphorylation (lower panel, respectively).

(E) Overlay of ChIP-qPCR and ChIP-seq signals. *WT* and *exo1Δ sgs1Δ* cells were arrested in M phase and analysed for γH2A phosphorylation after 4h of DSB induction. qPCR signals (red) are from the same experiment as in (B). Sequencing data (blue) is from the experiment plotted in Fig. 1C and Fig. S1C and S1D.

Figure S2

γH2A phosphorylation is not correlating with ssDNA signal strength – additional controls.

(A) DNA end resection (left panel) and γH2A phosphorylation (right panel) were measured by ChIP in *WT* strains or *exo1Δ sgs1Δ* strains with both mating type loci deleted, or intact HML or intact HML and HMR loci. All strains used in this study were HML hmrΔ if not indicated differently. Samples were analysed after 4 h of DSB induction.

(B) Also at an independent locus (ARS607), γH2A phosphorylation around a DSB is not showing a response that correlates with the ssDNA signal. ChIP-qPCR analysis of strains carrying an ectopic HO cutsite on ARS607 arrested in G1 (left panels) or M phase (right panels). RPA enrichment (upper panels) and γH2A phosphorylation (lower panels) were analysed at indicated times.

(C) Manipulation of DNA end resection by de-regulation of the Sgs1 helicase does not affect γH2A phosphorylation. ChIP-qPCR analysis of a *WT strain* arrested in G1 (left panels) or in M phase (middle panels) and an *sgs1-ss* mutant strain in M phase (right panels). Resection (upper panels) and γH2A phosphorylation (lower panels) were analysed at indicated times.

(D) Rtt107 is associating with a DSB in a resection-independent manner. Rtt107 recruitment to a DSB was measured at indicated times in *WT* strains arrested in G1 (left panel) or in M phase (middle panel), or in *exo1Δ sgs1Δ* cells arrested in M phase (right panel). Rtt107 was tagged with a C-terminal 3FLAG tag and detected by a ChIP directed against the FLAG tag.

Figure S3

615 DNA damage checkpoint signalling can be subdivided in two separate, Mec1-dependent
616 signaling circuits. Models of local **(A)** and global **(B)** checkpoint signalling circuits.
617 **(A)** Mec1-Ddc2 (orange) bound to RPA (red) phosphorylates γH2A as a substrate of the local
618 checkpoint signalling circuit (green) in a resection-independent manner.
619 **(B)** Mec1-Ddc2 (orange) bound to RPA (red) phosphorylates the checkpoint proteins of the 9-1-
620 1 axis (Ddc1, Dpb11, Rad9 and Rad53, shades of blue) as substrates of the global checkpoint
621 signalling circuit, which depends on DNA end resection and culminates in the activation of the
622 Rad53 effector kinase.
623
624 **Figure S4**
625 γH2A phosphorylation is strongly dependent on Mec1, but only weakly on Tel1, and is not
626 influenced by specific Mec1 activators.
627 **(A)** γH2A and Rad53 phosphorylation after phleomycin treatment are strongly decreased in
628 cells lacking Mec1, but almost unaffected in cells lacking Tel1. Western blot analysis of Rad53
629 phosphorylation (upper panels, respectively), γH2A phosphorylation (middle panels,
630 respectively) and PGK1 as a control for protein levels (lower panels, respectively) in *WT* cells or
631 *exo1Δ sgs1Δ*, *mec1Δ sml1Δ*, *exo1Δ sgs1Δ mec1Δ sml1Δ*, *tel1Δ*, *exo1Δ sgs1Δ tel1Δ* mutant cells
632 arrested in M phase after treatment with 50 μg/ml phleomycin for the indicated times.
633 **(B)** γH2A formation at a DSB strongly depends on the Mec1 kinase. IP/input ratios of the ChIP-
634 qPCR analysis of γH2A (upper panels) and RPA (lower panels) after indicated times of DSB
635 induction in M phase-arrested cells. *sml1Δ mec1Δ* cells (right panels, respectively) were
636 compared to *sml1Δ* cells (left panels, respectively).
637 **(C)** Damage-independent levels of γH2A phosphorylation at two independent loci on non-
638 broken chromosomes are reduced in cells lacking Mec1. γH2A ChIP IP/input ratios from two
639 loci on distinct, undamaged chromosomes are plotted. The values are from the same experiment
640 as in (B).
641 **(D)** γH2A phosphorylation is not influenced by the absence of a specific Mec1 activator after
642 phleomycin treatment. Western blot analysis of γH2A phosphorylation (upper panels,
643 respectively) and PGK1 as a control for protein concentrations (lower panels, respectively) in
644 *WT* cells or *ddc1Δ, dpb11ΔC* or *dna2-WYAA* mutant cells, either in a *WT* background or a *tel1Δ*
645 background arrested in M phase. Samples were analysed at indicated time points.
646
647 **Figure S5**

Regulators of the global checkpoint circuit (9-1-1 axis) differentially localize to a DSB in G1 and M phase-arrested cells.

(A) Recruitment of 9-1-1 (Ddc1), Dpb11 and Rad9 is enhanced in M phase. ChIP-qPCR of *WT* strains arrested in G1 (left panels) or M phase (right panels) at indicated times. For detection, Ddc1, Dpb11 and Rad9 were tagged with a C-terminal 3FLAG tag, and ChIPs were directed against the FLAG tag.

(B)-(D) Additional information to the microscopical Ddc1- and RPA- foci analysis in Fig. 3D-G.

(B) Representative microscopy images from the Rfa1- and Ddc1-foci analysis in G1-arrested cells. A DSB was induced at the MAT locus in G1 phase-arrested cells using Gal-HO and cells were microscopically analysed for Ddc1-YFP foci (yellow, left panel) and Rfa1-CFP foci (blue, second to the left panel) from 4h timepoint. An overlay of both imaging channels is shown in panel three and a bright field image of the yeast cells in the right panel.

(C) FACS analysis of G1 arrest. Cells were fixed for FACS analysis before addition of alpha-factor at 0, 2 and 4 hours of DSB induction. The graphs show the DNA content per cell.

(D) Normalization of Rfa1 and Ddc1 foci intensity against Rad52 as a standard. YFP and CFP intensities were quantified throughout the nucleus and the total number of tagged molecules was calculated by comparing the values to the intensity of the respectively tagged Rad52 molecules.

Figure S6

The *Rad9-dpb11ΔN* fusion is partly dependent on Ddc1 phosphorylation.

(A) ChIP-qPCR analysis of DNA resection (upper panels) and Rad9 recruitment (lower panels) in WT cells, *Rad9-dpb11ΔN fusion* cells and *Rad9-dpb11ΔN fusion ddc1-T602A* cells. All strains were arrested in M phase and samples were taken at indicated time points. For detection, Rad9 and the Rad9 fusion were tagged C-terminally with a 3FLAG tag and the ChIPs were directed against the 3FLAG tag. The data in the left and middle panels is identical to the data shown in Fig. 4C.

(B) The same strains as in (A) were analysed for checkpoint activation in a Rad53 Western Blot, including a *ddc1-T602A* mutant strain. The Western Blot samples are from the same experiment as shown in Fig. 4D.

680 **References:**

681

682 1. Harrison, J. C. & Haber, J. E. Surviving the breakup: the DNA damage checkpoint. *Annu.*
683 *Rev. Genet.* **40,** 209–235 (2006).
684 2. Finn, K., Lowndes, N. F. & Grenon, M. Eukaryotic DNA damage checkpoint activation in
685 response to double-strand breaks. *Cell. Mol. Life Sci.* **69,** 1447–1473 (2011).
686 3. Villa, M., cassani, C., Gobbini, E., Bonetti, D. & Longhese, M. P. Coupling end resection with
687 the checkpoint response at DNA double-strand breaks. *Cell. Mol. Life Sci.* **73,** 3655–3663
688 (2016).
689 4. Branzei, D. & Foiani, M. The Rad53 signal transduction pathway: Replication fork
690 stabilization, DNA repair, and adaptation. *Exp. Cell Res.* **312,** 2654–2659 (2006).
691 5. Lukas, J., Lukas, C. & Bartek, J. More than just a focus: The chromatin response to DNA
692 damage and its role in genome integrity maintenance. *Nat. Cell Biol.* **13,** 1161–1169
693 (2011).
694 6. Kinner, A., Wu, W., Staudt, C. & Iliakis, G. Gamma-H2AX in recognition and signaling of
695 DNA double-strand breaks in the context of chromatin. *Nucleic Acids Res.* **36,** 5678–5694
696 (2008).
697 7. Nakada, D., Matsumoto, K. & Sugimoto, K. ATM-related Tel1 associates with double-
698 strand breaks through an Xrs2-dependent mechanism. *Genes Dev.* **17,** 1957–1962 (2003).
699 8. Lee, J.-H. & Paull, T. T. ATM activation by DNA double-strand breaks through the Mre11-
700 Rad50-Nbs1 complex. *Science* **308,** 551–554 (2005).
701 9. Falck, J., Coates, J. & Jackson, S. P. Conserved modes of recruitment of ATM, ATR and DNA-
702 PKcs to sites of DNA damage. *Nature* **434,** 605–611 (2005).
703 10. Zou, L. & Elledge, S. J. Sensing DNA damage through ATRIP recognition of RPA-ssDNA
704 complexes. *Science* **300,** 1542–1548 (2003).
705 11. Deshpande, I. *et al.* Structural Basis of Mec1-Ddc2-RPA Assembly and Activation on
706 Single-Stranded DNA at Sites of Damage. *Mol. Cell* **68,** 431–445.e5 (2017).
707 12. Symington, L. S. End Resection at Double-Strand Breaks: Mechanism and Regulation. *Cold*
708 *Spring Harbor Perspectives in Biology* **6,** a016436–a016436 (2014).
709 13. Sogo, J. M., Lopes, M. & Foiani, M. Fork reversal and ssDNA accumulation at stalled
710 replication forks owing to checkpoint defects. *Science* **297,** 599–602 (2002).
711 14. Sanchez, Y. *et al.* Regulation of RAD53 by the ATM-like kinases MEC1 and TEL1 in yeast
712 cell cycle checkpoint pathways. *Science* **271,** 357–360 (1996).
713 15. de Oliveira, F. M. B. *et al.* Phosphoproteomics Reveals Distinct Modes of Mec1/ATR
714 Signaling during DNA Replication. *Mol. Cell* 1–10 (2015).
715 doi:10.1016/j.molcel.2015.01.043
716 16. Downs, J. A., Lowndes, N. F. & Jackson, S. P. A role for Saccharomyces cerevisiae histone
717 H2A in DNA repair. *Nature* **408,** 1001–1004 (2000).
718 17. Lisby, M., Barlow, J. H., Burgess, R. C. & Rothstein, R. Choreography of the DNA damage
719 response: spatiotemporal relationships among checkpoint and repair proteins. *Cell* **118,**
720 699–713 (2004).
721 18. Majka, J. & Burgers, P. M. J. Yeast Rad17/Mec3/Ddc1: a sliding clamp for the DNA damage
722 checkpoint. *Proceedings of the National Academy of Sciences* **100,** 2249–2254 (2003).
723 19. Majka, J., Binz, S. K., Wold, M. S. & Burgers, P. M. J. Replication protein A directs loading of
724 the DNA damage checkpoint clamp to 5'-DNA junctions. *J. Biol. Chem.* **281,** 27855–27861
725 (2006).
726 20. Melo, J. A., Cohen, J. & Toczyski, D. P. Two checkpoint complexes are independently
727 recruited to sites of DNA damage in vivo. *Genes Dev.* **15,** 2809–2821 (2001).
728 21. Puddu, F. *et al.* Phosphorylation of the Budding Yeast 9-1-1 Complex Is Required for

Dpb11 Function in the Full Activation of the UV-Induced DNA Damage Checkpoint. *Mol. Cell. Biol.* **28,** 4782–4793 (2008).
22. Pfander, B. & Diffley, J. F. X. Dpb11 coordinates Mec1 kinase activation with cell cycle-regulated Rad9 recruitment. *EMBO J.* **30,** 4897–4907 (2011).
23. Durocher, D., Henckel, J., Fersht, A. R. & Jackson, S. P. The FHA domain is a modular phosphopeptide recognition motif. *Mol. Cell* **4,** 387–394 (1999).
24. Wang, H. & Elledge, S. J. Genetic and physical interactions between DPB11 and DDC1 in the yeast DNA damage response pathway. *Genetics* **160,** 1295–1304 (2002).
25. Mordes, D. A., Nam, E. A. & Cortez, D. Dpb11 activates the Mec1-Ddc2 complex. *Proc. Natl. Acad. Sci. U.S.A.* **105,** 18730–18734 (2008).
26. Navadgi-Patil, V. M. & Burgers, P. M. Yeast DNA Replication Protein Dpb11 Activates the Mec1/ATR Checkpoint Kinase. *Journal of Biological Chemistry* **283,** 35853–35859 (2008).
27. Germann, S. M. *et al.* Dpb11/TopBP1 plays distinct roles in DNA replication, checkpoint response and homologous recombination. *DNA Repair (Amst.)* **10,** 210–224 (2011).
28. Bonilla, C. Y., Melo, J. A. & Toczyski, D. P. Colocalization of sensors is sufficient to activate the DNA damage checkpoint in the absence of damage. *Mol. Cell* **30,** 267–276 (2008).
29. Ciccia, A. & Elledge, S. J. The DNA Damage Response: Making It Safe to Play with Knives. *Mol. Cell* **40,** 179–204 (2010).
30. Hoeijmakers, J. H. J. DNA damage, aging, and cancer. *N. Engl. J. Med.* **361,** 1475–1485 (2009).
31. Lee, S. E. *et al.* Saccharomyces Ku70, mre11/rad50 and RPA proteins regulate adaptation to G2/M arrest after DNA damage. *Cell* **94,** 399–409 (1998).
32. Symington, L. S. Mechanism and regulation of DNA end resection in eukaryotes. *Critical Reviews in Biochemistry and Molecular Biology* **51,** 195–212 (2016).
33. Zhu, Z., Chung, W.-H., Shim, E. Y., Lee, S. E. & Ira, G. Sgs1 helicase and two nucleases Dna2 and Exo1 resect DNA double-strand break ends. *Cell* **134,** 981–994 (2008).
34. Mimitou, E. P. & Symington, L. S. Sae2, Exo1 and Sgs1 collaborate in DNA double-strand break processing. *Nature* **455,** 770–774 (2008).
35. Gravel, S., Chapman, J. R., Magill, C. & Jackson, S. P. DNA helicases Sgs1 and BLM promote DNA double-strand break resection. *Genes Dev.* **22,** 2767–2772 (2008).
36. Clerici, M., Trovesi, C., Galbiati, A., Lucchini, G. & Longhese, M. P. Mec1/ATR regulates the generation of single-stranded DNA that attenuates Tel1/ATM signaling at DNA ends. *EMBO J.* **33,** 198–216 (2014).
37. Ira, G. *et al.* DNA end resection, homologous recombination and DNA damage checkpoint activation require CDK1. *Nature* **431,** 1011–1017 (2004).
38. Li, X. *et al.* Structure of C-terminal tandem BRCT repeats of Rtt107 protein reveals critical role in interaction with phosphorylated histone H2A during DNA damage repair. *Journal of Biological Chemistry* **287,** 9137–9146 (2012).
39. Bantele, S. C., Ferreira, P., Gritenaite, D., Boos, D. & Pfander, B. Targeting of the Fun30 nucleosome remodeller by the Dpb11 scaffold facilitates cell cycle-regulated DNA end resection. *eLife* **6,** e21687 (2017).
40. Chen, X. *et al.* The Fun30 nucleosome remodeller promotes resection of DNA double-strand break ends. *Nature* **489,** 576–580 (2012).
41. Costelloe, T. *et al.* The yeast Fun30 and human SMARCAD1 chromatin remodellers promote DNA end resection. *Nature* **489,** 581–584 (2012).
42. Eapen, V. V., Sugawara, N., Tsabar, M., Wu, W. H. & Haber, J. E. The Saccharomyces cerevisiae Chromatin Remodeler Fun30 Regulates DNA End Resection and Checkpoint Deactivation. *Mol. Cell. Biol.* **32,** 4727–4740 (2012).
43. Trovesi, C., Falcettoni, M., Lucchini, G., Clerici, M. & Longhese, M. P. Distinct Cdk1 requirements during single-strand annealing, noncrossover, and crossover

779 recombination. *PLoS Genet.* **7,** e1002263 (2011).
780 44. Granata, M. *et al.* Dynamics of Rad9 Chromatin Binding and Checkpoint Function Are
781 Mediated by Its Dimerization and Are Cell Cycle–Regulated by CDK1 Activity. *PLoS Genet.*
782 **6,** e1001047 (2010).
783 45. di Cicco, G., Bantele, S. C. S., Reußwig, K.-U. & Pfander, B. A cell cycle-independent mode of
784 the Rad9-Dpb11 interaction is induced by DNA damage. *Nature Publishing Group* **7,**
785 11650 (2017).
786 46. Moran, L., Norris, D. & Osley, M. A. A yeast H2A-H2B promoter can be regulated by
787 changes in histone gene copy number. *Genes Dev.* **4,** 752–763 (1990).
788 47. Clerici, M., Trovesi, C., Galbiati, A., Lucchini, G. & Longhese, M. P. Mec1/ATR regulates the
789 generation of single-stranded DNA that attenuates Tel1/ATM signaling at DNA ends.
790 *EMBO J.* n/a–n/a (2013). doi:10.1002/embj.201386041
791 48. Majka, J., Niedziela-Majka, A. & Burgers, P. M. J. The checkpoint clamp activates Mec1
792 kinase during initiation of the DNA damage checkpoint. *Mol. Cell* **24,** 891–901 (2006).
793 49. Kumar, S. & Burgers, P. M. Lagging strand maturation factor Dna2 is a component of the
794 replication checkpoint initiation machinery. *Genes Dev.* (2013).
795 doi:10.1101/gad.204750.112
796 50. Navadgi-Patil, V. M. & Burgers, P. M. The unstructured C-terminal tail of the 9-1-1 clamp
797 subunit Ddc1 activates Mec1/ATR via two distinct mechanisms. *Mol. Cell* **36,** 743–753
798 (2009).
799 51. Aymard, F. *et al.* Genome-wide mapping of long-range contacts unveils clustering of DNA
800 double-strand breaks at damaged active genes. *Nat. Struct. Mol. Biol.* **24,** 353–361 (2017).
801 52. Hauer, M. H. *et al.* Histone degradation in response to DNA damage enhances chromatin
802 dynamics and recombination rates. *Nat. Struct. Mol. Biol.* **24,** 99–107 (2017).
803 53. Seeber, A., Dion, V. & Gasser, S. M. Checkpoint kinases and the INO80 nucleosome
804 remodeling complex enhance global chromatin mobility in response to DNA damage.
805 *Genes Dev.* **27,** 1999–2008 (2013).
806 54. Dion, V., Kalck, V., Horigome, C., Towbin, B. D. & Gasser, S. M. Increased mobility of
807 double-strand breaks requires Mec1, Rad9 and the homologous recombination
808 machinery. *Nat. Cell Biol.* **14,** 502–509 (2012).
809 55. Miné-Hattab, J. & Rothstein, R. Increased chromosome mobility facilitates homology
810 search during recombination. *Nat. Cell Biol.* **14,** 510–517 (2012).
811 56. Miné-Hattab, J., Recamier, V., Izeddin, I., Rothstein, R. & Darzacq, X. Multi-scale tracking
812 reveals scale-dependent chromatin dynamics after DNA damage. *Mol. Biol. Cell* **28,** 3323–
813 3332 (2017).
814 57. Lisby, M., Mortensen, U. H. & Rothstein, R. Colocalization of multiple DNA double-strand
815 breaks at a single Rad52 repair centre. *Nat. Cell Biol.* **5,** 572–577 (2003).
816 58. Dubrana, K., van Attikum, H., Hediger, F. & Gasser, S. M. The processing of double-strand
817 breaks and binding of single-strand-binding proteins RPA and Rad51 modulate the
818 formation of ATR-kinase foci in yeast. *Journal of Cell Science* **120,** 4209–4220 (2007).
819 59. Chen, R. & Wold, M. S. Replication protein A: single-stranded DNA's first responder:
820 dynamic DNA-interactions allow replication protein A to direct single-strand DNA
821 intermediates into different pathways for synthesis or repair. *BioEssays* **36,** 1156–1161
822 (2014).
823 60. Lukas, C., Falck, J., Bartkova, J., Bartek, J. & Lukas, J. Distinct spatiotemporal dynamics of
824 mammalian checkpoint regulators induced by DNA damage. *Nat. Cell Biol.* **5,** 255–260
825 (2003).
826 61. Piya, G. *et al.* Characterization of the interaction between Rfa1 and Rad24 in
827 Saccharomyces cerevisiae. *PLoS ONE* **10,** e0116512 (2015).
828 62. Bartkova, J. *et al.* DNA damage response as a candidate anti-cancer barrier in early

human tumorigenesis. *Nature* **434,** 864–870 (2005).
63. Halazonetis, T. D., Gorgoulis, V. G. & Bartek, J. An Oncogene-Induced DNA Damage Model for Cancer Development. *Science* **319,** 1352–1355 (2008).
64. Janke, C. *et al.* A versatile toolbox for PCR-based tagging of yeast genes: new fluorescent proteins, more markers and promoter substitution cassettes. *Yeast* **21,** 947–962 (2004).
65. Silva, S., Gallina, I., Eckert-Boulet, N. & Lisby, M. Live cell microscopy of DNA damage response in Saccharomyces cerevisiae. *Methods Mol. Biol.* **920,** 433–443 (2012).
66. Zierhut, C. & Diffley, J. F. X. Break dosage, cell cycle stage and DNA replication influence DNA double strand break response. *EMBO J.* **27,** 1875–1885 (2008).
67. Lisby, M., Rothstein, R. & Mortensen, U. H. Rad52 forms DNA repair and recombination centers during S phase. *Proceedings of the National Academy of Sciences* **98,** 8276–8282 (2001).

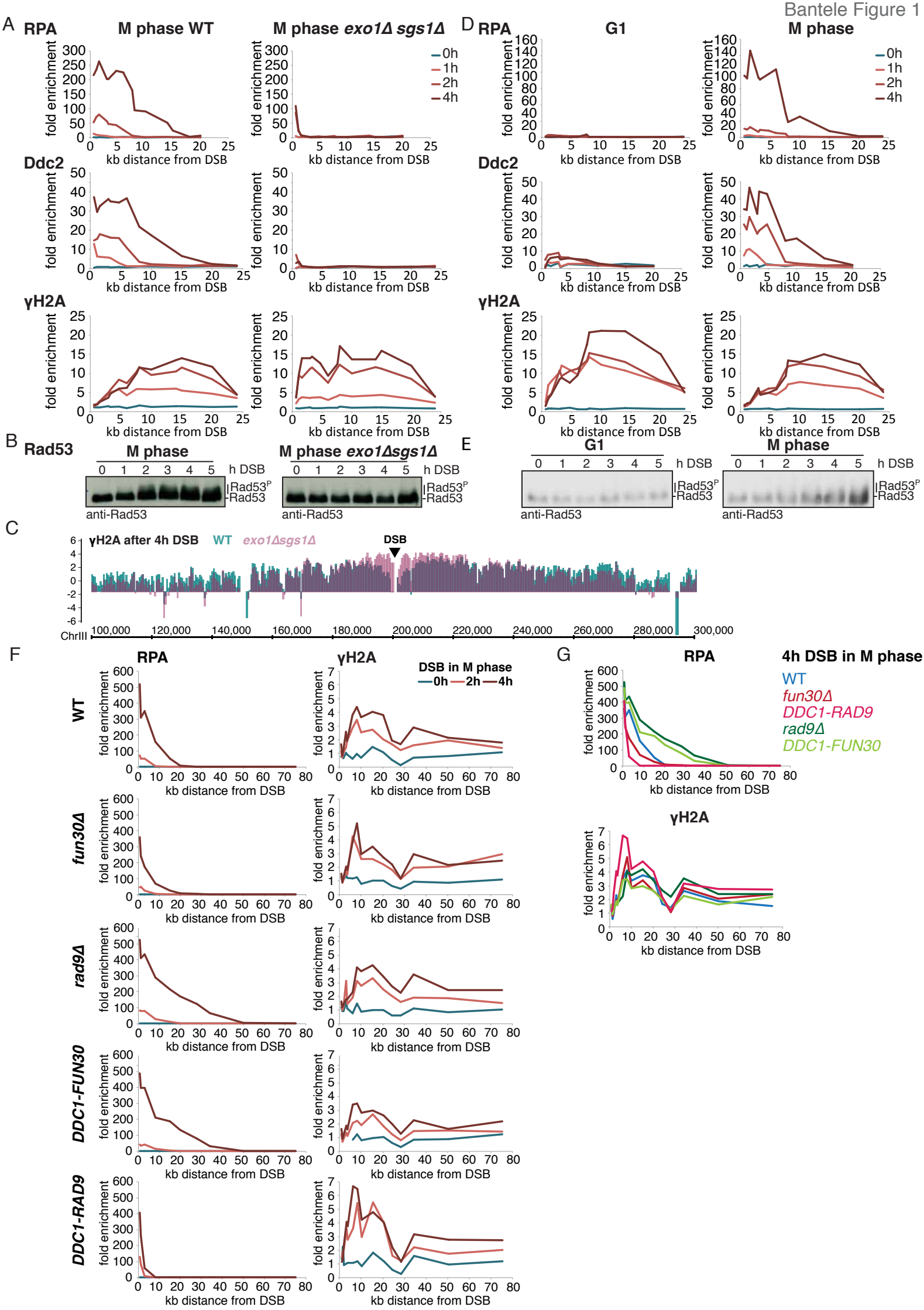
A
RPA
M phase WT
M phase exo1Δ sgs1Δ
0h
1h
2h
4h
fold enrichment
kb distance from DSB
Ddc2
γH2A
D
G1
M phase
B
Rad53
h DSB
Rad53P
Rad53
anti-Rad53
E
C
γH2A after 4h DSB
WT
exo1Δsgs1Δ
DSB
ChrIII
F
DSB in M phase
WT
fun30Δ
rad9Δ
DDC1-FUN30
DDC1-RAD9
G
4h DSB in M phase
WT
fun30Δ
DDC1-RAD9
rad9Δ
DDC1-FUN30

A

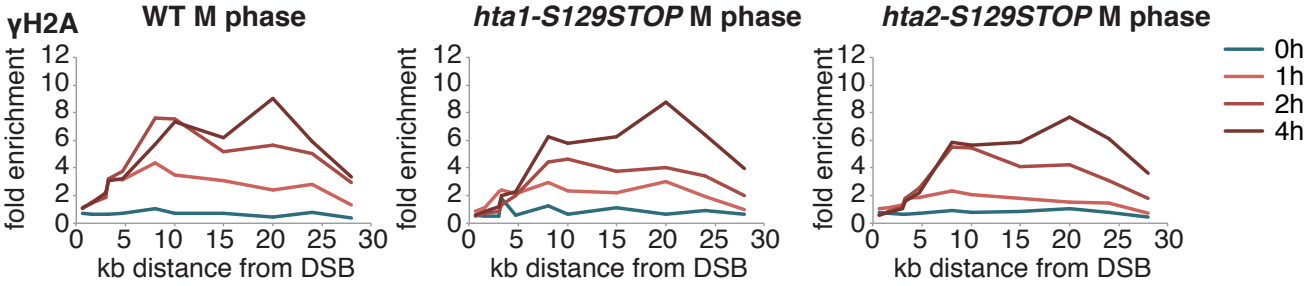
γH2A
WT M phase
hta1-S129STOP M phase
hta2-S129STOP M phase
fold enrichment
kb distance from DSB
0h
1h
2h
4h

B

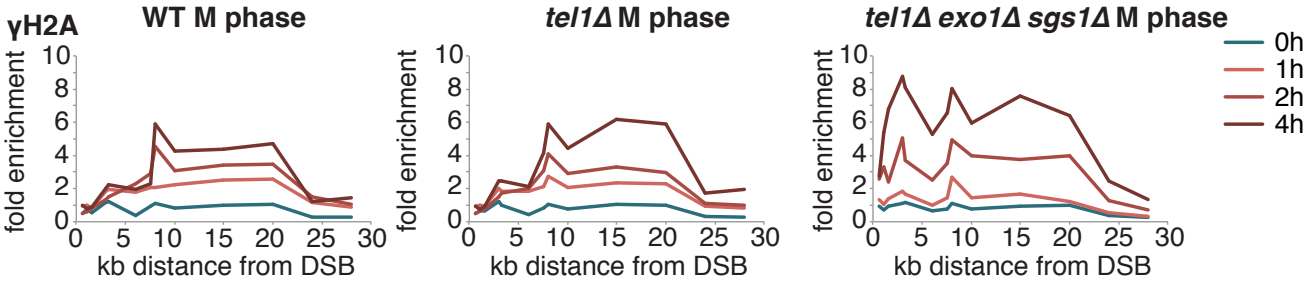
γH2A
WT M phase
tel1Δ M phase
tel1Δ exo1Δ sgs1Δ M phase
fold enrichment
kb distance from DSB
0h
1h
2h
4h

C

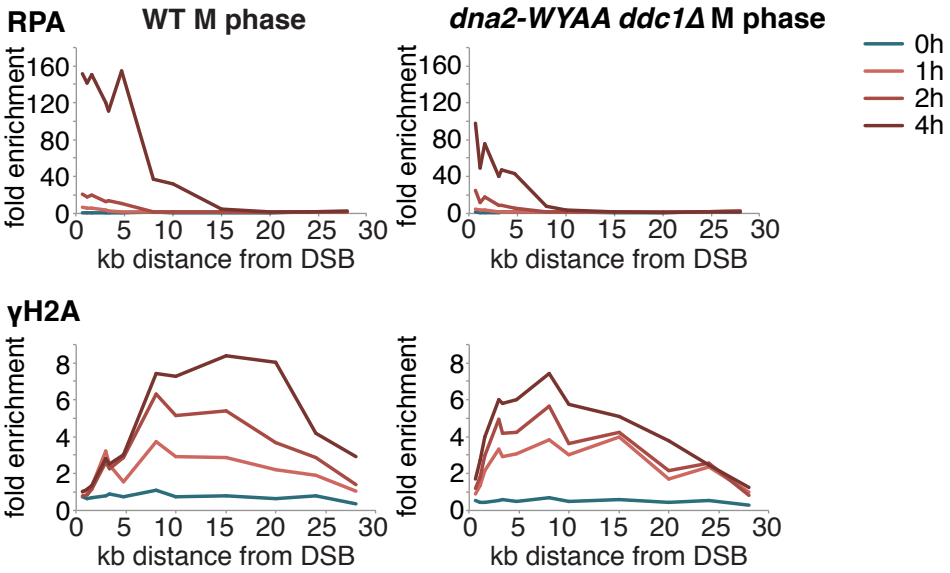
RPA
WT M phase
dna2-WYAA ddc1Δ M phase
γH2A
fold enrichment
kb distance from DSB
0h
1h
2h
4h

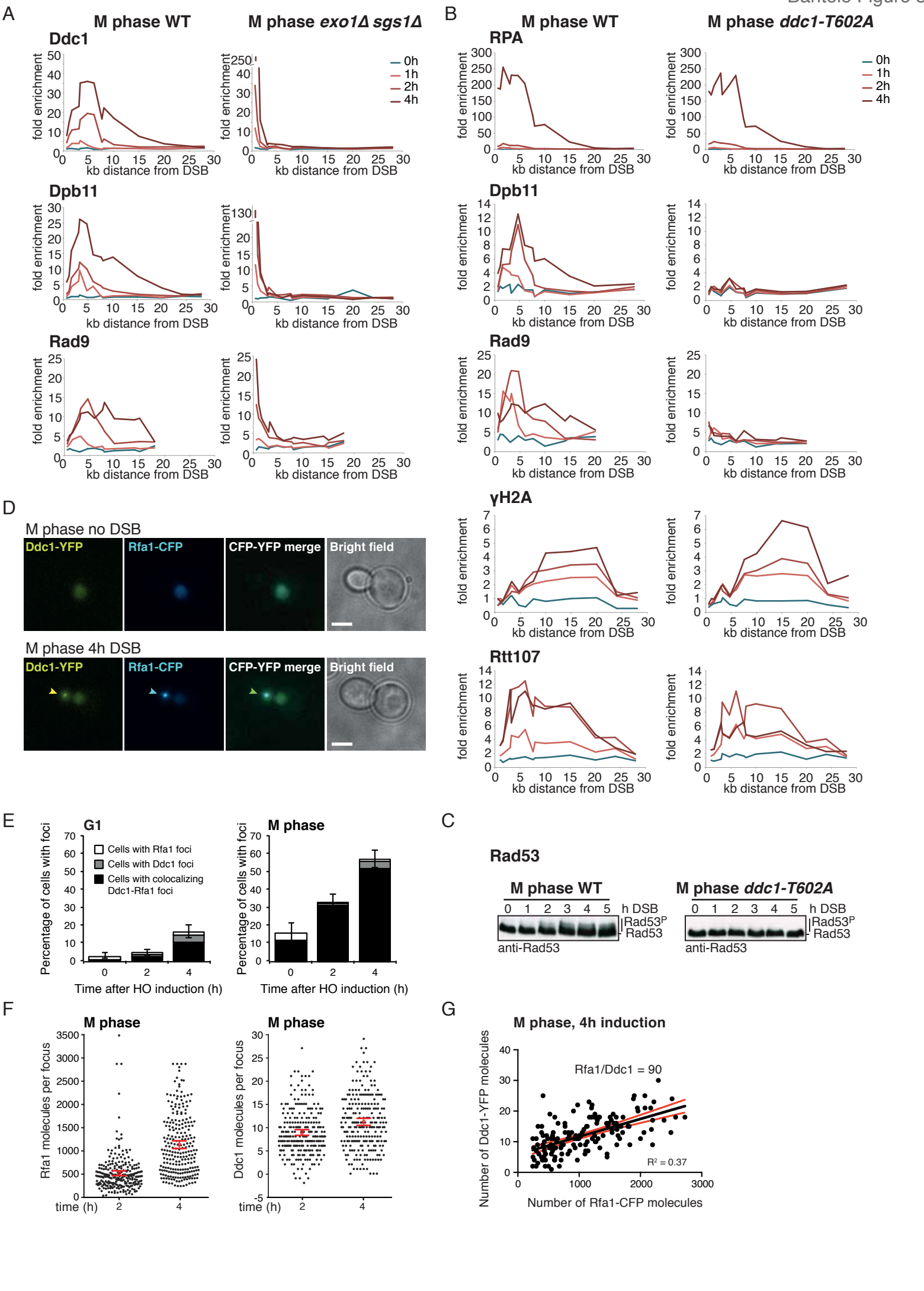
A
M phase WT
M phase exo1Δ sgs1Δ
Ddc1
Dpb11
Rad9
fold enrichment
kb distance from DSB
0h
1h
2h
4h
B
M phase WT
M phase ddc1-T602A
RPA
Dpb11
Rad9
γH2A
Rtt107
D
M phase no DSB
M phase 4h DSB
Ddc1-YFP
Rfa1-CFP
CFP-YFP merge
Bright field
E
G1
M phase
Cells with Rfa1 foci
Cells with Ddc1 foci
Cells with colocalizing Ddc1-Rfa1 foci
Percentage of cells with foci
Time after HO induction (h)
C
Rad53
M phase WT
M phase ddc1-T602A
h DSB
Rad53P
Rad53
anti-Rad53
F
M phase
Rfa1 molecules per focus
Ddc1 molecules per focus
time (h)
G
M phase, 4h induction
Rfa1/Ddc1 = 90
R² = 0.37
Number of Ddc1-YFP molecules
Number of Rfa1-CFP molecules

A

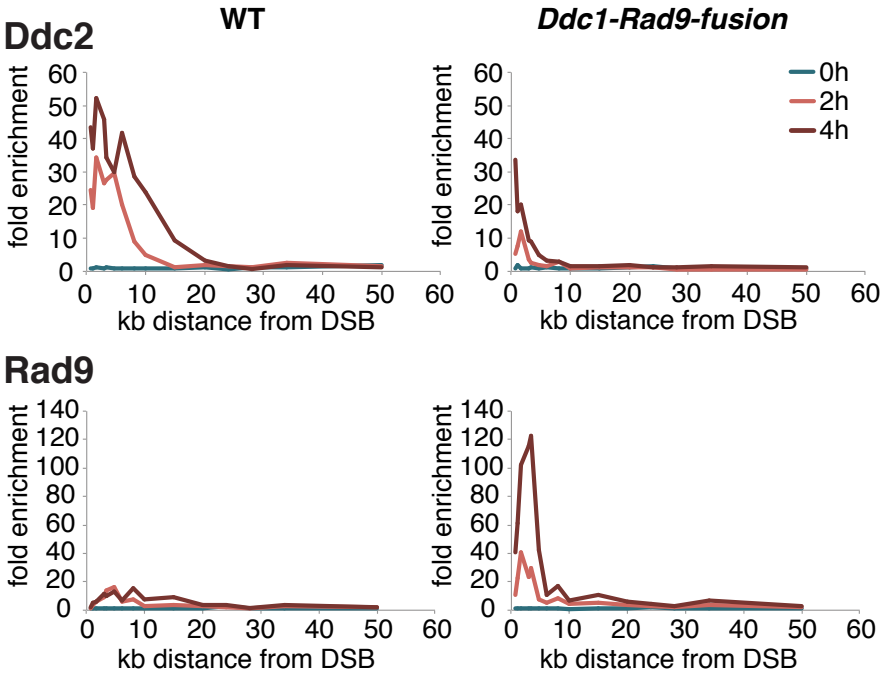
WT
Ddc1-Rad9-fusion
Ddc2
Rad9
fold enrichment
kb distance from DSB
0h
2h
4h

B

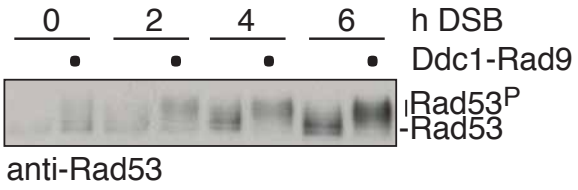
Rad53
0
2
4
6
h DSB
Ddc1-Rad9
Rad53P
Rad53
anti-Rad53

C

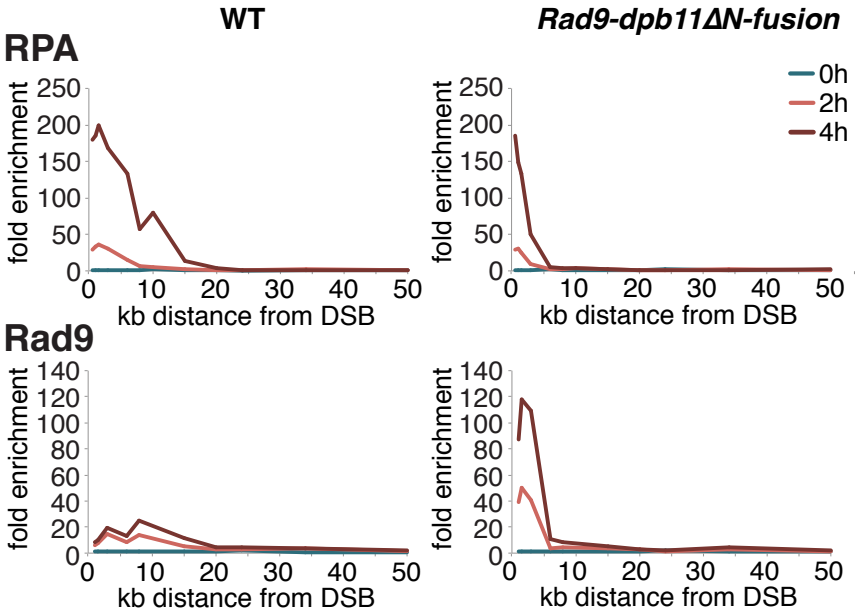
WT
Rad9-dpb11ΔN-fusion
RPA
Rad9
fold enrichment
kb distance from DSB
0h
2h
4h

D

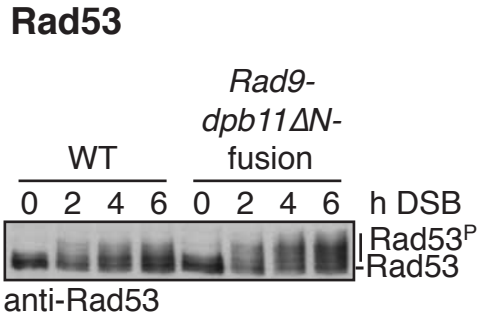
Rad53
Rad9-
dpb11ΔN-
fusion
WT
0 2 4 6 0 2 4 6
h DSB
Rad53P
Rad53
anti-Rad53

Supplementary Material to

Bantele, Lisby and Pfander **– Quantitative signalling mechanisms in response to DNA damage**

Contents:

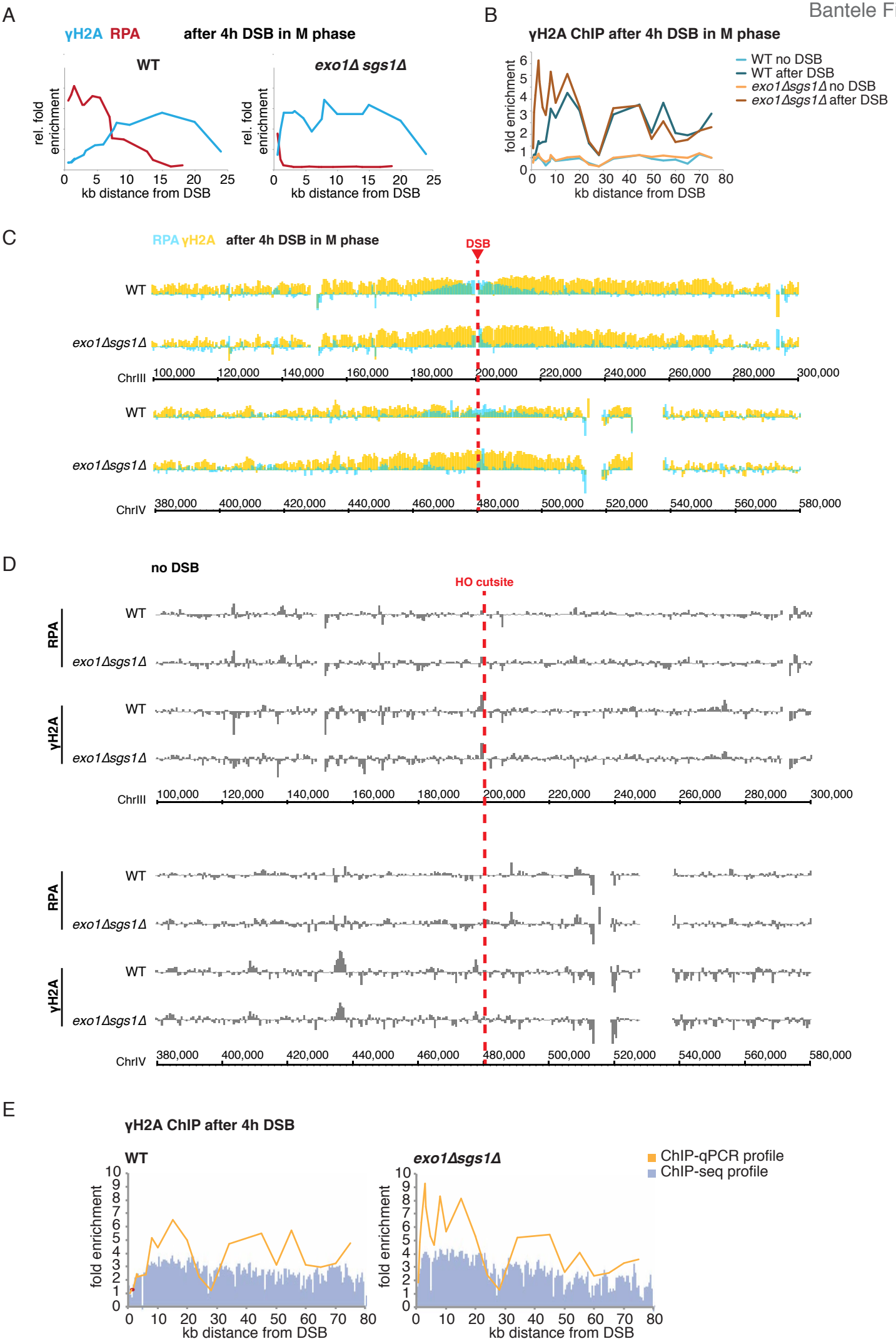
A
γH2A RPA after 4h DSB in M phase
WT
exo1Δ sgs1Δ
rel. fold enrichment
kb distance from DSB
B
γH2A ChIP after 4h DSB in M phase
WT no DSB
WT after DSB
exo1Δsgs1Δ no DSB
exo1Δsgs1Δ after DSB
fold enrichment
kb distance from DSB
C
RPA γH2A after 4h DSB in M phase
DSB
WT
exo1Δsgs1Δ
ChrIII
ChrIV
D
no DSB
HO cutsite
RPA
γH2A
WT
exo1Δsgs1Δ
ChrIII
ChrIV
E
γH2A ChIP after 4h DSB
WT
exo1Δsgs1Δ
ChIP-qPCR profile
ChIP-seq profile
fold enrichment
kb distance from DSB

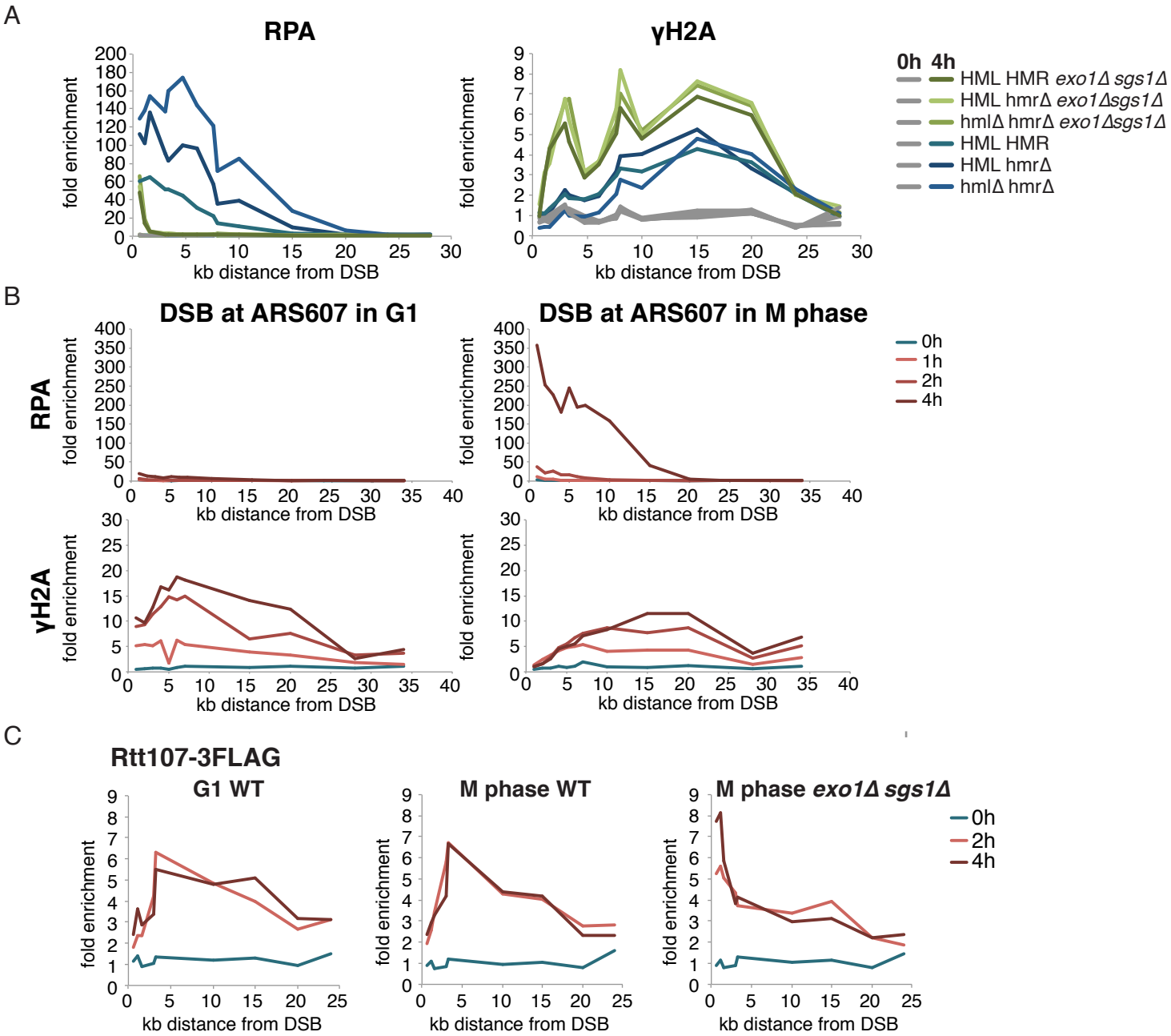
A
RPA
γH2A
fold enrichment
kb distance from DSB
0h 4h
HML HMR exo1Δ sgs1Δ
HML hmrΔ exo1Δsgs1Δ
hmlΔ hmrΔ exo1Δsgs1Δ
HML HMR
HML hmrΔ
hmlΔ hmrΔ
B
DSB at ARS607 in G1
DSB at ARS607 in M phase
RPA
γH2A
0h
1h
2h
4h
C
Rtt107-3FLAG
G1 WT
M phase WT
M phase exo1Δ sgs1Δ
0h
2h
4h

A

Model of the **local** checkpoint signalling circuit

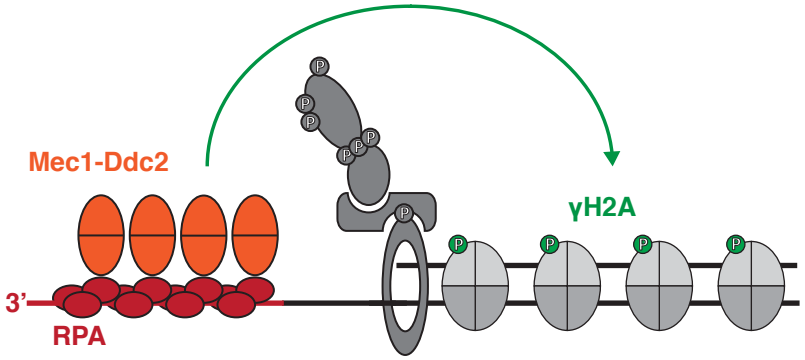

B

Model of the **global** checkpoint signalling circuit

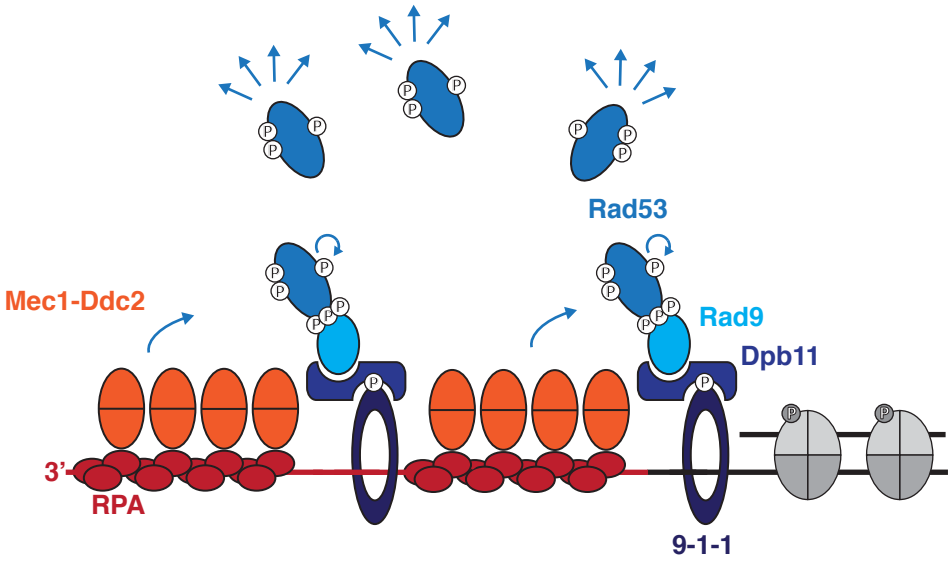

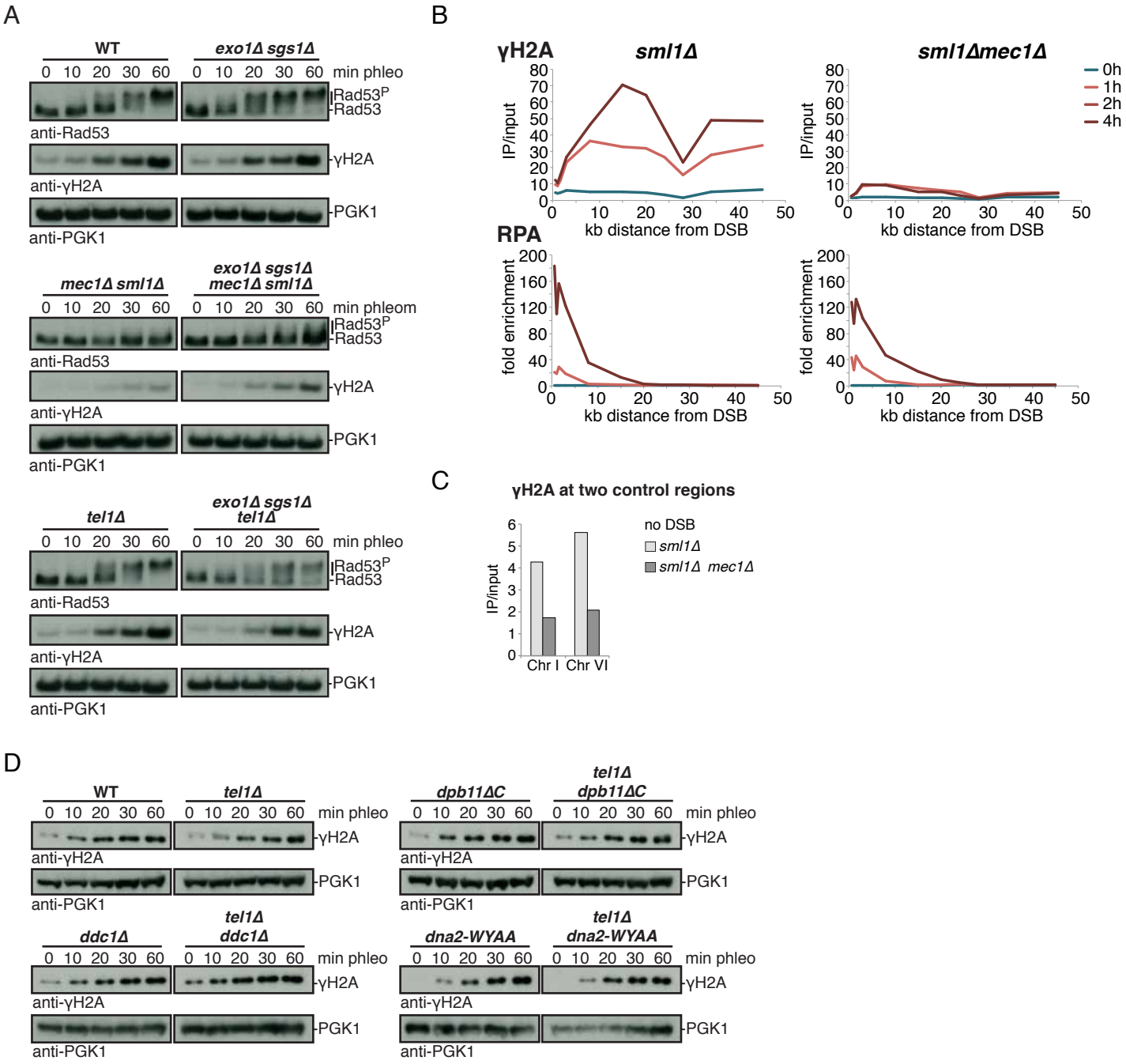
A
WT
exo1Δ sgs1Δ
0 10 20 30 60
0 10 20 30 60 min phleo
Rad53P
Rad53
anti-Rad53
γH2A
anti-γH2A
PGK1
anti-PGK1
mec1Δ sml1Δ
exo1Δ sgs1Δ mec1Δ sml1Δ
min phleom
tel1Δ
exo1Δ sgs1Δ tel1Δ
B
γH2A
sml1Δ
sml1Δmec1Δ
IP/input
kb distance from DSB
0h
1h
2h
4h
RPA
fold enrichment
C
γH2A at two control regions
no DSB
sml1Δ
sml1Δ mec1Δ
Chr I
Chr VI
D
dpb11ΔC
tel1Δ dpb11ΔC
ddc1Δ
tel1Δ ddc1Δ
dna2-WYAA
tel1Δ dna2-WYAA

A

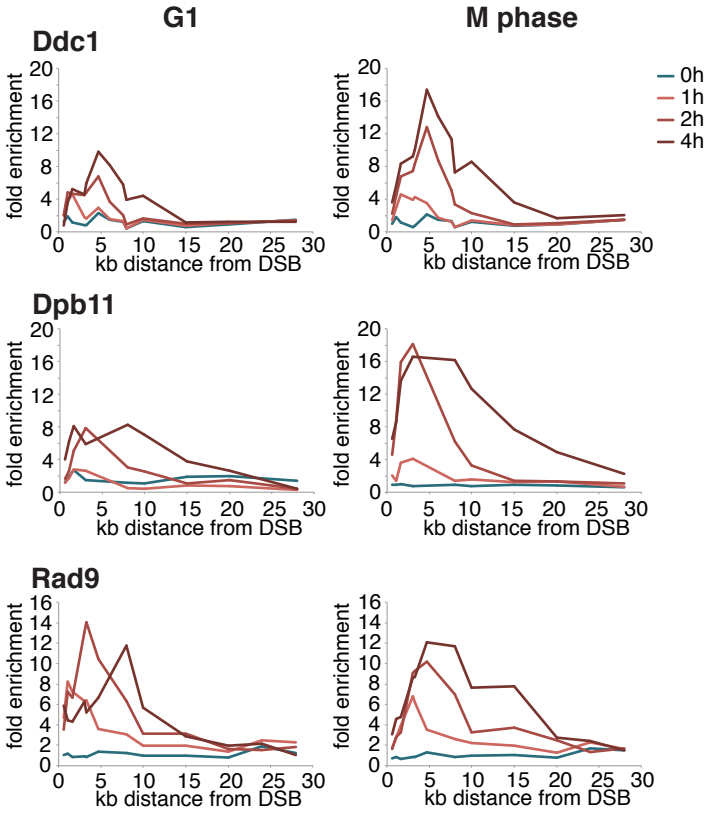
G1
M phase
Ddc1
Dpb11
Rad9
fold enrichment
kb distance from DSB
0h
1h
2h
4h

B

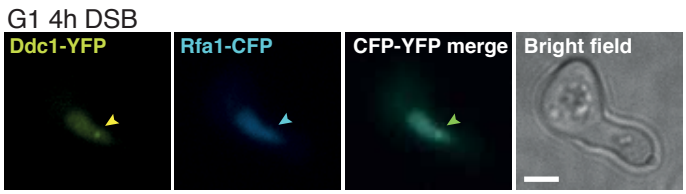
G1 4h DSB
Ddc1-YFP
Rfa1-CFP
CFP-YFP merge
Bright field

C

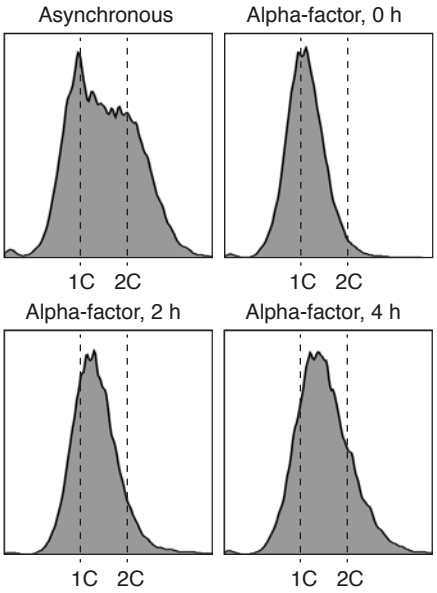
Asynchronous
Alpha-factor, 0 h
Alpha-factor, 2 h
Alpha-factor, 4 h
1C
2C

D

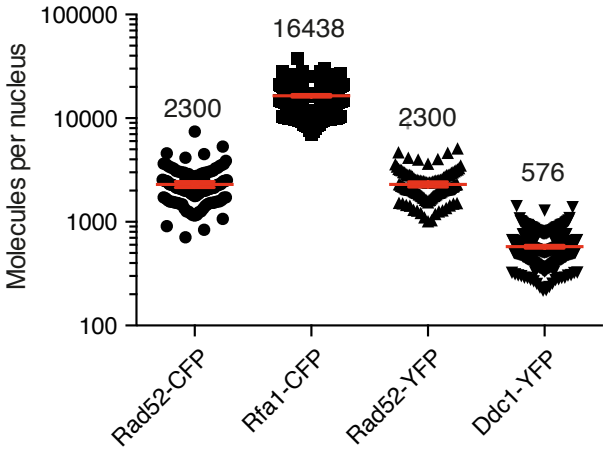
Molecules per nucleus
2300
16438
2300
576
Rad52-CFP
Rfa1-CFP
Rad52-YFP
Ddc1-YFP

A

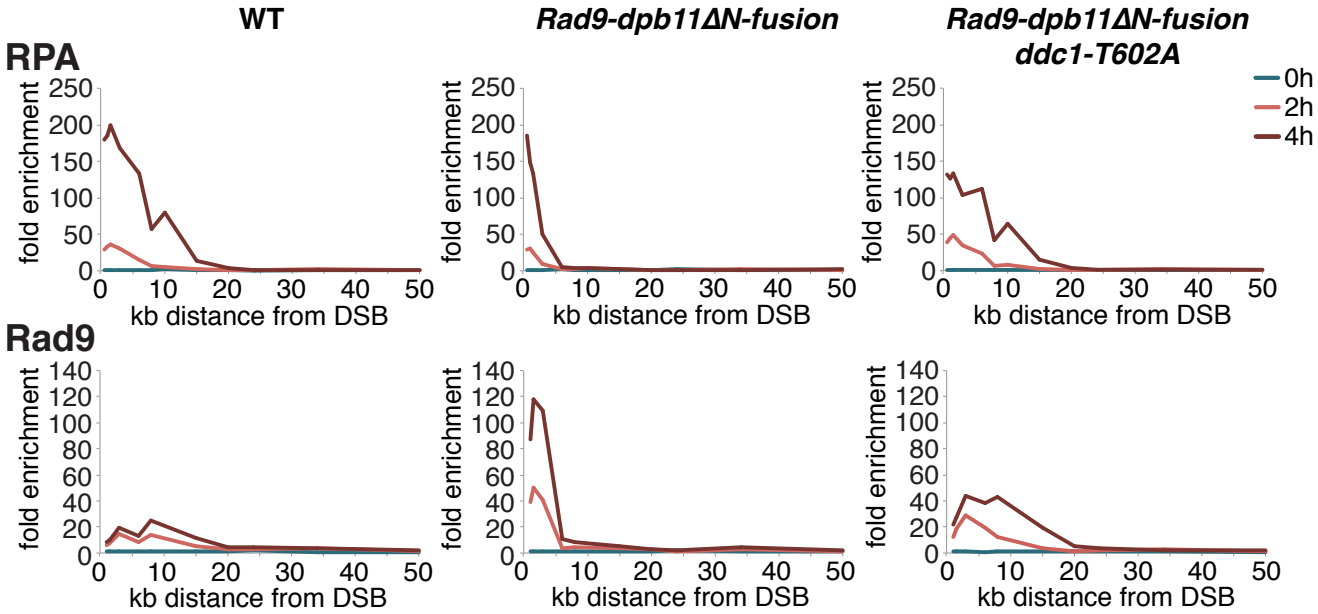
WT
Rad9-dpb11ΔN-fusion
Rad9-dpb11ΔN-fusion ddc1-T602A
RPA
Rad9
fold enrichment
kb distance from DSB
0h
2h
4h

B

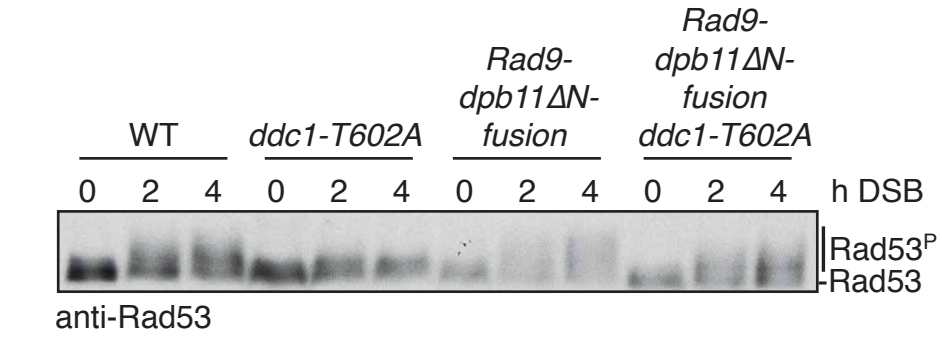
Rad53
WT
ddc1-T602A
Rad9-dpb11ΔN-fusion
Rad9-dpb11ΔN-fusion ddc1-T602A
0 2 4 0 2 4 0 2 4 0 2 4 h DSB
Rad53P
Rad53
anti-Rad53

Supplemental Figure Legends:

Figure S1

γH2A phosphorylation is not correlating with ssDNA signal strength.

(A) RPA and γH2A enrichments around a DSB are anti-correlated, suggesting that resection as read by RPA enrichment evicts histones and thereby the substrate for γH2A phosphorylation. Overlay of RPA (red) and γH2A (blue) ChIP signals after 4h of DSB in *WT* (left panel) and *exo1Δ sgs1Δ* cells (right panel) cells arrested in M phase.

(B) γH2A phosphorylation spreads over a large distance from a DSB (>75 kb) in *WT* and *exo1Δ sgs1Δ cells.* With the exception of the area of resection (Fig. S1A), resection has no influence on γH2A phosphorylation. ChIP-qPCR analysis of *WT* cells or *exo1Δ sgs1Δ* cells after 4h of DSB induction.

γH2A phosphorylation and RPA enrichment around two distinct DSBs anti-correlate in ChIP-seq experiments (C) and depend on the presence of the DSBs (D).

(C) Overlay of ChIP-seq profiles from the same experiment as shown in Fig. 1C. RPA enrichments are plotted in blue, γH2A phosphorylation is plotted in yellow. The positions of the HO-induced DSBs on chromosome 3 (upper two panels) and chromosome 4 (lower two panels) are indicated by the red dotted line. *WT* cells (upper traces) are compared with *exo1Δ sgs1Δ* mutant cells (lower traces).

(D) ChIP-seq profiles of the 0h time point before induction of DSB. Samples were obtained in the same experiment as data shown in Fig. 1B and Fig. S1A. Analysis of the enrichment of RPA (upper panel, respectively) and γH2A phosphorylation (lower panel, respectively).

(E) Overlay of ChIP-qPCR and ChIP-seq signals. *WT* and *exo1Δ sgs1Δ* cells were arrested in M phase and analysed for γH2A phosphorylation after 4h of DSB induction. qPCR signals (red) are from the same experiment as in (B). Sequencing data (blue) is from the experiment plotted in Fig. 1C and Fig. S1C and S1D.

Figure S2

γH2A phosphorylation is not correlating with ssDNA signal strength – additional controls.

(A) DNA end resection (left panel) and γH2A phosphorylation (right panel) were measured by ChIP in *WT* strains or *exo1Δ sgs1Δ* strains with both mating type loci deleted, or intact HML or intact HML and HMR loci. All strains used in this study were HML hmrΔ if not indicated differently. Samples were analysed after 4 h of DSB induction.

(B) Also at an independent locus (ARS607), γH2A phosphorylation around a DSB is not showing a response that correlates with the ssDNA signal. ChIP-qPCR analysis of strains carrying an ectopic HO cutsite on ARS607 arrested in G1 (left panels) or M phase (right panels). RPA enrichment (upper panels) and γH2A phosphorylation (lower panels) were analysed at indicated times.

(C) Manipulation of DNA end resection by de-regulation of the Sgs1 helicase does not affect γH2A phosphorylation. ChIP-qPCR analysis of a *WT strain* arrested in G1 (left panels) or in M phase (middle panels) and an *sgs1-ss* mutant strain in M phase (right panels). Resection (upper panels) and γH2A phosphorylation (lower panels) were analysed at indicated times.

(D) Rtt107 is associating with a DSB in a resection-independent manner. Rtt107 recruitment to a DSB was measured at indicated times in *WT* strains arrested in G1 (left panel) or in M phase (middle panel), or in *exo1Δ sgs1Δ* cells arrested in M phase (right panel). Rtt107 was tagged with a C-terminal 3FLAG tag and detected by a ChIP directed against the FLAG tag.

Figure S3

DNA damage checkpoint signalling can be subdivided in two separate, Mec1-dependent signaling circuits. Models of local **(A)** and global **(B)** checkpoint signalling circuits.

(A) Mec1-Ddc2 (orange) bound to RPA (red) phosphorylates γH2A as a substrate of the local checkpoint signalling circuit (green) in a resection-independent manner.

(B) Mec1-Ddc2 (orange) bound to RPA (red) phosphorylates the checkpoint proteins of the 9-1-1 axis (Ddc1, Dpb11, Rad9 and Rad53, shades of blue) as substrates of the global checkpoint signalling circuit, which depends on DNA end resection and culminates in the activation of the Rad53 effector kinase.

Figure S4

γH2A phosphorylation is strongly dependent on Mec1, but only weakly on Tel1, and is not influenced by specific Mec1 activators.

(A) γH2A and Rad53 phosphorylation after phleomycin treatment are strongly decreased in cells lacking Mec1, but almost unaffected in cells lacking Tel1. Western blot analysis of Rad53 phosphorylation (upper panels, respectively), γH2A phosphorylation (middle panels, respectively) and PGK1 as a control for protein levels (lower panels, respectively) in *WT* cells or *exo1Δ sgs1Δ*, *mec1Δ sml1Δ*, *exo1Δ sgs1Δ mec1Δ sml1Δ*, *tel1Δ*, *exo1Δ sgs1Δ tel1Δ* mutant cells arrested in M phase after treatment with 50 μg/ml phleomycin for the indicated times.

(B) γH2A formation at a DSB strongly depends on the Mec1 kinase. IP/input ratios of the ChIP-qPCR analysis of γH2A (upper panels) and RPA (lower panels) after indicated times of DSB

induction in M phase-arrested cells. *sml1Δ mec1Δ* cells (right panels, respectively) were compared to *sml1Δ* cells (left panels, respectively).

(C) Damage-independent levels of γH2A phosphorylation at two independent loci on non-broken chromosomes are reduced in cells lacking Mec1. γH2A ChIP IP/input ratios from two loci on distinct, undamaged chromosomes are plotted. The values are from the same experiment as in (B).

(D) γH2A phosphorylation is not influenced by the absence of a specific Mec1 activator after phleomycin treatment. Western blot analysis of γH2A phosphorylation (upper panels, respectively) and PGK1 as a control for protein concentrations (lower panels, respectively) in *WT* cells or *ddc1Δ, dpb11ΔC* or *dna2-WYAA* mutant cells, either in a *WT* background or a *tel1Δ* background arrested in M phase. Samples were analysed at indicated time points.

Figure S5

Regulators of the global checkpoint circuit (9-1-1 axis) differentially localize to a DSB in G1 and M phase-arrested cells.

(A) Recruitment of 9-1-1 (Ddc1), Dpb11 and Rad9 is enhanced in M phase. ChIP-qPCR of *WT* strains arrested in G1 (left panels) or M phase (right panels) at indicated times. For detection, Ddc1, Dpb11 and Rad9 were tagged with a C-terminal 3FLAG tag, and ChIPs were directed against the FLAG tag.

(B)-(D) Additional information to the microscopical Ddc1- and RPA- foci analysis in Fig. 3D-G.

(B) Representative microscopy images from the Rfa1- and Ddc1-foci analysis in G1-arrested cells. A DSB was induced at the MAT locus in G1 phase-arrested cells using Gal-HO and cells were microscopically analysed for Ddc1-YFP foci (yellow, left panel) and Rfa1-CFP foci (blue, second to the left panel) from 4h timepoint. An overlay of both imaging channels is shown in panel three and a bright field image of the yeast cells in the right panel.

(C) FACS analysis of G1 arrest. Cells were fixed for FACS analysis before addition of alpha-factor at 0, 2 and 4 hours of DSB induction. The graphs show the DNA content per cell.

(D) Normalization of Rfa1 and Ddc1 foci intensity against Rad52 as a standard. YFP and CFP intensities were quantified throughout the nucleus and the total number of tagged molecules was calculated by comparing the values to the intensity of the respectively tagged Rad52 molecules.

Figure S6

The *Rad9-dpb11ΔN* fusion is partly dependent on Ddc1 phosphorylation.

(A) ChIP-qPCR analysis of DNA resection (upper panels) and Rad9 recruitment (lower panels) in WT cells, *Rad9-dpb11ΔN fusion* cells and *Rad9-dpb11ΔN fusion ddc1-T602A* cells. All strains

were arrested in M phase and samples were taken at indicated time points. For detection, Rad9 and the Rad9 fusion were tagged C-terminally with a 3FLAG tag and the ChIPs were directed against the 3FLAG tag. The data in the left and middle panels is identical to the data shown in Fig. 4C.

(B) The same strains as in (A) were analysed for checkpoint activation in a Rad53 Western Blot, including a *ddc1-T602A* mutant strain. The Western Blot samples are from the same experiment as shown in Fig. 4D.

SCIENTIFIC REPORTS

OPEN

A cell cycle-independent mode of the Rad9-Dpb11 interaction is induced by DNA damage

Received: 20 July 2017
Accepted: 30 August 2017
Published online: 14 September 2017

Giulia di Cicco, Susanne C. S. Bantele, Karl-Uwe Reusswig & Boris Pfander

Budding yeast Rad9, like its orthologs, controls two aspects of the cellular response to DNA double strand breaks (DSBs) – signalling of the DNA damage checkpoint and DNA end resection. Rad9 binds to damaged chromatin via modified nucleosomes independently of the cell cycle phase. Additionally, Rad9 engages in a cell cycle-regulated interaction with Dpb11 and the 9-1-1 clamp, generating a second pathway that recruits Rad9 to DNA damage sites. Binding to Dpb11 depends on specific S/TP phosphorylation sites of Rad9, which are modified by cyclin-dependent kinase (CDK). Here, we show that these sites additionally become phosphorylated upon DNA damage. We define the requirements for DNA damage-induced S/TP phosphorylation of Rad9 and show that it is independent of the cell cycle or CDK activity but requires prior recruitment of Rad9 to damaged chromatin, indicating that it is catalysed by a chromatin-bound kinase. The checkpoint kinases Mec1 and Tel1 are required for Rad 9 S/TP phosphorylation, but their influence is likely indirect and involves phosphorylation of Rad9 at S/TQ sites. Notably, DNA damage-induced S/TP phosphorylation triggers Dpb11 binding to Rad9, but the DNA damage-induced Rad9-Dpb11 interaction is dispensable for recruitment to DNA damage sites, indicating that the Rad9-Dpb11 interaction functions beyond Rad9 recruitment.

DNA damage (such as double strand breaks (DSBs)) elicits cellular signalling pathways, collectively known as the DNA damage response (reviewed in ref. 1). Among these, checkpoint mechanisms control cell cycle progression as well as transcriptional and post-translational regulation of DNA repair and replication. Furthermore, local signalling events are critical in directing DNA repair pathway choice. Budding yeast Rad9 was the first checkpoint protein to be discovered[2]. Since then, it has become evident that Rad9, as well as its orthologs such as fission yeast Crb2[3,4] and human 53BP1 (reviewed in ref. 5), play a crucial role in the DNA damage response, having at least two functions: signal transduction in the DNA damage checkpoint (reviewed in ref. 1) and control of DNA end resection, a local process that critically determines DSB repair pathway choice (reviewed in ref. 6).

As checkpoint signalling mediator, Rad9 links the signal transduction from the apical kinase Mec1 to the effector kinase Rad53[7–12]. As such, it is essential for activation of Rad53 and therefore for the activation of a global checkpoint response upon DNA damage. Moreover, Rad9 is also an inhibitor of DNA end resection[13–16]. Since DNA end resection generates the DNA substrate for recombination-based repair and interferes with ligation-based repair, Rad9 is a critical regulator of DSB repair pathway choice. To fulfil these two functions, Rad9 engages in several protein-protein interactions that occur within damaged chromatin[17–22].

Rad9 binds to modified histones via two distinct domains. The TUDOR domain of Rad9 interacts with histone H3 in its K79-methylated form[19,22], a widespread modification of chromatin that is introduced by the methyltransferase Dot1[23,24]. The tandem-BRCT domain of Rad9 interacts with histone H2A in its S129-phosphorylated form (γH2A[21,25]), a DNA damage-specific chromatin mark introduced by the apical checkpoint kinases Mec1 and Tel1[26]. As such, Rad9 is a bivalent nucleosome binder, a feature that is conserved among Rad9 orthologs, even though different histone marks are being recognized[27–31].

Rad9 also binds to the scaffold protein Dpb11[17,18]. Dpb11 contains two pairs of BRCT domains, which provide two phospho-protein binding surfaces (reviewed in ref. 32). While Rad9 binds to BRCT1 + 2, Dpb11 also interacts with the 9-1-1 complex via BRCT3 + 4[17,33,34]. Physical and genetic interaction data suggest that these interactions generate a second pathway that recruits Rad9 to DNA damage sites: DNA damage-loaded 9-1-1 can tether Dpb11, which in turn can recruit Rad9[17,33]. Notably, the interaction of Dpb11 with Rad9 depends on Rad9 phosphorylation at S462 and T474 residues[17]. Both sites match the minimal consensus (S/TP) for phosphorylation

Max Planck Institute of Biochemistry, DNA Replication and Genome Integrity, Martinsried, Germany. Correspondence and requests for materials should be addressed to B.P. (email: bpfander@biochem.mpg.de)

by cyclin-dependent kinase (Cdc28, in the following referred to as CDK) and consistently a CDK-dependent interaction between Rad9 and Dpb11 can be observed in G2/M-arrested cells[17].

Furthermore, Rad9 binds to the checkpoint effector kinase Rad53[7,8,10,12]. This interaction involves phosphorylation of Rad9 in the S/TQ cluster domain (SCD), which is specifically bound by the FHA domains of Rad53. Rad9 is phosphorylated in the SCD by the apical kinases Mec1 and Tel1 upon association with damaged chromatin[7,12]. Current models suggest that Rad53 is transiently recruited to damaged chromatin by this mechanism (reviewed in ref. 1). Here, it becomes activated by Mec1/Tel1 phosphorylation, before it dissociates from the DNA damage site to set off the global DNA damage response.

Promoting Rad53 phosphorylation and activation offers a straightforward mechanism of how Rad9 mediates checkpoint signalling. In contrast, it is less clear by which mechanism Rad9 regulates DNA end resection[13,14], even though an antagonistic relationship between Rad9 and the resection-promoting nucleosome remodeller Fun30 has been demonstrated[35,36].

Rad9 recruitment to damaged chromatin occurs in all cell cycle phases[19]. However, individual Rad9 recruitment mechanisms are apparently under cell cycle control[17,33]. Previous data has therefore led to a model where in G1 only one Rad9 recruitment pathway (via interaction with modified nucleosomes, referred to as the 'histone pathway'[19–22,25]) is active, while outside of G1 a second Rad9 recruitment pathway (via Dpb11 and 9-1-1, referred to as the 'Dpb11 pathway') is additionally available[17,33]. However, the underlying reason for restricting the Rad9-Dpb11 interaction to specific cell cycle phases is not understood.

Here, we report new aspects in the regulation of Rad9 in the response to DSBs. We find that the Rad9 S/TP sites, which facilitate Dpb11-binding, are also phosphorylated upon DNA damage independently of the cell cycle phase. DNA damage-dependent phosphorylation of these sites can be detected even in G1 cells or upon inhibition of CDK. Notably, these phosphorylation events depend on prior chromatin-recruitment of Rad9 via the 'histone pathway' and on the integrity of the SCD domain of Rad9. Furthermore, the Rad9 phosphorylation facilitates the interaction between Rad9 and Dpb11, similarly to our previous results on the CDK-dependent mode of interaction. These findings suggest that Dpb11 and Rad9 can interact even in G1, where Dpb11 is not involved in recruiting Rad9 to damaged chromatin.

Results

DNA damage induces phosphorylation of Rad9 S/TP sites and binding of Rad9 to Dpb11.

Orthologs of Rad9 and Dpb11 were found to interact in different organisms[17,18,29,37]. In case of budding yeast, our previous work has shown that Rad9 specifically interacts with Dpb11 in cells arrested in M phase, but not in cells arrested in G1[17]. The cell cycle-regulation of the interaction is achieved by CDK-dependent phosphorylation of two S/TP motifs on Rad9 (S462 and T474, referred to as Rad9 S/TP sites hereafter), which are recognized by the BRCT1 + 2 domain of Dpb11[17].

We observed that Rad9^{9myc} from cell extracts of cells containing MMS-induced DNA damage showed increased interaction with ^{GST}Dpb11 in pulldown experiments (Fig. S1A). Strikingly, even when we used cells arrested in G1, we found that DNA damage treatment with the DSB-inducing agent phleomycin resulted in an increased interaction of Rad9^{9myc} with ^{GST}Dpb11 (Figs 1A and S1B). Phleomycin treatment causes Rad9 to undergo a phospho-shift (Fig. 1A)[8,10–12]. Notably, we found Dpb11 to associate with this hyperphosphorylated form of Rad9 (Fig. 1A). In contrast, in M phase cell extracts Rad9^{9myc} was able to interact with ^{GST}Dpb11 even in the absence of DNA damage treatment (Fig. 1A), consistent with our previous result on the CDK regulation of Rad9[17].

The interaction between Rad9 and Dpb11 critically depends on phosphorylation of S462 and T474 on Rad9[17]. We therefore tested, whether phosphorylation of these sites is also induced by DNA damage. To this end, we used our previously generated phosphorylation-specific antibodies directed against Rad9-epitopes containing either phosphorylated S462 or phosphorylated T474, respectively[17] (note that anti-Rad9-T474p is highly specific for the phosphorylated form, while anti-Rad9-S462p retains some binding to the unmodified form). When we purified Rad9 via IP from M phase cells, we observed that these Rad9 S/TP sites were phosphorylated in the presence as well as in the absence of DNA damage, consistent with these sites being modified by CDK (Figs 1B and S1C)[17]. Notably, we observed that the S/TP sites were also phosphorylated specifically in phleomycin-treated G1 cells, but not in the absence of DNA damage (Fig. 1B, note the phleomycin-induced phosphorylation shift). The anti-Rad9-T474p antibody can also detect Rad9 S/TP phosphorylation from cell extracts. Figure 1C shows Rad9-T474 phosphorylation in undamaged M phase cells, as well as damaged G1 and M phase cells, but not in undamaged G1 cells, corroborating the result of the IP experiment. Moreover, cells expressing the *rad9-ST462,474AA* variant (referred to as *rad9-AA* hereafter) did not show any reactivity with the Rad9-T474p antibody, confirming specificity (Figs 1C and S1D). We therefore conclude that there are two different modes of Rad9 S/TP phosphorylation: mode 1, which is cell cycle-regulated and depends on CDK[17], and mode 2, which is DNA damage-dependent.

In order to verify that the DNA damage-induced phosphorylation of Rad9 in G1 is CDK-independent, we used a *cdc28-as1* mutant strain, in which CDK activity was effectively inhibited by addition of 1-NM-PP1, but this did not abrogate Rad9-T474 phosphorylation after DNA damage (Figs 1D and S1E). We furthermore used the same strategy of CDK-inhibition in M phase-arrested cells and found that CDK-dependent phosphorylation of Rad9-T474 in undamaged cells was effectively inhibited in line with previous results (Figs 1E and S1F)[17]. Notably, phleomycin treatment efficiently stimulated phosphorylation of Rad9-T474 in M phase-arrested cells after CDK inhibition (Fig. 1E). Taken together, these data show that the damage-induced phosphorylation of the Rad9 S/TP sites occurs independently of the cell cycle phase and CDK activity (Fig. 1E).

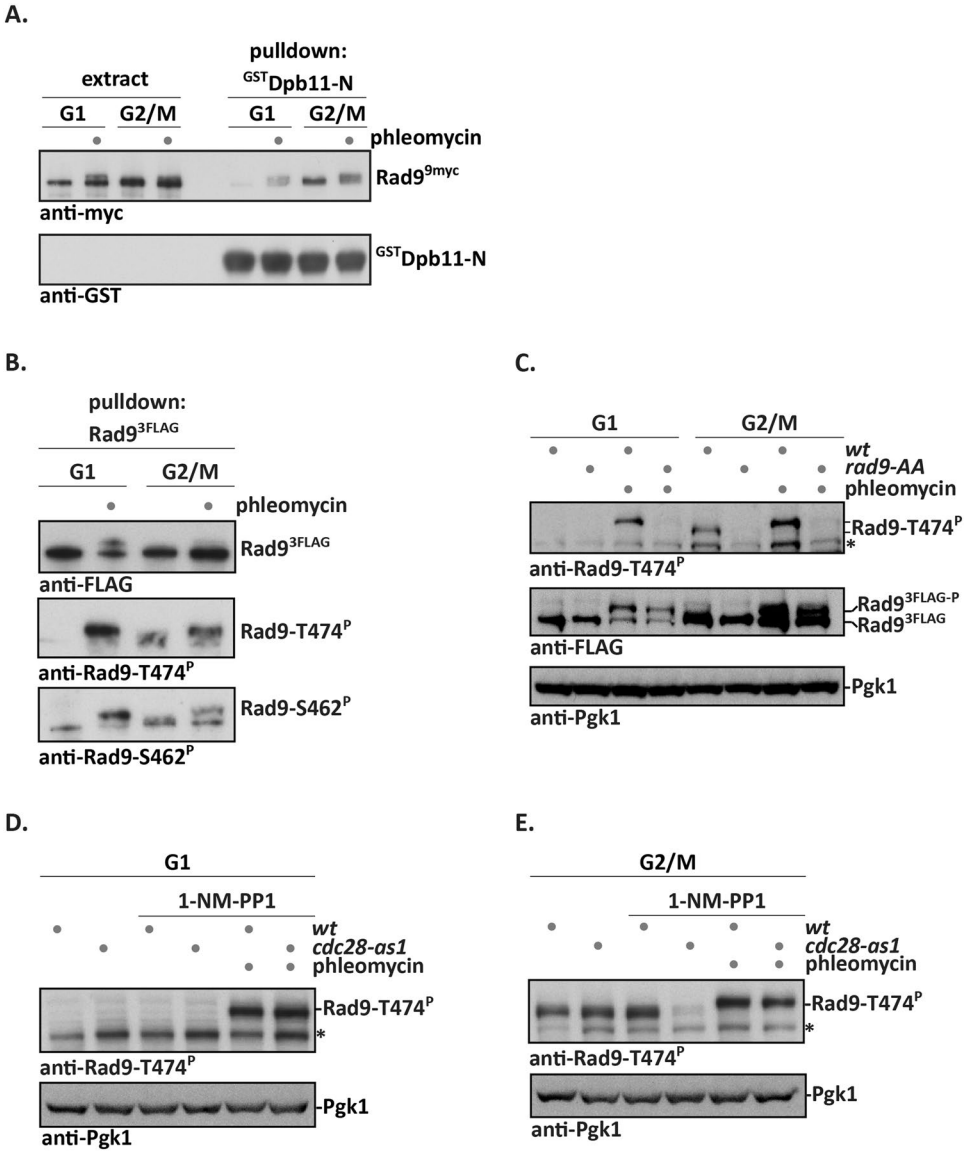

Figure 1. A CDK-independent, DNA damage-dependent mode of Rad9-S462 and -T474 phosphorylation and interaction with Dpb11. (**A**) DNA damage stimulates the Rad9-Dpb11 interaction in cell extracts. GST pulldown experiment with ^{GST}Dpb11-N (contains BRCT1 + 2, which is the Rad9 interaction site) and extracts from Rad9^{9myc}-expressing cells arrested in G1 (α-factor arrest) or M phase (nocodazole arrest) and treated with phleomycin or mock treated. FACS profiles in Fig. S1B. (**B**,**C**) Phosphorylation of Rad9-S462 and -T474 is stimulated by DNA damage in G1. (**B**) Rad9^{3FLAG} was purified from cells treated as in (**A**) by FLAG-IP. Phosphorylation of Rad9 S/TP sites was determined using Rad9-S462p and Rad9-T474p phosphorylation-specific antibodies. FACS profiles in Fig. S1C. **(C)** Cells treated as in **(A)** were used to prepare whole cell extract, which was probed with the Rad9-T474p phosphorylation-specific antibody. The *rad9-AA* strain (harbouring the S462A and T474A mutations) was used as specificity control. Pgk1 immunoblot serves as loading control. FACS profiles in Fig. S1D. (**D**,**E**) CDK inhibition does not affect damage-induced Rad9 S/TP phosphorylation. **(D)** 1-NM-PP1 was used to inhibit CDK in G1-arrested *cdc28-as1* cells, but this did not affect Rad9-T474 phosphorylation after DNA damage. FACS profiles in Fig. S1E. (**E**) As in (**D**), but with M phase-arrested cells. 1-NM-PP1 treatment abolished T474 phosphorylation in undamaged *cdc28-as1* cells, demonstrating that CDK is inhibited under these conditions. In contrast T474 is efficiently phosphorylated after phleomycin treatment, even after CDK inhibition. Pgk1 immunoblot serves as loading control. The asterisk denotes a crossreactive band. FACS profiles in Fig. S1F.

DNA damage-induced phosphorylation of the Rad9 S/TP sites depends on the apical checkpoint kinases Mec1 and Tel1 and the Rad9 SCD. Upon DNA damage, the apical checkpoint kinases Mec1 and Tel1 target several sites on Rad9[8, 11, 12]. Therefore, we tested whether also the phosphorylation of Rad9 S/TP sites would be dependent on Mec1 and Tel1. Notably, T474 phosphorylation in G1-arrested,

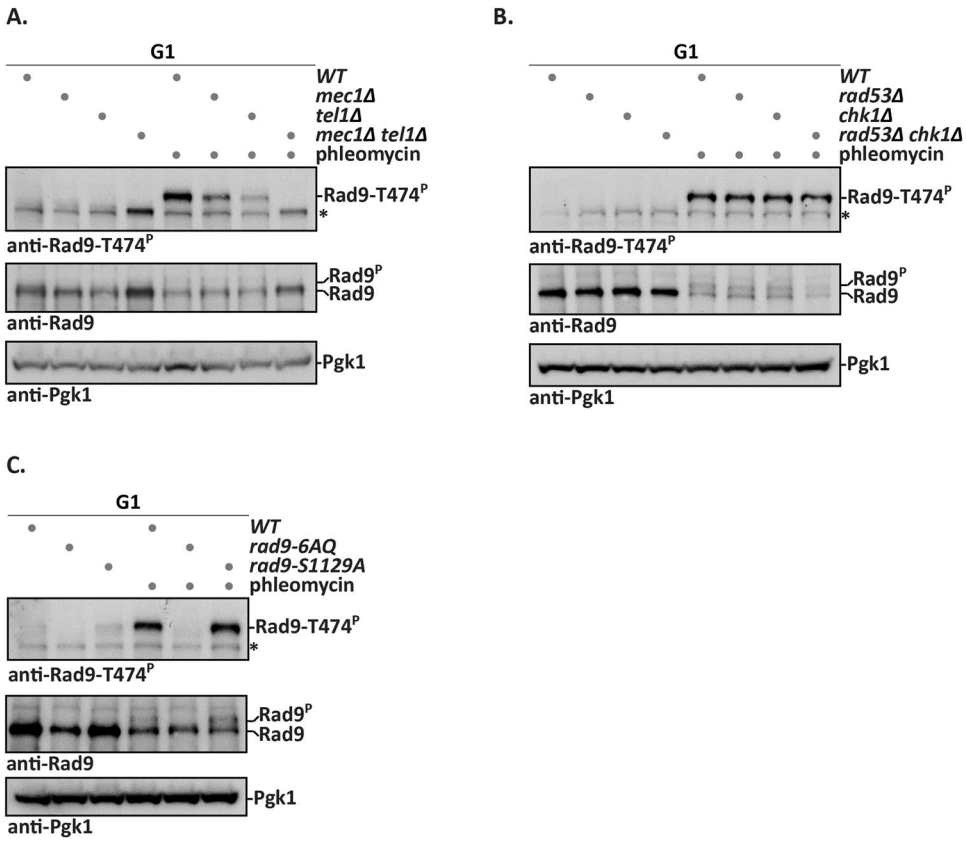

Figure 2. Mec1 and Tel1 are required for phosphorylation of Rad9 S/TP sites after DNA damage. (**A**) Rad9-T474 phosphorylation after DNA damage depends on the apical checkpoint kinases Mec1 and Tel1. G1-arrested cells with indicated genotypes were treated with phleomycin, Rad9-T474 phosphorylation was visualized by immunoblotting. Strains containing the *mec1Δ* mutation are in *sml1Δ* background. Pgk1 immunoblot serves as loading control. An asterisk denotes a crossreactive band. FACS profiles in Fig. S2A. (**B**) Rad9-T474 phosphorylation after DNA damage is independent of checkpoint effector kinases Chk1 and Rad53. G1-arrested cells with indicated genotypes were treated with phleomycin and subjected to analysis with immunoblots as in (**A**). Strains containing the *rad53Δ* mutation are in *sml1Δ* background. FACS profiles in Fig. S2B. (**C**) Integrity of the Rad9 SCD domain is important for damage-induced Rad9 S/TP phosphorylation. Treatment and immunoblotting of *WT*, *rad9-6AQ* and *rad9-S1129A* strains as in (**A**). FACS profiles in Fig. S2C.

phleomycin-treated cells was reduced in *mec1Δ* and *tel1Δ* mutant cells and completely abolished in a *mec1Δ tel1Δ* double mutant (Figs 2A and S2A). Therefore, phosphorylation of Rad9 S/TP sites shows a dependency on the apical checkpoint kinases, which is highly similar to overall damage-induced Rad9 phosphorylation (indicated by the phosphoshift, Fig. 2A). In contrast, the deletion mutants of the checkpoint effector kinases *RAD53* or *CHK1*, alone or in combination, did not affect T474 phosphorylation (Figs 2B and S2B).

It could thus be reasoned that Rad9 S/TP sites are themselves targeted by the apical checkpoint kinases Mec1 and Tel1, similarly to Rad9 S/TQ sites[8,11,12]. However, we did not obtain evidence that purified Mec1 would show activity towards Rad9 S/TP sites *in vitro* (data not shown). Therefore, we considered the option that the apical checkpoint kinases could promote Rad9 S/TP site phosphorylation indirectly. Possible mechanisms include a priming role of Rad9 S/TQ phosphorylation or Mec1/Tel1 promoting chromatin recruitment of a factor involved in S/TP site phosphorylation, such as the kinase acting on Rad9 or Rad9 itself (via γH2A). Indeed, we found that a Rad9 mutant harbouring six S/T to A exchanges in the S/TQ cluster domain (SCD) (*rad9-6AQ*)[12] abolished phleomycin-induced phosphorylation of Rad9 S/TP sites in G1 (Figs 2C and S2C). In contrast, CDK-dependent phosphorylation of these sites in M phase was unaffected by the *rad9-6AQ* mutant (Fig. S2D). Previous work has suggested that phosphorylation of the SCD would induce Rad9 dimerization[38]. However, we excluded dimerization as underlying cause for the SCD-dependency, as the dimerization-defective Rad9-S1129A variant[38] showed normal phosphorylation of Rad9-T474 both in G1 after DNA damage and in M phase (Figs 2C and S2D). Overall, we conclude that Mec1/Tel1-dependent phosphorylation of the SCD of Rad9 is required for phosphorylation of the Rad9 S/TP sites upon DNA damage, but additional direct and/or indirect roles of the apical checkpoint kinases are possible.

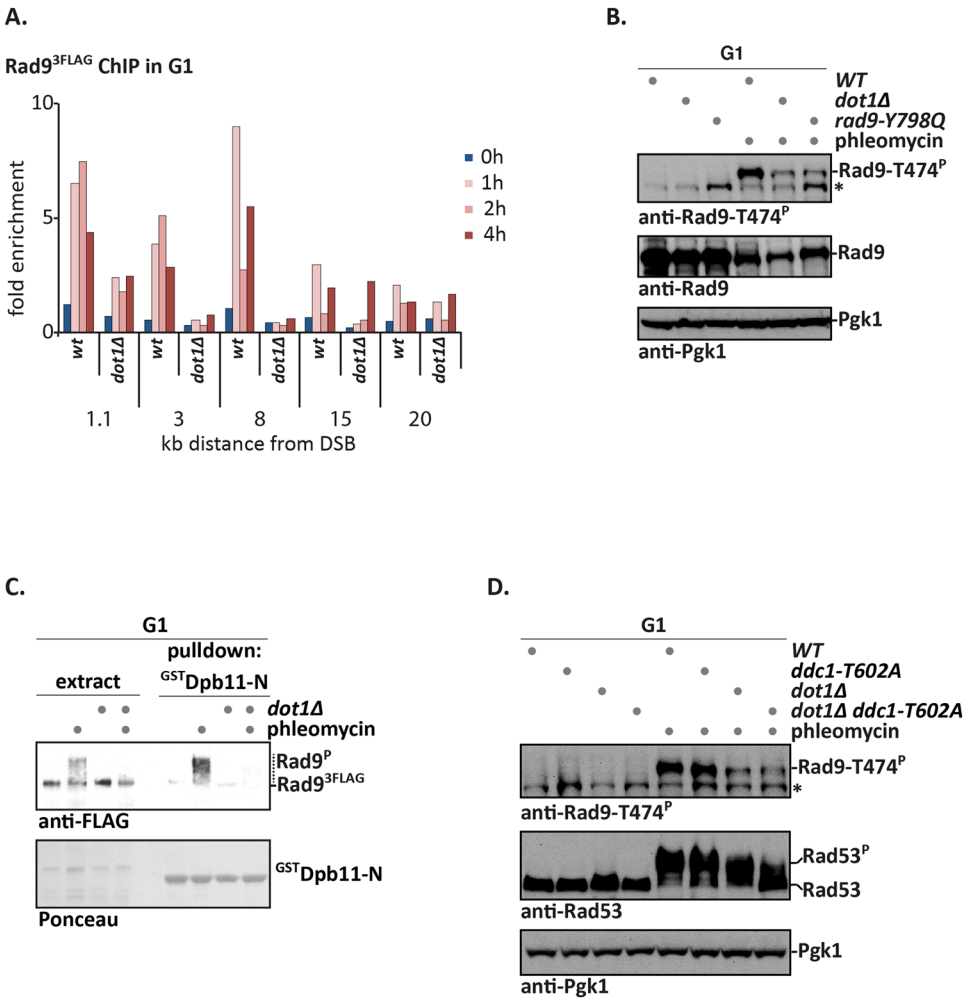

Figure 3. Dot1 is required for phosphorylation of Rad9 S/TP sites and interaction with Dpb11. (**A**) Dot1 is required for Rad9 association with a double strand break (DSB). Induction of an non-repairable DSB at *MAT* locus using galactose-induced HO. ChIP against Rad9^{3FLAG} to regions from 1.1 kb to 8 kb distal of the DSB site and 1, 2 and 4 h after DSB induction. FACS profiles in Fig. S3A. (**B**–**D**) The 'histone pathway' is required for efficient damage-induced phosphorylation of Rad9-T474 and binding to Dpb11. (**B**) Phleomycin-induced T474 phosphorylation is reduced in *dot1Δ* or *rad9-Y789Q* cells (deficient in TUDOR domain-dependent binding to K79-methylated H3). Experiment as in Fig. 2A, but with *WT*, *dot1Δ* and *rad9-Y789Q* cells. Pgk1 immunoblot serves as loading control. An asterisk denotes a crossreactive band. FACS profiles in Fig. S3D. (**C**) Dpb11 does not bind to Rad9 from extracts of G1-arrested, phleomycin-treated *dot1Δ* cells. GST-Dpb11-N pulldown as in Fig. 1A (**D**) DNA damage-induced Rad9-T474 phosphorylation in G1 as in (**B**), but with *WT, ddc1-T602A, dot1Δ* or *dot1Δ ddc1-T602A* strains. FACS profiles in Fig. S3E.

Chromatin-recruitment of Rad9 is required for phosphorylation of the Rad9 S/TP sites. Previous studies suggest two possible pathways by which Rad9 is recruited to damaged chromatin ('histone pathway'[19–22, 25] and 'Dpb11 pathway'[17, 33]). In G1 cells, however, the 'histone pathway' is apparently uniquely required[17, 33]. Given our findings, we re-investigated the possibility that the 'Dpb11 pathway' may be contributing to Rad9 recruitment and also tested the alternative model that the damage-induced Rad9-Dpb11 interaction in G1 may rely on the 'histone pathway'.

A critical element of the 'histone pathway' is K79-methylation of H3, which is catalysed by the Dot1 methyltransferase[23] and recognized by the TUDOR domain of Rad9[19, 22]. We therefore tested Rad9 binding to damaged chromatin by ChIP in G1-arrested cells and used the GAL-HO system to induce a site-specific, non-repairable DSB at the *MAT* locus[39]. While Rad9 became enriched in the chromatin region surrounding the DSB in *WT* cells after DSB induction, Rad9 enrichment was strongly decreased in *dot1Δ* cells (Figs 3A and S3A). Consistent with a lack of Rad9 recruitment to damaged chromatin, we observed that damage-induced phosphorylation of Rad9 S/TP sites was reduced in G1 cells lacking Dot1 (Figs 3B and S3D).

Intriguingly, deletion of *DOT1* caused a strong reduction of Rad9-T474 phosphorylation in phleomycin-treated G1 cells (Fig. 3B). To ascertain that this effect originated from a defect in the interaction of Rad9 with nucleosomes (i.e. a deficient 'histone pathway'), we introduced the corresponding H3 K79-binding-defective mutation in the Rad9 TUDOR domain (*rad9-Y798Q*[19]) and observed a highly similar

reduction in Rad9-T474 phosphorylation in this background (Fig. 3B). This effect was again specific for the DNA damage-induced phosphorylation of Rad9 S/TP sites (mode 2), as neither a *dot1Δ* nor a *rad9-Y798Q* mutation diminished CDK-dependent phosphorylation of Rad9-T474 in M phase (Fig. S3B,C).

We expected that a lack of Rad9 S/TP phosphorylation would translate into an inability to bind to Dpb11. Indeed, we observed a reduced association of Rad9 in ^{GST}Dpb11 pulldowns in the absence of Dot1, when the Rad9-Dpb11 association was induced by phleomycin-treatment of G1-arrested cells (Fig. 3C).

We observed that *dot1Δ* as well as *rad9-Y798Q* cells showed minor residual Rad9-T474 phosphorylation in G1 (Fig. 3B), which responded dose-dependently to phleomycin (Fig. S3D). Since M phase cells could compensate a defect in the 'histone pathway' by Dpb11-dependent Rad9 recruitment ('Dpb11 pathway'[17,33]), we tested if the 'Dpb11 pathway' would be responsible for the residual phosphorylation of Rad9. However, we did not observe any additional defect in Rad9-T474 phosphorylation, when we introduced the Dpb11-binding-deficient *ddc1-T602A* allele either alone or in combination with *dot1Δ* (Figs 3D and S3E). Therefore, we conclude that Rad9 S/TP site phosphorylation after DNA damage as well as the interaction of Dpb11 and Rad9 are dependent on the 'histone pathway'.

Forced Rad9 recruitment to damaged chromatin allows efficient Rad9 S/TP site phosphorylation. The 'histone pathway' facilitates Rad9 recruitment to damaged chromatin. We reasoned that the dependency of the damage-induced Rad9 S/TP-phosphorylation on the 'histone pathway' could be easily explained, if Rad9 needed to localize to damaged chromatin in order to become phosphorylated. We therefore aimed to create a cellular scenario, which forces Rad9 localization to damaged chromatin independently of the 'histone pathway'.

We have previously shown that covalent protein-fusions containing the BRCT3 + 4 domain of Dpb11 localized efficiently and cell cycle-independently to damaged chromatin[36]. In case of Rad9, this fusion protein (Rad9-Dpb11ΔN, referred to as Rad9-Dpb11 fusion) hyperactivates DNA damage checkpoint signalling[17]. To ascertain that this fusion acts by forcing Rad9 localization to damaged chromatin, we measured inhibition of DNA end resection by Rad9 as a read-out of Rad9 function[13,14]. Therefore, we tested the extent of resection at an HO-induced DSB using ChIP against the ssDNA-binding protein RPA. In the presence of the Rad9-Dpb11 fusion, the spreading of resection was strongly reduced independently of the cell cycle phase and the functionality of the 'histone pathway' (Figs 4A and S3A,B). These data therefore suggest a model whereby the Rad9-Dpb11 fusion forces enhanced Rad9 recruitment to damaged chromatin, where it causes hyperactivation of the DNA damage checkpoint, as well as inhibition to DNA end resection, consistent with previous results[17,40].

Next, we used the Rad9-Dpb11 fusion to test its effects on Rad9 S/TP site phosphorylation. We found that after DNA damage induction Rad9-T474 phosphorylation was enhanced in the context of the Rad9-Dpb11 fusion and even present to low levels without induction of exogenous damage (Figs 4B and S4C,D). Importantly, in the context of the fusion Rad9-T474 phosphorylation was largely independent of Dot1 (Fig. 4B), while it still showed dependency on the apical kinases Mec1 and Tel1 (Figs 4C and S4E). Overall, these data suggest that the function of the 'histone pathway' in damage-induced Rad9 S/TP phosphorylation lies entirely in the recruitment of Rad9 to damaged chromatin.

Rad9 S/TP phosphorylation in G1 is dispensable for DNA end resection and the DNA damage checkpoint. Outside of G1, CDK-phosphorylation of Rad9 S/TP sites provides a pathway of Rad9 recruitment to damaged chromatin[17]. However, in case of the damage-induced Rad9 phosphorylation mode, our data rather suggest a function downstream of recruitment (Figs 3 and 4). So far, Rad9 is known to have two functions – (A) inhibition of DNA end resection and (B) activation of the DNA damage checkpoint. Therefore, we tested if the *rad9-AA* variant would show a G1-specific defect in any of these functions.

To measure DNA end resection, we again used the GAL-HO system and ChIP against RPA. Consistent with previous studies[13,14], we observed enhanced spreading of the RPA-ChIP signal away from the site of the DSB in *rad9Δ* and *dot1Δ* strains, indicating enhanced DNA end resection in the absence of chromatin-bound Rad9 (Figs 5A and S5A). However, we did not observe any significant change in DNA end resection in G1-arrested *rad9-AA* cells, even in the absence of Yku70, suggesting that the Rad9-Dpb11 interaction on its own is not required for regulation of DNA end resection in G1 (Figs 5A,B and S5B).

For checkpoint activation, we have previously shown that the *rad9-AA* mutant on its own does not induce any defects in the phosphorylation of the Rad53 effector kinase in G1 cells[17] (see also Figs 5C and S5C). We therefore considered the possibility that a defect in damage-induced Rad9 S/TP phosphorylation may be compensated by other factors. Specifically, we tested compensation by the 9-1-1 complex, since both Rad9 and 9-1-1 could in principle serve to recruit Dpb11 to sites of DNA damage. Therefore, we combined the *rad9-AA* mutant with the *ddc1-T602A* mutant, which abolishes the 9-1-1-Dpb11 interaction. However, while the *ddc1-T602A* mutation strongly reduced Dpb11 association with a site-specific DSB in G1-arrested cells, the *rad9-AA* mutant did not induce a measurable defect (Fig. S5D). Consistently, checkpoint activation was still largely functional in the *rad9-AA* mutant, even in the *ddc1-T602A* background (Fig. 5C).

Overall, the functional relevance of the damage-induced mode of Rad9 S/TP phosphorylation therefore remains unclear. Given the high degree of redundancy in the checkpoint signalling network, it is highly likely that a defect in the *rad9-AA* mutant is compensated, perhaps by phosphorylation of an additional factor or by other phosphorylation sites in Rad9.

Discussion

S/TP site phosphorylation has been shown to be an important cellular mechanism that facilitates cell cycle controls (see ref. 41 for a review on control of the DNA damage response by S/TP phosphorylation). Our study provides experimental evidence for DNA damage-dependent, but cell cycle-independent phosphorylation of the budding yeast checkpoint protein Rad9 at S/TP sites. These sites have previously been shown to be phosphorylated

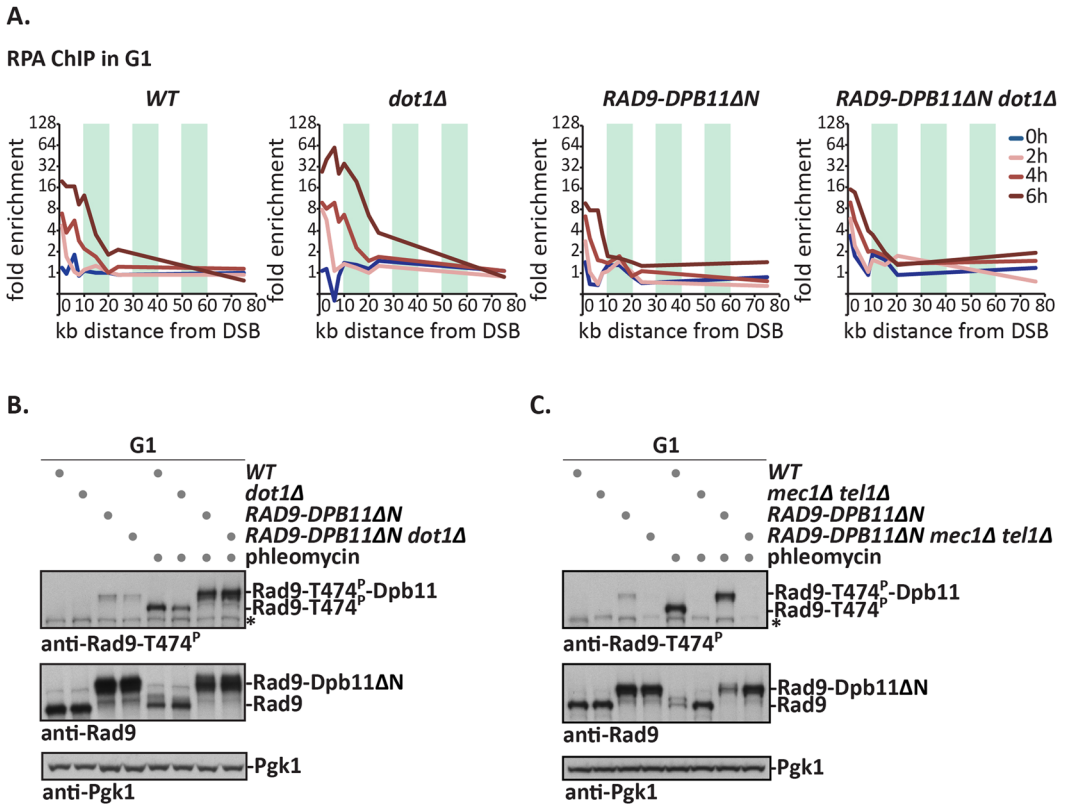

Figure 4. A Rad9-Dpb11 fusion forces Rad9 recruitment to DSBs and T474 phosphorylation independently of the 'histone pathway'. (**A**) The Rad9-Dpb11 fusion blocks resection, also in the absence of Dot1. RPA-ChIP at the indicated positions from an HO-induced DSB (0, 2, 4 and 6 h after HO induction) in *WT*, *dot1Δ*, *RAD9-DPB11ΔN* and *RAD9-DPB11ΔN dot1Δ* indicates the extent of DNA end resection. FACS profiles in Fig. S4A. (**B**,**C**) The Rad9-Dpb11 fusion bypasses the requirement for Dot1, but not for Mec1 and Tel1. Measurement of Rad9-T474 phosphorylation as in Fig. 2A, but in G1-arrested cells expressing the Rad9-Dpb11 fusion in (**B**) *WT* and *dot1Δ* background or (**C**) *WT* and *mec1Δ tel1Δ* background. Immunoblotting against Rad9 or Rad9-T474 phosphorylation. A Pgk1 immunoblot serves as loading control. An asterisk denotes a crossreactive band. FACS profiles in Fig. S4C and E respectively. Strains containing the *mec1Δ* mutation are in *sml1Δ* background.

by CDK and to facilitate interaction with Dpb11[17,42]. Notably, we found that also the DNA damage-induced, CDK-independent phosphorylation of Rad9 leads to an interaction with Dpb11. When testing the attributes of DNA damage-induced phosphorylation, we found that it requires the histone methyltransferase Dot1, indicating a dependency on the 'histone pathway', which is known to target Rad9 to damaged chromatin[19–22,25]. Moreover, the covalent Rad9-Dpb11 fusion, which is known to tether Rad9 to damaged chromatin[17,40], bypasses this dependency on the 'histone pathway'.

We found that damage-induced Rad9 S/TP phosphorylation is abolished, when Rad9 cannot be recruited to damaged chromatin. In this regard, damage-induced Rad9 S/TP phosphorylation is highly similar to Rad9 S/TQ phosphorylation[19–23], which can be measured as an overall Rad9 phosphorylation shift. Conversely, we observed that forced localization of Rad9 to chromatin, reinstates S/TP phosphorylation, suggesting that Rad9 has to be recruited to damaged chromatin in order to become phosphorylated for both damage-induced S/TP phosphorylation and S/TQ phosphorylation.

Our data therefore suggest that Rad9 S/TP sites are targeted by a chromatin-localized kinase. The apical checkpoint kinases Mec1 and Tel1 would fulfil this requirement, as they are specifically active at damaged chromatin[43]. Consistently, we found that damage-induced Rad9 S/TP phosphorylation is abolished in a *mec1Δ tel1Δ* double mutant. However, this influence could also be indirect, since Mec1 and Tel1 are necessary for efficient phosphorylation of the Rad9 SCD, which itself is required for damage-induced phosphorylation of Rad9 S/TP sites. Moreover, we could not find any *in vitro* evidence to support that Mec1 or Tel1 would directly target S/TP motifs. Currently, the best candidates for this novel mode of Rad9 S/TP phosphorylation, are the transcriptional kinases of the CDK family – Kin28, Srb10, Bur1 and Ctk1 – given their similarity to Cdc28 and their chromatin-localization. In the future, it will therefore be interesting to test the connection between transcriptional CDKs and the DNA damage checkpoint.

Several studies have collectively suggested a model of cell cycle-regulated Rad9 recruitment and activation in budding yeast[17,33,42] and fission yeast[4]. These models suggest that the 'histone pathway' is exclusively required for Rad9 recruitment to damaged chromatin in G1, while in M phase both 'histone pathway' and 'Dpb11 pathway' are active. While our study suggests that Rad9 and Dpb11 can interact in G1 as well, this view of Rad9

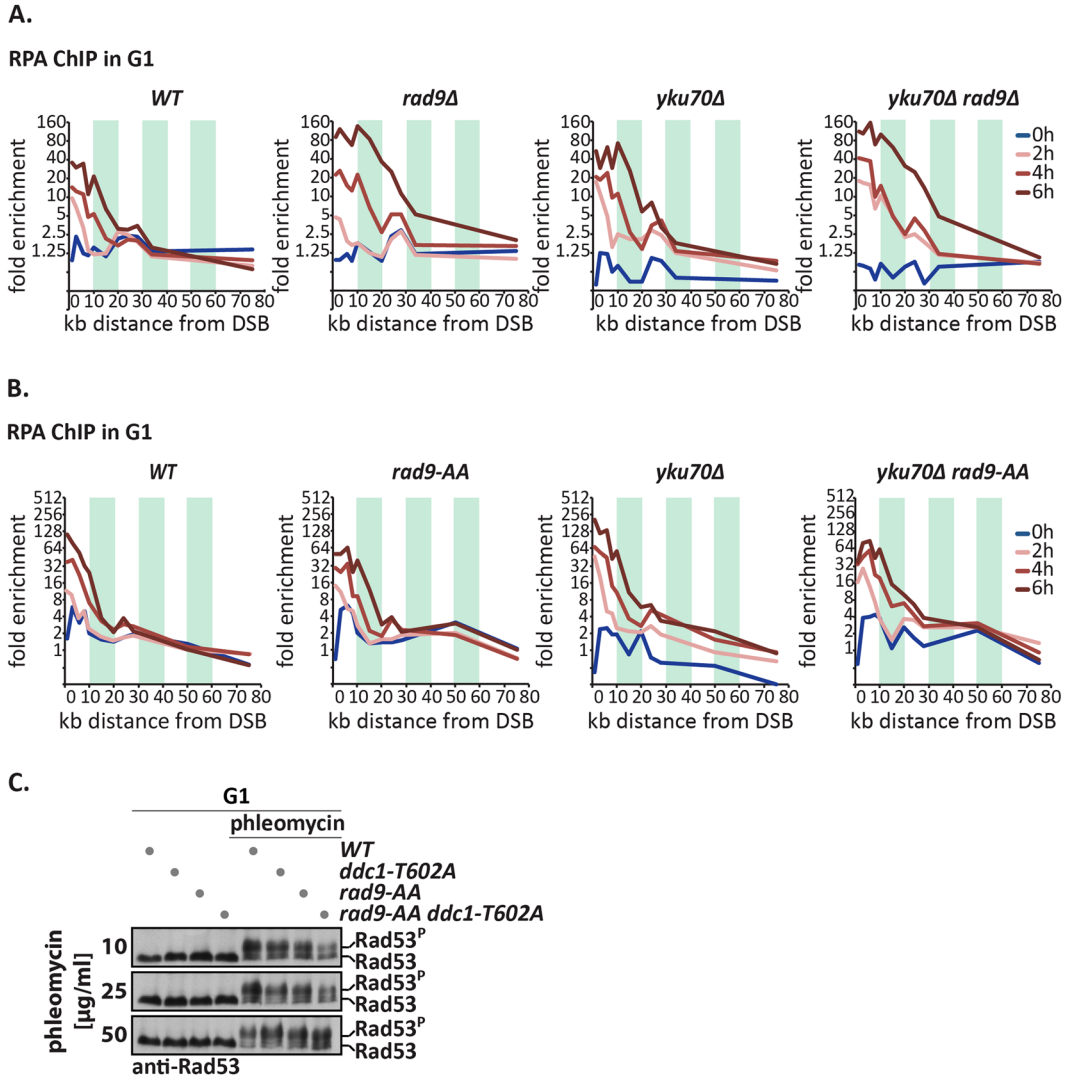

Figure 5. Lack of damage-induced Rad9 S/TP phosphorylation does not directly affect checkpoint signalling or DNA end resection. (**A**,**B**) The *rad9-AA* mutant – in contrast to the *rad9Δ* mutant – does not induce hyper-resection in G1-arrested cells. A site-specific DSB was induced at the *MAT* locus using galactose-induced HO in G1-arrested cells. DNA end resection is shown by ChIP against RPA at 0, 2, 4 and 6 h after HO induction within 0–80 kb distance to the DSB. (**A**) Resection was measured in *WT*, *rad9Δ*, *yku70Δ* and *rad9Δ yku70Δ* strains. FACS profiles in Fig. S5A. (**B**) as (**A**), but with *WT*, *rad9-AA*, *yku70Δ* and *rad9-AA yku70Δ* strains. FACS profiles in Fig. S5B. (**C**) The *rad9-AA* mutant does not induce apparent defects in checkpoint activation in G1 even in the background of the *ddc1-T602A* mutation. Hyperphosphorylation of Rad53 induced by different concentrations of phleomycin added to the growth medium is used as measure of checkpoint activation. FACS profiles in Fig. S5C.

recruitment pathways is not affected, since Rad9 recruitment via the 'histone pathway' is upstream of and required for damage-induced Rad9 S/TP site phosphorylation and the Rad9-Dpb11 interaction in G1. Dpb11, therefore, does apparently not function as Rad9 recruiter in G1. As such, it is currently unresolved what function the damage-induced phosphorylation of Rad9 S/TP sites and subsequent binding to Dpb11 could have. We have not found any phenotypes in the G1 checkpoint or in the control of DNA end resection in G1, when we used the *rad9-AA* mutant. So far, we have investigated possible redundancies in Dpb11 recruitment (using the *ddc1-T602A* allele, Fig. 5) and Rad9 recruitment (using the *dot1Δ* allele, ref. 17), but also this did not reveal a defect. Therefore, the damage-induced Rad9 phosphorylation at S/TP sites may either act redundantly with a currently unknown factor or mediate an entirely new function.

Eukaryotic orthologs of Rad9 have been shown to be recruited to damaged chromatin by related mechanisms[4,27–31,44–47]. Specifically, both fission yeast Crb2 and human 53BP1 were found to interact with the respective Dpb11 orthologs[29,37]. Notably, in human cells 53BP1 and TOPBP1 were found to interact specifically in G1[37]. This interaction, therefore, does seemingly not require CDK-phosphorylation, but would rather be consistent with a DNA damage-induced mode of interaction as described here. The phosphorylation sites on 53BP1 that mediate

TOPBP1-binding are currently unknown and it remains to be established whether the DNA damage-induced mode of the Rad9-Dpb11 interaction is evolutionary conserved.

Given the abundance of target proteins that are modified at S/TP sites by CDK[48], S/TP site phosphorylation is often interpreted as phosphorylation by CDK. Our results caution, however, that this may be an oversimplified view. It will be interesting to see if CDK-independent S/TP site phosphorylation is a general phenomenon that can be observed on other proteins as well. Phosphoproteomic experiments in human cells treated with etoposide or γ-irradiation have rather suggested an opposite trend, as S/TP phosphorylation was generally decreased[49]. However, this decrease is caused by the inhibition of Cdk1 and Cdk2 after DNA damage in human cells. In order to test whether a substantial number of S/TP phosphorylation substrates become modified specifically after DNA damage, a system would be required, where CDK is not generally downregulated after DNA damage. While budding yeast fulfils this requirement, previous phosphoproteomic studies of the DNA damage response in budding yeast have primarily focussed on damage-induced S/TQ phosphorylation and checkpoint kinase dependencies[50,51]. A systematic investigation of DNA damage-induced S/TP phosphorylation, as well as the involved kinases, therefore appears worthwhile.

Methods

Materials. All yeast strains used in this study were derived from W303 MATa and were constructed using standard methods[52]. Cells were grown in YP glucose or YP raffinose media at 30 °C. All strains used in this study are listed in Supplementary Table 1, all antibodies in Supplementary Table 2.

Measurement of Rad9 and Rad53 phosphorylation. Cells were grown in YP glucose media at 30 °C or 24 °C. Cell cycle synchronization was performed using α-factor (5 μg/ml or 0.25 μg/ml for *bar1Δ* mutants) or nocodazole (5 μg/ml) for 2–3 hours. To inhibit CDK, a strain containing the *cdc28-as1* allele[53] was treated with 1 μM 1-NM-PP1. To induce DNA damage, phleomycin (Invivogen) was added to the medium to a final concentration of 50 μg/ml - or concentrations as indicated. Denaturing cell extracts were prepared by alkaline lysis followed by trichloroacetic acid (TCA) precipitation and precipitated proteins were collected by centrifugation and resuspended in SDS-PAGE sample buffer containing 8 M urea for subsequent SDS-PAGE analysis.

To detect Rad9 phosphorylation on S462 and T474, previously described phospho-specific antibodies were used[17]. Rad53 phospho-shifts were resolved on 10% acrylamide gels.

Rad9 Immunoprecipitations. For Rad9^{3FLAG} IPs cell extracts were prepared from 200 OD yeast cells treated as above for cell cycle arrest and DNA damage. Cells were harvested, washed in ice-cold sorbitol buffer (1 M sorbitol, 25 mM Hepes pH 7.6), and resuspended in a 1:1 ratio with lysis buffer supplemented with protease and phosphatase inhibitors (100 mM Hepes, 200 mM KOAc, 0.1% NP-40, 10% glycerol, 2 mM β-mecaptoethanol, 100 nM okadaic acid, 10 mM NaF, 20 mM β-glycerophosphate, 400 μM PMSF, 4 μM aprotinin, 4 mM benzamidin, 400 μM leupeptin, 300 μM pepstatin A), snap-frozen to liquid nitrogen and lysed using a Spex Sample Prep cryo mill. The extracts were cleared by centrifugation and incubated with anti-FLAG agarose resin (Sigma) for 1 hour (4 °C, rotation). After five washes with lysis buffer, Rad9^{3FLAG} was eluted twice with 0.5 mg/ml 3xFLAG peptide (Sigma). The elutions were pooled and proteins were precipitated with TCA prior to analysis on 4–12% NuPAGE gels (Invitrogen) and standard western blotting.

GST-Dpb11 pulldowns. The Dpb11-Rad9 interaction was tested as described[17]. GST, GST-Dpb11 FL or a GST-Dpb11 fragment containing BRCT1 + 2 were immobilized on glutathione sepharose 4B (GE Healthcare) and incubated with 600 ml ammonium sulphate-precipitated (57%) cell extracts (in 200 mM KOAc, 100 mM Hepes pH 7.6, 10% glycerol, 0.02% NP-40, 2 mM β-mercaptoethanol, 20 mM β-glycerophosphate, 10 mM NaF, 100 mM okadaic acid, protease inhibitors) corresponding to 50 OD yeast cells. The pulldown was incubated 1 hour (4 °C, rotation), washed and eluted by boiling in SDS-PAGE sample buffer.

Chromatin Immunoprecipitation (ChIP) to a DSB and qPCR analysis. For chromatin immunoprecipitation of Rad9, RPA and Dpb11, cells were grown in YP raffinose to an OD of 0.5 and cell cycle arrest was induced with α-factor or nocodazole. A single double strand break at the *MAT* locus was introduced by inducing the HO endonuclease from the galactose promoter by addition of galactose to the cultures to a 2% final concentration. 100 ODs of cells were crosslinked with formaldehyde (final 1%) for 16 minutes at timepoints as indicated and the reaction was quenched with glycine. Cells were harvested by centrifugation, washed in ice-cold PBS and snap-frozen. Cell pellets were resuspended in 800 μl lysis buffer (50 mM HEPES KOH pH 7.5, 150 mM NaCl, 1 mM EDTA, 1% Triton X-100, 0.1% Na-deoxycholate, 0.1% SDS) and lysed with zirconia beads using a bead beating device. The chromatin was sonified to shear the DNA to a size of 200–500 bp. The obtained extracts were cleared by centrifugation, 1% was taken as input sample and 40% were incubated with either anti-FLAG-M2 magnetic beads (Sigma) for 2 hours (Rad9^{3FLAG} ChIPs) or with anti-RPA antibody (AS07-214, Agrisera) followed by 30 min with Dynabeads ProteinA (Invitrogen, for RPA ChIPs). The beads were washed 3x in lysis buffer, 2x in lysis buffer with 500 mM NaCl, 2x in wash buffer (10 mM Tris-Cl pH 8.0, 0.25 M LiCl, 1 mM EDTA, 0.5% NP-40, 0.5% Na-deoxycholate) and 2x in TE pH 8.0. DNA-protein complexes were eluted in 1% SDS, proteins were removed via proteinase K digestion (3 h, 42 °C) and crosslinks were reversed (8 h or overnight, 65 °C). The DNA was subsequently purified using phenol-chloroform extraction and ethanol precipitation and quantified by quantitative PCR (Roche LightCycler480 System, KAPA SYBR FAST 2x qPCR Master Mix, KAPA Biosystems) at indicated positions with respect to the DNA double strand break. As a control, 2-3 control regions on other chromosomes were quantified.

References

1. Finn, K., Lowndes, N. F. & Grenon, M. Eukaryotic DNA damage checkpoint activation in response to double-strand breaks. *Cell. Mol. Life Sci.* **69**, 1447–1473 (2011).
2. Weinert, T. A. & Hartwell, L. H. The RAD9 gene controls the cell cycle response to DNA damage in Saccharomyces cerevisiae. *Science* **241**, 317–322 (1988).
3. Saka, Y., Esashi, F., Matsusaka, T., Mochida, S. & Yanagida, M. Damage and replication checkpoint control in fission yeast is ensured by interactions of Crb2, a protein with BRCT motif, with Cut5 and Chk1. *Genes Dev.* **11**, 3387–3400 (1997).
4. Du, L.-L., Nakamura, T. M. & Russell, P. Histone modification-dependent and -independent pathways for recruitment of checkpoint protein Crb2 to double-strand breaks. *Genes Dev.* **20**, 1583–1596 (2006).
5. Panier, S. & Boulton, S. J. Double-strand break repair: 53BP1 comes into focus. *Nat. Rev. Mol. Cell Biol.* **15**, 7–18 (2014).
6. Symington, L. S. End Resection at Double-Strand Breaks: Mechanism and Regulation. *Cold Spring Harbor Perspectives in Biology* **6**, a016436–a016436 (2014).
7. Sweeney, F. D. *et al*. Saccharomyces cerevisiae Rad9 acts as a Mec1 adaptor to allow Rad53 activation. *Current Biology* **15**, 1364–1375 (2005).
8. Vialard, J. E., Gilbert, C. S., Green, C. M. & Lowndes, N. F. The budding yeast Rad9 checkpoint protein is subjected to Mec1/Tel1-dependent hyperphosphorylation and interacts with Rad53 after DNA damage. *EMBO J.* **17**, 5679–5688 (1998).
9. Durocher, D., Henckel, J., Fersht, A. R. & Jackson, S. P. The FHA domain is a modular phosphopeptide recognition motif. *Mol. Cell* **4**, 387–394 (1999).
10. Sun, Z., Hsiao, J., Fay, D. S. & Stern, D. F. Rad53 FHA domain associated with phosphorylated Rad9 in the DNA damage checkpoint. *Science* **281**, 272–274 (1998).
11. Emili, A. MEC1-dependent phosphorylation of Rad9p in response to DNA damage. *Mol. Cell* **2**, 183–189 (1998).
12. Schwartz, M. F. *et al*. Rad9 phosphorylation sites couple Rad53 to the Saccharomyces cerevisiae DNA damage checkpoint. *Mol. Cell* **9**, 1055–1065 (2002).
13. Lazzaro, F. *et al*. Histone methyltransferase Dot1 and Rad9 inhibit single-stranded DNA accumulation at DSBs and uncapped telomeres. *EMBO J.* **27**, 1502–1512 (2008).
14. Trovesi, C., Falcettoni, M., Lucchini, G., Clerici, M. & Longhese, M. P. Distinct Cdk1 requirements during single-strand annealing, noncrossover, and crossover recombination. *PLoS Genet.* **7**, e1002263 (2011).
15. Ferrari, M. *et al*. Functional Interplay between the 53BP1-Ortholog Rad9 and the Mre11 Complex Regulates Resection, End-Tethering and Repair of a Double-Strand Break. *PLoS Genet.* **11**, e1004928 (2015).
16. Lydall, D. & Weinert, T. Yeast checkpoint genes in DNA damage processing: implications for repair and arrest. *Science* **270**, 1488–1491 (1995).
17. Pfander, B. & Diffley, J. F. X. Dpb11 coordinates Mec1 kinase activation with cell cycle-regulated Rad9 recruitment. *EMBO J.* **30**, 4897–4907 (2011).
18. Granata, M. *et al*. Dynamics of Rad9 Chromatin Binding and Checkpoint Function Are Mediated by Its Dimerization and Are Cell Cycle–Regulated by CDK1 Activity. *PLoS Genet.* **6**, e1001047 (2010).
19. Wysocki, R. *et al*. Role of Dot1-dependent histone H3 methylation in G1 and S phase DNA damage checkpoint functions of Rad9. *Mol. Cell. Biol.* **25**, 8430–8443 (2005).
20. Javaheri, A. *et al*. Yeast G1 DNA damage checkpoint regulation by H2A phosphorylation is independent of chromatin remodeling. *Proceedings of the National Academy of Sciences* **103**, 13771–13776 (2006).
21. Hammet, A., Magill, C., Heierhorst, J. & Jackson, S. P. Rad9 BRCT domain interaction with phosphorylated H2AX regulates the G1 checkpoint in budding yeast. *EMBO Rep.* **8**, 851–857 (2007).
22. Grenon, M. *et al*. Docking onto chromatin via the Saccharomyces cerevisiae Rad9 Tudor domain. *Yeast* **24**, 105–119 (2007).
23. Giannattasio, M., Lazzaro, F., Plevani, P. & Muzi-Falconi, M. The DNA damage checkpoint response requires histone H2B ubiquitination by Rad6-Bre1 and H3 methylation by Dot1. *J. Biol. Chem.* **280**, 9879–9886 (2005).
24. van Leeuwen, F., Gafken, P. R. & Gottschling, D. E. Dot1p modulates silencing in yeast by methylation of the nucleosome core. *Cell* **109**, 745–756 (2002).
25. Toh, G. W.-L. *et al*. Histone H2A phosphorylation and H3 methylation are required for a novel Rad9 DSB repair function following checkpoint activation. *DNA Repair (Amst)* **5**, 693–703 (2006).
26. Downs, J. A., Lowndes, N. F. & Jackson, S. P. A role for Saccharomyces cerevisiae histone H2A in DNA repair. *Nature* **408**, 1001–1004 (2000).
27. Fradet-Turcotte, A. *et al*. 53BP1 is a reader of the DNA-damage-induced H2A Lys 15 ubiquitin mark. *Nature* **499**, 50–54 (2013).
28. Wilson, M. D. *et al*. The structural basis of modified nucleosome recognition by 53BP1. *Nature* **536**, 100–103 (2016).
29. Du, L. L. Histone modification-dependent and -independent pathways for recruitment of checkpoint protein Crb2 to double-strand breaks. *Genes Dev.* **20**, 1583–1596 (2006).
30. Sanders, S. L. *et al*. Methylation of histone H4 lysine 20 controls recruitment of Crb2 to sites of DNA damage. *Cell* **119**, 603–614 (2004).
31. Botuyan, M. V. *et al*. Structural Basis for the Methylation State-Specific Recognition of Histone H4-K20 by 53BP1 and Crb2 in DNA Repair. *Cell* **127**, 1361–1373 (2006).
32. Leung, C. C. Y. & Glover, J. N. M. BRCT domains. *Cell Cycle* **10**, 2461–2470 (2014).
33. Puddu, F. *et al*. Phosphorylation of the Budding Yeast 9-1-1 Complex Is Required for Dpb11 Function in the Full Activation of the UV-Induced DNA Damage Checkpoint. *Mol. Cell. Biol.* **28**, 4782–4793 (2008).
34. Gritenaite, D. *et al*. A cell cycle-regulated Slx4-Dpb11 complex promotes the resolution of DNA repair intermediates linked to stalled replication. *Genes Dev.* **28**, 1604–1619 (2014).
35. Chen, X. *et al*. The Fun30 nucleosome remodeller promotes resection of DNA double-strand break ends. *Nature* **489**, 576–580 (2012).
36. Bantele, S. C., Ferreira, P., Gritenaite, D., Boos, D. & Pfander, B. Targeting of the Fun30 nucleosome remodeller by the Dpb11 scaffold facilitates cell cycle-regulated DNA end resection. *eLife* **6**, e21687 (2017).
37. Cescutti, R., Negrini, S., Kohzaki, M. & Halazonetis, T. D. TopBP1 functions with 53BP1 in the G1 DNA damage checkpoint. *EMBO J.* **29**, 3723–3732 (2010).
38. Usui, T., Foster, S. S. & Petrini, J. H. J. Maintenance of the DNA-damage checkpoint requires DNA-damage-induced mediator protein oligomerization. *Mol. Cell* **33**, 147–159 (2009).
39. Lee, S. E. *et al*. Saccharomyces Ku70, mre11/rad50 and RPA proteins regulate adaptation to G2/M arrest after DNA damage. *Cell* **94**, 399–409 (1998).
40. Liu, Y. *et al*. TOPBP1 Dpb11plays a conserved role in homologous recombination DNA repair through the coordinated recruitment of 53BP1 Rad9. *J. Cell Biol.* **33**, jcb.201607031–17 (2017).
41. Ferretti, L. P., Lafranchi, L. & Sartori, A. A. Controlling DNA-end resection: a new task for CDKs. *Frontiers in Genetics* **4**, 1–7 (2013).
42. Wang, G., Tong, X., Weng, S. & Zhou, H. Multiple phosphorylation of Rad9 by CDK is required for DNA damage checkpoint activation. *Cell Cycle* **11**, 3792–3800 (2012).
43. Gobbini, E., Cesena, D., Galbiati, A., Lockhart, A. & Longhese, M. P. Interplays between ATM/Tel1 and ATR/Mec1 in sensing and signaling DNA double-strand breaks. *DNA Repair (Amst.)* **12**, 791–799 (2013).

44. Wakeman, T. P., Wang, Q., Feng, J. & Wang, X.-F. Bat3 facilitates H3K79 dimethylation by DOT1L and promotes DNA damage-induced 53BP1 foci at G1/G2 cell-cycle phases. *EMBO J.* **31**, 2169–2181 (2012).
45. Huyen, Y. *et al.* Methylated lysine 79 of histone H3 targets 53BP1 to DNA double-strand breaks. *Nature* **432**, 406–411 (2004).
46. Greeson, N. T., Sengupta, R., Arida, A. R., Jenuwein, T. & Sanders, S. L. Di-methyl H4 lysine 20 targets the checkpoint protein Crb2 to sites of DNA damage. *J. Biol. Chem.* **283**, 33168–33174 (2008).
47. Pellegrino, S., Michelena, J., Teloni, F., Imhof, R. & Altmeyer, M. Replication-Coupled Dilution of H4K20me2 Guides 53BP1 to Pre-replicative Chromatin. *CellReports* **19**, 1819–1831 (2017).
48. Holt, L. J. *et al.* Global analysis of Cdk1 substrate phosphorylation sites provides insights into evolution. *Science* **325**, 1682–1686 (2009).
49. Beli, P. *et al.* Proteomic investigations reveal a role for RNA processing factor THRAP3 in the DNA damage response. *Mol. Cell* **46**, 212–225 (2012).
50. Smolka, M. B., Albuquerque, C. P., Chen, S.-H. & Zhou, H. Proteome-wide identification of *in vivo* targets of DNA damage checkpoint kinases. *Proceedings of the National Academy of Sciences* **104**, 10364–10369 (2007).
51. de Oliveira, F. M. B. *et al.* Phosphoproteomics Reveals Distinct Modes of Mec1/ATR Signaling during DNA Replication. *Mol. Cell* 1–10, https://doi.org/10.1016/j.molcel.2015.01.043 (2015).
52. Janke, C. *et al.* A versatile toolbox for PCR-based tagging of yeast genes: new fluorescent proteins, more markers and promoter substitution cassettes. *Yeast* **21**, 947–962 (2004).
53. Bishop, A. C. *et al.* A chemical switch for inhibitor-sensitive alleles of any protein kinase. *Nature* **407**, 395–401 (2000).

Acknowledgements

We thank J. Diffley, M.P. Longhese, J. Petrini for antibodies, plasmid constructs and strains, members of the Jentsch and Pfander labs for stimulating discussion and critical reading of the manuscript. This work was supported by the German Research Council (DFG; project grant PF794/1-1, to BP) and the Max Planck Society (to BP).

Author Contributions

B.P. initiated the study. G.D.C. and B.P. conducted all experiments. S.C.S.B. and K.U.R. provided preliminary data and materials. All authors analysed the data. B.P. wrote the paper, all authors commented on the manuscript

Additional Information

Supplementary information accompanies this paper at https://doi.org/10.1038/s41598-017-11937-z.

Competing Interests: The authors declare that they have no competing interests.

Publisher's note: Springer Nature remains neutral with regard to jurisdictional claims in published maps and institutional affiliations.

Supplementary material

A cell cycle-independent mode of the Rad9-Dpb11 interaction is induced by DNA damage

Giulia di Cicco, Susanne C. S. Bantele, Karl-Uwe Reusswig, and Boris Pfander

- **Supplementary figures S1-S14**
- **Supplementary figure legends**
- **Supplementary tables S1-S2**

Figure S1

A.

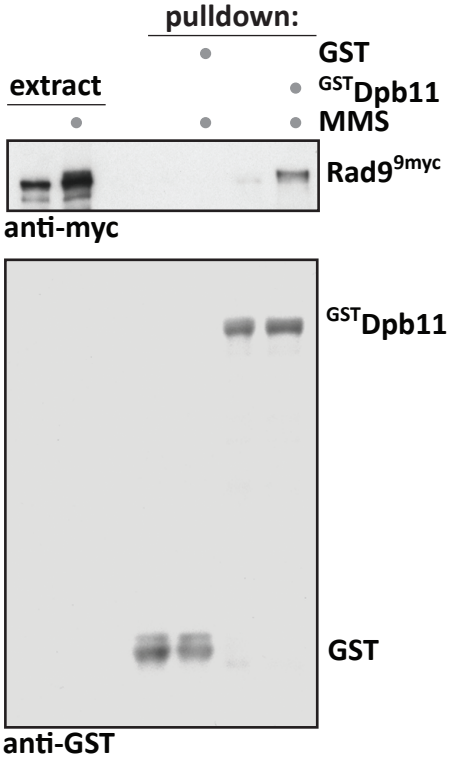

B.

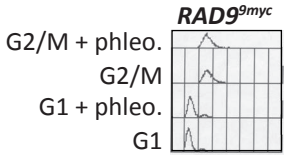

C.

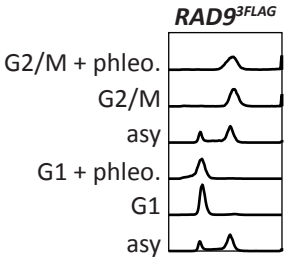

D.

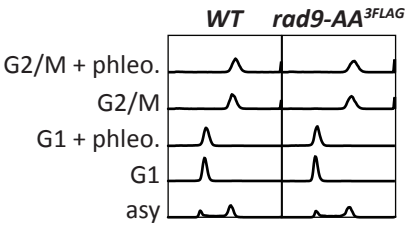

E.

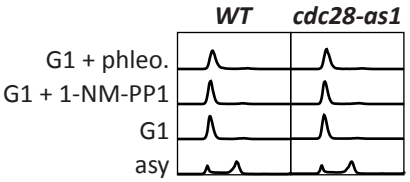

F.

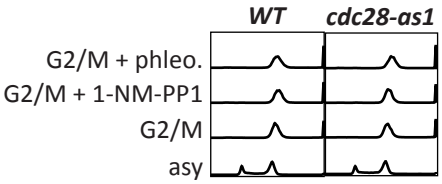

Figure S2

A.

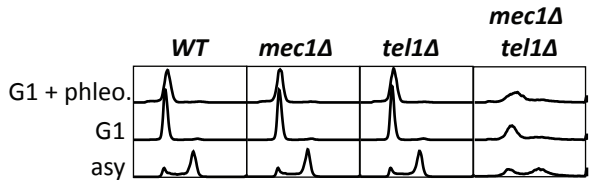

B.

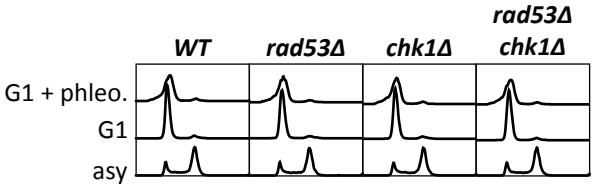

C.

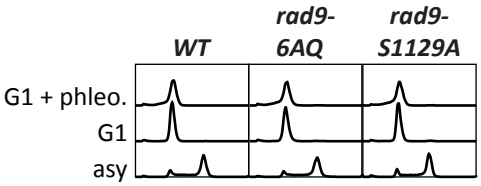

D.

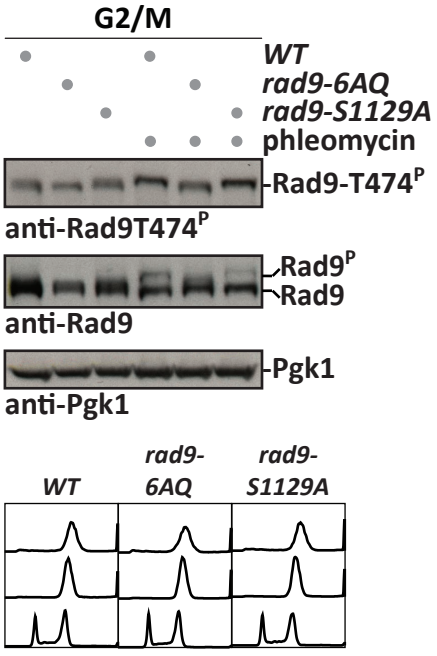

Figure S3

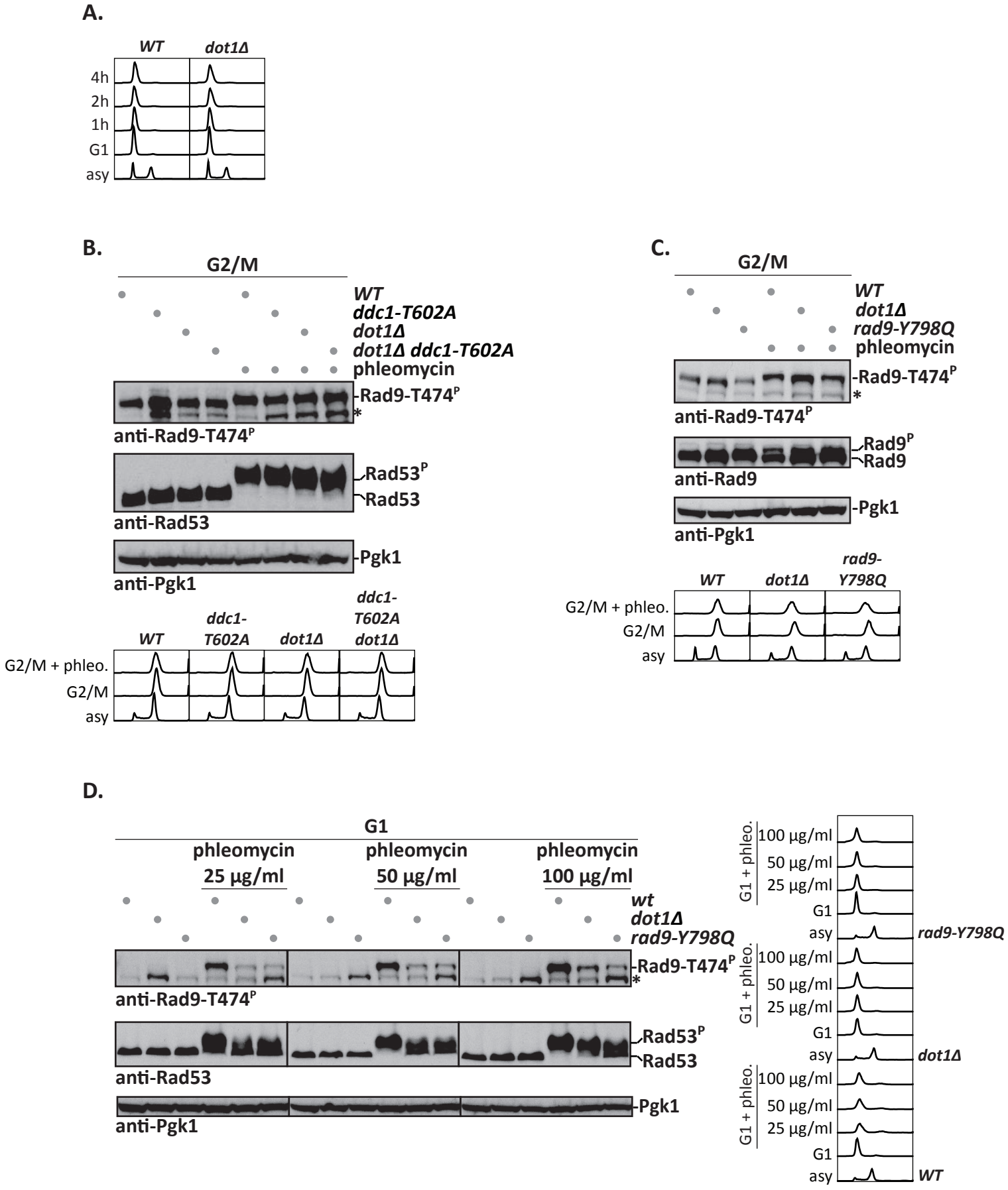
A.
WT
dot1Δ
4h
2h
1h
G1
asy
B.
G2/M
WT
ddc1-T602A
dot1Δ
dot1Δ ddc1-T602A
phleomycin
Rad9-T474P
*
anti-Rad9-T474P
Rad53P
Rad53
anti-Rad53
Pgk1
anti-Pgk1
WT
ddc1-T602A
dot1Δ
ddc1-T602A dot1Δ
G2/M + phleo.
G2/M
asy
C.
G2/M
WT
dot1Δ
rad9-Y798Q
phleomycin
-Rad9-T474P
*
anti-Rad9-T474P
Rad9P
Rad9
anti-Rad9
-Pgk1
anti-Pgk1
WT
dot1Δ
rad9-Y798Q
G2/M + phleo.
G2/M
asy
D.
G1
phleomycin 25 µg/ml
phleomycin 50 µg/ml
phleomycin 100 µg/ml
wt
dot1Δ
rad9-Y798Q
Rad9-T474P
*
anti-Rad9-T474P
Rad53P
Rad53
anti-Rad53
Pgk1
anti-Pgk1
G1 + phleo.
100 µg/ml
50 µg/ml
25 µg/ml
G1
asy
rad9-Y798Q
dot1Δ
WT
E.
WT
ddc1-T602A
dot1Δ
ddc1-T602A dot1Δ
G1 + phleo.
G1
asy

Figure S4

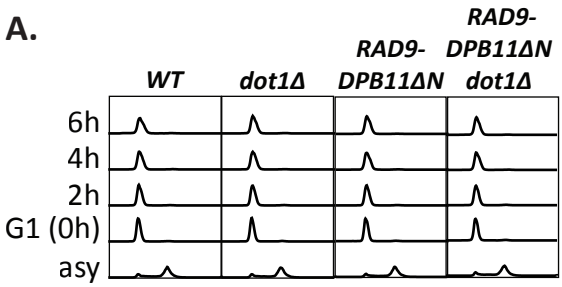
A.
WT
dot1Δ
RAD9-DPB11ΔN
RAD9-DPB11ΔN dot1Δ
6h
4h
2h
G1 (0h)
asy

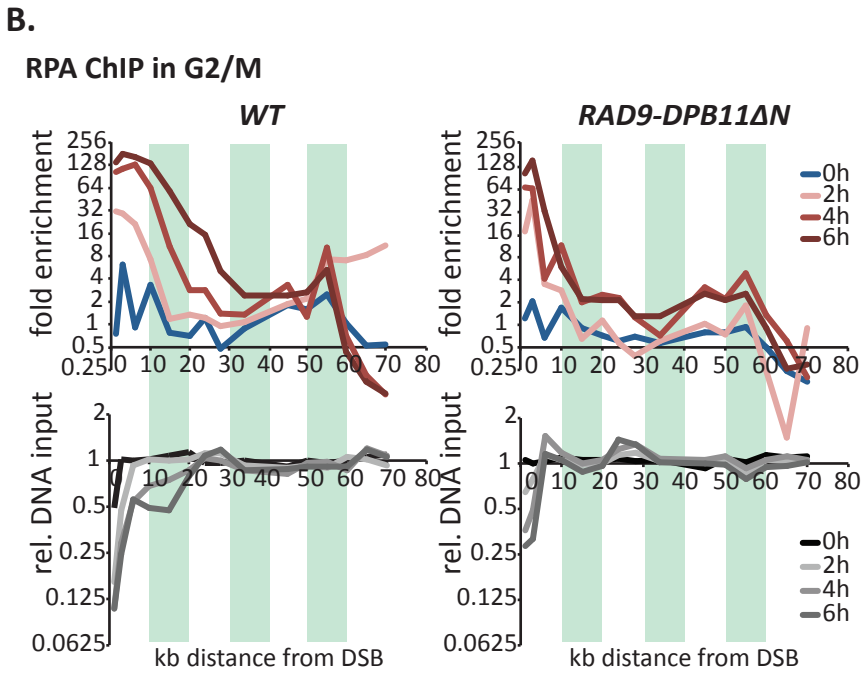
B.
RPA ChIP in G2/M
WT
RAD9-DPB11ΔN
fold enrichment
rel. DNA input
kb distance from DSB
0h
2h
4h
6h

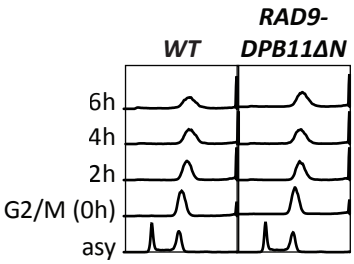
WT
RAD9-DPB11ΔN
6h
4h
2h
G2/M (0h)
asy

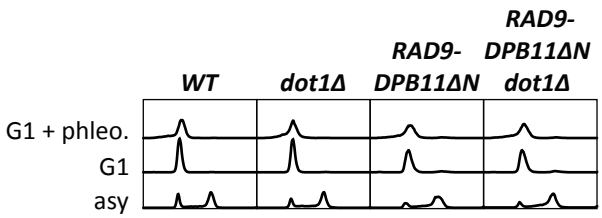
C.
WT
dot1Δ
RAD9-DPB11ΔN
RAD9-DPB11ΔN dot1Δ
G1 + phleo.
G1
asy

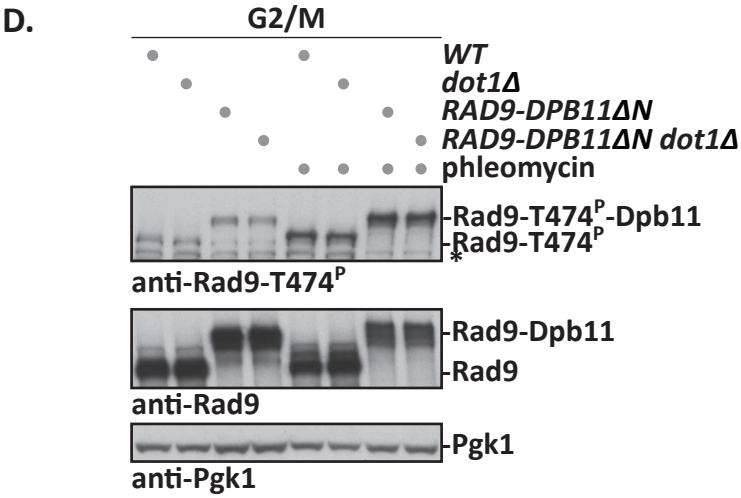
D.
G2/M
WT
dot1Δ
RAD9-DPB11ΔN
RAD9-DPB11ΔN dot1Δ
phleomycin
Rad9-T474P-Dpb11
Rad9-T474P
*
anti-Rad9-T474P
Rad9-Dpb11
Rad9
anti-Rad9
Pgk1
anti-Pgk1

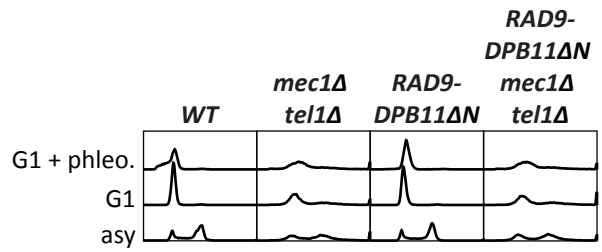
E.
WT
mec1Δ tel1Δ
RAD9-DPB11ΔN
RAD9-DPB11ΔN mec1Δ tel1Δ
G1 + phleo.
G1
asy

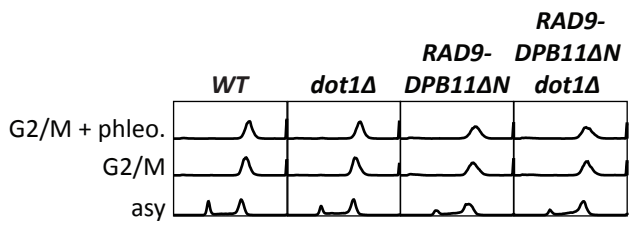
WT
dot1Δ
RAD9-DPB11ΔN
RAD9-DPB11ΔN dot1Δ
G2/M + phleo.
G2/M
asy

Figure S5

A.

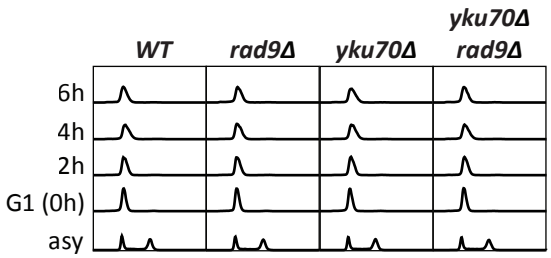

B.

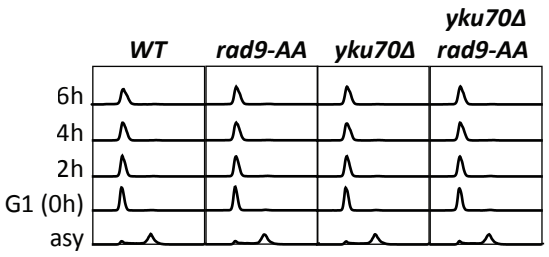

C.

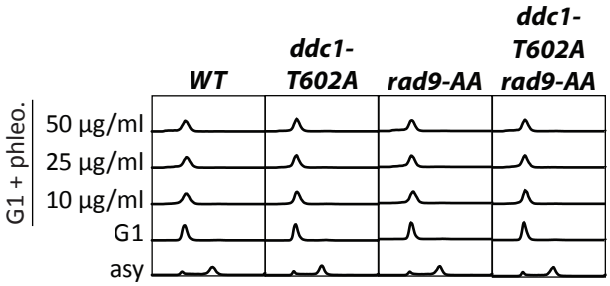

D.

Dpb11^{3FLAG} ChIP in G1

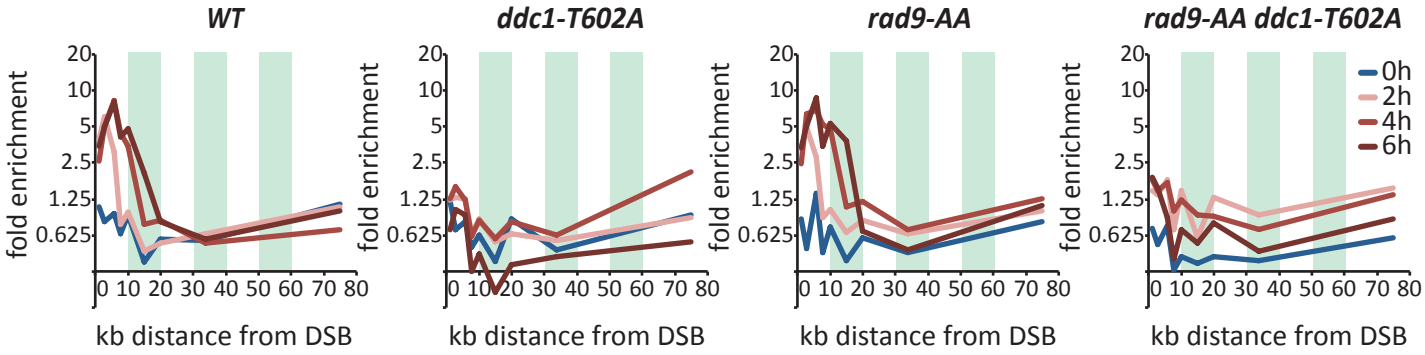

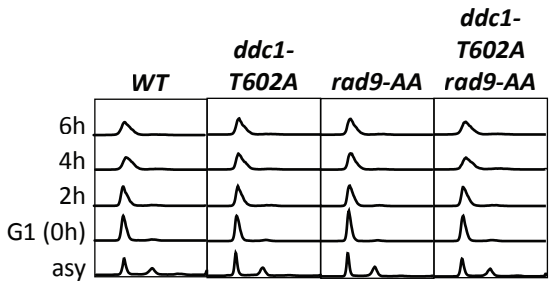

Figure S6

A. relates to Fig. 1A

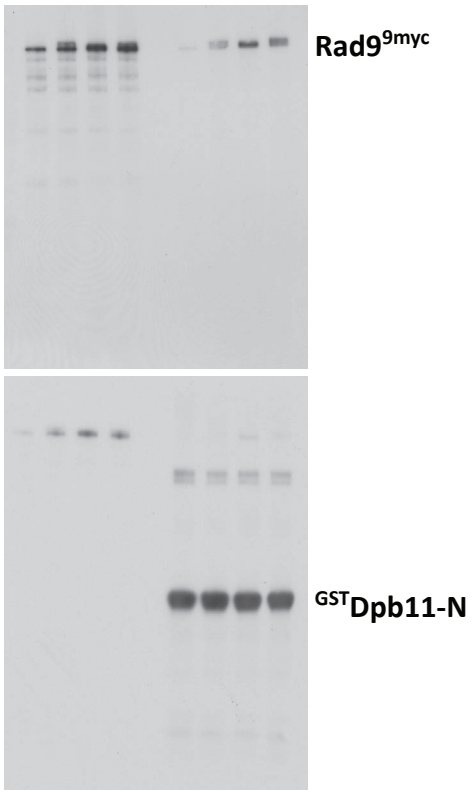

B. relates to Fig. 1B

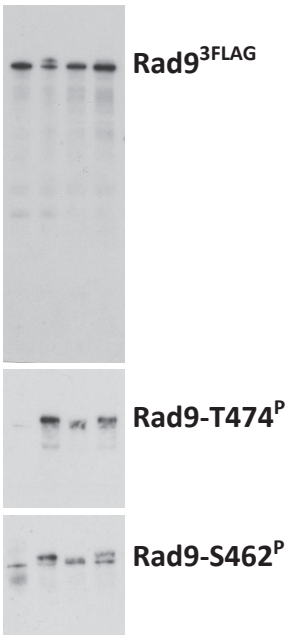

C. relates to Fig. 1C

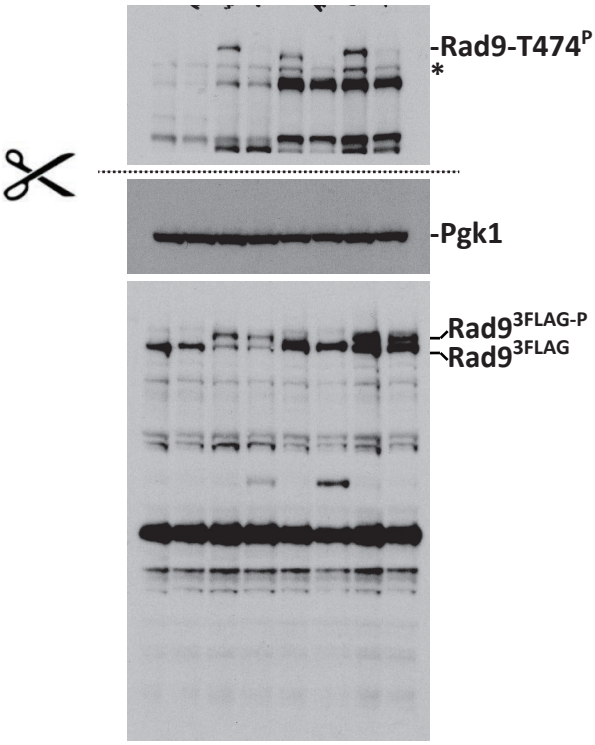

D. relates to Fig. 1D

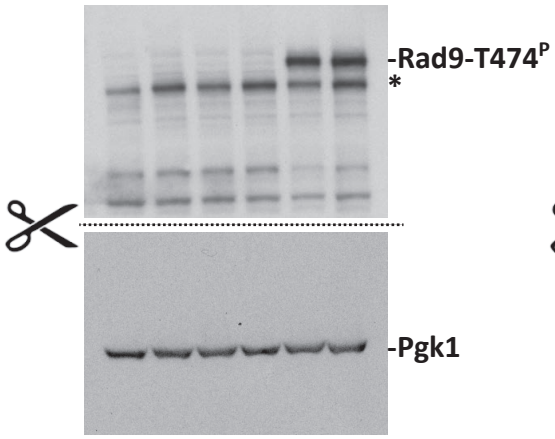

E. relates to Fig. 1E

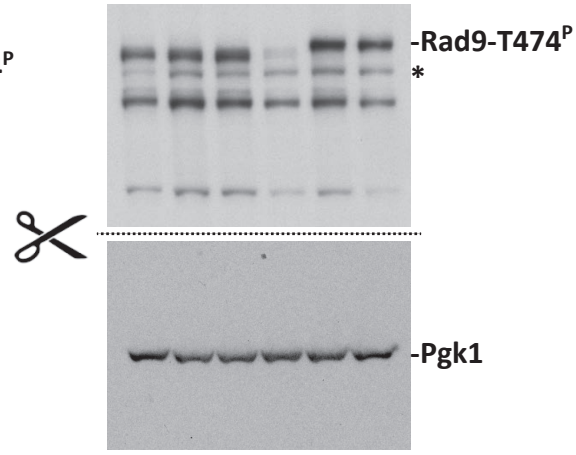

Figure S7

A. relates to Fig. S1A

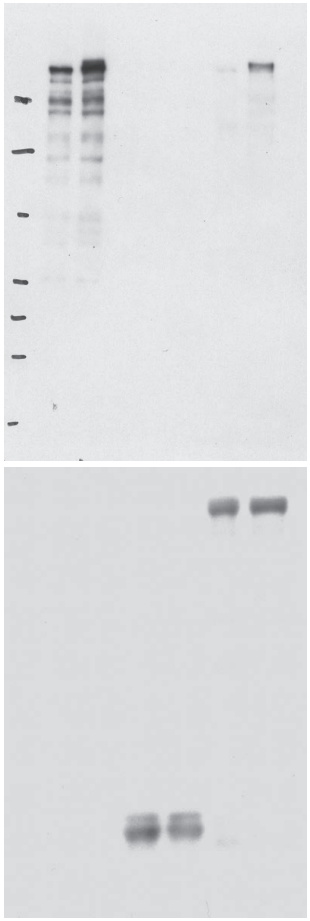

Figure S8

A. relates to Fig. 2A

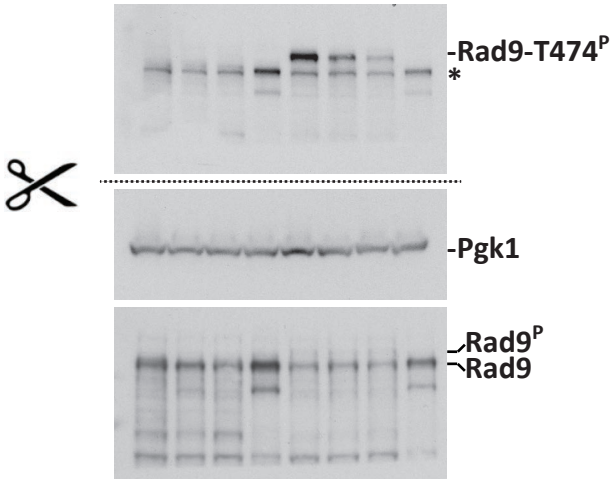

B. relates to Fig. 2B

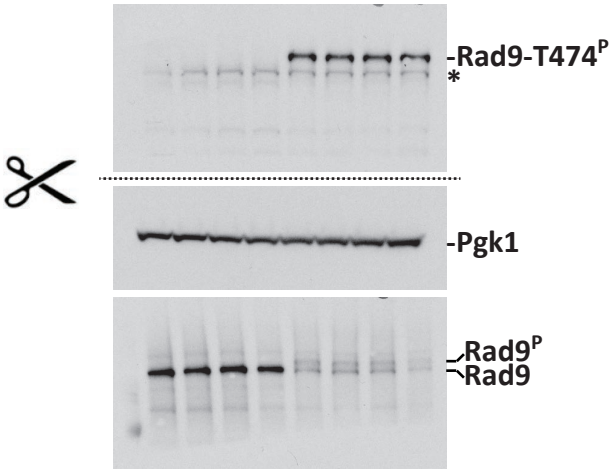

C. relates to Fig. 2C

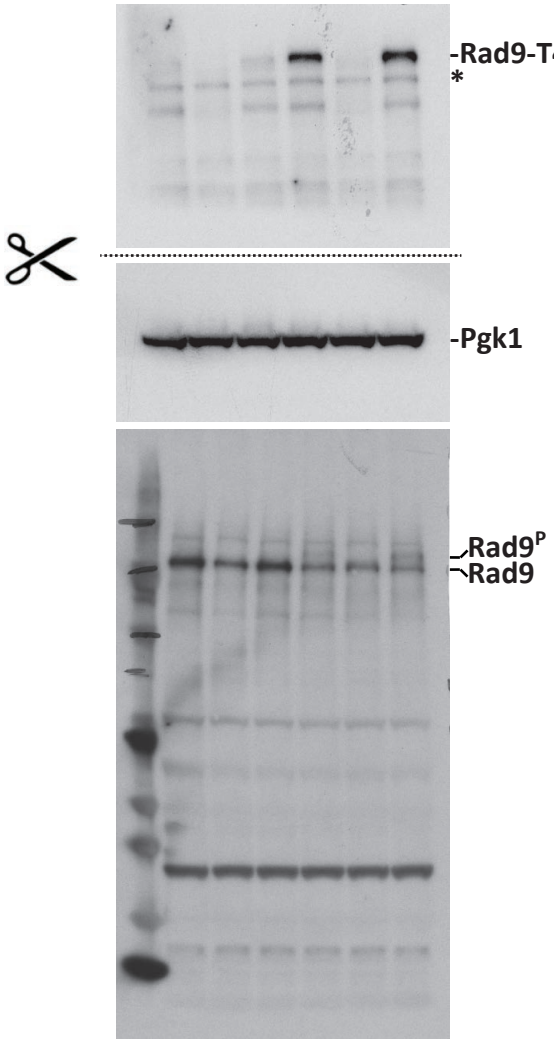

Figure S9

A. relates to Fig. S2D

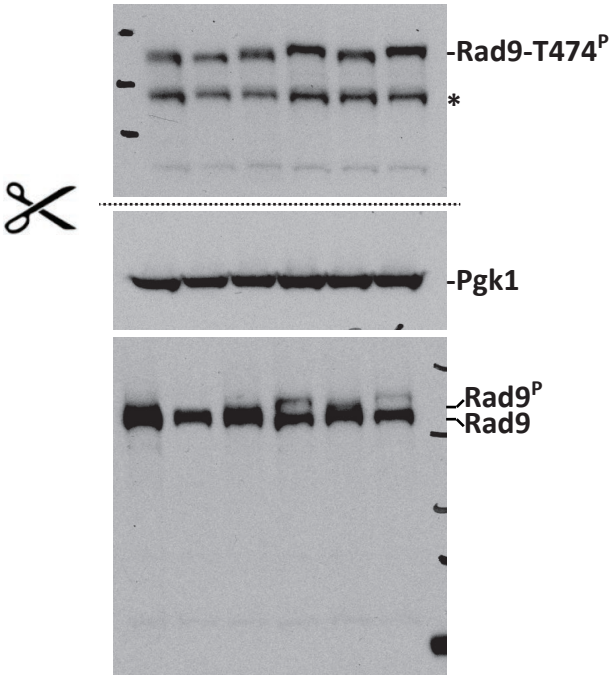

Figure S10

A. relates to Fig. 3B

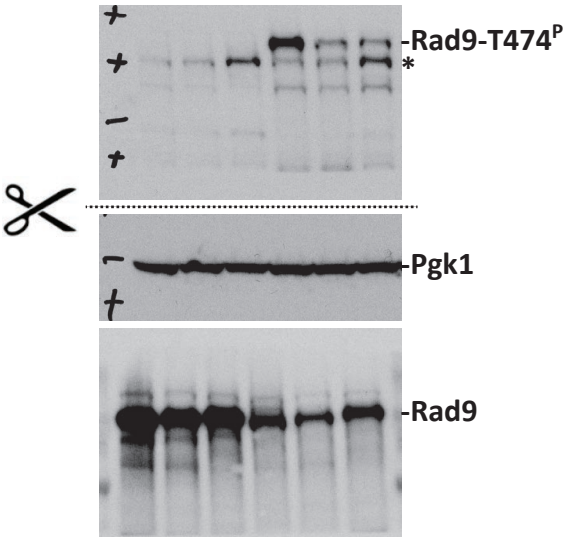

B. relates to Fig. 3C

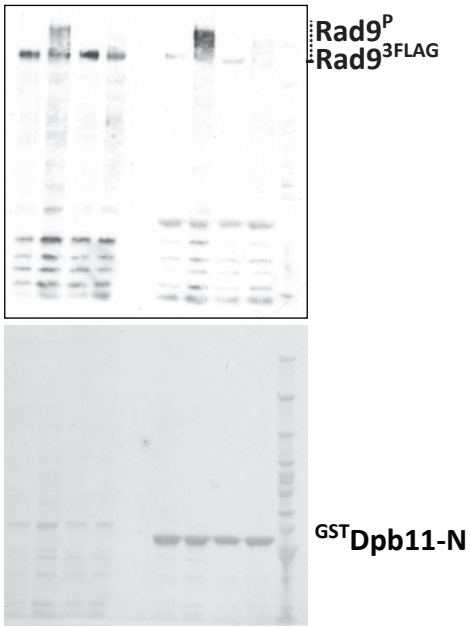

C. relates to Fig. 3D

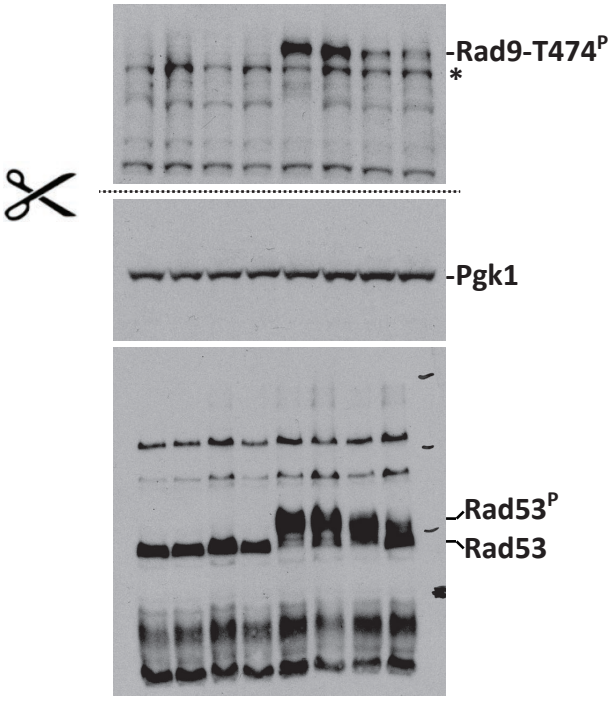

Figure S11

A. relates to Fig. S3B

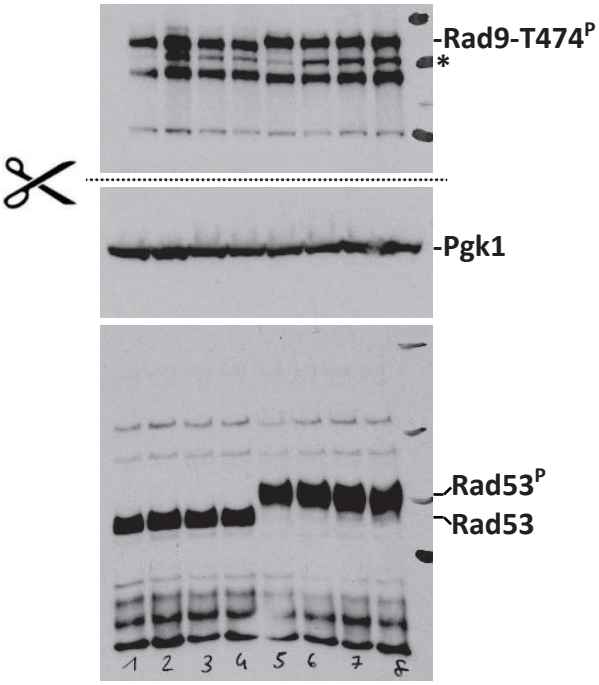

B. relates to Fig. S3C

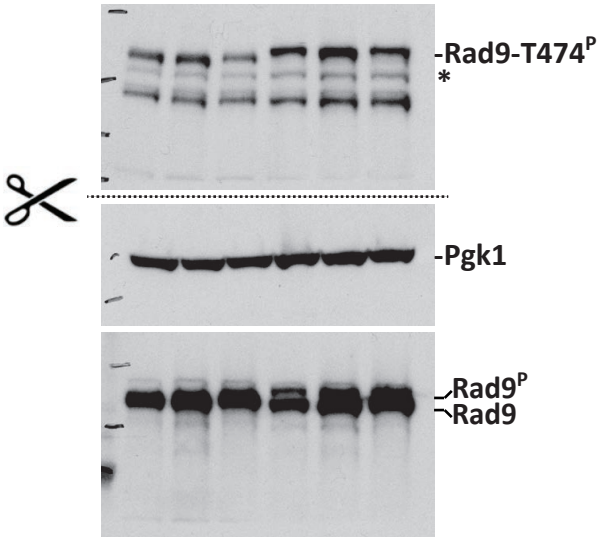

C. relates to Fig. S3D

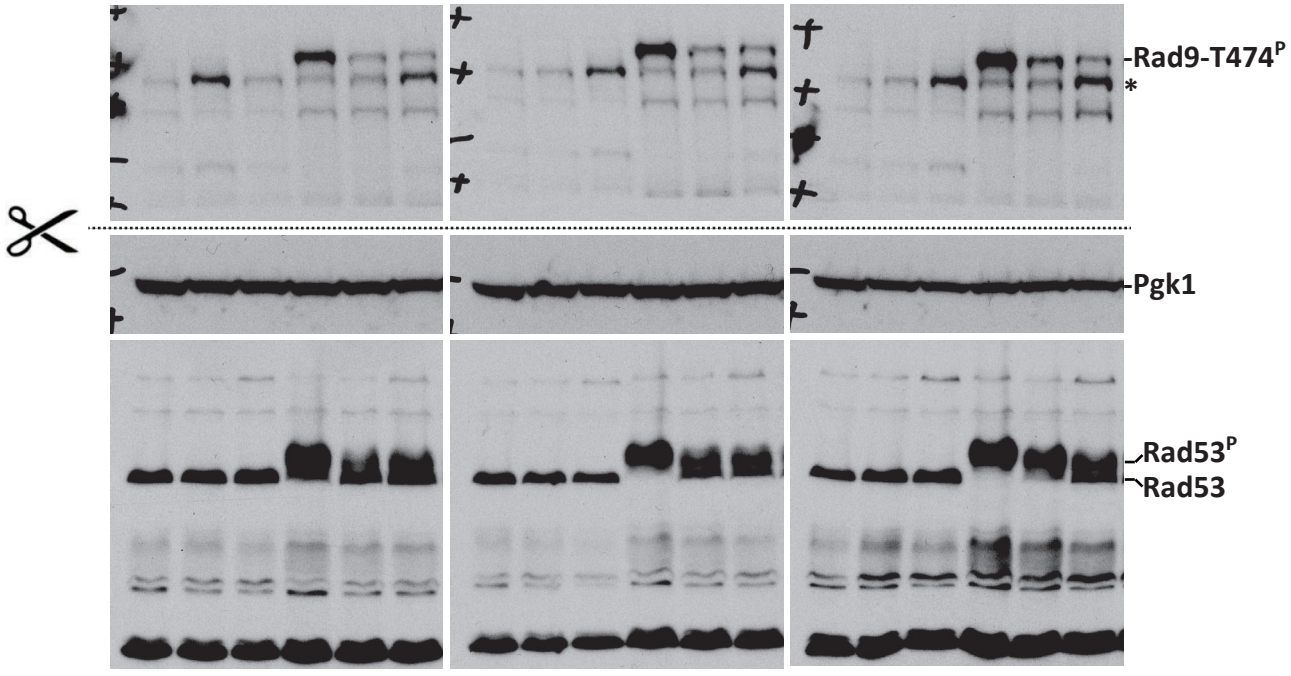

Figure S12

A. relates to Fig. 4B

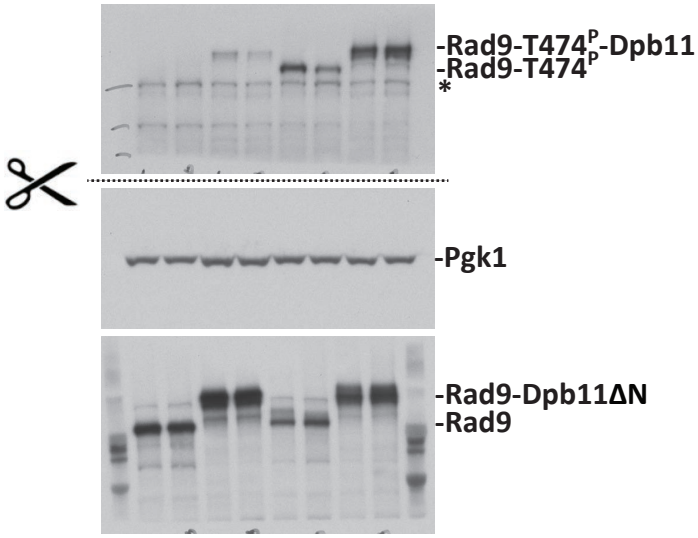

B. relates to Fig. 4C

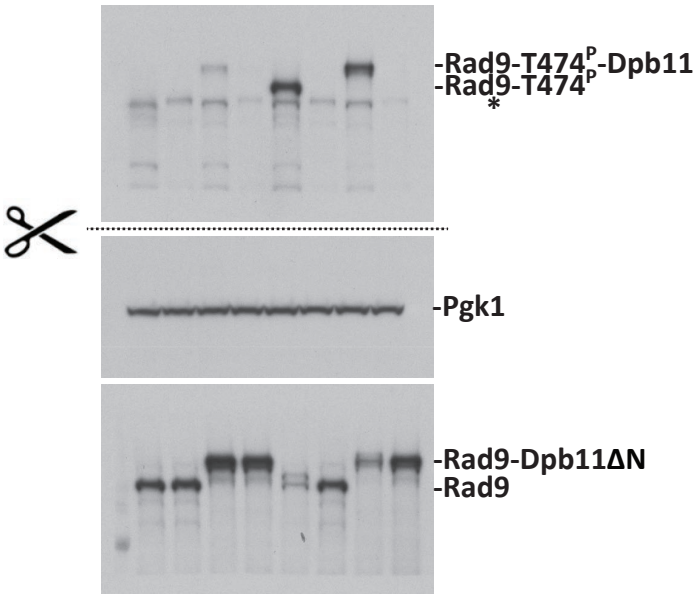

Figure S13

A. relates to Fig. S4D

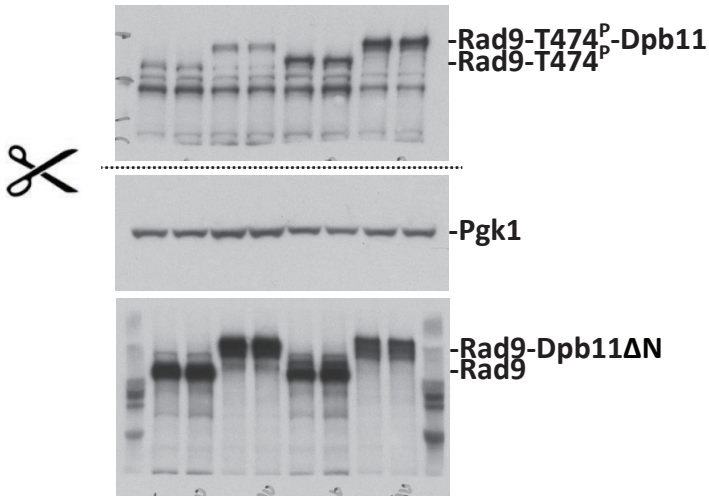

Figure S14

A. relates to Fig. 5C

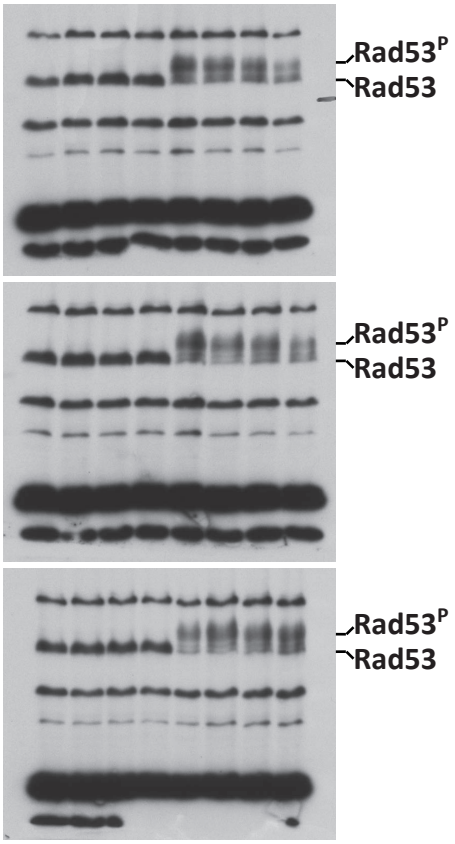

Figure S1:
Damage-induced interaction of Dpb11 and Rad9.
(A) Pulldown with recombinant GST-Dpb11 and extracts of asynchronous cells after MMS treatment shows damage-induced interaction of Rad9 and Dpb11.
(B) FACS-based DNA content measurement of experiment in Figure 1A.
(C) FACS-based DNA content measurement of experiment in Figure 1B.
(D) FACS-based DNA content measurement of experiment in Figure 1C.
(E) FACS-based DNA content measurement of experiment in Figure 1D.
(F) FACS-based DNA content measurement of experiment in Figure 1E.

Figure S2:
Involvement of checkpoint kinases in Rad9-T474 phosphorylation.
(A) FACS-based DNA content measurement of experiment in Figure 2A.
(B) FACS-based DNA content measurement of experiment in Figure 2B.
(C) FACS-based DNA content measurement of experiment in Figure 2C.
(D) Cell extracts of G2/M-arrested cells treated with phleomycin or mock-treated were probed with indicated antibodies. The Rad9-T474p phosphospecific antibody detects cell cycle-specific Rad9 phosphorylation in all mutant backgrounds. FACS-based DNA content measurement below.

Figure S3:
Involvement of Rad9-recruitment pathways in Rad9-T474 phosphorylation.
(A) FACS-based DNA content measurement of experiment in Figure 3A.
(B) *dot1Δ* cells retain S/TP phosphorylation of Rad9 in G2/M. Extracts from G2/M-arrested and phleomycin-treated cells of the indicated mutant background were probed with the indicated antibodies. FACS-based DNA content measurement below.
(C) A defect in the Rad9 TUDOR-domain (*rad9-Y798Q*) does not abolish Rad9 T474 phosphorylation S/TP phosphorylation in G2/M cells after DNA damage. Experiment as (B), FACS-based DNA content measurement below.
(D) *RAD9* mutant backgrounds impairing its recruitment to chromatin (*dot1Δ* and *rad9-Y798Q*) lead to defects in Rad9-T474 phosphorylation and Rad53 phosphorylation, when arrested in G1. Rad53 activation measured by detecting its phospho-shift on 10% SDS-gels using anti-rad53 antibodies. Right: FACS-based DNA content measurement.
(E) FACS-based DNA content measurement of experiment in Figure 3D.

Figure S4:
Influence of a Rad9-Dpb11 fusion on Rad9 function and phosphorylation.
(A) FACS-based DNA content measurement of experiment in Figure 4A.
(B) RPA ChIPs demonstrate inhibition of resection in the presence of the *RAD9-DPB11ΔN* fusion. RPA recruitment was measured at positions spanning 1.1 to 70 kb from an HO-induced DSB at the indicated time-points in G2/M arrested cells. Lower panel: DNA loss visualized by ChIP-DNA inputs (input DNA at each position relative to controls outside of the affected region). Right: FACS-based DNA content measurement.
(C) FACS-based DNA content measurement of experiment in Figure 4B.

(D) S/TP phosphorylation of Rad9 occurs in G2/M arrested cells independently of *RAD9-DPB11ΔN*. Extracts were probed with indicated phosphospecific antibodies. FACS-based DNA content measurement below.
(E) FACS-based DNA content measurement of experiment in Figure 4C.

Figure S5:
Phenotypic analysis of the *rad9-AA* mutant, deficient in binding to Dpb11.
(A) FACS-based DNA content measurement of experiment in Figure 5A.
(B) FACS-based DNA content measurement of experiment in Figure 5B.
(C) FACS-based DNA content measurement of experiment in Figure 5C.
(D) Dpb11 binding to DSBs in G1 as visualized by Dpb11-3FLAG ChIPs is abolished in *ddc1-T602* cells, but not in the *rad9-AA* cells. Dpb11 enrichment and spreading was measured starting from 1.1kb until 75kb away from an HO-induced DSB at the indicated time-points. FACS-based DNA content measurement below.

Figure S6:
(A) Original Western blots relating to Figure 1A
(B) Original Western blots relating to Figure 1B
(C) Original Western blots relating to Figure 1C
(D) Original Western blots relating to Figure 1D
(E) Original Western blots relating to Figure 1E

Figure S7:
(A) Original Western blots relating to Figure S1A

Figure S8:
(A) Original Western blots relating to Figure 2A
(B) Original Western blots relating to Figure 2B
(C) Original Western blots relating to Figure 2C

Figure S9:
(A) Original Western blots relating to Figure S2D

Figure S10:
(A) Original Western blots relating to Figure 3B
(B) Original Western blots relating to Figure 3C
(C) Original Western blots relating to Figure 3D

Figure S11:
(A) Original Western blots relating to Figure S3B
(B) Original Western blots relating to Figure S3C
(C) Original Western blots relating to Figure S3D

Figure S12:
(A) Original Western blots relating to Figure 4B
(B) Original Western blots relating to Figure 4C

Figure S13:
(A) Original Western blots relating to Figure S4D

Figure S14:
(A) Original Western blots relating to Figure 5C

Table 1:

strain	Relevant genotype	reference
W303	MATa leu2-3,112 trp1-1 can1-100 ura3-1 ade2-1 his3-11,15 [phi+]	Thomas and Rothstein, 1989
JPY923	MATa FLAG-rad53::LEU2 bar1 Δ::hisG cdc13-1 cdc15-2	Usui et al., 2008
JPY993	MATa FLAG-rad53::LEU2 bar1Δ::hisG cdc13-1 cdc15-2 rad9S1129A::URA3	Usui et al., 2008
JPY3344	MATa FLAG-rad53::LEU2 bar1Δ::hisG cdc13-1 cdc15-2 rad9-6AQ	Usui et al., 2008
YBP61	MATa RAD9-9myc::hphNT1	Pfander & Diffley, 2011
YBP109	MATa dot1Δ::kanMx4	Pfander & Diffley, 2011
YBP269	MATa ddc1-T602A::his3Mx6	Pfander & Diffley, 2011
YBP270	MATa ddc1-T602A::his3Mx6 dot1Δ::kanMx4	Pfander & Diffley, 2011
YBP366	MATa rad9Δ::natNT2 TRP1::RAD9-3FLAG::HISMx6 pep4::hphNT1	Pfander & Diffley, 2011
YBP388	MATa pep4Δ::LEU2	Pfander & Diffley, 2011
YBP390	MATa bar1Δ::TRP1	Pfander & Diffley, 2011
YBP403	MATa rad9Δ::natNT2 TRP1::rad9-3FLAG::HIS3Mx6 pep4Δ::LEU2 dot1 Δ::kanMx4	Pfander & Diffley, 2011
YBP406	MATa rad9Δ::NATNT2 TRP1::rad9AA-3FLAG::HIS3Mx6 pep4Δ::LEU2	Pfander & Diffley, 2011
YGD030	MATa rad9Δ::NATNT2 bar1Δ::HISMX6 trp1::RAD9-DPB11ΔN::TRP1	This study
YGD031	MATa RAD9-3FLAG::hphNT1 hml::pRS hmr::pRS bar1Δ::TRP1 pGal-HO::ADE3	This study
YGD032	rad9Δ::hphNT1 hml::pRS hmr::pRS bar1 Δ::TRP1 pGal-HO::ADE3	This study
YGD034	MATa rad9Δ::hphNT1 LEU2::RAD9AA-3FLAG hml::pRS hmr::pRS bar1::TRP1 pGal-HO::ADE3	This study
YGD035	MATa RAD9-3FLAG::hph dot1 Δ::kanMX4 hml::pRS hmr::pRS bar1Δ::TRP1 pGal-HO::ADE3	This study
YGD036	MATa rad9Δ::NATNT2 trp1-1::RAD9-DPB11ΔN::TRP1 mec1Δ::LEU2 tel1Δ::hphNT1 bar1Δ::HISMX6 sml1Δ::URA3	This study
YGD037	MATa trp1-1::RAD9-DPB11::TRP1 mec1Δ::LEU2 bar1Δ::HISMX6 rad9Δ::NATNT2 sml1Δ::URA3	This study
YGD038	MATa mec1Δ::LEU2 tel1Δ::NATNT2 bar1Δ::TRP1 sml1Δ::URA3	This study
YGD039	MATa rad53Δ::kanMX4 chk1Δ::NATNT2 bar1Δ::TRP1	This study
YGD040	MATa yku70::NAT rad9Δ::hphNT1 hml::pRS hmr::pRS bar1Δ::TRP1 pGal-HO::ADE3	This study

YGD041	MATa yku70::NATNT2 dot1Δ::kanMX4 hml::pRS hmr::pRS bar1Δ::TRP1 pGal-HO::ADE3	This study
YGD042	MATa RAD9-DPB11ΔN-3FLAG::hphNT1 hml::pRS hmr::pRS bar1Δ::TRP1 pGal-HO::ADE3	This study
YGD043	MATa RAD9-DPB11ΔN-3FLAG::hphNT1 dot1Δ::kanMX4 hml::pRS hmr::pRS bar1Δ::TRP1 pGal-HO::ADE3	This study
YGD044	MATa rad9Δ::hphNT1 leu2-3::Rad9AA-3FLAG::LEU2 yku70Δ::NATNT2 hml::pRS hmr::pRS bar1Δ::TRP1 pGal-HO::ADE3	This study
YGD045	MATa hml::pRS hmr::pRS bar1Δ::TRP1 pGal-HO::ade3 dpb11-3FLAG::kanMX4 rad9-AA::NATNT2	This study
YGD046	MATa hml::pRS hmr::pRS bar1Δ::TRP1 pGal-HO::ADE3 ddc1-T602A::hphNT1 DPB11-3FLAG::kanMX4 rad9-AA::NATNT2	This study
YKR112	MATa cdc28-F88G	Reusswig et al., 2016
YSB95	MATa mec1Δ::LEU2 bar1Δ::TRP1 sml1Δ::URA3	This study
YSB96	MATa rad53Δ::hphNT1 bar1Δ::TRP1 sml1Δ::URA3	This study
YSB97	MATa tel1Δ::NATNT2 bar1Δ::TRP1	This study
YSB98	MATa chk1Δ::NATNT2 bar1Δ::TRP1	This study
YSB189	MATa rad9Δ::NATNT2 pep4Δ::kanMX4 leu2-3::rad9-Y798Q-3FLAG::LEU2	This study
YSB517	MATa hml::pRS hmr::pRS bar1Δ::TRP1 pGal-HO::ADE3	Bantele et al. 2017
YSB812	MATa hml::pRS hmr::pRS bar1Δ::TRP1 pGal-HO::ADE3 dpb11-3FLAG::kanMX4	This study
YSB816	MATa hml::pRS hmr::pRS bar1Δ::TRP1 pGal-HO::ADE3 ddc1-T602A::hphNT1	This study

Table 2:

Antibody	**Antigen**	**Source**
Mouse anti-Pgk1	Pgk1	Invitrogen
Rabbit anti-Rad9	Rad9	F. Lowndes EMBO J. 1998
Rabbit anti-Rad9-S462P	Rad9 S462P peptide	Pfander, B. & J. Diffley EMBO J. 2010
Rabbit anti-Rad9-T474P	Rad9 T474P peptide	Pfander, B. & J. Diffley EMBO J. 2010
Rabbit anti-Rad53	Rad53	Abcam
Rabbit anti-RPA	Rfa1, Rfa2, Rfa3	Agrisera
Rabbit anti-FLAG	Synthetic FLAG sequence containing peptide DYKDDDDK-GC	Sigma
Mouse anti-myc	myc aa410-420	Millipore
Rabbit anti-GST-Dpb11	GST-Dpb11 555-C	Pfander, B. & J. Diffley EMBO J. 2010

A cell cycle-regulated Slx4–Dpb11 complex promotes the resolution of DNA repair intermediates linked to stalled replication

Dalia Gritenaite,[1,7] Lissa N. Princz,[1,7] Barnabas Szakal,[2] Susanne C.S. Bantele,[1] Lina Wendeler,[1] Sandra Schilbach,[1,6] Bianca H. Habermann,[3] Joao Matos,[4] Michael Lisby,[5] Dana Branzei,[2] and Boris Pfander[1,8]

[1]DNA Replication and Genome Integrity, Max-Planck Institute of Biochemistry, 82152 Martinsried, Germany; [2]Fondazione IFOM, Istituto FIRC di Oncologia Molecolare, 20139 Milan, Italy; [3]Computational Biology, Max-Planck Institute of Biochemistry, 82152 Martinsried, Germany; [4]Institute of Biochemistry, Eidgenössische Technische Hochschule Zürich, 8093 Zürich, Switzerland; [5]Department of Biology, University of Copenhagen, 2200 Copenhagen, Denmark

A key function of the cellular DNA damage response is to facilitate the bypass of replication fork-stalling DNA lesions. Template switch reactions allow such a bypass and involve the formation of DNA joint molecules (JMs) between sister chromatids. These JMs need to be resolved before cell division; however, the regulation of this process is only poorly understood. Here, we identify a regulatory mechanism in yeast that critically controls JM resolution by the Mus81–Mms4 endonuclease. Central to this regulation is a conserved complex comprising the scaffold proteins Dpb11 and Slx4 that is under stringent control. Cell cycle-dependent phosphorylation of Slx4 by Cdk1 promotes the Dpb11–Slx4 interaction, while in mitosis, phosphorylation of Mms4 by Polo-like kinase Cdc5 promotes the additional association of Mus81–Mms4 with the complex, thereby promoting JM resolution. Finally, the DNA damage checkpoint counteracts Mus81–Mms4 binding to the Dpb11–Slx4 complex. Thus, Dpb11–Slx4 integrates several cellular inputs and participates in the temporal program for activation of the JM-resolving nuclease Mus81.

[*Keywords*: DNA damage response; cell cycle; post-replicative repair; homologous recombination; joint molecule resolution]

Supplemental material is available for this article.

Received February 24, 2014; revised version accepted June 4, 2014.

Intrinsically and extrinsically induced DNA lesions can compromise the integrity of the genetic information and threaten cell viability. DNA lesions are particularly dangerous during S phase, when faithful DNA replication relies on two intact DNA strands. DNA lesions hamper the progression of replication forks and thereby the complete duplication of chromosomes. Moreover, replication forks that are stalled at DNA lesion sites can collapse and cause chromosome breaks and genome instability (Branzei and Foiani 2010).

Eukaryotes possess two fundamentally different mechanisms to bypass DNA lesions that affect one of the parental DNA strands: translesion synthesis (TLS) and template switching. TLS employs specialized polymerases (translesion polymerases) that in many cases are able to replicate the damaged strand but with a reduced fidelity (Prakash et al. 2005). On the other hand, during template switching, the genetic information is copied from the newly synthesized, undamaged sister chromatid. This mechanism is therefore error-free in principle, yet its precise mechanism remains poorly understood. Template switching is a complex process that can be initiated by different recombination-based mechanisms (homologous recombination [HR] and error-free post-replicative repair [PRR]) (Branzei et al. 2008). The choice between the different bypass mechanisms is regulated by ubiquitin and SUMO modifications

[6]Present address: Max-Planck Institute of Biophysical Chemistry, Molecular Biology, 37077 Göttingen, Germany.
[7]These authors contributed equally to this work.
[8]Corresponding author
E-mail bpfander@biochem.mpg.de
Article is online at http://www.genesdev.org/cgi/doi/10.1101/gad.240515.114.

of the replication protein PCNA at sites of stalled replication forks (Pfander et al. 2005).

Template switch mechanisms involve the formation of DNA joint molecules (JMs; also referred to as sister chromatid junctions [SCJs] or X molecules) as repair intermediates (Branzei et al. 2008). In order to allow completion of DNA replication and faithful chromosome segregation, these X-shaped DNA structures need to be disentangled before sister chromatids are separated during mitosis. To date, three enzymatic activities—the topoisomerase-containing Sgs1–Top3–Rmi1 complex (STR) as well as the Mus81–Mms4 and Yen1 structure-specific endonucleases—were shown to process JMs in budding yeast (Liberi et al. 2005; Blanco et al. 2010; Mankouri et al. 2011; Szakal and Branzei 2013). These three activities can be distinguished by their mechanism (termed dissolution for STR and resolution for Mus81–Mms4 and Yen1) (Gaillard et al. 2003; Ip et al. 2008; Cejka et al. 2010) but show a partial functional overlap. Moreover, they are differentially regulated during the cell cycle: Whereas the STR activity appears to be cell cycle-independent, the activity of Mus81–Mms4 is stimulated by CDK-mediated and Cdc5 (budding yeast Polo-like kinase)-mediated phosphorylation and peaks in mitosis (Matos et al. 2011, 2013; Gallo-Fernández et al. 2012; Szakal and Branzei 2013). Accordingly, the Mus81 regulation is assumed to create a hierarchy, with STR acting as a primary resolution pathway and Mus81–Mms4 acting as a salvage pathway. How Mus81–Mms4 phosphorylation by cell cycle kinases facilitates this temporal regulation of JM resolution pathways remains hardly understood.

The bypass of DNA lesions during replication is additionally regulated by the DNA damage checkpoint, the main cellular signaling pathway in response to DNA damage (Harrison and Haber 2006). As the primary purpose of the checkpoint is the stabilization of stalled replication forks (Branzei and Foiani 2010), its activation is a fundamental requirement for all fork repair and reactivation reactions. Notably, the checkpoint has been suggested to be involved in the choice of the JM resolution pathway, since precocious activation of the Mus81–Mms4 endonuclease is observed in checkpoint-deficient mutants (Szakal and Branzei 2013). However, it remains to be clarified how this second layer of regulation of JM resolution is achieved on a molecular level and how it is linked to cell cycle regulation.

Here, we identify an evolutionarily conserved protein complex comprising two scaffold proteins, Slx4 and Dpb11/TopBP1, as an important regulator of JM resolution by Mus81–Mms4. We show that the formation of the Slx4–Dpb11 complex is regulated by the cell cycle stage. An *slx4* mutant, compromised specifically in Dpb11 binding, exhibits hypersensitivity to the replication fork-stalling drug MMS, a delay in the resolution of X-shaped DNA JMs, and a reduced propensity to form crossovers (COs). The function of the Slx4–Dpb11 scaffold in JM resolution correlates with the finding that Dpb11 binds to the Mus81–Mms4 endonuclease. This association is restricted to mitosis, since it is dependent on the mitotic kinase Cdc5. Moreover, the checkpoint acts antagonistically to the regulation of JM resolution by Slx4 and Dpb11, as we found that partial inactivation of the DNA damage checkpoint can compensate for defects in formation of the Slx4–Dpb11 scaffold complex.

Results

An evolutionarily conserved and phosphorylation-dependent interaction between Slx4 and Dpb11/TopBP1

Dpb11 and its human homolog, TopBP1, are critical regulators of the cellular DNA damage response and interact with several DNA replication, repair, and checkpoint proteins (Garcia et al. 2005; Germann et al. 2011). In these protein complexes, Dpb11/TopBP1 specifically binds to phosphorylated proteins via its tandem BRCT domains (Yu 2003; Garcia et al. 2005). A key role of Dpb11/TopBP1 is to function as a scaffold, bringing together specific sets of proteins via several interaction surfaces. In budding yeast, two Dpb11 complexes have been described in detail, which regulate replication initiation (with Sld3 and Sld2) (Tanaka et al. 2007; Zegerman and Diffley 2007) and the DNA damage checkpoint (with Rad9, the 9-1-1 complex, and Mec1–Ddc2) (Mordes et al. 2008; Navadgi-Patil and Burgers 2008; Puddu et al. 2008; Pfander and Diffley 2011), respectively (Fig. 1A). Recently, a third Dpb11 complex with Slx4 and Rtt107 was identified (Ohouo et al. 2010, 2012). In this latter complex, Slx4 appears to inhibit the formation of the Dpb11 DNA damage checkpoint complex (Ohouo et al. 2012).

In the course of our studies of Dpb11 function, we identified an interaction between a Dpb11 fragment that includes the tandem BRCT repeats 3 and 4 (BRCT3+4) and Slx4 using a two-hybrid screen. To confirm this finding, we tested the binding of different Dpb11 constructs to Slx4 and known Dpb11 binders. As observed before (Puddu et al. 2008; Pfander and Diffley 2011), we found that Rad9 binds to BRCT1+2 of Dpb11, whereas Ddc1 binds to BRCT3+4 (Fig. 1B). For Slx4, we found an interaction with full-length Dpb11 and the BRCT3+4 fragment but not with the BRCT1+2 domain (Fig. 1B). When we tested binding of Slx4 from cell extracts to recombinant, purified fragments of Dpb11, Slx4 also bound to BRCT3+4, albeit weaker than to the full-length protein (Supplemental Fig. S1A). Moreover, ablation of Dpb11 Thr451, which is predicted to be part of the BRCT3+4 phospho-protein-binding surface (Rappas et al. 2011), partially inhibited the Slx4–Dpb11 interaction (Supplemental Fig. S1B). A recent report suggested that the Dpb11 BRCT1+2 domain is involved in Slx4 binding (Ohouo et al. 2012). However, although our data do not rule out a contribution of BRCT1+2 in overall binding, our two independent lines of evidence clearly demonstrate that BRCT3+4 of Dpb11 significantly contributes to Slx4 binding.

Next, we mapped the Dpb11-binding site on Slx4 starting from a fragment (amino acids 461–738) that was common to all Slx4 clones identified in our initial Dpb11 two-hybrid screen. Truncated variants that begin at amino acid 490 failed to interact with Dpb11 (Supplemental Fig. S1C),

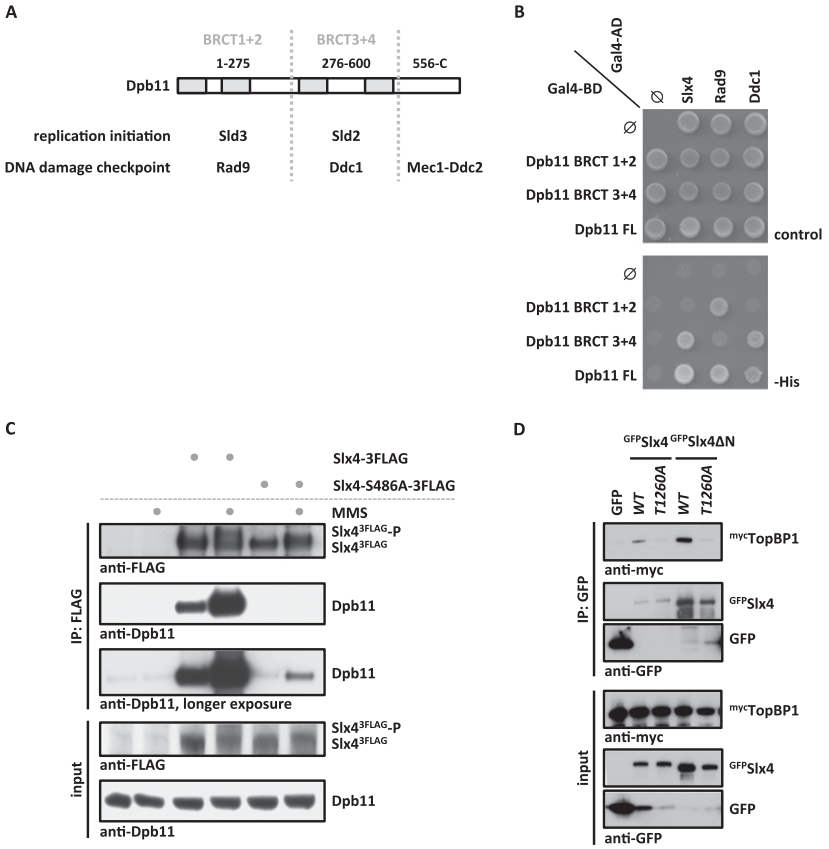

Figure 1. An evolutionarily conserved, phosphorylation-dependent interaction between Slx4 and Dpb11/TopBP1. (*A*) Schematic diagram of Dpb11 domain structure depicted with its interaction partners in replication initiation and DNA damage checkpoint. (*B*) Slx4 binds to the BRCT3+4 domain of Dpb11. Two-hybrid analysis of GAL4-BD fused to full-length Dpb11 or to BRCT1+2 and BRCT3+4 fragments and of GAL4-AD fusions with Slx4, Rad9, and Ddc1. (*C*) The Slx4–Dpb11 interaction is reduced by mutation of Slx4 Ser486 and is regulated by DNA damage. Coimmunoprecipitation of endogenous Dpb11 with Slx4^{3Flag} or phosphorylation-deficient Slx4-S486A^{3Flag} from undamaged cells or cells treated for 30 min with 0.033% MMS. (*D*) Human TopBP1 and Slx4 interact dependent on Thr1260 of Slx4. Coimmunoprecipitation of human ^{myc}TopBP1 with ^{GFP}Slx4 or N-terminally truncated ^{GFP}Slx4ΔN after transient overexpression in HEK293T cells. Slx4 or Slx4ΔN was expressed either as wild type (WT) or a T1260A phosphorylation-deficient variant.

indicating that the region between amino acid 461 and amino acid 490 is important for Dpb11 interaction. As several examples indicate that Dpb11 binds phosphorylated S/TP motifs, we tested all S/TP motifs within the C-terminal part of Slx4 for their ability to mediate Dpb11 binding. Indeed, we found that alteration of Ser486 in Slx4 into a nonphosphorylatable alanine residue (*slx4-S486A* mutant) reduced Dpb11 binding in a two-hybrid system (Supplemental Fig. S1D). Moreover, whereas immunoprecipitation of wild-type Slx4 efficiently copurified endogenous Dpb11 from cell extracts, in particular following MMS treatment, the Slx4–Dpb11 interaction was strongly decreased in extracts from cells expressing the *slx4-S486A* mutant, even after induction of DNA damage (Fig. 1C; see also Ohouo et al. 2012). Furthermore, the phospho-S486-containing peptide was specifically enriched (17-fold), when Dpb11 immunoprecipitations were analyzed by quantitative mass spectrometry (MS) (Supplemental Fig. S4A). We therefore conclude that the Slx4–Dpb11 interaction involves the BRCT3+4 region of Dpb11 and a region of Slx4 harboring the phosphorylated residue S486.

We further tested whether also the human homologs TopBP1 and Slx4 are binding partners. Indeed, we detected a specific interaction of TopBP1 and Slx4 or an N-terminally truncated version of Slx4 after transient transfection in human embryonic kidney (HEK) 293T cells (Fig. 1D). In contrast to the yeast proteins, we did not observe a stimulation of TopBP1 binding to Slx4 by DNA damage (Supplemental Fig. S1E). Human Slx4 is substantially larger than yeast Slx4, with an overall sequence conservation of only 17.9%. Nonetheless, we identified a conserved short linear motif present in Slx4 proteins from different eukaryotes that comprises Ser486 in budding yeast and Thr1260 in humans (Supplemental Fig. S2). Mutation of Thr1260 to a nonphosphorylatable alanine (T1260A) in human Slx4 reduced the interaction with TopBP1 (Fig. 1D), suggesting that this residue may function analogously to Ser486 in budding yeast. These data suggest the presence of a novel, evolutionarily conserved motif in Slx4 that functions in Dpb11/TopBP1 binding.

Cdk1-dependent phosphorylation of Slx4 regulates binding to Dpb11

In order to unravel the regulation of the Slx4–Dpb11-binding surface, we quantified the relative amount of Ser486 phosphorylation under different cellular conditions using SILAC-based quantitative MS. We observed a specific increase of Ser486 phosphorylation in G2/M-arrested cells compared with G1-arrested cells, indicating that the analyzed Slx4 phosphorylation is cell cycle-regulated (Fig. 2A). In agreement with Ser486 matching the consensus target sequence for phosphorylation by cyclin-dependent kinase Cdk1 (S/TPxK) (Holt et al. 2009), we observed a marked reduction of Ser486 phosphorylation in G2/M-arrested cells when Cdk1 activity was abrogated using the *cdc28-as1* allele (Bishop et al. 2000) in combination with 1NM-PP1 inhibitor treatment (Fig. 2B). Notably, we also detected

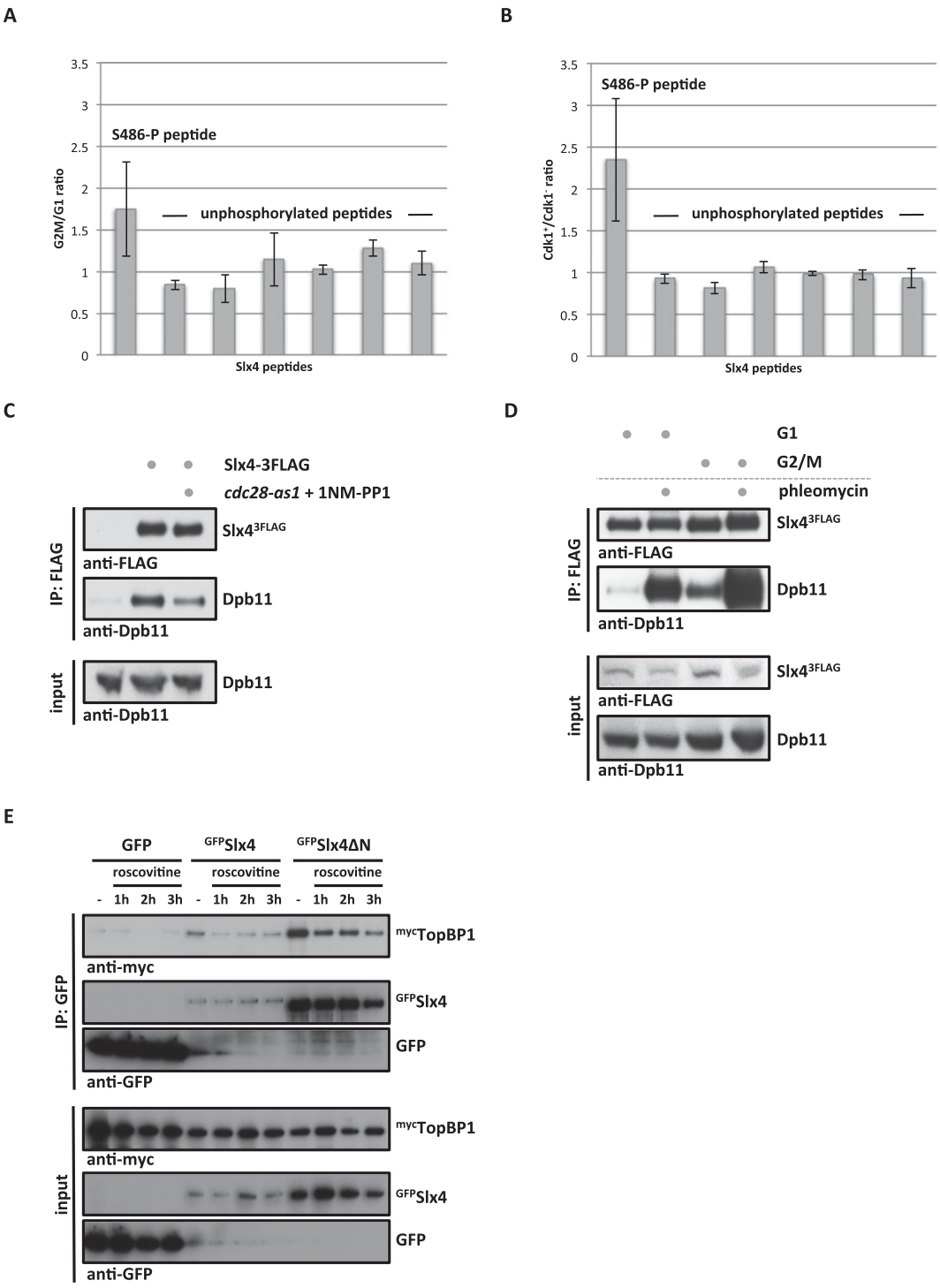

Figure 2. The Slx4–Dpb11/TopBP1-binding interface is cell cycle-regulated by Cdk1 phosphorylation of Slx4. (*A*) Ser486 phosphorylation is cell cycle-regulated. Relative abundance of the Slx4 480–489 phospho-peptide and six unmodified Slx4 peptides was measured by SILAC-based quantitative MS using $^{15}N_2{}^{13}C_6$ lysine (Lys8) and compared between Slx4 isolated from G1- and G2/M-arrested cells. H/L ratios for individual peptides were normalized to total Slx4 ratios. Error bars represent standard deviations from two independent experiments, including label switch. (*B*) S486 phosphorylation depends on Cdk1. Analysis as in *A* but comparing Slx4 from G2/M-arrested cells with normal Cdk1 activity with cells in which Cdk1 has been inactivated using the *cdc28-as1* allele and 500 nM 1NM-PP1. (*C*) The Slx4–Dpb11 interaction is regulated by CDK. Coimmunoprecipitation of Dpb11 and Slx4^{3Flag} from G2/M-arrested cells or G2/M-arrested cells in which Cdk1 has been inactivated as in *B*. (*D*) The Slx4–Dpb11 interaction is regulated by cell cycle phase and DNA damage. Experiment as in *C* but with G1- and G2/M-arrested cells, which were either damaged by 50 μg/mL phleomycin or left untreated. (*E*) Binding of human Slx4 and TopBP1 is regulated by CDK phosphorylation. Coimmunoprecipitation of ^{myc}TopBP1 with ^{GFP}Slx4 and ^{GFP}Slx4ΔN after transient overexpression in HEK293T cells. Cells were left untreated or treated with 10 μg/mL roscovitine for the indicated times to inhibit CDK activity.

reduced Slx4 binding to Dpb11 when Cdk1 was inhibited (Fig. 2C).

In addition to cell cycle-dependent regulation, we also observed a stimulation of Slx4–Dpb11 binding by DNA damage (Figs. 1C, 2D, Supplemental Fig. S1F). When Slx4 binding to recombinant GST-Dpb11 was tested, the DNA damage-dependent stimulation was less pronounced (Supplemental Fig. S1A), substantiating the notion that the Slx4–Dpb11 interaction may be additionally regulated by a damage-induced post-translational modification of Dpb11. On the other hand, Slx4 harbors several sites that can be targeted by kinases of the DNA damage checkpoint pathway. Mutation of seven sites in Slx4 partially inhibits its binding to Dpb11 (Ohouo et al. 2010), and the corresponding mutant shows phenotypes similar to those of *slx4-S486A* (Supplemental Fig. S3). As we cannot fully exclude pleiotropic defects for this mutant, we focused our analysis on *slx4-S486A*.

Taken together, our findings suggest that the Slx4–Dpb11 complex integrates at least two cellular signals: (1) cell cycle state through Cdk1 phosphorylation of Slx4 at Ser486 and (2) the presence of DNA damage through checkpoint kinase phosphorylation of several sites on Slx4 and perhaps on Dpb11.

Interestingly, the CDK regulation of this interaction is conserved between yeast and humans, since addition of the CDK inhibitor roscovitine reduced binding of Slx4 and TopBP1 (Fig. 2E).

The Slx4–Dpb11 complex is required for the response to replication fork stalling

Budding yeast Slx4 is known to bind to several DNA repair proteins (Slx1, Rtt107, and Rad1–Rad10) (Mullen et al. 2001; Roberts et al. 2006; Flott et al. 2007; Ohouo et al. 2010). However, whether these interaction partners are part of only one or several distinct complexes is unknown. While Slx4 has several independent DNA repair functions in budding yeast (Flott et al. 2007), until now, a detailed phenotypic characterization has only been conducted for *slx4Δ* deletion mutants. To test the specificity of the Dpb11-binding-deficient *slx4-S486A* phosphorylation site mutant, we compared its binding partners with those of wild-type Slx4 using quantitative proteomics. Indeed, we found that the mutant protein (Slx4-S486A^{3Flag}) displayed eightfold reduced binding to Dpb11 (Fig. 3A). This variant still bound Slx1 and Rtt107 as efficiently as wild-type Slx4, indicating that Ser486 phosphorylation is specifically relevant for the Dpb11 interaction (Fig. 3A; see Supplemental Fig. S4A for specific Slx4 interactors). We thus took advantage of the *slx4-S486A* separation-of-function mutant to reveal a specific role of the Slx4–Dpb11 complex.

Using different DNA-damaging agents, we observed that the *slx4-S486A* mutant is particularly sensitive to MMS and, to a lesser extent, 4-NQO (Fig. 3B; Supplemental Fig. S4B), two reagents that create toxicity through replication fork stalling. Notably, the mutant was not sensitive to reagents that generate DNA strand breaks or interstrand cross-links, consistent with a recombination rate that was similar to wild type (Supplemental Fig. S4B,C). Remarkably, expression of a fusion protein of the phospho-site mutant variant of Slx4 with Dpb11 (Dpb11–Slx4-S486A) rescued the MMS hypersensitivity phenotype almost to wild-type levels (Fig. 3B), suggesting that binding of Slx4 to Dpb11 is crucial for tolerance of replication fork-stalling lesions.

Next, we tested whether the response to stalled replication forks is aberrant in the *slx4-S486A* mutant. To this end, we treated synchronized cells with a pulse of MMS in early S phase. Under these conditions, the *slx4-S486A* mutant completed DNA replication with slightly slower kinetics compared with wild-type cells (Fig. 3C, 1-h time point). Also, the appearance of fully replicated and repaired chromosomes, as visualized by pulsed-field gel electrophoresis, was delayed (Fig. 3D, 1-h time point). This finding indicates that stalled replication fork structures or repair intermediates persist longer in the absence of the Slx4–Dpb11 complex. Additionally, the DNA damage checkpoint activation was prolonged in *slx4-S486A* cells (Fig. 3E), as determined by the phosphorylation status of the checkpoint kinase Rad53. This effect was specific for MMS treatment and could not be observed in cells in which double-strand breaks were induced by zeocin or phleomycin inside or outside of S phase (Supplemental Fig. S4D).

Defects in a checkpoint-antagonistic pathway (checkpoint "dampening") (Ohouo et al. 2012) in *slx4* mutants could, in principle, lead to prolonged checkpoint activation and could thereby indirectly lead to slow S-phase kinetics and DNA damage hypersensitivity. Alternatively, persistence of unrepaired DNA lesions or DNA repair intermediates could lead to very similar phenotypes. In order to discriminate between the two possibilities, we examined the DNA damage levels during recovery from an MMS pulse in wild-type and *slx4-S486A* cells. To this end, we investigated the appearance and disappearance of nuclear foci formed by the ssDNA-binding protein RPA after MMS treatment in S phase. Indeed, *slx4-S486A* cells contained more RPA foci, which persisted longer than in wild-type cells (Fig. 3F). Therefore, we conclude that unrepaired DNA lesions or DNA repair intermediates that contain ssDNA persist in *slx4-S486A* mutants. This finding does not necessarily exclude a role of Slx4 as a regulator of the DNA damage checkpoint yet strongly suggests an additional direct function of the Slx4–Dpb11 complex in the repair of replication fork structures.

The Slx4–Dpb11 complex promotes Mus81–Mms4-dependent JM resolution

As our findings pointed to a function of the Slx4–Dpb11 complex in the response and repair of MMS-induced lesions, we next investigated whether the complex is involved in the DNA damage bypass. Therefore, we tested possible functions in HR and error-prone or error-free PRR. From several lines of genetic evidence, we conclude that the Slx4–Dpb11 complex is not exclusively involved in either PRR or HR (Supplemental Fig. S5). First, the *slx4-S486A* mutation enhanced the MMS hypersensitivity of mutants defective in error-free PRR (double mutant with either *mms2Δ*, *rad5-KT538,539AA*,

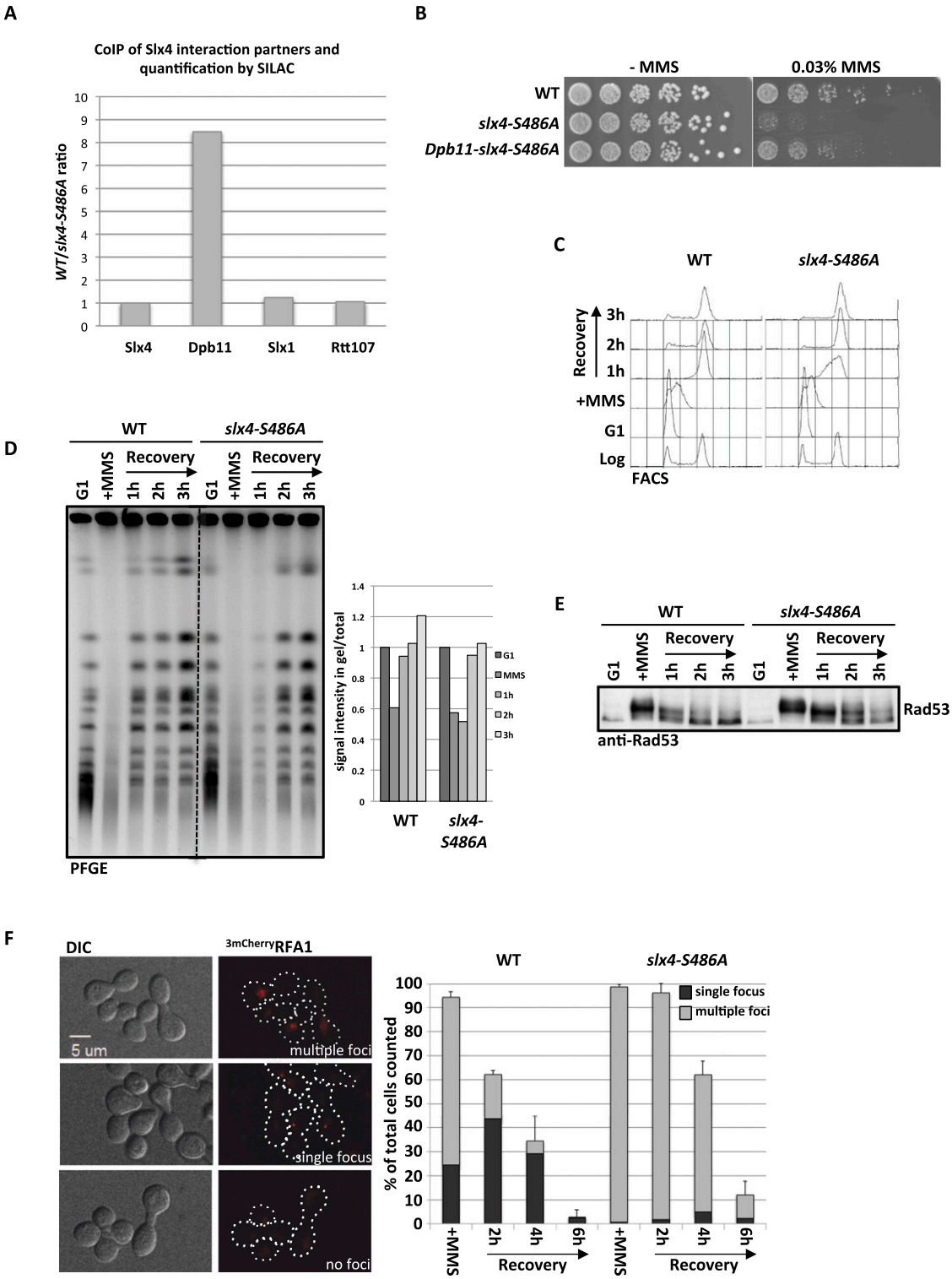

Figure 3. Mutation of *slx4-S486A* results in a specific defect in binding to Dpb11 and the response to stalled replication forks. (*A*) The *slx4-S486A* mutant leads to a specific defect in binding to Dpb11. Relative enrichment of Slx4 interactors (see Supplemental Fig. S4A) found in purifications of wild-type (WT) $Slx4^{3Flag}$ versus $Slx4\text{-}S486A^{3Flag}$ as determined by SILAC-based quantitative MS. Values >1 indicate a reduced binding to the Slx4-S486A relative to wild-type Slx4. (*B*) The *slx4-S486A* mutant, but not a *Dpb11–slx4-S486A*-fusion, is hypersensitive to MMS. Wild type or strains expressing *slx4-S486A* or the *Dpb11–slx4-S486A*-fusion from the *SLX4* promoter as only a copy of *SLX4* were spotted in fivefold serial dilutions on MMS-containing medium and assayed for growth after 2 d. (*C*,*D*) Replication fork stalling is prolonged in the *slx4-S486A* mutant. Cells were treated with a pulse of MMS during S phase, and recovery was analyzed by FACS (*C*; to measure cellular DNA content) and pulsed-field gel electrophoresis (*D*; to measure intact, fully replicated chromosomes). (*D*) For quantification, the fluorescence signal of chromosomes that migrated into the gel was divided by the total signal, including the pocket, and all signals were normalized to the G1 sample from each strain. (*E*) The DNA damage checkpoint is inactivated with reduced kinetics in the *slx4-S486A* mutant. Cells were treated as in *C*, and checkpoint activity was determined by anti-Rad53 Western blot. (*F*) The *slx4-S486A* mutant shows increased DNA damage foci and delayed recovery after transient MMS treatment in S phase. DNA damage sites were visualized by the ssDNA-binding $RFA1^{3mCherry}$ after transient MMS treatment during S phase. Cells were sorted into three categories: multiple, dispersed RFA1 foci; one RFA1 focus; and no RFA1 foci. Values are from two independent experiments, counting 100–150 cells per strain and time point. Error bars represent standard deviations.

or *rad5-C914S*), error-prone PRR (double mutant with either *rev1Δ*, *rev3Δ*, or *rad30Δ*), or HR (double mutant with *rad51Δ*) (Supplemental Fig. S5A). Second, spontaneous mutagenesis, a hallmark of error-prone PRR, was not significantly altered in *slx4-S486A* mutants (Supplemental Fig. S5B). Third, recombination rates, as determined by a direct repeat recombination assay, were similar between wild-type and *slx4-S486A* strains (Supplemental Fig. S4C). Fourth, *siz1Δ* or *srs2ΔC* mutations, which cause an upregulation of HR at stalled replication forks (Pfander et al. 2005), did not alleviate the MMS hypersensitivity of *slx4-S486A* mutants (Supplemental Fig. S5C).

The nonepistatic relationship of the *slx4-S486A* mutant to PRR or HR pathways could be explained if Slx4 and Dpb11 participated in a step common to both error-free PRR and HR because, in such a scenario, both pathways would be affected by the *slx4-S486A* mutation. Both HR and error-free PRR operate via template switching in order to bypass the replication fork-stalling lesion by copying the undamaged information from the sister chromatid. A critical step in template switching is the final removal of X-shaped DNA intermediates (JMs) that link the two sister chromatids (Mankouri et al. 2013). JM removal pathways act, in principle, independently of the pathway by which JMs have been created (Branzei et al. 2008; for *mus81Δ* phenotypes, see Interthal and Heyer 2000; Li and Brill 2005). To test whether the Slx4–Dpb11 complex is involved in this late step, we visualized these DNA intermediates in an *sgs1Δ* mutant (deficient in JM dissolution) by two-dimensional (2D) gel electrophoresis (Liberi et al. 2005; Mankouri et al. 2011). In this mutant, MMS treatment in S phase leads to enhanced levels of JMs, which subsequently disappear during late S, G2, and M phase (Szakal and Branzei 2013). The additional mutation of *slx4-S486A* in the *sgs1Δ* background does not alter the formation of JMs, indicating that the Slx4–Dpb11 complex is not required at early steps (Supplemental Fig. S6A). Interestingly, however, during the recovery from the MMS treatment, JMs are more slowly resolved in the *sgs1Δ slx4-S486A* double mutant compared with the *sgs1Δ* single mutant (Fig. 4A). A similar effect can be observed using an *slx4Δ* mutant and conditionally inactivated *SGS1* in the same experimental setup (Supplemental Fig. S6B). Consistently, we observed an enhanced MMS sensitivity for the *sgs1Δ slx4-S486A* double mutant compared with the respective single mutants (Fig. 4B). From these experiments, we conclude that the Slx4–Dpb11 complex is involved in the resolution of JMs that are supposedly intermediates arising from a template switch reaction and that this complex functions in a pathway parallel to dissolution by the STR complex.

To elucidate a potential role of the Slx4–Dpb11 complex in a resolution mechanism, we investigated the genetic interaction with Mus81–Mms4. Indeed, the MMS sensitivities of *slx4-S486A mms4Δ* or *slx4-S486A mus81Δ* double mutants were identical to those of *mms4Δ* or *mus81Δ* single mutants (Fig. 4C). This suggests that the Slx4–Dpb11 complex acts in the Mus81–Mms4 pathway. The same epistatic relationship was seen between *mms4Δ* and *slx4-S486A* when we investigated JM resolution by 2D gel electrophoresis when the STR complex was inactivated using the *Tc-sgs1* allele (Supplemental Fig. S6C). We note that the MMS hypersensitivity and the JM resolution defect of the *slx4-S486A* mutant are less pronounced compared with the deletion mutants that fully abolish Mus81 function (Fig. 4C; Supplemental Fig. S6C), suggesting that not all functions of the Mus81–Mms4 endonuclease depend on the Slx4–Dpb11 complex.

We also tested the involvement of other structure-specific endonucleases (Slx1, Rad1–Rad10, and Yen1) (Tomkinson et al. 1993; Fricke and Brill 2003; Coulon 2006; Ip et al. 2008), specifically of Slx1, as it associates with the Slx4–Dpb11 complex (Supplemental Fig. S4A). We found that *rad1Δ* showed an additive phenotype with *slx4-S486A*, while *slx1Δ* and *yen1Δ* mutants were not hypersensitive to MMS (Supplemental Fig. S6D; Fricke and Brill 2003; Coulon 2006; Blanco et al. 2010). We therefore conclude that these factors either are not involved in the resolution of template switch intermediates by Mus81 and the Slx4–Dpb11 complex or (in case of Slx1 and Yen1) have a function that can be taken over by a redundant pathway in the respective deletion mutant. Interestingly, the *yen1Δ* mutation caused an increase of MMS sensitivity specifically of the *sgs1Δ slx4-S486A* double mutant (Supplemental Fig. S6E), suggesting that Yen1 function becomes specifically important if the STR complex is inactive and function of the Slx4–Dpb11 complex is reduced.

The balance between STR-dependent JM dissolution and Mus81-dependent JM resolution is reflected in the ratio of CO to non-CO (NCO) products (Ira et al. 2003; Ho et al. 2010; Mankouri et al. 2013), since STR-mediated dissolution will not yield COs, while Mus81-mediated resolution can generate CO products. We therefore analyzed the rates of CO formation in the *slx4-S486A* mutant with a recombination assay using interchromosomal *arg4* heteroalleles (Robert et al. 2006; Szakal and Branzei 2013). Despite a slight increase in overall recombination rates, we measured a reduction in CO rates in the *slx4-S486A* mutant compared with wild-type cells (Fig. 4D). We therefore conclude that the Slx4–Dpb11 complex is an important regulator of JM removal pathways and that it acts by stimulating JM resolution, inhibiting JM dissolution, or both.

Persistent JMs interfere with the separation of sister chromatids in mitosis. Under circumstances in which JMs are not resolved before anaphase, these repair intermediates are thought to give rise to anaphase bridges between the dividing DNA masses (Chan et al. 2007; Mankouri et al. 2013). Consistent with a role in the resolution of JMs, Dpb11 localizes to DNA bridges between the separated chromosome masses in anaphase (Germann et al. 2014). Dpb11-containing anaphase bridges can be observed with a low frequency in undamaged cells (<5%) and are induced upon MMS treatment, suggesting that they arise from replication fork stalling (Germann et al. 2014). Interestingly, the occurrence of Dpb11 bridges is increased in *sgs1Δ* cells (Germann et al. 2014), indicating that the localization of Dpb11 to chromatin bridges reflects its action in a resolution mechanism. We observed a pro-

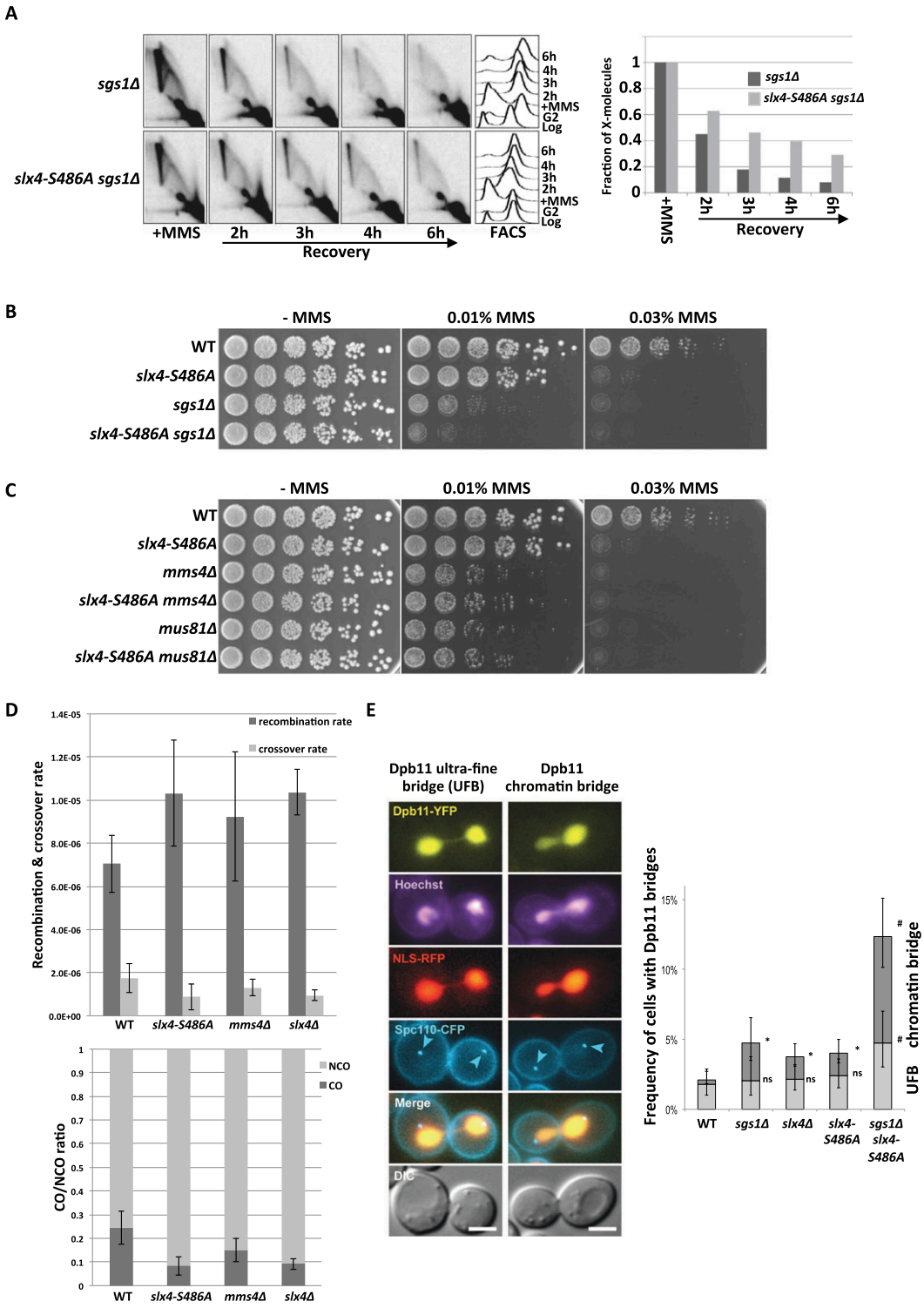

Figure 4. The Dpb11 binding-deficient *slx4-S486A* mutant causes defects in the Mus81–Mms4-dependent JM resolution. (*A*) JM structures are resolved slower in *sgs1Δ slx4-S486A* cells. X-shaped JMs were visualized as spike signal in 2D gels in *sgs1Δ* and *sgs1Δ slx4-S486A* cells that have been treated with a pulse of MMS in S phase. (*B*) MMS sensitivity is enhanced in the *sgs1Δ slx4-S486A* double mutant compared with each single mutant. Analysis of the MMS hypersensitivity phenotype as in Figure 3B. (*C*) The MMS hypersensitivity of *mms4Δ* and *mus81Δ* mutants is not further enhanced by an additional *slx4-S486A* mutation. Experiment as in *B*. (*D*) The *slx4-S486A* mutation leads to a reduced CO formation. COs and NCOs from an interchromosomal recombination assay using *arg4* heteroalleles on chromosome V and VIII (Robert et al. 2006) were determined using a PCR-based strategy. (*Top* panel) Recombination and CO rates were determined by fluctuation analysis using a maximum likelihood approach. (*Bottom* panel) CO ratio is quotient of CO rate and overall recombination rate. Error bars represent standard deviations of two to 11 independent experiments. (*E*) Dpb11 anaphase bridge structures occur more frequently when JM dissolution and the Dpb11–Slx4 interaction are defective. (*Right* panel) Quantification of Dpb11 ultrafine bridges (UFBs) or chromatin bridges in wild-type (WT), *sgs1Δ*, *slx4Δ*, *slx4-S486A*, and *slx4-S486A sgs1Δ* strains. Cells express Dpb11-YFP, NLS-RFP as a marker of the nucleoplasm and Spc110-CFP as a marker of the spindle pole body. DNA is stained with Hoechst. (*Left* panel) Images of representative anaphase cells are shown. Bar, 3 μm. Error bars indicate 95% confidence intervals. Significance is as follows: (*) $P < 0.01$ (compared with wild type); (#) $P < 0.01$ (compared with the single mutants); (ns) not significantly different from wild type.

nounced increase of cells containing Dpb11 bridges when the *sgs1Δ* and *slx4-S486A* mutants were combined (Fig. 4E). The genetic requirements for Dpb11 bridges are therefore highly similar to those for persistent JMs (Fig. 4A), supporting a role for Dpb11 and Slx4 in JM resolution. In line with this model, we observed frequent colocalization of either $Slx4^{YFP}$ or $Mus81^{YFP}$ with $Dpb11^{CFP}$-positive bridges that is further enhanced in *sgs1Δ* cells (Supplemental Fig. S7A). We also noticed a colocalization of Slx4, Mus81, and Dpb11 in DNA damage foci yet to a lesser extent (Supplemental Fig. S7B). Overall, the data in Figure 4 provide strong support for an involvement of the Slx4–Dpb11 complex in JM resolution by Mus81–Mms4.

Mus81–Mms4 interacts with the Slx4–Dpb11 complex during mitosis in a Cdc5-dependent fashion

To elucidate how the Slx4–Dpb11 complex regulates Mus81 function, we investigated a possible physical interaction. In previous studies using asynchronously growing yeast cells, no binding of Slx4 to Mus81–Mms4 was detectable (Schwartz et al. 2012). However, we detected Mms4 as a cell cycle-specific interactor if $Slx4^{3Flag}$ immunoprecipitations were investigated by SILAC MS (such as in Fig. 2A). Moreover, when we arrested cells in G2/M by nocodazole treatment, immunopurification of $Mms4^{3Flag}$ copurified Dpb11 and Slx4 (Fig. 5A). Notably, this interaction is highly cell cycle-specific, as it could not be observed in G1- or S-phase cells (Fig. 5A). We determined, using an unbiased SILAC MS approach, that Dpb11, Slx4, and Rtt107 are among the best interactors of Mus81–Mms4 in G2/M-arrested cells (Supplemental Fig. S8A).

Next, we tested whether Dpb11, Slx4, and Mus81–Mms4 form a single protein complex. Indeed, the three proteins comigrated at a size of ~33 S (Supplemental Fig. S8B, fractions 18–20, apparent molecular weight 1.1–1.2 MDa) when the eluate of an $Mms4^{3Flag}$ purification from G2/M cells was subjected to a glycerol gradient centrifugation. When we analyzed the complex architecture by a two-hybrid approach, we detected a direct interaction of Dpb11 and Mms4 that is independent of Slx4 (Supplemental Fig. S8C). Moreover, when we immunoprecipitated $Mms4^{3Flag}$ in the *slx4-S486A* background, we observed a reduction of Slx4, but not Dpb11, binding to $Mms4^{3Flag}$ (Fig. 5B). These findings thus suggest that Dpb11, Slx4, and Mus81–Mms4 are part of a multiprotein complex in which Dpb11 acts as a bridge between Slx4 and Mus81–Mms4.

We observed that Dpb11 and Slx4 could be partially eluted from Mms4-containing beads using λ-phosphatase treatment (Supplemental Fig. S8D), suggesting that the binding is at least in part dependent on protein phosphorylation. Previous work has established that Mus81 activity is decisively up-regulated in mitosis in response to a sequential phosphorylation of Mms4 by CDK and the Polo-like kinase Cdc5 (Matos et al. 2011; Gallo-Fernández et al. 2012; Saugar et al. 2013; Szakal and Branzei 2013). We therefore used two systems to interfere with Cdc5 activity: the *cdc5-as1* analog-sensitive allele, which we inhibited using chloromethylketone (CMK) (Snead et al. 2007), and transcriptional shutoff of *pGAL-CDC5* using glucose repression. Both types of Cdc5 inactivation resulted in a loss of the slower-migrating species of Mms4 in gels and at the same time diminished the binding of Dpb11 and Slx4 to $Mms4^{3Flag}$ (Fig. 5C; Supplemental Fig. S9A). In order to rule out indirect effects, we tested whether Cdk1 activity was uninfluenced under conditions of Cdc5 inhibition/shutoff and saw that neither the interaction between Slx4 and Dpb11 nor phosphorylation of a CDK target site on Rad9 (T474) (Pfander and Diffley 2011) was influenced by Cdc5 inactivation (Supplemental Fig. S9B,C). Together with our results on the architecture of the Slx4–Dpb11–Mms4–Mus81 complex, these experiments suggest that binding of Mms4 to Dpb11 is regulated by Cdc5 phosphorylation.

We also tested whether the formation of the Slx4–Dpb11–Mms4–Mus81 was regulated upon DNA damage. We found that $Mms4^{3Flag}$ bound similar amounts of Dpb11 and Slx4 after phleomycin or mock treatment of G2/M-arrested cells (Supplemental Fig. S9D). Moreover, we could also observe formation of the Slx4–Dpb11–Mms4–Mus81 complex during recovery from MMS pulse treatment during S phase (Fig. 5D). However, this binding occurred only once Cdc5 became active, as visualized by the slower-migrating form of Mms4, indicating that even after DNA damage, the Dpb11–Mms4 interaction is dependent on Cdc5 (Fig. 5D).

Given that the cell cycle regulation of Mus81 activity and the cell cycle regulation of the Slx4–Dpb11–Mms4–Mus81 complex formation have the same requirements, we tested whether the up-regulation of Mus81 nuclease activity requires Slx4 and Dpb11. We analyzed in vitro resolution of nicked Holliday junctions, Holliday junctions, and model replication fork structures on immunopurified Mus81–Mms4 and found that the enhanced activity of mitotic Mus81 is similar, independently of whether Mus81 was purified from wild-type or *slx4-S486A* cells (Fig. 5E; Supplemental Fig. S9E). Therefore, we conclude that cell cycle kinases regulate Mus81 by at least two mechanisms: direct up-regulation of the catalytic activity, which can be reconstituted in vitro, and an up-regulation through formation of an Slx4–Dpb11–Mms4–Mus81 complex, which could be seen in vivo.

The DNA damage checkpoint regulates the Slx4–Dpb11-dependent Mus81 function

The DNA damage checkpoint prevents collapse of stalled replication forks and thereby is fundamentally required for all aspects of the response to stalled replication forks (Branzei and Foiani 2010). Moreover, the checkpoint was also suggested to counteract Cdc5-dependent Mus81 activation, since premature Mms4 phosphorylation by Cdc5 was observed after MMS treatment of checkpoint-deficient cells (Szakal and Branzei 2013). Possible explanations for this phenomenon are a faster S-phase progression in the checkpoint mutants or a direct inhibition of Cdc5 activity by the checkpoint (Zhang et al. 2009).

To address these possibilities, we investigated the influence of the DNA damage checkpoint on Slx4–Dpb11–Mms4–Mus81 complex function. Interestingly, we found

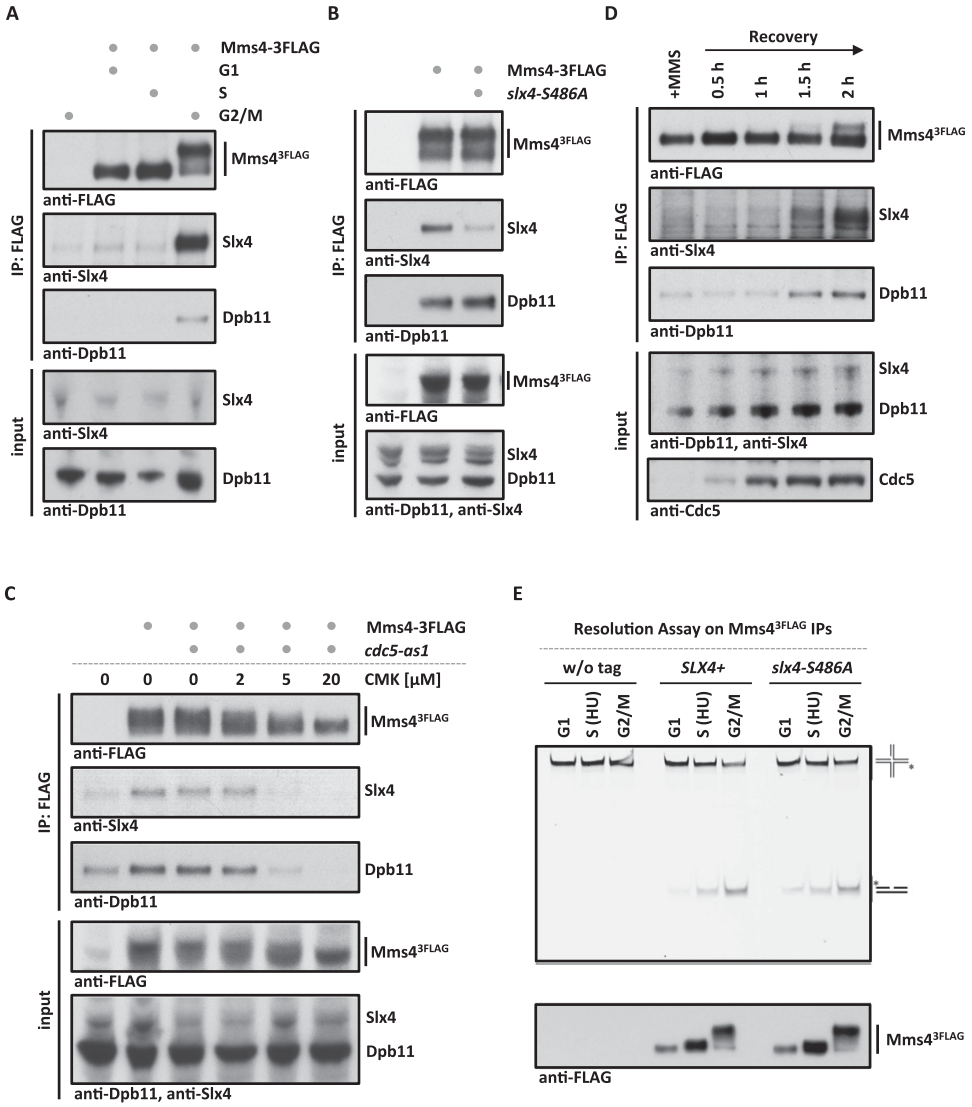

Figure 5. Slx4, Dpb11, and Mus81–Mms4 form a Cdc5-dependent complex at the G2/M cell cycle stage. (*A*) Mms4 binds to Dpb11 and Slx4 specifically in G2/M. Coimmunoprecipitation samples of Mms4^{3Flag} from G1, S, or G2/M cells were tested for binding to Dpb11 and Slx4. (*B*) Slx4-S486A is partially lost from the Slx4–Dpb11–Mms4–Mus81 complex, suggesting that Dpb11 bridges the interaction between Mms4 and Slx4. Mms4^{3Flag} coimmunoprecipitation were carried out as in *A* but from G2/M-arrested wild-type (WT) or *slx4-S486A* mutant cells. (*C*) The Dpb11–Mms4 interaction is dependent on the Polo-like kinase Cdc5. *cdc5-as1* was inhibited by 2, 5, and 20 μM CMK in G2/M-arrested cells. Mms4^{3Flag} coimmunoprecipitation was performed as in *A*. (*D*) Cdc5 hyperphosphorylated Mus81–Mms4 binds to Slx4 and Dpb11 during recovery from MMS damage. Cells were treated with a 30-min pulse of 0.03% MMS. Mms4^{3Flag} coimmunoprecipitations were performed from samples after 0, 30, 60, 90, and 120 min of recovery in nocodazole-containing medium. (*E*) Cell cycle regulation of Mus81–Mms4 nuclease activity remains intact in the *slx4-S486A* mutant. Mms4^{3Flag} and control immunoprecipitations (see the *bottom* panel for immunoprecipitation samples) from cells arrested in their cell cycle by α factor, HU, or nocodazole were incubated with a fluorescence-labeled nicked Holliday junction substrate.

that a partial defect in DNA damage checkpoint signaling alleviated the phenotypes of the *slx4-S486A* mutant (Fig. 6A,B; Supplemental Fig. S10A,B; see also Ohouo et al. 2012). In these experiments, we used three distinct mutants, which were partially impaired in checkpoint signaling: *ddc1-T602A* (defective in Dpb11-dependent Rad9 recruitment (Puddu et al. 2008), *dot1Δ* (defective in chromatin-dependent Rad9 recruitment) (Giannattasio et al. 2005), and *rad53-3HA* (a hypomorphic Rad53 allele) (Cordon-Preciado et al. 2006). All three mutants partially suppressed the hypersensitivity of *slx4-S486A* to chronic exposure of MMS (Fig. 6A; Supplemental Fig. S10A). Furthermore, the recovery from MMS treatment as judged by the reappearance of fully replicated chromosomes in PFGE and reappearance of unphosphorylated Rad53 was enhanced in *slx4-S486A ddc1-T602A* cells compared with *slx4-S486A* cells (Fig. 6B; Supplemental Fig. S10B).

A plausible interpretation of these results is that a partial inactivation of the checkpoint may compensate for a reduced or delayed formation of the Slx4–Dpb11–Mms4–

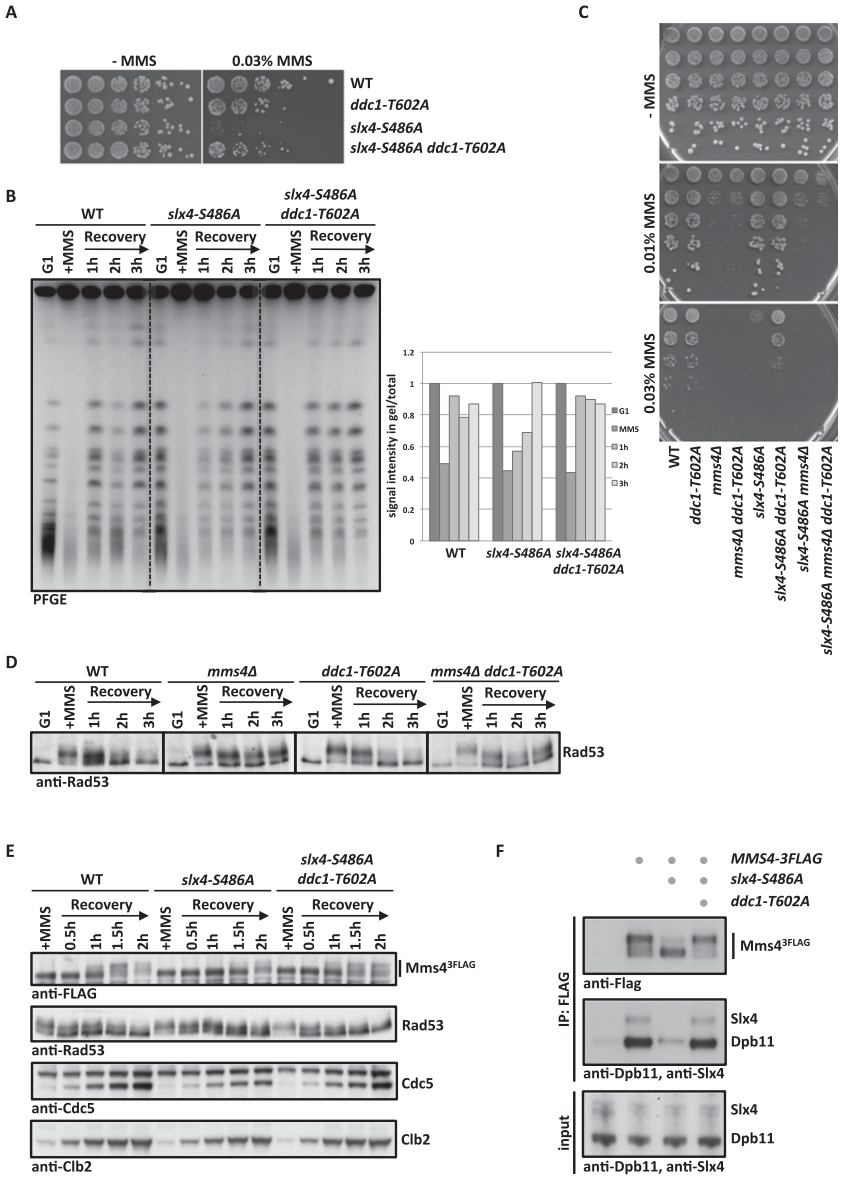

Figure 6. Partial inactivation of the DNA damage checkpoint rescues *slx4-S486A* phenotypes in an *MMS4*-dependent manner. (*A*) The DNA damage repsonse defect of *slx4-S486A* is suppressed by partial inactivation of the DNA damage checkpoint. Wild type (WT), *slx4-S486A*, the partial checkpoint mutant *ddc1-T602A*, and the *slx4-S486A ddc1-T602A* double mutant were spotted in fivefold serial dilutions on MMS-containing plates. (*B*) The prolonged replication fork stalling of the *slx4-S486A* mutant is rescued by the *ddc1-T602A* mutation. Cells were cell cycle-synchronized and treated with a 30-min pulse of 0.033% MMS in S phase. Recovery of fully replicated chromosomes was analyzed by pulsed-field gel electrophoresis. Quantification as in Figure 3D. (*C*) A complete defect in Mus81 activity (*mms4Δ*) cannot be rescued by checkpoint inactivation. The MMS hypersensitivity phenotypes of *slx4-S486A*, *mms4Δ*, and *ddc1-T602A* mutants and double and triple mutant combinations were analyzed as in *A*. (*D*) The checkpoint recovery defect of *mms4Δ* mutants is not rescued by a partial checkpoint mutant. Cells were treated as in *B*, and checkpoint activity was measured by Rad53 phosphorylation. (*E*,*F*) Cdc5-dependent hyperphosphorylation of Mms4 and concomitant binding to Dpb11 and Slx4 occur earlier during recovery from replication fork stalling in *slx4-S486A ddc1-T602A* double mutants compared with *slx4-S486A* mutants. (*E*) Cells were treated with a 40-min pulse of 0.033% MMS in S phase. The Cdc5-dependent $Mms4^{3Flag}$ phosphorylation shift was measured by anti-Flag Western blot, checkpoint activity was measured by Rad53 phosphorylation, and cell cycle progression was followed by anti-Clb2 and anti-Cdc5 Westerns. (*F*) Wild-type, *slx4-S486A*, and *slx4-S486A ddc1-T602A* cells that contain $MMS4^{3Flag}$ were harvested during the recovery phase (2.5 h after MMS removal) and subjected to anti-Flag immunoprecipitation. Coimmunoprecipitation samples were tested for binding to Dpb11 and Slx4.

Mus81 complex. Such compensation may occur by either a direct up-regulation of the Slx4–Dpb11–Mms4–Mus81 complex or hyperactivation of a Mus81-independent salvage pathway. We therefore tested whether the observed rescue would depend on Mms4. Consistent with a direct influence of the checkpoint on the Slx4–Dpb11–Mms4–Mus81 complex, a partial inactivation of the checkpoint did not rescue the MMS hypersensitivity of the *mms4Δ* or *mms4Δ slx4-S486A* mutants (Fig. 6C). In contrast, the *sgs1Δ slx4-S486A* or *yen1Δ slx4-S486A* double mutants could be rescued by additional mutation of *ddc1-T602A* (Supplemental Fig. S10C), suggesting that neither STR nor Yen1 activity is required for the rescue. Furthermore, *mms4Δ ddc1-T602A* mutants show a slow checkpoint recovery after a pulse of MMS in S phase that is similar to *mms4Δ* cells (Fig. 6D). These results suggest that the rescue of *slx4-S486A* mutants upon partial checkpoint inactivation is due to the action of Mms4–Mus81.

Furthermore, when we transiently exposed cells to MMS during S phase and released them into a G2/M arrest, we observed that the Cdc5-dependent phosphorylation shift of Mms4, which in this experiment serves as a marker for the interaction with Slx4–Dpb11, was slightly delayed in *slx4-S486A* cells compared with wild-type cells (Fig. 6E), probably because of a slower S-phase progression (see Fig. 3C). Importantly, the additional partial inactivation of the checkpoint (*slx4-S486A ddc1-T602A*) (Fig. 6E,F) allowed Cdc5-dependent Mms4 phosphorylation to occur earlier. Concomitantly, the binding of Mms4 to Dpb11 and Slx4 was rescued by partial checkpoint inactivation when immunoprecipitations were performed during the recovery phase (Fig. 6F). The occurrence of Mms4 phosphorylation

in the two mutants inversely correlated with DNA damage checkpoint activation (Rad53 phosphorylation) (Fig. 6E). It needs to be emphasized that Slx4–Dpb11 interaction is reduced, but not abolished, in the *slx4-S486A* mutant (Figs. 1B, 3A). The results in Figure 6, E and F, therefore suggest that the Slx4–Dpb11–Mms4–Mus81 complex can form earlier and potentially to a larger extent in the *slx4-S486A ddc1-T602A* mutant compared with the *slx4-S486A* single mutant. This offers a straightforward explanation for the rescue of the *slx4-S486A* mutant phenotypes by partial inactivation of the DNA damage checkpoint.

Taken together, we therefore identified an intricate regulatory mechanism of the Mus81 endonuclease, which critically depends on the formation of an Slx4–Dpb11–Mms4–Mus81 complex. The formation of this complex is activated by cell cycle stage-specific signaling and antagonized by the DNA damage checkpoint. Remarkably, complex formation and the direct control of Mus81 catalytic activity occur with similar timing, at the G2/M transition (Fig. 7).

Discussion

In this study, we describe a new facet of JM resolution following the bypass of DNA damage via template switch recombination. We describe a multiprotein complex containing Slx4, Dpb11, and Mus81–Mms4. This complex is cell cycle-controlled by at least two mechanisms: Cdk1-dependent phosphorylation of Slx4 and Cdc5-dependent phosphorylation of Mms4, and Dpb11 acts as a reader of both modifications. The conservation of the Slx4–Dpb11/TopBP1 interaction and its cell cycle regulation suggests that a similar complex may be involved in JM resolution in human cells. Importantly, the inhibition of Slx4 binding to Dpb11 causes phenotypes that are indicative of JM resolution defects, and we therefore infer that the association with Slx4 and Dpb11 promotes Mus81 function.

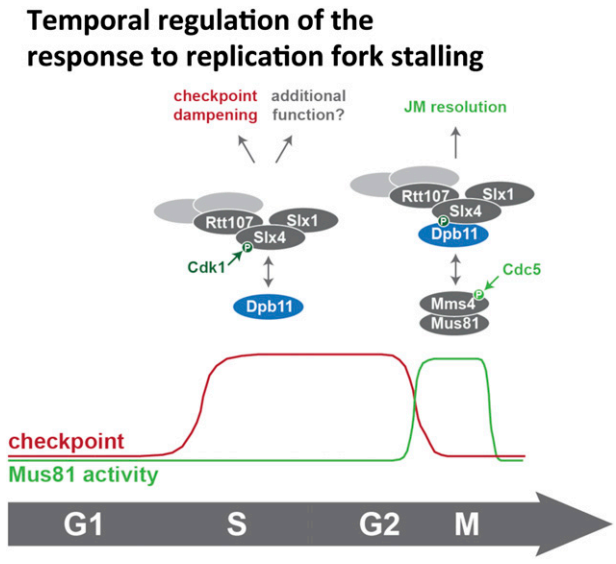

Figure 7. Model of the temporal response to replication fork stalling and its regulation by Slx4–Dpb11 complexes.

Slx4–Dpb11 multiprotein complex formation correlates with DNA JM resolution

The starting point of our analysis was a multiprotein complex containing Slx4, Dpb11, Slx1, and Rtt107 (Ohouo et al. 2010, 2012). In order to characterize a putative function of this complex in DNA repair, we tested whether the Slx4–Dpb11 complex would transiently interact with DNA repair enzymes and found an interaction with the Mus81–Mms4 structure-specific endonuclease specifically in mitotic cells. Based on the findings that the *slx4-S486A* mutant impairs complex formation and results in JM resolution defects, we propose that the Slx4–Dpb11 complex regulates Mus81–Mms4 activity. Our binding studies furthermore indicate a direct Dpb11–Mms4 interaction. Given the nature of Dpb11 as a scaffold protein, it appears likely that Dpb11 operates by tethering Mus81 to other activities that collaborate in the resolution reaction or targeting Mus81 to JM structures.

An intricate feature of the Slx4–Dpb11 complex is its complexity, as it involves four scaffold proteins: Dpb11, Slx4, Rtt107, and Mms4. An obvious advantage of such a multiscaffold complex is that its formation depends on several interaction surfaces, which offer numerous possibilities for regulation. The assembly of the complex therefore allows the integration of different cellular signals (for example, cell cycle and DNA damage), or one specific signal may control complex assembly by several mechanisms. Such a setup includes features of multisite phosphorylation systems, which have the ability to create switch-like transitions (Nash et al. 2001). Moreover, a multiscaffold complex may allow the assembly and coordination of different enzymatic activities (see below).

Our work has identified Mus81 as one catalytically active component of the Slx4–Dpb11 complex; a second one could potentially be Slx1. Recently, the Mus81 and Slx1 endonucleases from humans and mice have been shown to cooperate in the resolution of Holliday junctions in an Slx4-dependent manner (Wyatt et al. 2013). While our results suggest that also in budding yeast, Mus81 and Slx1 may be part of the same complex, we did not observe any specific defects in the response to MMS-induced replication fork stalling for *slx1Δ* cells (Supplemental Fig. S6D). Therefore, we conclude that either Slx1 is not involved in Mus81-dependent JM resolution in budding yeast or a functionally redundant nuclease compensates for the defects of the *slx1Δ* mutant.

Cell cycle regulation of the response to replication fork stalling and JM resolution

The cellular response to replication fork-stalling DNA lesions is intimately linked to the progression of the cell cycle. First, the primary problem, fork stalling, arises specifically in S phase. Moreover, the cells are required to finish the repair/bypass process at the latest in mitosis, when sister chromatids need to be accurately separated, and any remaining links between the chromatids have to be resolved.

In this study, we characterized two Dpb11 interactors: Slx4 and Mms4. Both proteins are phosphorylation tar-

gets of CDKs; however, Mms4 is additionally phosphorylated by the Polo-like kinase Cdc5 (Matos et al. 2011; Gallo-Fernández et al. 2012; Szakal and Branzei 2013). Interestingly, the Slx4–Dpb11 and Mms4–Dpb11 interactions display distinct cell cycle specificities: We observed a strong Slx4–Dpb11 interaction in asynchronous cultures as well as in S-phase and mitotic cells (Figs. 1C, 2C), while the Mms4–Dpb11 interaction was highly specific for mitosis (Fig. 5A). Accordingly, we found that the Mms4–Dpb11 interaction requires Cdc5, suggesting that Dpb11 can act as a reader of phosphorylation events that are initiated by different cell cycle kinases.

The cell cycle regulation of the Mus81–Mms4 association with the Slx4–Dpb11 complex correlates exactly with the known activity profile of Mus81 (Matos et al. 2011). Notably, the multiprotein complex is not the only mechanism of cell cycle regulation: Our in vitro resolution assays suggest that Cdc5 phosphorylation of Mus81–Mms4 directly stimulates Mus81 independently of complex formation. Therefore, we conclude that at least two parallel pathways of cell cycle regulation exist that promote appropriate Mus81 function in mitosis.

To date, it remains uncertain why cells restrict the activity of Mus81 until mitosis. The temporal regulation of Mus81 channels a large proportion of JMs into the Sgs1–Top3–Rmi1 dissolution pathway (Matos et al. 2011; Szakal and Branzei 2013). It has therefore been speculated that Sgs1-dependent dissolution, which leads to a NCO outcome (Ira et al. 2003), may be beneficial for cells dividing by a mitotic cell cycle. A second reason for restricting Mus81 activity may be the necessity to achieve temporal separation of the lesion bypass reaction and the JM resolution reaction (Saugar et al. 2013). Mus81 could impede the bypass reaction, given its relatively broad substrate specificity to a range of DNA structures (e.g., replication forks, D-loop structures, and Holliday junctions).

Intriguingly, the differences in the temporal regulation of the Slx4–Dpb11 and Mms4–Dpb11 interactions suggest that the composition of the Slx4–Dpb11 complex changes from the replication-associated template switch to the resolution reaction. Supporting the idea of several distinct Slx4–Dpb11 complexes is the fact that not all features of the Slx4–Dpb11 interaction (for example, enhanced binding after DNA damage) are seen in the Slx4–Dpb11–Mms4–Mus81 complex. It therefore appears plausible that Slx4–Dpb11 may associate with stalled replication forks already in S phase, while Mus81–Mms4 joins the complex in mitosis. It is tempting to speculate that the Slx4–Dpb11 complex may chaperone the DNA lesion site/repair intermediates until resolution (Fig. 7).

Regulation of JM resolution by the DNA damage checkpoint

The DNA damage checkpoint antagonizes JM resolution by Mus81 (Fig. 6; Szakal and Branzei 2013), and it has been suggested that Slx4 may act as negative regulator ("dampener") of the checkpoint by competing with binding of the checkpoint mediator Rad9 to Dpb11 (Ohouo et al. 2012). The JM resolution phenotypes of the *slx4-S486A* mutant could therefore, in principle, be explained by an indirect effect arising from checkpoint hyperactivation. Given the extensive ties between checkpoint and DNA repair pathways, the presented in vivo experiments cannot rule out a contribution of checkpoint misregulation to the observed JM resolution phenotypes.

We favor, however, a more direct role of Slx4 and Dpb11 in JM resolution for two reasons. First, the formation of the Slx4–Dpb11–Mms4–Mus81 complex and its regulation correlate with the temporal activation of Mus81. Second, the "dampener" model cannot account for all observed phenotypes. For example, the rescue of the MMS hypersensitivity of the *slx4-S486A* mutant by a covalent fusion with Dpb11 cannot be explained by competition, since in the fusion mutant, cells express two copies of full-length Dpb11 (one endogenous, one fused to Slx4), and therefore even more Dpb11 molecules (not less) are able to engage in checkpoint signaling complexes. Moreover, our analysis of RPA foci suggests that DNA lesions or repair intermediates persist and accumulate in the absence of a functional Slx4–Dpb11 complex, indicative of a role for Slx4 and Dpb11 in DNA repair.

Importantly, we found that the checkpoint regulates the formation of the Slx4–Dpb11–Mms4–Mus81 complex: Partial inhibition of the checkpoint enables Cdc5-dependent hyperphosphorylation of Mms4, which allows Dpb11 binding to occur earlier during the recovery from an MMS pulse and thereby reverses the effect of the *slx4* mutant. These findings suggest that at least in the *slx4-S486A* mutant background, the DNA damage checkpoint antagonizes the Slx4–Dpb11–Mms4–Mus81 complex. Partial inactivation of the checkpoint may therefore extend the temporal window during which Mus81 is active, which we propose to be beneficial in mutants with reduced JM resolution activity such as *slx4-S486A*. Whether this inhibitory mechanism takes place on the level of Cdc5 regulation in general (Zhang et al. 2009; Matos et al. 2013) or by specifically regulating Mms4 phosphorylation by Cdc5 remains to be determined. The important implication of this finding is that the activation of Mus81 is temporally restricted by two pathways: activation by cell cycle kinases and inhibition by the DNA damage checkpoint.

The Slx4–Dpb11 complex is conserved among eukaryotes

In addition to the mechanistic studies of the budding yeast Slx4–Dpb11 complex, we also provide the first evidence that at least parts of this complex may be found in human cells as well, since Slx4 and TopBP1 interact in a manner that depends on CDK phosphorylation of Slx4. It is worth noting that not all aspects of the protein network that controls resolution of JMs are conserved through evolution: While in human cells, Slx4 binds directly to Mus81–Eme1, this interaction appears to be absent in budding yeast (Fekairi et al. 2009; Muñoz et al. 2009; Svendsen et al. 2009; Schwartz et al. 2012). Given that both Slx4 and Mms4 bind to Dpb11, our data suggest that Dpb11 may serve as a bridge between the two proteins. Although a direct interaction between Slx4 and Mus81–Mms4 cannot be definitively

excluded, it appears as if the bridging interaction with Dpb11 in yeast may replace the direct interaction of Slx4 and Mus81 in human cells. Importantly, similar to our results in yeast, a stimulation of Slx4 binding to Mus81–Eme1 after phosphorylation by CDK and Polo-like kinase was observed in mitotic human cells as well (Wyatt et al. 2013). At this point, it seems therefore very likely that in both systems, JM resolution is promoted by a cell cycle-regulated complex containing several scaffold proteins.

Materials and methods

Yeast strains

All yeast strains are based on W303. Genotypes are listed in Supplemental Material.

Interaction assays

Coimmunoprecipitations of yeast extracts were performed using anti-Flag agarose resin (Sigma). Bound proteins were eluted with 3× Flag-peptide (Sigma).

For GST pull-downs, GST-Dpb11 or GST-tagged protein fragments were recombinantly expressed and purified as described (Pfander and Diffley 2011). Pull-downs were performed with ammonium sulphate-precipitated (57%) yeast extracts on glutathione sepharose 4B (GE Healthcare).

For coimmunoprecipitations from HEK293T, GFP-tagged proteins were transiently overexpressed and precipitated using GFP-Trap magnetic beads (Chromotek).

Nuclease activity assays

Nuclease assays on $Mms4^{3Flag}$ immunoprecipitations were done as described (Matos et al. 2011).

DNA gel electrophoresis

PFGE and 2D gel analysis of DNA intermediates were performed as previously described (Karras and Jentsch 2010; Szakal and Branzei 2013).

Mutation and recombination assays

Mutation rates were determined using a *CAN1* forward mutation assay. Interchromosomal recombination rates were determined using a direct repeat system using *leu2* heteroalleles (Aguilera and Klein 1988). CO rates were determined using a system harboring two *arg4* alleles on chromosome V and VIII (Robert et al. 2006; Szakal and Branzei 2013). In all, rates were determined by fluctuation analysis using a maximum likelihood approximation (Pfander et al. 2005).

Microscopy and immunofluorescence

Microscopy experiments were carried out as described (Germann et al. 2014).

A detailed methods description is provided in the Supplemental Material.

Acknowledgments

We thank U. Kagerer for excellent technical assistance, and C. Biertümpfel, J. Diffley, and H. Klein for providing plasmids, strains, and antibodies. We are grateful to Z. Storchova for help with microscopy analysis of RPA foci and thank S. Jentsch, M. Räschle, Z. Storchova, and members of the Jentsch and Pfander laboratories for stimulating discussion and critical reading of the manuscript. We thank the Max-Planck Institute of Biochemistry core facility for MS analysis. This work was supported by the Max-Planck Society and the German Research Council (Deutsche Forschungsgemeinschaft) to B.P.; the European Research Council, the Italian Association for International Cancer Research, and The Italian Foundation for Cancer Research (FIRC) to D.B.; and the Danish Agency for Science, Technology, and Innovation, the Villum Kann Rasmussen Foundation, the Lundbeck Foundation, and the European Research Council to M.L. S.C.S.B. is supported by a fellowship from the German Chemical Industry Association (VCI). B.S and D.B. performed the 2D gel experiments of Figure 4A and Supplemental Figure S6A–C and analyzed the data. M.L. performed the imaging experiments of Figure 4E and Supplemental Figure S7 and analyzed the data. J.M. performed the in vitro nuclease assays of Figure 5E and Supplemental Figure S9E and analyzed the data. B.H.H. did the bioinformatics analysis of Supplemental Figure S2. All other experiments were performed and analyzed by D.G., L.N.P., S.C.S.B, L.W., S.S., and B.P. B.P. wrote the paper, and all authors commented on the manuscript.

References

Aguilera A, Klein HL. 1988. Genetic control of intrachromosomal recombination in *Saccharomyces cerevisiae*. I. Isolation and genetic characterization of hyper-recombination mutations. *Genetics* **119:** 779–790.

Bishop AC, Ubersax JA, Petsch DT, Matheos DP, Gray NS, Blethrow J, Shimizu E, Tsien JZ, Schultz PG, Rose MD, et al. 2000. A chemical switch for inhibitor-sensitive alleles of any protein kinase. *Nature* **407:** 395–401.

Blanco MG, Matos J, Rass U, Ip SCY, West SC. 2010. Functional overlap between the structure-specific nucleases Yen1 and Mus81–Mms4 for DNA-damage repair in *S. cerevisiae*. *DNA Repair (Amst)* **9:** 394–402.

Branzei D, Foiani M. 2010. Maintaining genome stability at the replication fork. *Nat Rev Mol Cell Biol* **11:** 208–219.

Branzei D, Vanoli F, Foiani M. 2008. SUMOylation regulates Rad18-mediated template switch. *Nature* **456:** 915–920.

Cejka P, Plank JL, Bachrati CZ, Hickson ID, Kowalczykowski SC. 2010. Rmi1 stimulates decatenation of double Holliday junctions during dissolution by Sgs1–Top3. *Nat Struct Mol Biol* **17:** 1377–1382.

Chan K-L, North PS, Hickson ID. 2007. BLM is required for faithful chromosome segregation and its localization defines a class of ultrafine anaphase bridges. *EMBO J* **26:** 3397–3409.

Cordon-Preciado V, Ufano S, Bueno A. 2006. Limiting amounts of budding yeast Rad53 S-phase checkpoint activity results in increased resistance to DNA alkylation damage. *Nucleic Acids Res* **34:** 5852–5862.

Coulon S. 2006. Rad22Rad52-dependent repair of ribosomal DNA repeats cleaved by Slx1–Slx4 endonuclease. *Mol Biol Cell* **17:** 2081–2090.

Fekairi S, Scaglione S, Chahwan C, Taylor ER, Tissier A, Coulon S, Dong M-Q, Ruse C, Yates JR, Russell P, et al. 2009. Human SLX4 is a Holliday junction resolvase subunit that binds multiple DNA repair/recombination endonucleases. *Cell* **138:** 78–89.

Flott S, Alabert C, Toh GW, Toth R, Sugawara N, Campbell DG, Haber JE, Pasero P, Rouse J. 2007. Phosphorylation of Slx4 by Mec1 and Tel1 regulates the single-strand annealing mode of DNA repair in budding yeast. *Mol Cell Biol* **27:** 6433–6445.

Fricke WM, Brill SJ. 2003. Slx1–Slx4 is a second structure-specific endonuclease functionally redundant with Sgs1–Top3. *Genes Dev* **17:** 1768–1778.

Gaillard P-HL, Noguchi E, Shanahan P, Russell P. 2003. The endogenous Mus81–Eme1 complex resolves Holliday junctions by a nick and counternick mechanism. *Mol Cell* **12:** 747–759.

Gallo-Fernández M, Saugar I, Ortiz-Bazán MÁ, Vázquez MV, Tercero JA. 2012. Cell cycle-dependent regulation of the nuclease activity of Mus81–Eme1/Mms4. *Nucleic Acids Res* **40:** 8325–8335.

Garcia V, Furuya K, Carr AM. 2005. Identification and functional analysis of TopBP1 and its homologs. *DNA Repair (Amst)* **4:** 1227–1239.

Germann SM, Oestergaard VH, Haas C, Salis P, Motegi A, Lisby M. 2011. Dpb11/TopBP1 plays distinct roles in DNA replication, checkpoint response and homologous recombination. *DNA Repair (Amst)* **10:** 210–224.

Germann SM, Schramke V, Pedersen RT, Gallina I, Eckert-Boulet N, Oestergaard VH, Lisby M. 2014. TopBP1/Dpb11 binds DNA anaphase bridges to prevent genome instability. *J Cell Biol* **204:** 45–59.

Giannattasio M, Lazzaro F, Plevani P, Muzi-Falconi M. 2005. The DNA damage checkpoint response requires histone H2B ubiquitination by Rad6–Bre1 and H3 methylation by Dot1. *J Biol Chem* **280:** 9879–9886.

Harrison JC, Haber JE. 2006. Surviving the breakup: the DNA damage checkpoint. *Annu Rev Genet* **40:** 209–235.

Ho CK, Mazón G, Lam AF, Symington LS. 2010. Mus81 and Yen1 promote reciprocal exchange during mitotic recombination to maintain genome integrity in budding yeast. *Mol Cell* **40:** 988–1000.

Holt LJ, Tuch BB, Villén J, Johnson AD, Gygi SP, Morgan DO. 2009. Global analysis of Cdk1 substrate phosphorylation sites provides insights into evolution. *Science* **325:** 1682–1686.

Interthal H, Heyer WD. 2000. MUS81 encodes a novel helix–hairpin–helix protein involved in the response to UV- and methylation-induced DNA damage in *Saccharomyces cerevisiae*. *Mol Gen Genet* **263:** 812–827.

Ip SCY, Rass U, Blanco MG, Flynn HR, Skehel JM, West SC. 2008. Identification of Holliday junction resolvases from humans and yeast. *Nature* **456:** 357–361.

Ira G, Malkova A, Liberi G, Foiani M, Haber JE. 2003. Srs2 and Sgs1–Top3 suppress crossovers during double-strand break repair in yeast. *Cell* **115:** 401–411.

Karras GI, Jentsch S. 2010. The RAD6 DNA damage tolerance pathway operates uncoupled from the replication fork and is functional beyond S phase. *Cell* **141:** 255–267.

Li M, Brill SJ. 2005. Roles of SGS1, MUS81, and RAD51 in the repair of lagging-strand replication defects in *Saccharomyces cerevisiae*. *Curr Genet* **48:** 213–225.

Liberi G, Maffioletti G, Lucca C, Chiolo I, Baryshnikova A, Cotta-Ramusino C, Lopes M, Pellicioli A, Haber JE, Foiani M. 2005. Rad51-dependent DNA structures accumulate at damaged replication forks in sgs1 mutants defective in the yeast ortholog of BLM RecQ helicase. *Genes Dev* **19:** 339–350.

Mankouri HW, Ashton TM, Hickson ID. 2011. Holliday junction-containing DNA structures persist in cells lacking Sgs1 or Top3 following exposure to DNA damage. *Proc Natl Acad Sci* **108:** 4944–4949.

Mankouri HW, Huttner D, Hickson ID. 2013. How unfinished business from S-phase affects mitosis and beyond. *EMBO J* **32:** 2661–2671.

Matos J, Blanco MG, Maslen S, Skehel JM, West SC. 2011. Regulatory control of the resolution of DNA recombination intermediates during meiosis and mitosis. *Cell* **147:** 158–172.

Matos J, Blanco MG, West SC. 2013. Cell-cycle kinases coordinate the resolution of recombination intermediates with chromosome segregation. *Cell Rep* 1–11.

Mordes DA, Nam EA, Cortez D. 2008. Dpb11 activates the Mec1–Ddc2 complex. *Proc Natl Acad Sci* **105:** 18730–18734.

Mullen JR, Kaliraman V, Ibrahim SS, Brill SJ. 2001. Requirement for three novel protein complexes in the absence of the Sgs1 DNA helicase in *Saccharomyces cerevisiae*. *Genetics* **157:** 103–118.

Muñoz IM, Hain K, Déclais A-C, Gardiner M, Toh GW, Sanchez-Pulido L, Heuckmann JM, Toth R, Macartney T, Eppink B, et al. 2009. Coordination of structure-specific nucleases by human SLX4/BTBD12 is required for DNA repair. *Mol Cell* **35:** 116–127.

Nash P, Tang X, Orlicky S, Chen Q, Gertler FB, Mendenhall MD, Sicheri F, Pawson T, Tyers M. 2001. Multisite phosphorylation of a CDK inhibitor sets a threshold for the onset of DNA replication. *Nature* **414:** 514–521.

Navadgi-Patil VM, Burgers PM. 2008. Yeast DNA replication protein Dpb11 activates the Mec1/ATR checkpoint kinase. *J Biol Chem* **283:** 35853–35859.

Ohouo PY, Bastos de Oliveira FM, Almeida BS, Smolka MB. 2010. DNA damage signaling recruits the Rtt107–Slx4 scaffolds via Dpb11 to mediate replication stress response. *Mol Cell* **39:** 300–306.

Ohouo PY, de Oliveira FMB, Liu Y, Ma CJ, Smolka MB. 2012. DNA-repair scaffolds dampen checkpoint signalling by counteracting the adaptor Rad9. *Nature* **493:** 120–124.

Pfander B, Diffley JFX. 2011. Dpb11 coordinates Mec1 kinase activation with cell cycle-regulated Rad9 recruitment. *EMBO J* **30:** 4897–4907.

Pfander B, Moldovan GL, Sacher M, Hoege C, Jentsch S. 2005. SUMO-modified PCNA recruits Srs2 to prevent recombination during S phase. *Nature* **436:** 428–433.

Prakash S, Johnson RE, Prakash L. 2005. Eukaryotic translesion synthesis DNA polymerases: specificity of structure and function. *Annu Rev Biochem* **74:** 317–353.

Puddu F, Granata M, Di Nola L, Balestrini A, Piergiovanni G, Lazzaro F, Giannattasio M, Plevani P, Muzi-Falconi M. 2008. Phosphorylation of the budding yeast 9-1-1 complex is required for Dpb11 function in the full activation of the UV-induced DNA damage checkpoint. *Mol Cell Biol* **28:** 4782–4793.

Rappas M, Oliver AW, Pearl LH. 2011. Structure and function of the Rad9-binding region of the DNA-damage checkpoint adaptor TopBP1. *Nucleic Acids Res* **39:** 313–324.

Robert T, Dervins D, Fabre F, Gangloff S. 2006. Mrc1 and Srs2 are major actors in the regulation of spontaneous crossover. *EMBO J* **25:** 2837–2846.

Roberts TM, Kobor MS, Bastin-Shanower SA, Ii M, Horte SA, Gin JW, Emili A, Rine J, Brill SJ, Brown GW. 2006. Slx4 regulates DNA damage checkpoint-dependent phosphorylation of the BRCT domain protein Rtt107/Esc4. *Mol Biol Cell* **17:** 539–548.

Saugar I, Vazquez MV, Gallo-Fernandez M, Ortiz-Bazan MA, Segurado M, Calzada A, Tercero JA. 2013. Temporal regulation of the Mus81–Mms4 endonuclease ensures cell survival under conditions of DNA damage. *Nucleic Acids Res* **41:** 8943–8958.

Schwartz EK, Wright WD, Ehmsen KT, Evans JE, Stahlberg H, Heyer WD. 2012. Mus81–Mms4 functions as a single heterodimer to cleave nicked intermediates in recombinational DNA repair. *Mol Cell Biol* **32:** 3065–3080.

Snead JL, Sullivan M, Lowery DM, Cohen MS, Zhang C, Randle DH, Taunton J, Yaffe MB, Morgan DO, Shokat KM. 2007. A coupled chemical-genetic and bioinformatic approach to

Polo-like kinase pathway exploration. *Chem Biol* **14:** 1261–1272.

Svendsen JM, Smogorzewska A, Sowa ME, O'Connell BC, Gygi SP, Elledge SJ, Harper JW. 2009. Mammalian BTBD12/SLX4 assembles a Holliday junction resolvase and is required for DNA repair. *Cell* **138:** 63–77.

Szakal B, Branzei D. 2013. Premature Cdk1/Cdc5/Mus81 pathway activation induces aberrant replication and deleterious crossover. *EMBO J* **32:** 1155–1167.

Tanaka S, Umemori T, Hirai K, Muramatsu S, Kamimura Y, Araki H. 2007. CDK-dependent phosphorylation of Sld2 and Sld3 initiates DNA replication in budding yeast. *Nature* **445:** 328–332.

Tomkinson AE, Bardwell AJ, Bardwell L, Tappe NJ, Friedberg EC. 1993. Yeast DNA repair and recombination proteins Rad1 and Rad10 constitute a single-stranded-DNA endonuclease. *Nature* **362:** 860–862.

Wyatt HDM, Sarbajna S, Matos J, West SC. 2013. Coordinated actions of SLX1–SLX4 and MUS81–EME1 for Holliday junction resolution in human cells. *Mol Cell* **52:** 234–247.

Yu X. 2003. The BRCT domain is a phospho-protein binding domain. *Science* **302:** 639–642.

Zegerman P, Diffley JFX. 2007. Phosphorylation of Sld2 and Sld3 by cyclin-dependent kinases promotes DNA replication in budding yeast. *Nature* **445:** 281–285.

Zhang T, Nirantar S, Lim HH, Sinha I, Surana U. 2009. DNA damage checkpoint maintains Cdh1 in an active state to inhibit anaphase progression. *Dev Cell* **17:** 541–551.

A cell cycle-regulated Slx4–Dpb11 complex promotes the resolution of DNA repair intermediates linked to stalled replication

Dalia Gritenaite, Lissa N. Princz, Barnabas Szakal, et al.

Genes Dev. 2014, **28:**
Access the most recent version at doi:10.1101/gad.240515.114

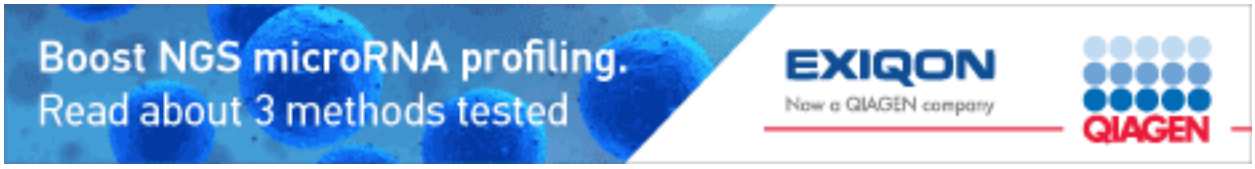

Supplemental Information – Outline

- Supplemental Figures
- Supplemental Figure Legends
- Supplemental Methods
- References

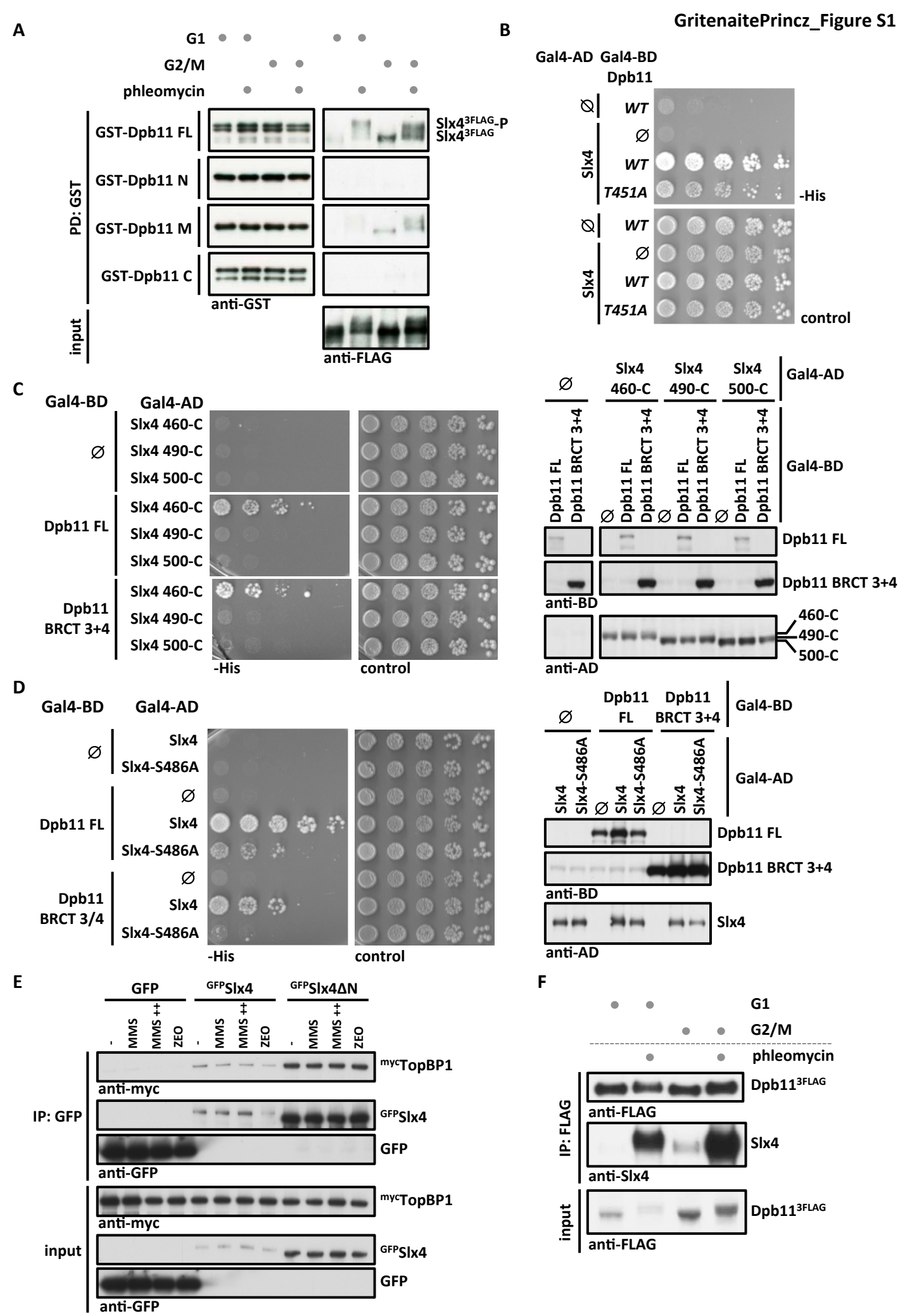
A
G1
G2/M
phleomycin
PD: GST
GST-Dpb11 FL
GST-Dpb11 N
GST-Dpb11 M
GST-Dpb11 C
anti-GST
input
anti-FLAG
Slx4^3FLAG-P
Slx4^3FLAG
B
Gal4-AD
Gal4-BD
Dpb11
Slx4
WT
T451A
-His
control
C
Gal4-BD
Gal4-AD
Slx4 460-C
Slx4 490-C
Slx4 500-C
Dpb11 FL
Dpb11 BRCT 3+4
-His
control
D
Gal4-BD
Gal4-AD
Slx4
Slx4-S486A
Dpb11 FL
Dpb11 BRCT 3/4
-His
control
E
GFP
GFPSlx4
GFPSlx4ΔN
-
MMS
MMS ++
ZEO
IP: GFP
anti-myc
anti-GFP
input
mycTopBP1
GFPSlx4
GFP
F
G1
G2/M
phleomycin
IP: FLAG
input
anti-FLAG
anti-Slx4
Dpb11^3FLAG
Slx4

Dpb11/TopBP1 interaction motif in Slx4 proteins from different eukaryotes

```
Sp   156 GFYYHR-----KPQLFEKSLEKLGNK---SIEA-NR---SPLIKELC 190
Sc   458 QFFTPN--TSPLDGIIDLTQE--------SFKA-VRSLISPLKVENN 493 (S486)
Kl   372 KTKREYSRANINDQLINISQT--------SYDV-VSSIVSPMKAQRT 409
Ec   347 PDESPDNLPIHEDTVIDLTQE--------TFRA-VSNIASPVKATSR 384
Nc   494 SQSPTPGTSPQQDEIIDLTQE--------SFKA-VGRLISPVRPPTL 531
Ka   374 SIFSAHPSPEKPDNIIDLSVG--------SFKA-VKSLVSPIKPDVV 411
Td   282 QFYTPR--TTPPDEIIDLTQE--------SFKV-VKSLISPLKD--- 314
Zr   305 DAGTPKTAHSPSDGVIDLTNG--------SFKV-VKSLISPLK---- 338
Vp   391 QFFTADG--NMVDGVIDLTQG--------SFKA-VTKLFSPLKVDTL 426
Lt   385 HTYRTPSGLAGRDQLIDLTQC--------SFNA-VKSLISPLKS--- 419
Hs  1236 WLFCDRESSPSEASTTDTSW---------LVPA-TP-LASRSRDCSS 1271 (T1260)
Sb  1196 WLFCDRESSPEEGSTTDTSW---------LVPA-TP-LAGRSRDCSS 1231
Mm  1038 WLLCSQKTSLDEDSATDTSW---------LVPA-TP-GVSRSRDCSS 1073
Rn  1242 WLFCSQTPSLGEDSATESSW---------LVPA-TP-GASKSRDRSS 1277
Sh  1214 RPVTRHE----ESSTTDTSW---------LVPA-TP-LTNRSHDCSS 1245
Tm  1250 QLFCKAESSP-EASTTDTSW---------LVPA-TP-LASRGCHRSS 1284
Oo  1244 QLFCDPKISGDEDSTTDTSW---------LVPA-TP-LASRSRDCSS 1279
Xt  1129 EVPQIST--IQSAFHYN-SLSPPL-----LSPAKSP-AKPLSPPVSP 1166
Dr  1168 DVSRASTMGHLAQGVPQPSSSTP------VHSVGS--LQRKILFDSP 1207
Dm   281 EGPIDDLESYYVTDLFEVSRTPAHHLLKNWAAI-QGRDFSPERETQK 326
Dg   283 EESLANLSAYYVQDLFEVSRTPAHHLLKNWAAI-QGRDLSPKRPSKE 328
Dw   276 EDPIELN-VYYVKDLIEISYTPAEHLLKDWSAI-QGRDLSPKRLNPK 320
Cc   325 DEHRANLDEFYVRSLFEVANVQAGYLLKDWHAI-EGRDKSPKHRPNK 370
Ag   343 LPSEQLMEMYYVPELLEANPAPVGCMLKDWSKI-PGRECTPERELDG 388
```

A

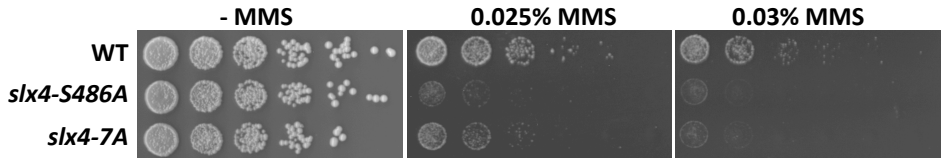
- MMS
0.025% MMS
0.03% MMS
WT
slx4-S486A
slx4-7A

B

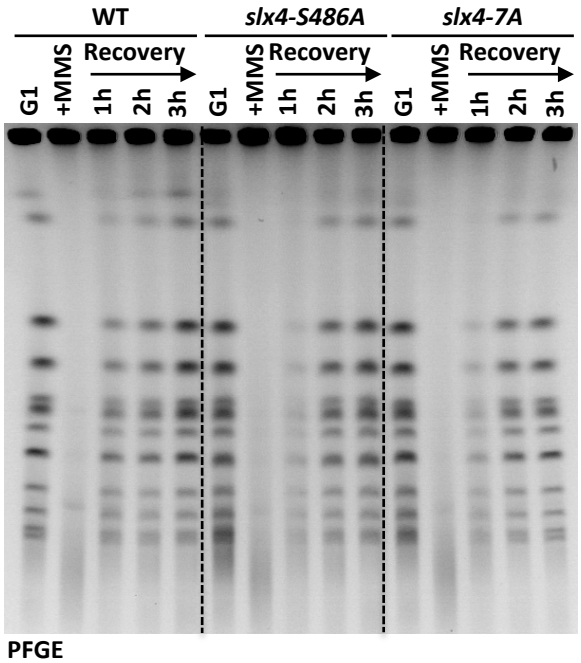
WT
slx4-S486A
slx4-7A
Recovery
G1
+MMS
1h
2h
3h
PFGE

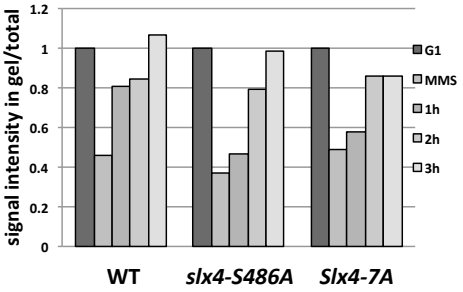
signal intensity in gel/total
1.2
1
0.8
0.6
0.4
0.2
0
G1
MMS
1h
2h
3h
WT
slx4-S486A
Slx4-7A

C

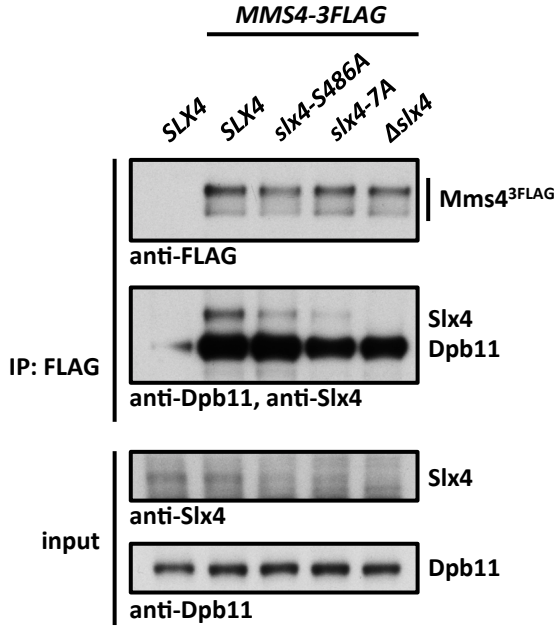
MMS4-3FLAG
SLX4
SLX4
slx4-S486A
slx4-7A
Δslx4
Mms4^3FLAG
anti-FLAG
IP: FLAG
Slx4
Dpb11
anti-Dpb11, anti-Slx4
input
Slx4
anti-Slx4
Dpb11
anti-Dpb11

A

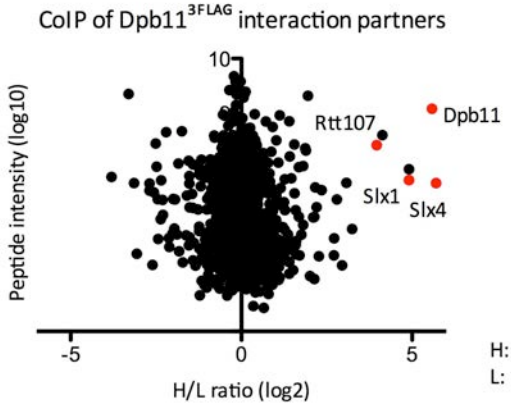

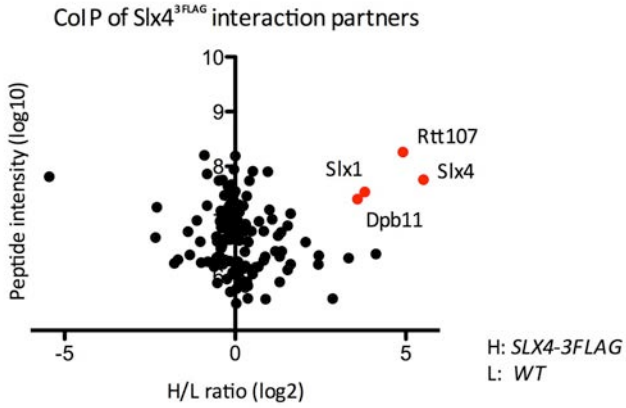

Best scoring MS-MS spectrum of SLX4 phospho-S486 peptide from Dpb11 3FLAG CoIP :

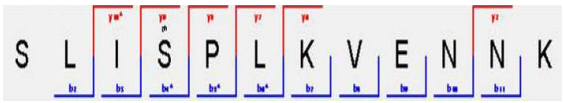

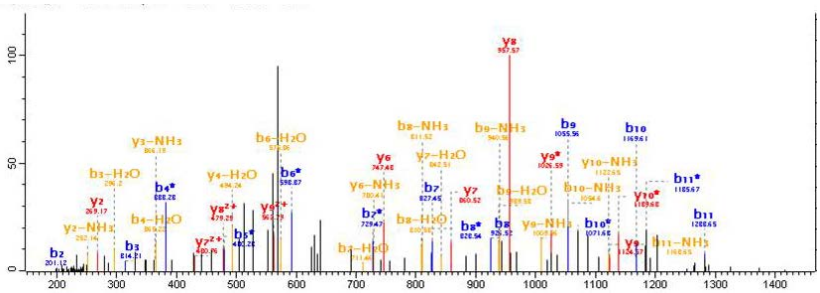

B

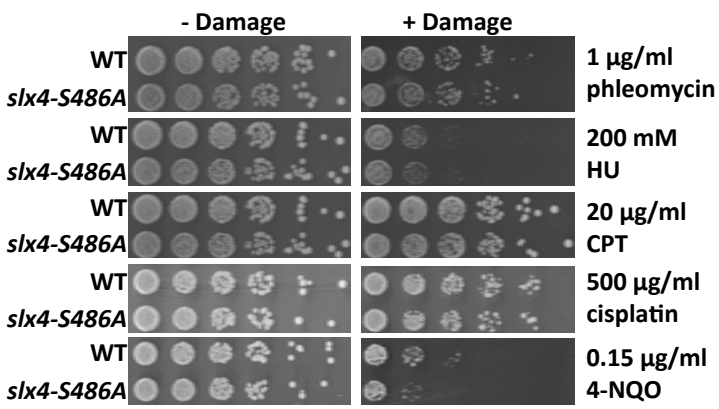

C

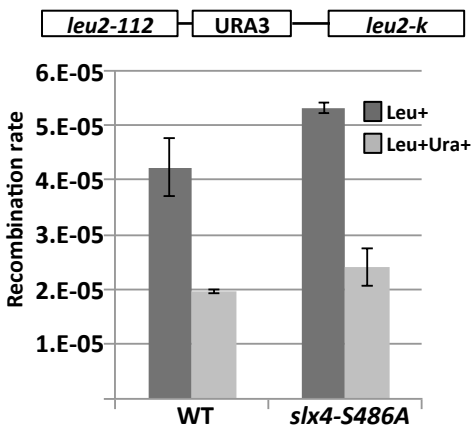

D

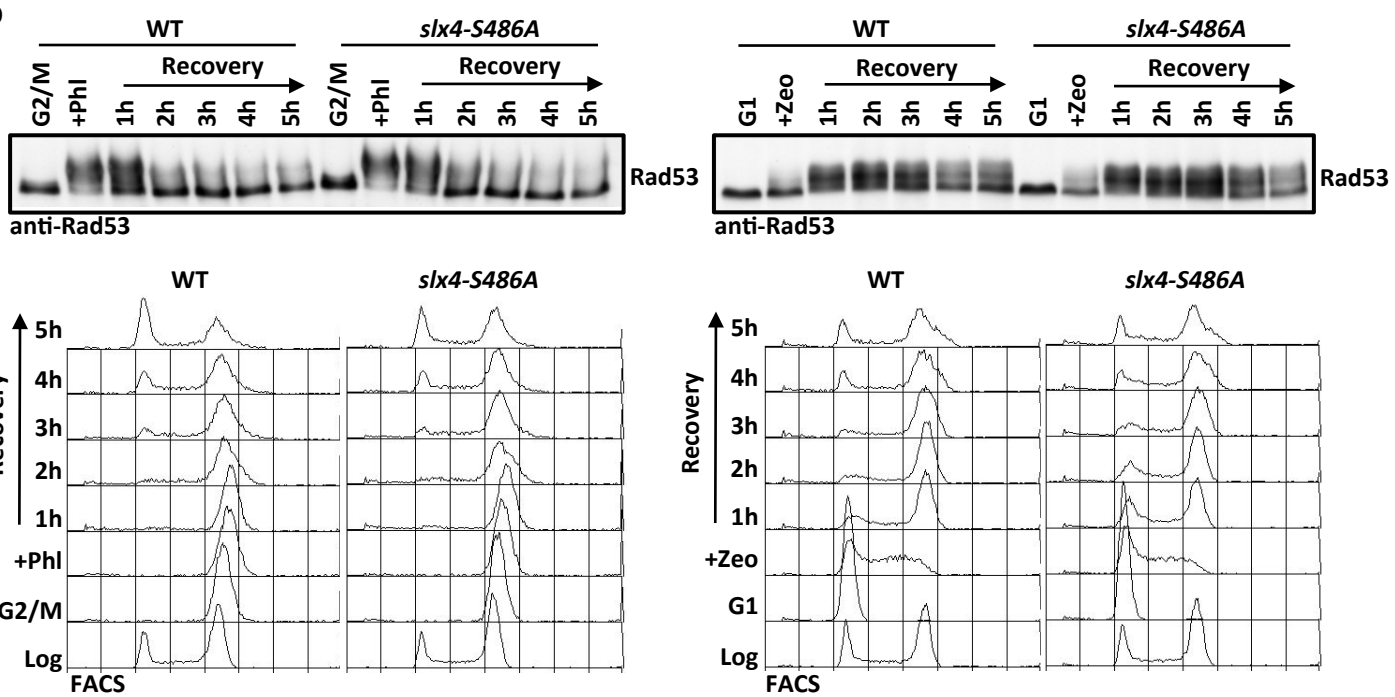

A

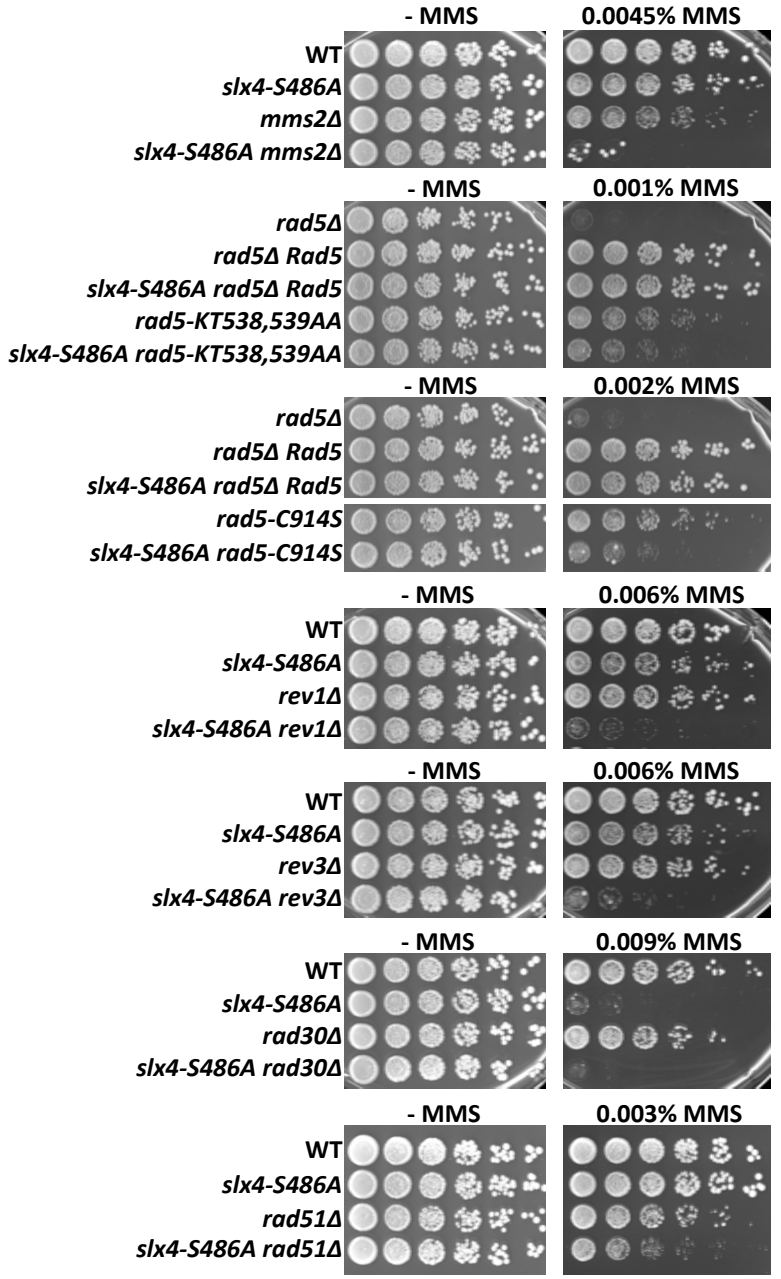
- MMS
0.0045% MMS
WT
slx4-S486A
mms2Δ
slx4-S486A mms2Δ
- MMS
0.001% MMS
rad5Δ
rad5Δ Rad5
slx4-S486A rad5Δ Rad5
rad5-KT538,539AA
slx4-S486A rad5-KT538,539AA
- MMS
0.002% MMS
rad5Δ
rad5Δ Rad5
slx4-S486A rad5Δ Rad5
rad5-C914S
slx4-S486A rad5-C914S
- MMS
0.006% MMS
WT
slx4-S486A
rev1Δ
slx4-S486A rev1Δ
- MMS
0.006% MMS
WT
slx4-S486A
rev3Δ
slx4-S486A rev3Δ
- MMS
0.009% MMS
WT
slx4-S486A
rad30Δ
slx4-S486A rad30Δ
- MMS
0.003% MMS
WT
slx4-S486A
rad51Δ
slx4-S486A rad51Δ

B

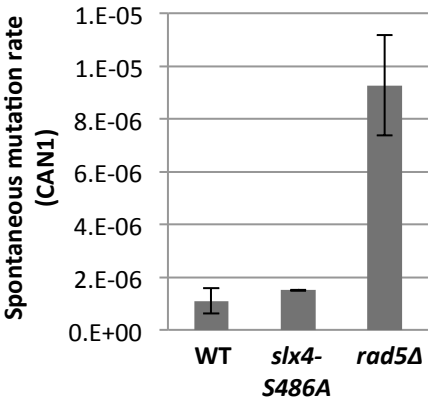
Spontaneous mutation rate (CAN1)
1.E-05
1.E-05
8.E-06
6.E-06
4.E-06
2.E-06
0.E+00
WT
slx4-S486A
rad5Δ

C

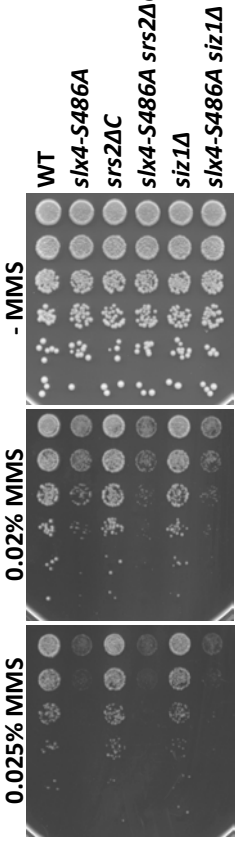
WT
slx4-S486A
srs2ΔC
slx4-S486A srs2ΔC
siz1Δ
slx4-S486A siz1Δ
- MMS
0.02% MMS
0.025% MMS

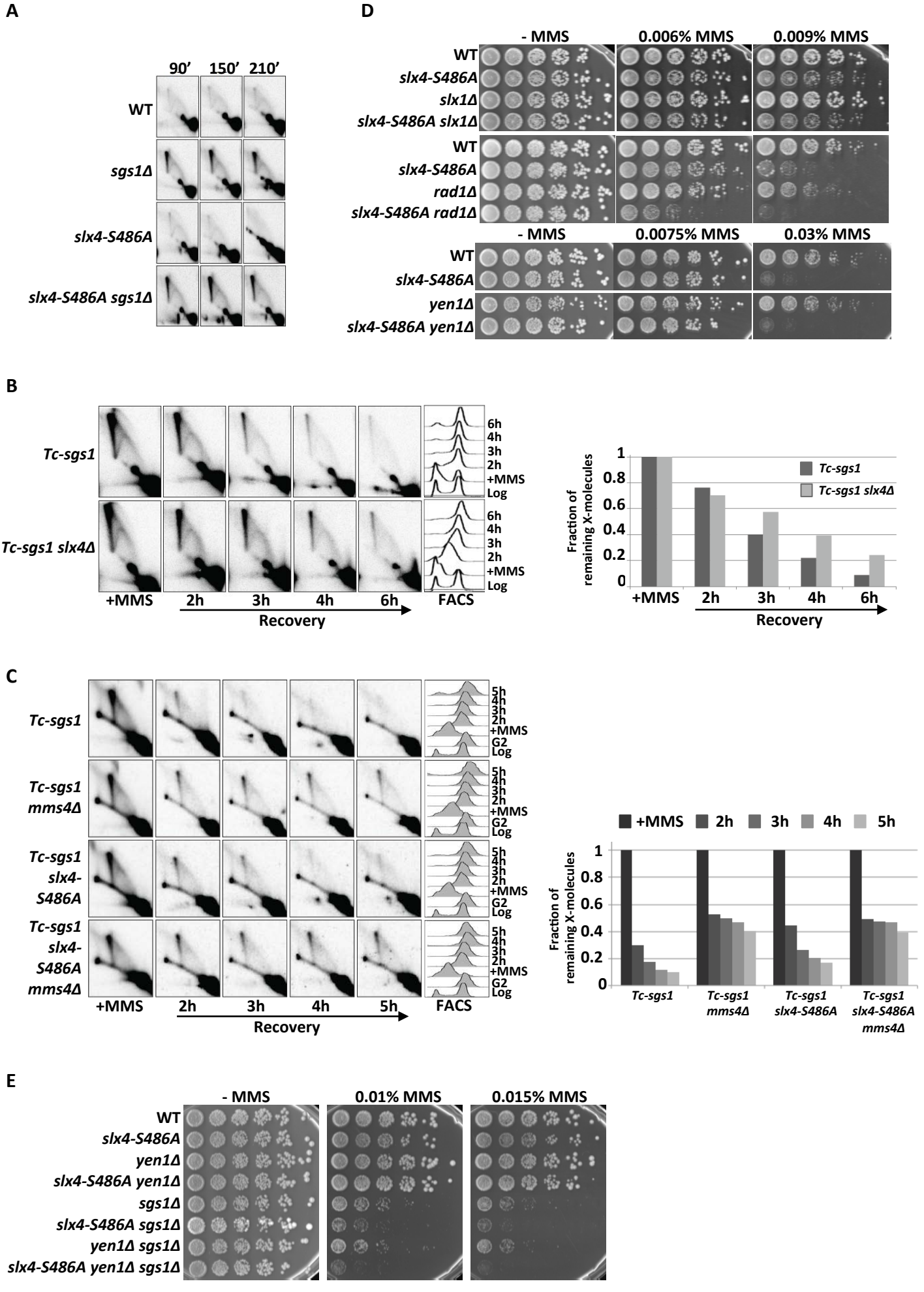
A
90'
150'
210'
WT
sgs1Δ
slx4-S486A
slx4-S486A sgs1Δ
D
- MMS
0.006% MMS
0.009% MMS
WT
slx4-S486A
slx1Δ
slx4-S486A slx1Δ
WT
slx4-S486A
rad1Δ
slx4-S486A rad1Δ
- MMS
0.0075% MMS
0.03% MMS
WT
slx4-S486A
yen1Δ
slx4-S486A yen1Δ
B
Tc-sgs1
Tc-sgs1 slx4Δ
6h
4h
3h
2h
+MMS
Log
FACS
+MMS
2h
3h
4h
6h
Recovery
Fraction of remaining X-molecules
Tc-sgs1
Tc-sgs1 slx4Δ
C
Tc-sgs1
Tc-sgs1 mms4Δ
Tc-sgs1 slx4-S486A
Tc-sgs1 slx4-S486A mms4Δ
5h
4h
3h
2h
+MMS
G2
Log
FACS
+MMS
2h
3h
4h
5h
Recovery
Fraction of remaining X-molecules
Tc-sgs1
Tc-sgs1 mms4Δ
Tc-sgs1 slx4-S486A
Tc-sgs1 slx4-S486A mms4Δ
E
- MMS
0.01% MMS
0.015% MMS
WT
slx4-S486A
yen1Δ
slx4-S486A yen1Δ
sgs1Δ
slx4-S486A sgs1Δ
yen1Δ sgs1Δ
slx4-S486A yen1Δ sgs1Δ

A

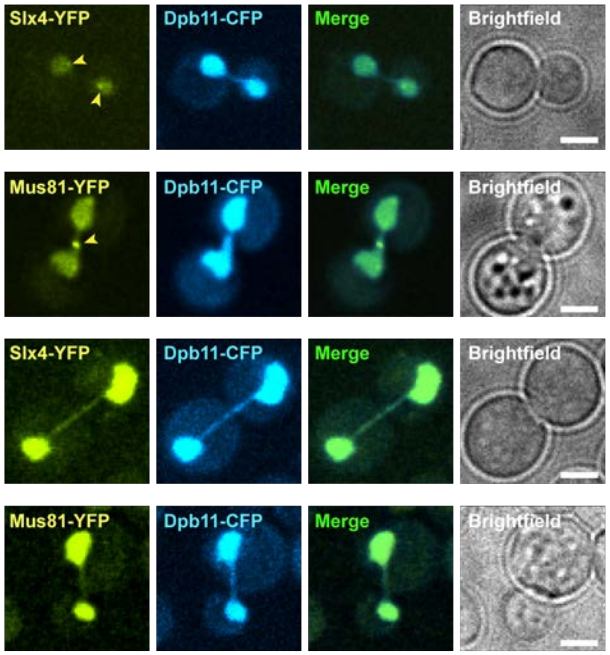
Slx4-YFP
Dpb11-CFP
Merge
Brightfield
Mus81-YFP
Dpb11-CFP
Merge
Brightfield
Slx4-YFP
Dpb11-CFP
Merge
Brightfield
Mus81-YFP
Dpb11-CFP
Merge
Brightfield

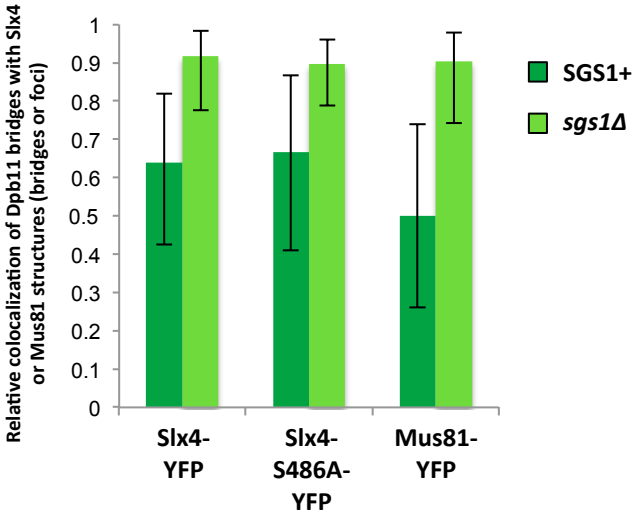
Relative colocalization of Dpb11 bridges with Slx4 or Mus81 structures (bridges or foci)
0
0.1
0.2
0.3
0.4
0.5
0.6
0.7
0.8
0.9
1
Slx4-YFP
Slx4-S486A-YFP
Mus81-YFP
SGS1+
sgs1Δ

B

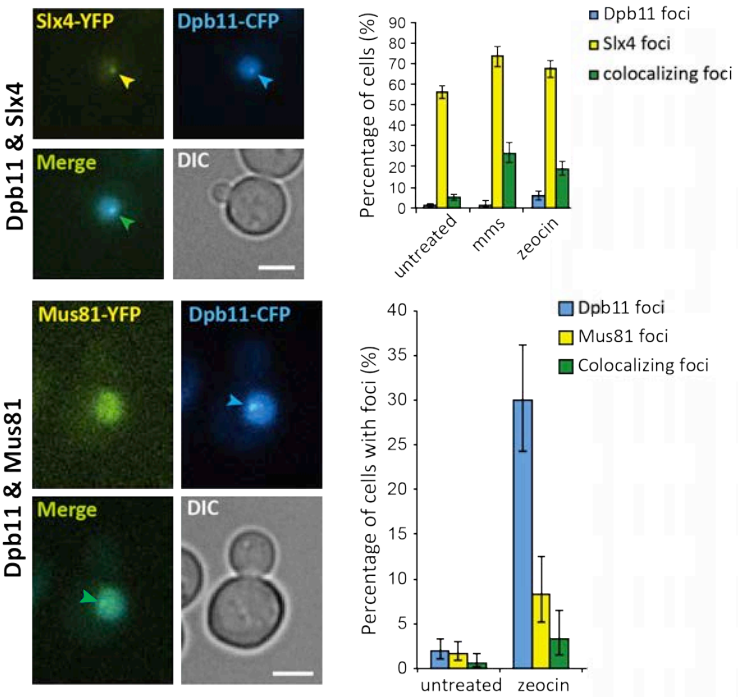
Dpb11 & Slx4
Slx4-YFP
Dpb11-CFP
Merge
DIC
Percentage of cells (%)
Dpb11 foci
Slx4 foci
colocalizing foci
untreated
mms
zeocin
Dpb11 & Mus81
Mus81-YFP
Dpb11-CFP
Merge
DIC
Percentage of cells with foci (%)
Dpb11 foci
Mus81 foci
Colocalizing foci
untreated
zeocin

A

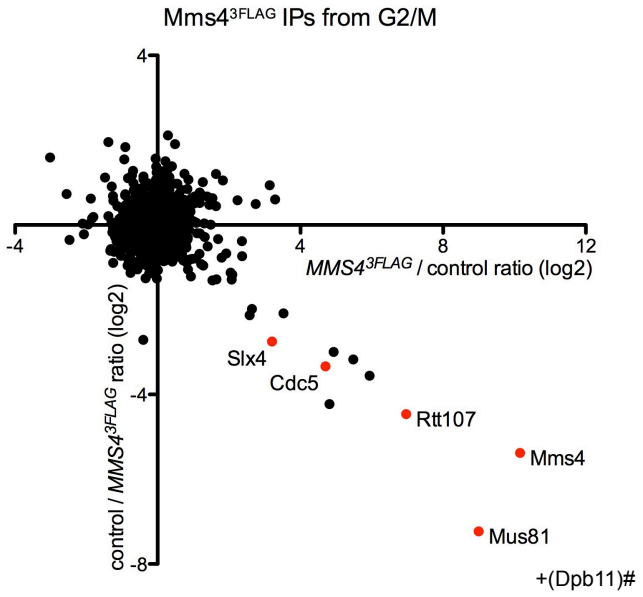
Mms4^3FLAG IPs from G2/M
MMS4^3FLAG / control ratio (log2)
control / MMS4^3FLAG ratio (log2)
Slx4
Cdc5
Rtt107
Mms4
Mus81
+(Dpb11)#

C

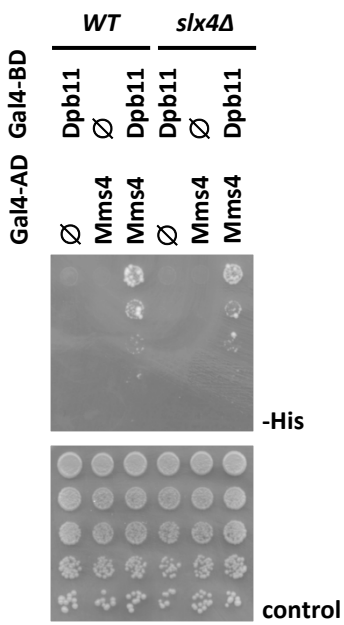
WT
slx4Δ
Gal4-BD
Dpb11
∅
Dpb11
Dpb11
∅
Dpb11
Gal4-AD
∅
Mms4
Mms4
∅
Mms4
Mms4
-His
control

B


glycerol gradient
10%
30%
input
1 2 3 4 5 6 7 8 9 10 11 12 13 14 15 16 17 18 19 20 21 22
Mms4^3FLAG
anti-FLAG
Slx4
Dpb11
anti-Dpb11,
anti-Slx4

D

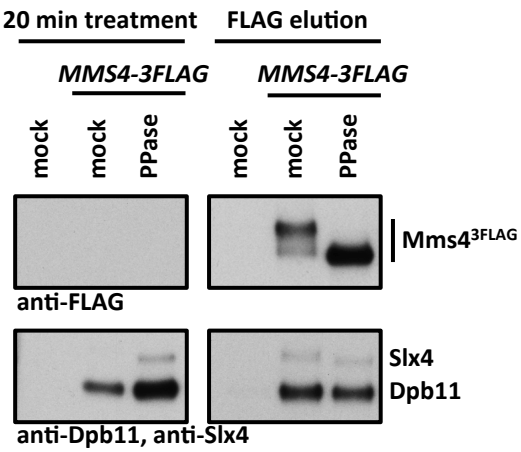
20 min treatment
FLAG elution
MMS4-3FLAG
MMS4-3FLAG
mock
mock
PPase
mock
mock
PPase
Mms4^3FLAG
anti-FLAG
Slx4
Dpb11
anti-Dpb11, anti-Slx4

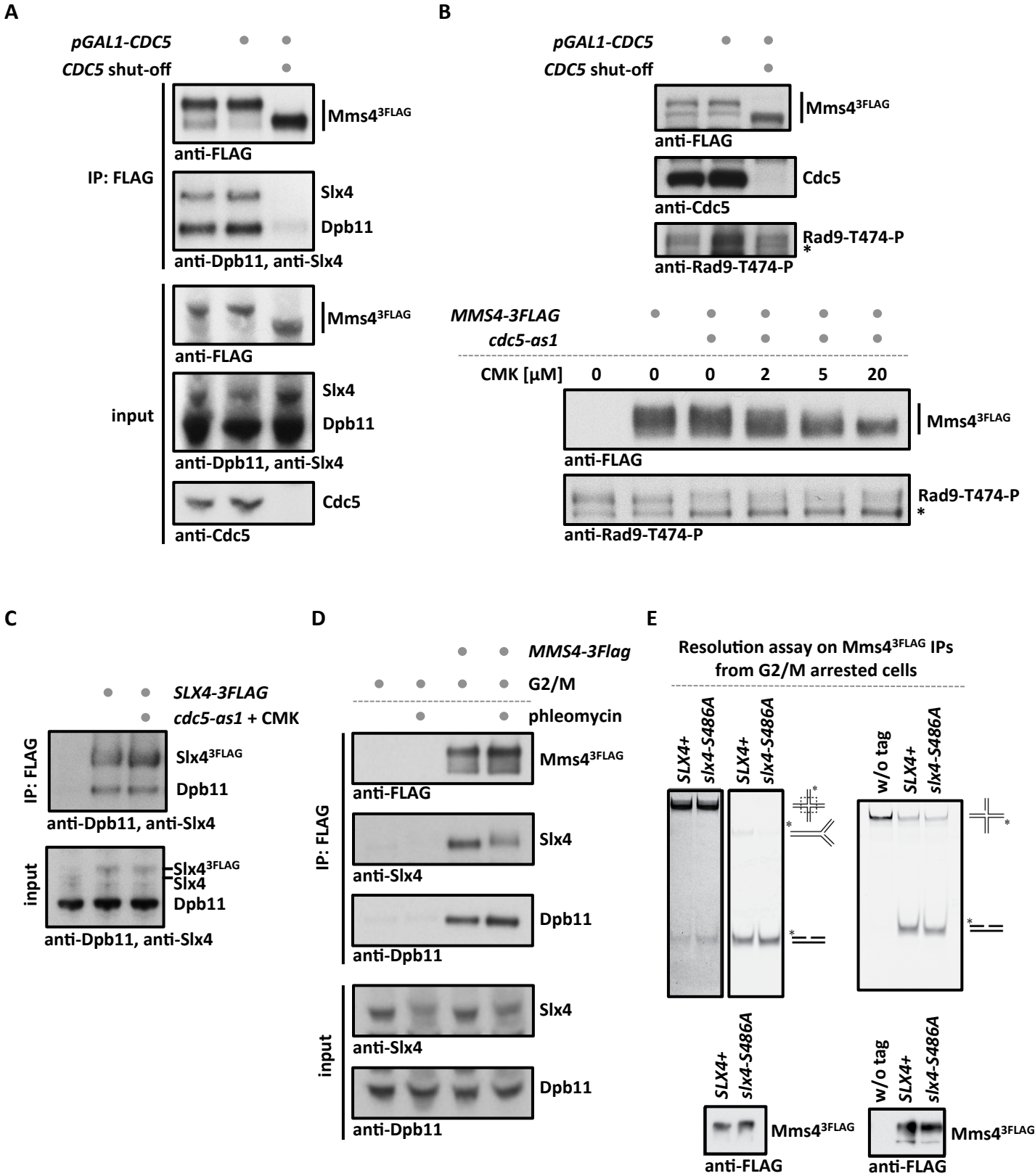
A
pGAL1-CDC5
CDC5 shut-off
Mms4^3FLAG
anti-FLAG
IP: FLAG
Slx4
Dpb11
anti-Dpb11, anti-Slx4
input
Cdc5
anti-Cdc5
B
pGAL1-CDC5
CDC5 shut-off
Mms4^3FLAG
anti-FLAG
Cdc5
anti-Cdc5
Rad9-T474-P
anti-Rad9-T474-P
MMS4-3FLAG
cdc5-as1
CMK [μM] 0 0 0 2 5 20
C
SLX4-3FLAG
cdc5-as1 + CMK
Slx4^3FLAG
Dpb11
Slx4
D
MMS4-3Flag
G2/M
phleomycin
E
Resolution assay on Mms4^3FLAG IPs from G2/M arrested cells
SLX4+
slx4-S486A
w/o tag

A

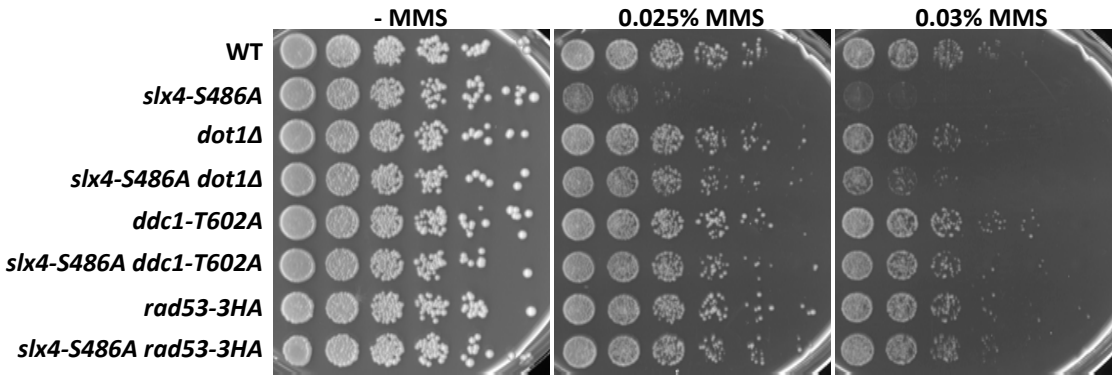
- MMS
0.025% MMS
0.03% MMS
WT
slx4-S486A
dot1Δ
slx4-S486A dot1Δ
ddc1-T602A
slx4-S486A ddc1-T602A
rad53-3HA
slx4-S486A rad53-3HA

B

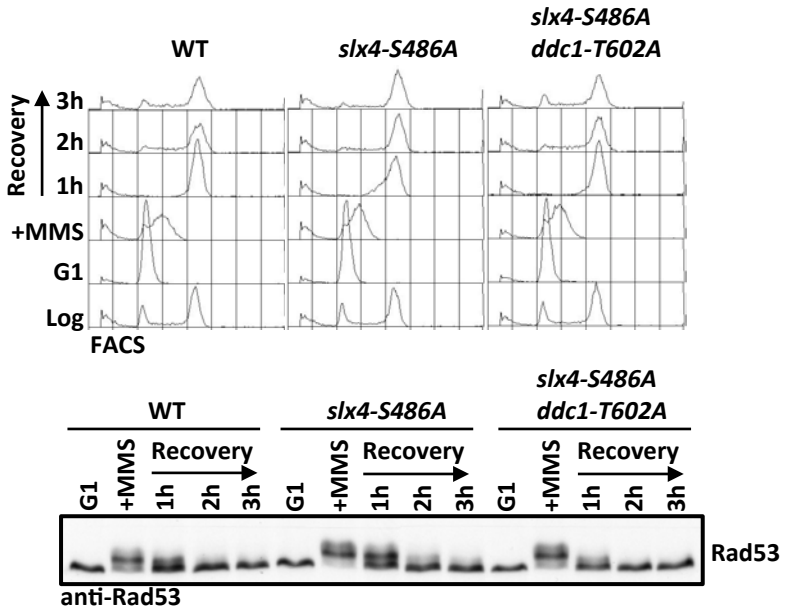
WT
slx4-S486A
slx4-S486A ddc1-T602A
Recovery
3h
2h
1h
+MMS
G1
Log
FACS
WT
slx4-S486A
slx4-S486A ddc1-T602A
G1
+MMS
Recovery
1h
2h
3h
Rad53
anti-Rad53

C

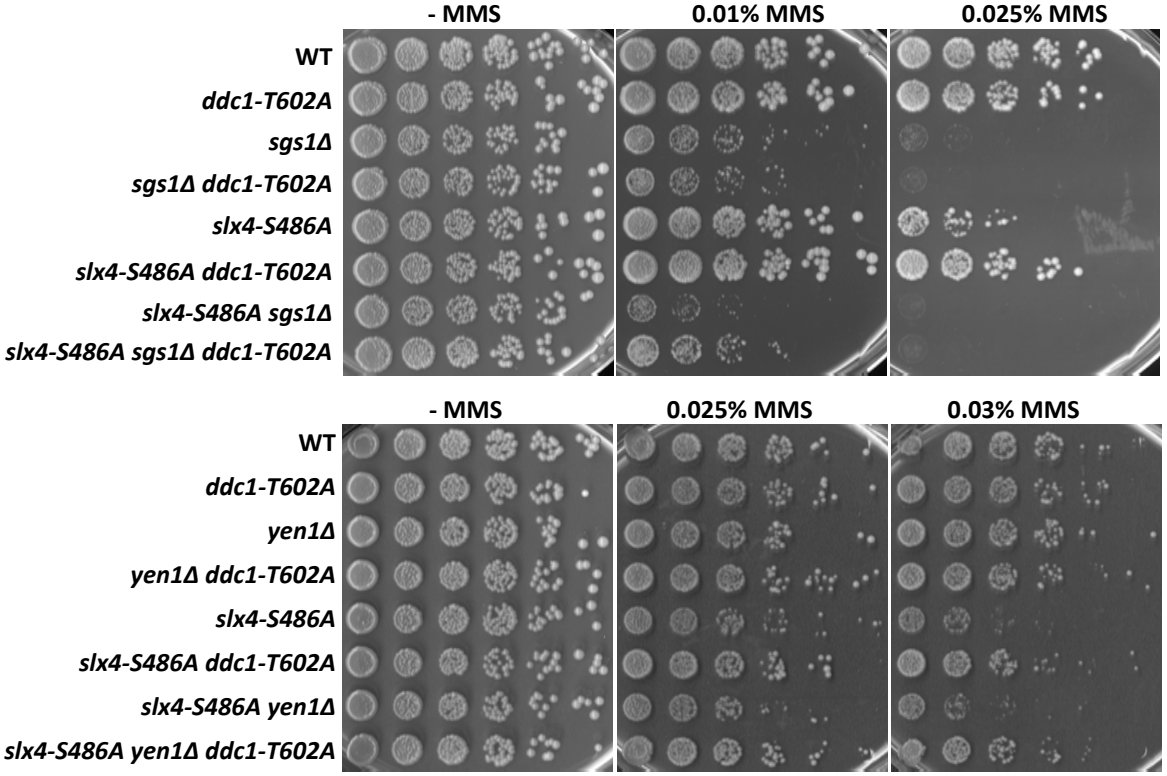
- MMS
0.01% MMS
0.025% MMS
WT
ddc1-T602A
sgs1Δ
sgs1Δ ddc1-T602A
slx4-S486A
slx4-S486A ddc1-T602A
slx4-S486A sgs1Δ
slx4-S486A sgs1Δ ddc1-T602A
- MMS
0.025% MMS
0.03% MMS
WT
ddc1-T602A
yen1Δ
yen1Δ ddc1-T602A
slx4-S486A
slx4-S486A ddc1-T602A
slx4-S486A yen1Δ
slx4-S486A yen1Δ ddc1-T602A

Supplemental Figure Legends

Figure S1.

The binding surface of the evolutionary conserved Slx4 and Dpb11 complex contains BRCT3+4 of Dpb11 and S486 of Slx4 in *S. cerevisiae*. **A** Slx4 binds to Dpb11 fragments containing BRCT3+4. Pulldown of Slx4 from undamaged or phleomycin-treated G1 or G2/M cell extracts using GST-Dpb11 fragments (N: aa 1-275, M: aa 276-600, C: aa 556-764, ΔC: aa 1-600). **B** Mutation of the Dpb11 BRCT3+4 phospho-protein binding surface reduces Slx4 binding to Dpb11. Two-hybrid analysis of GAL4-BD fused to *WT* Dpb11 or to Dpb11-T451A, and GAL4-AD fusions with Slx4. **C** A region in Slx4 sequence between aa 461 and aa 490 is important for Dpb11 interaction. Two-hybrid analysis of GAL4-BD (left panel) fused to *WT* Dpb11 or to the BRCT3+4 fragment, and GAL4-AD fusions with Slx4 C-terminal fragments. Expression of the constructs was verified by western blot analysis (right panel). **D** Mutation of S486 in Slx4 to a non-phosphorylatable alanine residue reduces Dpb11 binding. Two-hybrid analysis of GAL4-BD (left panel) fused to *WT* Dpb11 or to the BRCT3+4 fragment, and GAL4-AD fusions with *WT* Slx4 or with Slx4-S486A. Expression of the constructs was verified by western blot analysis (right panel). **E** The presence of DNA damage does not stimulate TopBP1 binding to Slx4 in human cells. Co-immunoprecipitation of ^{myc}TopBP1 with ^{GFP}Slx4 and ^{GFP}Slx4ΔN after transient overexpression in HEK 293T cells. Cells were left untreated or treated with 0.001% or 0.003% (++) MMS or 100 µg/ml zeocin for 30 min to induce DNA damage. **F** The Slx4-Dpb11 interaction is regulated by cell cycle phase and DNA damage. Co-

immunoprecipitation of Slx4 and Dpb11^{3FLAG} from G1 or G2/M arrested cells, which were either damaged by 50 µg/ml phleomycin or left untreated.

Figure S2.

A phosphorylation-dependent Dpb11/TopBP1 binding motif in eukaryotic Slx4 proteins.

Slx4 proteins from different eukaryotes comprise a conserved, short linear motif, which harbours serine 486 in budding yeast and threonine 1260 in humans. Multiple sequence alignment of the Dpb11/TopBP1 interaction motif. Conserved residues in more than one class are highlighted in yellow. Phosphorylation sites in *Saccharomyces cerevisiae* and *Homo sapiens*, as well as predicted sites as inferred from homology are indicated in red, alternative sites with unclear homology in light green. Species abbreviations, as well as accession numbers are listed in Supplementary Table 2.

Figure S3.

Mutation of seven SQ/TQ motifs in the C-terminus of Slx4 leads to similar phenotypes as the *slx4-S486A* mutation.

A The *slx4-S486A* and *slx4-7A* mutants are hyper-sensitive to MMS. *WT* or strains expressing *slx4-S486A* or the *slx4-7A* as only copy of Slx4 from the *SLX4* promoter were spotted in 5-fold serial dilutions on MMS-containing media and assayed for growth after two days. **B** Replication fork stalling is prolonged in the *slx4-S486A* and *slx4-7A* mutant. Cells were treated with a pulse of MMS during S-phase and recovery was analysed by pulsed-field gel electrophoresis to measure intact, fully replicated chromosomes. For

quantification, the fluorescence signal of chromosomes that migrated into the gel was divided by the total signal including the pocket and all signals normalized to the G1 sample from each strain. **C** The *Slx4-7A* and *Slx4-S486A* mutant proteins show reduced binding to Mms4 and Dpb11. Co-immunoprecipitation of endogenous Dpb11 and Slx4 with Mms4^{3FLAG} in combination with phosphorylation-deficient mutants of Slx4, S486A or 7A, or Slx4 deletion from G2/M arrested cells.

Figure S4.

Analysis of composition and function of the Slx4-Dpb11 complex.

A Slx4 and Dpb11 are part of a multi-protein complex containing Rtt107 and Slx1. Co-immunoprecipitations of Dpb11^{3FLAG} (left panel) and Slx4^{3FLAG} (right panel) were compared to purifications from untagged control strains using a SILAC setup. Cells were treated with 0.033% MMS, whereby strains containing Dpb11^{3FLAG}/Slx4^{3FLAG} were grown in heavy ($^{15}N_2$ $^{13}C_6$ lysine (Lys8) and $^{15}N_4$ $^{13}C_6$ arginine (Arg10)) medium, untagged control strains in light medium. Proteins shown in red are enriched in both purifications (Dpb11, Slx4, Rtt107, Slx1). The best scoring MS-MS spectra of the Slx4 peptide containing phosphorylated S486A from the Dpb11^{3FLAG} CoIP is shown. This peptide showed an H/L ratio of 17 in the Dpb11^{3FLAG} pulldown. **B** The *slx4-S486A* mutant is slightly sensitive to 4-NQO (in addition to MMS (Fig. 3B)), but not to other DNA damaging drugs. *WT* cells or the *slx4-S486A* mutant were spotted in 5-fold serial dilutions on media containing phleomycin, HU, CPT, cisplatin and 4-NQO and assayed for growth after two days. **C** The *slx4-S486A* mutant has a similar recombination rate compared to *WT*.

Recombination rates were measured using an intrachromosomal direct-repeat system (*leu2-112*::URA3::*leu2-k*, Aguilera and Klein 1988). Fluctuation analysis was performed using 10 independent cultures and recombinants were determined by plating on plates lacking leucine or leucine and uracil. Single colonies were counted and recombination rates were calculated using a maximum-likelihood method. The shown values represent means of three independent experiments. Error bars represent standard deviations. **D** The checkpoint response after treatment with DSB-inducing agents is similar in *WT* and *slx4-S486A* cells. Cells were treated with a 30 min pulse of 50 µg/ml phleomycin or zeocin during G2/M- or S-phase (see samples +Phl/+Zeo) and recovery was analysed by checkpoint activity as determined by anti-Rad53 western blot (upper panel) and by cellular DNA content as determined by FACS (lower panel).

Figure S5.

The Slx4-Dpb11 complex is not exclusively involved in either post-replicative repair (PRR) or homologous recombination (HR).

A A defect in the Dpb11-Slx4 complex further enhances the hyper-sensitivity of PRR and HR mutants. Strains expressing *slx4-S486A* as endogenous copy of Slx4 alone or in combination with mutants defective in error-free PRR (*mms2Δ*, *rad5-KT538,539AA* and *rad5-C914S*), error-prone PRR (*rev1Δ*, *rev3Δ* and *rad30Δ*) or HR (*rad51Δ*) were spotted in 5-fold serial dilutions on MMS-containing media and assayed for growth after two days. **B** The spontaneous mutagenesis rate of the *slx4-S486A* mutant is similar to *WT*. A forward mutagenesis assay was performed using a *CAN1* tester strain and

resistance to canavanine. Fluctuation analysis was carried out with 10 independent cultures. Colonies on canavanine-containing plates were counted and mutation rates were determined using a maximum-likelihood approach. The mean from 2 independent experiments is shown. Error bars represent standard deviations. **C** Up-regulation of HR at replication forks does not rescue the MMS hyper-sensitivity of *slx4-S486A* mutants. Strains expressing *WT* Slx4 or *slx4-S486A* in combination with *siz1Δ* or *srs2ΔC* were spotted as in A.

Figure S6.

The Slx4-Dpb11 complex is involved in JM resolution by Mus81-Mms4 and functions separately from Sgs1, Yen1 and Rad1-Rad10.

A DNA joint molecules form to a similar extent in *sgs1Δ* and *sgs1Δ slx4-S486A*. Cells were treated with 0.033% MMS in S-phase and after 90', 150' and 210' X-shaped JMs were visualized as spike signals in 2D gels. **B** JM structures are resolved slower in *slx4Δ tc-sgs1* cells. A conditional *sgs1* (*tc-sgs1)* allele was used because of *sgs1Δ slx4Δ* lethality (Mullen et al. 2001). In the *tc-sgs1* allele, Sgs1 translation is prevented upon addition of tetracycline (Gonzalez-Huici et al. 2014). *C*ells were treated with a pulse of MMS in S-phase and the profile of recombination intermediates was examined 0 h, 2 h, 3 h, 4 h and 6 h after release from MMS. X-shaped JMs were visualized as spike signal in 2D gels in *tc-sgs1* and *slx4Δ tc-sgs1* mutants. **C** The JM resolution defect in *slx4-S486A* mutants is weaker than in *mms4Δ* and both mutants show epistasis. *Tc-sgs1* inactivation and experiment as in B, but

samples were examined 0 h, 2 h, 3 h, 4 h and 5 h after release from MMS. **D** The Slx4-Dpb11 complex function in response to MMS is not related to the structure-specific endonucleases Rad1-Rad10, Slx1 or Yen1. Strains expressing *slx4-S486A* as endogenous copy of Slx4 alone or in combination with *rad1Δ, slx1Δ* and *yen1Δ* were spotted in 5-fold serial dilutions on MMS-containing media and assayed for growth after two days. **E** The *yen1Δ* increases MMS sensitivity of the *sgs1Δ slx4-S486A* double mutant, but not of either single mutant. *yen1Δ*, *sgs1Δ*, *slx4-S486A* mutants alone and double and triple mutant combinations were spotted as in D.

Figure S7.

Slx4 and Mus81 structures co-localize with Dpb11 anaphase bridge. A Quantification of Slx4 and Mus81 foci and bridges at Dpb11 anaphase bridges. *WT* or *sgs1*Δ cells expressing Dpb11^{CFP} and Slx4^{YFP}, Slx4-S486A^{YFP} or Mus81^{YFP} were subjected to live cell fluorescence microscopy. Representative examples of Slx4 and Mus81 foci and bridges co-localizing with Dpb11 anaphase bridges are shown. Scale bar, 3 μm. Yellow arrowhead marks foci. Error bars correspond to 95% confidence intervals. **B** Slx4^{YFP} and Mus81^{YFP} show a partial co-localization with Dpb11^{CFP} in spontaneous and DNA damage induced foci. Cells were treated with 0.03% MMS or 200 μg/ml zeocin for 1 h and co-localization (green arrow) of Dpb11^{CFP} with Slx4^{YFP} (top panel) and Mus81^{YFP} (lower panel) in foci was scored manually. Error bars correspond to 95% confidence intervals. Arrowheads mark foci.

Figure S8.

Mus81-Mms4 forms a complex with Dpb11 and Slx4.

A Mus81-Mms4 from mitotic cells binds specifically to Dpb11, Slx4 and Rtt107. A SILAC MS experiment comparing an Mms4^{3FLAG} IP to a control IP from an untagged strain using $^{15}N_2$ $^{13}C_6$ lysine (Lys8) and Lys-C digestion is shown. All cells were arrested in mitosis by nocodazole. H/L ratios from two label-switch experiments without ratio count cut-off are plotted. #, as the only protein of the analysis Dpb11 displayed exclusively peptides, which were derived from the Mms4^{3FLAG} IP samples, but not the control samples, making Dpb11 a highly specific interactor of Mus81-Mms4. **B** Slx4, Dpb11 and Mus81-Mms4 are part of one multi-protein complex. Mms4^{3FLAG} immunoprecipitates (as in A) from G2/M arrested cells were subjected to glycerol gradient (10%-30%) centrifugation. Slx4, Dpb11 and Mms4 co-migrate in fractions 18-20 (marked by box), corresponding to a multi-protein complex with an apparent molecular weight of 1-1.5 MDa. Arrowheads indicate elution peaks of single proteins. **C** The Dpb11-Mms4 interaction is independent of Slx4. Two-hybrid analysis in WT and *slx4Δ* cells with Gal4-BD-Dpb11 and Gal4-AD-Mms4. **D** Dpb11 and Slx4 binding to Mms4 is partially phosphatase-sensitive. Mms4^{3FLAG} immunoprecipitates (as in A) from G2/M arrested cells were either mock treated or treated with 24,000 U/ml λ-phosphatase for 20 min at 4°C. Shown is the phosphatase eluate and a 3xFLAG peptide-eluate of the remaining bound material.

Figure S9.

Mus81-Mms4 show a Cdc5-dependent association with Slx4-Dpb11 in mitosis. A Mms4 interaction with the Slx4-Dpb11 complex is dependent on Polo-like kinase Cdc5 activity. *CDC5* was expressed from a pGAL1-10 promoter. Cells were grown in raffinose-containing medium, arrested in G1, then expression was either induced in G1 by switching cells to galactose-containing medium prior to G2/M arrest (lane 2) or shut-off in G1 by switching cells to glucose-containing medium (lane 3). Co-immunoprecipitations of Mms4^{3FLAG} were performed from the corresponding cell extracts and tested for binding to Dpb11 and Slx4. **B** CDK activity is not influenced by interfering with Cdc5 activity. TCA samples of experiments shown in Fig. 5C and Fig. S9A were tested for CDK-mediated phosphorylation of Rad9-T474 by using a phospho-specific antibody in western blot analysis. The asterisk denotes a cross-reactive band. **C** The Slx4-Dpb11 interaction is not dependent on the Polo-like kinase Cdc5. Co-immunoprecipitation of Dpb11 and Slx4^{3FLAG} from G2/M arrested cells or G2/M arrested cells, in which Cdc5 has been inactivated by using the *cdc5-as1* allele and 10 µM CMK. **D** The formation of the Slx4-Dpb11-Mms4-Mus81 complex is not influenced by the presence of DNA damage. Co-immunoprecipitation samples of Mms4^{3FLAG} cell extracts from G2/M arrested cells, which were either damaged by 50 µg/ml phleomycin or left untreated, were tested for binding to Dpb11 and Slx4. **E** Cell cycle regulation of Mus81-Mms4 nuclease activity remains intact in the *slx4-S486A* mutant. Mms4^{3FLAG} and control IPs from cells arrested at G2/M with nocodazole (see lower panel for the inputs) were incubated with

fluorescence-labelled Holliday junction, replication fork and nicked Holliday junction substrates.

Figure S10.

Partial inactivation of the DNA damage checkpoint rescues the defects of the *slx4-S486A* mutant in response to MMS.

A A partial defect in DNA damage checkpoint signalling suppresses the *slx4-S486A* mutant hyper-sensitivity to MMS. Strains expressing *slx4-S486A* in combination with mutants defective in DNA damage checkpoint signalling (*dot1Δ, ddc1-T602A* and *rad53-3HA)* were spotted in 5-fold serial dilutions on MMS-containing media and assayed for growth after two days. **B** The *slx4-S486A* mutant recovers faster after a partial inactivation of the DNA damage checkpoint. *WT*, *slx4-S486A* and *slx4-S486A ddc1-T602A* mutant cells were treated with a pulse of 0.033% MMS during S-phase, and recovery was analysed by cellular DNA content as determined by FACS (upper panel) and by checkpoint activity as determined by anti-Rad53 western blot (lower panel). **C** Yen1 and Sgs1 are not required for the rescue of the *slx4-S486A* MMS hyper-sensitivity by partial checkpoint inactivation. MMS hyper-sensitivity phenotypes of *slx4-S486A*, *sgs1Δ*, *yen1Δ*, *ddc1-T602A* mutants and double or triple mutant combinations were spotted in 5-fold serial dilutions on MMS-containing media and assayed for growth after two (lower panel) or three (upper panel) days.

Supplemental Methods

Yeast strains

All yeast strains are based on W303 (Thomas and Rothstein 1989). Genotypes are listed below. All biochemical experiments were performed in a W303-1A *pep4Δ* background. The genetic studies in Fig. 3B-E, 4, 6A-E and Fig. S3A-B, S4B-D, S5, S6, S10 were performed in a W303 *RAD5+* background to exclude any effect from a partial defect of the *rad5-535* allele, but similar results were obtained using W303-1A. Two-hybrid analyses were performed in the strain PJ69-7A (James et al. 1996).

S. cerevisiae strains were prepared by genetic crosses and transformation techniques. Deletion of particular genes and endogenous protein tagging were performed as described (Knop et al. 1999). Correct integrations were checked by genotyping PCR. Denaturing cell extracts were prepared by alkaline lysis and TCA precipitation (Knop et al. 1999). The *slx4-S486A* allele was generated using site-directed mutagenesis and integrated as a linear plasmid at the TRP1 locus.

List of strains used in this study.

Strain	Full genotype	Relevant genotype	Source
1093-5A	MATa *ADE2+ RAD5+ CAN1+ ura3-1 his3-11,15 trp1-1 leu2-3,112*	*CAN1+*	Klein lab
FY1060	MATa *RAD5+ ade2-1 ura3-1 his3-11,15 trp1-1 leu2-3,112 can1-100 GAL PSI+ sgs1::HIS3*	*sgs1*	Branzei lab
HY4021	MATa *RAD5+ ade2-1 trp1-1 leu2-3,112 his3-11,15 ura3-1 can1-100 sgs1::pADH1-tc3-3xHA-Sgs1*	*Tc-SGS1*	Branzei lab

	(NATMX)		
HY4072	MATa *RAD5+ ade2-1 trp1-1 leu2-3,112 his3-11,15 ura3-1 can1-100 slx4::HIS3 sgs1::pADH1-tc3-3xHA-Sgs1 (HPHMX4)*	*slx4 Tc-SGS1*	Branzei lab
ML664-10A	MATa *tTA(tetR-VP16)-tetO$_2$-DPB11-4ala-YFP*::*KanMX NLS-yEmRFPrv::URA3 SPC110-CFP::KAN*	*DPB11-YFP SPC110-CFP*	Lisby lab
ML678-12B	MATa *tTA(tetR-VP16)-tetO$_2$-DPB11-4ala-YFP*::*KanMX NLS-yEmRFPrv::URA3 SPC110-CFP::KanMX sgs1::HIS3*	*DPB11-YFP SPC110-CFP sgs1*	Lisby lab
ML779-4A	MATa *tTA(tetR-VP16)-tetO$_2$-DPB11-4ala-YFP*::*KanMX NLS-yEmRFPrv::URA3 SPC110-CFP::KanMX slx4::KanMX*	*DPB11-YFP SPC110-CFP slx4*	Lisby lab
ML781-8D	MATa *tTA(tetR-VP16)-tetO$_2$-DPB11-4ala-YFP*::*KanMX NLS-yEmRFPrv::URA3 SPC110-CFP::KanMX slx4::KanMX trp1-1::slx4-S486A::TRP1*	*DPB11-YFP SPC110-CFP slx4 slx4-S486A*	Lisby lab
ML798-4C	MATa *tTA(tetR-VP16)-tetO$_2$-DPB11-4ala-YFP*::*KanMX NLS-yEmRFPrv::URA3 SPC110-CFP::KanMX slx4::KanMX trp1-1::slx4-S486A::TRP1 sgs1::HIS3*	*DPB11-YFP SPC110-CFP slx4 slx4-S486A sgs1*	Lisby lab
ML789-7D	MATa *ade2-1 ura3-1 his3-11,15 trp1-1 leu2-3,112 can1-100 tTA(tetR-VP16)-tetO$_2$-DPB11-4ala-CFP::KanMX SLX4-4ala-YFP*	*DPB11-CFP SLX4-YFP*	Lisby lab
ML799-2C	MATa *tTA(tetR-VP16)-tetO$_2$-DPB11-4ala-CFP*::*KanMX SLX4-YFP sgs1::HIS3*	*DPB11-CFP SLX4-YFP sgs1*	Lisby lab
ML806-3C	MATa *tTA(tetR-VP16)-tetO$_2$-DPB11-4ala-CFP*::*KanMX slx4-S486A-YFP*	*DPB11-CFP slx4-S486A-YFP*	Lisby lab
ML806-3A	MATa *tTA(tetR-VP16)-tetO$_2$-DPB11-4ala-CFP*::*KanMX slx4-S486A-YFP sgs1::HIS3*	*DPB11-CFP slx4-S486A-YFP sgs1*	Lisby lab
ML792-2D	MATa *ade2-1 ura3-1 his3-11,15 trp1-1 leu2-3,112 can1-100*	*DPB11-CFP MUS81-YFP*	Lisby lab

	tTA(tetR-VP16)-tetO$_2$-DPB11-4ala-CFP::KanMX MUS81-4ala-YFP		
ML800-9A	MATa *tTA(tetR-VP16)-tetO$_2$-DPB11-4ala-CFP*::*KanMX MUS81-YFP sgs1::HIS3*	*DPB11-CFP MUS81-YFP sgs1*	Lisby lab
Y2050	MATα *ade2-1 trp1-1 his3-11 his3-15 can1-100 leu2-112::URA3::leu2-k*	*leu2-112::URA3::leu2-k*	Jentsch lab
YBP388	MATa *ade2-1 ura3-1 his3-11,15 leu2-3,112 can1-100 leu2-3,112::pep4::LEU2*	*pep4*	This study
YBP392	MATa *ade2-1 ura3-1 his3-11,15 leu2-3,112 can1-100 trp1-1::bar1::TRP1 leu2-3,112::pep4::LEU2*	*bar1 pep4*	This study
YBP418-1	MATa *ade2-1 ura3-1 his3-11,15 can1-100 lys1::NAT-NT2 arg4::hph-NT1 trp1-1::bar1::TRP1 leu2-3,112::pep4::LEU2 SLX4-3FLAG::KanMx4*	*lys1 SLX4-3FLAG*	This study
YBP420	MATa *ade2-1 ura3-1 his3-11,15 can1-100 arg4::hph-NT2 lys1::NAT-NT1 leu2-3,112::pep4::LEU2 trp1-1::bar1::TRP1*	*lys1 arg4*	This study
YBP422	MATa *ade2-1 ura3-1 his3-11,15 can1-100 arg4::hph-NT2 lys1::NAT-NT1 leu2-3,112::pep4::LEU2 trp1-1::bar1::TRP1 DPB11-3FLAG::KanMx*	*lys1 arg4 DPB11-3FLAG*	This study
YDG40	MATα *ade2-1 ura3-1 his3-11,15 leu2-3,112 can1-100 slx4::kanMx4 trp1-1::slx4-S486A::TRP1*	*slx4-S486A*	This study
YDG66	MATa *ade2-1 ura3-1 his3-11,15 trp1-1 leu2-3,112 can1-100 rad51::natNT2*	*rad51*	This study
YDG96	MATα *ade2-1 trp1-1 his3-11 his3-15 can1-100 leu2-112::URA3::leu2-k slx4::kanMx slx4-S486A::TRP1*	*leu2-112::URA3::leu2-k slx4-S486A*	This study

YDG126	MATa *ade2-1 ura3-1 his3-11,15 trp1-1 leu2-3,112 can1-100 rad1::hphNTI*	*rad1*	This study
YDG134	MATa *ade2-1 ura3-1 his3-11,15 trp1-1 leu2-3,112 can1-100 slx1::hphNTI*	*slx1*	This study
YDG135	MATa *ade2-1 ura3-1 his3-11,15 leu2-3,112 can1-100 slx4::KanMx trp1-1::slx4-S486A::TRP1 slx1::hphNTI*	*slx4-S486A slx1*	This study
YDG150	MATa *ade2-1 ura3-1 his3-11,15 trp1-1 leu2-3,112 can1-100 mms2::hphNTI*	*mms2*	This study
YDG151	MATα *ade2-1 ura3-1 his3-11,15 leu2-3,112 can1-100 slx4::kanMx trp1-1::slx4-S486A::TRP1 mms2::hphNTI*	*slx4-S486A mms2*	This study
YDG175	MATa *ade2-1 ura3-1 his3-11,15 trp1-1 leu2-3,112 can1-100 rad5::hphNTI*	*rad5*	This study
YDG182	MATa *ade2-1 ura3-1 his3-11,15 leu2-3,112 can1-100 slx4::kanMx trp1-1::slx4-S486A::TRP1 rad51::hphNT1*	*slx4-S486A rad51*	This study
YDG183	MATa *ade2-1 ura3-1 his3-11,15 trp1-1 leu2-3,112 can1-100 rev1::hphNT1*	*rev1*	This study
YDG184	MATa *ade2-1 ura3-1 his3-11,15 leu2-3,112 can1-100 slx4::kanMx trp1-1::slx4-S486A::TRP1 rev1::hphNT1*	*slx4-S486A rev1*	This study
YDG185	MATa *ade2-1 ura3-1 his3-11,15 trp1-1 leu2-3,112 can1-100 rev3::hphNT1*	*rev3*	This study
YDG186	MATa *ade2-1 ura3-1 his3-11,15 leu2-3,112 can1-100 slx4::kanMx trp1-1::slx4-S486A::TRP1 rev3::hphNT1*	*slx4-S486A rev3*	This study
YDG187	MATa *ade2-1 ura3-1 his3-11,15 trp1-1 leu2-3,112 can1-100 rad30::hphNT1*	*rad30*	This study
YDG188	MATa *ade2-1 ura3-1 his3-11,15 leu2-3,112 can1-100 slx4::kanMx*	*slx4-S486A rad30*	This study

	trp1-1::slx4-S486A::TRP1 rad30Δ::hphNT1		
YDG189	MATa *RAD5+ ade2-1 ura3-1 leu2-3,112 can1-100 slx4::kanMx trp1-1::slx4-S486A::TRP1 his3-11,15::sgs1::HIS3*	*slx4-S486A sgs1*	This study
YDG190	MATa *RAD5+ ade2-1 ura3-1 his3-11,15 leu2-3,112 can1-100 slx4::kanMx trp1-1::slx4-S486A::TRP1*	*slx4-S486A*	This study
YDG206	MATα *RAD5+ CAN1+ ADE2+ ura3-1 his3-11,15 leu2-3,112 slx4::kanMx4 trp1-1::slx4-S486A::TRP1*	*CAN1+ slx4-S486A*	This study
YDG207	MATa *CAN1+* ADE2+ *ura3-1 his3-11,15 trp1-1 leu2-3,112 rad5::hphNT1*	*CAN1+ rad5*	This study
YDG209	MATa *ade2-1 his3-11,15 trp1-1 leu2-3,112 can1-100 rad5::hphNT1 ura3-1::RAD5+::URA3*	*rad5 RAD5+*	This study
YDG211	MATa *ade2-1 his3-11,15 trp1-1 leu2-3,112 can1-100 rad5::hphNT1 ura3-1::rad5+-C914S::URA3*	*rad5+-C914S*	This study
YDG212	MATa *ade2-1 his3-11,15 leu2-3,112 can1-100 slx4::kanMx4 trp1-1::slx4-S486A::TRP1 rad5::hphNT1 ura3-1::RAD5+::URA3*	*slx4-S486A rad5Δ RAD5+*	This study
YDG214	MATa *ade2-1 his3-11,15 leu2-3,112 can1-100 slx4::kanMx4 trp1-1::slx4-S486A::TRP1 rad5::hphNT1 ura3-1::rad5+-C914S::URA3*	*slx4-S486A rad5+-C914S*	This study
YDG217	MATa *RAD5+ ade2-1 his3-11,15 trp1-1 ura3-1 leu2-3,112 can1-100 srs2ΔC::hphNT1*	*srs2ΔC*	This study
YDG218	MATa *RAD5+ ade2-1 his3-11,15 ura3-1 leu2-3,112 can1-100 slx4::kanMx4 trp1-1::slx4-S486A::TRP1 srs2ΔC::hphNT1*	*slx4-S486A srs2ΔC*	This study
YDG219	MATa *RAD5+ ade2-1 his3-11,15*	*siz1*	This

	trp1-1 ura3-1 leu2-3,112 can1-100 siz1::hphNT1		study
YDG220	MATa *Rad5+ ade2-1 his3-11,15 ura3-1 leu2-3,112 can1-100 slx4::kanMx4 trp1-1::slx4-S486A::TRP1 siz1::hphNT1*	*slx4-S486A siz1*	This study
YDG240	MATa *ade2-1 his3-11,15 trp1-1 leu2-3,112 can1-100 rad5::hphNT1 ura3-1::rad5+-KT538,539AA::URA3*	*rad5+-KT538,539AA*	This study
YDG241	MATa *ade2-1 his3-11,15 leu2-3,112 can1-100 rad5::hphNT1 ura3-1:rad5+-KT538,539AA::URA3 slx4::kanMx4 trp1-1::slx4-S486A::TRP1*	*slx4-S486A rad5+-KT538,539AA*	This study
YDG251	MATa *RAD5+ ade2-1 leu2-3,112 ura3-1 trp1-1 can1-100 his3-11,15::rad53-3HA::HIS3*	*rad53-3HA*	This study
YDG252	MATa *RAD5+ ade2-1 leu2-3,112 ura3-1 can1-100 slx4Δ::kanMx4 trp1-1::slx4-S486A::TRP1 his3-11,15::rad53-3HA::HIS3*	*slx4-S486A rad53-3HA*	This study
YDG287	MATa *RAD5+ ade2-1 his3-11,15 leu2-3,112 ura3-1 can1-100 slx4::kanMx4 trp1-1::slx4-S486A::TRP1 dot1::natNT2*	*slx4-S486A dot1*	This study
YDG288	MATa *RAD5+ ade2-1 his3-11,15 leu2-3,112 ura3-1 can1-100 slx4::kanMx4 trp1-1::slx4-S486A::TRP1 ddc1-T602A::natNT2*	*slx4-S486A ddc1-T602A*	This study
YDG289	MATa *RAD5+ ade2-1 his3-11,15 leu2-3,112 trp1-1 ura3-1 can1-100 mms4::hphNT1*	*mms4*	This study
YDG290	MATa *RAD5+ ade2-1 his3-11,15 leu2-3,112 ura3-1 can1-100 slx4::kanMx4 trp1-1::slx4-S486A::TRP1 mms4::hphNT1*	*slx4-S486A mms4*	This study
YDG291	MATa *RAD5+ ade2-1 his3-11,15 leu2-3,112 trp1-1 ura3-1 can1-100 yen1::hphNT1*	*yen1*	This study
YDG292	MATa *RAD5+ ade2-1 his3-11,15*	*slx4-S486A yen1*	This

	leu2-3,112 ura3-1 can1-100 slx4::kanMx4 trp1-1::slx4-S486A::TRP1 yen1::hphNT1		study
YDG293	MATa *RAD5+ ade2-1 his3-11,15 leu2-3,112 ura3-1 can1-100 slx4::kanMx trp1-1::DPB11-slx4-S486A::TRP1*	*DPB11-slx4-S486A*	This study
YDG295	MATa *RAD5+ ade2-1 his3-11,15 leu2-3,112 ura3-1 can1-100 slx4::kanMx4 trp1-1::slx4-S486A::TRP1 ddc1-T602A::natNT2 yen1::hphNT1*	*slx4-S486A ddc1-T602A yen1*	This study
YDG296	MATa *RAD5+ ade2-1 his3-11,15 leu2-3,112 trp1-1 ura3-1 can1-100 ddc1-T602A::natNT2 yen1::hphNT1*	*ddc1-T602A yen1*	This study
YDG329	MATa *RAD5+ ade2-1 ura3-1 his3-11,15 trp1-1 leu2-3,112 can1-100 sgs1::hphNT1*	*sgs1*	This study
YDG303	MATa *Rad5+ ade2-1 his3-11,15 leu2-3,112 trp1-1 ura3-1 can1-100 ddc1-T602A::natNT2*	*ddc1-T602A*	This study
YDG304	MATa *RAD5+ ade2-1 his3-11,15 leu2-3,112 trp1-1 ura3-1 can1-100 dot1::natNT2*	*dot1*	This study
YDG309	MATa *RAD5+ ade2-1 his3-11,15 leu2-3,112 ura3-1 can1-100 slx4::kanMx4 trp1-1::slx4-S486A::TRP1 ddc1-T602A::natNT2 mms4::hphNT1*	*slx4-S486A ddc1-T602A mms4*	This study
YDG310	MATa *RAD5+ ade2-1 his3-11,15 leu2-3,112 trp1-1 ura3-1 can1-100 ddc1-T602A::natNT2 mms4::hphNT1*	*ddc1-T602A mms4*	This study
YDG313	MATa *RAD5+ ade2-1 his3-11,15 leu2-3,112 ura3-1 can1-100 slx4::kanMx4 trp1-1::slx4-S486A::TRP1 ddc1-T602A::natNT2 sgs1::hphNT1*	*slx4-S486A ddc1-T602A sgs1*	This study
YDG314	MATa *RAD5+ ade2-1 his3-11,15 leu2-3,112 trp1-1 ura3-1 can1-100 ddc1-T602A::natNT2 sgs1::hphNT1*	*ddc1-T602A sgs1*	This study

YDG335	MATa *RAD5+ ade2-1 ura3-1 his3-11,15 leu2-3,112 trp1-1 can1-100 mus81Δ::hphNT1*	*mus81*	This study
YDG336	MATa *RAD5+ ade2-1 ura3-1 his3-11,15 leu2-3,112 can1-100 slx4::kanMx4 trp1-1::slx4-S486A::TRP1 mus81::hphNT1*	*slx4-S486A mus81*	This study
YDG339	MATa *RAD5+ ade2-1 ura3-1 his3-11,15 trp1-1 leu2-3,112 can1-100 MMS4-3FLAG::hphNTI*	*MMS4-3FLAG*	This study
YDG340	MATa *RAD5+ ade2-1 ura3-1 his3-11,15 leu2-3,112 can1-100 slx4::kanMx trp1-1::slx4-S486A::TRP1 MMS4-3FLAG::hphNTI*	*slx4-S486A MMS4-3FLAG*	This study
YDG355	MATa *RAD5+ ade2-1 his3-11, 15 trp1-1 ura3-1 can1-100 mms4::hphNTI leu2-3,112::mms4SS184,201AA::LEU2*	*mms4-SS184,201AA*	This study
YDG356	MATa *RAD5+ ade2-1 trp1-1 ura3-1 can1-100 mms4::hphNTI leu2-3,112::mms4SS184,201AA::LEU2 his3-11,15::sgs1::HIS3*	*mms4-SS184,201AA sgs1*	This study
YDG366	MATa *RAD5+ ade2-1 his3-1,15 leu2-3,112 ura3-1 can1-100 slx4::kanMx trp1-1::slx4-S486A::TRP1 ddc1-T602A::natNT2 MMS4-3FLAG::hphNTI*	*slx4-S486A ddc1-T602A MMS4-3FLAG*	This study
YDG375	MATa *RAD5+ ade2-1 ura3-1 his3-11,15 leu2-3,112 can1-100 slx4::NAT trp1-1::slx4-7A::TRP1*	*slx4-T457A, T474A, S499A, T597A, S627A, S659A, S725A*	This study
YDG376	MATa *RAD5+ ade2-1 ura3-1 his3-11,15 trp1-1 leu2-3,112 can1-100 yen1::hphNT1 sgs1::natNT2*	*yen1 sgs1*	This study
YDG377	MATa *RAD5+ ade2-1 ura3-1 his3-11,15 leu2-3,112 can1-100 slx4::kanMx trp1-1::slx4-S486A::TRP1 yen1Δ::hphNT1 sgs1::natNT2*	*slx4-S486A yen1 sgs1*	This study

YKR44	MATa *ade2-1 ura3-1 his3-11 his3-15 can1-100 trp1-1::bar1::TRP1 leu2-3,112::pep4::LEU2 DPB11-9myc::KanMX4*	*DPB11-9myc*	This study
YLP15	MATa *ade2-1 ura3-1 his3-11 his3-15 can1-100 trp1-1::bar1::TRP1 leu2-3,112::pep4::LEU2 lys1::nat-NT2*	*lys1*	This study
YLP18	MATa *ade2-1 ura3-1 can1-100 trp1-1::bar1::TRP1 leu2-3,112::pep4::LEU2 lys1::nat-NT2 his3-11,15::SLX4-3FLAG::HisMx*	*lys1 SLX4-3FLAG*	This study
YLP30	MATa *ade2-1 ura3-1 trp1-1 leu2-3,112 can1-100 pep4::NAT slx4::KanMx his3-11,15::slx4-S486A-3FLAG::HISMx*	*slx4-S486A-3FLAG*	This study
YLP41	MATa *ade2-1 ura3-1 trp1-1 leu2-3,112 can1-100 his3-11,15::slx4-S486A-3FLAG::HisMx pep4::NAT lys1::hph*	*lys1 slx4-S486A-3FLAG*	This study
YLP42	MATa *ade2-1 his3-11 his3-15 can1-100 trp1-1::bar1::TRP1 leu2-3,112::pep4::LEU2 SLX4-3FLAG::KanMx4 ura3-1::cdc28as-1 F88G::URA3*	*SLX4-3FLAG cdc28-as1*	This study
YLP43	MATa *ade2-1 his3-11,15 can1-100 lys1::hph trp1-1::bar1::TRP1 leu2-3,112::pep4::LEU2 SLX4-3FLAG::KanMx4 ura3-1::cdc28as-1 F88G::URA*	*lys1 SLX4-3FLAG cdc28-as1*	This study
YLP47	MATa *ade2-1 ura3-1 can1-100 trp1-1::bar1::TRP1 leu2-3,112::pep4::LEU2 his3-11,15::DPB11-3Flag::HIS3*	*DPB11-3FLAG*	This study
YLP57	MATa *RAD5+ ade2-1 ura3-1 trp1-1 leu2-3,112 can1-100 MMS4-3Flag::hphNTI his3-11,15::pep4::HIS3*	*MMS4-3FLAG*	This study
YLP59	MATa *ade2-1 ura3-1 trp1-1 leu2-3,112 can1-100 MMS4-3Flag::hph-NT1 his3-11,15::pep4::HIS3Mx4 pGAL1-*	*MMS4-3FLAG pGal1-Cdc5*	This study

	CDC5::KanMx		
YLP62	MATa *ade2-1 ura3-1 leu2-3,112 can1-100 MMS4-3Flag::hph-NT1 his3-11,15::pep4::HIS3Mx4 slx4::KanMx trp1-1::slx4-S486A::TRP1*	*MMS4-3FLAG slx4-S486A*	This study
YLP63	MATa *RAD5+ ade2-1 ura3-1 trp1-1 leu2-3,112 can1-100 cdc5-as1 MMS4-3Flag::hph-NT1 his3-11,15::pep4::HIS3Mx4*	*MMS4-3FLAG cdc5-as1*	This study
YLP64	MATa *RAD5+ ade2-1 leu2-3,112 ura3-1 can1-100 slx4::kanMx trp1-1::slx4-S486A::TRP1 ddc1T602A:: natNT2 MMS4-3Flag::hphNTI his3-11,15::pep4::HIS3Mx4*	*MMS4-3FLAG slx4-S486A ddc1-T602A*	This study
YLP78	MATa *ade2-1 leu2-3,112 trp1-1 ura3-1 can1-100 MMS4-3Flag::hph-NT1 his3-11,15::pep4::HIS3Mx4 slx4::KanMx*	*MMS4-3FLAG slx4*	This study
YLP80	MATa *RAD5+ ade2-1 leu2-3,112 ura3-1 can1-100 MMS4-3Flag::hph-NT1 his3-11,15::pep4::HIS3Mx4 slx4::KanMx trp1-1::Slx4 T457A, T474A, S499A, T597A, S627A, S659A, S725A::TRP1*	*MMS4-3FLAG slx4-T457A, T474A, S499A, T597A, S627A, S659A, S725A*	This study
YLP83	MATa *RAD5+ ade2-1 his3-1,15 trp1-1 ura3-1 can1-100 leu2-3,112::pep4::LEU2 SLX4-3Flag::KanMx4 cdc5-as1*	*SLX4-3FLAG cdc5-as1*	This study
YLP87	MATa *RAD5+ ade2-1 leu2-3,112 trp1-1 ura3-1 can1-100 his3-11,15::pep4::HIS*	*pep4*	This study
YLP88	MATa *RAD5+ ade2-1 leu2-3,112 ura3-1 can1-100 slx4Δ::kanMx trp1-1::slx4-S486A::TRP1 MMS4-3Flag::hphNTI his3-11,15::pep4::HIS*	*MMS4-3FLAG slx4-S486A*	This study
YSB79	MATa *RAD5+ ade2-1 ura3-1 his3-11,15 leu2-3,112 trp1-1 can1-100 RFA1-*	*RFA1-3xmCherry*	This study

	3xmCherry::hphNT1		
YSB86	MATa *RAD5+ ade2-1 ura3-1 his3-11,15 leu2-3,112 trp1-1 can1-100 RFA1-3xmCherry::hphNT1 slx4::kanMx4 trp1-1:Slx4-S486A::TRP1*	*RFA1-3xmCherry slx4-S486A*	This study
YSS3	MATa *ade2-1 ura3-1 trp1-1 leu2-3,112 can1-100 MMS4-3Flag::hph-NT1 his3-11,15::pep4::HIS3Mx4*	*MMS4-3FLAG*	This study
YSS5	MATa *ade2-1 ura3-1 his3-11,15 can1-100 trp1-1::bar1::TRP1 leu2-3,112::pep4::LEU2 SLX4-3Flag::KanMx4*	*SLX4-3FLAG*	This study

Synchronization by α-factor and nocodazole

Logarithmic growing cells were synchronized in G2/M-phase by nocodazole (5 μg/ml), or in G1-phase by α-factor (5-10 μg/ml, or 167 ng/ml for *bar1* cells). The release from synchronization was performed by washing once in YPD, and suspending cells in YPD with 0.033% or 0.04% MMS. For recovery experiments, cells were washed after 30' (45' in Fig. 6E, S3B) of damage treatment, and suspended in drug free YPD media with (Fig. 5D, 6E-F) or without nocodazole.

Drug treatment

DNA damage in liquid cultures was induced by MMS (final concentration 0.033%, or 0.04% (Fig. 3C-E, 6D)) or phleomycin/zeocin (final concentration 50 μg/ml).

For solid media, concentrations of methyl methanesulfonate (MMS), hydroxyurea (HU), phleomycin, cisplatin, camptothecin (CPT) or 4-nitroquinoline 1-oxide (4-NQO) were as indicated in the figures.

FACS analysis

$1x10^7$ - $2x10^7$ cells were harvested by centrifugation and resuspended in 70% ethanol + 50 mM Tris pH 7.8. After centrifugation cells were washed with 1 ml 50 mM Tris pH 7.8 (Tris buffer) followed by resuspending in 520 µl RNase solution (500 µl 50 mM Tris pH 7.8 + 20 µl RNase A (10 mg/ml in 10 mM Tris pH 7.5, 10 mM $MgCl_2$) and incubation for 4 h at 37 °C. Next, cells were treated with proteinase K (200 µl Tris buffer + 20 µl proteinase K (10 mg/ml in 50% glycerol, 10 mM Tris pH 7.5, 25 mM $CaCl_2$) and incubated for 30' at 50 °C. After centrifugation cells were resuspended in 500 µl Tris buffer. Before measuring the DNA content, samples were sonified (5''; 50% CYCLE) and stained by SYTOX solution (999 µl Tris buffer + 1 µl SYTOX). Measurement was performed using FL1 channel 520 for SYTOX-DNA on a BD FACSCalibur system.

Interaction assays

After cell growth under the indicated conditions, yeast extracts were obtained by freezer mill lysis in lysis buffer (100 mM Hepes, 200 mM KOAc, 0.1 % NP-40, 10 % glycerol, 2 mM b-ME, protease inhibitors, 100 mM ocadaic acid, 10 mM NaF, 20 mM b-glycerophosphate). Co-IP was performed for 2 hours by head-over-tail rotation at 4 °C using anti-FLAG agarose resin (Sigma). Non-specific background was removed by six washes and bound proteins were

eluted by incubation with 0.5 mg/ml 3X FLAG-peptide (Sigma). The TCA precipitated eluates were resolved on 4-12% NuPAGE gradient gels (Invitrogen), and analyzed by standard Western blotting techniques.
For GST pulldowns (Fig. S1A), GST-Dpb11 or GST-tagged protein fragments were recombinantly expressed and purified as described (Pfander and Diffley 2011). Proteins were immobilizied on glutathione sepharose 4B (GE Healthcare) and incubated with ammonium sulphate-precipitated (57%) yeast extracts (lysis buffer as described above). Non-specific background was removed by five washes and bound proteins were eluted by Laemmli buffer.
For Co-IP from HEK 293T cells were lysed in lysis buffer (see yeast lysates) for 30' on ice. Protein concentrations were determined by Bradford. GFP-tagged proteins were precipitated using GFP-Trap magnetic beads (Chromotek) and incubated for 1.5 h with head-over-tail rotation. Non-specifically bound proteins were removed by 6 washes with lysis buffer using a magnetic rack, and specifically bound proteins were eluted by Laemmli buffer.

Analysis of interacting proteins by SILAC

For Co-IP experiments followed by mass spectrometry analysis, cells deficient in lysine biosynthesis were grown in synthetic complete (SC) medium supplemented with normal lysine ("light" medium) or heavy-isotope-labeled lysine (Lys8; "heavy" medium) from Cambridge Isotope Laboratories.
For SILAC Co-IP experiments shown in Fig. S4A, cells deficient in lysine and arginine biosynthesis were grown in synthetic complete (SC) medium supplemented with normal lysine and arginine ("light" medium) or heavy-

isotope-labeled lysine and arginine (Lys8, Arg10; “heavy” medium) from Cambridge Isotope Laboratories. All other SILAC experiments were done using lysine-only labeling.

Lysates were prepared by harvesting cells in equal amounts after growth under the indicated conditions. After co-IP, eluted proteins from light and heavy cultures were pooled, TCA precipitated and separated on 4-12% NuPAGE Bis-Tris gel (Invitrogen). The gel was stained with GelCode Blue (Thermo Scientific). The gel lane was excided into ten slices and peptides were analyzed by LC-MS/MS after in-gel Lys-C or trypsin digestion. Samples were measured on an LTQ-Orbitrap and analyzed using MaxQuant (Cox and Mann 2008).

Antibodies

Proteins were detected using specific antibodies: rabbit-anti-Rad53 (JD147, J. Diffley), rabbit-anti-Dpb11 (BPF19; Pfander and Diffley 2011), rabbit-anti-Rad9-T474-P (BPF25, Pfander and Diffley 2011), rabbit-anti-Slx4 (2057, Pfander lab), goat-anti-Cdc5 (sc-6733, Santa Cruz), rabbit-anti-Clb2 (sc-9071, Santa Cruz), rabbit-anti-FLAG (Sigma), rabbit-HRP-coupled-anti-GST (Z-5; sc-459, Santa Cruz), mouse-anti-myc (clone 4A6; Millipore), mouse-anti-GFP (B2; Santa Cruz), mouse-anti-Gal4-AD (TA-C10; Santa Cruz), mouse-anti-Gal4-BD (RK5C1; Santa Cruz).

Pulsed-field gel electrophoresis

In the recovery experiments (Fig. 3D, 6B, S3B) $8x10^7$ of cells were taken for every time point and centrifuged at 5,000 x g 10 min at 4 °C. Cells were

resuspended in 1 ml cold 0.1% sodium azide and centrifuged at 3,000 rpm for 3 min. Remaining pellets were resuspended in 50 µl zymolyase buffer (50 mM EDTA, 10 mM Tris pH 8.0, 20 mM NaCl, 1 mg/ml zymolyase (T100)) and mixed with equal amount of 2% agarose. The samples were transferred to the plug mold. The plugs were incubated in zymolyase buffer at 37 °C for 1 h, followed by treatment with proteinase K (0.5 M EDTA pH 8.0, 1 mg/ml proteinase K, 10 mg/ml sodium lauryl sarcosine) at 50 °C for 24-48 h. Next, the plugs were washed 3 times with 50 mM EDTA and loaded. Electrophoresis was performed using the CHEF-DRIII pulsed-field electrophoresis system (Bio-Rad) according to the manufacturer's instructions. The gel was stained with 1 µg/ml ethidium bromide and scanned under UV light. Quantification of PFGE signals was performed using ImageJ. For every time point the signal from the bands that have entered the gel was normalized to the total signal in the lane including that from the well, and the values from every time point were normalized relative to the G1 signal.

2D gel analysis and quantification of replication/recombination intermediates

The experiments were conducted as described previously (Szakal and Branzei, 2013). The DNA samples were digested with HindIII and EcoRV and analysed with probes for ARS305. In all, 200 ml cultures (2-4x10^9 cells) were arrested by addition of sodium azide (final concentration 0.1%) and cooled down in ice. Cells were harvested by centrifugation, washed in cold water, and incubated in spheroplasting buffer (1 M sorbitol, 100 mM EDTA pH 8.0, 0.1% b-ME, and 50 U zymolase/ml) for 1.5 h at 30 °C. In all, 2 ml water, 200

µl RNase A (10 mg/ml), and 2.5 ml Solution I (2% w/v cetyl-trimethyl-ammonium-bromide (CTAB), 1.4 M NaCl, 100 mM Tris-HCl pH 7.6, and 25 mM EDTA pH 8.0) were sequentially added to the spheroplast pellets and samples were incubated for 30 min at 50 °C. In all, 200 µl proteinase K (20 mg/ml) was then added and the incubation was prolonged at 50 °C for 1 h 30 min, and at 30 °C overnight. The sample was then centrifuged at 4,000 rpm for 10 min: the cellular debris pellet was kept for further extraction, while the supernatant was extracted with 2.5 ml chloroform/isoamylalcohol (24/1) and the DNA in the upper phase was precipitated by addition of 2 volumes Solution II (1% w/v CTAB, 50 mM Tris-HCl pH 7.6, and 10 mM EDTA) and centrifugation at 8,500 rpm for 10 min. The pellet was resuspended in 2 ml Solution III (1.4 M NaCl, 10 mM Tris-HCl pH 7.6, and 1 mM EDTA). Residual DNA in the cellular debris pellet was also extracted by resuspension in 2 ml Solution III and incubation at 50 °C for 30 min, followed by extraction in 1 ml chloroform/isoamylalcohol (24/1). The upper phase was pooled together with the main DNA preparation. Total DNA was then precipitated with 1 volume isopropanol, washed with 70% ethanol, air dried, and finally resuspended in TE 1X. Quantification of X-shaped intermediate signals was performed using the Image Quant software as previously described (Liberi et al. 2005; Branzei et al. 2008; Vanoli et al. 2010). For each time point, areas corresponding to the monomer spot (M), the X-spike signal and a region without any replication intermediates as background reference were selected and the signal intensities (SIs) in percentage of each signal were obtained. The values for the X and monomer were corrected by subtracting from the SI value the background value after the latter was multiplied for the ratio between the

dimension of the area for the intermediate of interest and for background. Thus, the values for X and M were calculated in the following way:
Value for X=SI (Xs)-(SI (background) (area (Xs)/area (background));
Value for M=SI (M)-(SI (background) (area (M)/area (background)).
The relative SI for the X was then determined by dividing the value for X with the sum of the total signals (the sum of the X and monomer values). The resulting values for X signals were then normalized. For instance, for recovery experiments the relative value of X obtained after MMS treatment was considered as 100% and the other X values were normalized to it.

Mutation and recombination assays

Mutation rates were determined using a *CAN1* forward mutation assay (Klein 2001). Interchromosomal recombination rates were determined using a direct-repeat system using *leu2* heteroalleles (Aquilera and Klein 1988) and crossover rates were determined using a system harbouring two *arg4* alleles on chromosome V and VIII (Robert et al. 2006, Szakal and Branzei 2013). In all cases mutation/recombination rates were determined using fluctuation analysis and a maximum-likelihood approach. Therefore, for each strain ten independent cultures originated from the single cell were analyzed. To get single colonies 100 cells were plated or streaked out for single colonies on YPD media plates and incubated for 2 days at 30 °C. The frequency of mutants/recombinants in all cultures was determined by plating on selective media. The total cell number was determined by plating an appropriate dilution on non-selective media. For determination of CO rates, for each culture ten ARG+ colonies were picked, analyzed by PCR for CO or NCO

events (Szakal and Branzei 2013) and the overall number of crossover recombinants was extrapolated. From the number of mutants/recombinants/crossover recombinants the number of mutational/recombinational/crossover events was determined using a maximum-likelihood approach and rates were determined by dividing by the number of cell divisions (Pfander et al. 2005). For each strain 2-10 independent experiments were performed to determine mean and standard deviation.

Microscopy and immunofluorescence

Yeast cells were grown in synthetic complete (SC) medium supplemented with 100 µg/ml adenine (SC+Ade) and processed for fluorescence microscopy as described (Eckert-Boulet et al. 2011). For staining of DNA in live yeast cells, 5 µg/ml of Hoechst 33258 (B2883, Sigma-Aldrich) were added to the culture 10-15 min prior to microscopy and washed out with fresh medium immediately prior to microscopy and imaged at 25 °C. Fluorophores used in yeast were cyan fluorescent protein (CFP, clone W7) (Heim and Tsien 1996) and yellow fluorescent protein (YFP, clone 10C) (Ormo et al. 1996). Microscopy was performed using an AxioImager Z1 (Carl Zeiss MicroImaging, Inc) equipped with a 100x objective lens (Zeiss PLAN-APO, NA 1.4), a cooled Orca-ER CCD camera (Hamamatsu, Japan), differential interference contrast (DIC), and a Zeiss HXP120C illumination source, or on a Deltavision Elite microscope (Applied Precision, Inc) equipped with a 100x objective lens (Olympus U-PLAN S-APO, NA 1.4), a cooled Evolve 512 EMCCD camera (Photometrics, Japan), and a Insight solid state illumination source (Applied

Precision, Inc). Images were acquired using Volocity (PerkinElmer) or softWoRx (Applied Precision, Inc) software. Images were acquired and processed using Volocity (PerkinElmer) software. Images were pseudocoloured according to the approximate emission wavelength of the fluorophores.

For analysis of RPA foci (Fig. 3F) cells were grown in SC media, arrested with α-factor and treated in S-phase with 0.033% MMS for 120 min, then released into the fresh SC media for recovery. For microscopy cells were fixed in FA for 30 min and quenched in 2.5 M glycine for 30 min. Cells were washed twice and resuspended in 50 mM Tris, pH 7.5. Images of cells were obtained using a fully automated Zeiss inverted microscope (AxioObserver Z1) equipped with a MS-2000 stage (Applied Scientific Instrumentation, USA), a CSU-X1 spinning disk confocal head (Yokogawa, Herrsching), LaserStack Launch with selectable laser lines (Intelligent Imaging Innovations, USA) and an X-CITE Fluorescent Illumination System. Images were captured using a CoolSnap HQ camera (Roper Scientific, Canada) under the control of the Slidebook software (Intelligent Imaging Innovations, USA). All fluorescence signals were imaged with a 63x oil objective.

Cell culture and transfection techniques

HEK 293T cells were cultured at 37 °C at 7.5% CO_2 in DMEM (GIBCO-BRL) supplemented with 10% FCS. Transient transfections were performed in 6-well plates (HeLa) using the calcium phosphate method. In general $5x10^5$ 293T cells per well were seeded and transfected the next day using 20 µg

total DNA. After 4-6 h incubation the TF medium was replaced with fresh growth medium, and cells were cultured for another 18-20 h.

Nuclease assays

5'-end-Cy3-labeled oligonucletides were used to prepare synthetic DNA substrates as described (Rass & West 2006). Nuclease assays were carried out with immobilized Mms4-FLAG. The Anti-FLAG immunoprecipitates were extensively washed and mixed with 10 µl reaction buffer (50 mM Tris-HCl pH 7.5, 3 mM $MgCl_2$) containing ~2.5 nM 5'-Cy3-end-labeled substrate (Matos et al 2011). Reactions were incubated for 15-45 min with gentle rotation at 30 °C and stopped by addition of 4 µl 10 mg/ml proteinase K and 2% SDS, and further incubation at 37 ºC for 1 h. Loading buffer was added and radiolabeled products were separated by 10% PAGE, and analyzed using a Typhoon scanner.

Sequence analysis

Close orthologues of budding yeast and human Slx4 were found by NCBI-BLAST (Altschul et al. 1997) and verified by reciprocal BLAST searches. Individual multiple sequence alignments of fungal and mammalian Slx4 were done using ClustalX (Chenna et al. 2003). The Profile Alignment feature was used in ClustalX to align the two profiles from mammalian and fungal Slx4 proteins. This identified the potential Dpb11/TopBP1 interaction motif in human Slx4. Slx4 proteins from further classes were identified by BLAST and first aligned with members of their individual class using ClustalX. Resulting multiple sequence alignments were manually analyzed for the occurrence of

the Dpb11/TopBP1 motif and subsequently manually aligned to the yeast and mammalian motif.

Species abbreviations and accession numbers for Figure S2.

Sp	Schizosaccharomyces pombe	NP_594064
Sc	Saccharomyces cerevisiae	NP_013236
Kl	Kluyveromyces lactis	XP_453790
Ec	Eremothecium cymbalariae	XP_003646141
Nc	Naumovozyma castellii	XP_003928518
Ka	Kazachstania naganashii	CCK71307 (emb)
Td	Toluraspora delbrueckii	XP_003682477
Zr	Zygosaccharomyces rouxii	XP_002497655
Vp	Vanderwaltozyma polyspora	XP_001647185
Lt	Lachancea thermotolerans	XP_002555561
Hs	Homo sapiens	NP_115820
Sb	Samiri b. boliviensis	XP_003928518
Mm	Mus musculus	NP_803423
Rn	Rattus norvegicus	XP_001079342
Sh	Sacrophilus harrisii	XP_003761955
Tm	Trichechus manatus latirostris	XP_004373478
Oo	Orcinus orca	XP_004270504
Xt	Xenopus tropicalis	XP_002932505
Dr	Danio rerio	XP_003201146
Dm	Drosophila melanogaster	NP_648104
Dg	Drosophila grimshawi	XP_001983575
Dw	Drosophila willistoni	XP_002062409
Cc	Ceratitis capitata	XP_004526156
Ag	Anopheles gambiae	XP_001687887

References

Aguilera A, Klein HL. (1988). Genetic control of intrachromosomal recombination in Saccharomyces cerevisiae. I. Isolation and genetic characterization of hyper-recombination mutations. Genetics. 119, 779-790.

Altschul SF, Madden TL, Schäffer AA, Zhang J, Zhang Z, Miller W, Lipman DJ. (1997). Gapped BLAST and PSI-BLAST: a new generation of protein database search programs. Nucleic Acids Res. 25, 3389-3402.

Branzei D, Vanoli F, Foiani M. (2008). SUMOylation regulates Rad18-mediated template switch. Nature. 7224, 915-920.

Chenna R, Sugawara H, Koike T, Lopez R, Gibson TJ, Higgins DG, Thompson JD. (2003). Multiple sequence alignment with the Clustal series of programs. Nucleic Acids Res. 31, 3497-3500.

Cox J, Mann M. (2008). MaxQuant enables high peptide identification rates, individualized p.p.b.-range mass accuracies and proteome-wide protein quantification. Nat Biotechnol. 26, 1367-1372.

Eckert-Boulet N, Rothstein R, Lisby M. (2011). Cell biology of homologous recombination in yeast. Methods Mol Biol. 745, 523-536.

Gonzalez-Huici V, Szakal B, Urulangodi M, Psakhye I, Castellucci F, Menolfi D, Rajakumara E, Fumasoni M, Bermejo R, Jentsch S, Branzei D. (2014).

DNA bending facilitates the error-free DNA damage tolerance pathway and upholds genome integrity. EMBO J. (Epub ahead of print).

Heim R, Tsien RY. (1996). Engineering green fluorescent protein for improved brightness, longer wavelengths and fluorescence resonance energy transfer. Curr Biol. 6, 178-182.

James P, Halladay J, Craig EA. (1996). Genomic libraries and a host strain designed for highly efficient two-hybrid selection in yeast. Genetics. 144, 1425-1436.

Klein HL. (2001). Mutations in recombinational repair and in checkpoint control genes suppress the lethal combination of srs2Delta with other DNA repair genes in Saccharomyces cerevisiae. Genetics. 157, 557-565.

Knop M, Siegers K, Pereira G, Zachariae W, Winsor B, Nasmyth K, Schiebel E. (1999). Epitope tagging of yeast genes using a PCR-based strategy: more tags and improved practical routines. Yeast. 15, 963-972.

Liberi G, Maffioletti G, Lucca C, Chiolo I, Baryshnikova A, Cotta-Ramusino C, Lopes M, Pellicioli A, Haber JE, Foiani M. (2005). Rad51-dependent DNA structures accumulate at damaged replication forks in sgs1 mutants defective in the yeast ortholog of BLM RecQ helicase. Genes Dev. 19, 339-350.

Matos J, Blanco MG, Maslen S, Skehel JM, West SC (2011) Regulatory control of the resolution of DNA recombination intermediates during meiosis and mitosis. Cell 147**:** 158-172

Mullen JR, Kaliraman V, Ibrahim SS, Brill SJ. (2001). Requirement for three novel protein complexes in the absence of the Sgs1 DNA helicase in Saccharomyces cerevisiae. Genetics. 157, 103-118.

Ormö M, Cubitt AB, Kallio K, Gross LA, Tsien RY, Remington SJ. (1996). Crystal structure of the Aequorea victoria green fluorescent protein. Science. 273, 1392-1395.

Pfander B, Moldovan GL, Sacher M, Hoege C, Jentsch S. (2005). SUMO-modified PCNA recruits Srs2 to prevent recombination during S phase. Nature. 7049, 428-433.

Rass U, West SC (2006) Synthetic junctions as tools to identify and characterise Holliday junction resolvases. In *Meth. Enzymol.*, Campbell JL, Modrich P (eds), Vol. 408, pp 485-501. San Diego: Elsevier

Robert T, Dervins D, Fabre F, Gangloff S. (2006). Mrc1 and Srs2 are major actors in the regulation of spontaneous crossover. EMBO J. 25, 2837-2846.

Szakal B, Branzei D. (2013). Premature Cdk1/Cdc5/Mus81 pathway activation induces aberrant replication and deleterious crossover. EMBO J. 32, 1155-1167.

Thomas BJ, Rothstein R. (1989). Elevated recombination rates in transcriptionally active DNA. Cell. 56, 619-630.

Vanoli F, Fumasoni M, Szakal B, Maloisel L, Branzei D. (2010). Replication and recombination factors contributing to recombination-dependent bypass of DNA lesions by template switch. PLoS Genet. 6: e1001205.